NATURAL VENTILATION OF ATRIUM SPACES

Rong Li, B.Arch.

A thesis submitted for the
Degree of Doctor of Philosophy

School of Architecture,
The University of Sheffield, UK

September, 2007

SUMMARY

This research is aimed to develop a series of design guidelines and relevant prediction tools for the incorporation of natural ventilation in atrium spaces as a passive cooling strategy. Focused on the geometrical and thermal characteristics of atrium buildings, four aspects related to this purpose are investigated in this work, including thermal comfort, wind-induced ventilation, buoyancy-induced ventilation, and combined buoyancy- and wind-driven ventilation.

In order to identify when passive cooling strategies are needed for atrium spaces, a new thermal comfort assessment method which enables the treatment of the solar radiation and non-uniform environment is developed using MATLAB as the data exchange platform. It is found that high mean radiant temperature (MRT) can be a more significant factor contributing to the thermal discomfort of the space compared to air temperature when the internal occupants' level is irradiated by the sun rays. It is also shown that the air temperature at the occupants' level is mostly affected by the temperatures of the surfaces at lower levels, and the temperatures at the roof level and the upper areas generally have little influence on the air temperature at the occupants' level.

The study of wind-induced ventilation is mainly concerned with the airflow through roof openings since the atrium is often placed in the centre of a building and the openings at lower levels may not be available as a result. In this way the air movement in the space is actually driven by the recirculation rather than the direct main flow from the wind. Three possible flow patterns, and related controlling forces for each flow pattern are defined first, based on which the impacts of the design parameters on the ventilation performance are investigated by CFD techniques and design guidelines are developed accordingly.

The effects of the location of heat source and the control of the neutral level are studied for buoyancy-driven natural ventilation of atrium spaces. The tendency of the heat source efficiency with the variation of its location is examined and the optimised location for the heat source is suggested, based on which the guidelines for the selection of materials for atrium internal surfaces are made. A series of new algorithms are also developed for the prediction of neutral level and airflow rate when bi-directional flows occur and they are verified with CFD simulations.

The investigation of the combined ventilation focuses on the condition where wind forces and buoyancy forces partly assist each other and partly oppose each other, and it is found that the phenomenon of solution multiplicity still exists for this condition and different solutions may have different ventilation performance depending on the initial conditions.

Based on the above investigations, a control diagram for the passive design of atrium spaces is developed finally and a new methodology for the design of large-volume spaces with non-uniform environment is proposed. It can also be concluded that CFD is a valuable tool for parametric studies associated with airflows and it is capable of dealing with very sophisticated characteristics of air movement, such as flow separation, bi-directional flows and solution multiplicity.

Key words: atrium buildings; natural ventilation; thermal comfort; CFD; design guidelines

ACKNOWLEDGEMENTS

Firstly, I would like to acknowledge the support of my supervisor, Dr Adrian Pitts. He inspired, challenged and motivated me throughout the whole PhD study, and his valuable suggestions and encouragement are very important to the completion of this thesis.

Special thanks go to a number of staff at School of Architecture, the University of Sheffield including Prof Steve Sharples, Prof Jian Kang and Mr Ian Ward for their invaluable advice and help on this research. I am also very grateful to Prof Yuguo Li at the Department of Mechanical Engineering, the University of Hong Kong, whom I visited for this project.

Thanks also extend to my colleagues at Faculty of Architectural Studies, the University of Sheffield, including Jijun Zhao, Xin Wu, Jianqiang Li, Xuemei Li, Linan Wang and Bing Chen, and my friends in China including Zengtao Ye, Jin Wang for their collaboration and friendship. I am also indebted to Martyn Fisher, who helped with the proofreading of this thesis.

I would like to express my warmest gratitude to my family in China including both my parents and my fiancée Guihua Jiang, whose unceasing love makes my study in the UK possible. Finally, the financial support from the Fee Waiver Scheme and the Excellence Exchange Scheme of the University of Sheffield, and the Henry Lester Trust is also gratefully acknowledged.

CONTENTS

LIST OF SYMBOLS

A	Area	$\{ m^2 \}$
B	Buoyancy flux	
C_D	Discharge coefficient	{}
C_p	Pressure coefficient	{}
c_p	Specific heat	$\{ J/KgK \}$
f	Surface area	$\{ m^2 \}$
F	View factor	{}
g	Gravitational acceleration	$\{ m/s^2 \}$
h	Vertical distance	$\{ m \}$
H	Height of a vertical surface	$\{ m \}$
h_c	Convection coefficient	{}
i, j	Grid indices in x and y directions	
k	Thermal conductivity or turbulence kinetic energy	$\{ m^2/s^2 \}$
L	a length scale	$\{ m \}$
M	Metabolic rate	$\{ W \}$
Nu	Nusselt number	$\{ m^2 \}$
P	pressure	$\{ Pa \}$
Pa	Atmospheric pressure	$\{ Pa \}$
PMV	Predicted mean vote	
PPD	Predicted percentage of dissatisfied	
Pr	Prandtl number	
q	Airflow rate	$\{ m^3/s \}$
Ra	Rayleigh number	
t	Time or temperature	$\{ s \}$ or $\{ K \}$
$\bar{t}_r$	Mean radiant temperature	$\{ K \}$
T	Temperature	$\{ K \}$
U_R	Reference velocity	$\{ m/s \}$
U	Velocity component in x-direction	$\{ m/s \}$
v	Velocity component in y-direction	$\{ m/s \}$
v_{ar}	Relative air velocity	$\{ m/s \}$

V	Volume	$\{ m^3 \}$
w	Velocity component in z-direction	$\{ m/s \}$
W	Activity level or building width or Effective mechanical power	$\{W/ m^2\}$ or $\{m\}$ or $\{ W/ m^2 \}$
u_j	Velocity components expressed in tensor notation	$\{ m/s \}$
x, y, z	Cartesian coordinates	
x_j	Cartesian coordinates expressed in tensor notation	

Greek Symbols

Γ	Turbulent heat diffusion	$\{ Pa \cdot s \}$
ρ	Fluid density	$\{ Kg/m^3 \}$
μ	Molecular viscosity	$\{ Pa \cdot s \}$
μ_t	Eddy viscosity	$\{ Pa \cdot s \}$
β	Thermal expansion coefficient of air	$\{ K^{-1} \}$
τ	Shear stress	$\{ N/m^2 \}$
α	Thermal buoyancy air change parameter	
γ	Wind air change parameter	
ε	Dissipation rate of turbulent energy	$\{ m^2/s^2 \}$
σ_t	Turbulent Prandtl number	
κ	von Karman's constant	$\{\}$

Subscripts

u	State at upper location of a vertical wall
l	State at lower location of a vertical wall
o	State of outdoor environment
i	State of indoor environment
b	State induced by buoyancy forces
w	State induced by wind forces
cl	State at clothes of human beings

INTRODUCTION

1.1 Development of atrium buildings

Atrium spaces, which nowadays are generally defined as "those protected or glazed winter-gardens within buildings" (Watson 1982)[1], have been incorporated as a design element with increased frequency over the last few decades. Large numbers of buildings with atria have been built all over the world, and ever since the late 1960s the atrium concept has been undergoing a great revival of interest among architects, clients and the general public (Bednar 1986). Both a great many ideas and much enthusiasm have been expressed with regard to this special type of space. First and the most important, atrium spaces can help with the enhancement of social and commercial activities because of their ability to attract shoppers and tenants and increase the level of communication between them. In addition, they can enable more surfaces to be "open" to nature and help occupants "reach" the outside without having to leave the building (Watson 1982; Aschehoug et al. 1990). Not only can they be adopted in newly-built public buildings as a cafeteria or as entrance space to facilitate the circulation of people, but they can also be used for the refurbishment of existing traditional and historical buildings as the link between neighbouring buildings. They can also be used for various other purposes: as summarised by Saxon (1983), atrium spaces can fulfil functions including economic, cultural, shelter, accommodation, etc. With the popularity of the use of glass, the atrium space has already become a common feature of modern public buildings. Indeed, the

[1] Whilst an accurate definition does not exist, this one is the most commonly and widely used. In this thesis, atria refer to those with large volumes and glazed roofs.

present time can be regarded as an epoch of atrium buildings and as has been pointed out by Bednar (1986), how long this epoch will last and whether the atrium will become a permanent spatial type still remains to be seen; however, what is known at this time is that the atrium is a vital and exciting feature of the present architectural era, making it highly worthy of study and analysis, both now and for the foreseeable future.

Over the past few years, one feature of atrium buildings concerned with energy and environmental issues has frequently been identified: they are often claimed to be able to offer passive benefits in terms of moderating outdoor climate and saving energy when properly incorporated (Saxon 1983; Setty 1983; Bednar 1986). With the realisation that fossil-fuel consumption releases the greenhouse gas CO_2 causing global warming, energy conservation has become an important issue and the appearance of atria seems to address this concern very pertinently. Atria have been stated as capable of improving indoor comfort level by natural climatic means created by architectural devices, such as passive heating, natural ventilation and daylight enhancement, mainly due to their internal greenhouse effect and the stack effect brought about by the skylights and large spatial volume. In addition, the natural ventilation brought about by buoyancy and wind forces in these spaces can effectively reduce the possibility of "sick building syndrome" (SBS) and significantly improve the indoor air quality. As a consequence, the design of this type of space has been attracting a large number of designers and researchers. Many recent buildings designed with the concern regarding sustainability issues have incorporated atrium type spaces such as the IONICA building at Cambridge, UK (Smith and Pitts 1997), the GSW office block in Berlin (Russell 2000) and National Trust Central Office Swindon (RIBA Awards, 2006).

However, atrium spaces are neither energy efficient automatically nor do they achieve this efficiency only by simply adopting large areas of glazing (Baker and Steemers 2000). As indicated by some researchers, the energy and environmental potential of atrium buildings has not been exploited to the full and it has been reported that many atrium buildings were even energy and money luxuries simply because of inappropriate design. Moreover, many atrium buildings, which are claimed as a buffer space, usually require large amounts of energy to service them due to the large spatial volume and are still found fully air conditioned (Watson 1982; Bednar 1986; Goulding et al. 1992). This is particularly true for those atrium spaces located in warm climates: they can usually perform quite well during winter as solar collectors because of greenhouse effect, but in summer, the space is very easily overheated thus necessitating the use of the air-conditioning system. Therefore, in order to make atrium buildings really energy efficient and sustainable, passive cooling strategies will have to be incorporated during warm period. Furthermore, the increasing level of concern regarding global warming makes the study of this issue even more imperative, since with this trend more and more new atrium buildings will experience the problems of overheating, even including those located in cold or moderate climates.

1.2 Passive cooling of atrium buildings

The main source of the problem of excessive energy consumption in atria in warm weather lies in the material invariably used inside as the envelope: glass. In other words, they may employ too much glazing inappropriately. Although the use of glass has become characteristic of modern buildings, glass can aid but does not equate to sustainability or energy saving. The abuse of glass in modern architecture has resulted in many negative effects and led to a lot of criticism. As stated by some researchers, fully glazed buildings are perhaps the most dangerous type of building from the point view of dull and uncritical replication: they are hardly sustainable even if well designed, and they are definitely unsustainable if poorly designed (Butera 2005).

Basically, the geometrical and thermal characteristics can result in significant change of the physical mechanism of the energy transfer and air movement of the internal atrium space, on which the design of passive cooling strategies are based. This can also be regarded as the reason why traditional passive cooling strategies are sometimes not easily adapted into atrium spaces, and consequently guidelines and tools for the use of these passive strategies in ordinary spaces are usually not applicable in atria.

In order to provide cooling effects for an overheated atrium space, an accurate and effective assessment of the indoor thermal comfort level is indispensable to diagnose the potential causes for the overheating and evaluate the effects of various cooling strategies. Compared to ordinary spaces, atrium type spaces can let in a much larger amount of solar radiation, which can significantly affect the mean radiant temperature (MRT) of the space and hence the thermal comfort level. If conventional approaches of predicting thermal comfort level are still used in atrium spaces and the impact of solar radiation is neglected (i.e. the air temperature is considered as the main indicator for the thermal comfort level of the space), there will be a significant delay of the adoption of suitable passive cooling strategies and thermal discomfort can be caused. As a consequence, a new approach for the evaluation of the thermal comfort level of atrium spaces is needed to take their thermal characteristics into account.

With regard to the cooling strategies, a number of passive cooling techniques can be considered at the early design stage in order to cope with the overheating problems in atrium spaces, such as the incorporation of shading devices, thermal mass, natural ventilation, etc. As an effective and favourable strategy to bring on cooling effects, natural ventilation in atrium spaces is of particular interest if the outside air is cooler than indoor air which is the normal case for most atria in warm weather, because not only will it enhance the convective heat transfer between the occupants and the surrounding air, it will also bring in cool outside air, both of which can improve the thermal comfort level of the space. Moreover, it is cheap and clean. There are two types of natural ventilation in terms of their physical mechanism: wind-induced

natural ventilation and buoyancy-driven natural ventilation. For the incorporation of natural ventilation, designers usually need to understand the impacts of design parameters on a number of ventilation indices for the evaluation of the ventilation performance at the early stage of design process, such as the airflow pattern, the air velocity and temperature distribution at occupants' level and the airflow rate.

Many of the design guidelines developed for other plain spaces regarding natural ventilation are still useful for atrium buildings, such as those for the incorporation of wind-induced cross ventilation and those for buoyancy-driven displacement ventilation with the heat source located at the bottom of the building. However, atrium spaces also have some special features for the use of natural ventilation related to their geometrical and thermal characteristics, which requires further development of the relevant design guidance. This issue is elaborated in terms of the mechanism driving the airflow as follows.

- *Wind-induced ventilation*

It is known that atrium spaces are often located at the centre of buildings to enhance the communication of occupants between adjacent buildings, such as those used in shopping malls and office blocks. This may lead to the unavailability of the openings towards the outside at the lower occupants' level in the atrium, and as a result openings at the roof level have to be incorporated in order to catch the wind. An example of using openings of skylights in a shopping mall is illustrated in Figure 1.1. In this situation, the ventilation performance of the atrium spaces will be very sensitive to the roof design including the roof shape and the characteristics of the openings in the roof, such as the location and the size of the openings. More interestingly, it should be noted that, under this circumstance, the internal air movement is driven by the recirculation flow, which is quite different from the cross ventilation of ordinary spaces which directly uses the main flow of the oncoming wind.

- *Buoyancy-driven ventilation*

Buoyancy-driven ventilation is easier to induce in atrium spaces compared to other ordinary types of spaces, as this kind of air flow can be enhanced by stack effect driven by the large height and the relatively higher temperature of atrium space due to the large glazing commonly employed. Nevertheless, one precondition of the incorporation for the buoyancy-driven ventilation is to make sure that the internal temperature will not be too high and cause thermal discomfort at the occupants' level. Fortunately, one advantage of an atrium space is that it usually has large height but only the bottom level is occupied. Thus it is possible to sacrifice the thermal comfort of the upper level which is not occupied, and use the surfaces at that level heated by the sun as the heat source to generate buoyancy-driven natural ventilation

for the whole space without compromising the thermal comfort level of the occupants at the bottom. In this way, cooling effects can be generated by heating processes and the atrium space functions as a solar chimney. From this above description, it can be seen that an important feature that distinguishes buoyancy-driven ventilation of atrium spaces from that of other spaces is the location of the heat source that drives the air movement. For ordinary spaces, the heat source is usually located as the bottom, such as the heat from occupants and appliances like computers or other equipment, but the most important and favourable heat source in atrium spaces is usually the surfaces irradiated by the sun, as the heat intensity from the solar radiation is much stronger compared to that from the appliances and occupants. This change may significantly influence the airflow inside the space and cause problems if a traditional prediction and design tool is used.

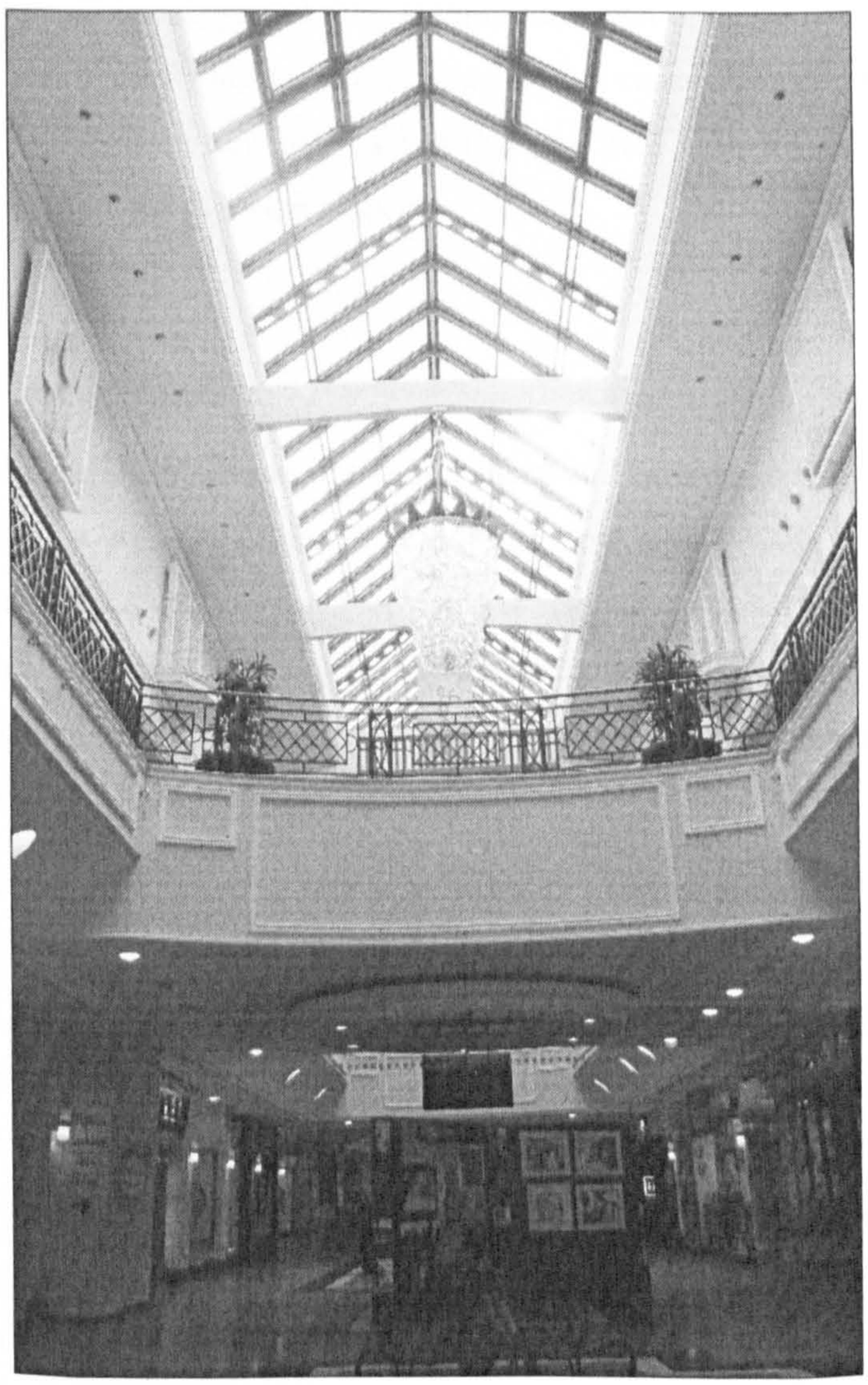

Figure 1.1: Internal view of the atrium in the shopping mall at Meadowhall, Sheffield, UK (see roof openings at the top of the picture)

Another feature for the buoyancy-driven ventilation in atrium spaces is that it can be designed for the enhancement of the airflow of the adjacent buildings as a buffer zone. Usually it is hoped that the warm air of the adjacent buildings can be sucked into the atrium and then expelled from the upper openings together with the hot air from the atrium space. For this purpose the level of the neutral plane of the atrium space where the internal pressure equals to the external pressure, should be designed to be very high, i.e. at least higher than the uppermost openings of the adjacent spaces (see Figure 1.2, otherwise the hot air in the atrium may get into the adjacent buildings causing thermal discomfort) and a common way of realising this is to enlarge the upper opening. It should be noted that, when the size of the upper opening is increased to certain extent, the height of the neutral plane will rise and it may intersect with the upper opening causing bi-directional flows. Conventional methods for the prediction of the neutral level are for small openings and they assume that each opening has a uniform pressure distribution. As a result they may be not applicable for cases with large openings and bi-directional flows, and therefore new approaches that can deal with the non-uniform pressure distribution of an opening need to be developed.

- *Combined wind and buoyancy driven ventilation*

This kind of natural ventilation in atrium spaces will take place when both outside wind forces and solar radiation are very intensive, and it has more significance in atrium spaces than in other type of spaces, because the buoyancy force is stronger in atria than in other spaces and may be similar in scale to wind forces. The two forces may assist each other, thus reinforcing the ventilation effects but it is also possible for them to oppose each other depending on the environmental and design scenarios.

Since the design for the situations where the two forces assist each other is generally straightforward, this research is particularly interested in the conditions when the two forces oppose each other. For some cases, one force may be totally overwhelmed by the other force and thus the ventilation is actually dominated by the stronger one. This is also the most popular basic model for the research in this area. However, there are a number of occasions where the two forces oppose each other but the stronger one cannot overwhelm the weaker one and even partly assist it. For instance, when bi-directional flow occurs for a large opening, which is the case for buoyancy-driven mixing flows, the wind will always support part of the airflow at the opening, no matter what the magnitude or direction of the wind velocity is (see Figure 1.3). This flow can also occur in atrium spaces quite often as large openings are usually employed and it will be the main concern of this research regarding this area.

The above analysis discusses different flow regimes that may take place in atrium spaces, and it can also be envisioned that the use of either wind-induced ventilation or buoyancy-driven ventilation or combined natural ventilation can be of great benefit, but it can also be of high risk if enough care is not taken during the design process. In order to take the use of different ventilation regimes into full advantage and avoid the risk of discomfort at the ground level, impacts of relevant design parameters on the ventilation performance of the space need to be made clear for the use of designers and engineers and this will be the main concern of the research.

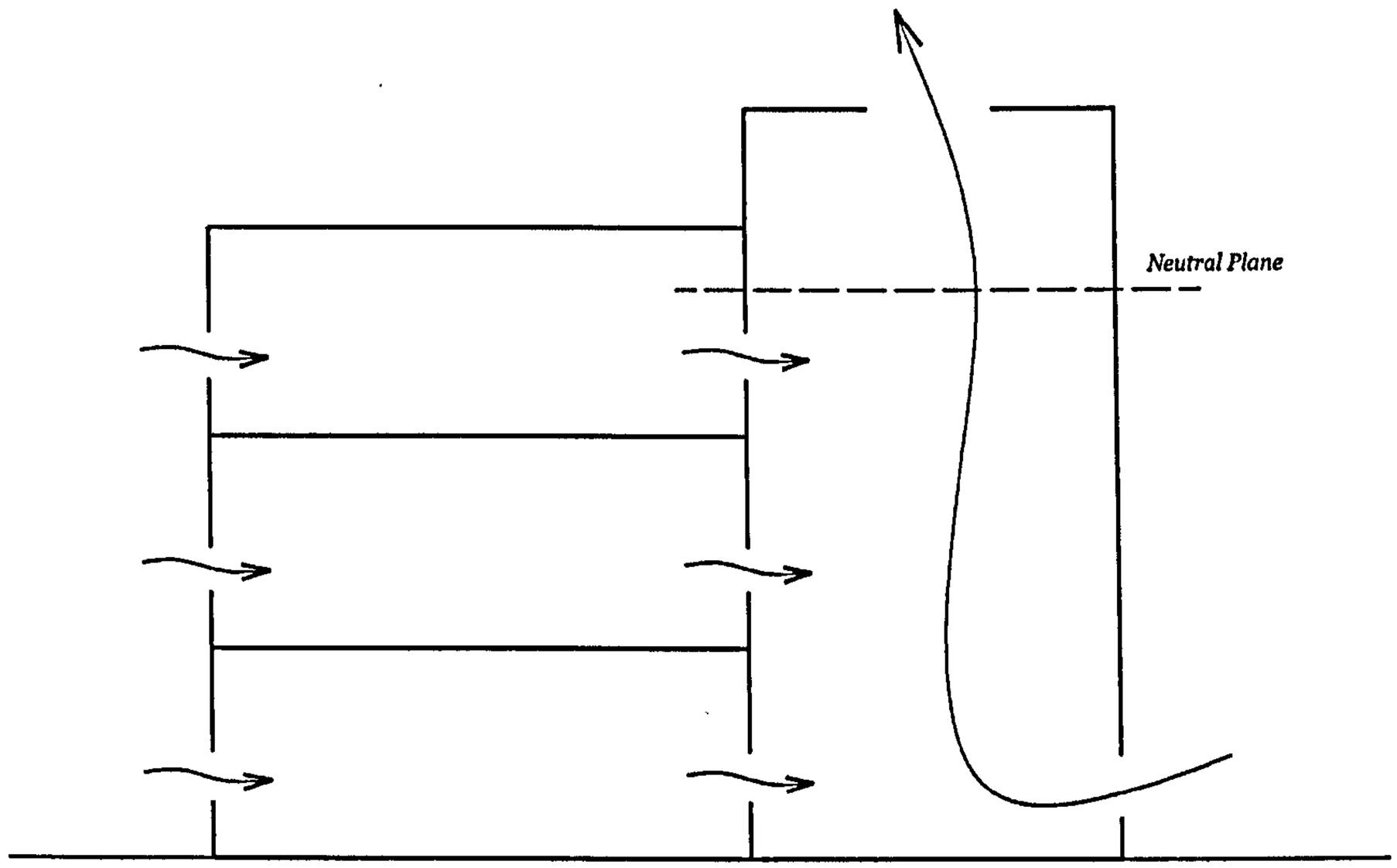

Figure 1.2: The use of the atrium space to assist the ventilation of adjacent buildings

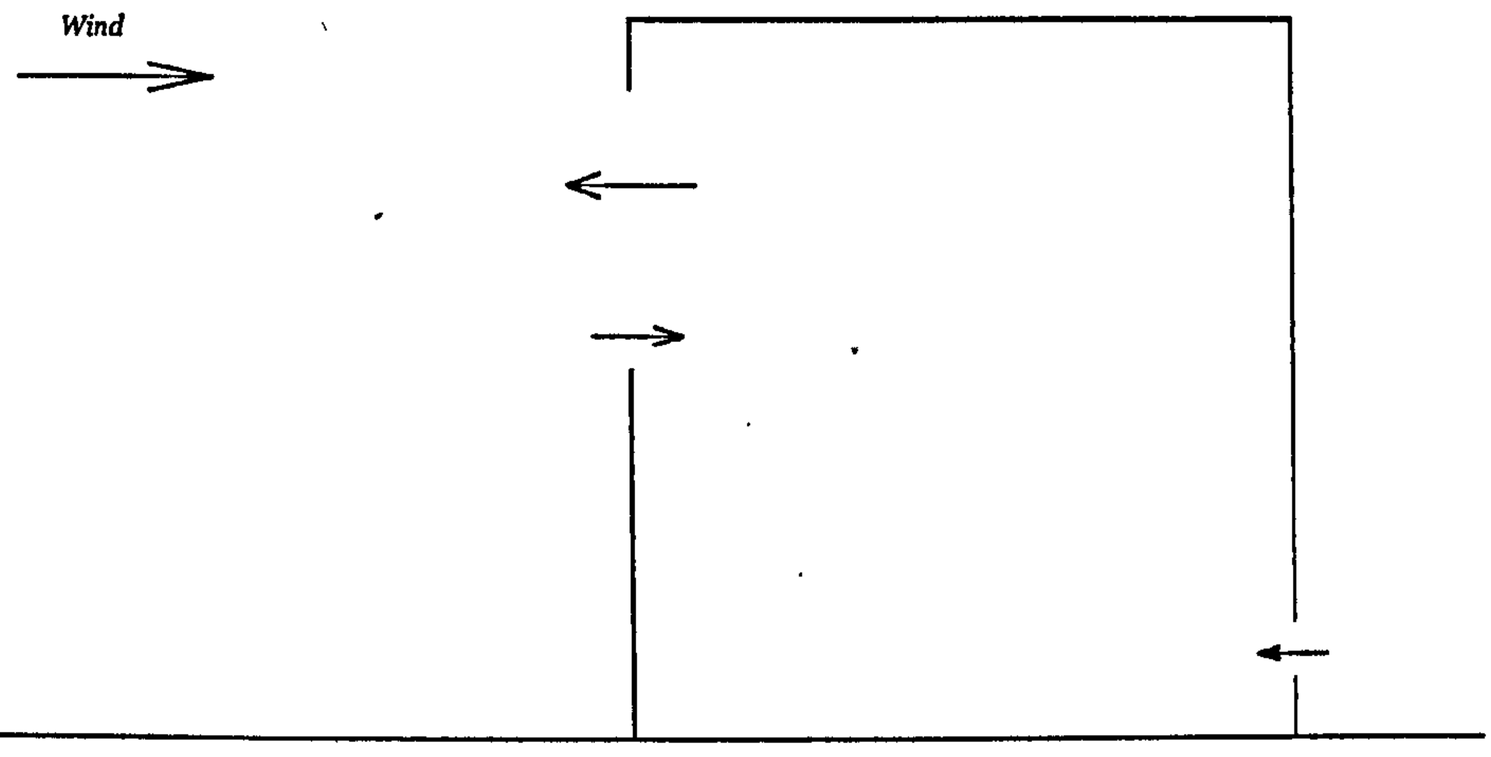

Figure 1.3: Illustration of an example where the wind forces and the buoyancy forces partly oppose and partly assist each other (when bi-directional flow occurs)

1.3 Research objectives and thesis outline

With the aim to develop appropriate guidelines for the design of natural ventilation at the early stage in order to provide passive cooling effects, this research will particularly try to deal with following issues:

- To develop a new approach for the thermal comfort assessment of atrium spaces taking the impacts of solar radiation into account;
- To investigate the wind-induced natural ventilation through roof openings of atrium spaces (this part of study will be the main emphasis of the research since wind is the most effective source driving the natural ventilation of atria);
- To study the effects of the heat sources on the buoyancy-driven natural ventilation and to develop algorithms for the control of the neutral level, especially when bi-directional flows are incurred;
- To examine the combined natural ventilation when buoyancy forces and wind forces partly oppose each other and partly assist each other.

This thesis records the major developments of the research and is organised into seven chapters:

- The research background and fundamentals of the whole research are reviewed in Chapter Two. It starts with the historical development of atrium buildings and traces the idea back to ancient times. The main technical facets that are associated with passive cooling strategies of atrium spaces, including the basic heat transfer process, energy use, thermal comfort and air movement, are then introduced with particular focus on the review of natural ventilation strategies, and the research direction is highlighted accordingly.
- Chapter Three discusses the methodology employed in the study with particular attention on the research methods of air movement, as the majority of the study is related to this area. Commonly-used methods are reviewed first and then an appropriate approach is selected and validated.
- Chapter Four focuses on the development of a new method for the thermal comfort assessment of atrium spaces. The approach that enables to take the special characteristics of atria, such as non-uniform environment and incident solar radiation into account is introduced first and then a case study is carried out for illustration. Finally, based on the new method, the impacts of related design parameters are studied and some guidelines are obtained as a result.

- Chapters Five to Seven systematically investigates different air flow regimes of the natural ventilation of atrium spaces including natural convection, buoyancy-driven ventilation, wind-induced ventilation and combined ventilation respectively. Emphasis for the investigation of each flow regime is not the same. Chapter Five studies the wind-induced natural ventilation in atrium spaces through roof openings and the main parameters chosen to be investigated include roof shape, opening characteristics such as location, size and opening methods, and adjacent buildings. Guidelines on the design of these parameters are also developed accordingly.

- Buoyancy-driven ventilation is discussed in Chapter Six and concentration is placed on the influences of the location of heat source and the treatment of large openings. Both displacement and mixing ventilation are studied. Design guidance on the selection of the materials for the atrium surfaces regarding buoyancy-driven ventilation is put forward finally and new algorithms for large openings are developed and compared with simulations.

- Chapter Seven deals with combined buoyancy and wind-driven natural ventilation of atrium spaces and discusses the design strategies when these two forces partly oppose each other. The airflow pattern, vertical temperature profile and the air velocity/temperature distribution at the occupants' level are studied for the conditions with different combinations of the buoyancy and wind forces, and the design guidance on the control of the two forces in order to achieve a better ventilation performance is developed.

- Chapter Eight concludes this research and recommendations are made for the future work.

2 REVIEW OF FUNDAMENTALS

2.1 Introduction

Chapter One has stated that the most serious problem for the energy efficiency of atrium buildings is that they can easily overheat in warm weather, and natural ventilation is a promising passive strategy to overcome this problem. As a review for the basics of the whole research, this chapter is intended to introduce the fundamental knowledge required for the investigation of the issues proposed in previous chapter from two perspectives: historical and technical.

This chapter begins with the introduction to the historical development of atrium buildings and traces the idea of using atrium space or courtyard to moderate climate back to ancient times. The role of climate in the design of energy efficiency of atrium spaces is discussed and particular attention is paid to the courtyards and atrium prototypes used in history for ventilation purposes to show the possibility and potential for the passive cooling of atrium spaces.

Technical facets in relation to the ventilative cooling strategies of atrium spaces are then described and the state-of-the-art research is also reviewed. Issues related to energy use, including the basic energy transfer process, resulting thermal characteristics and applications of atrium spaces are introduced first in Section 2.3, and subsequently, the thermal comfort issues are described in Section 2.4 including both the basic theory and the approaches for the

prediction of the thermal comfort level of atrium spaces. The basic physical mechanism of natural ventilation and its applications in atrium spaces are discussed in Section 2.5. Different flow regimes are dealt with respectively in the subsequent subsections and the impacts of design parameters and relevant prediction methods are reviewed, based on which the directions of this research are discussed in detail. Finally a summary is provided in Section 2.6.

2.2 Evolution of atrium spaces

The idea and concept of an atrium space can be traced back to climate sensitive and social use of a central room in ancient design. The antecedents of atria are evident in architecture since the beginning of recorded history. The review of its historical background will start from the origin of this concept so that its idea and concept can be fully understood. This part of work is mainly based on the work of Bednar (1986) and Saxon (1994). According to them, the whole history of the development of atria is not continuous and can be divided into four periods –

- Antique origins – the era of development of the idea of courtyard and central room up to the nineteenth century;
- First epoch – mainly the nineteenth century when the use of metal and glass as significant components in architecture began to develop;
- Second epoch – from the turning of nineteenth century to early twentieth century, when the atrium of the first epoch was improved;
- Third epoch – from the mid twentieth century up to now when the atrium concept has enjoyed a revival and greatly enhanced the economy and environment.

A brief review is carried out in the following section. The first three periods are reviewed in Section 2.2.1 and the last period is reviewed in Section 2.2.2.

2.2.1 Historical Development

• *Antique origins*

The idea of atrium can be traced back to the old concept of central room and courtyard in very ancient times and the reason why the concept and idea of atrium were developed is mainly three-fold:

First, it is the result of urban development. With the emergence of urban settlements, the courtyard concept, which had evolved from the encampments of nomadic peoples, was brought into the individual dwelling, thus creating the atrium house form. Because of some conditions of urbanism – the lack of privacy, limited land area, and limited exposure to

communal space, the atrium space was incorporated to plan a logical form. It addresses these problems while providing other positive amenities: a source of natural light and air, protection against the wind, etc.

Secondly, although the general conditions of urbanism can be considered as one basis for the development of the atrium plan, climatic control is equally important. Examples of adopting courtyards or quasi-atrium[1] spaces to alleviate outdoor severe climate can be found in quite a big range of climates. In hot and dry climates, courtyards are incorporated to provide cooling functions. In North Africa, for example, shallow low quasi-atria, one story high are utilised as collectors of cool night air and a source of shade in the daytime. In regions like southern Spain, quasi-atria with deeper cross sections are utilised for the same reasons but with great efficiency. In temperate climates with moderate winter seasons, like Rome, shallow quasi-atria serve both as passive solar collectors and as wind shelters. In warm-humid climates, shallow quasi-atria serve to generate wind-induced ventilation for cooling effects. It is shown by these examples that the atrium type space has the potential to incorporated passive cooling strategies, although these precedents cannot be copied to modern atrium design because the materials of the space and the physical mechanism behind have significantly changed.

The third reason is that the idea of atria or courtyards can lead to some social and cultural effects. Those courtyard houses, used in cultures which are both populous and hierarchic, serve the individual need to get away while still remaining within the familiar territory of the family (Rapoport 1969). The rooms surrounding the courtyard provide this separation of domains, and the courtyard provides communal precinct. This kind of courtyards can be found in China, Greece, Rome, India and many Islamic countries.

A great many examples of courtyard houses with this original idea have been found. The earliest according to archaeological exploration is perhaps the one found at Ur on the Euphrates River in Mesopotamia, which dates from the third millennium B.C (See Figure 2.1). Other examples include an ancient Greek house design, Le Grand Commun at Versailles by Mansart, the Pallazzo Farnese, etc.

[1] As clarified at the very beginning, 'atrium spaces' in this thesis refer to those with glazed roofs and large heights. Obviously there were no atrium spaces at this stage according to this definition because glass was not invented and hence the concept 'quasi-atrium' is used here.

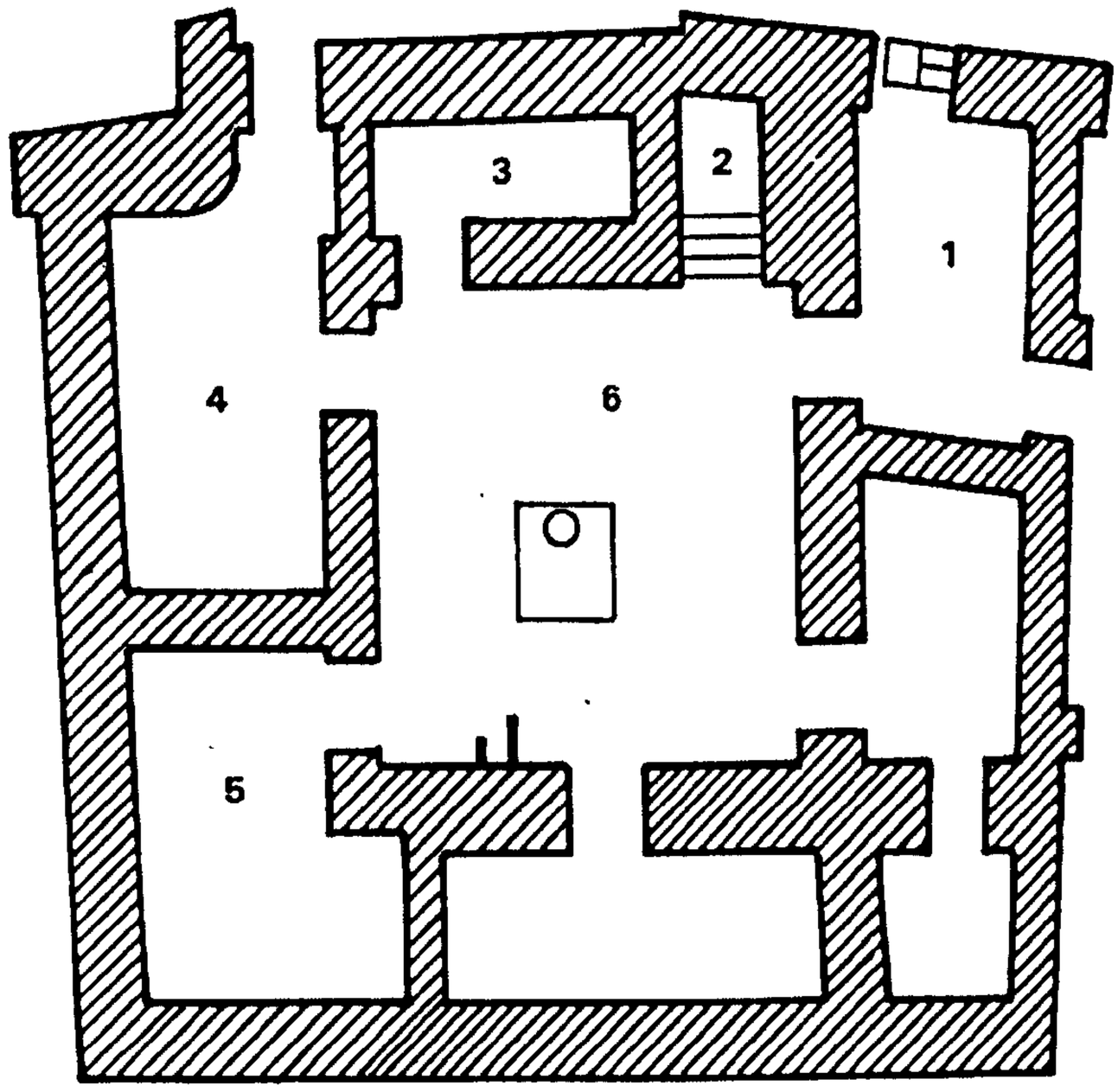

Figure 2.1: Plan of the House at Ur, Mesopotamia: (1) Entrance Hall; (2) Staircase; (3) Washroom; (4) Kitchen; (5) Storeroom; (6) Courtyard. (Bednar 1986)

• *First epoch*

In the early nineteenth century, the use of metal and glass as significant components in architecture began to develop, which greatly changed the old form of courtyards and developed the old idea of a courtyard house into the real concept of an atrium. Cast iron and wrought iron actually had been available since 1800, but they were not widely used. The search for greater structural spans and a concurrent development in glass manufacturing are the real motivations of the modern atrium idea. In 1855, Sir Henry Bessemer invented a new method of making steel which resulted in larger and stronger structural components, leading to ever greater spans of space. The fascination of these two new technologies resulted in the development of buildings incorporating iron and glass, which were utilised primarily in the public spaces of atrium buildings. Many classical examples (See Figure 2.2 for an example), which were used as conservatories, train stations, etc, were built in England and France and the culmination was the Crystal Palace in Hyde Park, London, by Joseph Paxon in 1851 (Hix 1974).

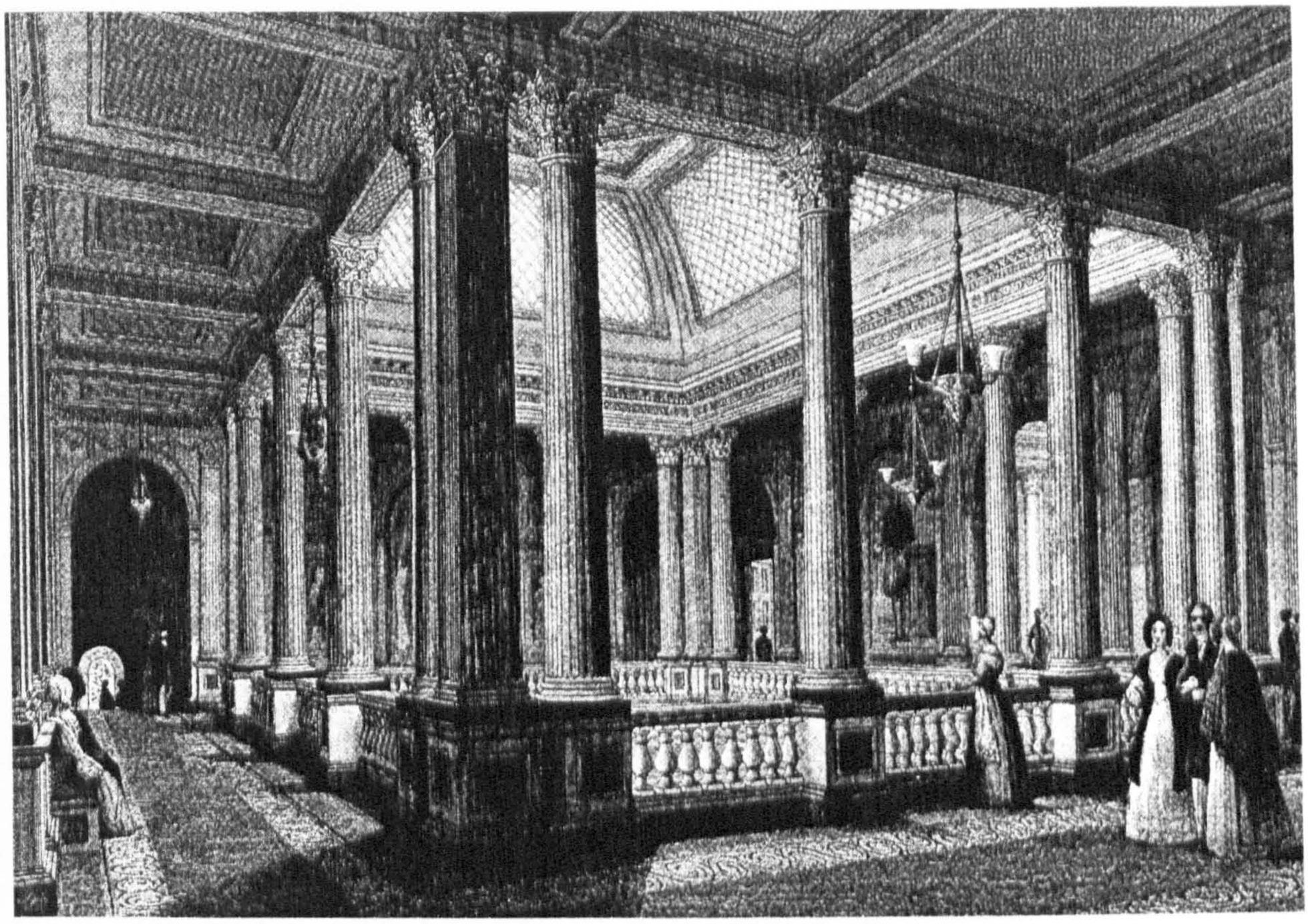

Figure 2.2: Drawing of saloon in the Reform Club, London, England (Bednar 1986)

Generally, there were two special types of atria during this time in terms of their geometry – one was linear atria, which can also be termed as the *arcade* with the other being the rectangular kind. The linear ones, or the arcade, incorporated a glass-covered passageway which connects two busy streets and is lined on both sides with shops (Geist 1983). Its invention was based on the specific needs of society during that century for a public space, protected from traffic and the weather, which would aid in marketing. Perhaps the best known of these arcades is the Galleria Vittorio Emanuele II in Milan, built in 1867 by Mengoni (See Figure 2.3). Cleveland Arcade in Ohio, the United States, built in 1890 by John Eisenmann and George Smith is another good example. The rectangular atria were more common and had much wider functional applications whereas the arcade was exclusively for commercial purposes. The Amsterdam Stock Exchange, designed by H. P. Berlage between 1898 and 1903, and London Coal Exchange on Lower Thames Street designed in the years 1846 to 1899 by J. B. Bunning are good cases.

However, the excitement in Europe began to wane toward the end of the century as architectural styles and forms began to change. The fire hazard was a real reason for the waning, as people discovered that iron or steel and glass structures could not withstand the intense heat of urban fires. Many of the iron and glass buildings burned and collapsed.

Figure 2.3: Interior view, Gallleria Vittorio Emanuele II, Milan, Italy (Bednar 1986)

• *Second epoch*

The second epoch of the atrium took place in the United States at the turn of the nineteenth century. The buildings from this era were based upon the earlier European models and as a group they were all masonry buildings on the exterior, with iron, steel, and glass being used only in the atrium space itself. More than likely, this design strategy was a response to the fire problems encountered in Europe. Some other reasons are probably incorporation of abundant light and air and some monumental civic use. On the one hand, architects had convinced their clients that bringing natural light and fresh air to the office workers was worth the sacrifice in additional office space. On the other hand, the use of the atrium was very appropriate to monumental civic buildings, such as courthouses and city halls, which had to accommodate large throngs of people requiring a multitude of services (Bednar 1986).

All of these atria were either square or rectangular in plan and multi-storeyed in section and they housed the same range of functions as their European models. Several examples are the Pension building in Washington, D.C designed by General Montgomery Meigs in 1882, the Bradbury Building in Los Angeles, designed by George Wyman in 1893 and John Wanamaker's Department Store in Phiadelphia by Burnham in 1902 – 1911. Figure 2.4 shows an example of this kind of atrium buildings in this period.

Figure 2.4: Atrium view, Larkin Building, Buffalo, New York by Frank Lloyd Wright (Bednar 1986)

The late nineteenth century and early twentieth century had been an era of great exuberance and architectural spirit that saw the atrium plan adapted to many different building types and utilised in buildings of many styles, including Italian Renaissance, Romanesque, Victorian, and Chicago school. However, this second epoch of the atrium came to an uncertain close in the years following World War I. Certainly the atria in the United States, like the atria in Europe, were plagued by fire hazards and probably were affected by other post war issues. The buildings which did incorporate the atrium during this era had a certain forthright presence and civic grandeur, a legacy which is being rediscovered in the present day.

2.2.2 Development of modern atria (the third epoch)

Ever since the late 60s the atrium space is currently enjoying an unparalleled sustained resurgence of interest and development after a period of dormancy in the mid twentieth century (Bednar 1996). The reason for its popularity is mainly two-fold: social and economical causes and technological ones. On one hand, economic and social issues are always of great importance for atrium design. In the early '70s and '80s, John Portman's first atrium hotels were soon followed by other architects, which somehow led the mainstream commercial development in North America to adopt the atrium concept more universally and believe in its economic value and "feasibility" (Saxon 1983). Besides, an atrium would always encourage play, people-watching, promenading, movement through space, enjoyment of nature, and social life (Watson 1982) and examples where atria have increased the profitability or occupancy rates are easily available. In the meanwhile, the atrium emerged as one of the most versatile and useful elements available for urban design. On the other hand, after the energy crisis in 1970s and consciousness for global warming in more recent times, more and more architects became aware of sustainability issues. The atrium space, which can be adopted as a buffer zone to improve building energy consumption and indoor environment, together with its special aesthetic characteristics, gave a very plausible response to these tricky issues and attracted many designers and clients. Examples of this epoch are found all around the world, including the Hyatt Regency Hotel by Edwards and Portman in 1967, the Ford Foundation Headquarters, etc (Bednar 1986). Figure 2.5 is a commercial building with an atrium in Japan. Unfortunately, few atrium buildings are really recognised as energy-efficient, and a few atrium buildings located in warm climate are found fully-conditioned (Watson 1982; Bednar 1986; Goulding et al. 1992). As identified by some researchers (Butera 2005), the problem is that atrium spaces incorporate too much glazing inappropriately causing serious overheating.

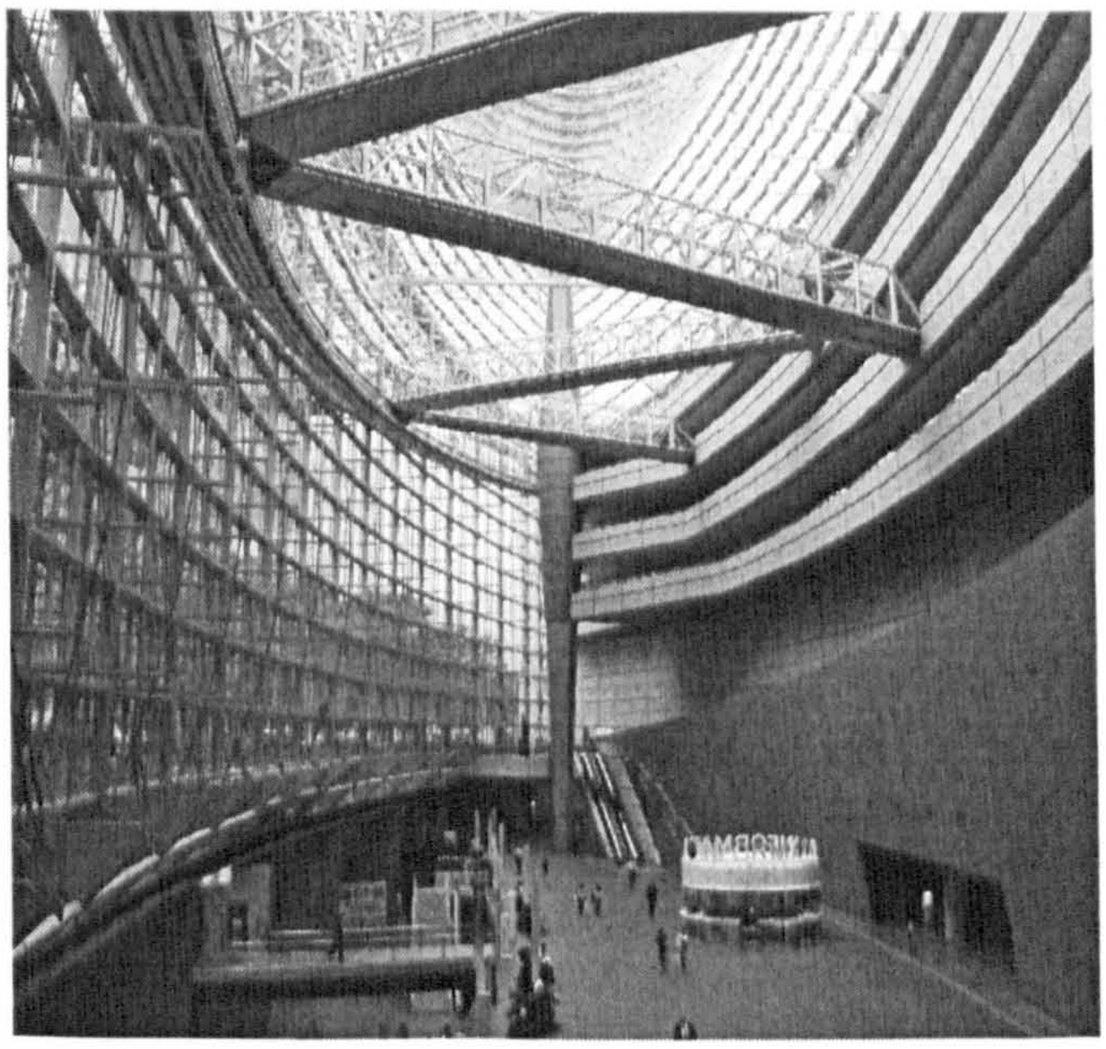

Figure 2.5: Tokyo Culture Centre, Japan

In this era, up to the present day, not only have an unprecedented number of atrium buildings been built, but the concept has also been adapted to new roles and extended to new kinds of development. In recent years, atria have been incorporated into hospitals, schools, libraries, etc. Atrium spaces are all around and for various reasons, their number is still increasing. As stated by Bednar (1986), how long this third epoch will last or whether the atrium will become a permanent spatial type remains to be seen. What is known at this time is that the atrium is a vital and exciting aspect of the present architectural era, making it highly worthy of study and analysis, now and for the foreseeable future.

In general, the key points of the historical development of atrium buildings can be summarised as follows:

- Atrium spaces are of great importance to modern building development and it is highly worthwhile to conduct research into both their social and technical features.
- Atrium spaces can bring a lot of benefits to economic and social activities and probably this is the most important reason for the great exuberance of this type of spaces at the present time.
- Their potential for saving energy is an important reason for their contemporary popularity and development.
- Atrium buildings in warm areas are easily overheated, but more and more are being built for marketing and economic purposes. This requires more research into passive cooling strategies for this kind of space in order to avoid energy waste for cooling.
- The idea of incorporating an atrium space as a passive energy strategy can be traced back to earlier times, and energy efficient atrium spaces ought to be very sensitive to the environment in which they are located and different places should have different spatial types of atrium spaces due to different climates. In earlier times, although atria were adopted in many areas, their forms were quite different from each other. Therefore, in order to take full advantage the energy potential of atrium buildings, careful design according to different climatic conditions is essential.
- Ventilative cooling strategies were incorporated in original quasi-atrium spaces and courtyards, which shows the possibility and potential for modern atrium spaces to be passively cooled by air movement, although the materials of construction and the physical mechanisms for this have significantly changed.

2.3 Energy flows in atrium spaces

In essence, the characteristics of the energy transfer process of atrium spaces are attributed to the physical features of this space type: large glazing and large height. Because of its large glazing, the solar radiation can be dominant among all other forms of heat transfer and greenhouse effect can be very significant. Due to the large height, the whole indoor environment cannot be regarded as uniform: the temperature stratification will be explicit and the distribution of the solar radiation will have to be taken into account.

This section reviews issues in relation to the energy use of atrium spaces, including the basic heat transfer process, their thermal characteristics and relevant applications, and finally the issues regarding to the passive cooling strategies of atrium spaces are discussed.

2.3.1 Basic heat transfer process

Generally speaking, the whole heat transfer process of an atrium during the daytime with solar radiation can be divided into three steps for ease of understanding, although these three steps take effect simultaneously. They are described as follows –

In the first step, the atrium space admits energy from solar radiation, conduction and convection from the outdoor environment, and long-wave radiation from the surroundings and atmosphere. Among all the forms of heat transfer, the gain of solar radiation certainly constitutes a very high proportion and is undoubtedly the most important: the intensity of solar radiation on a $1m^2$ horizontal flat surface can reach up to several hundreds watts while the conduction of the walls with the same area or the convection between the wall and the air is usually at the order of tens of watts (Givoni 1976). Glasses transmit radiation in varying degrees depending on the wave length of the radiation. It is known that glass is more transparent to short-wave solar radiation whilst it is more opaque to long-wave radiant energy. Consequently, solar radiation, which consists of a majority of short wave radiation and a smaller part of long wave radiation, impinges on the glass and enters the building with little obstruction, warming the surfaces that can "see" the sun; and then the warmed surfaces emit long-wave radiation, which cannot be transmitted back out. As a result, a majority of energy emitted by the sun impinging on the glass is absorbed by the space, and the indoor environment will gain heat and appear warmer than it would be without glass. This phenomenon is also known as the greenhouse effect. The average temperature of atria can easily be several few degrees higher than the outside temperature, and with better sealing and more insulated glazing system such as triple glazing, the temperature difference could be even larger (Wall 1996).

The second component is the heat exchange between surfaces and the air. The internal surfaces heated by the sun will transfer the energy to the air near each surface by convection and to other surfaces of the space by radiation respectively. The former part generally takes the

majority because the space contains a large volume of air that has a high thermal capacity, and the determinant of the radiation, the temperature difference between the surfaces is usually very small. The warmed air can also transfer some energy back to other cold surfaces and the indoor air also exchanges heat with outside air by convection and turbulent mixing if openings are available. As a consequence, for this stage, two things will be very beneficial for the cooling of the space: a cold surface can be provided as a cold sink so that air can transfer its energy to this, or the convection between inside and outside air can be enhanced by natural ventilation. It has been frequently demonstrated that the opening of atrium roof vents can immediately change the indoor thermal environment and as reported by other researchers, when the air change rate changes from 0 to 1.5 ach, the temperature of an atrium can drop 10 - 20 ℃ in winter (Wall 1996).

In the final step, the indoor air is re-distributed. As introduced in step two, after the surfaces are warmed by solar radiation, the surfaces warm the air nearby by convection. Due to different density of the air with different temperatures, convective currents inside the space will be set up: the warmer air with a lower density will float up and will be replaced by cooler air in the vicinity which has a relatively greater density. In this way the air will be re-distributed according to its temperature condition: warm air will occupy the top of the space while the bottom is taken up by cool air, and temperature stratification will result, which creates a non-uniform environment. It has been observed that, in an atrium building of dimensions $46m(width)\times10m(depth)\times17m(height)$, the temperature difference between 13m and 1.7m is 16℃ when the vents are closed, while the temperature difference is only 2℃ when roof vents are opened and ventilation is incorporated (Aschehoug et al. 1990).

2.3.2 Thermal characteristics of atrium spaces and applications

- *Thermal characteristics of atrium spaces*

Generally, the heat transfer process in atria introduced above exhibit three special thermal characteristics which other kinds of spaces do not have.

- Warmer Indoor Climate. Due to the greenhouse effect, the atria can let in and 'trap' more energy than other spaces, resulting in a warmer indoor climate, especially in those areas which have sufficient solar radiation. This thermal characteristic can contribute beneficially to the atrium thermal environment in winter but may cause overheating problems in summer. This is also the reason why successful energy-efficient atrium spaces are usually found in cold areas such as Scandinavia and Canada, whilst few good cases are reported in warm climates.
- Non-uniform thermal environment. Because of the intensive solar radiation penetrating into the space and the large height, strong vertical temperature

stratification can be formed. A temperature difference of 20 – 30℃ between the uppermost and lowest areas has been observed in a seven-storey atrium space in a situation where there is no ventilation and the intensity of solar radiation is very high (Barthakur 1996). On the other hand, because solar radiation plays an important role in affecting MRT, the MRT will also be non-uniformly distributed. This non-uniform character of atrium spaces can significantly influence the prediction of the parameters related to indoor thermal environment such as the thermal comfort level and energy consumption because the assumption of "well-mixed air" is employed in normal circumstances, whilst in an atrium the assumption cannot be made and new solutions are needed.

- Air movement. Stack effect can be very significant in atrium spaces due to the large height and air movement will be enhanced as a result. Frequently identified as a passive cooling strategy, stack effect can be put into effective use to release unwanted heat in summer if some openings are provided so that the warm air can escape and cool outside fresh air can enter, even if there is no wind outside. As can be envisioned, the openings at the roof level are much more efficient than openings at the floor level in removing energy in atrium spaces, since hot air occupies the upper area of the space. However, care should be taken as this characteristic can also lead to unnecessary air leakage and may cause discomfort due to the pressure difference acting on the building envelope if gaps exist.

• *Applications*

The three thermal characteristics at atrium spaces presented above are associated with a number of passive strategies addressing sustainability and energy efficiency issues of building industry and a great many efforts have been made by researchers and designers to utilise atrium spaces to improve the indoor thermal environment. Generally speaking, atria can be incorporated for three kinds of applications with respect to thermal and ventilation issues[1].

Atria as solar collectors

Even without auxiliary heating system, the average air temperature in atria will be higher than the ambient temperature due to the greenhouse effect, and hence in winter the atrium space can offset the energy used for heating and help with the energy savings of the building. As reported, a large number of atria have been incorporated into buildings in forms of communication spaces in public buildings, verandas and balconies in residential buildings, etc

[1] Atria can also be associated with other sustainable strategies such as daylighting enhancement. This thesis only focuses on the thermal issues and hence other issues are ignored.

(Wall 1996). Two examples are shown in Figure 2.6 and Figure 2.7. In a research on the atrium buildings in cold climate, the energy reduction of parent buildings can be as large as 50%, compared with buildings without atria (Goulding et al. 1992).

According to the heat transfer process introduced before, to take full advantage of atria as solar collectors, two things are quite important during the design process: firstly, sufficient solar radiation can be absorbed and stored by the space. In order to achieve this, an appropriate envelope material that allows enough sunshine to penetrate should be chosen. In addition, thermal mass may be used for the assistance of the storage of the energy absorbed and this is also the basic idea of Trombe Wall. Secondly, energy transfer from the indoor to outdoor environment, including convection between the indoor and outdoor air and the transmission from the indoor air to the cold surface should be prevented. To this end, the building should be well sealed and glazing with high insulation would be favourable, such as transparent insulation material (TIM) or other special types of glazing.

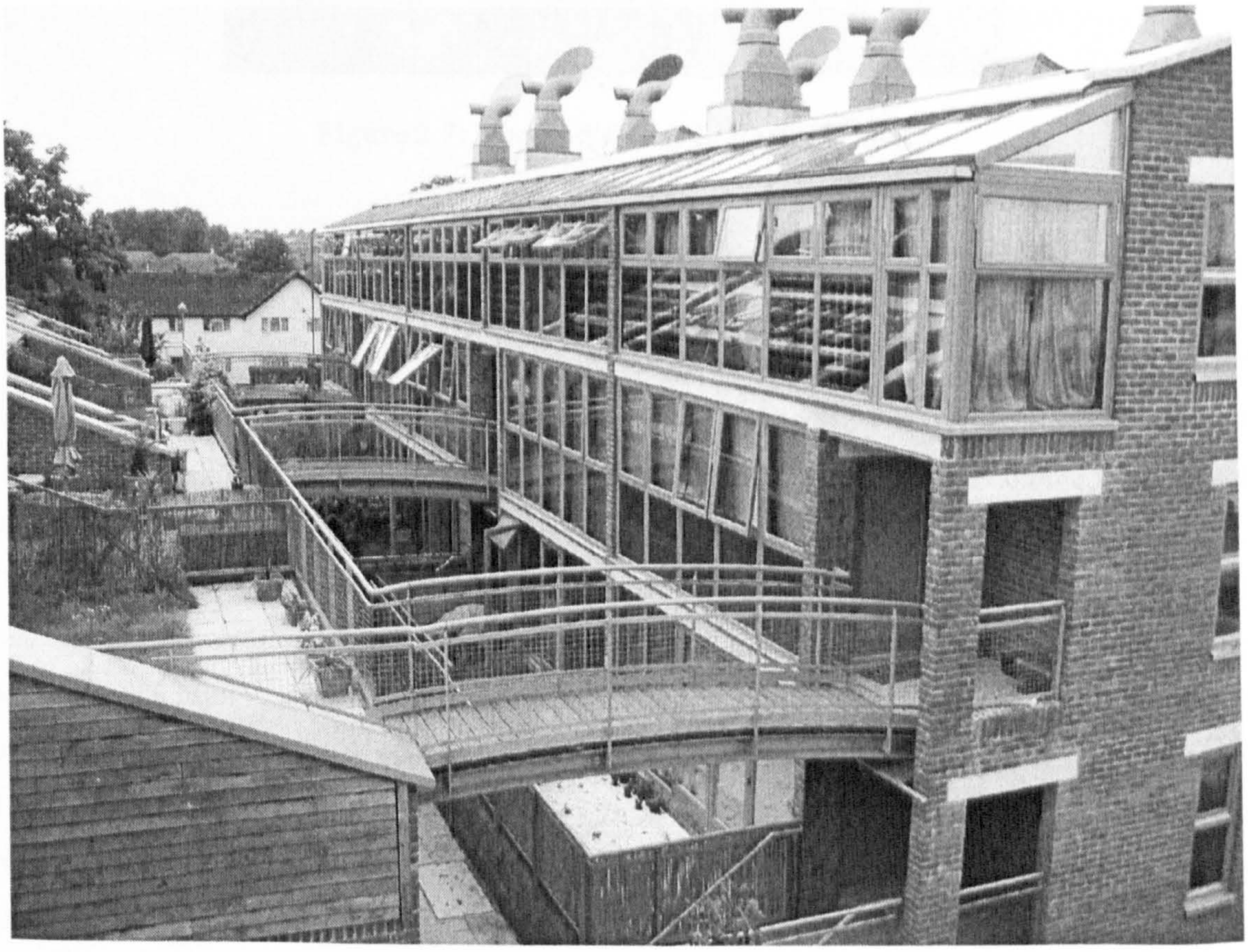

Figure 2.6: An example of the atrium incorporated in residential buildings (BEDZED)

Figure 2.7: Musée d'Orsay in Paris, France

Atria as buffer zones

Apart from use as a solar collector, atrium spaces can also be incorporated as buffer zones, providing a modestly insulated enclosure which reduces the convection and conduction heat loss of the parent buildings. The conductive heat loss mainly depends on the temperature difference of indoor and outdoor environment and the thermal property of the separating wall. Due to the greenhouse effect, the atrium air temperature is higher than the outside, which leads to a reduced conductive heat loss and thus the energy consumption of parent buildings can be reduced. In addition, atrium spaces can also be incorporated as part of the ventilation system of the parent buildings so that the convective heat loss of the building can be reduced as well. There are two ways of doing this. One way is to use the atrium as a pre-heater. Since atria are warmer than the outside, the energy requirement of heating the supply air to the required indoor temperature will be lower than when the air is taken directly from the outside. The other way is to use the extracted air from the parent buildings as the inlet air to the atrium space so that the heat can be 'stored' and the atrium spaces can be heated. A quantitative account of the energy savings for the atrium space as buffer zone under different circumstances can be illustrated in Figure 2.8. The biggest step is in the difference between the situation a and b, all due to the

reduced conductive heat loss. With the incorporation of atria as part of the ventilation system, more energy can be saved, as shown in the situation c, d and e. (Baker and Steemers 2000)

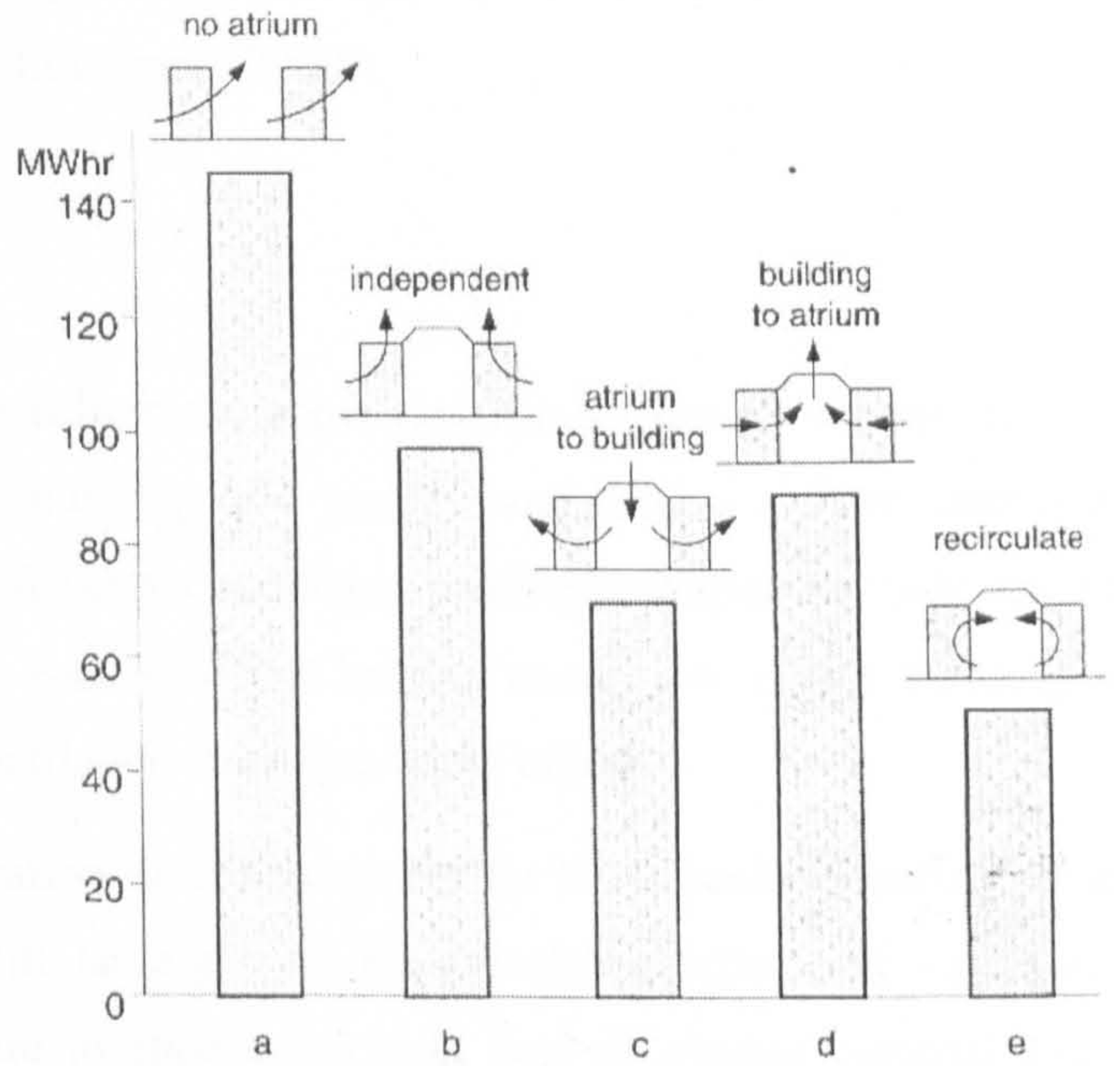

Figure 2.8: Heating Energy Consumption by a building with an atrium for different ventilation modes (Baker and Steemers 2000)

Atria for natural ventilation

Even when there is no wind outside, atrium spaces can also induce natural ventilation by stack effect. This is very important for "the worst situation" of atria: when there is strong solar radiation but no wind available. Under this situation, openings can help to improve the thermal comfort level of the space but care should be taken that the internal high temperature and solar radiation do not cause overheating problems and shading may be a better option.

If there is wind outside and if it is strong enough, forced ventilation will be dominant although buoyancy-driven ventilation by stack effect still operates. The thermal performance of buildings under forced ventilation cannot be studied independently and is dependent on many design and environmental parameters, such as the wind direction, the roof type, the opening position and the opening area (Ernest 1991). It has been found that the space with the largest opening area, the open courtyard, has a very weak ventilation performance compared with other opening situations, particularly when the oncoming wind direction is perpendicular to the courtyard (Sharples and Bensalem 2001).

In addition to aiding the cooling of the atrium space itself, the process can also help with the natural ventilation of its parent building. Most naturally ventilated buildings are designed with a shallow plan, as natural ventilation from an open window is considered to be effective in ventilating up to 6m into a room. This means that the width of a naturally ventilated building is

up to about 15m (6m from window to wall each side and 3m corridor in between), which is a major limitation for many buildings. Fortunately, the incorporation of atria can minimise this limitation and greatly enlarge the span of the building without compromising the effect of natural ventilation (Levermore 2000).

Discussion

It can be seen from the above description that the incorporation of an atrium space has potential to help a building save energy and achieve a more comfortable environment. An atrium can be used for either cooling or heating strategies: not only can it be employed as a solar collector or buffer zone to offset heating energy use of the building, it can also be used to generate natural ventilation to bring cooling effects.

The application of atrium spaces for basic passive heating strategies is generally very straightforward. With large glazing, the greenhouse effect will work automatically and the most important issues are to choose the right type of glazing material and avoid unnecessary air leakage. There is no real need to use any particular guidelines or prediction tools for the design of atrium spaces for this type of use, except in trying to assess overheating risk.

Compared to the use as solar collectors or as buffer zones for heating purposes, the application of atrium spaces in passive cooling strategies is much more complicated. Generally speaking, passive cooling strategies can be incorporated for two sorts of functions: either they may influence the energy flows, i.e. reduce the energy gain and increase the energy loss of the space, or they can directly impact on the factors affecting the thermal comfort level[1] such as air temperature, air velocity and MRT.

In order to reduce the solar gain, shading can be used, although this may not be the best option, as this will significantly reduce the daylighting performance of the building. A more advanced approach taking both thermal and daylighting aspects into consideration would be to incorporate Laser Cut Panels (LCPs) into the facades or/and the roof so that high elevation direct sunlight can be rejected, whilst the low elevation skylight can be redirected to occupants' level (Mabb 2001). Figure 2.9 illustrates the mechanism of the LCP.

Other passive cooling strategies for energy purposes include thermal mass, night cooling and the use of glass surface as heat sink. However, the methods used to develop guidelines for the use of these strategies in other spaces will not be applicable for atrium type buildings due to the special heat transfer processes of atrium spaces. As noted earlier, the atrium spaces are highly non-uniform and the solar radiation has much more significant impacts, which results in the unsuitability of the "well-mixed air" assumption that most conventional methods are based

[1] Detailed information in relation to thermal comfort will be introduced in Section 2.4.

upon. New approaches are therefore needed but this is beyond the topic of this research and will not be discussed any further.

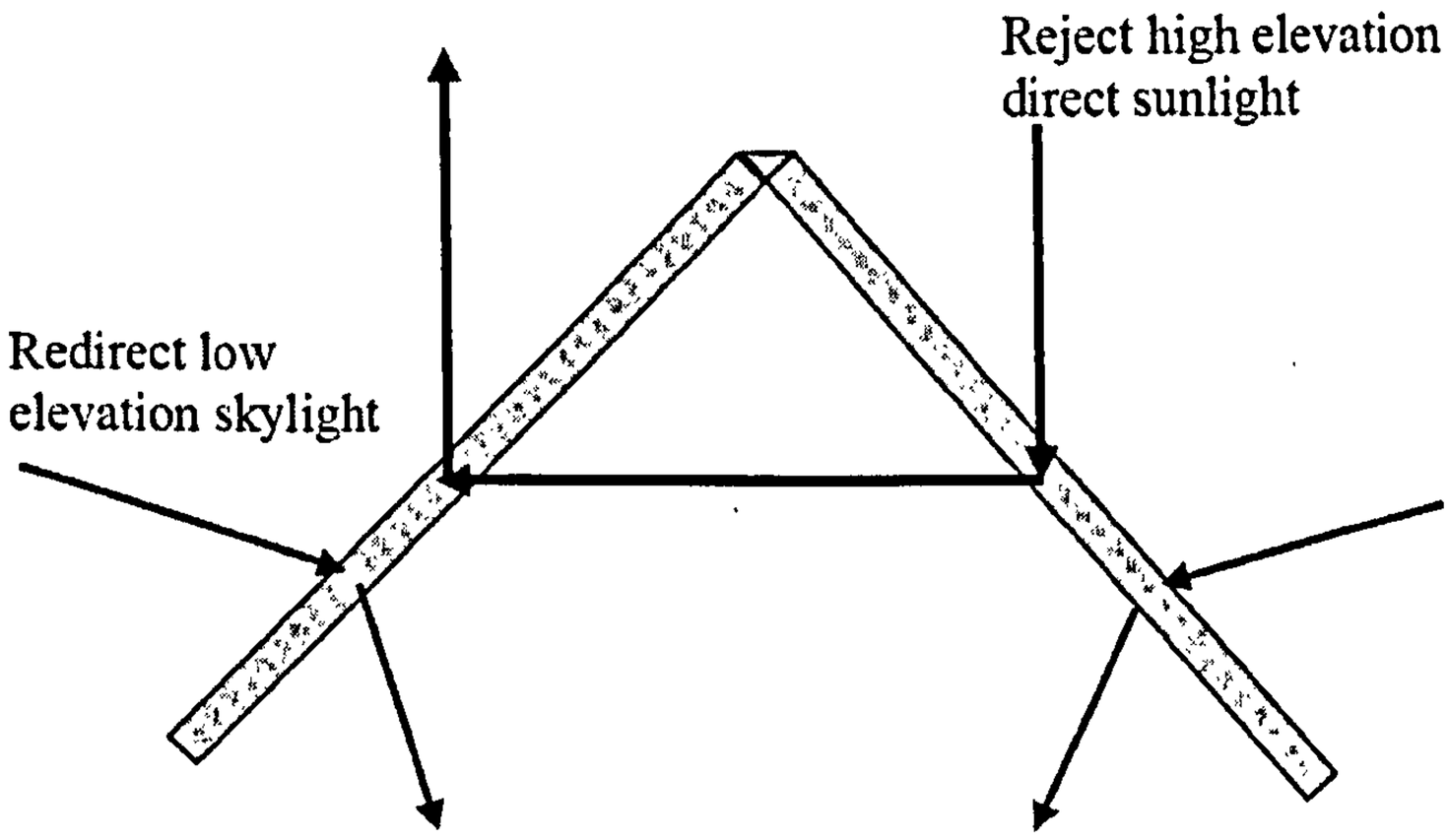

Figure 2.9: LCPs redirect light through pyramid skylights (Mabb 2001)

Apart from the use for the removal of the excessive heat in the space such as night time cooling, natural ventilation is also a very efficient strategy that can directly influence the factors related to the thermal comfort at the occupants' level in the space, because it can change the air temperature and velocity simultaneously. For the wind-induced ventilation, as introduced above, there are many design parameters involved in the problem and no parameter can be studied independently and in addition, the significance of the roof design for atrium spaces complicates the problem even more. Although the generation of buoyancy-driven ventilation in atrium spaces is easier than that of other spaces because of stack effect, one important premise of using buoyancy-driven ventilation is that this kind of ventilation relies on the hope that the high internal temperatures that occur will not cause comfort problems. This means that the heat source driving the airflow should not be located too close to the occupants and their effects on thermal comfort level of the space need to be evaluated at the early design stage. This topic will be introduced in next section. In addition, in order to help with the ventilation of adjacent buildings, it is necessary to control the height of the neutral level, and thus the controlling factors of the neutral level, including the sizes and locations of the openings become very crucial. As a consequence, the design of atrium spaces for natural ventilation purposes will demand guidance to achieve a balance between the issues mentioned above. The detailed review of the issues associated with natural ventilation in atrium spaces is provided in Section 2.5.

2.4 Thermal comfort in atrium spaces

Review of the energy flows of atrium spaces in Section 2.3 indicates that one of the thermal characteristics is that the temperature of atria can be raised easily due to the greenhouse effect, which may result in thermal discomfort. Chapter One has also suggested that solar radiation plays an important role on MRT of the occupants' level, which is significantly influential on the thermal comfort condition of the space as well. As a consequence, there are two potential causes for the overheating of atrium spaces – too high air temperature and too high MRT.

.In order to identify the main factor that causes overheating for a particular circumstance, it is necessary for architects or engineers to use a methodology to assess the thermal comfort level in atrium spaces at the early design stage. This is the main issue to be dealt with in this section. Section 2.4.1 is concerned with the introduction to the general basic theory of thermal comfort. The factors affecting occupants' thermal sensation and the methods for the evaluation of thermal comfort level are discussed. Then the discussion is extended to atrium spaces in Section 2.4.2 in which a methodology for the assessment of the thermal comfort level in atrium spaces is introduced.

2.4.1 Basic theory of thermal comfort

• *Factors affecting thermal sensation*

Thermal comfort has been defined as 'the condition of mind that expresses satisfaction with the thermal environment' (ISO7730 2005) . Alternatively, it is the state where the people are in thermal equilibrium: they are entirely unaware of their surroundings neither considering whether the space is too hot or too cold. For a body to be in thermal equilibrium, the amount of heat absorbed or produced must equal the heat dissipated. The various processes involved with the heat transfer between the body and its surroundings are shown as follows (see Figure 2.10).

- losses by evaporation (perspiration and sweating) and respiration ('g' in diagram);
- losses by convection ('c' in diagram);
- losses/gains by radiation (solar - 'a' in diagram and atmosphere – 'd' and 'e' in diagram);
- losses by conduction ('f' in diagram);
- gains from metabolic heat production ('b' in diagram).

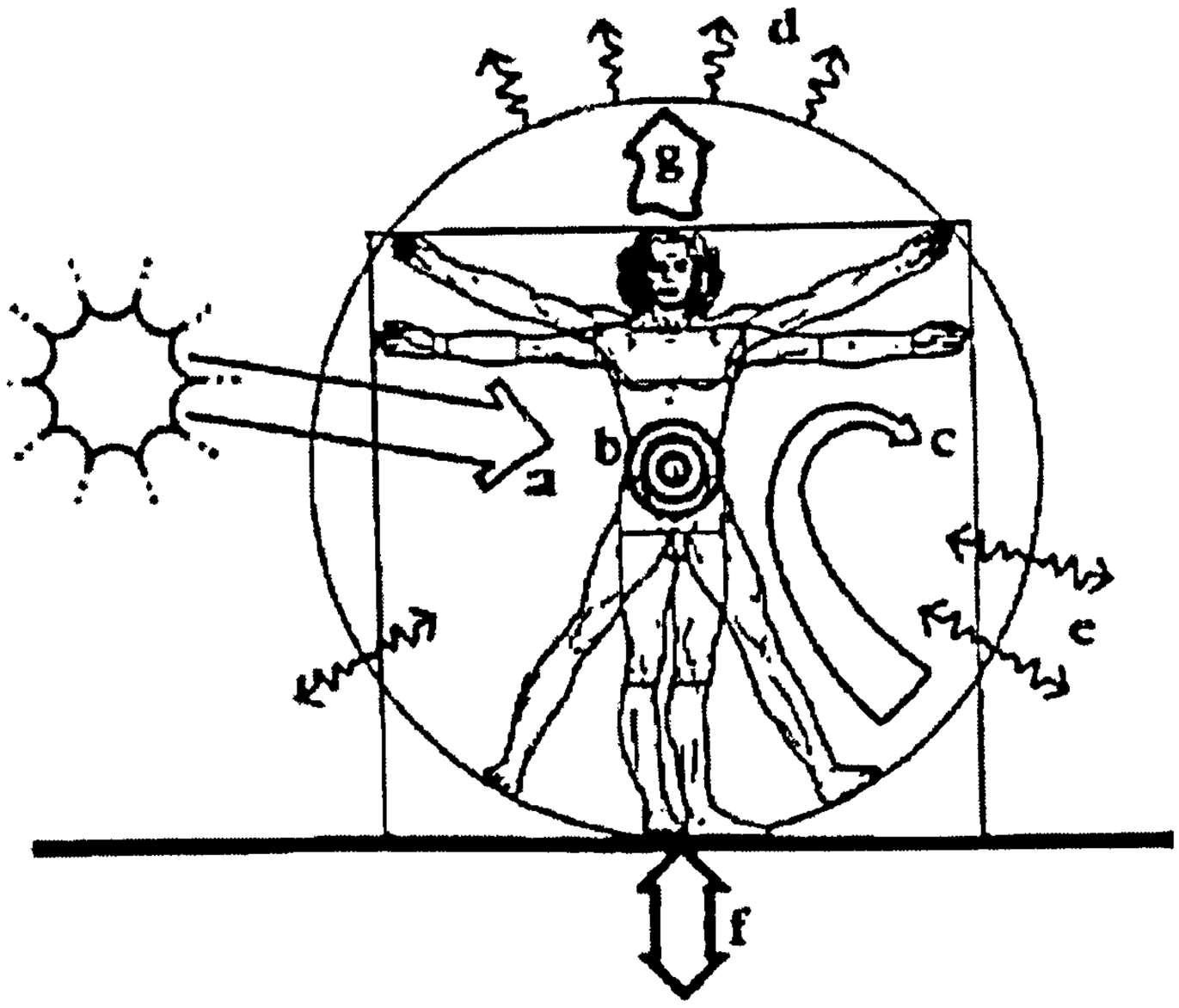

Figure 2.10: Heat exchange from a body to surroundings (Goulding et al. 1992)

In typical indoor conditions, convective losses account for some 35% of heat losses, radiative losses occupy the largest proportion which is about 45%, and evaporative losses are in the order of 20%.

Parameters that affect the heat transfer processes from the body to the environment are those which are most important in influencing thermal comfort. It has been widely recognised that occupants' thermal comfort level is primarily affected by four environmental parameters and two human parameters, although some secondary factors like sex, age may have some influence as well (ASHRAE 2001). The four environmental parameters are air temperature, air velocity, humidity and mean radiant temperature. The two human parameters are clothing and activity level.

These parameters influence the human thermal comfort conditions in different ways. Activity level affects internal metabolic heat production of the body. The higher the activity level, the more the metabolic heat generated and the more it needs to be dissipated from the body. Different types of clothing offer different insulation properties that prevent convective heat exchange between the body surface and the environment. Mean radiant temperature affects the radiative heat exchange of the body with all surroundings. Air temperature is the most important parameter for most situations directly influencing the heat transfer between occupants and the environment. Air velocity can take effect mainly through the convection process: it will increase the rate of convective heat transfer.

• *Thermal indices*

Thermal comfort can be achieved by many combinations of the aforementioned six environmental and human factors and it is almost impossible to consider the effect of any single factor in isolation. The combined thermal effect of these factors on human thermal sensation is the most important, and based on this idea, a number of thermal indices have been developed and used for the evaluation of the thermal comfort level under various circumstances, including effective temperature (Houghten and Yagloglou 1923), operative temperature (Winslow et al. 1937), index of thermal stress (Givoni 1969), Predicted Mean Vote (PMV) and Predicted Percentage of Dissatisfied (PPD) system (Fanger 1970), etc.

Among all the thermal indices, PMV and PPD index is the most widely applied. The PMV scale is a seven-point thermal sensation scale ranging from -3(cold) to +3(hot), where 0 represents the thermally neutral sensation. During design process, the PMV scale can be calculated using the following formula with all six factors known.

$$PMV = [0.303e^{-0.036M} + 0.028] \begin{Bmatrix} (M-W) - 3.05\times10^{-3}\times[5733 - 6.99(M-W) - Pa] - 0.42[(M-W) - 58.15] \\ -1.7\times10^{-5} M(5867 - Pa) - 0.0014M(34 - t_a) \\ -3.96\times10^{-8} f_{cl}[(t_{cl}+273)^4 - (\bar{t}_r+273)^4] - f_{cl}\times h_c(t_{cl} - t_a) \end{Bmatrix} \quad (2.1)$$

where

$$tcl = 35.7 - 0.028(M-W) - I_{cl}\left\{3.96\times10^{-8} f_{cl}[(t_{cl}+273)^4 - (\bar{t}_r+273)^4] + f_{cl}\times h_c(t_{cl} - t_a)\right\} \quad (2.2)$$

$$h_c = \begin{cases} 2.38|t_{cl} - t_a|^{0.25} & for\ 2.38|t_{cl} - t_a|^{0.25} > 12.1\sqrt{v_{ar}} \\ 12.1\sqrt{v_{ar}} & for\ 2.38|t_{cl} - t_a|^{0.25} > 12.1\sqrt{v_{ar}} \end{cases} \quad (2.3)$$

$$f_{cl} = \begin{cases} 1.00 + 1.290 I_{cl} & for\ I_{cl} \le 0.078 m^2 K/W \\ 1.05 + 0.645 I_{cl} & for\ I_{cl} > 0.078 m^2 K/W \end{cases} \quad (2.4)$$

With the use of the PMV index, it is possible to assess how various combinations of thermal conditions influence occupants' thermal sensation. Given the PMV value, the "Predicted Percentage of Dissatisfied" occupants can be determined by Equation (2.5).

$$PPD = 100 - 98\times e^{(-0.03353\times PMV - 0.2179\times PMV^2)} \quad (2.5)$$

This index thus predicts the percentage of dissatisfied occupants that can be expected at each PMV or under certain conditions. The minimum of 5% dissatisfied corresponds to a mean vote equal to zero (neutral), which means that there will always be some individuals who are dissatisfied with the comfort level, regardless of the fact that they are all dressed similarly and have the same level of activity: comfort evaluation differs a little from person to person.

For real applications in buildings, the use of PMV and PPD is generally too complicated for designers and engineers, and other simple indices such as effective temperature or operative temperature are usually used. These simple indices usually consider air temperature as the most important factor and combine the effects of air temperature, humidity and air velocity. However, the calculation of mean radiant temperature is simplified or even assumed to be equal to air temperature.

2.4.2 Assessment of the thermal comfort level in atrium spaces

As described earlier, most comfort level predictions used in real practice consider air temperature as the most important factor and assume MRT to be the same as air temperature for calculations. This assumption is still employed for the developments of the adaptive model for thermal comfort studies (Auliciems 1981) and also for other research in relation to atrium spaces, including those work by Ayoob and Izard (1994), Izard and Frusta (1998) and Douvlou (2003).

These conventional methods can generally achieve sensible results for ordinary spaces, and they may be even reasonable for the use of atrium spaces for some simple purposes. However, they may bring on serious errors if they are used to diagnose the main cause for overheating, because the effects of MRT cannot be ignored for this situation. In addition, as introduced in Section 2.3.2, atrium spaces are usually characterised with a non-uniform thermal environment and there may be strong vertical temperature stratification in the space, which may also cause local thermal discomfort due to vertical temperature difference and the too high/cold temperature of the wall heated by the sun/the glass. It is also worth mentioning that usually only the evaluation of the thermal comfort level at the bottom of the space is sensible, because this area may be only occupied area of the whole space.

The above problems have been separately identified by other researchers when they are dealing with their research projects and solutions to resolve them are proposed respectively. A generalised algorithm has been developed to take solar radiation into account for the calculation of MRT (Gennusa et al. 2006). CFD has been frequently identified as an invaluable tool to cope with the treatment of non-uniform environment and local thermal discomfort (Gan 1995). However, there is still no approach available that can integrate above two methods together and analyse the collective effects of the above issues. Thus the full assessment of the thermal comfort level in atrium spaces cannot yet be fulfilled.

2.5 Natural ventilation in atrium spaces

Natural ventilation plays a very important role in the thermal environment of a building. It can offer passive cooling effects for overcoming the overheating of atrium spaces, no matter what the real cause is. In addition, it can also contribute to the cooling of the structure and reduce the possibility of sick building syndrome (SBS) (Liddament 1996). Over recent decades, natural ventilation has been frequently identified as a cost-effective and environmentally friendly strategy if properly designed, especially in moderate or mild climates (Clements-Croome 1997). As pointed out earlier, due to their thermal characteristics, atrium spaces can help to induce natural ventilation under certain circumstances and hence offer passive cooling benefits. The primary purpose of this section is to review the state-of-the-art research in relation to this issue and highlight the directions for this research in this area.

The mechanics for natural ventilation is usually termed "Architectural Fluid Dynamics" (AFD) that concerns the air movement in and around buildings and can be considered as a cross between classical engineering fluid dynamics and geophysical fluid dynamics. As indicated by Prof. Paul Linden[1],

"*...Most engineering flows, such as in an internal combustion engine, or around a vehicle, are dominated by the geometry. They need to be calculated for the specific boundary conditions that the geometry imposes. Geophysical fluid dynamics, on the other hand, is a study of flows for which boundaries usually only play a minor role. The flows are governed by internal dynamics associated with buoyancy and Coriolis forces...In AFD the flows are determined both by the geometry and by the internal dynamics in about equal measure. The flow through a building is determined both by the internal geometry and the location and sizes of openings and also by pressure and buoyancy forces. This combination makes computation especially difficult. In addition, it is often desirable to make calculations of flows in the design phase when the building geometry is evolving – often quite radically...*"

This above passage suggests that, to accurately evaluate the natural ventilation performance in a space, it is essential that all of the influencing factors mentioned above, including the building and opening characteristics, distribution of the openings, pressure differences and heat sources, and flow regimes, etc, are known. However, this is rare to happen at the initial stage of the design process; and furthermore, even if all the parameters can be clarified, the calculation may still be difficult to perform due to the large number of variables involved and the tedious procedures of quantifying all of them. As a consequence, in order for ventilation strategies to achieve better performance, it is quite important to find out the most significant parameters and study the impacts of these parameters.

---

[1] Please refer to his academic website for details: http://maeresearch.ucsd.edu/linden/AFD/archfd.html

According to the type of forces determining flow regimes, the rest of this section is divided into three subsections, each of which is concerned with one type of flow, and the basic mechanism, the available design guidelines and tools, and the research work related to the flow regime are discussed. This review also provides an overview of the topics relevant to this research.

2.5.1 Wind-induced natural ventilation in atrium spaces

Wind-induced ventilation refers to the natural ventilation driven by wind and the air pressure difference resulting from temperature difference can be ignored for this situation. When wind is blowing against a building, the straight motion of the air is disturbed and deflected around and above the building. The air pressure on the sides facing the wind is elevated above atmospheric pressure (pressure zone) and on the leeward sides it is reduced (suction zone). In this way, pressure differences are created over the building and natural ventilation can be driven if openings are provided (Givoni 1969).

Wind-induced ventilation can be an effective passive cooling strategy for atrium spaces since the air with a lower outdoor temperature can help to remove excessive energy accumulated in the space in warm weather. This is extremely promising for the regions with mild climates where the temperature is acceptable even for the hottest period. In addition, atrium space is usually the tallest part of the building and hence openings are always possible to catch and incorporate wind into space.

- *Theoretical analysis*

The mechanism of wind-induced ventilation is very complicated because of the complex physics and the large number of variables involved. As a consequence, the theoretical analysis can only be performed for very simple cases. The most common type of wind-induced ventilation, i.e. cross ventilation, is shown below (See Figure 2.11).

For an opening of relatively larger free area, such as air vent and opening windows, the air flow through an opening tends to be approximately turbulent under normal pressures (Awbi 2003). In this case, the airflow rate approximates to a simple square root law as expressed in Equation (2.6) (Etheridge and Sandberg 1996):

$$q = C_D A\sqrt{2\Delta p / \rho} \tag{2.6}$$

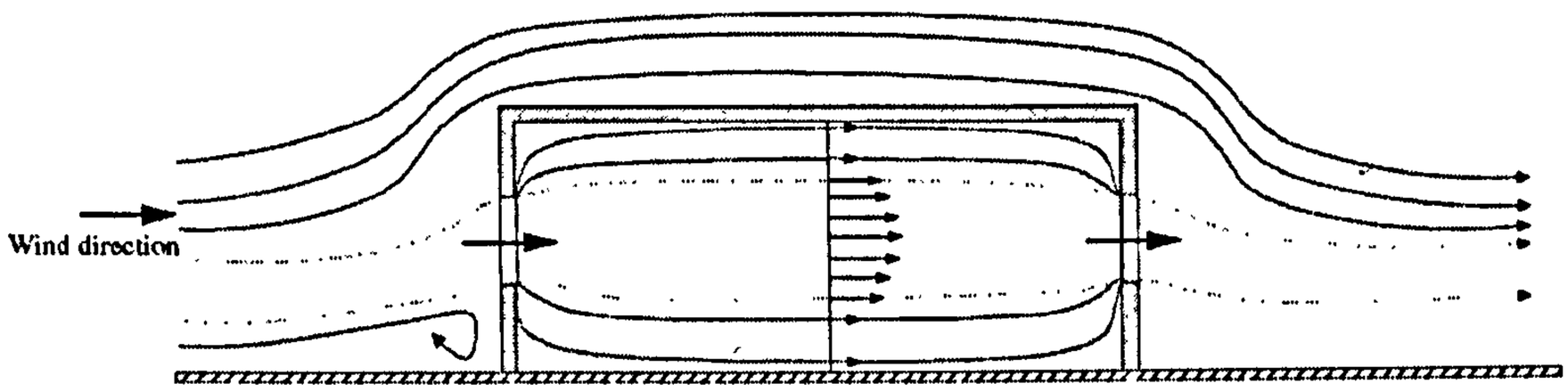

Figure 2.11: Illustration of cross wind-induced natural ventilation

For a given building in a given wind environment, the pressure difference usually increases with the square of the wind speed. More precisely, it is proportional to the so-called dynamic pressure $\frac{1}{2}\rho U_R^2$. It is often useful to make use of this by expressing the pressure difference in terms of a pressure coefficient ΔC_p:

$$\Delta p = \frac{1}{2}\rho U_R^2 \Delta C_p \tag{2.7}$$

Assuming that (a) two openings are of equal size, (b) pressure and velocity fields are uniform; (c) the room resistance is ignored; (d) the air velocities within the building are negligible, the airflow rate for cross ventilation illustrated in Figure 2.3 can be calculated by the following equation by combining Equations (2.6) and (2.7) (Note that the pressure differences across the openings are simply assumed to equal to half the pressure difference across the building):

$$q = C_D A U_R \sqrt{\Delta C_p / 2} \tag{2.8}$$

Although this simple equation is derived based on a number of assumptions and its use is limited to certain circumstances as it ignores certain physical phenomena such as turbulent fluctuation (Murakami et al. 1992; Seifert et al. 2006), it still shows the general relationship between airflow rate and influential parameters: the airflow rate is proportional to the opening area, the wind velocity, and the positioning of openings at areas with higher pressure difference can increase the airflow rate.

However, information provided by the above simple analysis may not be applicable for the wind-induced airflow model to be studied that was proposed in Chapter One, i.e. the ventilation through roof openings. In essence, their ways of incorporating ventilation are different: the cross ventilation model introduced above employs the openings at the occupants' level and thus the wind can come to the occupants directly, whilst the model to be studied in this research utilises openings higher on the top of the space and thus the wind is in fact indirectly used. In other words, recirculation rather than the main flow is used for ventilation through roof

openings. There has been still no theoretical analysis available regarding this model and the research relevant to this topic is reviewed below.

• *Review of the research in relation to wind-induced ventilation in atrium spaces*

Although few investigations have been carried out directly with respect to the wind-induced ventilation performance of atrium spaces through roof openings, research into spaces that have similar geometrical characteristics such as courtyards and street canyons, and that into particular components relevant to atrium spaces such as skylights, are also of some significance for the design of atrium type buildings. They are reviewed respectively as below.

A street canyon refers to a relatively narrow street in-between buildings that line up continuously along both sides and generally can be regarded as an atrium space without roof. The most important features of street canyon micro-climate are the wind-induced flow patterns such as air recirculation, which has a significant impact on the level of air pollution emitted from vehicles and also the thermal comfort of inhabitants (Li et al. 2006). The most important factor that determines the air flow pattern inside the street canyons is their geometries, in particular, the section aspect ratio, i.e., *H/W*, where *H* is the building height and *W* is the street width. Three different flow patterns were identified by Oke (1988) according to field measurements and mathematical modelling, as shown in Figure 2.12.

For widely spaced buildings ($H/W < 0.3$), the flow fields associated with the buildings do not interact resulting in the isolated roughness flow. At closer spacing ($0.3 < H/W < 0.7$), the wake behind the upwind building is disturbed by the recirculation created in front of the windward building and wake interference flow will occur. Further reducing spacing ($H/W > 0.7$) leads to skimming flow and a stable recirculation is decoupled from the flow above the street. More than one recirculation may be resulted if a section aspect ratio higher than 1.3 is introduced, which will induce very weak air movement at the bottom of the space (Jeong and Andrews 2002).

Apart from the geometries of the street canyons, other parameters can also influence the flow pattern. It has been found that the configurations of adjacent upwind and downwind buildings have significant impacts (e.g. Rafailidis 1997; Kastner-Klein and Plate 1999; Assimakopoulos et al. 2003). The effects of the street obstructions on flow process were also investigated (Gayev and Savory 1999). In addition, the ambient wind plays an important role in the flow pattern as well. Kim and Baik (1988) demonstrated that changes in ambient wind direction could make large differences in the mean flow recirculation and hence the pollutant distribution. Huang et al. (2000) found that wind speed also had an important effect and furthermore, the inflow turbulence intensities also have significant effects on the momentum and pollutant transfer of the mean flow, according to Kim and Baik (1988). Although the main

concern of these investigations is focused on the general flow pattern and pollutant dispersion rather than the factors affecting the thermal comfort level of the bottom such as air velocity and turbulence intensity, the above review still shows some important parameters that can have significant impacts, including the adjacent buildings, the building geometry, the ambient wind, etc.

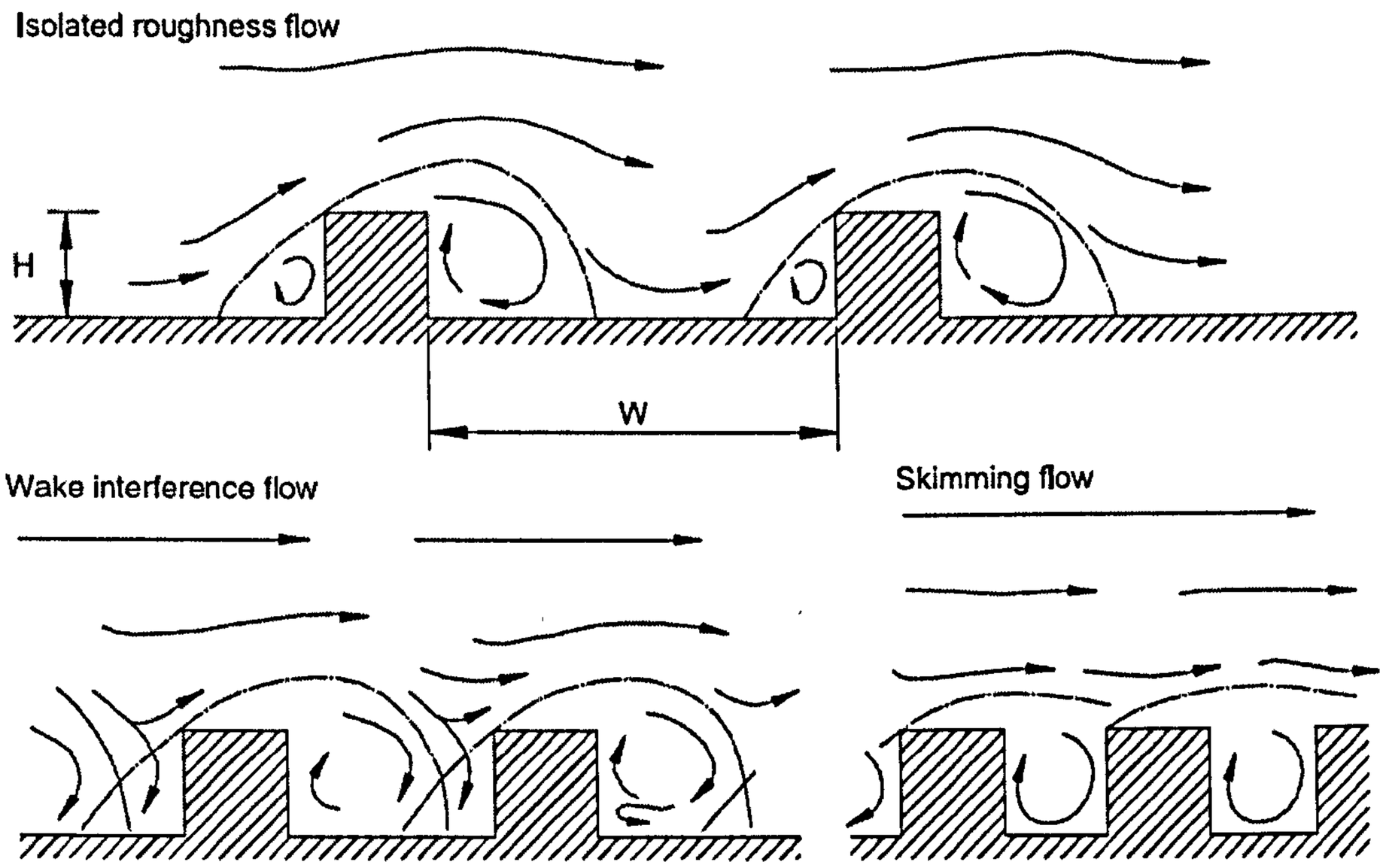

Figure 2.12: Three flow patterns associated with different section aspect ratio (Oke 1988)

With regarding to the impacts of roof, in fact, the idea of using such elements to enhance the ventilation of buildings is not new. Wind towers and wind catchers have been prevalent in the Middle East and North Africa for hundreds of years, and have formed a key component of the indigenous architecture of those regions. Recently vents and openings at roof level have also been incorporated into modern buildings and their effects are studied by a number of researchers. Bauman (1988) investigated a "jack roof" configuration using a wind tunnel and found that the jack roof can be effective in inducing internal air movement. It has also been indicated by other researchers that the shape of roof has a significant impact on the air flow patterns and air velocity distributions (Kindangen et al. 1997; Riskowski et al. 1998).

Research has also been carried out for courtyards. Walker et al (1993) and Shao et al (1993) performed CFD and wind tunnel studies of courtyards and Alvarez et al (1998) modelled airflow patterns in courtyards as a function of their depth and width ratios. Sharples and Bensalem (2001) compared several different opening scenarios (See Figure 2.13) under various wind circumstances using a wind tunnel and found that, with a roof that has biggest opening

(model A1), i.e. the courtyard, has a very weak ventilation performance, particularly when the wind is perpendicular to the courtyard without inclined angle.

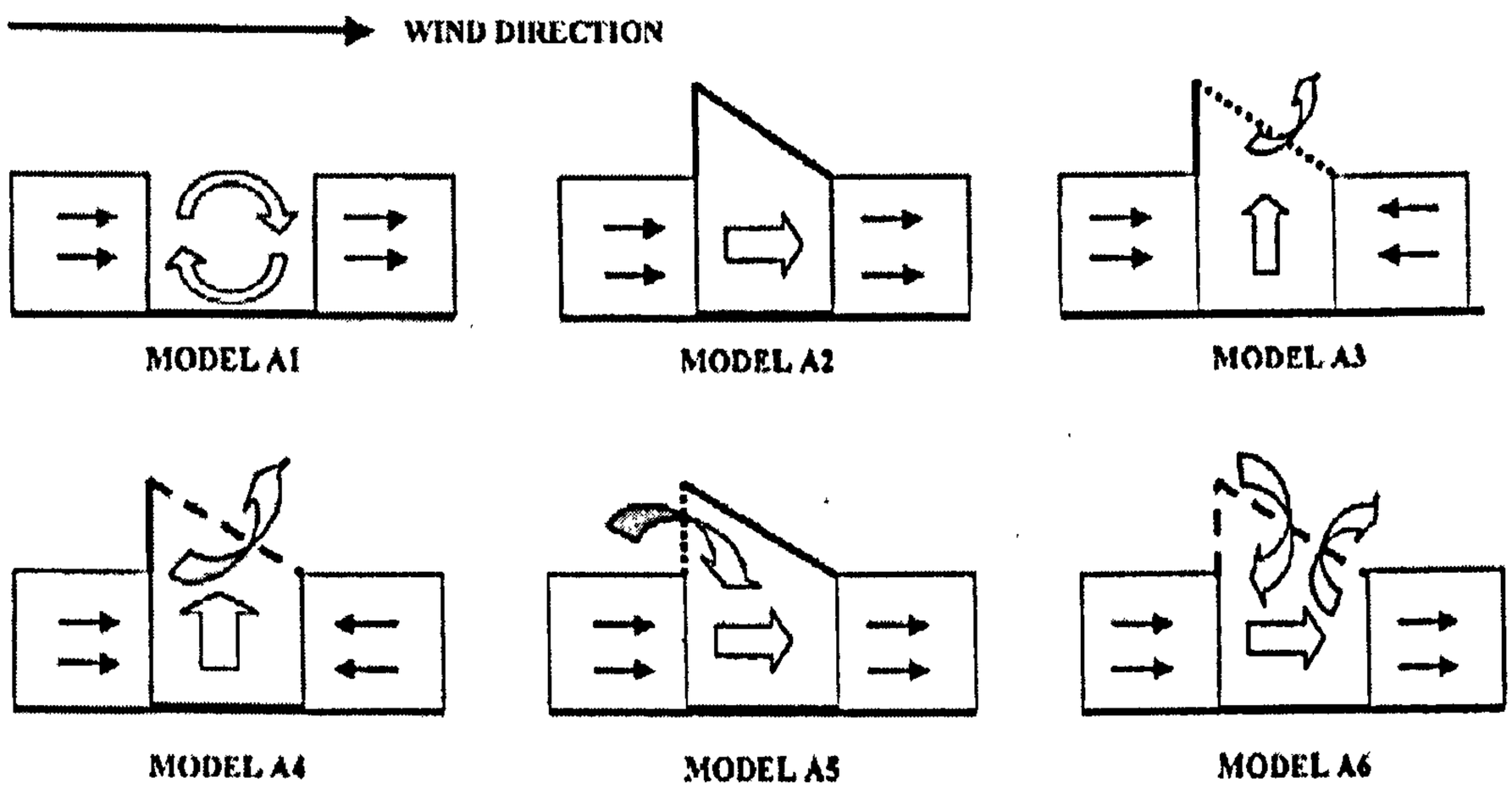

Figure 2.13: Different Opening Scenarios Studied in Sharples and Bensalem (2001)

It can be generally concluded from the above studies that the performance of wind-induced ventilation of atrium spaces is very sensitive to environmental parameters such as ambient wind, and design parameters such as adjacent buildings, roof shape, opening configurations, etc, although how these parameters impact on the thermal comfort level of the space still remains unknown. It is also shown that courtyards or street canyons without roofs usually do not have a good ventilation performance, which implies that the roof design can be of great importance to the ventilation performance at the bottom of the space. The discussions on the relationship between the recirculation and the building aspect ratio also suggests that the aspect ratio of the atrium building should be around 0.7 – 1.3 if the recirculation is going to be used for ventilation purposes.

2.5.2 Buoyancy-driven natural ventilation in atrium spaces

When the indoor and outdoor air temperatures are not the same, a difference is created between their densities and the vertical pressure gradients differ correspondingly in and out of doors. If there are openings provided at different levels (or one large opening is provided), then buoyancy-driven air movement will be induced. Due to the great height available and the large area of glazing causing greenhouse effect, the buoyancy-driven ventilation in atrium spaces will be much more significant than other spaces.

Two general kinds of buoyancy-driven ventilation in atrium spaces can be defined. These are "mixing ventilation" and "displacement ventilation" respectively, as illustrated in Figure 2.14 (Baker and Steemers 2000). Mixing ventilation takes place when bi-directional flow occurs for one opening and it can also be regarded as diluting ventilation, as outside cool air comes into the space and reduces the indoor air temperature by diluting the indoor air other than replacing it. If openings exist at both the roof and the floor level, displacement ventilation will take effect. Warm air leaves the upper opening and cooler air enters the lower opening.

Buoyancy-driven ventilation can be very important for the passive cooling of atrium spaces, especially for the 'worst situation' – when there is strong solar radiation and outside air temperature is very high but no wind is available. Under this circumstance, if openings can be provided, particularly at both higher and lower level, the thermal environment will be greatly improved.

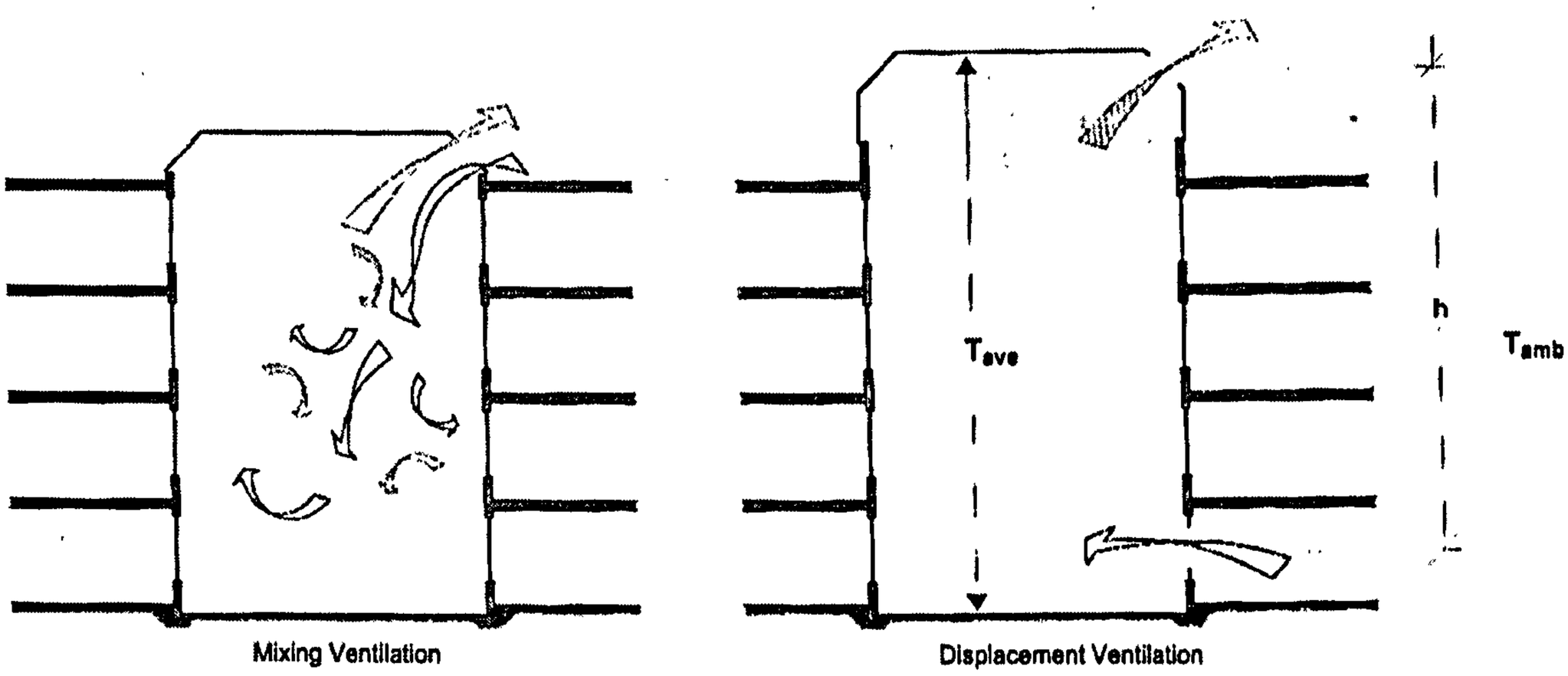

Figure 2.14: Buoyancy-driven natural ventilation in atrium spaces (Baker and Steemers 2000)

- *Theoretical analysis*

Two quantitative variables are usually important at the design stage for the evaluation of the performance of the buoyancy-driven ventilation in atrium spaces. In addition to the airflow rate, another variable that needs to be determined is the neutral level at which the pressure difference between the indoor and outdoor is zero. In essence, the height of the neutral level determines the flow pattern of the space, i.e. either displacement flow or mixing flow: for the former, the neutral level is located in-between the two openings while it intersects with an opening for the latter. Furthermore, if an additional opening is provided, the neutral level can help to determine the airflow direction through that new opening.

For ventilation driven by buoyancy forces, the equation determining the airflow rate (Equation 2.25) can still apply but the equation for the calculation of the pressure difference need to be altered. Figure 2.15 illustrates a simple case of buoyancy-driven displacement ventilation with a distributed heat source resulting in a uniform air temperature distribution. The pressure difference can be expressed with Equation (2.9) (Anderson 2003):

$$\Delta p = \Delta \rho g h = (\rho_o - \rho_i) g h \tag{2.9}$$

Then the airflow rate can be calculated by:

$$q = (C_D A)^* \sqrt{2(\rho_o - \rho_i) g h / \rho_o} \tag{2.10}$$

Assuming that the air temperature is inversely proportional to the pressure, the equation becomes:

$$q = (C_D A)^* \sqrt{2(T_i - T_o) g h / T_i} \tag{2.11}$$

where
$$(C_D A)^* = \left[\frac{1}{(C_{Du} A_u)^2} + \frac{1}{(C_{Dl} A_l)^2} \right]^{-\frac{1}{2}} \tag{2.12}$$

and the neutral height can be determined by:

$$h_n = \frac{\gamma^2}{1+\gamma^2} h \tag{2.13}$$

where γ is the opening ratio and is calculated by $\gamma = C_{Du} A_u / C_{Dl} A_l$. It can be seen from this equation that the neutral height is only determined by the vertical distance between the openings and the opening ratio, and it is not related to the pressure or air temperature. The Equation (2.12) for the calculation of the effective area $(C_D A)^*$ also suggests that the flow rate is more significantly influenced by the small opening as it determines the magnitude of the effective area (Hunt and Linden 1999). However, if the area of lower opening increases, γ will decrease and h_n will decrease as well according to Equation (2.13). Thus it is possible for the neutral level to intersect with the lower opening if the area of the lower opening continues to enlarge to certain extent. If this happens, the displacement ventilation and the mixing interaction will interact and the equations introduced above for the calculation of airflow rate and neutral height will be violated as the flow regime has changed.

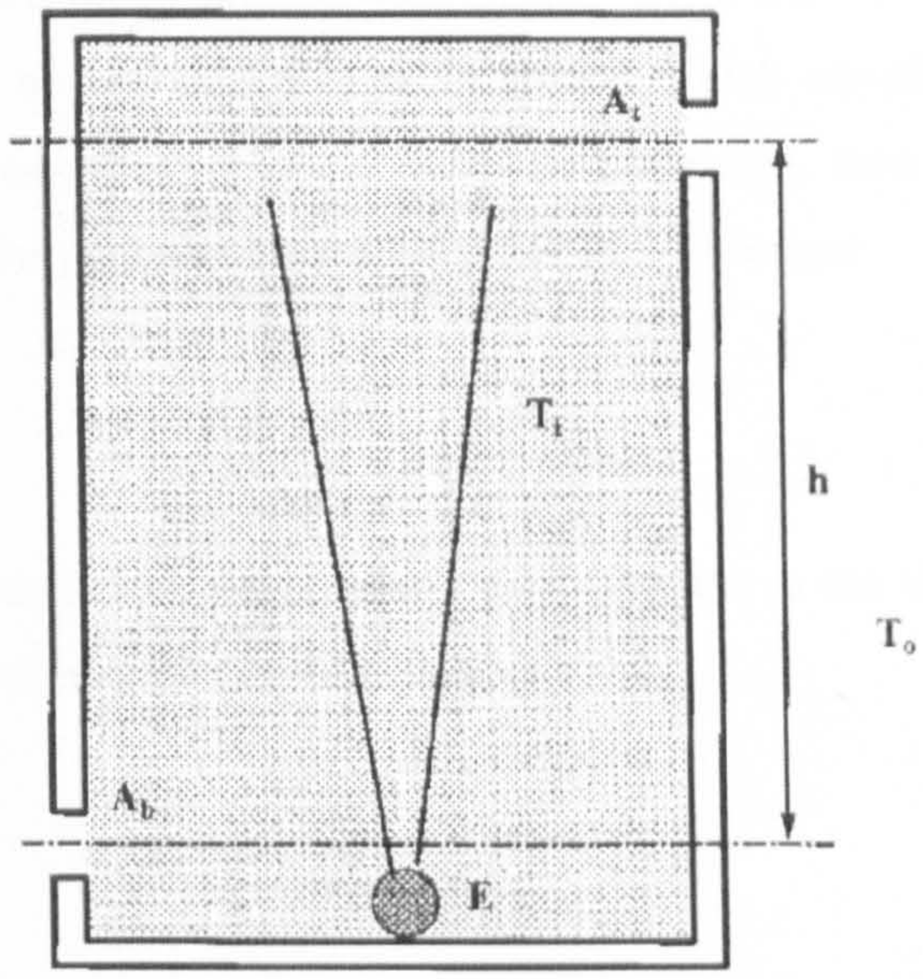

Figure 2.15: A simple case with buoyancy-driven ventilation (the interior air temperature is uniformly distributed) (Li 2000)

For atrium spaces, the air temperature is usually not uniformly distributed and there may be temperature stratification depending on the location of the heat source (Bryn and Schilfloe 1996). Thus, according to the loop equation method (Axley 1998), T_i in Equation (2.11) can be substituted by the integration of the air temperature along the vertical direction and Equation (2.11) becomes (See Appendix B for detailed deduction of the following two equation):

$$q = (C_D A)^* \sqrt{2gh(1 - \frac{1}{h}\int_0^h \frac{T_o}{T_j} dy)} \tag{2.14}$$

where T_j is the air temperature at point j.

The equation for the calculation of the neutral level for this circumstance will become:

$$\int_0^{h_n} (1 - \frac{T_o}{T_i}) dy = A_u^* (h - \int_0^h \frac{T_o}{T_j} dy) \tag{2.15}$$

where
$$A_u^* = \frac{(C_{Du} A_u)^2}{(C_{Du} A_u)^2 + (C_{Dl} A_l)^2} \tag{2.16}$$

Apparently the equation is very complicated and there has been no analytical solution for Equation (2.15) before the vertical air temperature distribution is made clear.

The above equations are only applicable for the use of displacement buoyancy-driven natural ventilation under specified conditions. The opening for mixing ventilation acts as both

inlet and outlet and bi-directional airflow will occur. With the assumption that the neutral pressure level lies in the middle of the opening height, which actually assumes that the big opening is consisted of two small openings with the same size, then the airflow rate can be calculated by integrating the pressure difference in vertical direction:

$$q = C_D A \int_0^{h/2} \sqrt{2\Delta p(y)/\rho} dy \tag{2.17}$$

Assuming that both indoor and outdoor air temperatures are uniformly distributed, the following equation will be obtained (Awbi 1996):

$$q = \frac{1}{3} C_D A \sqrt{\frac{(T_i - T_o) g h}{T_i}} \tag{2.18}$$

If the temperature cannot be assumed to be uniformly distributed, the theoretical analysis will not be able to be performed, as the position of the neutral pressure level is not known.

It can be revealed from the above theoretical analysis that, both displacement and mixing buoyancy-driven ventilation are significantly influenced by the opening area, the temperature difference between the indoor and outdoor environment and also opening characteristics. The vertical distance between the openings is very important for the displacement ventilation and this is very relevant to atrium spaces because of their large height commonly adopted. By comparing Equation (2.11) and (2.18), it is also shown that, with the same opening area, displacement ventilation should be much more efficient than the mixing ventilation, as the two openings of the mixing ventilation (actually they form one big opening but just divided by the neutral level) has the least distance compared to displacement ventilation.

In addition, the above analysis also suggests that the information associated with the heat source such as its location and intensity significantly affects the airflow rate of both types of ventilation, as it can impact on the air temperature distribution of the space (Bryn and Schilfloe 1996). Only with the air temperature distribution known, can the airflow rate and the neutral level be predicted.

The information provided by the theoretical analysis is very useful for the design of the buoyancy-driven ventilation of atrium spaces; however, there are a number of important assumptions for their application which may not be the case for atrium spaces, such as the uniformly distributed air temperature in the space, and moreover, the information regarding to the air velocity distribution at the occupants' level cannot be produced by above equations.

• *Review of the research in relation to buoyancy-driven ventilation in atrium spaces*

Buoyancy-driven ventilation has been widely and extensively investigated over recent years. The research relevant to the issues to be studied in this thesis, i.e. the impacts of the heat source and the neutral level is reviewed respectively as below.

Substantial work has been carried out for the buoyancy-driven ventilation with different settings of heat sources. Linden et al (1990) studied the impacts of a single plume-type heat source inducing buoyancy-driven natural ventilation by mathematical models and laboratory experiments. It was found that a strong temperature stratification develops consisting of two layers separated by a horizontal interface when displacement ventilation occurs. The lower layer is at uniform ambient temperature and the upper layer is also at a uniform but higher temperature. Whilst the strength of the temperature stratification and the magnitudes of the velocities depend on the source strength, the form of the stratification within the space depends on the entrainment caused by the convective elements (plumes) and is independent of the strength of the sources. A general algorithm was also presented to express the relationship between interface height, effective area and the vertical distance between the top and bottom openings.

Linden and Cooper (1996) and Cooper and Linden (1996) studied the natural ventilation of an enclosure containing two buoyancy sources. Two sources of unequal strength are found to produce a vertical density profile consisting of three distinct, fully mixed layers and theoretical models are produced for the prediction of the depth and densities of these layers.

This string of research was also extended to the situations that have multiple plumes (Hunt and Linden 1999). If there are n sources of equal strength present on the floor of the enclosure, again a stratification with two uniform layers forms, and since each source shares an equal fraction of the effective area, the interface height will be reduced. If n is an infinite number, the interface will reach the floor and the whole interior is at a uniform temperature. This is actually the case for the buoyancy-driven ventilation of spaces with heated floors. This result was also confirmed by the experiments of Gladstone and Woods (2001).

Li (2000) developed new theoretical models for the prediction of airflow rate and neutral level of buoyancy-driven displacement ventilation taking into consideration the impacts of temperature stratification for various temperature distribution conditions introduced above. Chen and Li (2002) extended the application of theoretical analysis to the spaces with multiple openings. Three flow modes for a single-zone building with three-level openings (one top, one bottom and the other intermediate level) were identified and they suggested that for certain ranges of building geometry, flow bifurcation may occur between the flow modes depending on the initial conditions according to their mathematical models. Fitzgerald and Woods (2004) performed similar research based on the same ventilation conditions and argued that the result of flow bifurcation numerically obtained by Chen and Li (2002) did not exist physically. The

impacts of the additional intermediate opening on the neutral height and flow rate were also investigated.

A theoretical model was also derived by Holford and Hunt (2003) with the attention focused on the capacity of atrium spaces to assist the ventilation of adjacent buildings and the result of the model was also compared with that from physical modelling. Guidelines were also obtained accordingly for the ventilation situations defined in the research.

The airflow performance of buildings with heating at multiple levels with various opening conditions was investigated by Livermore and Woods (2007). Theoretical models for building with two openings and three openings were developed. Laboratory experiments were also performed to verify the models obtained analytically. For three-opening circumstances, three different flow regimes were identified. The applications of the models were also introduced.

Compared to the fruitful research on the heat sources, very little research can be found in relation to the neutral level when the displacement ventilation and the mixing interact. One exception is the work performed by Haslavsky et al (2006), who observed that, in a full scale enclosure with upper and lower openings, the height of the neutral plane varies with the ratio between the opening heights (areas) of the upper and the lower openings and it was possible for the neutral level to intersect with the larger opening resulting in bi-directional flow. However, the generalised algorithms for the prediction of the neutral level and the airflow rate have not been proposed regarding to this condition.

Computer simulation was also applied to study buoyancy-driven ventilation. CFD with various settings was used by Jiang and Chen (2003)(2003) to investigate the buoyancy-driven single-sided natural ventilation and the results were compared with full-scale experiments in order to validate the turbulence models. Ji and Cook (2007) further demonstrated the capability of CFD for predicting buoyancy-driven ventilation airflows and some guidelines for the use of CFD for atrium spaces were provided by Schild (1995). The impacts of design parameters on the performance of single-sided mixing ventilation have been investigated by CFD methods (Papakonstantinou et al. 2000; Favarolo and Manz 2005). It was found that the vertical position of the opening was the most important parameter affecting ventilation performance, and other variables such as wall thickness, opening width could also be influential. CFD has also been employed for the study of displacement buoyancy-driven ventilation (Allocca et al. 2003). It was shown that the results obtained from CFD analysis are within a 10% difference from the semi-analytical results.

It can be seen that from the above review that the heat sources and the resulting temperature distributions are the key factors for the performance of the buoyancy-driven ventilation but little research is found related to the ventilation performance when solar radiation acts as the main heat source. In addition, most of these investigations are focused on

either mixing type of ventilation or displacement ventilation but the interaction between them when the neutral level intersects with one opening has not been well understood. It is also suggested that in the review that CFD is a valuable tool for the study of buoyancy-driven ventilation with appropriate settings.

2.5.3 Combined natural ventilation in atrium spaces

When wind-driven forces and the buoyancy forces in atrium spaces are significant simultaneously, combined natural ventilation will occur as a result. The two forces may operate in the same or in opposite directions, depending on the direction of the wind and on whether the internal or external temperature is the higher.

For simple spaces, the buoyancy force is usually very small in hot weather, as the temperature difference is generally not large, and the wind force will dominate the performance of combined natural ventilation. However, in atrium spaces, the buoyancy force can be very strong due to the large height and the intensive incident solar radiation and the two forces may be of similar magnitude. As introduced above, the two forces do not necessarily assist each other and may oppose one another (See Figure 2.16). Thus, in order to make better use of this phenomenon to provide passive cooling effects, it is of practical importance to understand its behaviour under various circumstances and the impacts of related design parameters.

• *Theoretical analysis*

Consider a simple one-zone building with combined ventilation as shown in Figure 2.16. Assume that the indoor air temperature is uniformly distributed. When the buoyancy force and wind force assist each other, as illustrated in (a), the pressure difference driving the airflow can be considered as that driven by the buoyancy forces in addition to that by wind forces. This can be expressed by the following equation:

$$\Delta p = \frac{\rho_o (T_i - T_o) g h}{T_o} + \Delta p_w \tag{2.19}$$

Thus, the calculation of the airflow rate can be obtained by integrating Equation (2.19) with Equation (2.6) as follows:

$$q = (C_D A)^* \sqrt{\frac{2(T_i - T_o) g h}{T_i} + 2\frac{\Delta p_w}{\rho_o}} \tag{2.20}$$

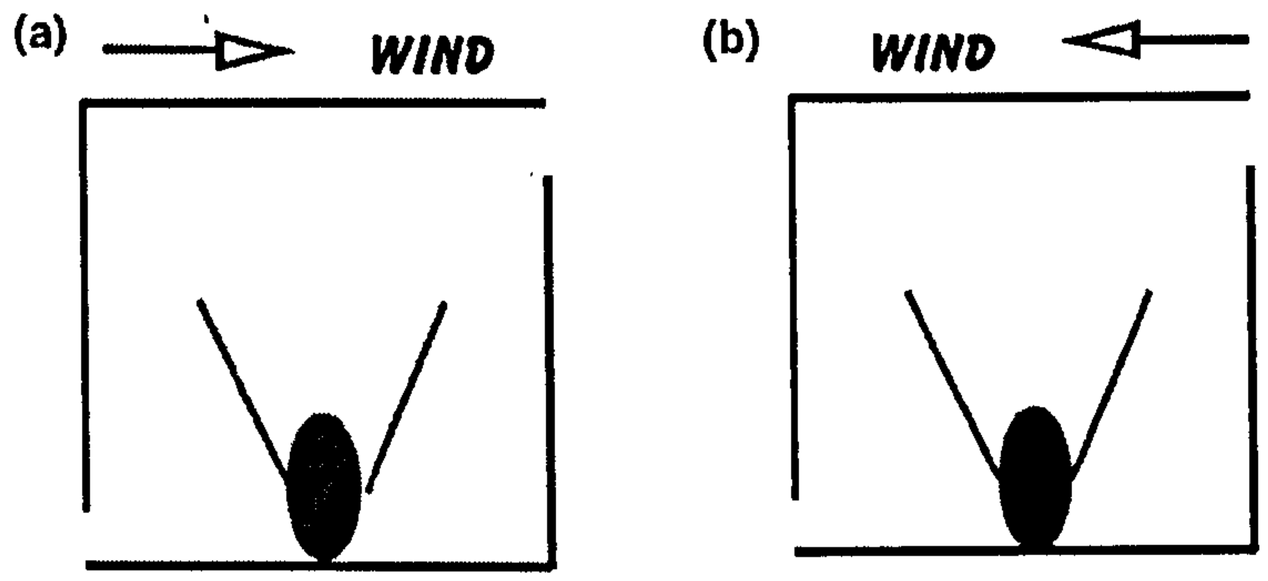

Figure 2.16: A schematic diagram illustrating the conditions for which wind and buoyancy forces assist (a) or oppose (b) each other (Heiselberg et al. 2004)

It is shown by this equation that, there is a Pythagorean relationship between the combined buoyancy and wind-driven velocity and the velocities which are produced by buoyancy and wind forces acting in isolation, i.e.:

$$q^2 = q_b^2 + q_w^2 \tag{2.21}$$

This result is also confirmed by laboratory experiments (Hunt and Linden 1999). Equation (2.21) also means that the airflow rate can be increased at most by 40% than it would be with the single force alone (when two forces are of equal magnitude).

When the two forces oppose each other, as illustrated in Figure 2.16 (b), the equation for the calculation of the airflow rate becomes:

$$q = (C_D A)^* \sqrt{\left| \frac{2(T_i - T_o)gh}{T_i} - 2\frac{\Delta p_w}{\rho_o} \right|} \tag{2.22}$$

Thus we have:

$$q^2 = \left| q_b^2 - q_w^2 \right| \tag{2.23}$$

It can be seen that the Pythagorean relationship can still apply, except that the role of the combined airflow rate has changed from hypotenuse to side. This equation also shows that the combined airflow rate can be considerably reduced if the two forces are in opposite direction and this should be avoided in practice.

For both assisted and opposed ventilation conditions, according to energy conservation, we have (assuming that all the energy is from heat source and all other parts of buildings are adiabatic):

$$E = \rho C_p q (T_i - T_o) \tag{2.24}$$

• *Review of the research in relation to combined ventilation in atrium spaces*

Following the above equations, one interesting question may be raised with regard to opposed ventilation: if the wind forces and the buoyancy forces are equal, then the airflow rate will be zero according to Equation (2.23), so how can Equation (2.24) be tenable and where will the energy from the heat source go?

A number of researchers have tried to address this problem. Li and Delsante (2001) obtained three possible solutions for one building with the opposed natural ventilation using theoretical analysis. Although one of them is not stable numerically, the other two are possible and valid depending on initial conditions. It was also found that the performance of opposed ventilation has hysteresis behaviour under certain circumstances, i.e., the airflow does not change continuously and some "jumps" may occur when two forces become of similar magnitude. It could be inferred that the airflow rate will never fall to zero when the two forces are equal, unless both of them are zero in the first place.

This result was further verified by laboratory experiments (Hunt and Linden 2004). For a space with a point type heat source on the floor, displacement ventilation will occur if two openings are provided at the top and bottom respectively and the indoor air temperature will also be stratified into two layers. For small opposing winds, a steady two-layer stratification and displacement ventilation is established. Exterior fluid enters through the lower leeward openings and buoyant interior fluid leaves through the upper windward openings. In this regime, the increase in wind speed increases the depth and temperature of the warm upper layer, and reduces the ventilation rate. If, on the other hand, the wind speed is very high, the reversed flow is maintained, the stratification is destroyed and mixing ventilation occurs. It was also observed that the transitions between these two flow patterns are not continuous and exhibit hysteresis. The change from displacement ventilation to mixing ventilation occurs at a higher Froude number (the dimensionless ratio between buoyancy force and wind force) than the transition from mixing to displacement.

Andersen (2007) further studied the multiplicity, stability and hysteresis of the solutions of opposed ventilation with an example in real practice. It was shown that unambiguous solutions could be obtained if the difference between indoor and outdoor air temperature was known at the start point, and the specific conditions, under which the discontinuities occur were also identified.

Examples of solution multiplicity in opposed ventilation were also illustrated by other experiments and CFD simulations (Li et al. 2001; Heiselberg et al. 2004) and consequently it was concluded that the setting of initial conditions for CFD analysis would be very crucial for the achievement of correct results.

Buoyancy and wind-driven assisting ventilation was also investigated by a number of researchers. Hunt and Linden (2001) examined the performance of displacement ventilation driven by a point source on the floor of an enclosure assisted by wind. The airflow rate was increased owing to the wind pressure and two-layer stratification and displacement ventilation were maintained over a range of wind speeds, even when the wind-induced flow far exceeded the flow induced by the buoyancy force. Increasing the wind speed raised the position of the interface and decreased the temperature of the upper layer. For significantly larger Froude number, the displacement flow broke down. The value of the initial Froude number at which the transition occurs was determined by Hunt and Linden (1999). The phenomenon of solution multiplicity or hysteresis has not been observed for buoyancy and wind-driven assisting ventilation.

However, it should be noted that most investigations introduced above are focused on the bulk flows and generally assume that the air movement in the space is ignorable and only small openings are employed. In fact, from the flow pattern point of view, the airflows driven by the two forces will never entirely assist each other everywhere in the flow field, even if the bulk flow has the same direction, simply because the directions of the driving forces are quite different: the wind forces are horizontal towards the direction of the wind whilst the buoyancy forces are vertical towards the sky. This may suggest that, even if the bulk flows of the two forces assist each other, those phenomena observed for opposed ventilation may still exist.

In addition, the above theoretical analysis seem to suggest that, the reason for the occurrence of the solution multiplicity and hysteresis is that the direction of the airflow at either opening has to change suddenly without reaching to zero in order to keep the conservation of energy. Thus, it would be interesting to know whether these phenomena still take place when large openings are incorporated where bi-directional flows can occur demolishing the sudden change of the flow direction.

These issues will be the main concern of this research regarding the combined ventilation of atrium spaces and in addition, the effects of solution multiplicity on the evaluation of the ventilation performance will also be examined, based on which design guidelines can be developed.

In order to take the flow pattern into account, computer simulation tools will have to be used. It has been found that, CFD has also been employed for the study of combined buoyancy and wind-driven ventilation. Examples include Allocca et al. (2003) and Cook et al.(2003) and the guidelines they developed for the settings of CFD provide important basis work for this research.

2.6 Summary

An overview of the fundamental knowledge in relation to the ventilative cooling of atrium spaces, including their historical development, the characteristics of their energy use, thermal comfort and natural ventilation, has been provided in this chapter. This is intended as a basis from which to develop the research embodied in the remainder of the thesis.

It has been clearly shown that, as a vital and exciting feature of the present architectural era, atrium type buildings are undergoing a great revival and have been incorporated as a design element with increased frequency for the last few decades. Early examples of atrium buildings in different climates imply that climate is an important factor for the incorporation of atrium spaces and atrium spaces have the potential to provide passive cooling effects.

The thermal environment of atrium spaces is usually characterised with warmer conditions than the external climate, and this is also accompanied by non-uniform distribution of thermal properties, and more significant air movement due to greenhouse and stack effects. They can be used in various ways: as solar collectors, buffer zones and also for natural ventilation. However, in spite of the benefits resulting from these characteristics, such as the success achieved in cold climates like Scandinavian areas, risks and difficulties can be brought on for ventilative cooling purposes, which will be the main problems to be solved in this research.

Aimed at the issues proposed in Chapter One, relevant research is reviewed in detail and the research topic is further refined as follows: the thermal comfort assessment needs to take some important factors of such type of space into consideration, such as the impacts of solar radiation on MRT and vertical air temperature stratification; the airflow for wind-induced ventilation of atrium spaces may be driven by recirculation rather than the main flow due to the unavailability of the openings at the occupants' level and thus the roof design is extremely important to achieve a better ventilation performance; the performance of the buoyancy-driven ventilation is sensitive to the conditions of heat sources, and a new approach for the prediction of the neutral level when the displacement ventilation and mixing ventilation interacts with each other is needed; with respect to combined ventilation, the existence of solution multiplicity and hysteresis will be tested for two common conditions of atria: (1) bulk flows of the two forces assist whilst the flow pattern is not the same; (2) bi-directional flow occurs, and the effects of these special phenomena on the evaluation of the ventilation performance will be studied. Focused on these problems, the next chapter will discuss the method to be employed for the investigation of this study.

3

AIRFLOW RESEARCH METHODOLOGY

3.1 Introduction

It has been clarified in Chapter One that the primary concern of this research is to deal with the thermal comfort assessment of atrium spaces and three types of ventilation strategies for cooling purposes including airflows driven by wind forces, buoyancy forces and combined forces, and the detailed research directions have been highlighted in Chapter Two. Although there is no universal method that can be applied for the study of both thermal comfort and natural ventilation, investigations of airflows are the key issue for both of them and this plays an important role of the whole research.

With the focus to choose the appropriate methodology for air movement study, this chapter starts with a review of the research methods that are commonly used for airflow studies (Section 3.2) and then describes the tool employed for this project according to the research purposes (Section 3.3), followed by validations. The settings of the tool adopted in the research are investigated in order to optimise its use for accurate and sensible results in Section 3.4 and a summary is finally provided in Section 3.5.

3.2 Review of the research methods for air movement studies

According to the type of information required about air movement and the level of accuracy and complexity, various research tools may be used ranging from simple theoretical algorithms for the calculation of the global airflow rate to sophisticated computerised fluid-

dynamic techniques solving Navier-Stokes equations. In general, research methods in relation to air flow can be categorised into three groups as follows: theoretical methods, experimental methods and numerical methods.

As introduced in Chapter One, the main concern of the study of air movement in this research is to understand the impacts of the design characteristics of atrium spaces and develop design guidelines accordingly. For this purpose, a parametric study that consists of a large number of tests regarding various design and environmental scenarios will be the basic requirement. In addition, it has also been mentioned in Chapter Two that precise control of some parameters, such as neutral level and airflow rate will also be investigated in the research. As a consequence, a method that can achieve fast solution but does not comprise accuracy has to be employed. Below is a review of the methods available for air movement study, and then based on the above criterion, the appropriate tool is selected and introduced further in detail.

3.2.1 Theoretical and semi-empirical methods

Generalised theoretical and semi-empirical methods mainly offer general correlations to calculate the bulk airflow rate, or the mean air velocity in the building zone (Santamouris et al. 1998). These integrate the airflow with a number of associated parameters, such as the wind velocity, temperature difference and basic building configuration. Simple methods of this group that are widely used include the British Standards method developed in the UK (BS5925 1991) and the ASHRAE method in the USA (ASHRAE 2001). Some theoretical models in relation to the natural ventilation in atrium spaces have also been introduced in Chapter Two. Recently this group of methods also extended to the calculation of more sophisticated situations, such as buoyancy-driven air flow in a thermally stratified one-zone building with different settings of openings (Li 2000; Zhai et al. 2002; Anderson 2003). Tables 3.1 and 3.2 from British Standard (1991) show schematically the proposed formulae for different airflow patterns under various conditions.

These tools are still the most widely used at the early stage of the design process because of their simplicity for implementation, and they are of great use because they offer a fast first estimation of the airflow rate or of the mean air velocity, but should always be used within limits of their applicability. Nevertheless, it is very difficult for theoretical methods to be employed for parametric studies of design characteristics, as they can only cope with simple geometries.

3.2.2 Experimental methods

Experiments can be performed on the level of either full size buildings or physical models in order to investigate impacts of different variables on air flow. Early work on building

ventilation in relation to wind-driven flows was, and still is, extensively studied in wind tunnels. For airflow driven by wind forces, the air flow pattern around the building is generally governed by inviscid dynamics, and in addition, separation is a major factor in determining the wind flow around the building, particularly downstream of the windward face. Most buildings have sharp corners and wind speed plays only a minor part in determining the flow pattern. As a result, the airflow pattern around buildings can be regarded as independent of Reynolds number, which is, of course, why wind-tunnel modelling has been so successful in determining airflow characteristics (Linden 1999).

When using this technique, pressure coefficients are determined by the measurement of each scenario and then used to calculate the air flow through vents at different locations on the facade (See Section 2.5.1 for further information on the correlation between pressure coefficients and flow characteristics). Nevertheless, it is difficult to obtain the detailed flow patterns in and around buildings by wind tunnel and there is usually little consideration of the mechanics of the flow.

Conditions	Schematic representation	Formula
(a) Due to wind	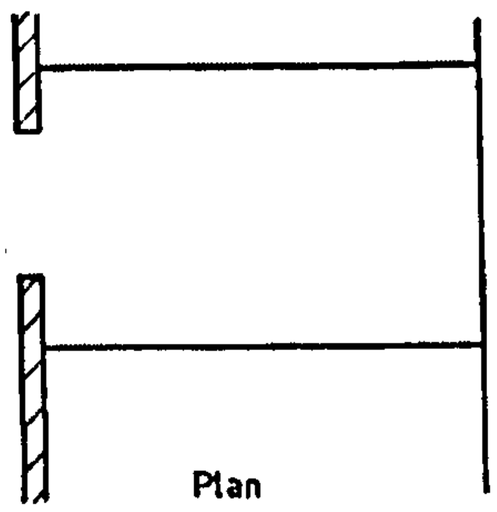	$Q = 0.025 A u_r$
(b) Due to temperature difference with two openings	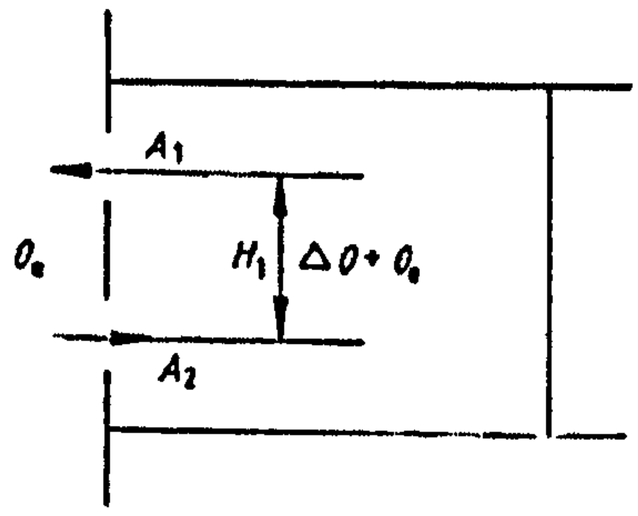	$Q = C_d A \left[\frac{\epsilon\sqrt{2}}{(1+\epsilon)(1+\epsilon^2)^{1/2}}\right] \left(\frac{\Delta\theta g H_1}{\bar{\theta}}\right)^{1/2}$ $\epsilon = \frac{A_1}{A_2}; A = A_1 + A_2$
(c) Due to temperature difference with one opening	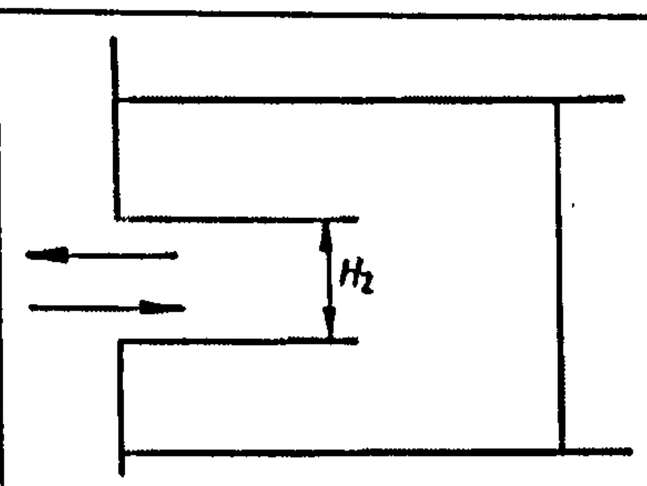	$Q = C_d \frac{A}{3} \left(\frac{\Delta\theta g H_2}{\bar{\theta}}\right)^{1/2}$ If an opening light is present $Q = C_d \frac{A}{3} J(\phi) \left(\frac{\Delta\theta g H_2}{\bar{\theta}}\right)^{1/2}$ Where $J(\phi)$ is given in Figure 7

Table 3.1: Formulae for single-sided ventilation (BS5925 1991)

Conditions	Schematic representation	Formula
(a) Wind only	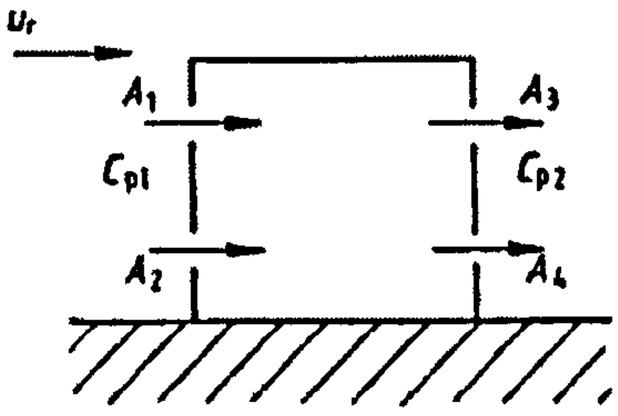	$Q_w = C_d A_w u_r (\Delta C_p)^{1/2}$ $\frac{1}{A_w^2} = \frac{1}{(A_1 + A_2)^2} + \frac{1}{(A_3 + A_4)^2}$
(b) Temperature difference only	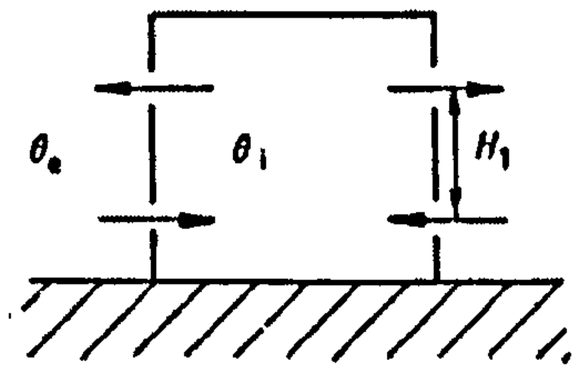	$Q_b = C_d A_b \left(\frac{2\Delta\theta g H_1}{\bar{\theta}}\right)^{1/2}$ $\frac{1}{A_b^2} = \frac{1}{(A_1 + A_3)^2} + \frac{1}{(A_2 + A_4)^2}$
(c) Wind and temperature difference together	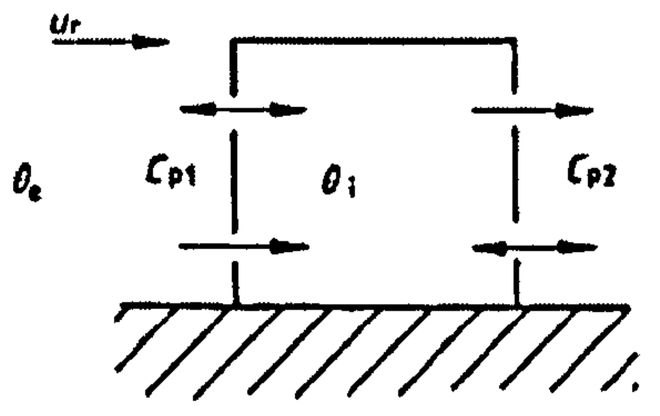	$Q = Q_b$ For $\frac{u_r}{\sqrt{\Delta\theta}} < 0.26 \left(\frac{A_b}{A_w}\right)^{1/2} \left(\frac{H_1}{\Delta C_p}\right)^{1/2}$ $Q = Q_w$ For $\frac{u_r}{\sqrt{\Delta\theta}} > 0.26 \left(\frac{A_b}{A_w}\right)^{1/2} \left(\frac{H_1}{\Delta C_p}\right)^{1/2}$
NOTE It should be appreciated that, in practice, some openings exist unintentionally, e.g. junctions between building components, and that such openings will contribute to the ventilation actually achieved.		

Table 3.2: Formulae for cross ventilation (BS5925 1991)

In contrast to wind-driven air flow, it was difficult to carry out studies of buoyancy-driven ventilation at small scale because of the increased importance of viscous effects at the low Reynolds numbers obtained. In recent years the group at Cambridge overcame this problem (Linden et al. 1990; Baker and Linden 1991) and developed the methodology of small-scale modelling using water as the working liquid. Buoyancy forces are produced by salinity differences within the fluid. This technique is widely adopted after development and some examples have already been introduced in the previous chapter regarding the buoyancy-driven ventilation in atrium spaces (See Section 2.5.2).

Experimental methods are very helpful because they are straight-forward and they can be performed without too much expertise on the theoretical mechanism of the air movement, especially when the mechanics of the flow is very clear. However, experimental methods are still not flexible enough for the parametric study due to the difficulty of changing physical modes. Furthermore, the discrepancy of the two methods for buoyancy-driven and wind-driven flows also means that it is not easy to make use of a single experiment to study a flow in which the two forces are equally important, which is usually the case for atrium type buildings.

3.2.3 Numerical methods

Numerical methods consider air flow in a different way: they admit that an analytical solution to airflow problems does not exist, because as a continuous fluid, air does not have a uniform behaviour and there are too many influential factors. As a result they divide the whole space into large numbers of small control volumes, each of which can be considered as having a uniform property and build up a string of equations based upon conservation laws. All the functions are then solved using iteration procedures. According to the level of modelling complexity, two different numerical approaches can be generally distinguished for the prediction of the air flow in buildings: zonal network methods and Computational Fluid Dynamics (CFD) models.

Developed in 1970s for the simulation of infiltration and internal airflow between spaces of one building (Lebrun 1970), zonal network models are usually adopted to simulate a building with a number of spaces based on the "well-mixed air" assumption. The whole building is represented by a grid that is formed by a number of nodes that stand for the simulated zones and the exterior environment. Interaction between various zones is denoted by flow paths linking their respective nodes. Thus, the spaces of a building are represented by nodes and the openings are represented by linking flow paths. Interaction with the outdoor environment is represented by flow paths linking interior and exterior nodes. All nodes are attributed a pressure value and are solved together. As stated earlier in Chapter Two (See Section 2.3.2), a significant feature of the thermal environment of atrium spaces is that there may be strong vertical temperature stratification and the indoor air cannot be regarded as uniform in this situation. As a consequence, the basic assumption of zonal network methods may not be valid for the use of atrium spaces, unless splitting vertically the space into a number of small zones that have generally the same air temperature (e.g. Laouadi and Atif 1999; Voeltzel et al. 2000; Laouadi et al. 2001; Laouadi et al. 2003).

Based on the solution of the Navier-Stokes conservation equations, namely, the mass, momentum and energy conservation equations, CFD programs allow the explicit calculation of the air temperature and velocity field of a flow as well as easy visualisation for post-processing. With the development of computing techniques, CFD methods have been greatly advanced and widely applied during the last few decades. They are versatile for the simulation of all kinds of flows including both steady and unsteady, both compressible and incompressible, both single- and multi-phases. It offers the potential of obtaining much richer details about the air flow and much lower cost than traditional laboratory experiments. More importantly, it provides a higher degree of flexibility for the use of designers and is suitable to perform parametric studies, as building parameters can be easily altered in modelling process. Some examples that use CFD to study the air movement issues associated with thermal comfort, natural ventilation and energy use in buildings have already been introduced in Chapter Two. In addition, as is widely

recognised, the turbulence intensity may have a significant impact on the assessment of thermal comfort (ISO7730 2005) and CFD is the only available tool to achieve this information at an early stage.

As described earlier, the main concern of the air flow study in this research is to investigate the impacts of design characteristics of atrium buildings on the performance of different flow regimes of air movement and to obtain information relevant for the study of thermal comfort and energy. Considering the flexibility and the versatility of the tool required by this research, CFD is the option to be employed and details are introduced in the following section.

3.3 Computational Fluid Dynamics (CFD)

3.3.1 CFD basics

• *Governing equations*

The fundamental governing equations of fluid dynamics, i.e. the continuity, momentum and energy equations are the mathematical statements of three fundamental physical principles, which are respectively conservation of mass, Newton's Second Law and conservation of energy. Room air flow can be considered incompressible as velocities tend to be low, in the order of metres or centimetres per second (air is considered incompressible at Mach numbers less than 0.3, about 100 m/s, which is impossible for ventilative cooling purposes). Air, like many common fluids such as water, is newtonian (newtonian fluids display a linear relationship between shear and strain rate). Given the above description on the properties of the fluid, the following set of differential equations can be written to describe room airflow. They are presented in the common Navier-Stokes formulation (Schlichting 1968) and in three-dimensional Cartesian coordinates.

Conservation of mass

$$\frac{\partial \rho}{\partial t}+\frac{\partial}{\partial x}(\rho u)+\frac{\partial}{\partial y}(\rho v)+\frac{\partial}{\partial z}(\rho w)=0 \qquad (3.1)$$

Conservation of momentum

$$\frac{\partial}{\partial t}(\rho u)+\frac{\partial}{\partial x}(\rho uu)+\frac{\partial}{\partial y}(\rho vu)+\frac{\partial}{\partial z}(\rho wu)=-\frac{\partial P}{\partial x}+\frac{\partial}{\partial x_j}\left[\mu\left(\frac{\partial u}{\partial x_j}+\frac{\partial u_j}{\partial x}\right)\right] \qquad (3.2)$$

$$\frac{\partial}{\partial t}(\rho v)+\frac{\partial}{\partial x}(\rho uv)+\frac{\partial}{\partial y}(\rho vv)+\frac{\partial}{\partial z}(\rho wv)=-\frac{\partial P}{\partial y}+\frac{\partial}{\partial x_j}\left[\mu\left(\frac{\partial v}{\partial x_j}+\frac{\partial u_j}{\partial y}\right)\right] \qquad (3.3)$$

$$\frac{\partial}{\partial t}(\rho w)+\frac{\partial}{\partial x}(\rho uw)+\frac{\partial}{\partial y}(\rho vw)+\frac{\partial}{\partial z}(\rho ww)=-\frac{\partial P}{\partial z}+\frac{\partial}{\partial x_j}\left[\mu\left(\frac{\partial w}{\partial x_j}+\frac{\partial u_j}{\partial z}\right)\right]-\rho g\beta(T_\infty-T) \qquad (3.4)$$

Conservation of energy

$$\frac{\partial}{\partial t}(\rho c_p T)+\frac{\partial}{\partial x}(\rho c_p u T)+\frac{\partial}{\partial y}(\rho c_p v T)+\frac{\partial}{\partial z}(\rho c_p w T)=\frac{\partial}{\partial x_j}\left(k\frac{\partial T}{\partial x_j}\right)+q''' \tag{3.5}$$

In essence, all these equations can be generally understood as (Patankar 1980),

unsteady terms + convection terms = diffusion terms + source terms

• *Turbulence modelling*

Most flows of practical interest experience some degree of random turbulent fluctuations. These fluctuations are caused by instabilities between inertial and viscous forces (Fox et al. 2006). As the turbulent fluctuations enhance the transport of momentum, heat, and pollutants, they must be considered in the formulation and solution of the equations of motion. Although the problem has been investigated for well over a century, there is still no general approach to the solution of turbulent flows and instead empirical data has to be resorted to (Tennekes and Lumley 1972).

The approaches to solving the flow equations for a turbulent flow field can be roughly divided into two classes according to their complexity and computational intensity (Versteeg and Malalasekera 1995). Some approaches, such as direct numerical simulations (DNS) and large eddy simulation (LES) attempt to resolve all of the spatial and temporal details of turbulent fluctuations with little or no assumption, which necessitates very fine grid and time steps. Examples of the applications of this group of methods that have been made include Nielson (1998), Emmerich and McGrattan (1998), Jiang and Chen (2003), etc. These methods still remain limited to very simple geometries (e.g., channel flows, jets and boundary layers) and are extremely computationally expensive to run. Jiang (2002) indicated that, with reduced number of grids, LES still require 4-5 days computing time of a fast workstation for the simulation of the wind-driven natural ventilation in a simple model, which is not acceptable for most practical applications.

The alternative to these approaches, which is also found in most CFD packages, is to solve the Reynolds Averaged Navier-Stokes (RANS) equations by treating random fluctuations with statistical methods mainly focused on time-averaged mean velocity and pressure. The equations of motion are filtered with respect to time, so that rather than modelling the details of the turbulent motion, these methods account for the influence of turbulence on the time-mean motion. The time filtering generates new terms in the equations, which approximates the impact of the high-frequency fluctuations on the time-mean motion.

If a turbulent flow is considered within RANS, each instantaneous variable in equation of (3.1 to 3.5) is replaced by the sum of a time-mean component and a fluctuating component, i.e.:

$$P=\bar{P}+P';\qquad u=\bar{u}+u';\qquad v=\bar{v}+v';\qquad w=\bar{w}+w';\qquad T=\bar{T}+T' \tag{3.6}$$

Substituting these expressions into equation (3.1) to (3.5) results in the Reynolds averaged form of the motion –

Conservation of mass

$$\frac{\partial\rho}{\partial t}+\frac{\partial}{\partial x}(\rho\bar{u})+\frac{\partial}{\partial y}(\rho\bar{v})+\frac{\partial}{\partial z}(\rho\bar{w})=0 \tag{3.7}$$

Conservation of momentum

$$\frac{\partial}{\partial t}(\rho\bar{u})+\frac{\partial}{\partial x}(\rho\bar{u}\bar{u})+\frac{\partial}{\partial y}(\rho\bar{v}\bar{u})+\frac{\partial}{\partial z}(\rho\bar{w}\bar{u})=-\frac{\partial\bar{P}}{\partial x}+\frac{\partial}{\partial x_j}\left[\mu\left(\frac{\partial\bar{u}}{\partial x_j}+\frac{\partial\bar{u}_j}{\partial x}\right)-\rho\overline{u'u_j'}\right] \tag{3.8}$$

$$\frac{\partial}{\partial t}(\rho\bar{v})+\frac{\partial}{\partial x}(\rho\bar{u}\bar{v})+\frac{\partial}{\partial y}(\rho\bar{v}\bar{v})+\frac{\partial}{\partial z}(\rho\bar{w}\bar{v})=-\frac{\partial\bar{P}}{\partial y}+\frac{\partial}{\partial x_j}\left[\mu\left(\frac{\partial\bar{v}}{\partial x_j}+\frac{\partial\bar{u}_j}{\partial y}\right)-\rho\overline{v'u_j'}\right] \tag{3.9}$$

$$\frac{\partial}{\partial t}(\rho\bar{w})+\frac{\partial}{\partial x}(\rho\bar{u}\bar{w})+\frac{\partial}{\partial y}(\rho\bar{v}\bar{w})+\frac{\partial}{\partial z}(\rho\bar{w}\bar{w})=$$
$$-\frac{\partial\bar{P}}{\partial z}+\frac{\partial}{\partial x_j}\left[\mu\left(\frac{\partial\bar{w}}{\partial x_j}+\frac{\partial\bar{u}_j}{\partial z}\right)-\rho\overline{w'u_j'}\right]-\rho g\beta(\bar{T}_\infty-\bar{T}) \tag{3.10}$$

Conservation of energy

$$\frac{\partial}{\partial t}(\rho c_p\bar{T})+\frac{\partial}{\partial x}(\rho c_p\bar{u}\bar{T})+\frac{\partial}{\partial y}(\rho c_p\bar{v}\bar{T})+\frac{\partial}{\partial z}(\rho c_p\bar{w}\bar{T})=\frac{\partial}{\partial x_j}\left(k\frac{\partial\bar{T}}{\partial x_j}-\rho c_p\overline{T'u_j'}\right)+q''' \tag{3.11}$$

The new terms appearing in the momentum equations ($-\rho\overline{u_i'u_j'}$) contain the high-frequency fluctuating velocity components and are known as Reynolds stresses. The new terms appearing in the energy equation ($-\rho c_p\overline{T'u_j}$) contain the fluctuating components of temperature and velocity, and are known as turbulent heat fluxes.

As the number of equations is still five but the number of variables has doubled, more equations are needed to close the system of above equations. According to the eddy-viscosity concept based on the analogy between molecular and turbulent diffusion proposed by Boussinesq (1877), the turbulent stresses are assumed to be proportional to the gradients of mean-velocity,

$$-\overline{u_i'u_j'}=\frac{\mu_t}{\rho}\left(\frac{\partial\bar{u}_i}{\partial x_j}+\frac{\partial\bar{u}_j}{\partial x_i}\right) \tag{3.12}$$

where μ_t is defined to be eddy viscosity. The molecular viscosity μ is a property of the fluid while μ_t is a property of the flow – it can differ significantly from one flow to another and can vary through a flow domain. Similarly, the turbulent heat fluxes are assumed to be proportional to the gradients of mean-temperature,

$$-\rho\overline{T'u'_j} = \Gamma\frac{\partial\bar{T}}{\partial x_i} \tag{3.13}$$

where Γ is the turbulent diffusivity of heat. Like the eddy viscosity, it is a property of the flow rather than of the fluid. Since turbulent transport of momentum and heat or mass is due to the same mechanism – eddy mixing – it is expected that the value of the turbulent diffusivity Γ is close to that of the turbulent viscosity μ_t. The turbulent Prandtl number, σ_t is introduced to relate the turbulent diffusivity of heat and the eddy viscosity and it is usually considered as constant,

$$\sigma_t = \frac{\mu_t}{\Gamma} \tag{3.14}$$

By substituting equations (3.12) to (3.14) into equations (3.8) to (3.11), the governing equations become the following.

Conservation of mass

$$\frac{\partial\rho}{\partial t}+\frac{\partial}{\partial x}(\rho\bar{u})+\frac{\partial}{\partial y}(\rho\bar{v})+\frac{\partial}{\partial z}(\rho\bar{w})=0 \tag{3.15}$$

Conservation of momentum

$$\frac{\partial}{\partial t}(\rho\bar{u})+\frac{\partial}{\partial x}(\rho\overline{uu})+\frac{\partial}{\partial y}(\rho\overline{vu})+\frac{\partial}{\partial z}(\rho\overline{wu})=-\frac{\partial\bar{P}}{\partial x}+\frac{\partial}{\partial x_j}\left[(\mu+\mu_t)\left(\frac{\partial\bar{u}}{\partial x_j}+\frac{\partial\bar{u}_j}{\partial x}\right)\right] \tag{3.16}$$

$$\frac{\partial}{\partial t}(\rho\bar{v})+\frac{\partial}{\partial x}(\rho\overline{uv})+\frac{\partial}{\partial y}(\rho\overline{vv})+\frac{\partial}{\partial z}(\rho\overline{wv})=-\frac{\partial\bar{P}}{\partial y}+\frac{\partial}{\partial x_j}\left[(\mu+\mu_t)\left(\frac{\partial\bar{v}}{\partial x_j}+\frac{\partial\bar{u}_j}{\partial y}\right)\right] \tag{3.17}$$

$$\frac{\partial}{\partial t}(\rho\bar{w})+\frac{\partial}{\partial x}(\rho\overline{uw})+\frac{\partial}{\partial y}(\rho\overline{vw})+\frac{\partial}{\partial z}(\rho\overline{ww})= -\frac{\partial\bar{P}}{\partial z}+\frac{\partial}{\partial x_j}\left[(\mu+\mu_t)\left(\frac{\partial\bar{w}}{\partial x_j}+\frac{\partial\bar{u}_j}{\partial z}\right)\right]-\rho g\beta(\bar{T}_\infty-\bar{T}) \tag{3.18}$$

Conservation of energy

$$\frac{\partial}{\partial t}(\rho c_p\bar{T})+\frac{\partial}{\partial x}(\rho c_p u\bar{T})+\frac{\partial}{\partial y}(\rho c_p v\bar{T})+\frac{\partial}{\partial z}(\rho c_p w\bar{T})=\frac{\partial}{\partial x_j}\left[\left(k+\frac{c_p\mu_t}{\sigma_t}\right)\frac{\partial\bar{T}}{\partial x_j}\right]+q''' \tag{3.19}$$

The new form of governing equations is nearly identical to that of the initial ones. The only differences are the momentum and heat diffusion coefficients. In order to calculate μ_t and hence make the solution of the above equation series possible, some algorithm has to be used and this is the job of turbulence models.

Depending on the number of equations used to calculate μ_t, the turbulence models can be classified into the following groups: zero-equation models (mixing length models), one-equation models such as the Spalart-Allmaras model, two-equation models such as k-ε models, algebraic stress models (ASM) and Reynolds stress models (RSM). The order also shows the sequence of computational cost from lowest to highest. A detailed review of this group of models is provided by Rodi (1980).

Despite its weakness when dealing with some complex flows, the standard k-ε model, proposed by Launder and Spalding (1974) is the most commonly used and validated turbulence model in small-scale applications such as rooms due to its robustness, relatively low computational costs and generally better numerical stability than other turbulence models. However, for large-scale applications such as urban wind studies, the standard k-ε model has clear disadvantages and over-predicts the turbulent kinetic energy in regions of stagnant flow (Franke et al. 2004). More advanced k-ε models such as the renormalization group (RNG) k-ε model (Yakhot et al. 1992) and the realizable k-ε model (Shih et al. 1995) are increasingly used as remedies.

Studies were, and are still being carried out to compare the performances of different turbulence models. Examples include Leschziner (1991), Murakami (1993), Chen (1995), Chen and Chao (1996), etc. There is still no evidence showing that any turbulence model can be universally applied for all kinds of flows, although the k-ε family is the most widely adopted. The selection of turbulence models for different flows is largely based on precedents and the relevant work carried out by others.

• *Boundary conditions*

The governing equations introduced above characterise the transient fluid motion and heat transfer throughout the air volume of the room's computational domain. However, a closed system of flow transport equations that can be solved mathematically has not been formed until the boundary conditions are specified at all the boundaries around the flow field. When boundary conditions are applied to define the domain boundary (e.g. wall surfaces, openings), the distribution of air flow and heat transfer within the room can be fully described. Essentially, the boundary conditions impose the influence of the domain's boundary upon the equations of motion.

Two things are the most important for the specification of boundary conditions of a flow. First is the location of the computational domain. Typically this is defined to encompass a single room's air volume and the domain boundary is placed at the internal surfaces of the fabric components (walls, windows, etc.), thus excluding the solid masses from the computational domain. As a result, the boundary conditions must accurately account for the

effect of the fabric components upon the room air, otherwise predictions of air flow and heat transfer throughout the room will suffer. However, sometimes part of the information on the boundary conditions of an air volume might not be available. For example, when dealing with natural ventilation of a space, what we know is the wind velocity of outside, but the air velocity at the openings is not clear. In this situation, the typical computational domain will not be applicable and the computational domain has to be extended to include some outdoor environment.

Another important issue that should be noted is that boundary conditions have to be expressed in such a way that they can reflect the reality and also be quantified and absorbed by next-to-wall air points. This becomes very tricky when the computational domain includes outdoor environment, as the boundaries will be entirely fictitious in this case. Furthermore, the nature of the airflow near the boundaries may be different flow other parts of the domain to be calculated and hence special near-wall handling techniques – so-called "wall function" will have to be applied. Detailed treatment of this issue will be introduced in the next section regarding the validation and settings of the tool for the use in this research (See Section 3.3.2 and 3.3.3).

• *Solution procedures*

The partial differential equations (3.15) to (3.19) given in the previous subsection fully describe room air flow and heat transfer. However, the equations are highly non-linear and strongly coupled: each momentum equation contains all three velocity components; temperature appears in Equation (3.4) and the energy equation contains the velocity components. Only simplest problems can be solved analytically (e.g. Lienhard 2004).

Numerical discretisation techniques are introduced to render the problem to a solvable level. Basically, this involves approximating the governing differential equations by one of the well-established numerical procedures such as Finite Volume Method (FVM) (Patankar 1980), Finite Difference Method (FDM) (Roache 1972) and Finite Element Method (FEM) (Baker 1983). The FVM is more popular than the other two, because not only does it reflect the physical phenomenon more realistically, it is also generally more robust and economical in computational time, and the majority of commercially available CFD codes use the FVM solution techniques.

With the FVM, the whole space is subdivided into finite volumes using a gridding system. Rather than solving over the continuum, all the dependent variables are calculated only at those discrete points located at the centre of each volume. In this way, all the partial differential equations are discretised and linearised into a set of simple algebraic relations.

There is still one difficulty before these equations can be solved: an approach is required to deal with pressure-velocity linkage and the lack of an equation for solving pressure.

One of the most widely used methods that link the velocity to the pressure is the SIMPLE (semi-implicit method for pressure-linked equations) procedure developed by Patankar and Spalding (1972). This method uses a staggered grid so that correction to the velocity components can be made using the pressure values at the neighbouring grid nodes.

The solution of all the discretised algebraic equations is based on iteration procedures – the calculation continues until convergence is achieved, that is, until further iteration produces no significant change in the solution variables. Various criteria can be used to judge whether a solution has converged, including a critical variable such as the heat flux of a specific surface or more commonly, the equation residuals for each grid point.

Above is a brief description of how CFD works. Some other approaches are also possible, but the techniques reviewed here are the most widely used for room airflow and heat transfer simulation, and are also those employed in this study.

3.3.2 CFD applications for air flow and heat transfer prediction in buildings

During the last two decades there has been great interest in both applying and developing CFD programs for building airflow and energy studies. For building applications, CFD can be used to analyse a wide range of important issues in relation to airflow including wind force, air temperature and velocity distribution, energy flows, thermal comfort and dispersion of pollutants. Nielsen (1974) was credited with the first application: the two-dimensional modelling of a room with flow driven by a supply air diffuser. Predictions of the jet's decay were found to agree well with experimental measurements. Modelling was soon extended to three-dimensional and other kinds of flows and significant success was achieved. Detailed review of the application of this tool is provided by Whittle (1986), Nielsen (1989), Liddament (1991), Jones and Whittle (1992), Moser (1992), Chen and Jiang (1992), Emmerich (1997) and Spengler and Chen (2000). These reviews conclude that CFD is powerful in predicting building air movement, although users' knowledge, experience and skills with CFD are essential for the accuracy of the simulation results.

The applications of CFD for building simulations can be generally divided into two strings in terms of the scale of the computational domain: applications in enclosed rooms and applications in open spaces. Features of the use of CFD regarding each of them are described in the subsequent two subsections.

• *CFD application in enclosed rooms*

For this kind of CFD application, the computational domain is usually defined to be the same as the air volume of the building to be simulated. One very interesting trend is revealed in the literature of room applications: the vast majority of the successful applications have been for

predicting room air flow. Attempts to predict room heat transfer, in particular convective heat transfer at internal surfaces for natural convection, have met with much less success. The crux of this dichotomy concerns with the nature of building air flows and the modelling of turbulent motion (Beausoleil-Morrison 2000). As described before, the standard k-ε turbulence model is usually employed for room applications, and for the near-wall regions where viscous force is dominant, the log-law wall function method (Launder and Spalding 1974) is used. The standard k-ε model was actually based on the experimental observation of fully-developed turbulence and strictly speaking, it is therefore valid for fully turbulent flows but it is not known whether it is suitable for other flow regimes. However, indoor airflow is not necessarily fully turbulent and errors can incur due to this mismatch. Another weakness is that the performance of the log-law wall-function is highly dependent on the gridding of the near-wall regions, because they are based on the logarithmic velocity profile with zero streamwise pressure gradient and thus they cannot accurately model boundary conditions that have a different velocity profile, such as mixed or natural convection or wall-jet flows (Chen et al. 1990).

Beausoleil-Morrison (2000) studied the impacts of implementation of the standard k-ε model in a weakly turbulent flow simulation based on a model of IEA Annex 20, and it was found that the k-ε model may over-predict the eddy viscosity μ_t of the weakly turbulent area. The over-prediction of μ_t may have very different effects on air flow and heat transfer calculations: it can be ignored for the former but may result in significant error for the latter. This can be explained by examining the diffusion terms of momentum and energy equations (see equation 3.16 to 3.19). For weakly turbulent area, the diffusion of momentum is generally weak in comparison with the convection of momentum and hence the over-prediction can be tolerant; but if this area has large temperature gradient and the diffusion of energy is quite strong, the over-prediction will lead to significant mistakes.

In spite of this shortcoming noted above, the standard form of the k-ε model in conjunction with the log-law wall functions has been applied more than any other turbulence modelling approach for predicting room air flow and heat transfer, although some other alternate methods also exist, such as low-Reynolds number k-ε model (Lam and Bremhorst 1981), Yuan wall functions plus k-ε model (Yuan et al. 1993), new type of zero equation turbulence model (Chen and Xu 1998), etc. However, considering the expensive computing cost that these sophisticated methods have to take, they are still mainly used in laboratory settings and are not widely employed.

With respect to log-law wall functions, most researchers improve the simulation of heat transfer by adjusting the gridding system of the model. Niu and van der Kooi (1992) suggested that the dimensionless spacing to the next-to-wall grid point (y^+) was the most important and the optimum value of y^+ was recommended to be 9.2 for the best performance of natural

convection simulation. A similar research project was also conducted by Awbi (1998) and the optimum distance of the first grid for calculating heat transfer was found to be 0.5*mm*. Schild (1997) reported that the log-law wall function fits the experimental data poorly for values of local Reynolds numbers in the range $8 < y^+ < 40$, whilst the fit is good in the range of $y^+ < 8$ and $y^+ > 40$. Other researchers (Beausoleil-Morrison 2000; Zhai and Chen 2004) also noticed that the size of the first grid has significant impacts for the prediction of convective heat transfer.

One important premise for the CFD application in enclosed rooms is that the conditions for the inlets and outlets should be made clear before the implementation of the simulation, as they are part of the boundaries. This is easy for enclosed spaces with internal natural convection or air-conditioned rooms; however, this may be problematic for the study of natural ventilation in and around buildings: as introduced earlier, under certain conditions the air temperatures or velocities at the openings on the envelope may not be easily obtained before the simulation and have to be treated as unknowns. For this situation, the computational domain may have to be extended and encompass part of the outside environment, and in this way the building is placed in an open space actually. This will be the topic of next subsection.

• *CFD application in open spaces*

In addition to the definition of the computational domain, the difficulties associated with the applications of CFD in open spaces also lie in other aspects such as turbulence models. As introduced before, the standard k-ε model is usually not applicable in large scale situations, although it may produce reasonable results sometimes only "fortuitously" because of its overproduction of turbulent kinetic energy in the regions of stagnant flow (Franke et al. 2004). More advanced turbulence models will need to be employed as a result. The most widely used one to take the place of the standard k-ε model is the RNG k-ε turbulence model. It has been employed in a number of CFD applications in open spaces and urban scale for both buoyancy-driven and wind-induced airflows, including those by Ferreira et al.(2002), Allocca et al.(2003), Seifert et al.(2006), etc.

In this study, the computational domain, as introduced earlier, has to include some outside environment. Therefore, a question will arise: how far should the domain be extended from the building? Additionally, this setting can also result in problems of the specification of boundary conditions, as the boundaries for this type of applications are entirely fictitious.

It is suggested by the research in relation to this issue, that the settings for the use of CFD in open urban scale are highly dependent on the regimes of the airflow, i.e., different flow regimes need to employ different computational domains and different types of boundary conditions. Generally speaking, the rule of thumb for the computational domain of wind-induced airflow is that, the bigger the domain, the better the result, except that the inlet is too far

from the building so that the boundary layer cannot be maintained up to the building because of the decay (Hargreaves and Wright 2006). Most guidelines available are focused on the smallest computational domain in order to achieve the balance between the accuracy and the expensive time cost. According to Hall (1997), the inlet, the top and the lateral boundary should be $5H$ away from the building, where H is the height of the building. The outflow boundary should be positioned at least 8-10H behind the building to allow for flow development, as fully developed flow is normally used as a boundary condition. With respect to the inlet boundary conditions, a wind profile such as a power law or log law is usually specified; the top is prescribed symmetry enforcing a parallel flow. In order to obtain accurate results, the minimal grid resolution should be 10 cells per cube root of a building volume and 10 cells per building separation.

As regards the buoyancy-driven ventilation, the size of the computational domain can be slightly smaller then the one employed for wind-induced ventilation. In the research carried out by Allocca et al.(2003) for the study of single-sided buoyancy-driven ventilation, the building was placed in the centre of a domain with double width, double length and one and a half height of the building size. Boundary conditions for the outside environment were specified as follows: solid plates with slip boundary conditions and a temperature equal to the outdoor air for all the side boundaries, zero pressure boundary at the outdoor air temperature for the upper boundary, and solid adiabatic plate with non-slip boundary for the lower boundary. Cook and Lomas (1997) used a domain with double width, length and height of the building for a simulation of buoyancy-driven displacement ventilation and all the boundary conditions for the domain are specified as zero pressure inlets for the approximation of the outside environment. Unlike the wind-induced ventilation in open spaces, there are still no guidelines available on the settings of the size of the computational domain and of the boundary conditions.

Another problem for the buoyancy-driven natural ventilation is that it may be difficult for the solution to reach convergence using the default settings for solution techniques and under-relaxation factors because the driving force of the airflow is very small which leads to numerical instabilities (Cook 1998). Strategies have to be implemented in order to overcome this problem and one of the most popular is to use a time-dependent approach to obtain a steady-state solution (FLUENT 1996). This approach has also been adopted by a number of researchers simulating buoyancy-driven airflows, including Cook et al.(2003), Cook et al.(2005) and Ji et al.(2007).

An alternative approach is also suggested for the simulation of buoyancy-driven natural ventilation, i.e. to directly use the building itself as the computational domain and both vents are modelled as outlets at zero pressure and zero gradients for other variables. Generally speaking, the former method is preferable than this approach for two reasons. First, the result obtained with the former approach is much more accurate (Allocca et al. 2003), as its condition is more similar to the real environment. Another disadvantage of this latter method is that, by

specifying the uniform zero pressure on an opening, it is difficult to simulate bi-directional flows for large openings, which was the case for mixed flows introduced in Section 2.5.2 and will be one of the main concerns to be investigated in a later chapter.

The settings of CFD for the simulation of combined ventilation are generally a mixture of the settings for buoyancy-driven ventilation and those for wind-induced ventilation. The computational domain for combined ventilation should be similar to the one employed for wind-induced ventilation in order to make sure that the wind profile is maintained and well developed, but the boundary conditions should also include the information of outdoor air temperature. One feature that distinguishes the settings of combined ventilation study from those of wind or buoyancy-driven ventilation is that the settings of initial conditions should be taken into account. As introduced in Chapter Two, multiple solutions may exist for one condition of combined ventilation and the right solution for that moment depends on the initial conditions.

The above analysis indicates that CFD is a valuable tool for the simulation of air flow and heat transfer but the result can be very sensitive to its settings, especially those of computational domain, boundary conditions, turbulence models, gridding system, etc. It is therefore very essential that any program and related settings need to be validated before intensive use. A commercially available CFD program, FLUENT is employed in this study to perform the calculation procedures introduced above. It is described in more detail in the following section.

3.3.3 FLUENT

Initiated and partly developed at the University of Sheffield, UK in the early 1980s, FLUENT is one of the most popular CFD programs used all over the world. It has been successfully applied in various kinds of applications in relation to fluid dynamics such as aircraft aerodynamics, meteorology, biomedical engineering, nuclear engineering, building engineering, etc. It is also a useful research tool for building energy and ventilation studies to predict room air flow and heat transfer. A large number of research projects in literature have been accomplished with FLUENT (e.g. Wang and Wong 2006; Ayata et al. 2007).

The general procedures to use FLUENT (1996) consist of:

- Creating model geometry and grid;
- Choosing the basic equations to be solved;
- Specifying material and boundary properties;
- Setting the solution control parameters;

- Calculating and saving the results;
- Refine the grid, or make revisions of the numerical or physical models, if necessary;
- Post-processing the results.

3.4 Settings and validation of FLUENT for this research

As stated in section 3.2.2, CFD programs may introduce intolerant mistakes if inappropriately set and hence their settings have to be validated before intensive use. General validation of FLUENT can be easily found in literature, and in particular, they have ever been extensively employed for the study of the thermal and ventilation issues in greenhouses used for agriculture (e.g. Montero et al. 2001; Bartzanas et al. 2004; Khaoua et al. 2006). Although different focuses are placed for agricultural purposes, this still shows that this tool is capable of dealing with spaces with similar characteristics of greenhouses such as large volume, strong temperature stratification and roof openings, which are also the geometrical and thermal characteristics atrium spaces may have.

As reviewed in Chapter Two, a variety of flow regimes will be simulated and investigated in this research. Since the settings for them are not identical, the following subsections will present those of the three basic flow regimes respectively, including wind-induced ventilation, buoyancy-driven ventilation, and combined ventilation with particular attention on the settings of computational domain, boundary conditions, meshing and turbulence modelling. In addition, the settings of FLUENT for the simulation of internal natural convection also need to be validated in order to accurately model the heat transfer from the heat source for both buoyancy airflows and thermal comfort studies. Simulations with these settings will be performed with results compared to experimental or empirical data for the verification of their validity. Before doing these, the validation methodology, including the commonly used approaches and the general criterion, is introduced first as the basis for the whole validation process.

3.4.1 Validation methodology

Simulation errors can be classified into two groups consisted of seven categories (Beausoleil-Morrison 2000) as follows:

External errors:

- Differences between the actual microclimate affecting the building and the weather input used by the program;

• Differences between the actual schedules, control strategies, and effects of occupant behaviour and those assumed by the program user;

• User error in deriving building input files;

• Differences between the actual thermal and physical properties of the building and those input by the user.

Internal errors:

• Differences between the actual mechanisms taking place in the real building and the simplified model of those physical processes in the simulation;

• Errors or inaccuracies in the mathematical solution of the models;

• Coding errors.

The external errors principally relate to user factors that are outside the domain of the simulation program, and the internal sources of error are the focus of consideration in the context of the current research. Due to the physical complexity of buildings and the nearly infinite possible data input combinations, the comprehensive validation of a detailed simulation program is an impossible task. Judkoff and Neymark (1995) proposed a pragmatic approach composed of three primary validation constructs to check for internal errors. These are:

• Analytical verification;

• Empirical validation;

• Comparative testing.

With analytical verification, the program (or subroutine) output is compared to a well-known analytical solution for a problem that isolates a single heat transfer mechanism. As suggested in the review of the research methods, typically this necessitates very simple geometries and boundary conditions. Although analytical verification is limited to simple cases for which analytic solutions are known, it provides an exact standard for comparison.

Program outputs are compared to monitored data with empirical validation. The measurements can be made in real buildings, controlled test cells, or in a laboratory. The design and operation of experiments leading to high-quality data sets is complex and expensive, thus restricting this approach to a limited number of cases. The characterisation of some of the more complex physical processes, such as detailed turbulence structure, is often excluded due to measurement difficulties and uncertainty.

A program is compared to itself or other programs with comparative testing, which usually includes both sensitivity testing and inter-modal comparisons. For CFD validations, usually the independence of the grid system needs to be checked for this step.

It can be seen from the above description that, the general procedures for the validation of the CFD settings are consisted of the comparisons with other research methods introduced earlier including generalised analytical algorithms and the experiments. These procedures will also be implemented for the validation of the CFD settings for each flow regime. The criteria used for the justification of each validation in this research can be described as follows:

• Qualitatively, the CFD simulation should show the same tendency as the other analytical algorithms and experimental data when a building or environmental parameter varies;

• Quantitatively, the discrepancies between the results of the CFD simulations and those from other sources should be less than 30%;

Only when both of the above criteria are satisfied, can the CFD settings be adopted for further use in the research. These criteria have also been widely applied by other researchers, such as (Zhai 2003).

3.4.2 Settings of FLUENT for internal natural convection (heat transfer)

The simulation of internal natural ventilation has two purposes in this research. The first is to predict the air temperature and velocity distribution at the occupants' level for the thermal comfort evaluation; secondly, the settings for the internal natural convection will also be used for the simulation of the heat source in buoyancy-driven natural ventilation.

• *Settings of FLUENT*

For most situations in buildings, *Ra* number is usually about 10^9-10^{10}, and it can be even higher in atrium spaces due to strong solar radiation and large height. Therefore, natural convection in atrium enclosures is turbulent rather than laminar and the standard k-ε turbulence model is employed. As suggested before, the size of the first grid is very important to the accuracy of simulation results and it is specified to be $5mm$, which yields the y^+ value of around 7-10. The computational domain for the study is identical to the boundary of the air volume of the space without any outdoor environment included. The coupled implicit scheme is used for discretisation of the flow. The internal surface heated by the sun, which works as the heat source, is specified with a constant temperature and other surfaces are specified as adiabatic or the same temperature according to the research need. As the temperature difference is small - generally from a few degrees to several tens of degrees, boussinesq approximation is employed to express the relation between the change of density and that of temperature. All the data

regarding to the thermophysical properties of air used in this research can be found in Appendix B, such as the air density, viscosity, etc. Convergence criteria of all variables are set to be 10^{-3}.

• *Empirical validation*

A validation is performed using the experimental data from literature to investigate the performance of the above settings. The case chosen to be tested is the experiment carried out by Olson et al (1990). The experiment included measurement of natural convection in both a full-size room and a physical model. Figure 3.1 shows the configuration of the full-scale room with the opposing hot and cold side walls. The small-scale model was geometrically similar, had the same *Ra* number, and had the same dimensionless side wall temperature as the full-scale room. The experiment found good agreement between the full-scale room and the scale model in flow patterns, velocity levels, temperature distributions, and heat transfer. It is also used by other researchers for CFD validation purposes. This study is focused on the convective heat transfer at the hot and cold walls and compares the simulation results with the experimental results of the physical modelling.

The simulation results are shown in Figure 3.2. It can be seen that, qualitatively, the dimensionless number indicating the convective heat transfer coefficient, *Nu*, from both measurement and simulation, has the same trend with the increase of the Ra number indicating the ratio between the strength of buoyancy and viscous forces; quantitatively, the results from the simulation and the experiments are in good agreement and the discrepancy is less than 15%.

• *Grid independence study and comparison with semi-empirical algorithms*

As analysed previously, the quality of the gridding system also have significant impacts on the simulation results. Thus it is essential to perform a study to ensure that the meshing system adopted is reasonably independent. A prototype atrium space of this study, based on which other design alternatives are created, is simulated to investigate the influence of the grids. The geometry of the space is illustrated in Figure 3.3 and it is 12*m* wide and 12*m* tall with a roof angle of 45°. The upper part of the right-hand side wall heated by the sun and the temperature difference between the heated wall and other parts is assumed to be 20°C. All other surfaces are assumed to be adiabatic.

Figure 3.4 presents the results of the convective heat transfer coefficient and y^+ of the heated wall calculated by FLUENT for different gridding system (See Table 3.3). The convective heat transfer coefficient from the simulation is also compared with the coefficients from other semi-empirical algorithms. It can be seen that the results from the simulation lie in somewhere in-between other results calculated from those well-known semi-empirical algorithms, which significantly increases the credibility of the settings described before for the

use of this study and it can be concluded that the settings introduced above can be used to obtain satisfactory results for heat transfer simulation. It is also observed that there is fluctuation of the convective heat transfer coefficient predicted by CFD and y^+ keeps increasing before gridding system No.5 but the results can be generally considered independent of the gridding system after that. As a consequence, grid No.5 is chosen for this study (See Figure 3.5 for detailed illustration of the gridding system).

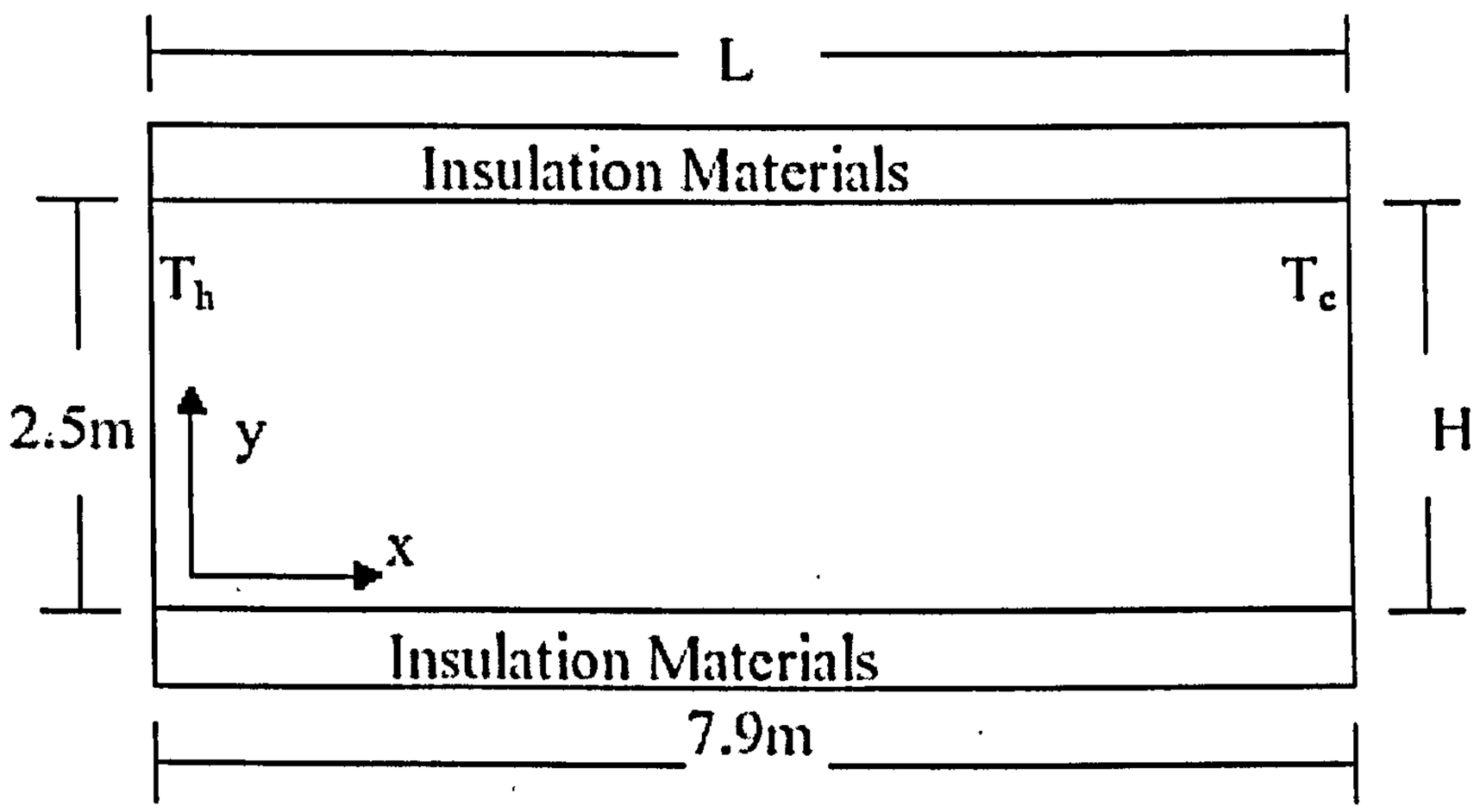

Figure 3.1: Configuration of the test case (Olson et al., 1990)

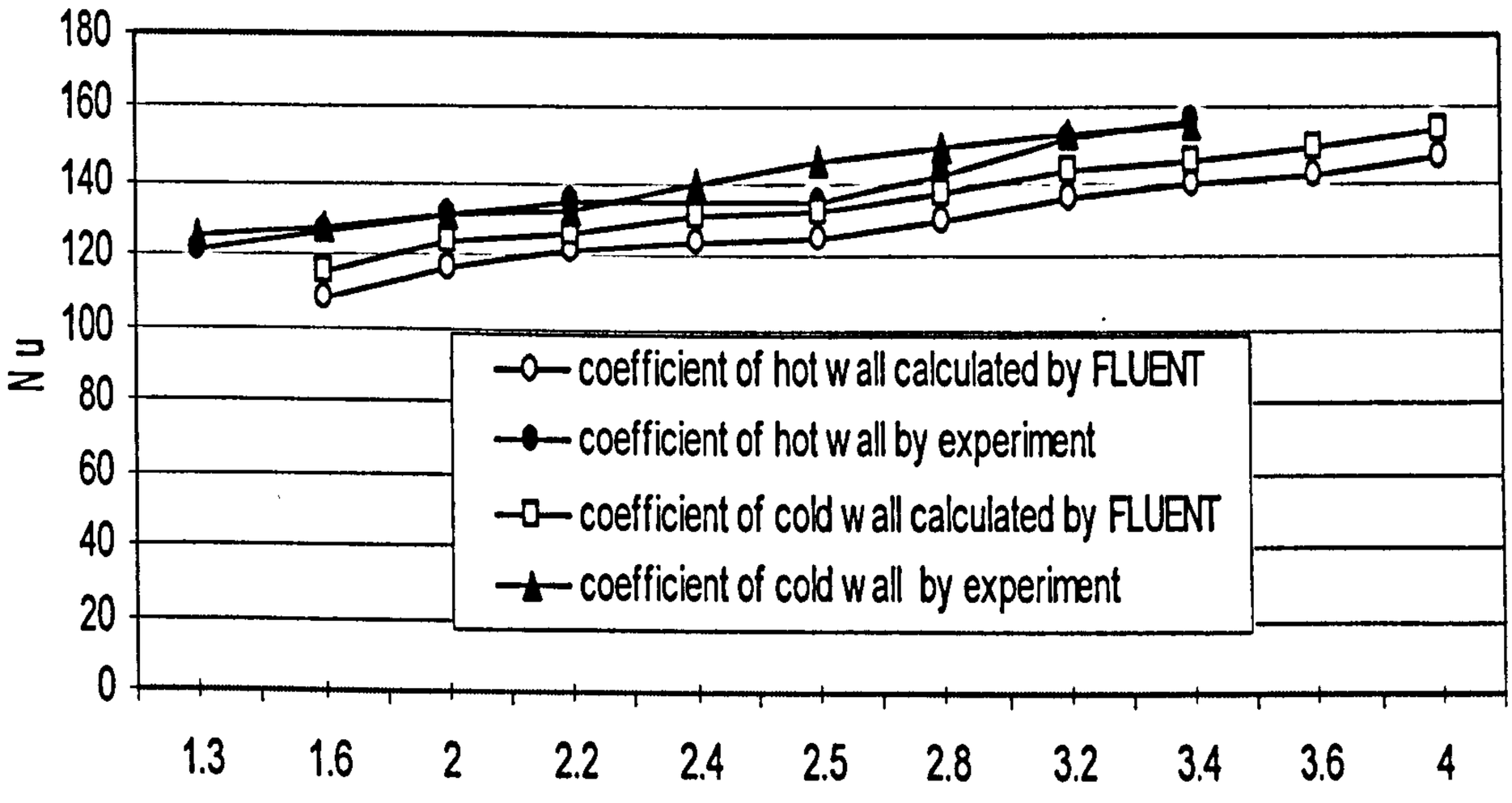

Figure 3.2: Comparison of the convective heat transfer coefficients calculated by FLUENT and the experiment

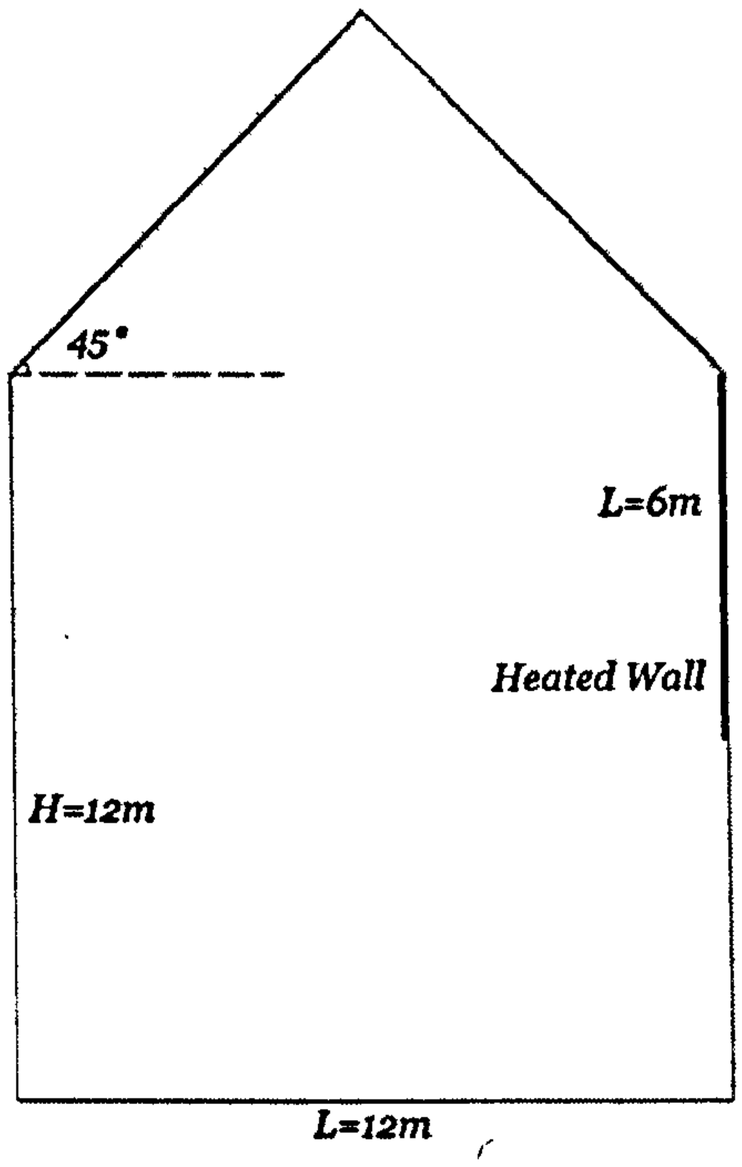

Figure 3.3: The geometry and environment definition of the primary study

Table 3.3: Different gridding systems for internal natural convection study

No.	1	2	3	4	5	6	7	8	9
Number of grids (horizontal edge × vertical edge)	160×160	200×200	200×240	240×240	240×280	280× 280	320×320	360×360	400×400

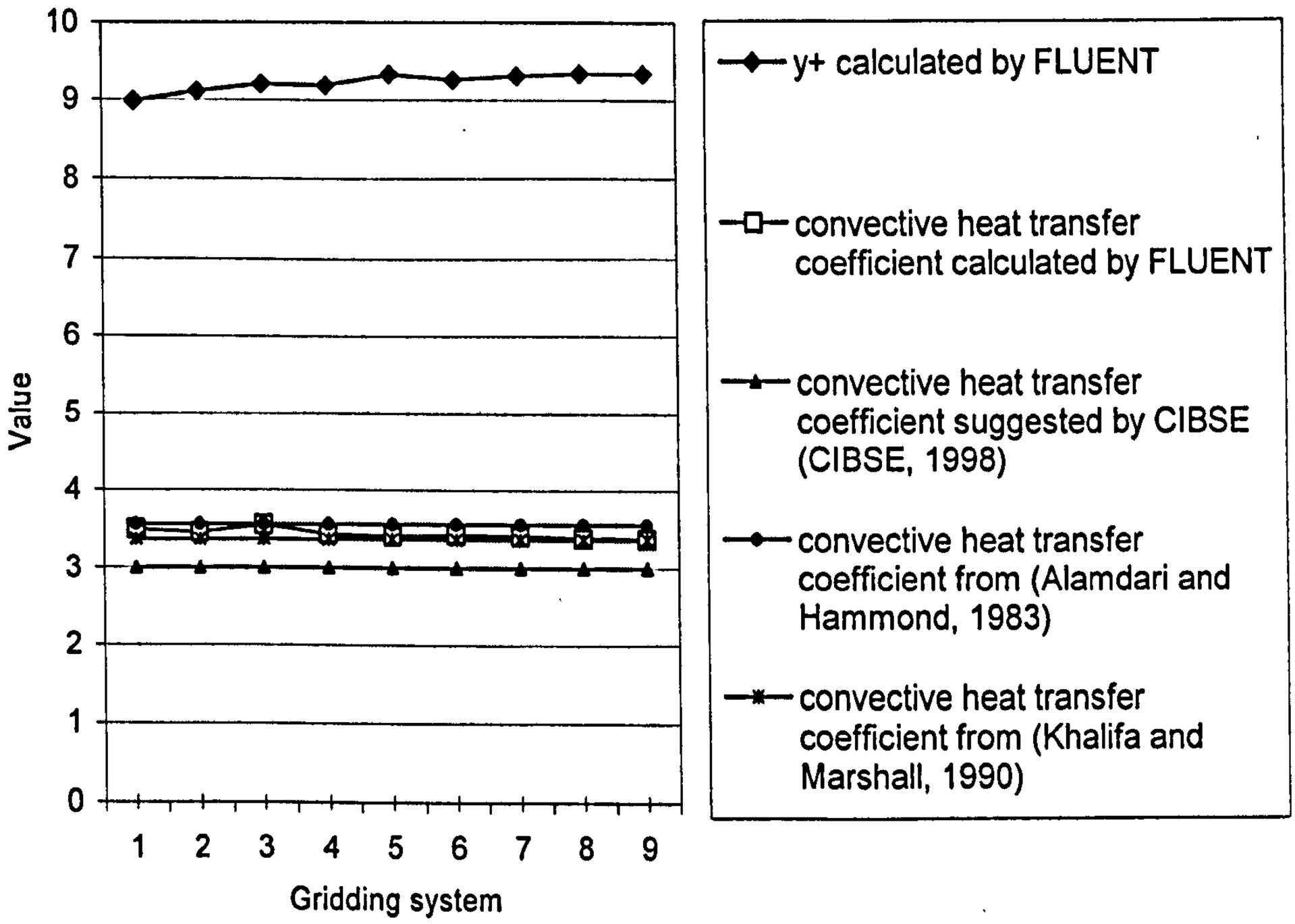

Figure 3.4: y^+ and the convective heat transfer coefficient of the heated wall of the prototype

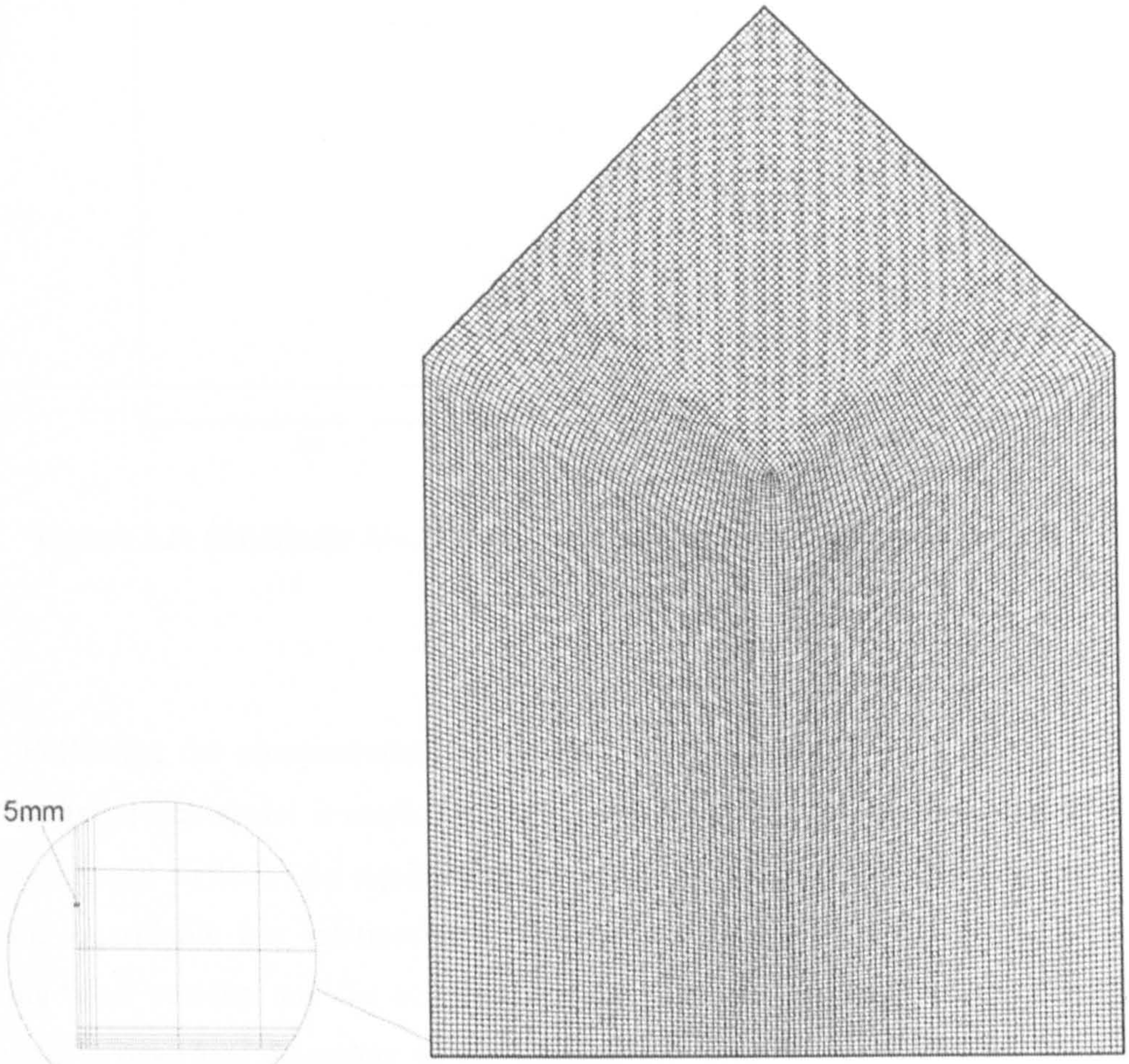

Figure 3.5: The grid system employed for internal natural convection study in this research

3.4.3 Settings of FLUENT for wind-induced ventilation study

The wind-induced ventilation study is aimed to investigate the impacts of design parameters such as adjacent buildings, roof shape and opening characteristics on the ventilation performance. It is assumed that the buoyancy force is negligible and hence the heat transfer will not be simulated. Only two-dimensional (2-D) study is performed in this research and hence the settings introduced below are all made for 2-D situations.

• *Settings of FLUENT*

As introduced previously in the review of CFD applications in open spaces, the computational domain for the wind-induced ventilation study has to be extended from the building itself to include part of the outside environment. This is illustrated by the Figure 3.6 as follows.

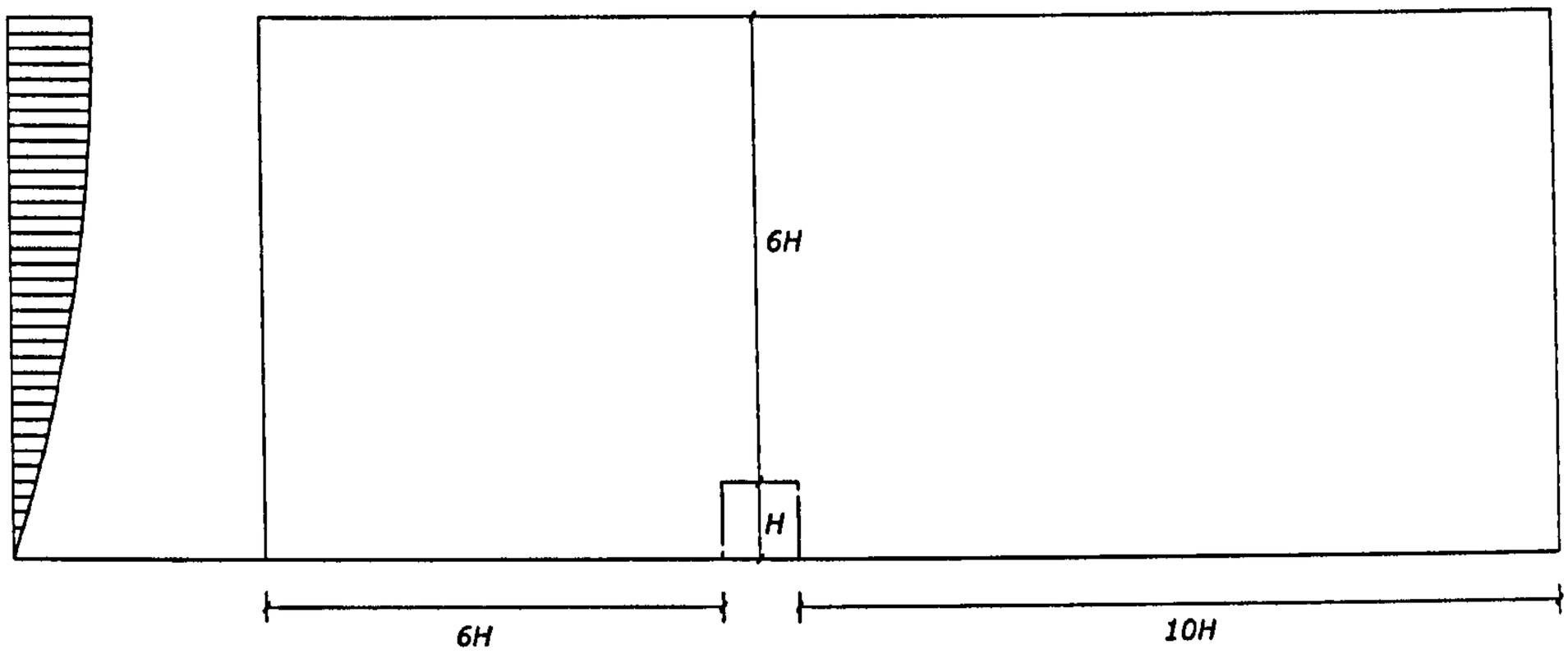

Figure 3.6: Schematic illustration of the computational domain for wind-induced ventilation study

Following the recommendations of many other researchers (See Section 3.3.2), the RNG k-ε turbulence model is employed for the simulation of the turbulence characteristics of the wind-induced airflow. An equilibrium boundary layer is prescribed for the inlet. Unless specified, logarithmic law relationship (Etheridge and Sandberg 1996) is specified for the oncoming wind velocity and the boundary condition for the turbulent kinetic energy and its dissipation is described according to the formula provided by Richards and Hoxey (1993). These can be expressed by Equation (3.20) to (3.22):

$$U = \frac{U_*}{\kappa} \ln\left(\frac{z_o + y}{z_o}\right) \tag{3.20}$$

$$k = \frac{U_*^2}{\sqrt{Cu}} \tag{3.21}$$

$$\varepsilon = \frac{U_*^2}{\kappa(z_o + y)} \tag{3.22}$$

where z_o is the surface roughness and is specified as $1.05m$ to represent the conditions for urban areas and the reference height is chosen as that of the roof level of the building. As introduced before, the outlet is specified with outflow type boundary condition and the upper boundary is prescribed as symmetry.

Since heat transfer is not considered for wind-induced ventilation, all the walls are regarded as adiabatic. The distance of the first grid is specified to achieve 30-60 for the value of y^+ in order to achieve the best performance of the wall function and thus improve the accuracy of the simulation for near-wall treatment (FLUENT 1996). This is realised by grid adaptation after each run until the value of y^+ falls into the region requested. Second order

approximations are used for the solution of algebraic equations. More strict convergence criteria, rather than those of default settings, i.e., the residuals of 10^{-6} for all variables, are adopted.

• *Validation*

One empirical validation with respect to the use of FLUENT with the settings introduced above for the simulation of wind-induced ventilation has been reported by Seifert et al. (2006). The wind-induced ventilation around a cubic box is simulated and the wind pressure coefficients obtained from the simulation are compared with the measurement from (Castro 2003). It is shown in Figure 3.5 that the simulation results generally show the same trend as the measurement and good agreement is achieved. It can also be seen that the RNG k-ε turbulence model has a better performance than the standard k-ε model, especially for the simulation of top and lateral surfaces.

As this research will be mainly focused on the general flow pattern and ventilation performance under various conditions other than aspects with respect to pressure coefficients, another two further simulation runs are carried out addressing these two issues. Figure 3.7 shows the general flow pattern around a cubic box from a 2D simulation. According to the simulation, the oncoming flow will separate at the corner of the leeward wall and the roof; the wind stagnation in front of the building will cause a standing vortex at the bottom; a reverse flow will be incurred on the roof due to the wind separation and after some distance the flow will reattach the roof; there is a strong recirculation flow behind the building. All these significant flow characteristics observed comply with other measurements and numerical studies for the building under the same condition.

Nevertheless, the horizontal length of the recirculation behind the building might be too long compared to some other studies, such as (Tutar and Oguz 2002). This is attributed to two reasons. Firstly, the size of recirculation is significantly affected by the inflow characteristics (Zhang et al. 1993; Castro 2003), i.e. the settings about wind, which is determined by a lot of factors including local conditions such as density, ground roughness, etc and there are no general settings available for all kinds of oncoming wind. Thus, different settings of wind usually result in very different size for the recirculation zone. Secondly, the simulation is only a 2D study and it is expected that the horizontal length of recirculation zone is longer in a 2D simulation than in a 3D simulation (Boyer and Kim 1988; Castro 2003).

Apart from the validation with experiments, an analytical verification is also performed. Figure 3.8 shows the detailed flow field of a building with the same geometry as those studied in the previous simulation but two openings are added: one on windward wall located half a meter above the ground and the other on the leeward wall at the position half a meter lower than

the roof. Both openings have a height of one meter. The X-coordinate air velocities for the inlet, together with their positions are plotted in Figure 3.9. By averaging the velocity at each position, it can be obtained that the bulk flow rate is approximately 1.06*m/s*. A simple calculation can also be made based on Equation (2.8) and by using the pressure coefficients shown in Figure 3.6 and assuming that the discharge coefficient of both openings is 0.61, which is the normal expectation for windows. It can be obtained that the airflow rate is 1.02*m/s*. This means that the airflow rates predicted by both methods are generally agreeable with a discrepancy less than 5%.

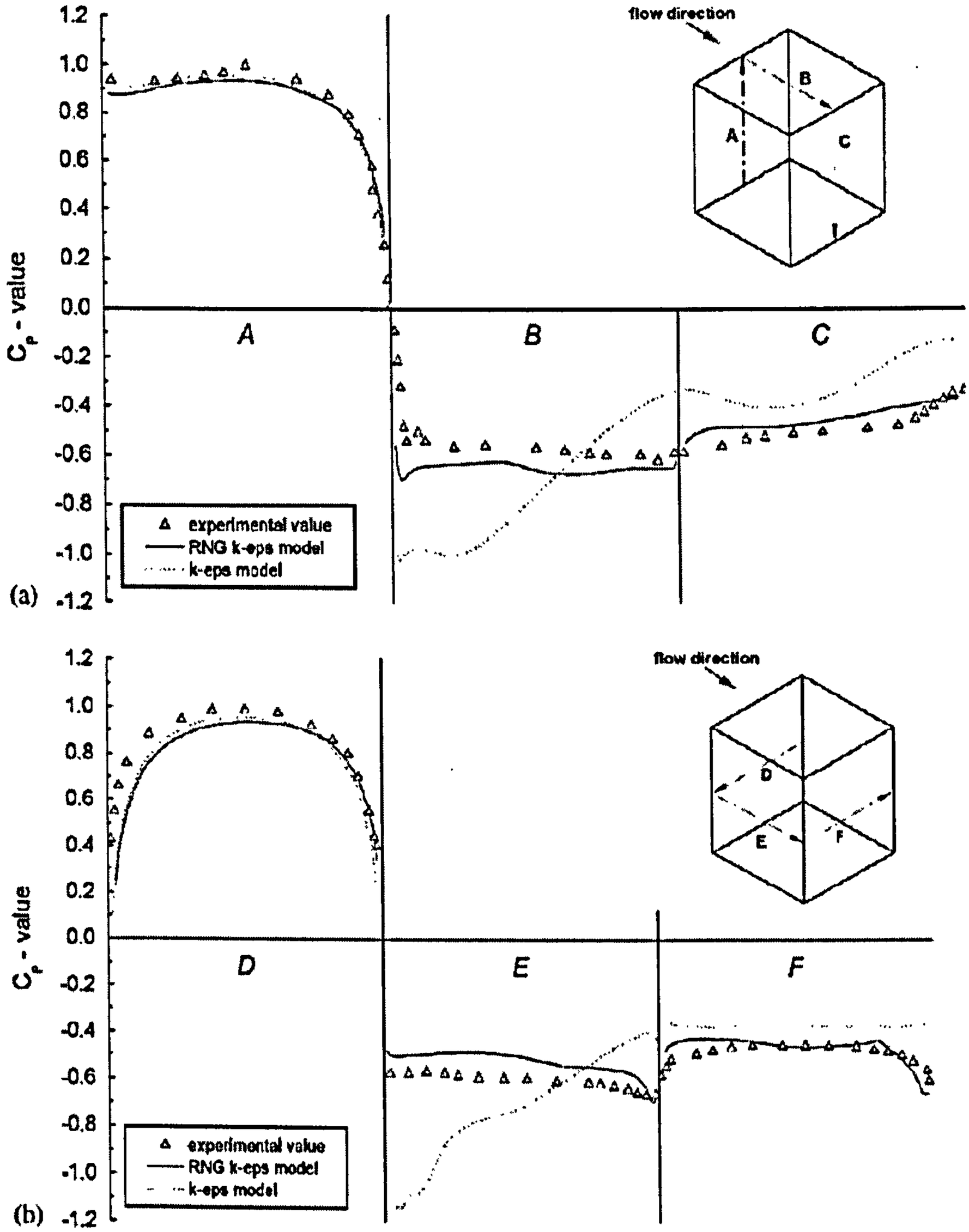

Figure 3.6: Comparison of wind pressure coefficients on the cube between CFD simulation and measurement (Seifert et al. 2006)

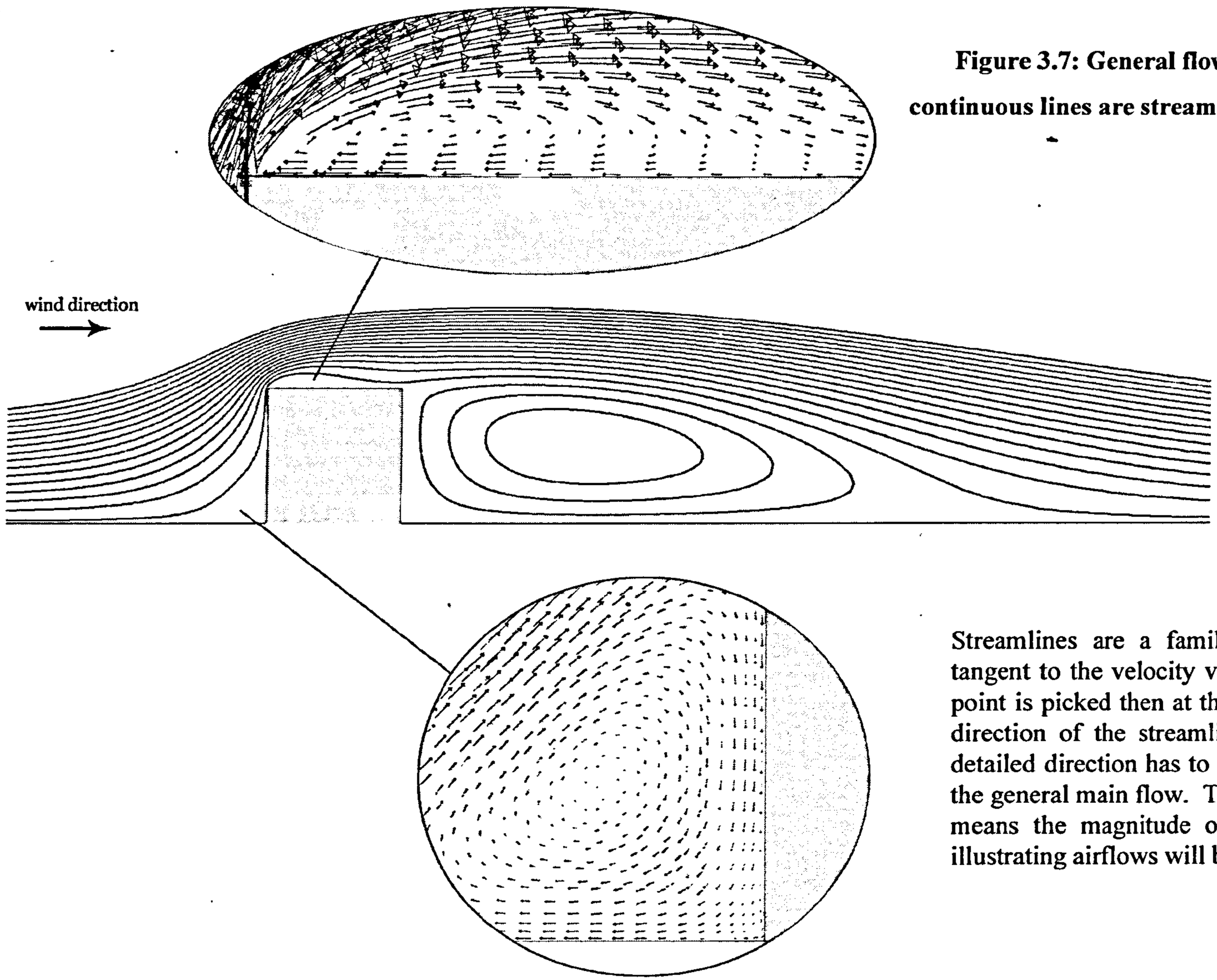

Figure 3.7: General flow pattern around a cubic building (the continuous lines are stream lines and the arrows are velocity vectors)

Streamlines are a family of curves that are instantaneously tangent to the velocity vector of the flow. This means that if a point is picked then at that point the flow moves in a tangential direction of the streamline that the point is on, although the detailed direction has to be judged according to the direction of the general main flow. The density of streamlines at a point also means the magnitude of the velocity there. This method of illustrating airflows will be extensively used in this research.

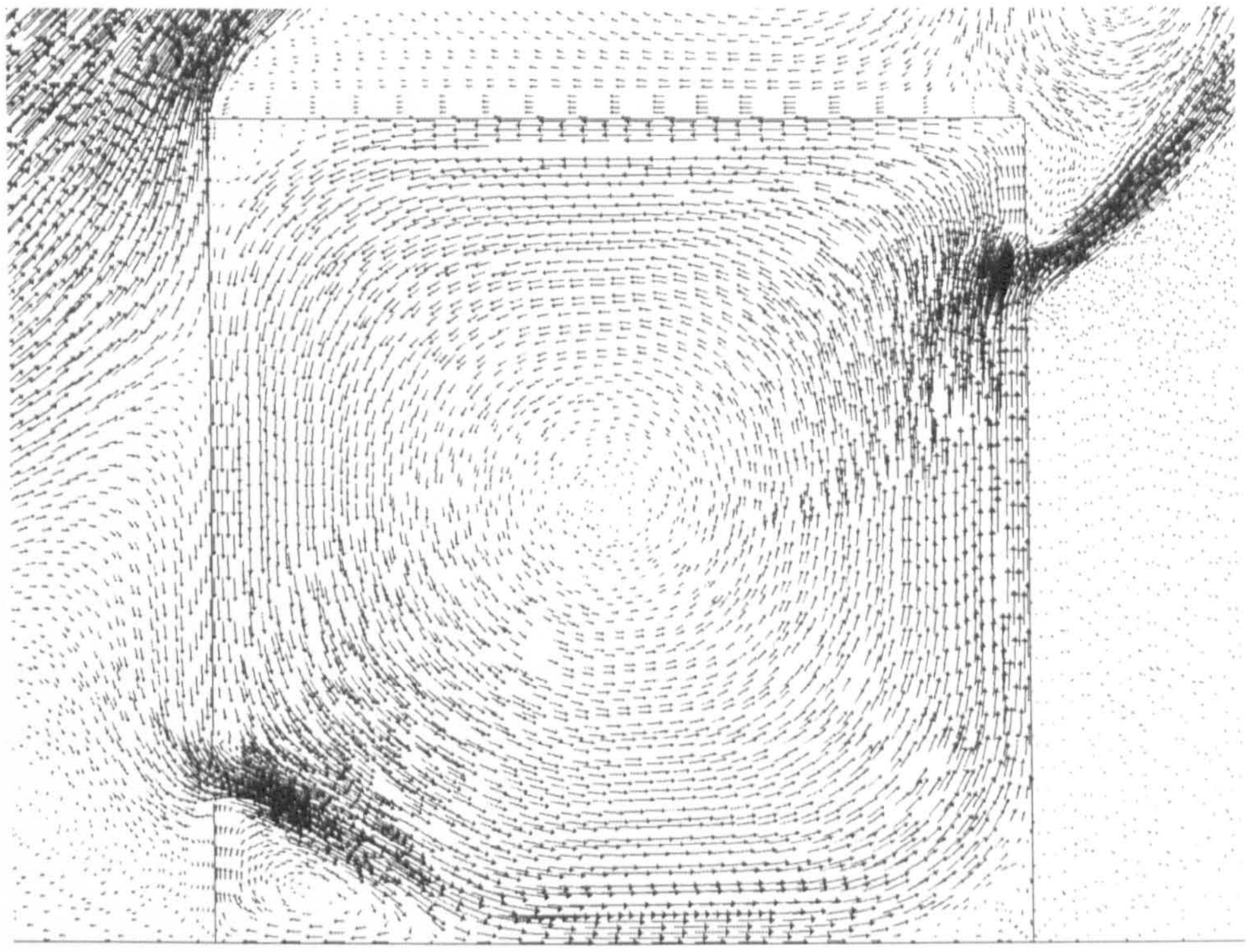

Figure 3.8: Detailed flow field of a cubic building with two openings (arrows are velocity vectors)

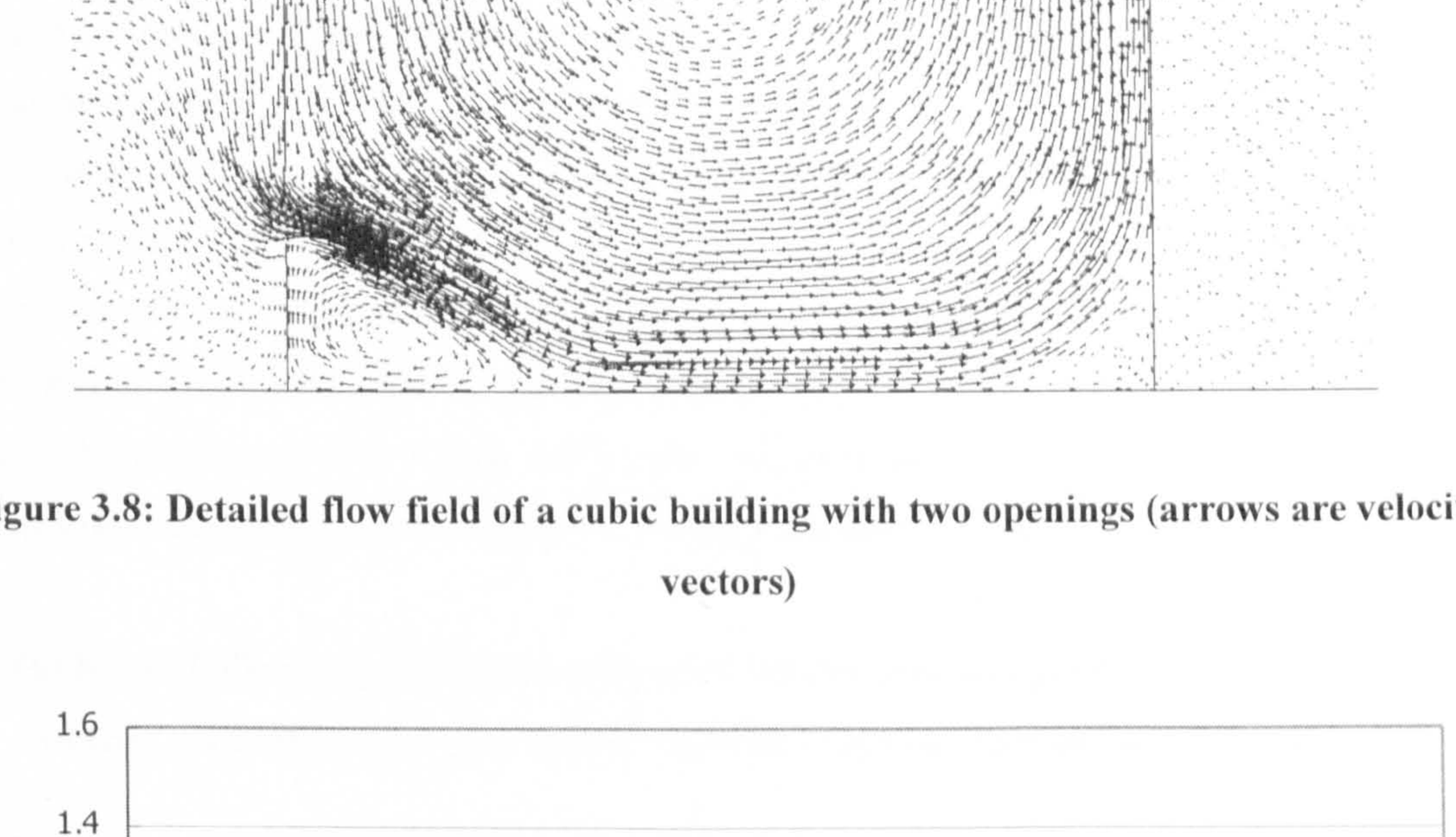

Figure 3.9: The distribution of X-coordinate air velocities at the inlet for the wind-induced ventilation of a cubic building

• *Grid independence study*

For wind-induced ventilation, the size of the first grid and the grid density of the whole computational domain are still the main concerns of the grid independence study. The first grid size is specified as 20cm to achieve a value of 30-60 for y^+ and the grid is adapted after each run according to the y^+ value to make sure its average for the whole building surface is neither too high nor too low. As regards the grid density, in order to calculate the airflow rate across the building, a relatively large number of grids are placed near the opening, and to avoid highly skewed grids, the grid density in the space and around the vicinity of the space should not be reduced too quickly. These conditions actually have already made the grid density in the whole computational domain higher than the guidelines suggested by other researchers (e.g. Hall 1997; Franke et al. 2004) and it should be already high enough for this study. This is further verified by a number of simulations for the same prototype used for the study of internal natural convection with different grid density shown in Figure 3.3. Two openings are placed at the roof level, and one on windward side with the other on leeward side. They occupy one third of the area of the whole roof (See Figure 3.13). The reference wind velocity $U = 4m/s$. The gridding systems that are tested in the independence study are listed in Table 3.4.

Table 3.4: Different gridding systems used for the grid independence study of wind-induced ventilation (the grid density of other edges are half of that of the opening)

No.	1	2	3	4	5
Number of grids for each opening	10	15	20	25	30

Figure 3.10 compares the air velocity distributions at the occupants' level predicted by the five different gridding systems and those at roof level are shown in Figure 3.11. Generally they agree on with each other very well both quantitatively and qualitatively. By increasing the grid density from No.1 to No.5 (three times as shown in Table 3.4), the velocity change is less than 15%. This accuracy is sufficient for a parametric study, and it is also acceptable for the design and engineering use, especially at the early stage. Moreover, gridding system with a density higher than No.5 will take a very long time to reach convergence, i.e. usually about 16-20 hours. This will not be suitable for a parametric study which requires running a large number of simulations. Considering both accuracy and time cost, No.3 is chosen as the typical grid system for this project, as shown in Figure 3.12. The general flow pattern is shown in Figure 3.13.

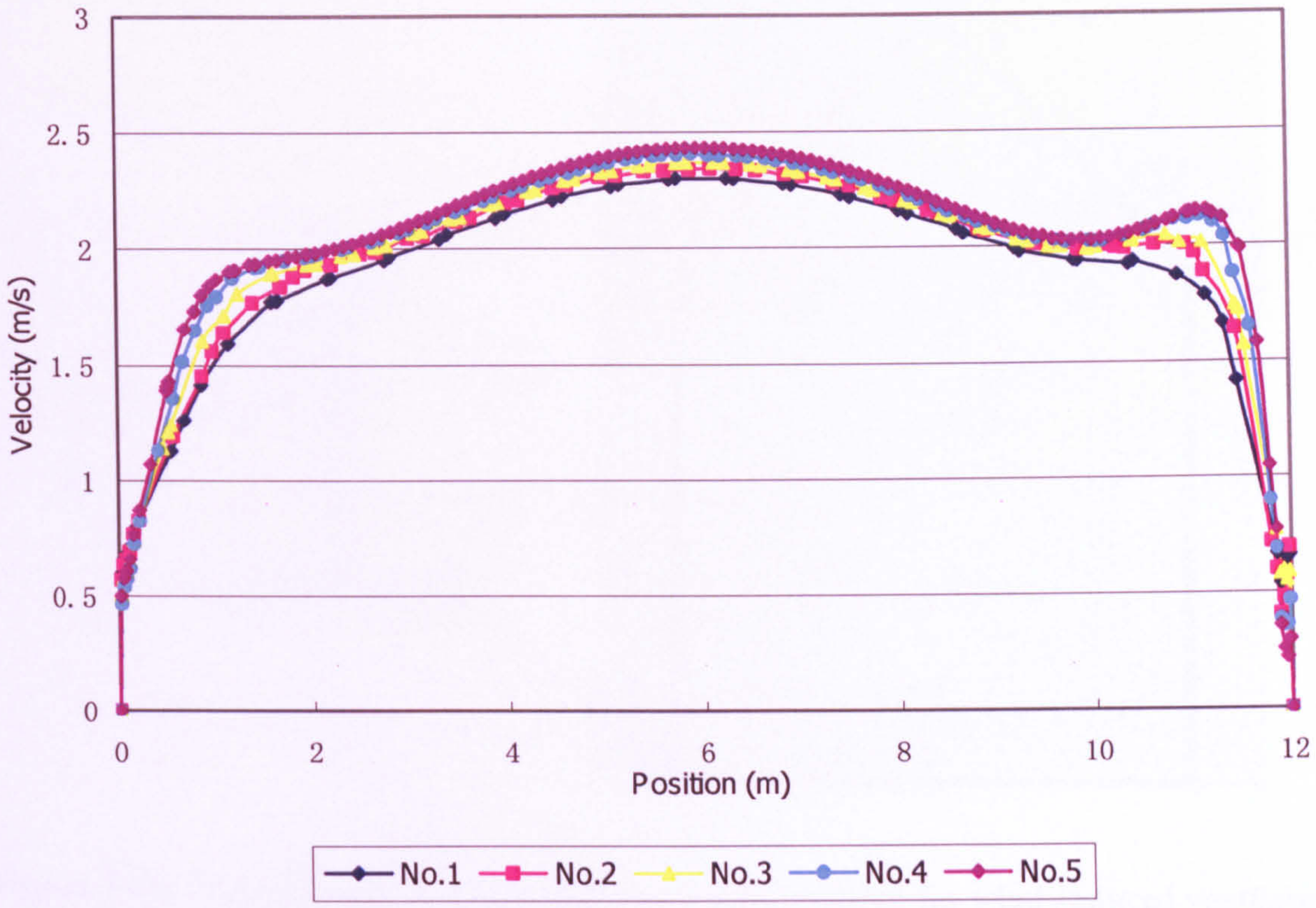

Figure 3.10: The air velocities at the occupants' level (y=1.6m) simulated for grid independence study of wind-induced ventilation

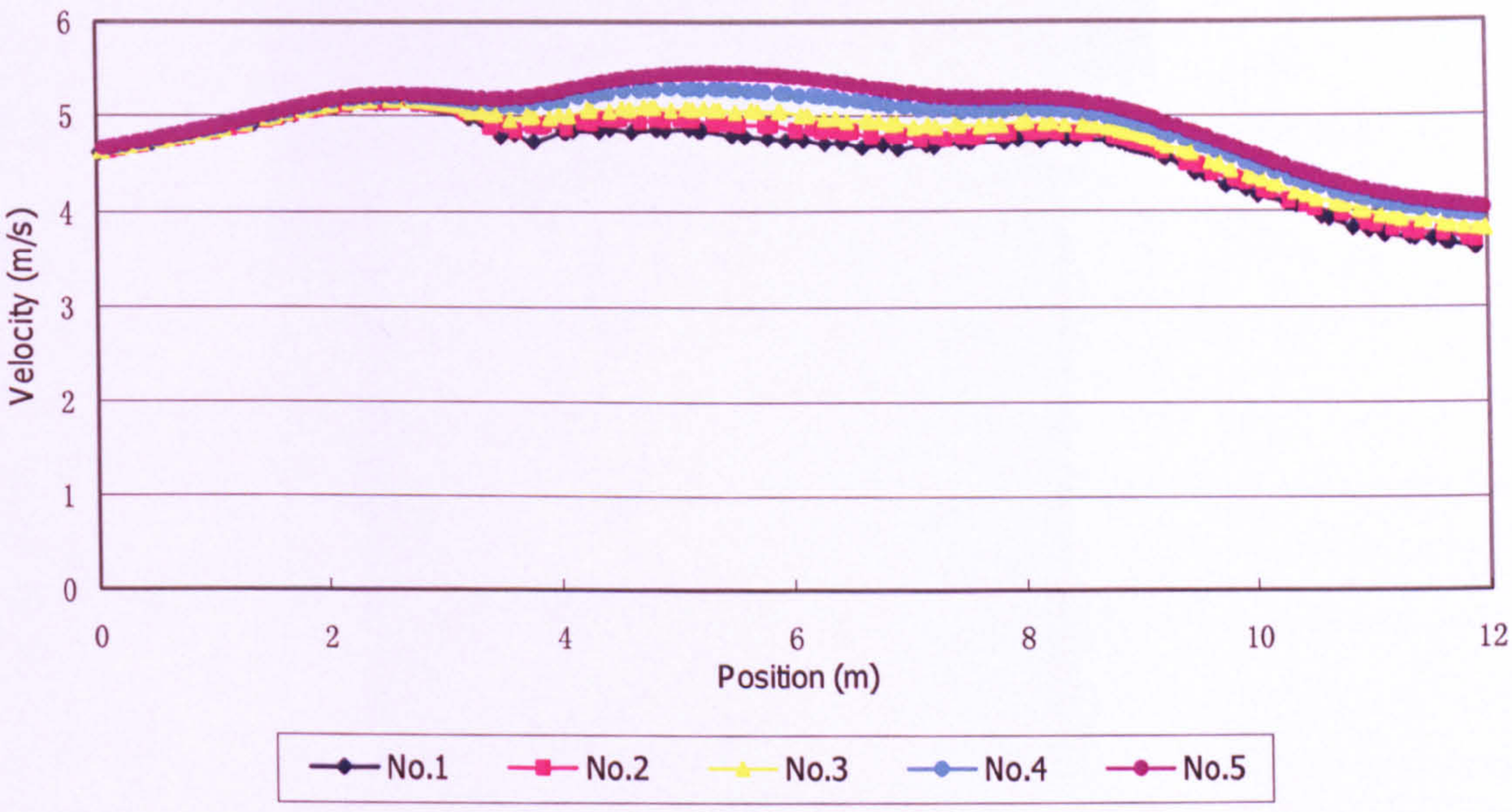

Figure 3.11: The air velocities at the roof level (y=15m) simulated for grid independence study of wind-induced ventilation

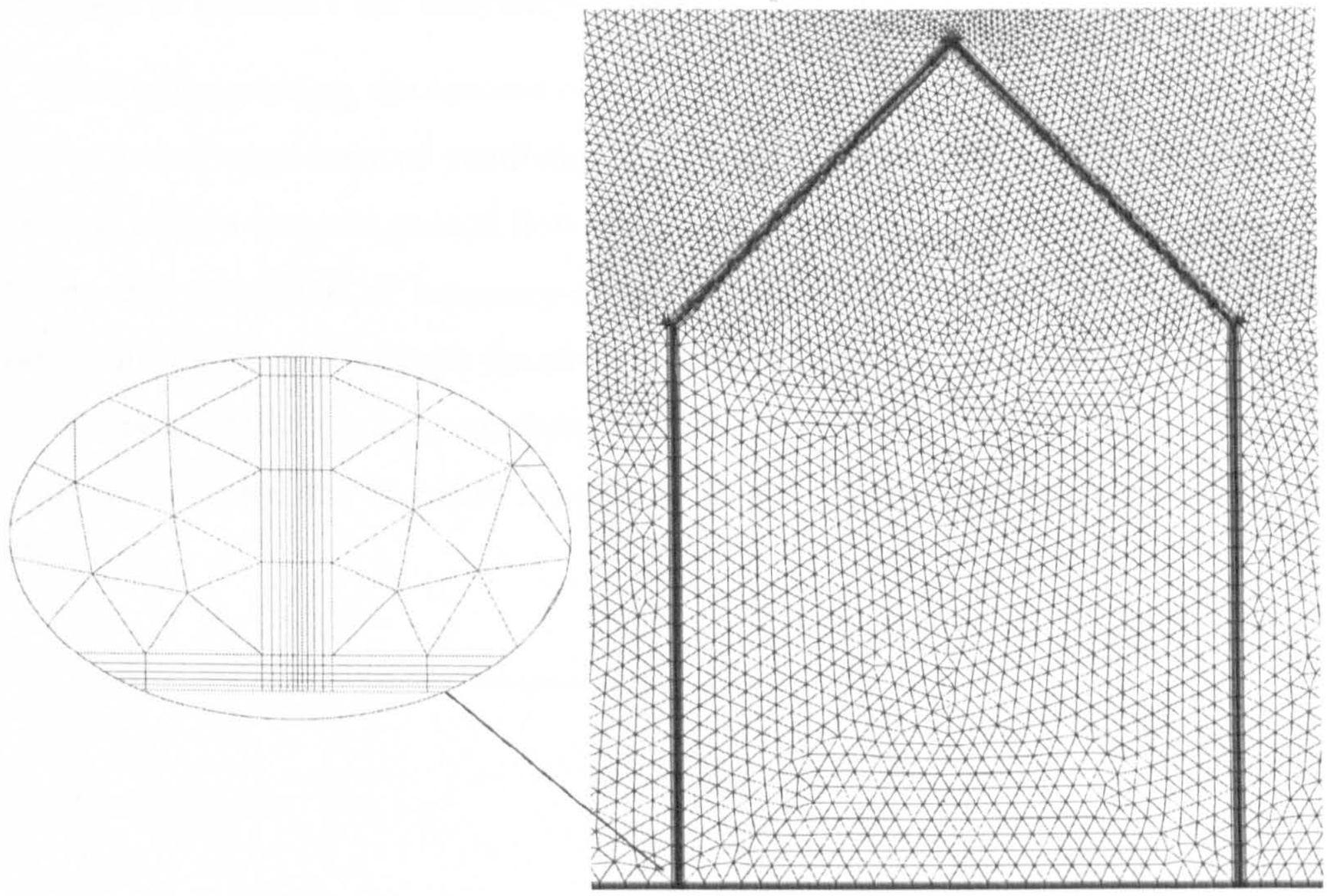

Figure 3.12: The typical grid system adopted in this research for wind-induced ventilation study

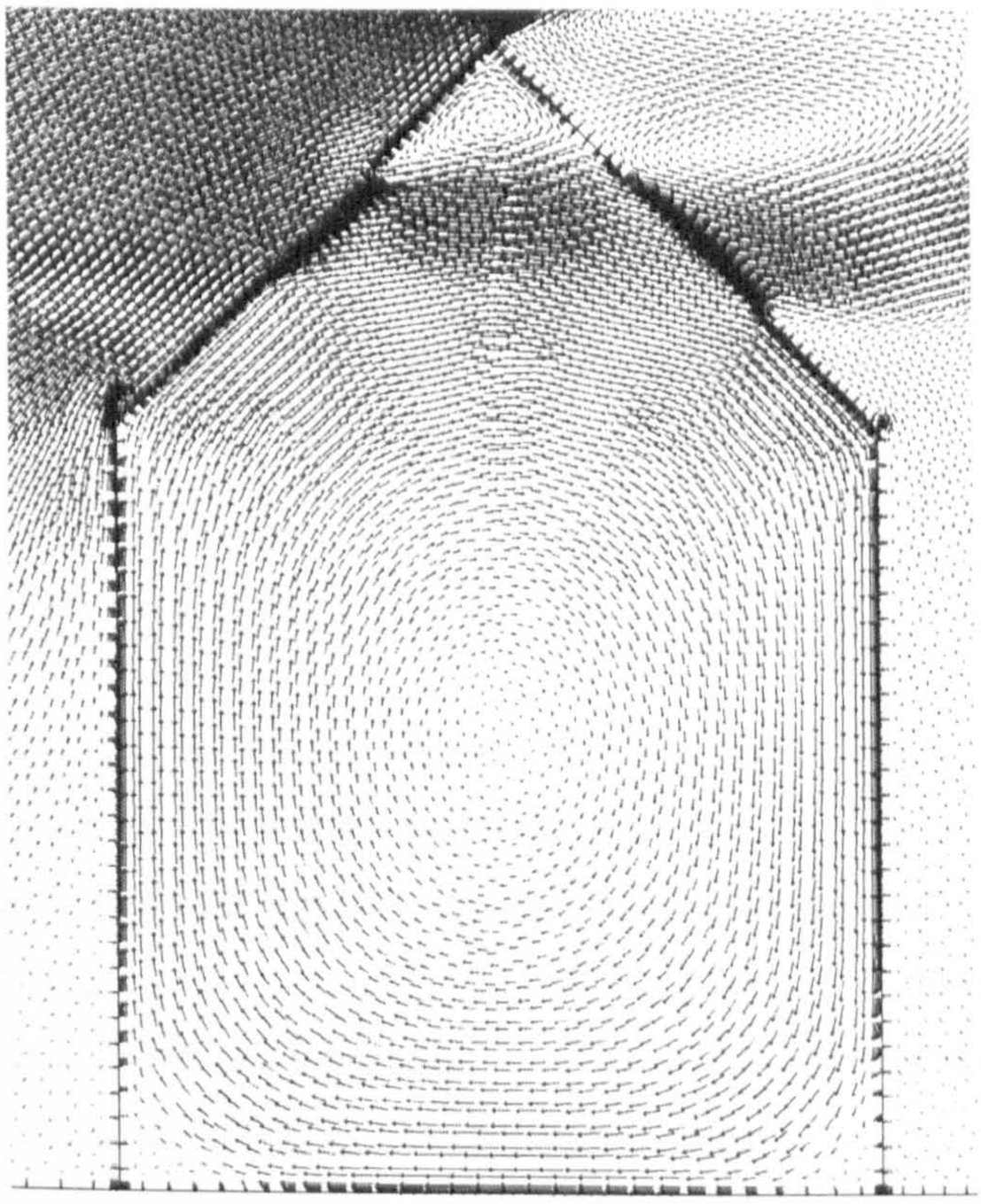

Figure 3.13: The flow field obtained from the simulation for the grid independence study for wind-induced ventilation (the No.3 grid system is used)

3.4.4 Settings of FLUENT for buoyancy-driven ventilation study

Generally speaking, the concern of buoyancy-driven ventilation study in this research is the same as that of wind-induced ventilation, i.e. to investigate the air velocity distribution at the bottom, bulk airflow rate and general flow pattern. In addition, also similar to the wind-induced ventilation, the simulation of buoyancy-driven ventilation has to be realised by placing the building in an open scale, because the air velocities at the openings are not known in the first place. However, unlike the large numbers of references that are found for the CFD settings of wind-induced airflows, the literature relevant to those of buoyancy-driven ventilation is quite limited.

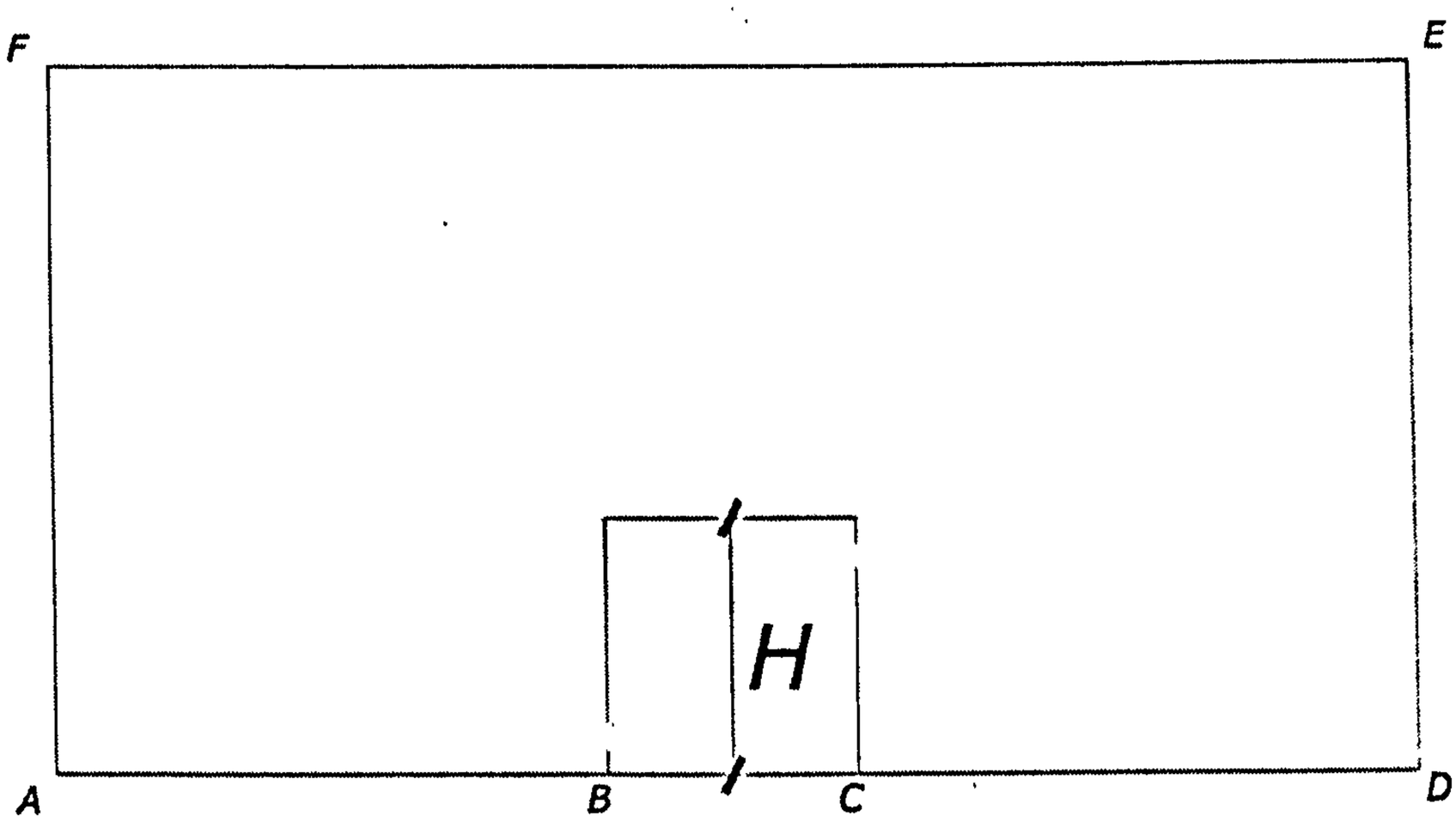

Figure 3.14: Schematic illustration of the computational domain for buoyancy-driven ventilation study

• *Settings of FLUENT*

Following the review in Section 3.2.2, the RNG k-ε turbulence model will be used; the Boussinesq model is used to approximate the relationship between the density and temperature change; all the building walls are regarded as adiabatic except the heat source part; of ground AB and CD shown in Figure 3.14 are also specified as adiabatic; "fictitious walls" AF and DE are specified as slip walls with the temperature being the same as the outside air temperature; the upper boundary EF is specified as zero-pressure boundary with outside air temperature. However, there is no clear guidance on the settings of the size the computational domain, i.e. the appropriate lengths of AB, CD and DE are unknown, and this will be the topic of next subsection.

With regard to the numerical settings, in order to achieve convergence, an unsteady-state approach is used to obtain a steady-state solution and the time scale for each step is calculated according to (Bejan 1995):

$$\Delta t \approx \frac{\tau}{4} = \frac{L}{4\sqrt{g\beta\Delta TL}} \tag{3.23}$$

Second order approximations are used for the solution of algebraic equations. The default settings of convergence criteria, i.e. the residuals of 10^{-3} for all variables, are adopted.

• *Study of computational domain*

A successful computational domain for buoyancy-driven ventilation should be capable of leading to a stable and sensible solution and more importantly, those fictitious walls should not have any direct "contact" with the main flow in the simulation results, as they do not exist physically in reality and their function in CFD is no more than providing temperature for the outdoor air.

Figure 3.15 compares the results from simulations with different computational domains for the simple cubic building shown in Figure 3.14. One opening is placed at the lower left wall and another opening located at the upper right wall. The floor is heated as the source driving the flow.

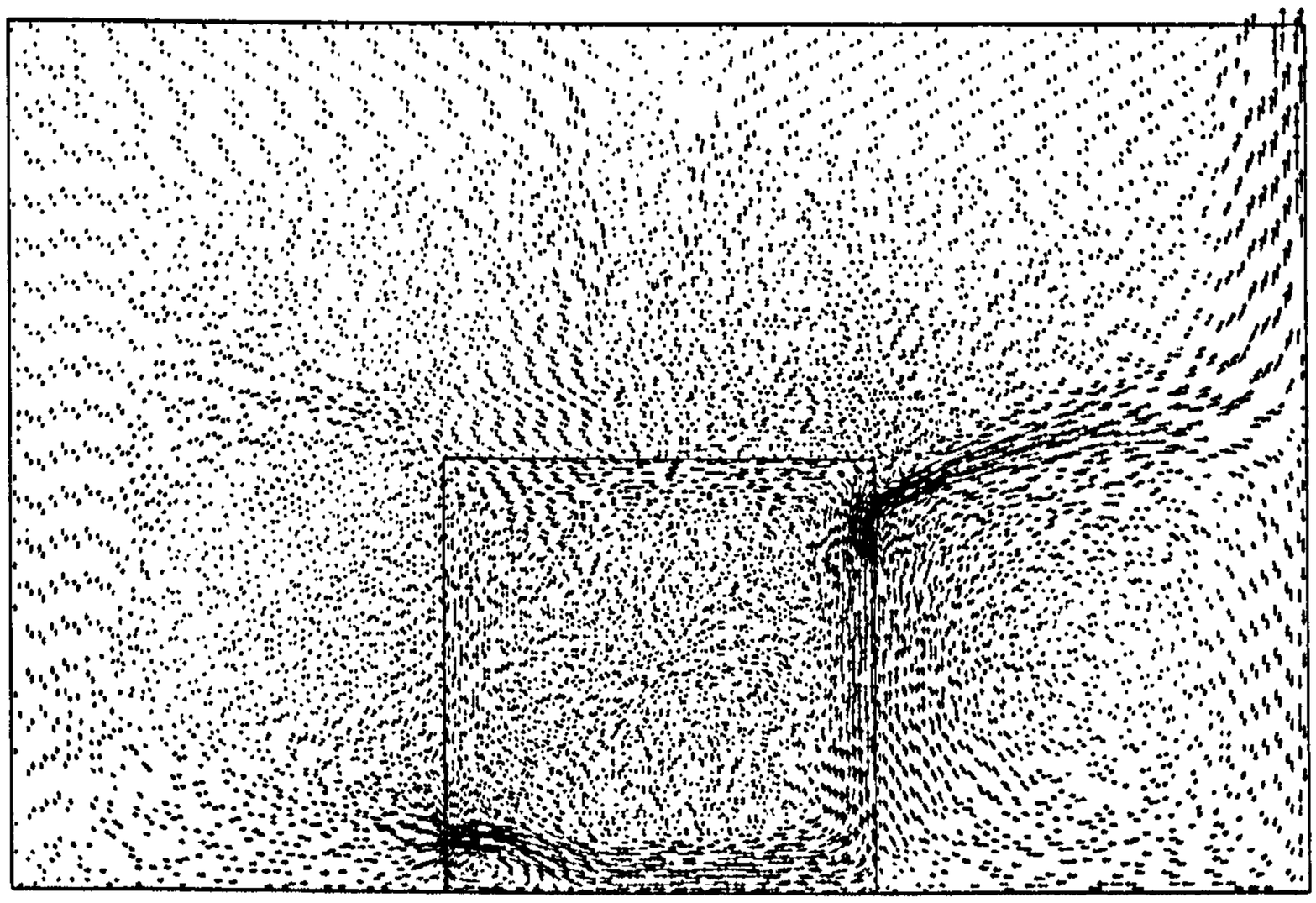

Figure 3.15 (a): The flow field of a cubic building with two openings (computational domain: AB = CD = *H*, DE = *2H*)

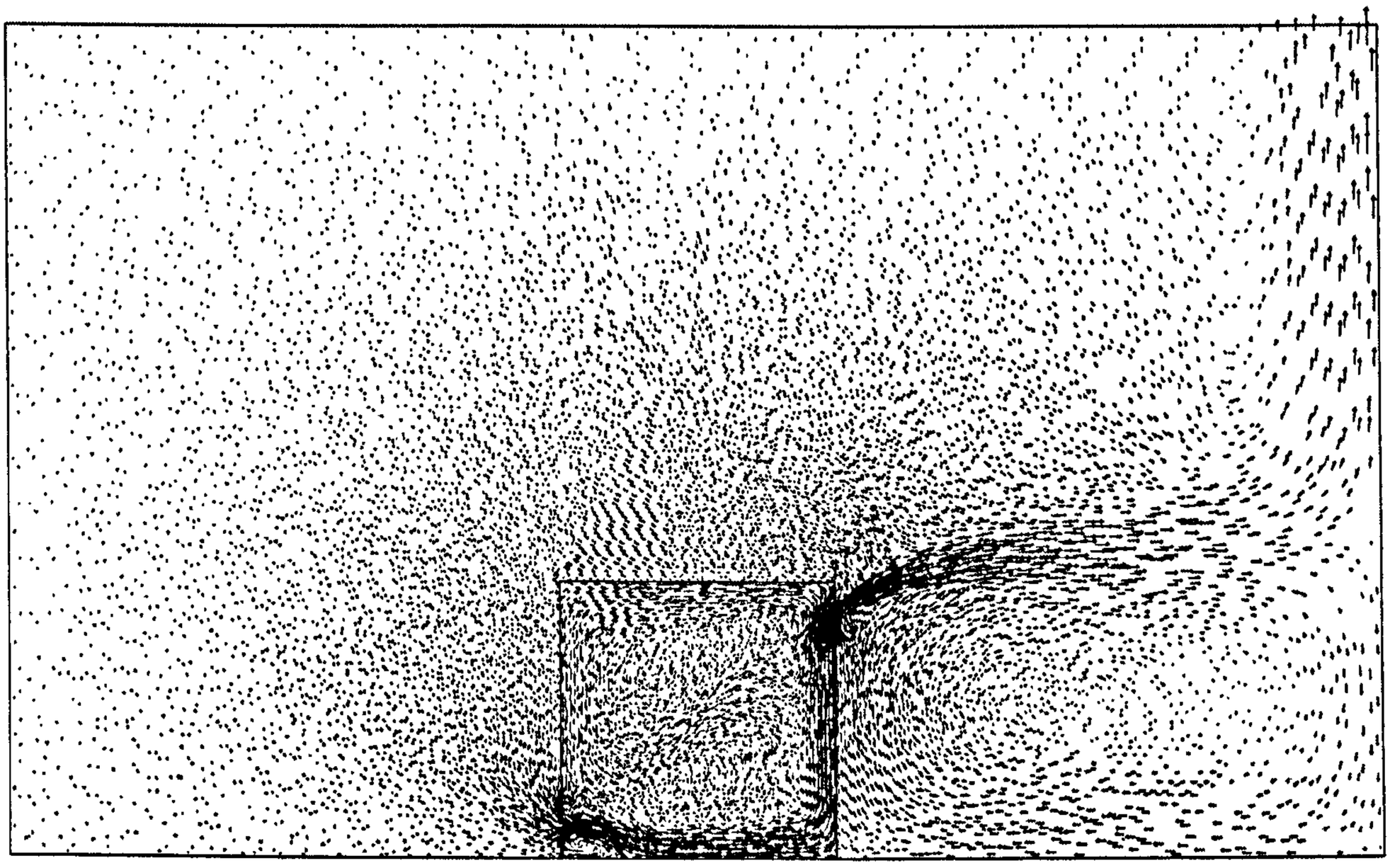

Figure 3.15 (b): The flow field of a cubic building with two openings (computational domain: AB = CD = 2*H*, DE = 3*H*)

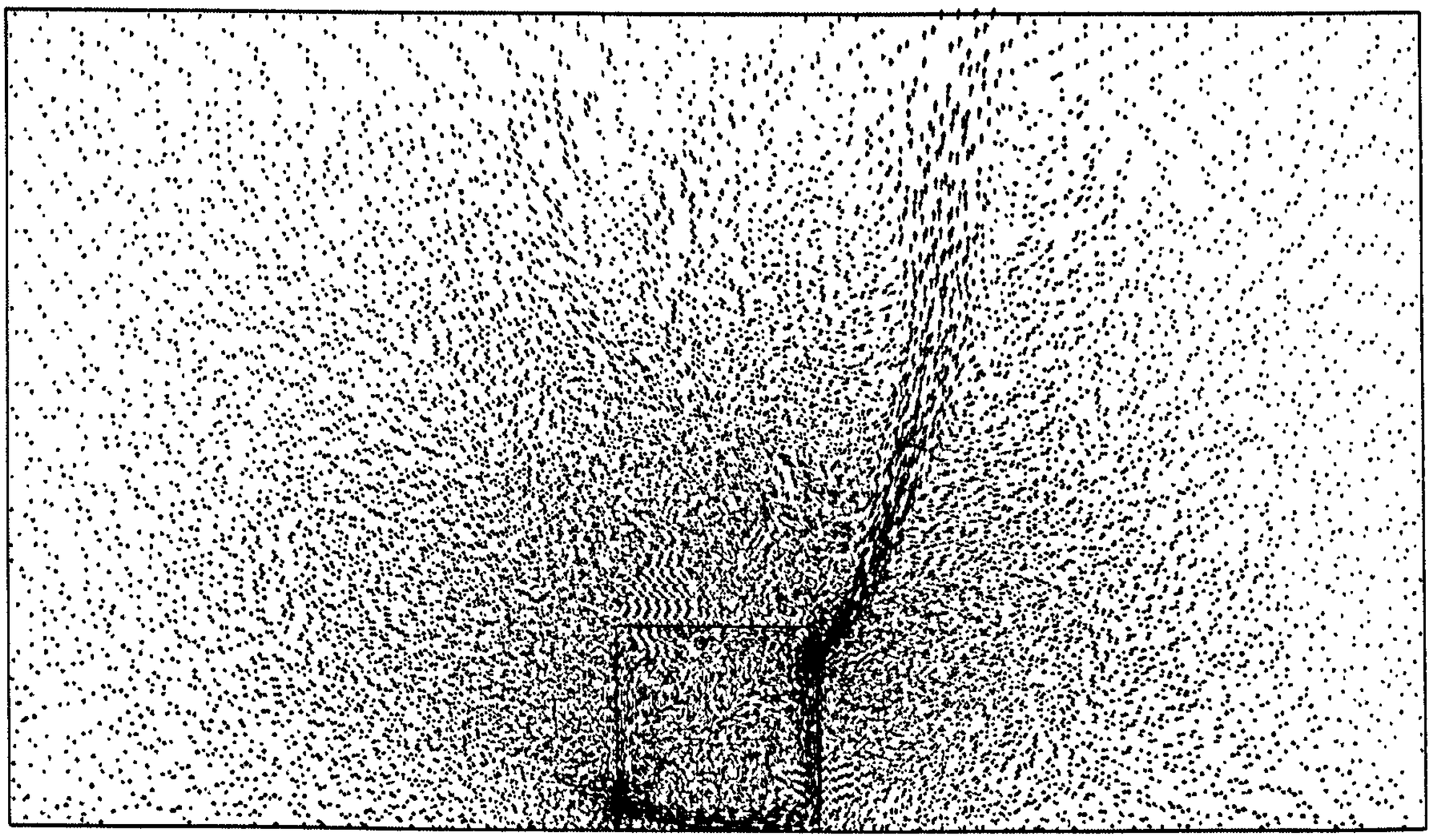

Figure 3.15 (c): The flow field of a cubic building with two openings (computational domain: AB = CD = 3*H*, DE = 4*H*)

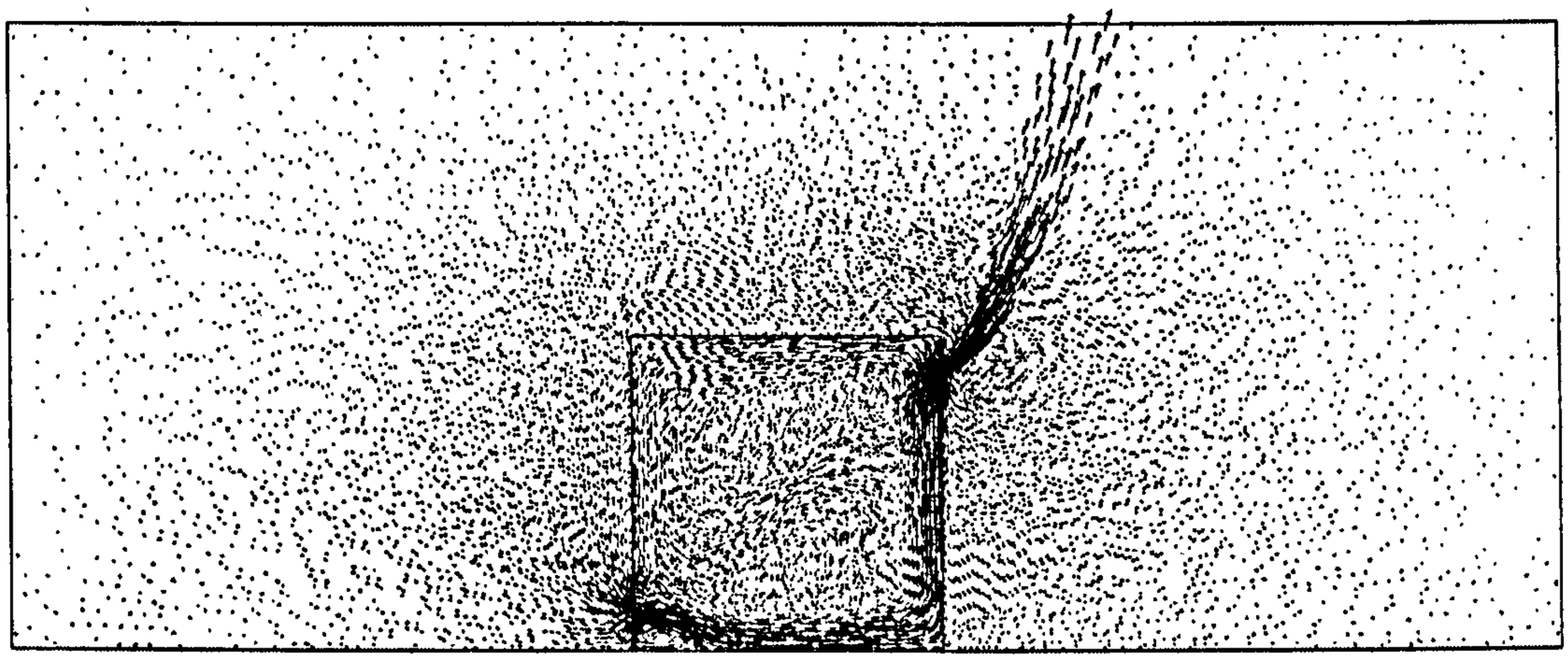

Figure 3.15 (d): The flow field of a cubic building with two openings (computational domain: AB = CD = 2*H*, DE = 2*H*)

It can be seen from above figures that, according to the criterion set at the beginning of this subsection, the computational domains of (a) and (b) are not appropriate, because the main flow attaches the right wall in the upper part of the domain showing that there is an interaction between them. Field flows of simulation with computational domains (c) and (d) are more close to the reality, as the "fictitious walls" are independent of the flow. Although the inside flows simulated by all different domains are very similar, the flow out of the building also have some influence. For instance, the outflow direction near the outlet undoubtedly will be very important for the analysis of opening methods of the outlet.

Figure 3.15 also suggests that a bigger size does help to obtain the correct solution (See (a) to (c)), which is also the rule-of-thumb for wind-induced ventilation study, a more effective way to achieve that is to modify the aspect ratio of the computational domain. Essentially the idea of using "fictitious walls" is based on the premise that they should be far away enough from the building and main flow in order to provide information about temperature only. However, the upper boundary does not necessarily have to be placed very far away from the building. In fact, locating the upper boundary too far from the building will not only result in expensive computational time cost but also bring on more risk because the main flow expands because of entrainment thus becomes nearer to external side wall. Having considered these issues, the computational domain illustrated in Figure 3.15 (d) is employed in this research for buoyancy-driven natural ventilation study.

• *Validation*

A number of validations for the use of CFD have been reported with respect to different kinds of buoyancy-driven airflows, such as (Cook and Lomas 1997) for the displacement

ventilation of a room with one plume heat source at the bottom, (Ji et al. 2007) for the displacement of an enclosure connected to an atrium space. The approach adopted in these two projects was to compare the simulation with the generalised algorithm developed based on physical experiments.

The above validations will not be repeated here with FLUENT, because basically the mechanism for different CFD programs is the same. Instead, another validation is made below for another type of buoyancy-driven ventilation, i.e. the displacement ventilation of a space with heated floor. Compared to those validations carried out for plume type heat sources, the displacement ventilation of a room with heated floor will be more relevant to this research, as the sun patch on the wall, which is a plane source other than a point source, will be the main heat source for atrium spaces in most situations.

As introduced in Section 2.5.2, under this circumstance, the temperature of the whole space can be regarded as uniformly distributed, and algorithm for the calculation of the airflow rate of this type of ventilation has been developed as follows (which can also be deduced with Equation 2.30 and 2.44):

$$q = \left[(C_D A)^* \right]^{\frac{2}{3}} (Bh)^{\frac{1}{3}} \tag{3.24}$$

where

$$B = \frac{Eg}{\rho c_p T_o} \tag{3.25}$$

This algorithm was also verified with the experiments performed by Gladstone and Woods (2001).

The building geometry used for the study of the size of the computational domain is still employed for this validation. The lower opening is located one metre above the ground while the upper opening is positioned one metre below the roof level. Both openings are one metre high. As the whole building has a height of $12m$, thus the vertical distance between two openings is $9m$. The outside temperature is specified as 17℃ ($290K$) and the interior floor is 32℃ ($305K$), thus 15℃ warmer than the outside[1]. The convective heat transfer coefficient is specified as 4.15, according to (Denton and Wood 1979). This value also complies with other references such as (CIBSE 1988) and (Khalifa and Marshall 1990). The discharge coefficient, C_D, is assumed to be 0.61, which is commonly used in other research. With all these data, it can be calculated that the bulk airflow rate should be $0.39m/s$.

[1] To comply with the boundary conditions used in the physical experiments by Gladstone and Woods (2001), constant temperature boundary condition is also used in CFD. However, constant heat flux is used as the boundary condition of heat sources for the buoyancy-driven ventilation studies in chapter five of this thesis in order to avoid the inefficiency of the constant temperature boundary condition to reproduce the heat flux.

Figure 3.16 shows the distribution of X-velocities at the inlet opening from the simulation and the average airflow rate is 0.37m/s. Thus, the discrepancy between simulation and the calculation by Equation (3.34) is only about 5%.

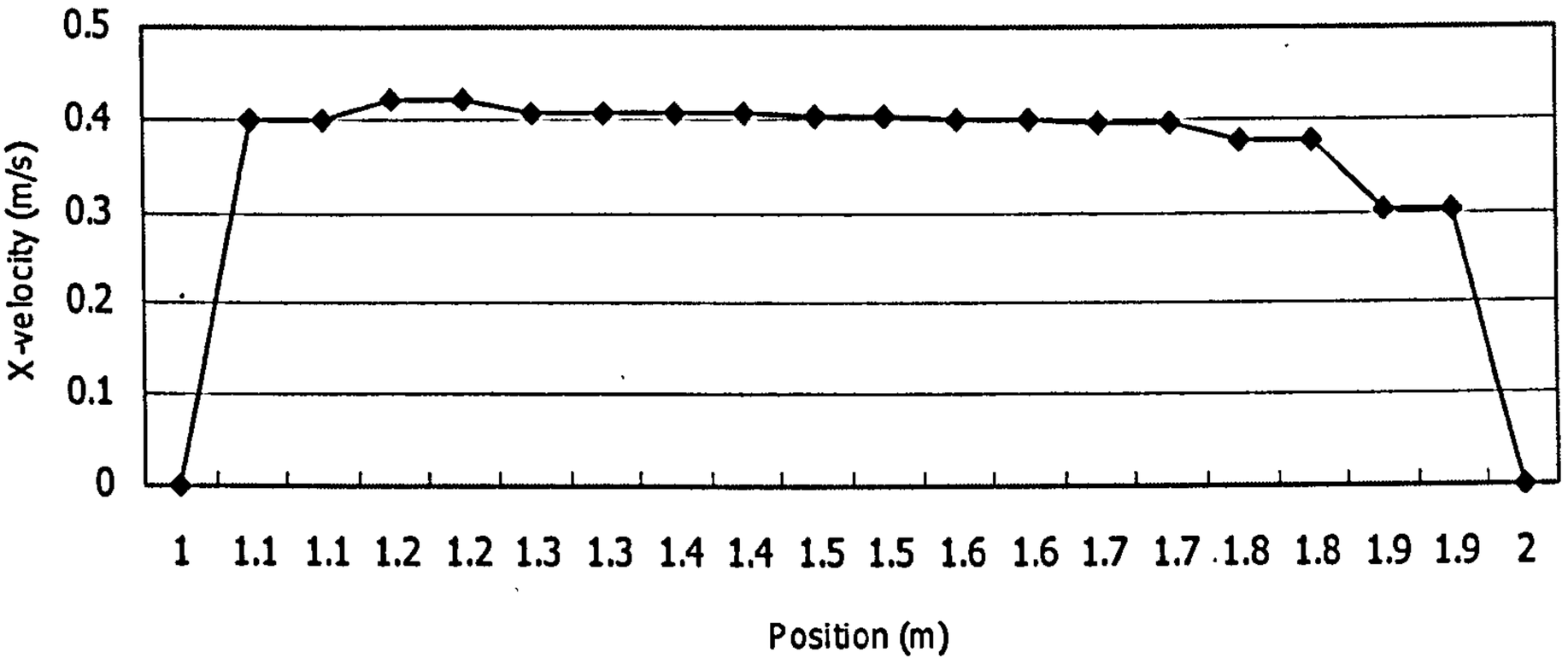

Figure 3.16: The distribution of X-coordinate air velocities at the inlet for the displacement ventilation of a room with a heated floor

Figure 3.17 illustrates the vertical temperature distribution for the central line of the space. It could be seen that, only for the area very near to the heat source (lower than 1.1*m*), the air temperature is significantly influenced by the heat source. Areas above that all have the same air temperature, which means that there is no vertical stratification. This is agreeable with the review and the observations in the experiments of Gladstone and Woods (2001).

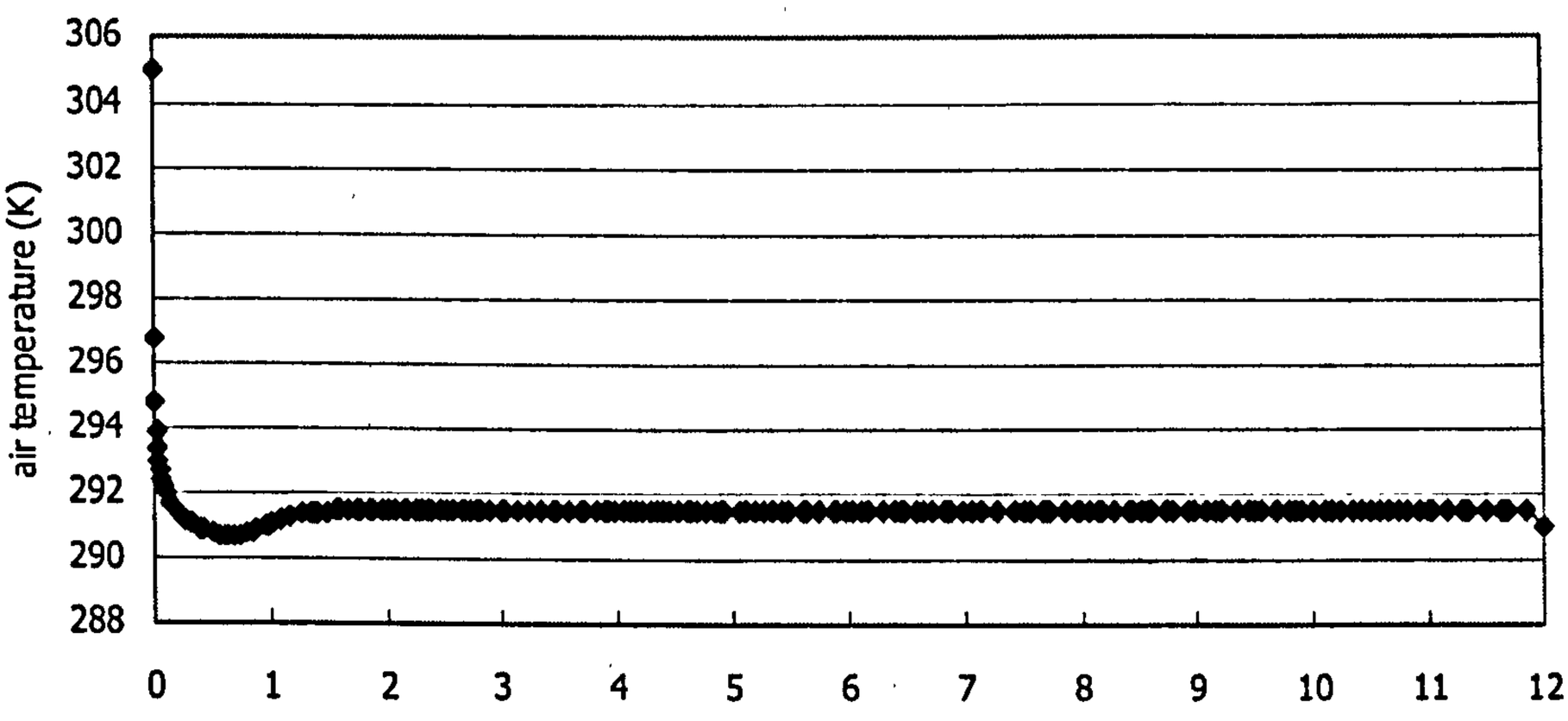

Figure 3.17: The vertical air temperature distribution of the central line for the displacement ventilation of a room with a heated floor

• *Grid independence study*

The concern of this grid independence study is still with the general grid density and the value of y^+. The characteristics of settings on y^+ are a combination of those on internal natural convection and those on wind-induced ventilation. For the heat source, in order to accurately simulate the amount of heat transferred, the settings of the internal natural convection should be adopted, i.e. the value of y^+ should be controlled to be around 9. As for other surfaces, then y^+ should be around 30 – 60, which is also the requirement for wind-induced ventilation.

For the study of grid density, the same prototype used before is simulated with five different gridding systems. Two openings are incorporated at different heights, as shown in Figure 3.20. Other conditions and settings are the same as those for validation study. The tested gridding systems are listed in Table 3.5. Figure 3.18 compares the air temperature distributions of the simulations with different grid densities and the air velocity distributions are illustrated in Figure 3.19.

Table 3.5: Different gridding systems used for the grid independence study of buoyancy-driven ventilation (the grid density of other edges are half of that of the opening)

No.	1	2	3	4	5
Number of grids for each opening	10	15	20	25	30

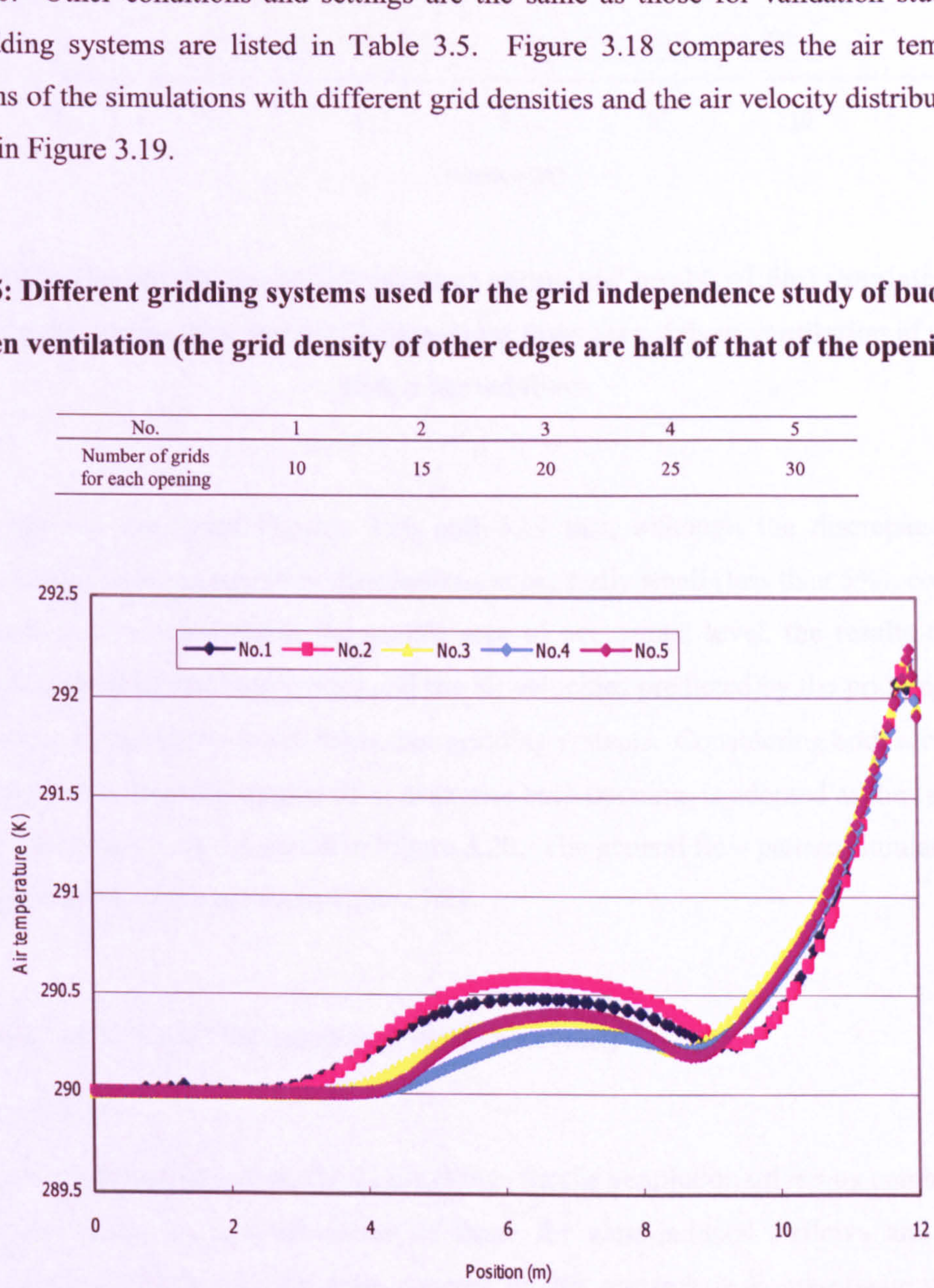

Figure 3.18: The air temperature distribution at occupants' level (y=1.6m) simulated with different gridding systems for the displacement buoyancy-driven ventilation of a room with a heated floor

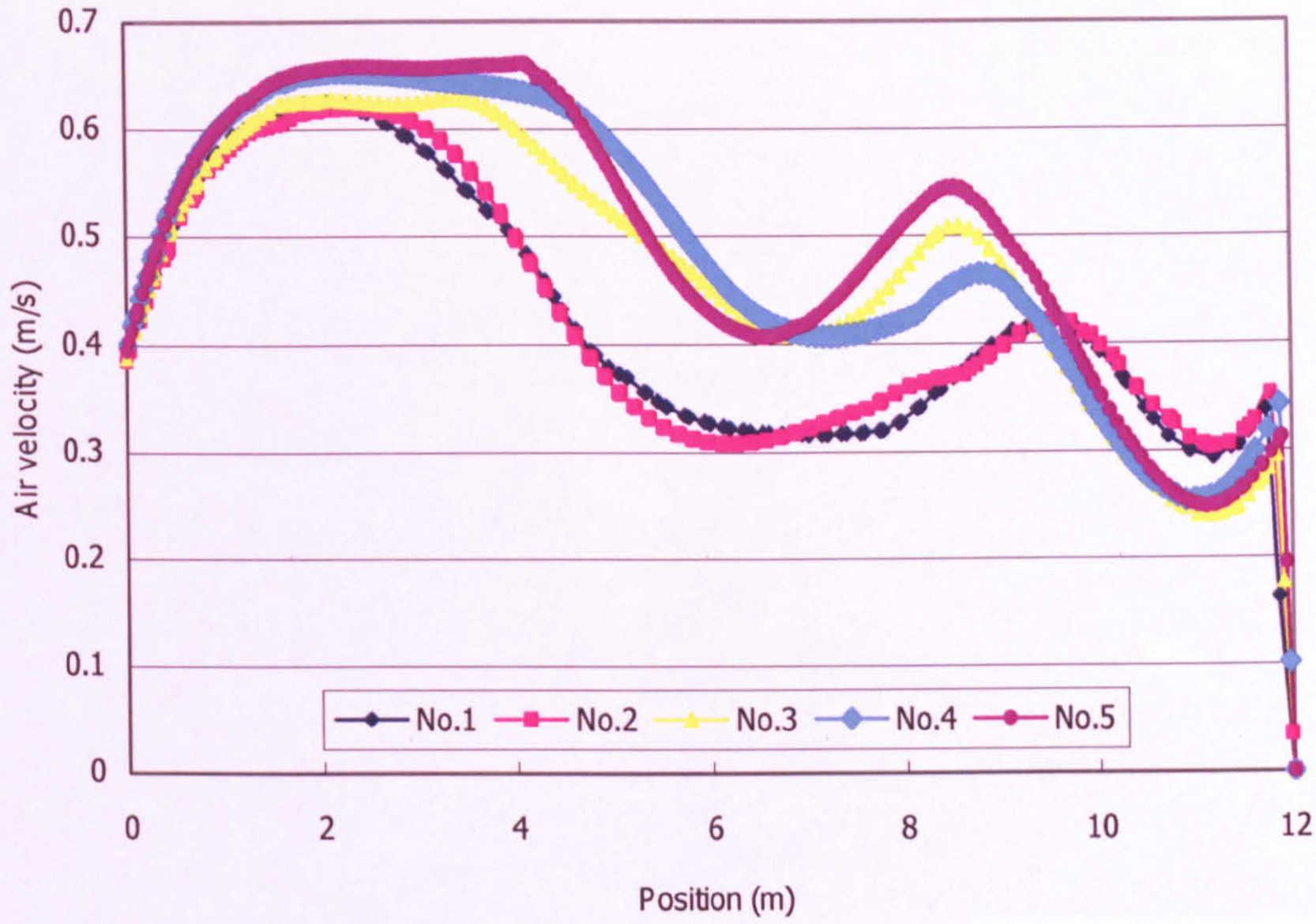

Figure 3.19: The air velocity distributions at occupants' level (y=1.6m) simulated with different gridding systems for the displacement buoyancy-driven ventilation of a room with a heated floor

It can be seen from Figures 3.18 and 3.19 that, although the discrepancy of the simulation results on air temperature distributions is generally small (less than 5%), coarse grids underestimate the air velocities at the middle area of occupants' level: the results of all five simulations are divided into two groups and the air velocities predicted by the gridding systems No. 1 and No.2 are generally lower than other gridding systems. Considering both accuracy and time cost, No.3, i.e. 20 grids are placed to discretise each opening, is adopted as the typical grid system for this research, as illustrated in Figure 3.20. The general flow pattern simulated for the grid independence study is shown in Figure 3.21.

3.4.5 Settings of FLUENT for combined ventilation study

• *FLUENT settings*

As has been stated earlier, the CFD settings for the ventilation driven by combined wind and buoyancy forces are a combination of those for wind-induced airflows and those for buoyancy-driven airflows. As the main concern of this research is to investigate the airflow when the two forces oppose each other, only the settings for this condition will be introduced.

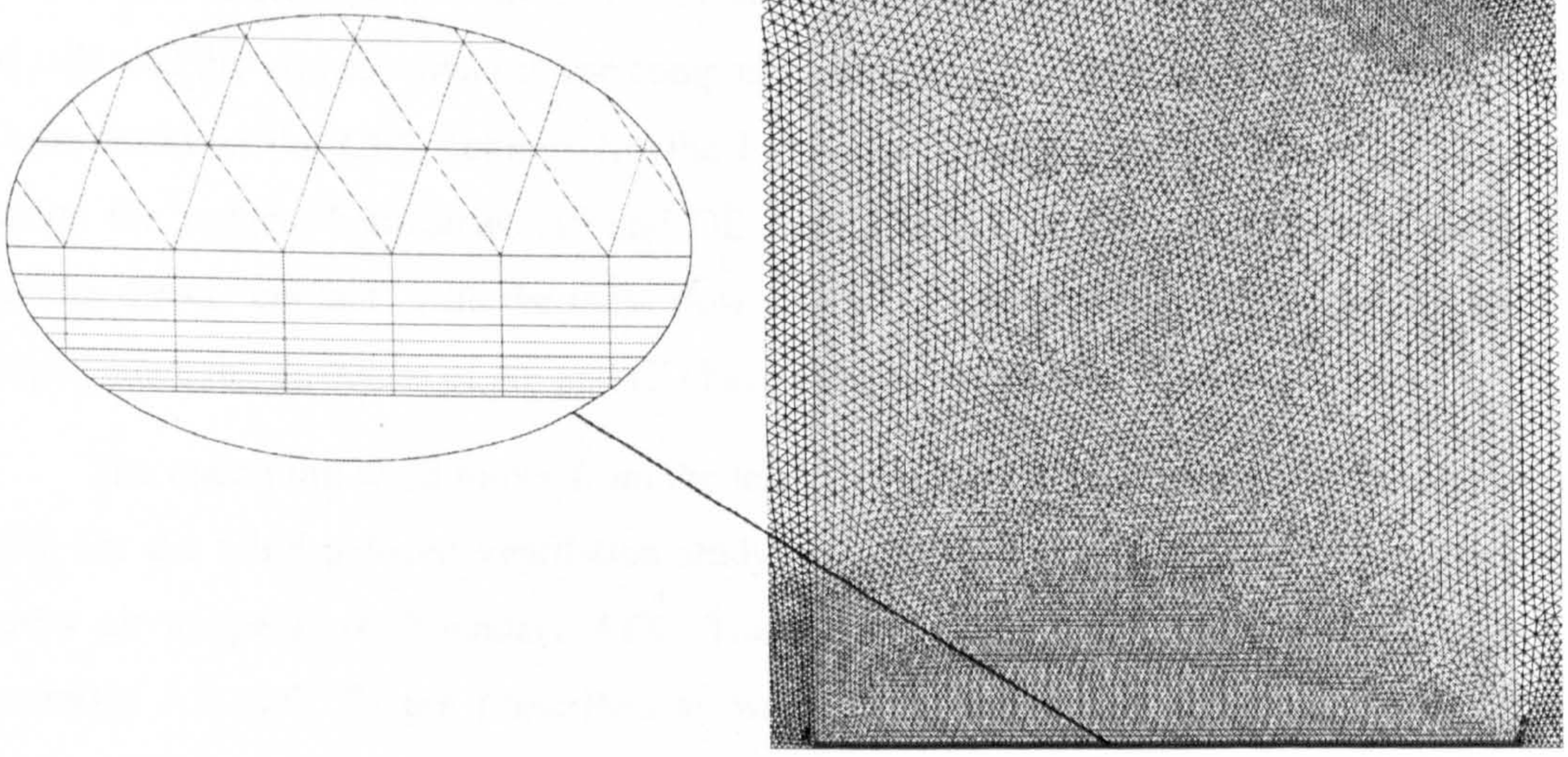

Figure 3.20: The typical grid system used in the simulation of buoyancy-driven ventilation

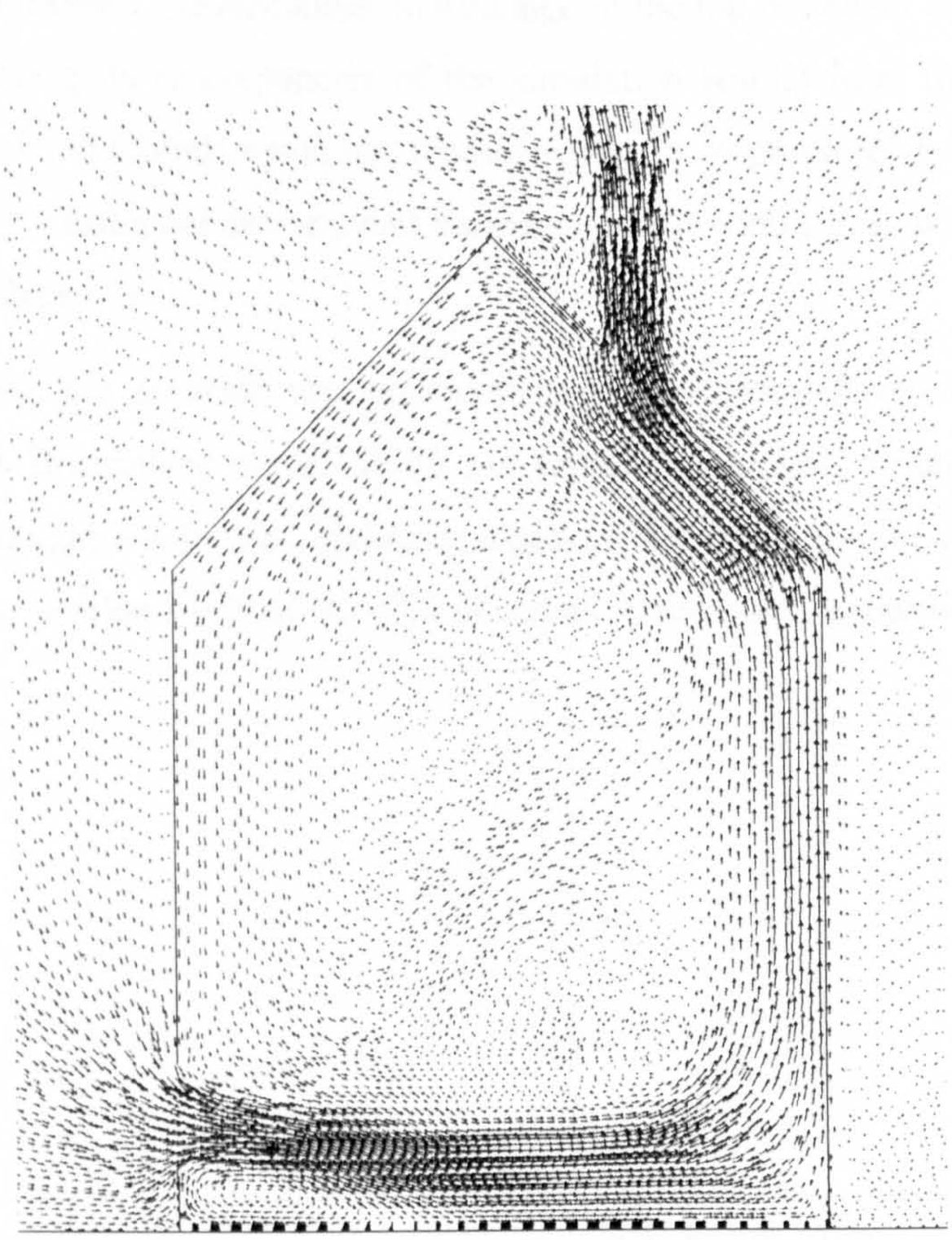

Figure 3.21: The flow field obtained from the simulation for the grid independence study for buoyancy-driven ventilation (the No.3 grid system is used)

Figure 3.22 illustrates the computational domain employed for the opposed ventilation study in this research. Most distances of the computational domain are identical to those for the wind-induced ventilation study, such as AF and CD. However, it should be noted that the distance AB is prolonged to 10*H*. This is because, when the buoyancy forces are much stronger than the wind forces, the air will move out of the building from the upper opening on the left hand side and the air movement in the computational domain is dominated by buoyancy forces. As introduced in the CFD settings for the buoyancy-driven airflows (Section 3.4.3), in this situation the vertical boundaries AF and DE should be placed far away from the building to avoid the direct "contact" with the main flow. As a consequence, the distance of AF has to be enlarged since the distances of AF and CD have already reached the minimum.

The oncoming wind blows from the left hand side and the wind profile used is the same of that for the wind-induced ventilation study, except that the temperature is specified as the outdoor air temperature (boundary AF). The boundary DE is still specified as outflow, and boundaries AB and CD are prescribed as walls with the outdoor air temperature. The top boundary EF cannot be specified as symmetry any longer, as the air may go through it when the buoyancy forces are dominant. As a result a zero-pressure boundary with the outside air temperature is used instead. Nevertheless, this change of the top boundary of the computational domain may also bring on discrepancies of the simulation results from those obtained from wind tunnels, since wind tunnels could not reproduce the "zero-pressure" boundary for the top. This will significantly influence the relevant validation when wind forces dominate the airflow, which will be introduced later.

Other settings are generally the same as those for buoyancy-driven airflow simulations, such as the use of Boussinesq model, RNG k-ε turbulence model, unsteady-state approach, second order approximations for the solution of algebraic equations and the convergence criteria. Readers can refer to Section 3.4.3 for detailed information regarding to these issues.

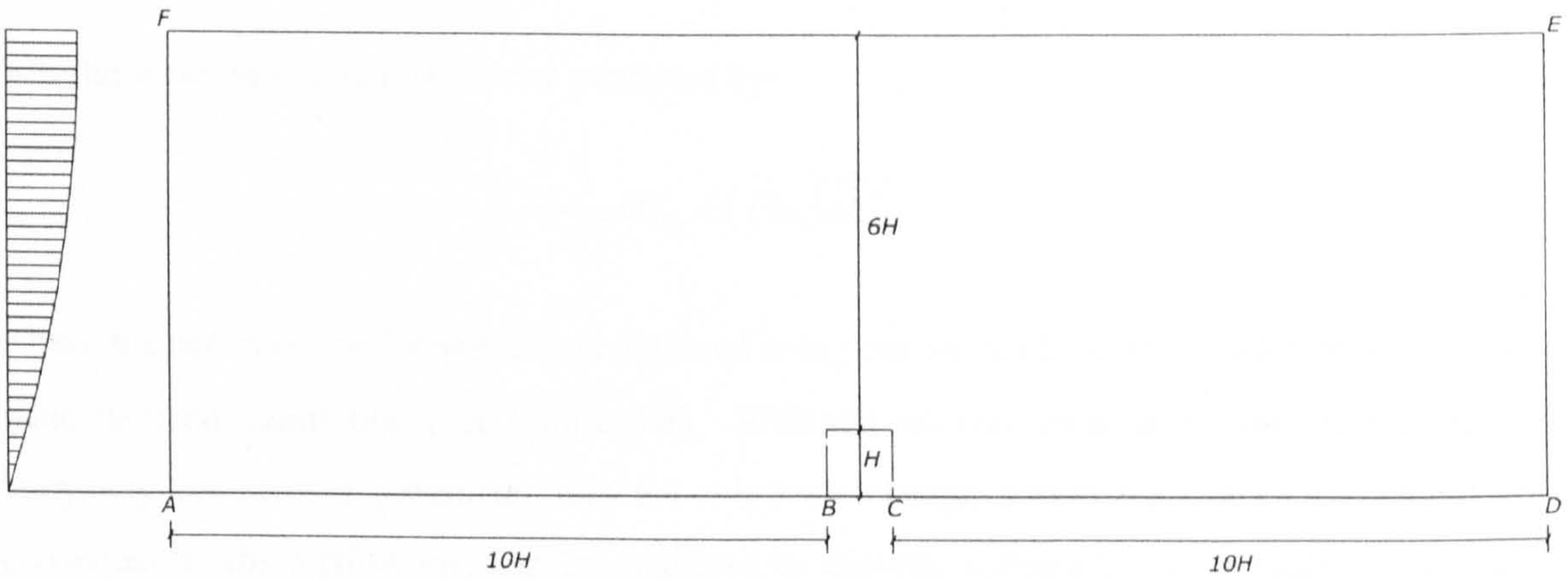

Figure 3.22: Schematic illustration of the computational domain for combined ventilation study

• *Validation*

As has been introduced in Chapter Two, there are a number of research projects that have already used CFD to investigate the combined ventilation, including Allocca et al. (2003), Cook et al.(2003), and Heiselberg et al.(2004), and it has been shown CFD is capable of studying some important characteristics of the problems with airflows with opposed forces, such as solution multiplicity.

The CFD settings introduced above will be further validated with a case more pertinent to this study compared to other references in the literature: that is, when the floor is heated as the heat source driving the buoyancy forces whilst the oncoming wind blows from the upper opening side. Generally the environmental conditions of this model are the same as those used for the buoyancy-driven validation study, except the presence of the wind. The building geometry and the openings' locations and sizes are also the same as those employed for buoyancy-driven validation study. Constant heat flux is specified as the boundary condition for the floor which emits energy of $50 W/m^2$. In order to simulate both the conditions where wind forces control the airflow and the conditions where buoyancy forces are determinant, the reference wind velocity increases from 0 to 1m/s with a step of 0.1m/s.

A generalised algorithm has been developed for the calculation of the airflow rate based on the equations of energy and mass conservations for combined airflows introduced in Chapter 2 (Section 2.5.3), which can be expressed as follows (Li and Delsante 2001; Andersen 2007):

$$q = \pm\sqrt{\left|\frac{2\alpha^3}{|q|} - 3\gamma^2\right|} \tag{3.26}$$

where α is defined as the thermal buoyancy air change parameter and can be calculated as:

$$\alpha = \left[(C_D A)^*\right]^{\frac{2}{3}} (Bh)^{\frac{1}{3}} \tag{3.27}$$

γ is the wind air change parameter predicted by:

$$\gamma = \frac{1}{\sqrt{3}} (C_D A)^* U_R \sqrt{\Delta C_P} \tag{3.28}$$

where the pressure coefficient ΔC_P is obtained using the results from the validation study of the wind-induced ventilation (see Figure 3.6). With the relevant parameters known, the thermal buoyancy air change parameter and the wind air change parameter can be calculated and consequently the airflow rate can be predicted by directly solving Equation (3.26). It can also be seen from Equation (3.26) that multiple solutions may exist due to the multiple selections for the symbols for the absolute value. This analytical approach has also been validated with the experiments carried out by Gladstone and Woods (2001).

As has been introduced earlier, special attention has to be paid to the settings of the initial conditions in order for the CFD simulation to find the multiple solutions. A two-way approach is employed for this purpose (Duan and Li 2005). Firstly, conventional zero initialisation is used to simulate a situation where wind forces are much stronger than the buoyancy forces, such as reference wind velocity is 1m/s and the heat source is kept constant as $50W/m^2$. Next the wind velocity is gradually reduced with a step of 0.1m/s and the previous simulation result was used as the initial condition for the next simulation. Secondly, simulation is started again from a buoyancy-dominated case: when the reference wind velocity is zero, and gradually increase the wind velocity by a step of 0.1m/s. The results of the simulations together with those from algorithms are plotted in Figure 3.23.

It can be seen from Figure 3.23 that, the results predicted by CFD and by the algorithms generally show the same trend with the increase of the reference wind velocity. Quantitatively, the discrepancies between the two approaches are quite small (less than 20%) when the wind velocity is below 0.6m/s. Nevertheless, when the wind dominates the airflow, the discrepancies become very large. As has been described earlier, the reason for this is the use of the "zero-pressure" condition for the top boundary of the computational domain, which is quite different from the real conditions employed for the experiments and those for the development of the algorithm. It should be noted that, however, as the main concern of this project is about multiple solution that takes place when the two opposing forces are in similar scale, the inefficiency of the settings for the simulation of wind-dominant flows would not bring significant problems for this research.

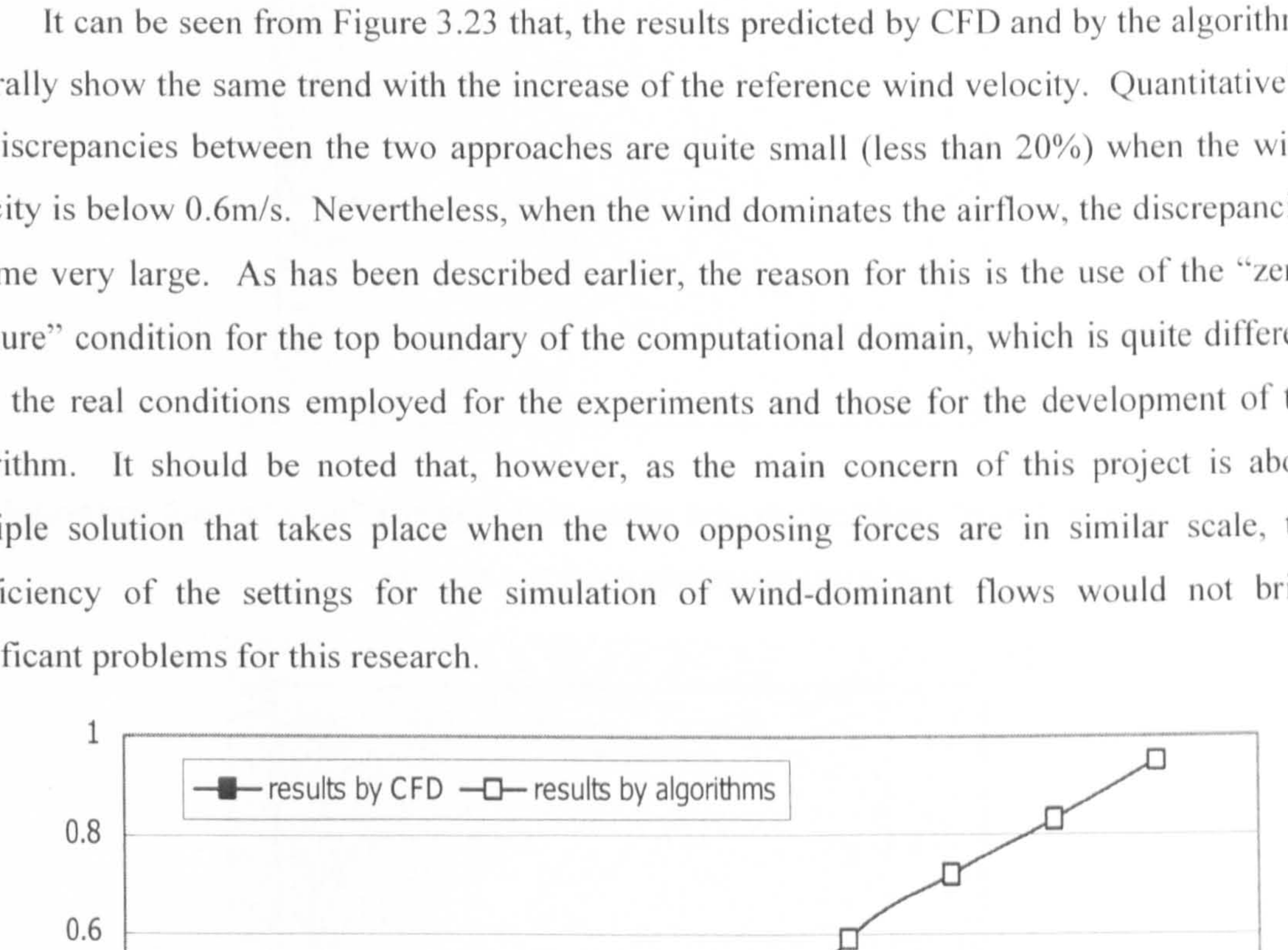

Figure 3.23: Comparison between the airflow rates predicted by CFD and by algorithms

Figure 3.23 also shows that, when the reference wind velocity is 0.5m/s, multiple solutions exist for different initial conditions. The airflow fields for the two solutions are further illustrated in Figure 3.24. It can be observed from Figure 3.23 that more multiple solutions can be obtained by using generalised algorithms but they only exist mathematically rather than physically.

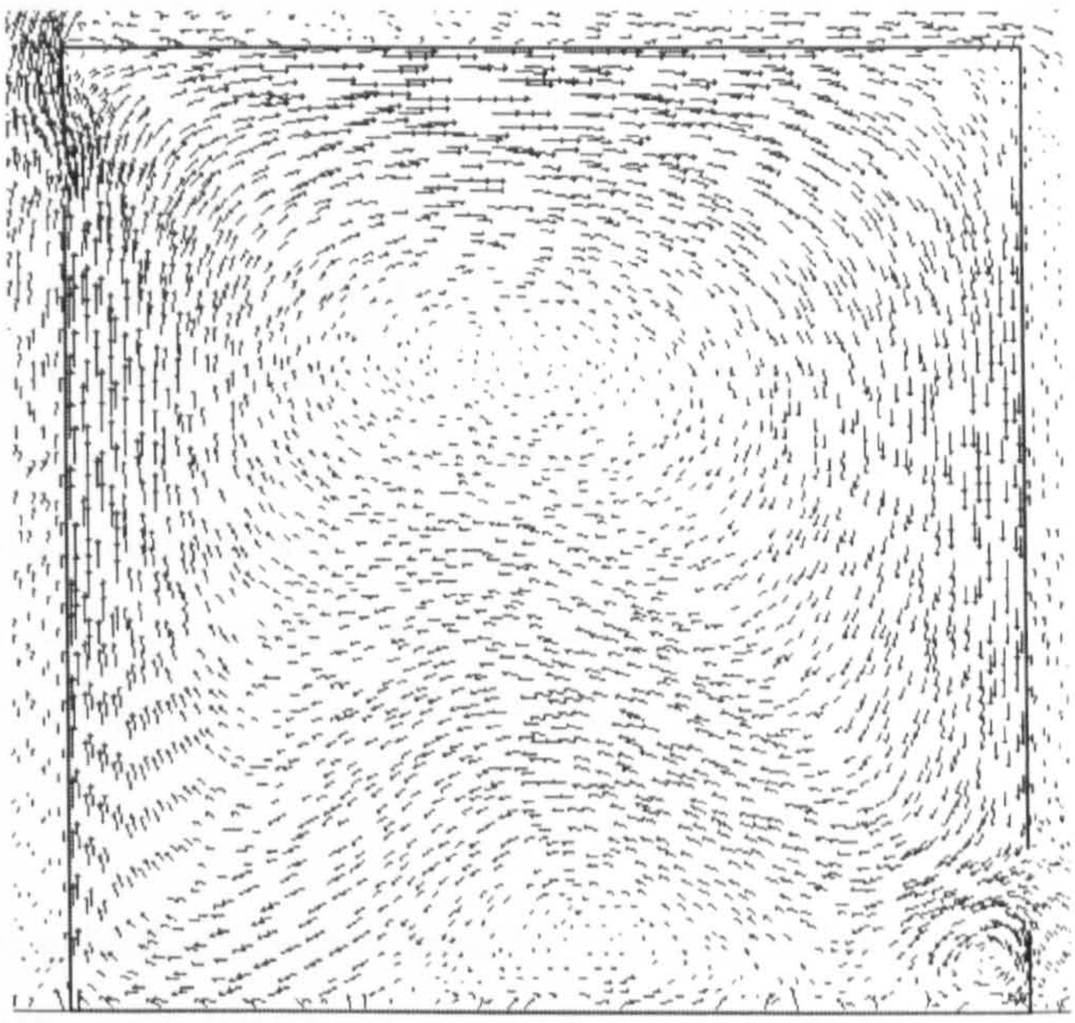

(a) buoyancy forces "look" stronger (air comes into the building from the lower opening and get out from the upper opening)

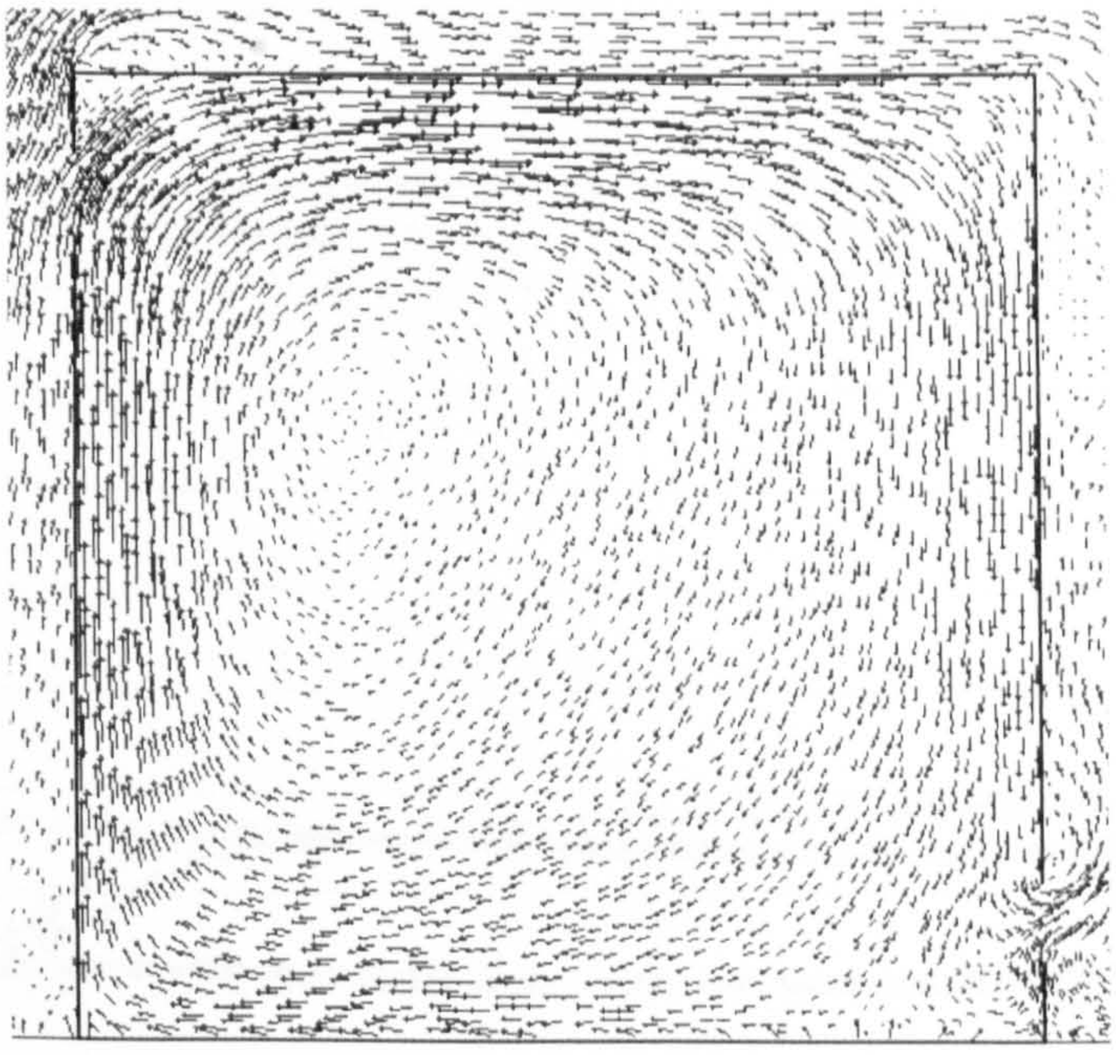

(b) wind forces "look" stronger (air comes into the building from the upper opening and get out from the lower opening)

Figure 3.24: Airflow fields for the multiple solutions when the reference wind velocity is 0.5m/s

• *Grid independence study*

It has been introduced that the computational domain for the simulation of combined ventilation is much larger than that for either wind-induced ventilation or buoyancy-driven ventilation, which means more significance for the use of grids with less density to save the computing time cost.

The building configuration used above for the validation study will also be used for grid independence study. All the environmental conditions, including the wind profile, the location and intensity of the heat source remain the same as those used for previous validation studies. A scenario where the buoyancy forces dominate the air movement (the reference wind velocity is 0.1m/s) is simulated for comparison of different gridding systems listed in Table 3.6. The air velocity distributions and the vertical temperature profiles simulated by different gridding systems are compared in Figures 3.25 and 3.26 respectively.

Table 3.6: Different gridding systems used for the grid independence study of combined ventilation (the grid density of other edges are half of that of the opening)

No.	1	2	3	4	5
Number of grids for each opening	5	8	10	12	15

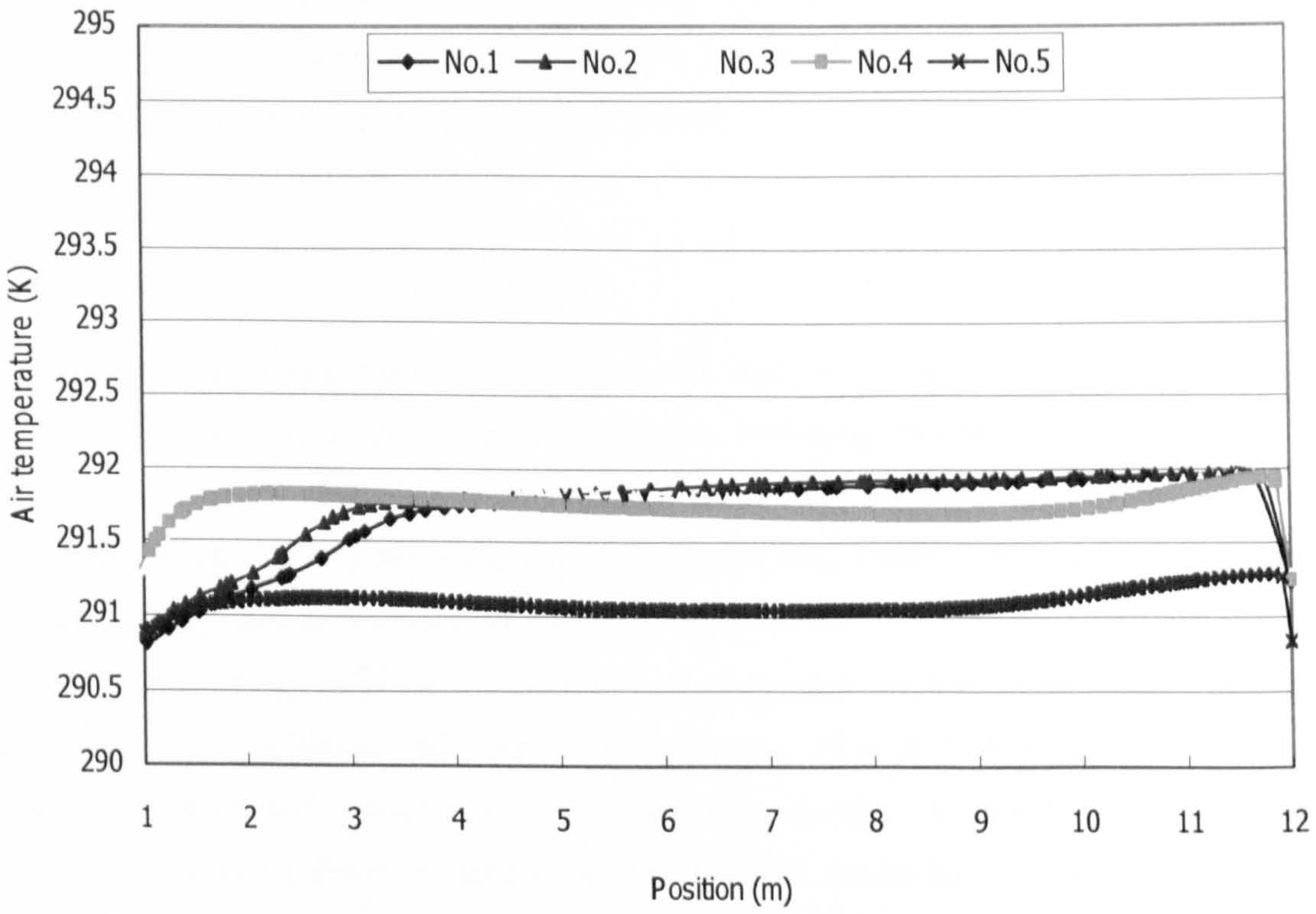

Figure 3.24: Vertical air temperature profiles of CFD simulations with different gridding systems for combined ventilation

• *Grid independence study*

It has been introduced that the computational domain for the simulation of combined ventilation is much larger than that for either wind-induced ventilation or buoyancy-driven ventilation, which means more significance for the use of grids with less density to save the computing time cost.

The building configuration used above for the validation study will also be used for grid independence study. All the environmental conditions, including the wind profile, the location and intensity of the heat source remain the same as those used for previous validation studies. A scenario where the buoyancy forces dominate the air movement (the reference wind velocity is 0.1m/s) is simulated for comparison of different gridding systems listed in Table 3.6. The air velocity distributions and the vertical temperature profiles simulated by different gridding systems are compared in Figures 3.25 and 3.26 respectively.

Table 3.6: Different gridding systems used for the grid independence study of combined ventilation (the grid density of other edges are half of that of the opening)

No.	1	2	3	4	5
Number of grids for each opening	5	8	10	12	15

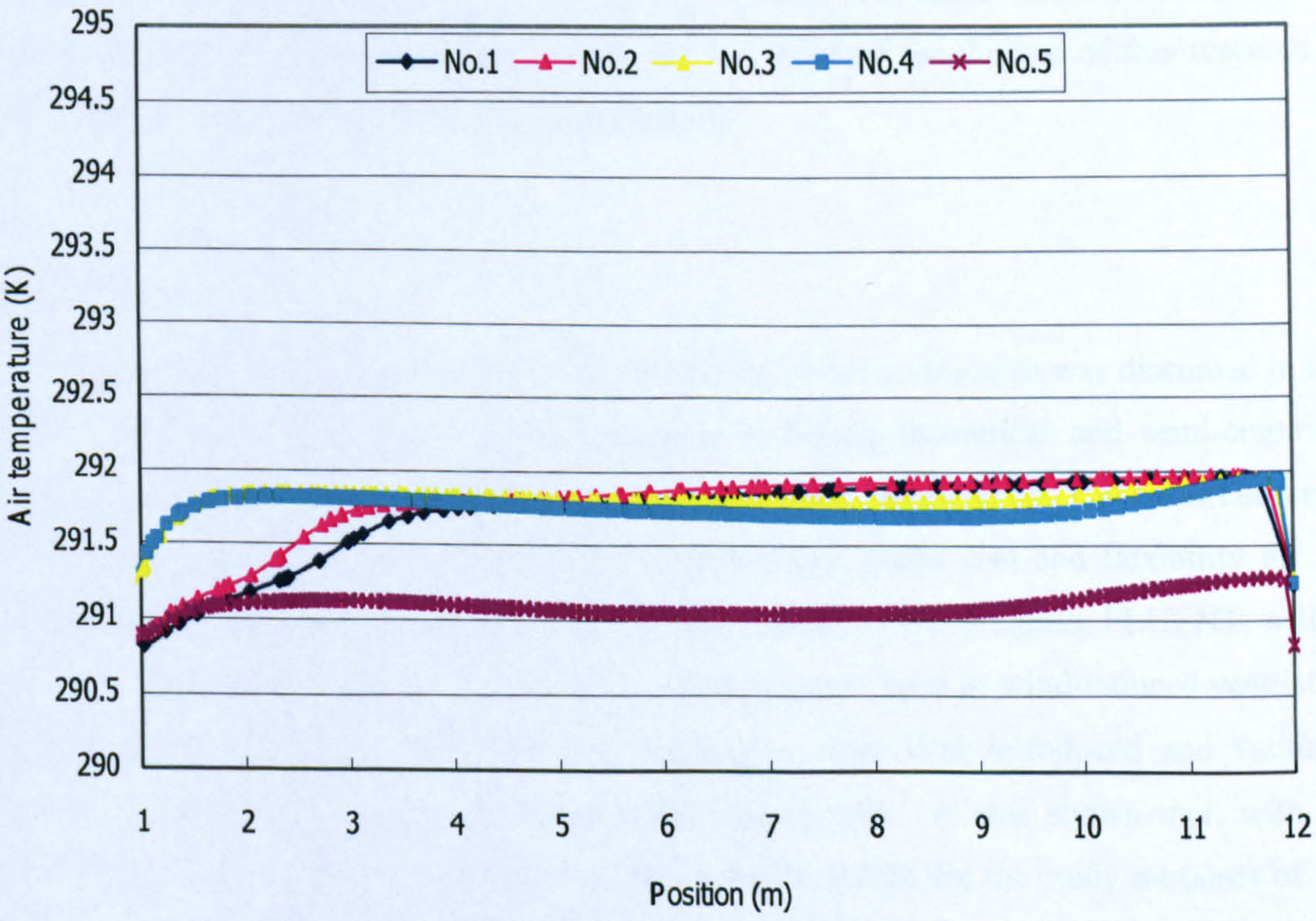

Figure 3.24: Vertical air temperature profiles of CFD simulations with different gridding systems for combined ventilation

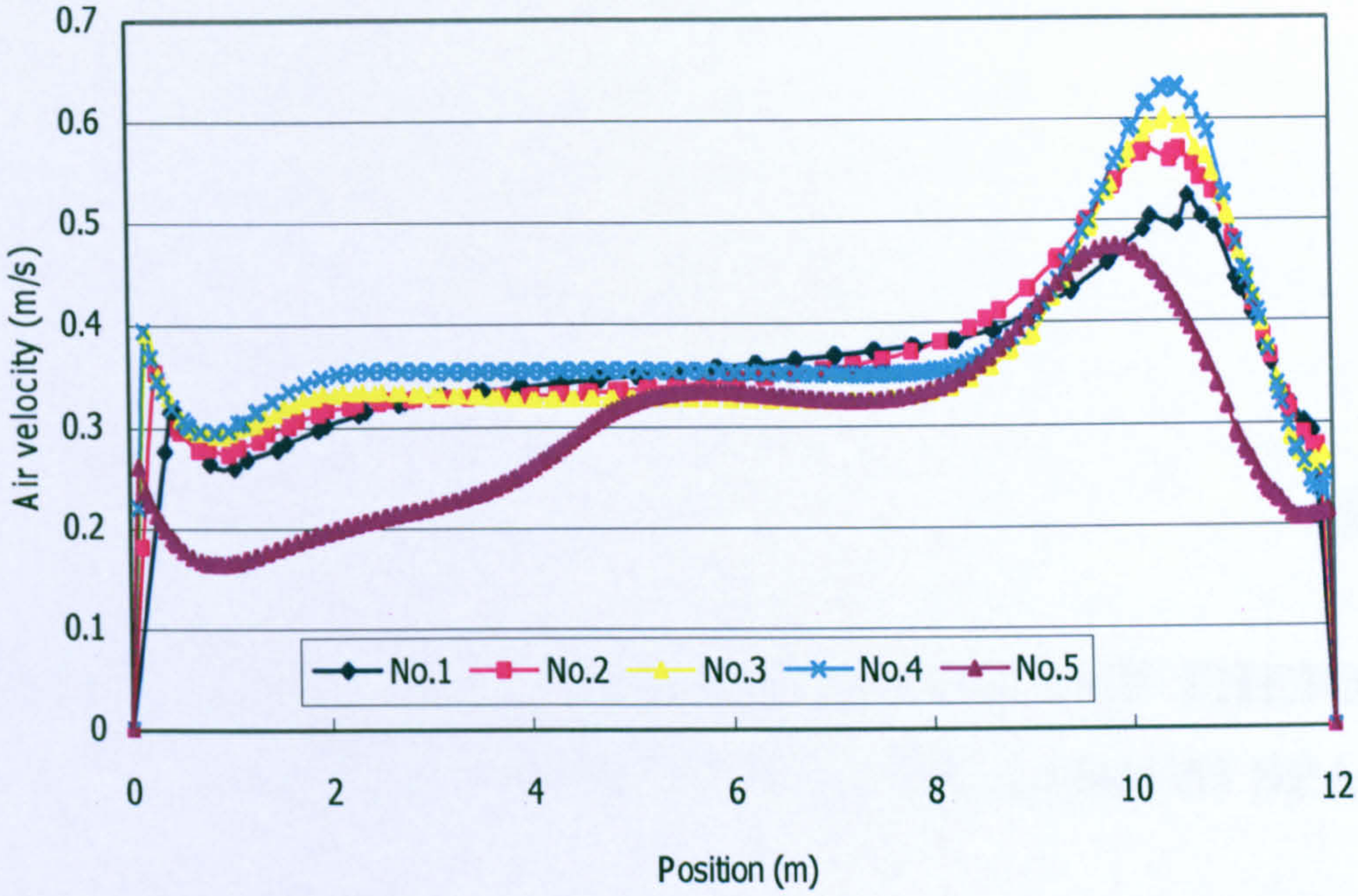

Figure 3.25: Air velocity distributions at the occupants' level of CFD simulations with different gridding systems for combined ventilation

It is shown that, the results predicted by different gridding systems are generally very similar with a discrepancy of less than 5%, although too dense grids may under-predict the air temperatures and velocities of some areas in the space (see Figure 3.24 and 3.25 respectively). Figure 3.24 also shows that the first two gridding systems may underestimate the air temperatures near the ground level of the space. Considering these issues and the balance between accuracy and time cost, grid system No.3 is selected for the use of this research to investigate the combined ventilation in atrium spaces.

3.5 Summary

The method employed for the air movement study of this research was discussed in this chapter. The commonly used research methods, including theoretical and semi-empirical methods, experimental methods and numerical methods were reviewed and CFD was chosen as the main approach for this research, due to its robustness, cheap cost and flexibility for the investigation of design parameters. A commercially available CFD program, FLUENT, will be employed. The settings of FLUENT for various flow regimes, such as wind-induced ventilation, buoyancy-driven ventilation and combined ventilation, were then introduced and validated against well-established theories and recognised experiments. It was shown that, with the settings introduced, CFD can be used to achieve sensible results for the study purposes of this research on air movement in and around buildings, and consequently this tool will be extensively implemented in the next few chapters.

DEVELOPING A NEW METHOD FOR THE THERMAL COMFORT ASSESSMENT OF ATRIUM SPACES

4.1 Introduction

It was stated in Chapter Two that conventional methods for the thermal comfort evaluation in buildings had two difficulties dealing with atrium spaces: firstly, they cannot take solar radiation into account and thus underestimate the mean radiant temperature (MRT) as a result; secondly, the indoor environment has to be assumed as uniform and temperature stratification cannot be accounted for in the space. Focusing on the above issues, this chapter sets out to develop a new method enabling the thermal comfort assessment of atrium spaces.

In order to do this, the environmental parameters of atrium spaces that affect the thermal sensation of occupants, including MRT, air temperature and velocity, should be modelled first and this is dealt with in Section 4.2 with particular attention on the contribution of solar radiation to MRT and the treatment of non-uniform temperature distribution. Since several different techniques are used for the environmental modelling, Section 4.3 describes the approach to integrate the data obtained from various sources in the modelling process in order to realise the assessment. A case study is carried out in Section 4.4 for the demonstration of the application of the new method, and finally Section 4.5 provides a summary for the whole chapter.

4.2 Modelling of the environmental parameters of atrium spaces

It has been made clear in the review chapter that occupants' thermal comfort level is primarily affected by four environmental parameters, which are air temperature, air velocity, mean radiant temperature (MRT) and moisture content (See Section 2.4 for details). Generally speaking, the passive strategies, such as natural ventilation and shading, can modify the first three parameters but their influence on moisture content can be ignored. As a consequence, moisture content is usually considered as constant and obtained from weather station, whilst the air temperature and velocity and MRT need to be modelled.

The following parameters are used as the input for the modelling, and in practice these parameters can be easily accessed at the early stage by measurement or from other prediction tools:

- The building geometry and orientation;
- The sun's position and radiation intensity including that of both diffuse and direct radiation;
- The temperature of each surface;
- The location of glass and its thermophysical properties.

The thermal comfort condition at the lower occupants' level (1.6m high from the ground) will be the only focus for modelling since usually that is the only area occupied. As introduced in Chapter Two, a new code has to be developed for the MRT modelling accounting for the solar radiation and CFD can be used for the modelling of air velocity and air temperature. These two modelling procedures will be introduced respectively in Subsection 4.2.1 and 4.2.2.

As described in the previous chapter, the mechanism for CFD requires discretising the whole computational domain into a large number of small elements, and equations for each element are then derived based on the conservation laws. In order to keep the consistency with CFD for the further assessment of thermal comfort, the MRT code has to use the similar approach to divide the plane at the occupants' level for MRT calculation and the two gridding systems employed by the MRT code and CFD should be the same for the final integration.

4.2.1 Modelling of MRT

Traditional MRT calculation method is based on the radiation transfer mechanism and only the radiative heat transfer from the walls are taken into account. It is derived by using absolute surface temperature and the view factor of each surrounding surface, which can be expressed by the following equation:

$$T_{mrt}^4 = \sum_{i=1}^{j} (F_i \, T_i^4) \tag{4.1}$$

where T_{mrt} is the mean radiant temperature, F_i is the view factor from the point interested to the surface i, T_i is the temperature of surface i and j is the total number of internal surfaces. This formula does not consider the influence of solar radiation and thus cannot be applied to atrium spaces with large areas of glazing.

La Gennusa et al. (2005) derived a new MRT calculation algorithm taking solar radiation into account (assuming that there are only 6 internal surfaces), as shown in Equation (4.2):

$$T_{mrt} = \sqrt[4]{\sum_{i=1}^{6} (F_i \, T_i^4) + \frac{C_{dn}}{\varepsilon\sigma} (\alpha_{irr,d} \sum_{j=1}^{M} F_j \, I_{d,j} + C_s \alpha_{irr,b} f_p I_b)} \tag{4.2}$$

where T_{mrt} is the mean radiant temperature for the grid to be calculated, F_i is the view factor from the grid to the surface i; F_j is the view factor from the grid to the glass surface j; T_i is the temperature of surface i; C_{dn} is day-night coefficient (equal to 1 in the daytime and to 0 in the night time); C_s is the shading coefficient (equal to 1 when the point is hit by the solar beam and to 0 in other cases); ε is the emissivity of the human body; σ is the Stefan-Boltzmann constant; $\alpha_{irr,d}$ and $\alpha_{irr,b}$ are the human beings' absorption coefficient for diffuse and direct solar radiation respectively; $I_{d,j}$ and I_b are the diffuse and direct solar radiation the grid to be calculated receives; f_p is the effective area of the projected area of a person.

Apparently the above equation is too complicated to be solved analytically, thus numerical methods have to be resorted to, i.e. the occupants' level has to be divided into a number of small grids and then the MRT is calculated for each of them respectively, which also means that a computer code has to be used to mitigate the tedious task. The following part will introduce the factors to be determined for the realisation of the thermal comfort assessment and the related approaches for this purpose.

It could be seen from the above equation that the radiant heat transfer generally consists of three parts: the long-wave radiation from the wall, the direct short-wave solar radiation from the sun that penetrates the glass and the short-wave solar radiation diffused from other surfaces. The first part about the radiation from the wall is the same as the traditional method and is determined by the view factor and the surface temperature of each wall. The latter two parts are about the radiation from the sun and the factors to be determined include the day-night coefficient C_{dn} and shading coefficient C_s, the view factors for diffusion radiation calculation

and the solar radiation intensity at the grid. A diagram for the calculation process can be shown as below in Figure 4.1. The procedures for the determination of these factors are introduced as follows.

The determination of the coefficient C_{dn} is straightforward because it is only related to time and the main difficulty will lie in the coefficient C_s, which can be determined by the following approach: with the sun position and space orientation known, a line parallel to the sun rays can be drawn from each grid by the basic knowledge of analytical geometry (one point and one slope determine a line). Then whether this line intersects with the plane of glass is checked and the value of C_s can be designated accordingly: its value will be specified as 1 if they intersect, otherwise it is specified as 0 (as shown in Figure 4.2).

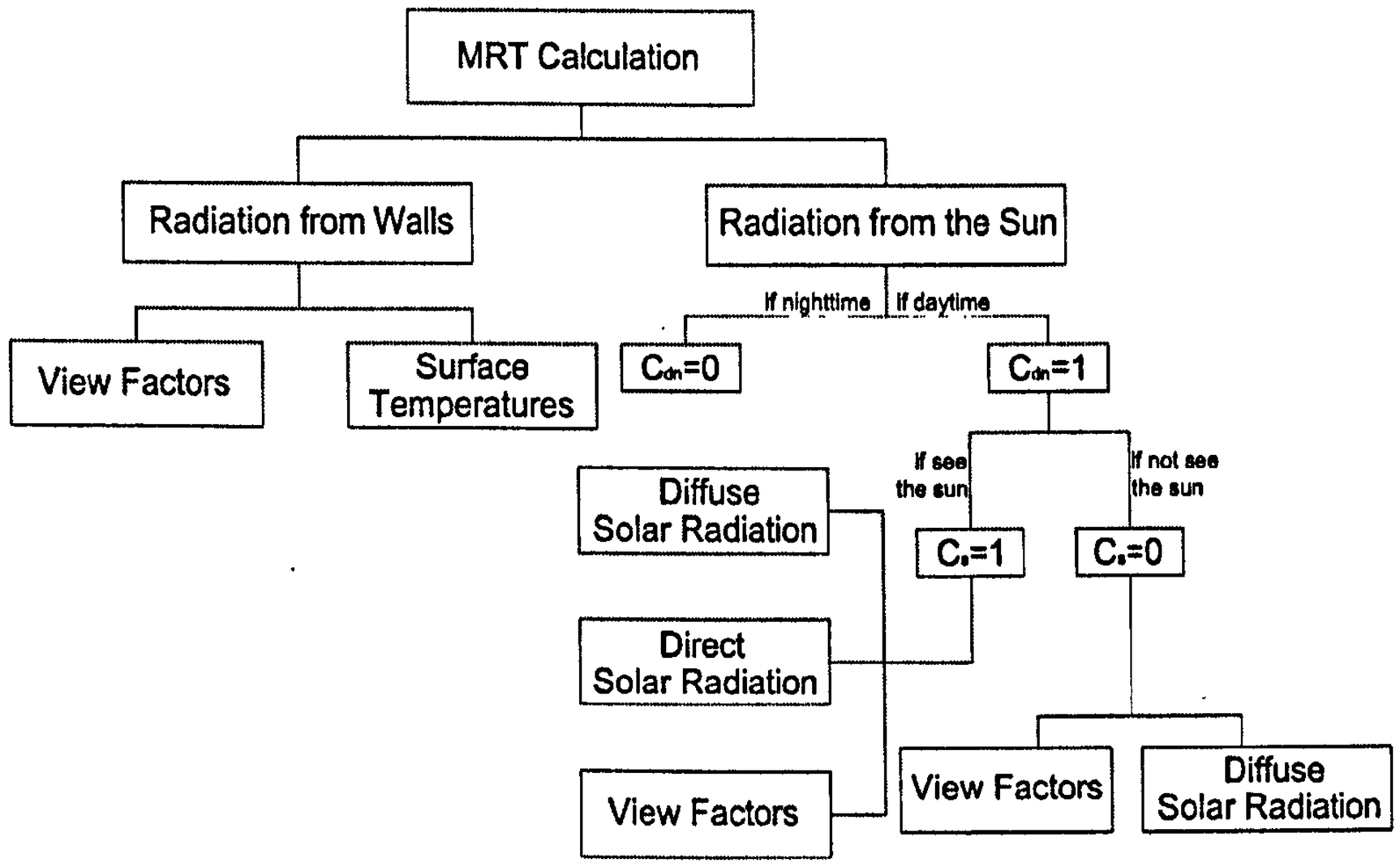

Figure 4.1: A diagram illustrating the process of MRT calculation for atrium spaces

Algorithms for the view factors calculations are based on the work of Hamilton and Morgan (1952). Since only a simple hexahedral building is considered, two kinds of algorithms are needed: one is for horizontal surfaces, i.e. roof and floor, whilst the other is for vertical surfaces, i.e. walls (only the horizontal receiving surfaces are considered in this thesis but the method developed in this chapter can be easily extended for vertical receiving surfaces). View factors for other complicated configurations are also available from other sources[1] but are not discussed here.

For the walls (see Figure 4.3), the view factor for a small element at the occupants' level can be calculated as:

[1] A cataloge of radiation heat transfer view factors can be accessed on the website: http://www.me.utexas.edu/~howell/

$$F = \frac{1}{2\pi}\left[\tan^{-1}\left(\frac{1}{C}\right) - \frac{C}{Y}\tan^{-1}\left(\frac{1}{Y}\right)\right] \tag{4.3}$$

where $A = a/b; C = c/b; Y = \left(A^2 + C^2\right)^{0.5}$.

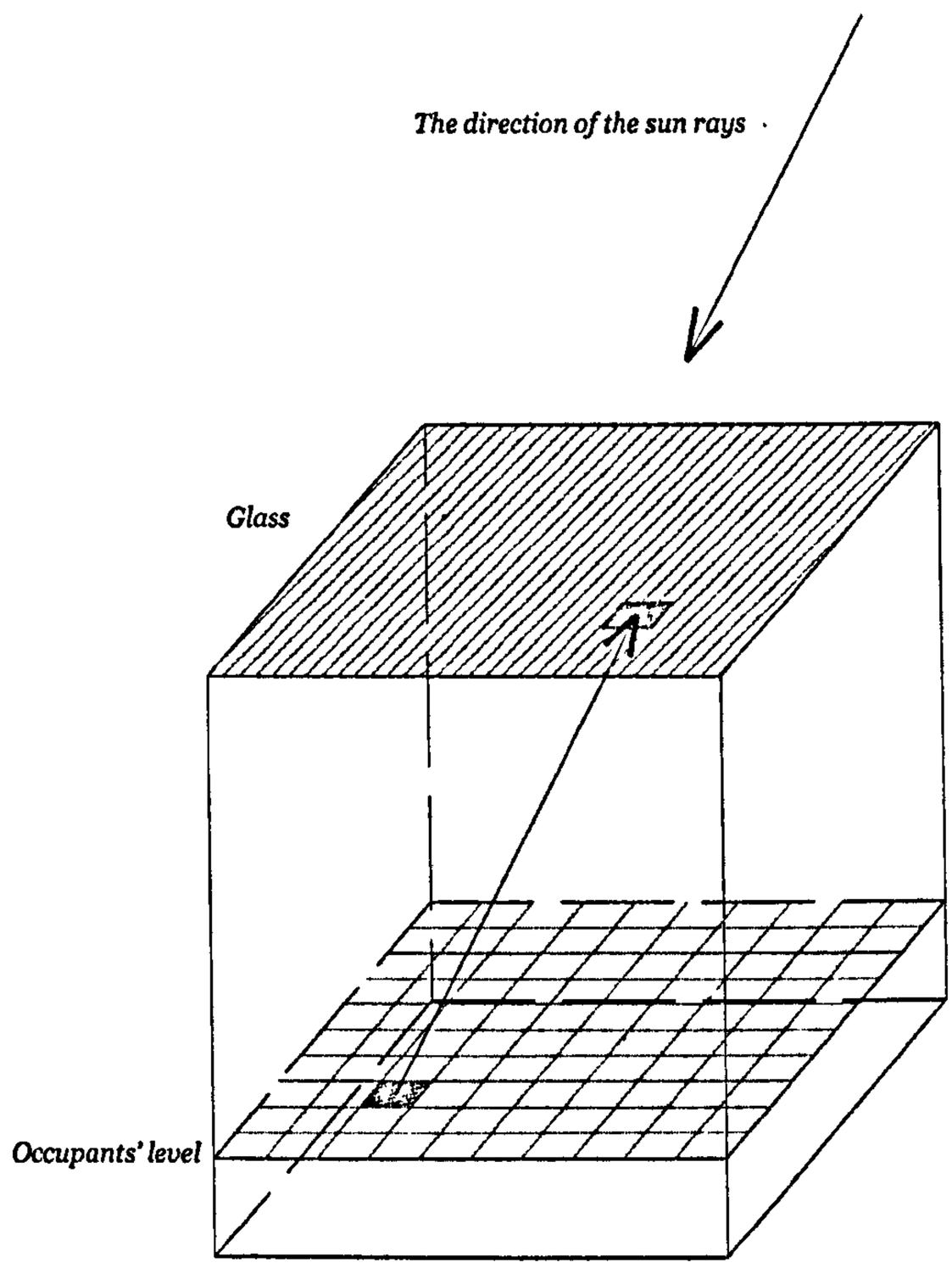

Figure 4.2: A diagram illustrating the process of determining the coefficient C_r (the figure shows an example where the line drawn from the shaded grid at the occupants' level intersects with the top glass surface and thus C_r should be designated as 1)

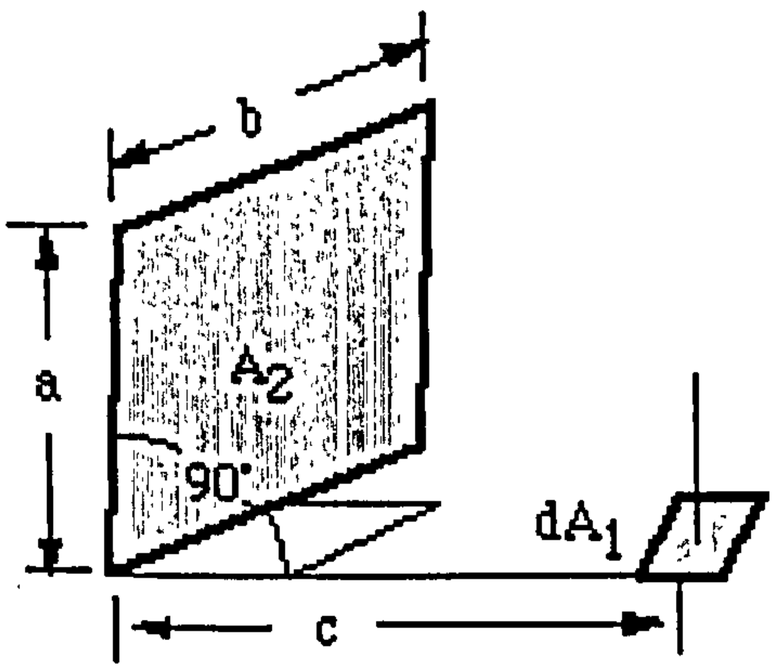

Figure 4.3: Illustration of the view factor calculation for walls

For the view factors to the roof and floor (see Figure 4.4), the following calculation formula can be used:

$$F = \frac{1}{2\pi}\left\{\begin{array}{l} \dfrac{A}{(1+A^2)^{0.5}}\tan^{-1}\left[\dfrac{B}{(1+A^2)^{0.5}}\right] \\ +\dfrac{R}{(1+B^2)^{0.5}}\tan^{-1}\left[\dfrac{A}{(1+B^2)^{0.5}}\right] \end{array}\right\} \tag{4.4}$$

where $A = a/c; B = b/c$.

The solar radiation from the sun that influences the thermal comfort level of an atrium building generally includes two parts: direct radiation from solar beams and radiation diffused from adjacent buildings or surfaces. The heat transfer process when the solar radiation meets transparent surface of a building is illustrated in Figure 4.5, which shows that the solar radiation that is incident on a glass will be separated into several parts, including the reflected, absorbed, penetrated and diffused respectively. The relative proportion of each part is determined by the thermophysical properties of the glass and has been addressed by a number of sources such as (van Straaten 1967; Givoni 1976) but for ordinary glass used in buildings the penetrated part is usually larger than the others. As a consequence, if the sun's position, the radiation intensity and the glass thermophysical properties have been made known at the initial stage, the direct and diffuse solar radiation at the occupants' level can be calculated at an earlier stage. Nevertheless, it should be noted that only the diffused radiation through the glass is taken into account whilst that diffused or reflected short-wave radiation from the walls is ignored. This simplification can be regarded as valid for the MRT calculation since most energy incident on the walls will be absorbed and then transferred as long-wave radiation, whilst the diffused or reflected short-wave radiation only occupies a very small proportion.

Based upon the above analysis, a code is developed to perform the procedures introduced for the MRT calculations at the occupants' level by dividing the occupants' level into a number of small rectangular elements. The detailed code can be found in Appendix C.

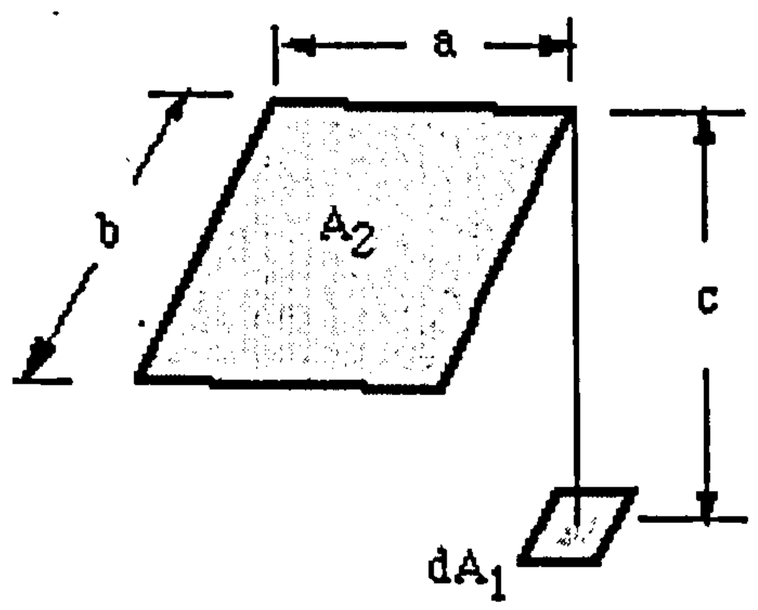

Figure 4.4: Illustration of the view factor calculation for roof and floor

4.2.2 Modelling of air temperature and velocity

The modelling of the air temperature and velocity will be implemented by CFD and the related settings are very similar to those introduced in the validation studies in Chapter Three for different flow regimes. Mostly the evaluation of the thermal comfort level is more significant for sealed atria without ventilation, because when ventilation is incorporated, the air temperature at the occupants' level will be similar to the outside air temperature and consequently the thermal conditions for this circumstance are generally the same as the outdoors (this will be demonstrated in Chapter 6, see Figures 6.4&6.9). For this reason, this subsection is focused on the modelling of sealed atria without ventilation, although the method to be introduced is also applicable for atria with all other types of airflows.

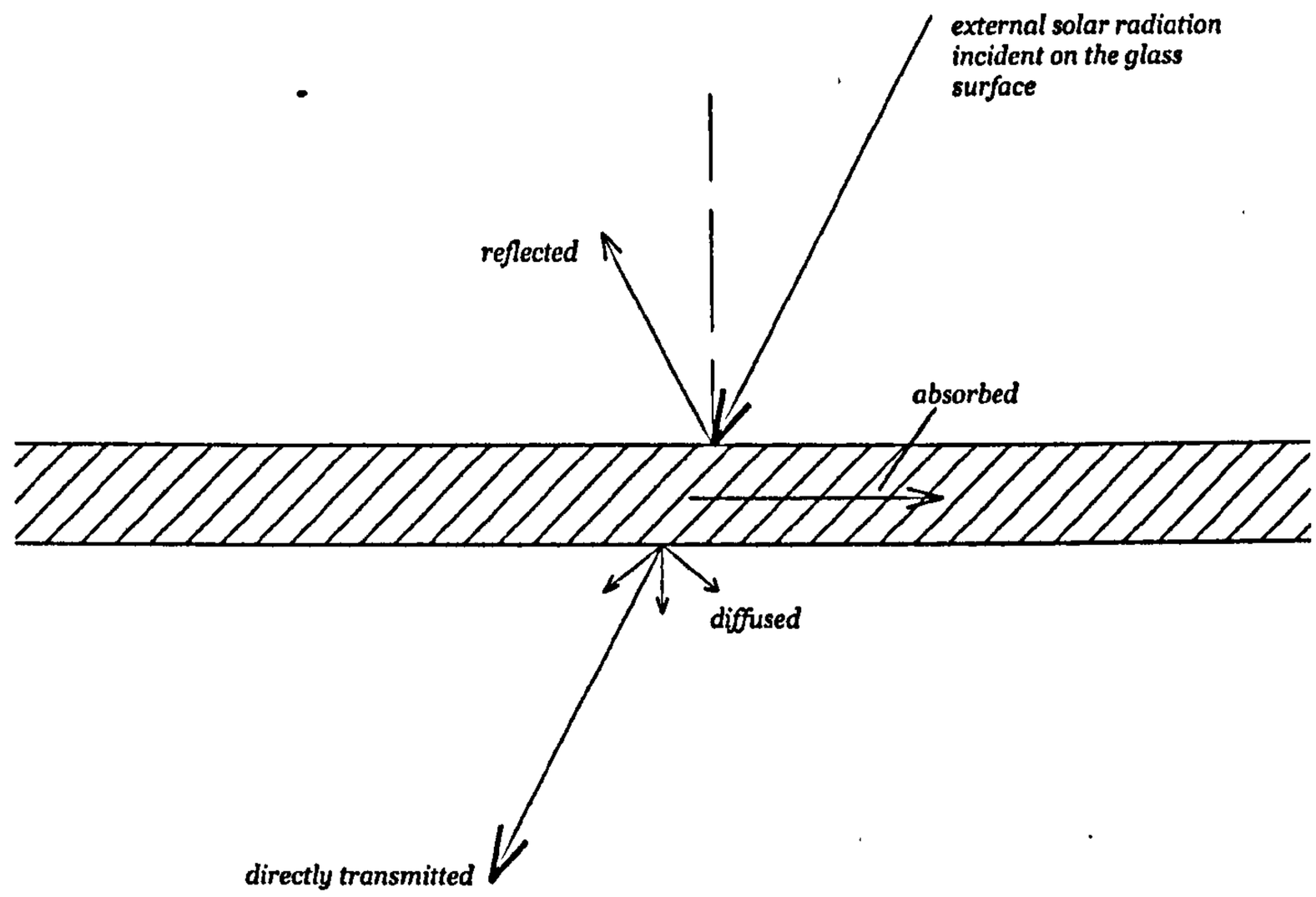

Figure 4.5: Illustration of the heat transfer process when solar radiation impinges on a glass surface

All CFD settings described in the previous chapter for the simulation of internal natural convection are used for this part of study. It should be noted that a non-uniform gridding system was used with dense grids near the boundaries and coarse grids in the middle of the space to achieve more accurate results; nevertheless, this is very difficult to realise for the MRT code and in fact will not be very sensible for the thermal comfort evaluation since the areas in the middle of the space are more likely to be occupied than those at the corners and therefore of more significance from thermal comfort point of view. Fortunately, as the length of the boundary layer near the surfaces are very small compared to that of the edge of building (recall that the grid size near each surface is only 0.5mm and the width of the building is 12m), the

whole gridding system can still be considered as uniform and the environmental data for the boundary layers will be ignored and not used for thermal comfort assessment.

The above subsections introduced the methods and related underlying assumptions for the calculation of MRT and air temperature/velocity respectively. Nevertheless, it should be mentioned that these environmental parameters are actually interrelated in reality: the radiant heat transfer which determines MRT, is also involved in the heat transfer process for walls and air influencing the air temperature and velocity prediction. However, this interaction is generally very small and is usually ignored in practice. This assumption is also adopted in this research to make the problem tractable.

4.3 Thermal comfort assessment of atrium spaces

It was introduced earlier that most thermal comfort indices only consider air temperature as the main factor and ignore the effects of solar radiation. In order to account for this issue, a widely applied thermal comfort indicator that can take the effects of both radiant temperature and air temperature into consideration, PMV/PPD system, will be employed. The detailed calculation formulae are Equations 2.1 to 2.5 in Section 2.4.1.

From the earlier analysis, the air temperature and velocity field at the occupants' level can be obtained from CFD and the MRT field can be computed from the code developed. All other influential factors are assumed to be known. However, a platform is still needed in order to integrate the data from the two analyses. As a high-level language and interactive environment capable of performing computationally intensive tasks, in particular the calculation in relation to matrix, MATLAB is used for this purpose. FLUENT can export the data of air velocities and temperatures from the calculation in ASCII format and then the data can be imported to MATLAB. The code for the calculation for MRT calculation can be directly developed in the MATLAB environment. Thus, all the data obtained can be finally placed together for the PMV/PPD calculation. The code for the PMV/PPD prediction can be seen in Appendix D. An application of these procedures for the thermal comfort assessment of atrium spaces is shown in the following section.

4.4 Application of the new method

4.4.1 A case study

- *Case description*

The geometrical configuration of the case chosen for the demonstration of the new tool is shown below in Figure 4.6. It is an enclosed atrium space surrounded by adjacent parts. The

length, width and height of the space are all 12m. A typical summer daytime, from 9am to 5pm is considered and the main purpose for the study is to diagnose whether air temperature or MRT is the most important factor possibly leading to overheating. The relative humidity is assumed as 50%. As no ventilation is incorporated, air infiltration will be the most significant factor influencing the air velocity at the occupants' level, which is assumed as 0.1m/s. For the PMV/PPD calculation, both of the activity and clothing levels are assumed as 1. Other important data, such as the sun position, solar radiation intensity the surface temperatures for every two hours are listed in Table 4.1.

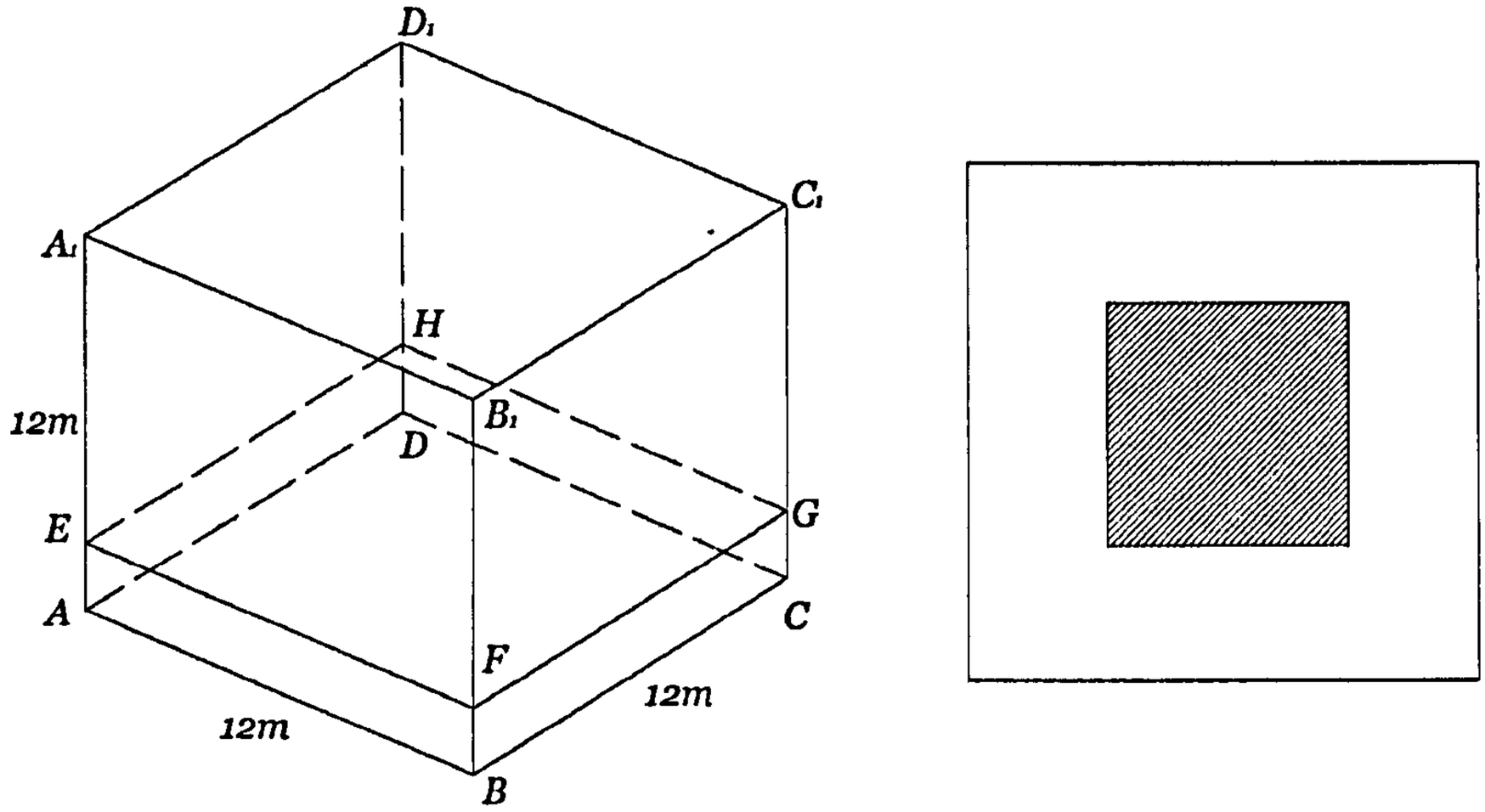

Figure 4.6: Geometrical configurations of the atrium space that is to be used for the illustration of the new method for the thermal comfort assessment (EFGH is the occupants' level)

Table 4.1:Data relevant to the case study

	Surface temperatures (°C)					
	top	bottom	left	right	back	front
9am	21.2	25.3	24.2	23.1	23.8	22.6
11am	35.6	27.2	27.8	26.9	28.2	25.8
1pm	48.7	29.0	32.6	30.7	33.5	28.7
3pm	40.2	28.0	29.3	30.3	31.7	27.6
5pm	36.8	27.2	26.8	28.7	27.8	25.9

	Solar radiation incident on the roof (Wm^{-2})		Sun position	
	direct	diffuse	Azimuth	Altitude
9am	353	102	113.7	43.5
11am	443	186	153.8	56.3
1pm	443	186	-154.7	56.5
3pm	353	102	-115.3	43.8
5pm	86	20	-88.4	26.4

- *MRT calculation*

The results of the MRT calculation for each time step are shown below in Figures 4.7 to 4.11. It can be seen that, the MRT of the areas that the sun can irradiate is much higher than that of the area that the sun does not irradiate: usually 10°C or even higher depending on the radiation intensity and surface temperatures. If the whole surface is not irradiated (e.g. Figure 4.11), the MRT distribution has very small variation: only 2 degrees. This actually suggests that, solar radiation has a more significant contribution to the MRT than the surface temperatures. By comparing the MRT distribution at 9am and 3pm (or 11am and 1pm) when the solar radiation for both is the same, the increase of MRT is generally much smaller than that of roof temperature; and when there is no solar radiation, the MRT reduces significantly: the maximum MRT can reach up to around 310K when where is solar radiation at the occupants' level (see Figures 4.7 to 4.10) whilst the maximum MRT is only 302.2K when the sun cannot irradiate the occupants' level.

It is also observed that, the position with the highest MRT is usually in the middle for both shaded areas and irradiated areas when the roof temperature is the highest among all surfaces or intensive heat transfer is diffused at the roof glass: this is because these areas have the largest view factor to the roof surface at this level of height. The position with the lowest MRT is located at the shaded corner between two walls with the lowest surface temperatures.

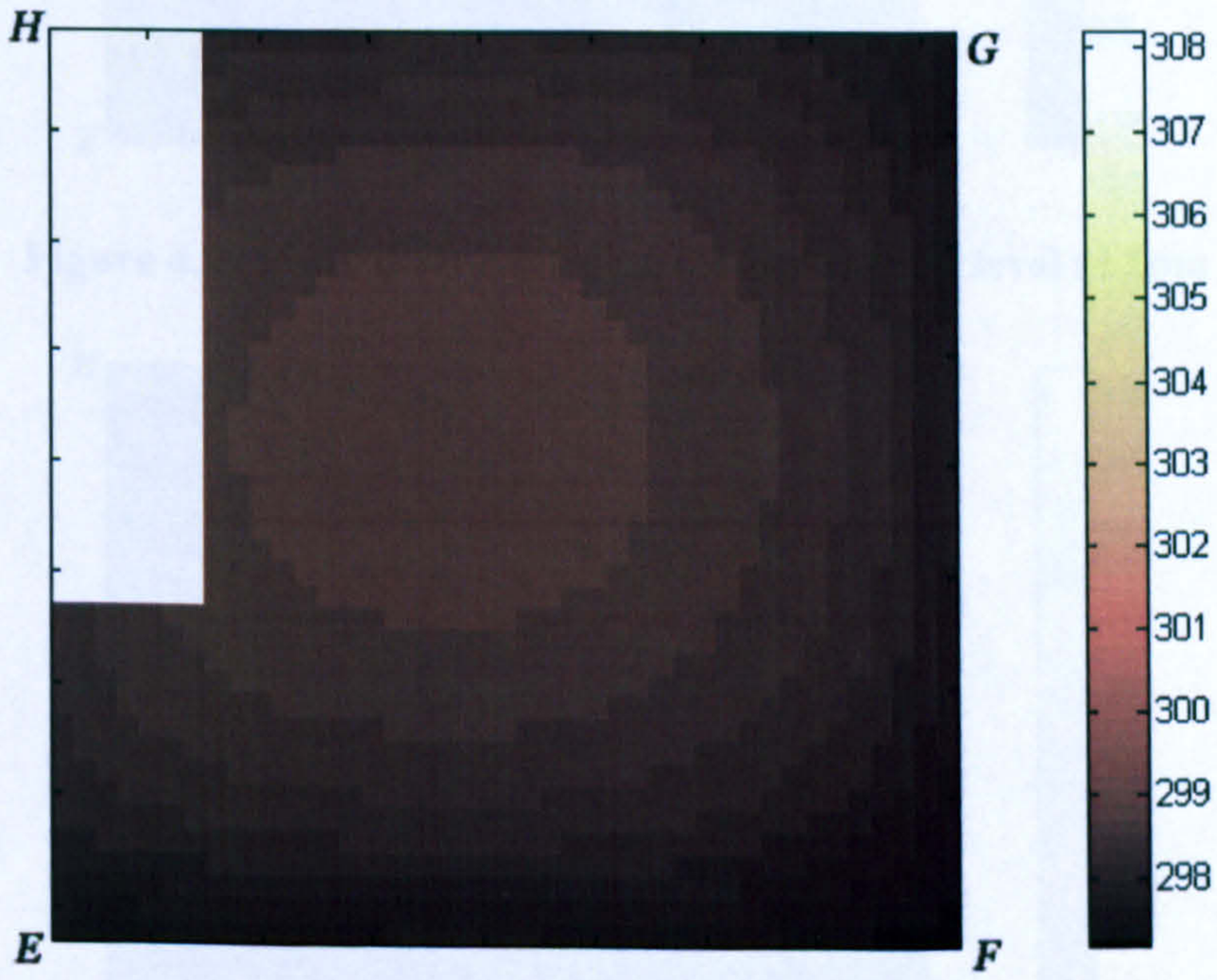

Figure 4.7: MRT distribution at the occupants' level at 9am

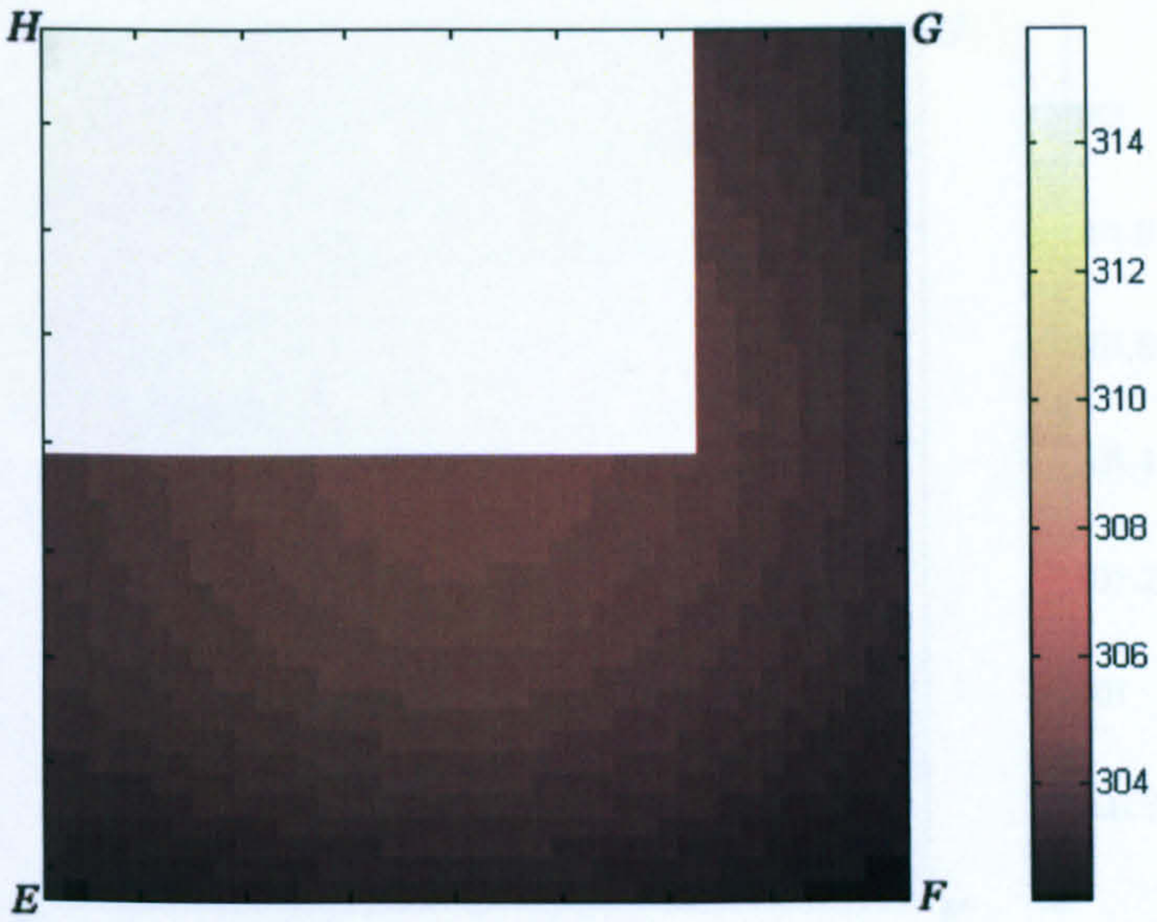

Figure 4.8: MRT distribution at the occupants' level at 11am

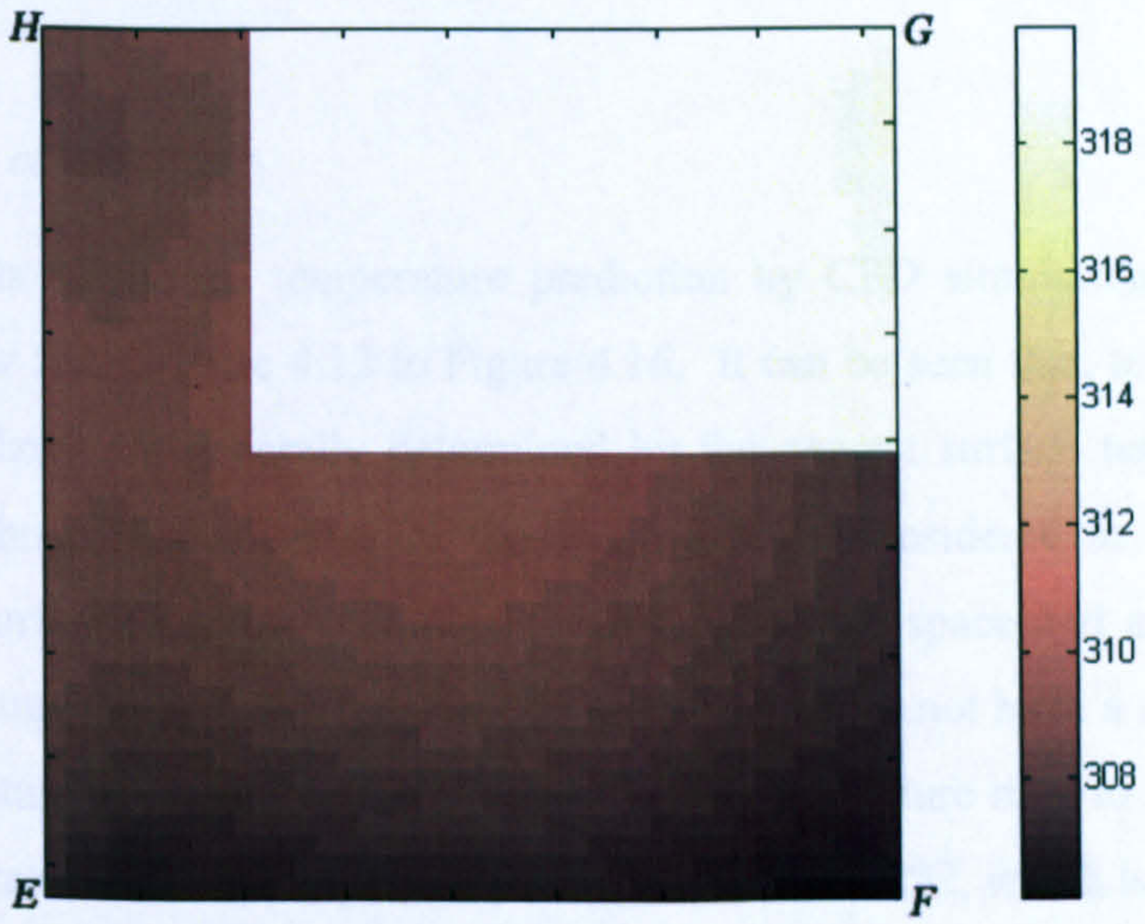

Figure 4.9: MRT distribution at the occupants' level at 1pm

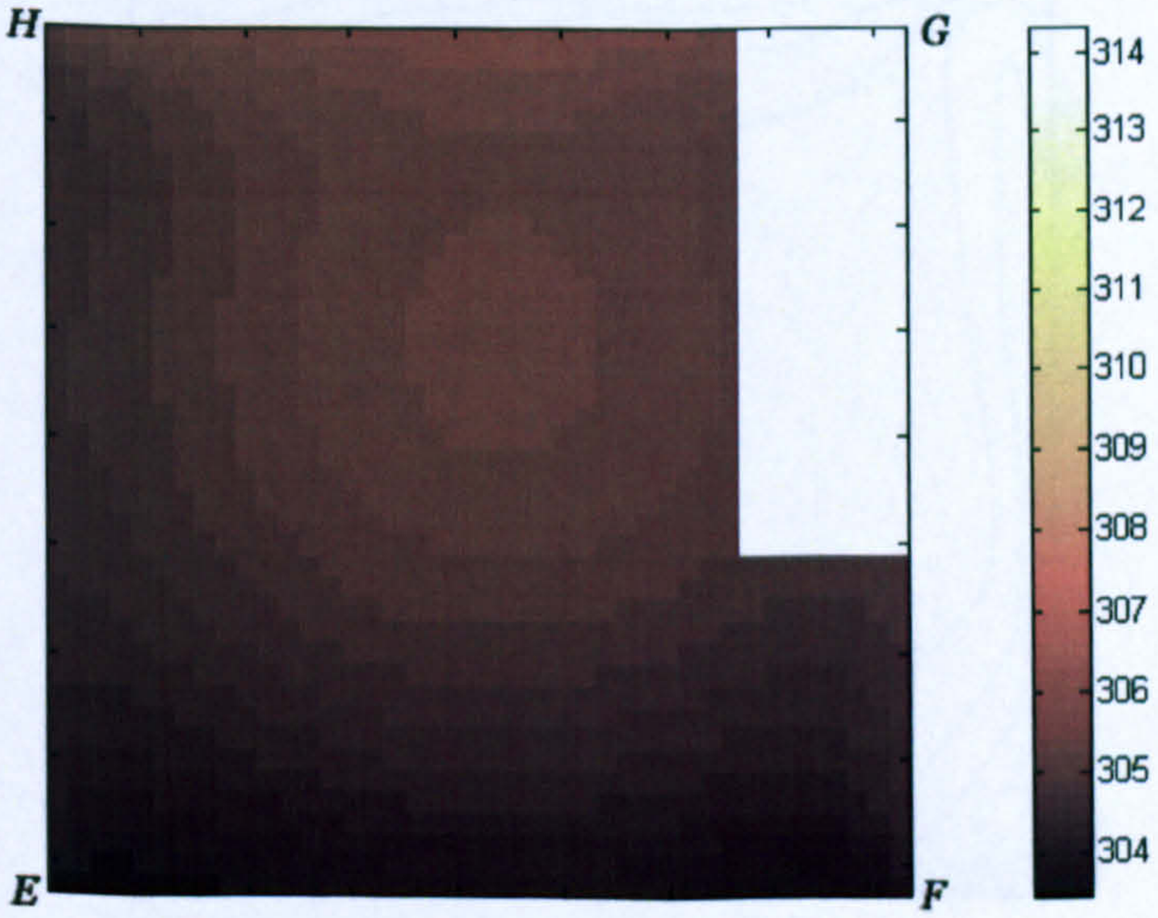

Figure 4.10: MRT distribution at the occupants' level at 3pm

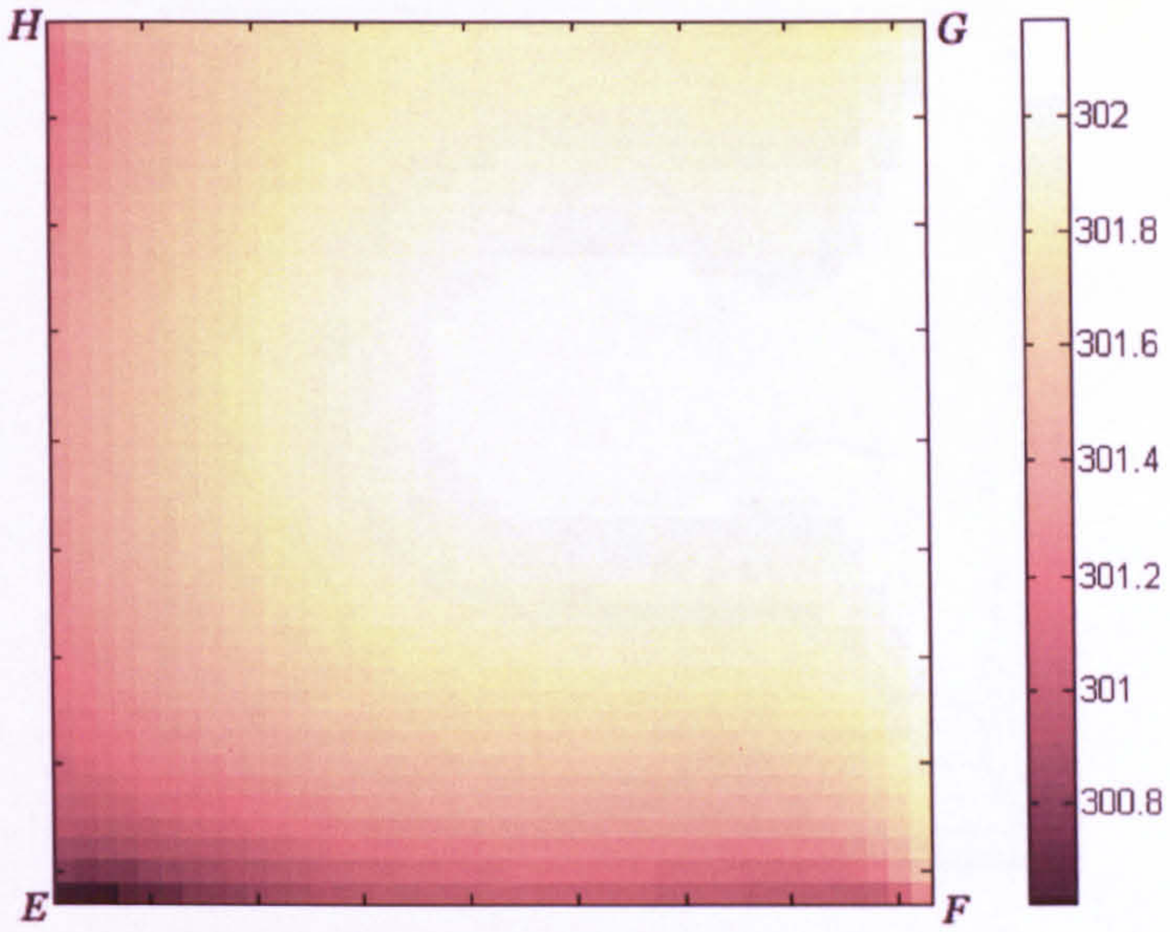

Figure 4.11: MRT distribution at the occupants' level at 5pm

- *Air temperature calculation*

The results of the air temperature prediction by CFD simulation for each time are presented as below from Figure 4.12 to Figure 4.16. It can be seen that, temperatures of those grids at the periphery are generally determined by the nearest surface temperatures, and the temperatures of those in the centre of the space can be considered as the average of the temperatures of surfaces nearby, including the bottom of the space and also the surrounding walls. This also suggests that, the temperature of the roof does not have a significant influence on the air temperature at occupants' level. Even if the temperature rises to nearly 50°C at 1pm, the highest temperature of the occupants' level is still around 32°C, which is close to the highest surface temperature at that time (the temperature of the back surface is 33.5 °C).

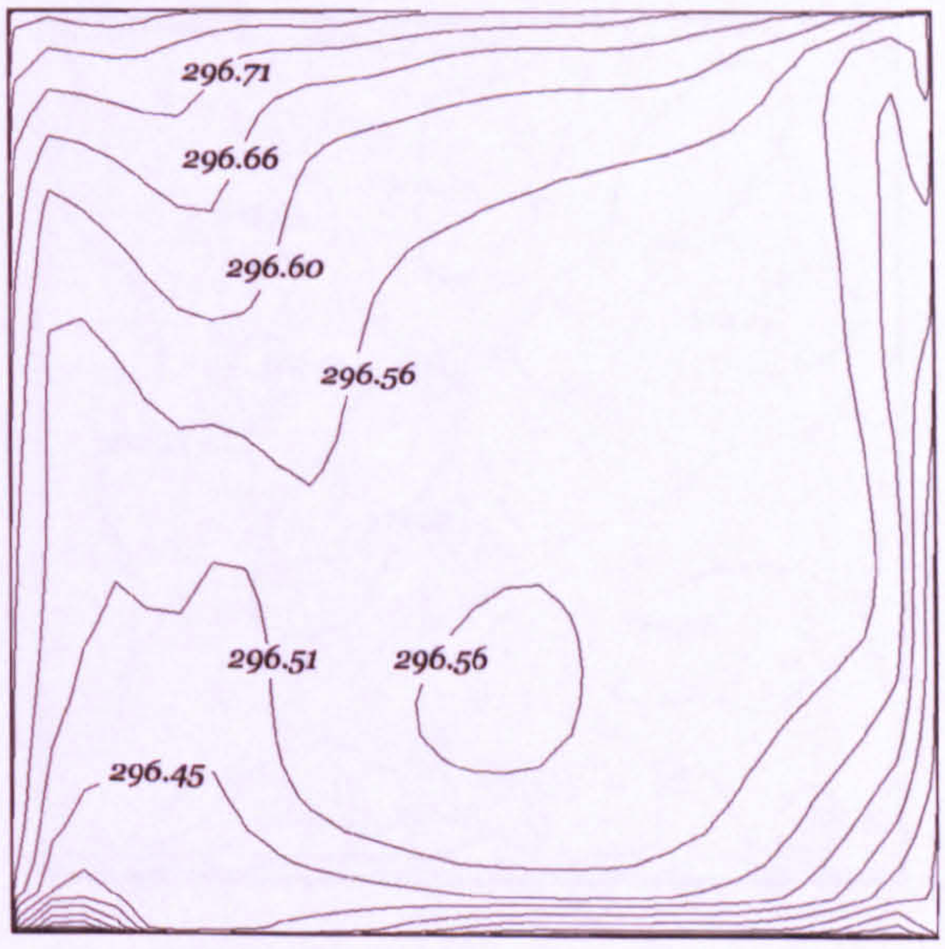

Figure 4.12: Air temperature distribution at the occupants' level at 9am

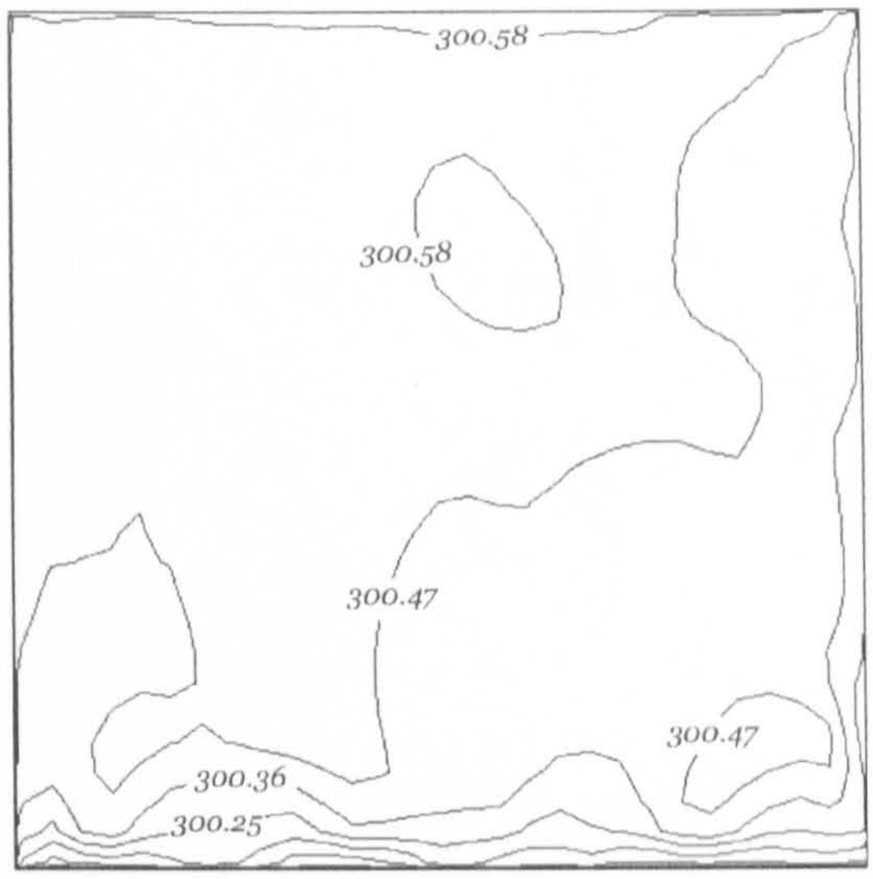

Figure 4.13: Air temperature distribution at the occupants' level at 11am

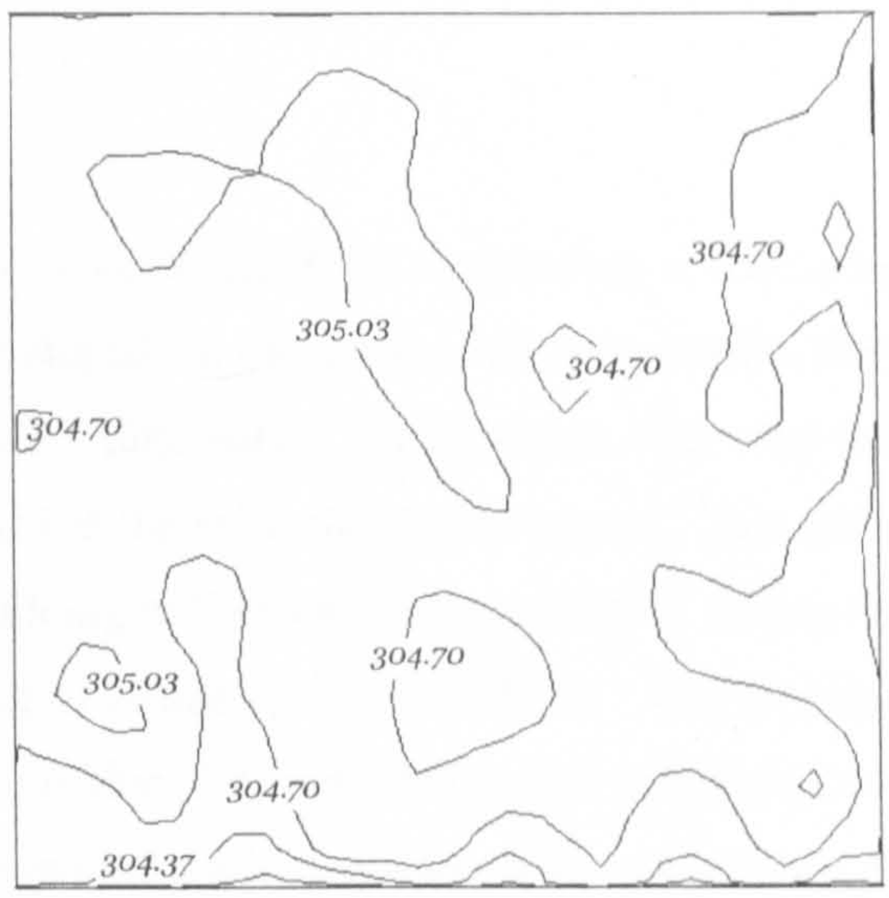

Figure 4.14: Air temperature distribution at the occupants' level at 1pm

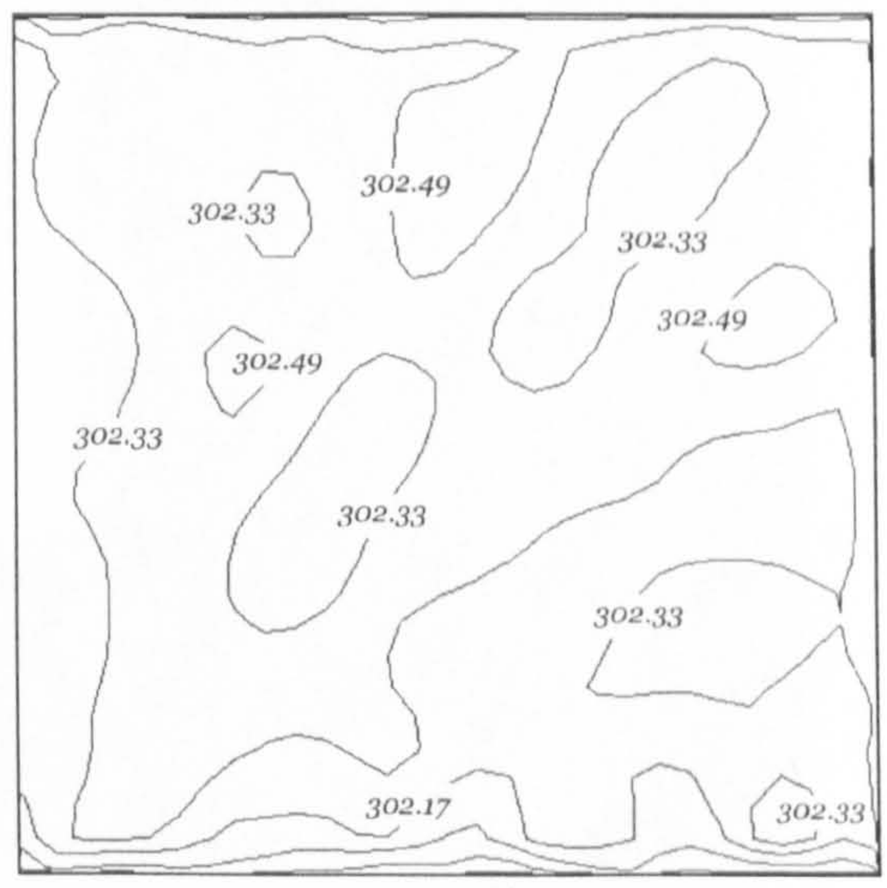

Figure 4.15: Air temperature distribution at the occupants' level at 3pm

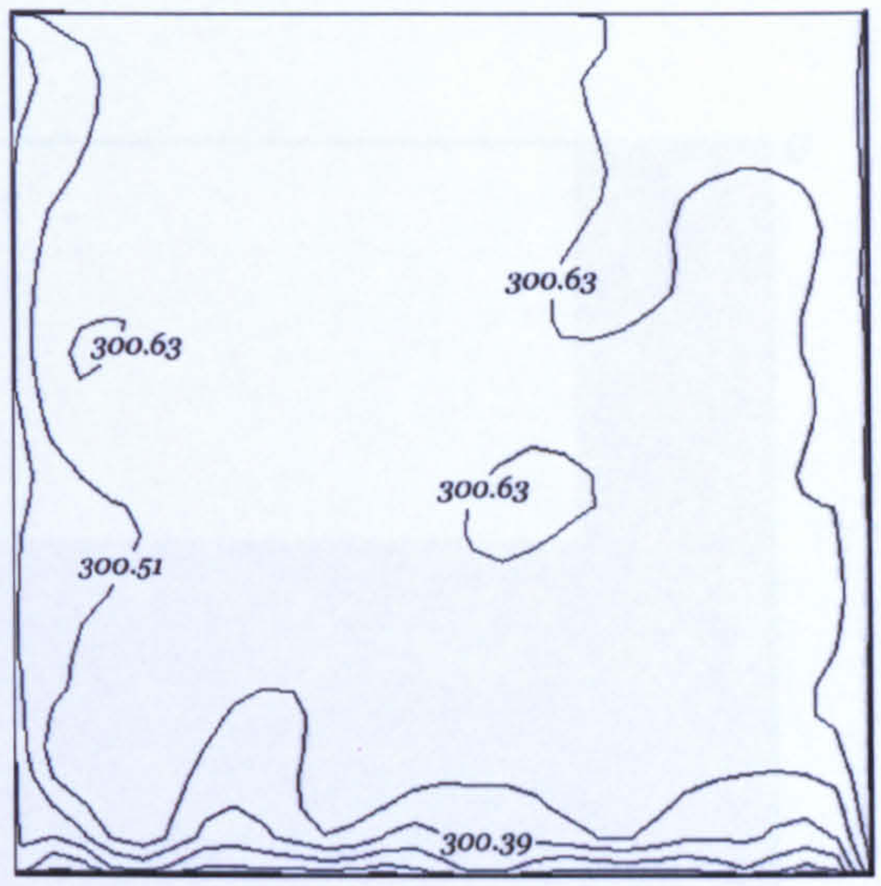

Figure 4.16: Air temperature distribution at the occupants' level at 5pm

- *PMV/PPD calculation*

Figures 4.17 to 4.21 show the PMV distribution at the occupants' level for each time step by using the tool developed. It can be seen from the results that the PMV distribution has the same pattern as the MRT distribution, which means that solar radiation that comes into the building through the glass has the most significant impact. This also suggests that, without any passive strategies, this building will experience overheating during the period simulated and the main cause of overheating of atrium space is the MRT. The greenhouse effect, that used to be considered as the biggest problem for overheating, also contributes to the thermal discomfort, as it raises the surface temperatures and hence internal air temperature, but its significance is much weaker.

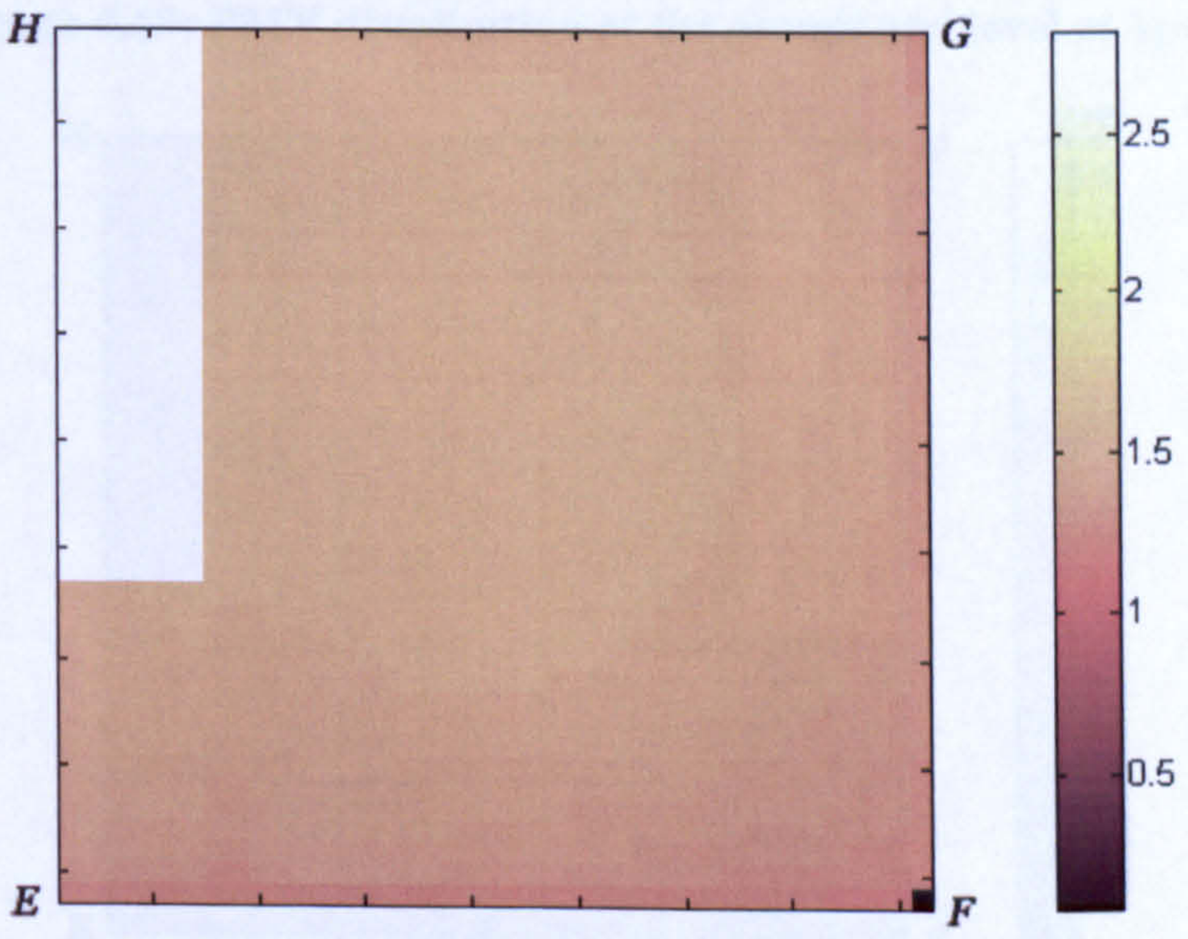

Figure 4.17: PMV distribution at the occupants' level at 9am

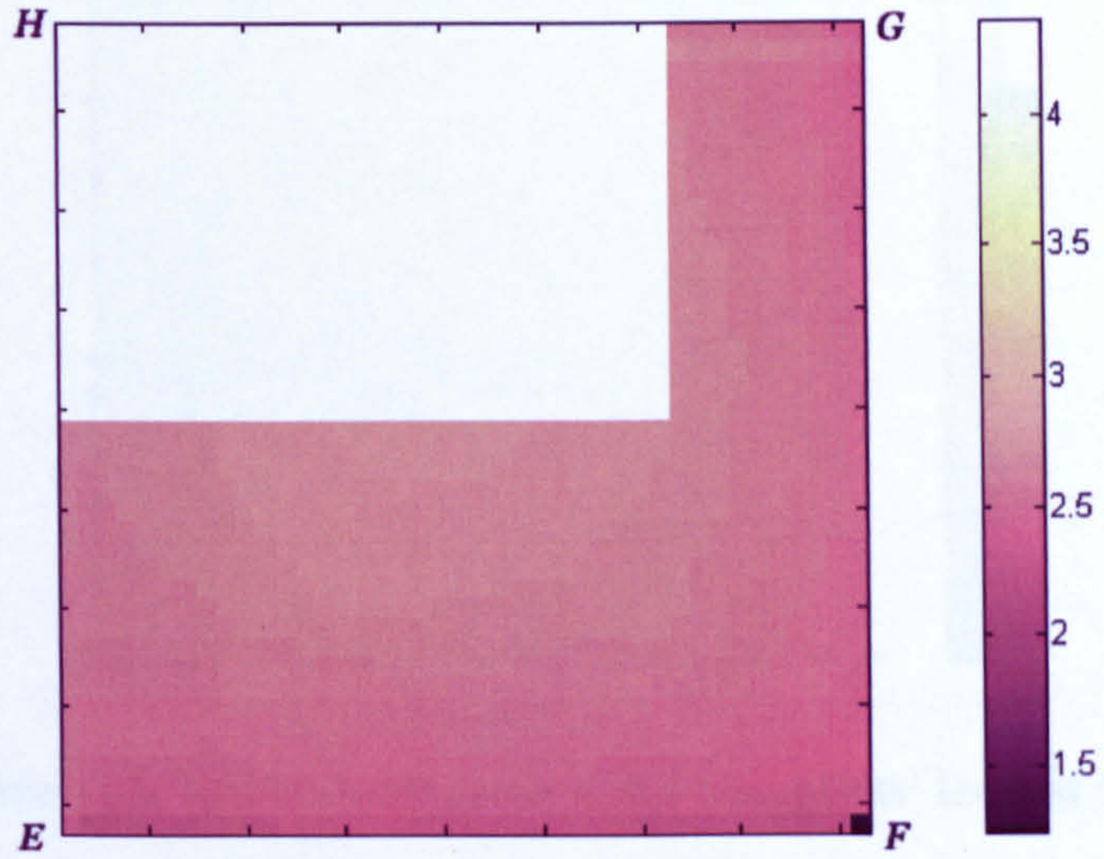

Figure 4.18: PMV distribution at the occupants' level at 11am

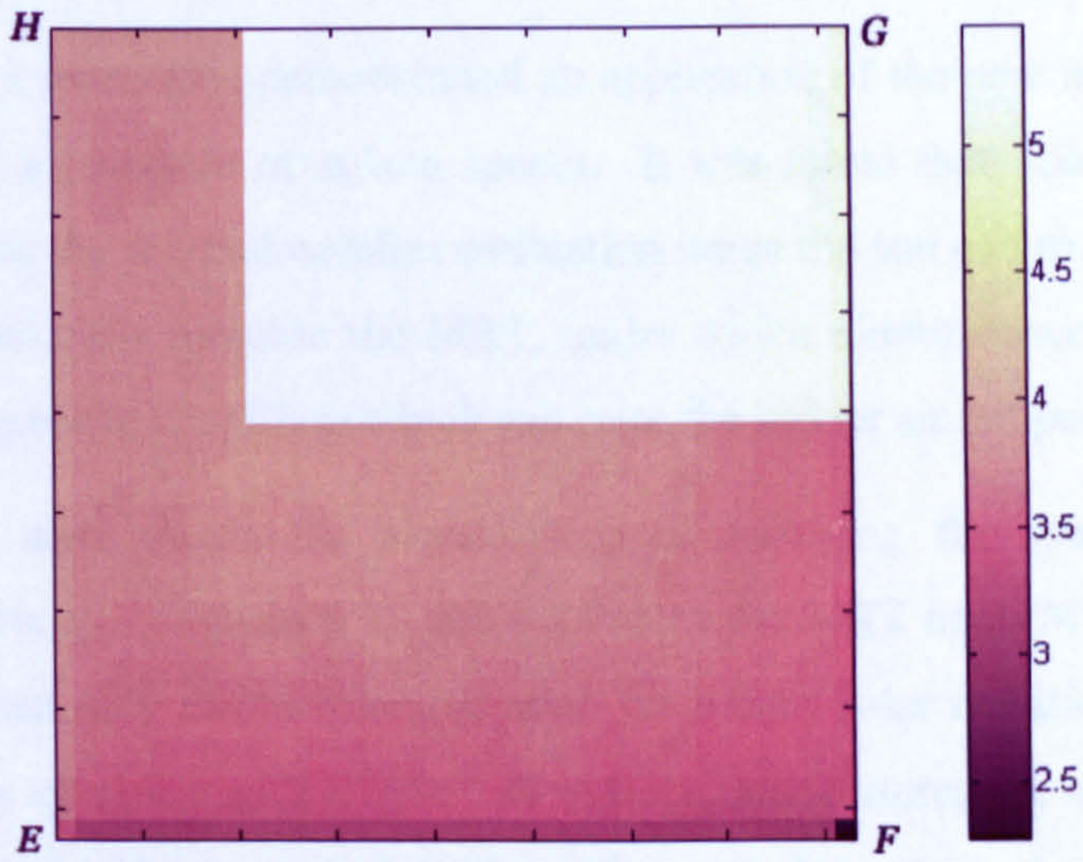

Figure 4.19: PMV distribution at the occupants' level at 1pm

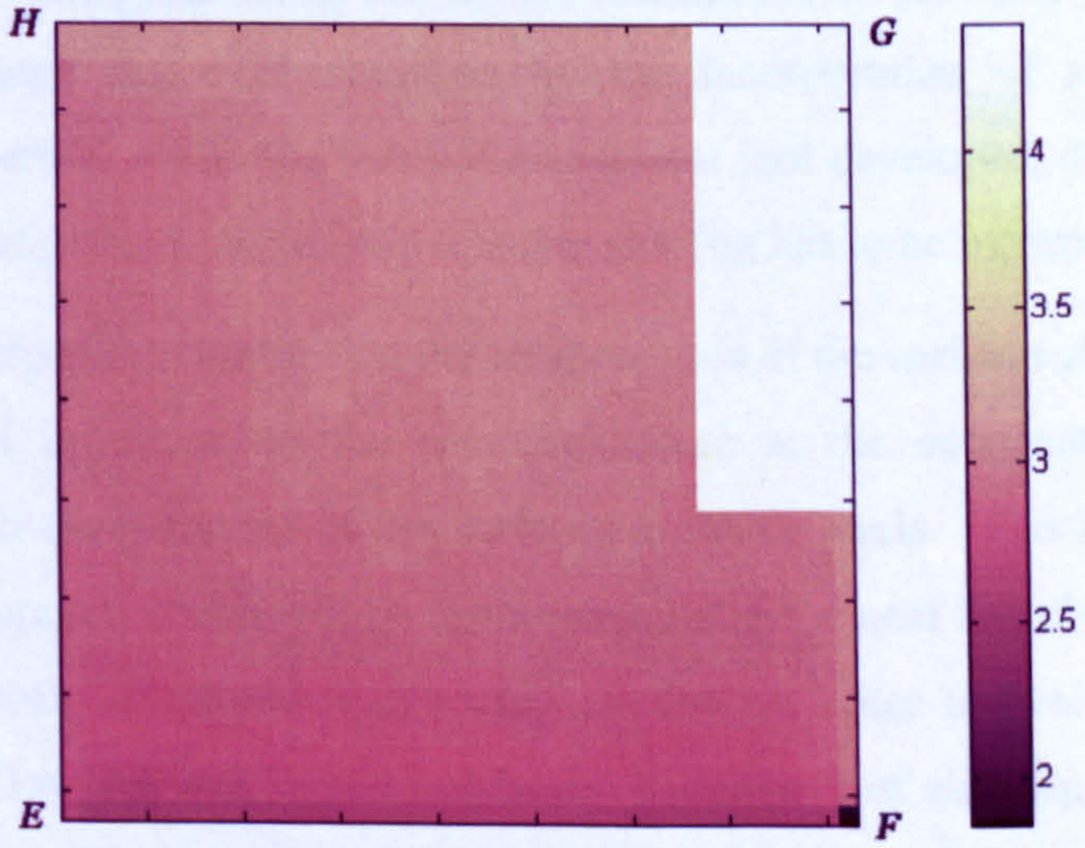

Figure 4.20: PMV distribution at the occupants' level at 3pm

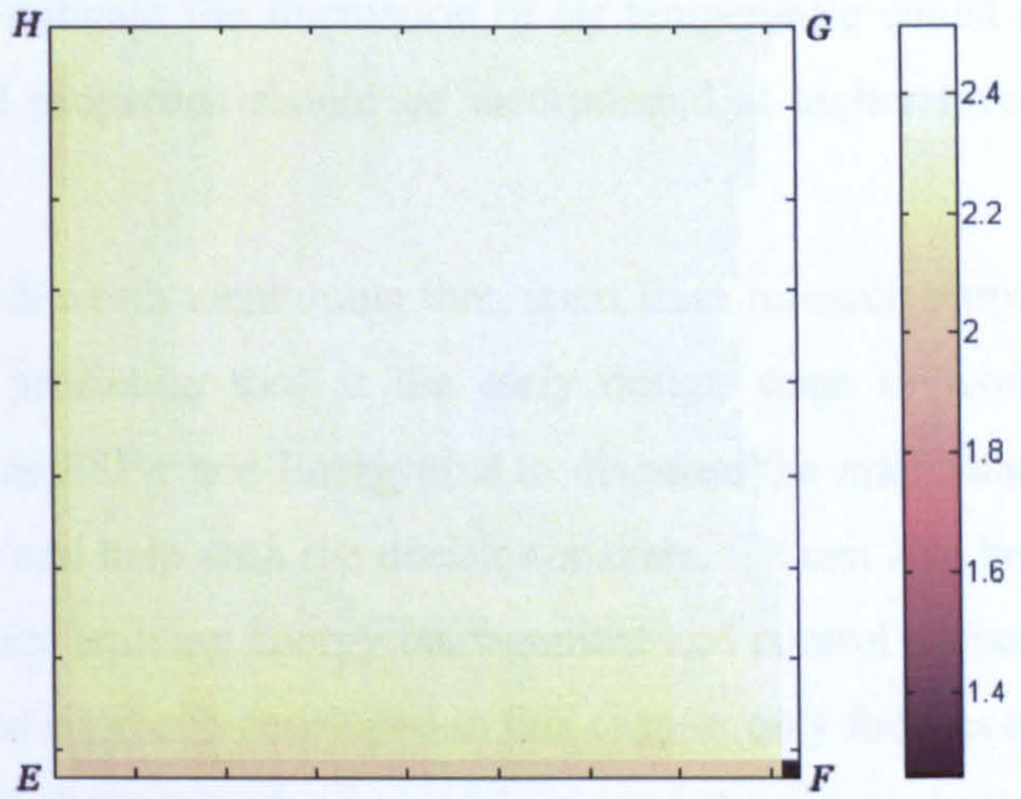

Figure 4.21: PMV distribution at the occupants' level at 5pm

4.4.2 Discussions

The previous subsection demonstrated an application of the new method developed for the thermal comfort assessment of atrium spaces. It was found that, solar radiation has very significant impacts on the thermal comfort evaluation when the sun can irradiate the occupants' level as it can dramatically increase the MRT, under which circumstance its effects are more influential than the greenhouse effects which can raise the indoor air temperature.

This result also shows the significance of selecting the glass with appropriate thermophysical properties. Figures 4.22 and 4.23 show the MRT and PMV distributions at the occupants' level when only direct solar radiation or diffuse solar radiation is considered (the radiation intensity is specified as $300W/m^2$; all surface temperatures are assumed as 24 °C and all other environmental and geometrical configurations are the same as the case study for 11am). It is shown that thermal discomfort will occur when the direct radiation is $300W/m^2$ (see Figure 4.22) but it does not take place when the diffuse radiation is of the same intensity (see Figure 4.23), and this change can easily realised by the incorporation of a glass with certain thermophysical properties. With the thermal assessment tool developed, designers will be able to decide what type of glass is needed and whether shading has to be incorporated.

It was also brought to notice that the temperatures of the surfaces at the upper levels did not have significant influence on the air temperature at the occupants' level: it is only determined by the air temperatures of the surfaces at lower levels. This is also the fact when ventilation is incorporated, which will be further studied in the next few chapters. This finding, together with the result introduced above suggests that, in order to avoid overheating in the space, the design of lower levels should emphasise the control of air temperature whilst that of upper levels should emphasise that of the MRT. As a consequence, in order to maintain the thermal comfort at the occupants' level, thermal mass should be used as the main materials for

the lower surfaces to mitigate the fluctuation of air temperature whilst shading or glass with proper thermophysical properties should be incorporated at higher levels to avoid too much direct solar radiation.

In addition, it is worth mentioning that, apart from research purposes, this new method can be applied as a prediction tool at the early design stage to work with other thermal simulation tools such as ESP-r and Energyplus to diagnose the main causes of the overheating problems of buildings and help with the decision-makers. It can also be used as a monitoring tool in real buildings for building energy management and control purposes. It should also be noted that, although the approach developed in this chapter only focuses on the thermal comfort level at the bottom of the space, it is possible to use the same strategy to deal with other conditions where the emphasis is changed to other parts of the large volume space.

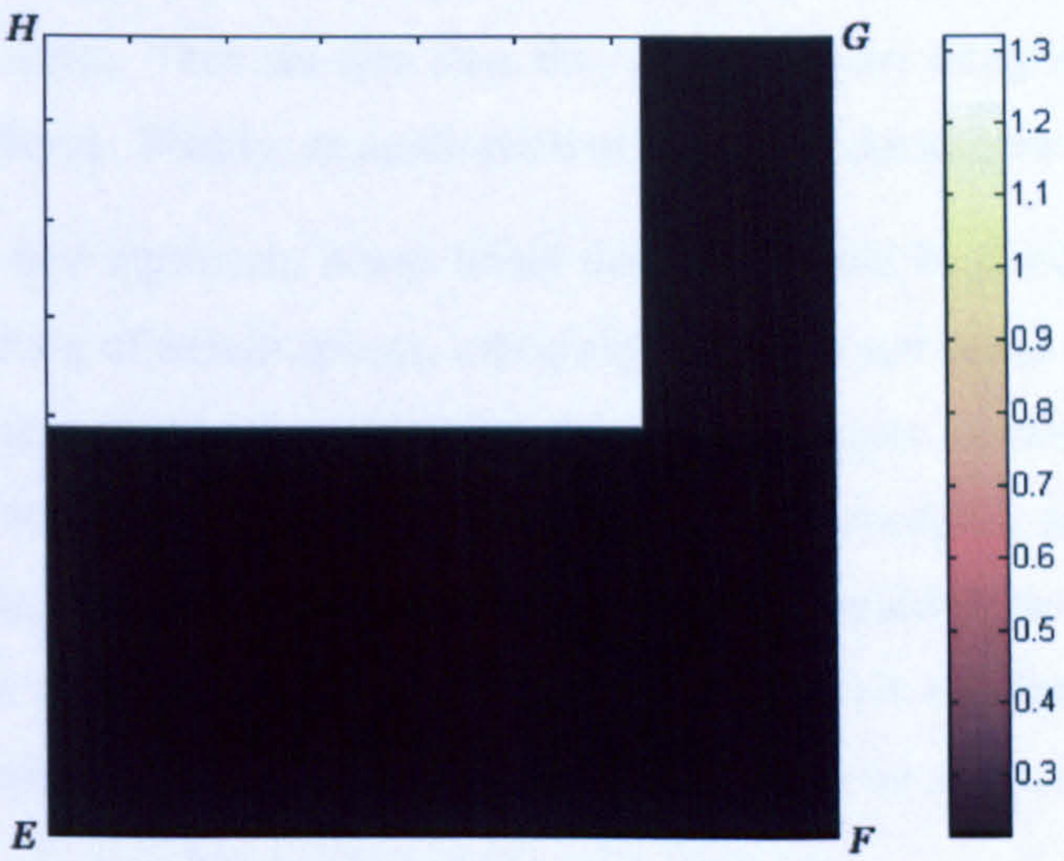

Figure 4.22: PMV distribution at the occupants' level when the direct solar radiation intensity is 300 W/m^2 and the diffuse solar radiation intensity is 0

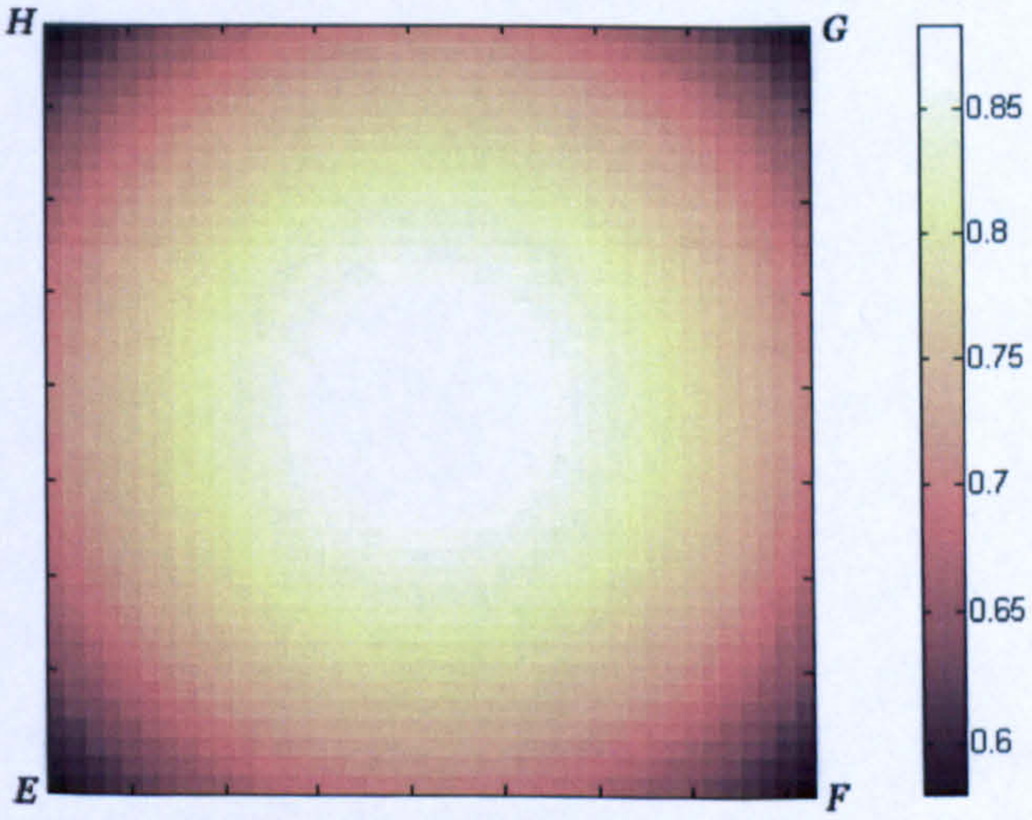

Figure 4.22: PMV distribution at the occupants' level when the diffuse solar radiation intensity is 300 W/m^2 and the direct solar radiation intensity is 0

Furthermore, it is also hoped that the findings in this chapter can help to develop new adaptive thermal comfort models in atrium spaces. It has already been mentioned that the adaptive models are focused on the air temperature as the primary indicator, but in atrium spaces the MRT will be equally important. Therefore, if adaptive models are going to be developed for free-running atrium buildings, MRT should be incorporated in the models.

4.5 Summary

A new tool for the evaluation of thermal comfort level in atrium spaces has been developed in this chapter. The temperature and velocity field is obtained from CFD and a code is developed for MRT calculation based upon the combination of solar radiation and radiant heat transfer from the walls. Then the data from the two sources are integrated using MATLAB as the exchanging platform. Finally, an application of the tool is demonstrated by a case study.

Based on this new approach, it was found that MRT could be a more significant factor leading to the overheating of atrium spaces, especially when the sun could directly irradiate the occupants' level, which means that the most important passive cooling strategy for this circumstance would be the provision of shading devices or changing glass thermophysical properties. In addition, it was also shown that the air temperature at the occupants' level is mostly affected by the temperatures of the surfaces at lower levels and the temperatures at the roof level and the upper areas generally have little influence on the air temperature at the occupants' level.

WIND-INDUCED NATURAL VENTILATION IN ATRIUM SPACES

5.1 Introduction

Having developed a new method for the thermal comfort assessment of atrium spaces in Chapter Four, the next three chapters will be focused on the study of natural ventilation as a passive cooling strategy for atrium buildings with the tool selected and validated in Chapter Three. This chapter concentrates on the investigation of wind-induced natural ventilation, and the subsequent two chapters will deal with buoyancy-driven natural ventilation and combined ventilation respectively.

Chapter One demonstrated that airflow pattern, air velocity distribution and turbulence intensity are the key factors for the evaluation of the ventilation performance of a space, and as introduced in Chapter Two, the most important design parameters that influence these factors include roof shape, adjacent buildings and opening characteristics. The investigation of the impacts of these parameters will be the main concern of this chapter, and in particular, the effects of the roof design will be the primary emphasis. Nevertheless, considering the large numbers of possible variations consisted of the above parameters, a thorough study of all scenarios is next to impossible. As a result, a basic configuration, based on which alterations can be made for comparison, is employed for the parametric study, as shown in Figure 5.1. It is a composition of a cubic building with a width of $12m$ and a height of $12m$ and a roof, and there are two openings at the roof level. Research will be extended to other atria with more complicated configurations when the basic version has been sufficiently understood.

This chapter starts with a basic analysis of the airflow around a cubic building in Section 5.2 and tries to identify the possible flow patterns in atrium spaces, based on which the effects of the design parameters can be studied. Sections 5.3 to 5.6 investigate the design parameters and each section deals with one parameter respectively. Design guidelines are produced in Section 5.7 based on the outcomes of the investigations and the findings are also extended to other related scenarios.

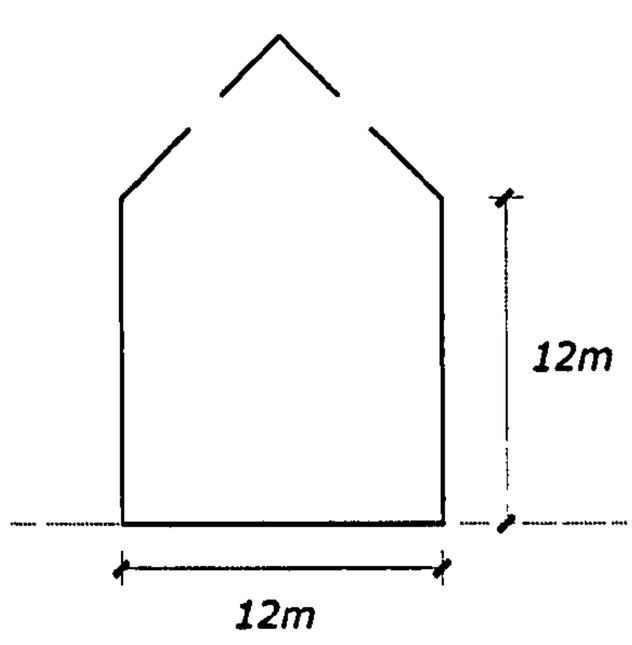

Figure 5.1: Schematic illustration of the basic configuration for wind-induced natural ventilation study

5.2 Preliminary analysis

In order to better understand the driving forces for the air movement in atrium spaces, a basic analysis of the airflow around a cubic building is first carried out based on which the possible flow patterns in atrium spaces with two roof openings can be defined.

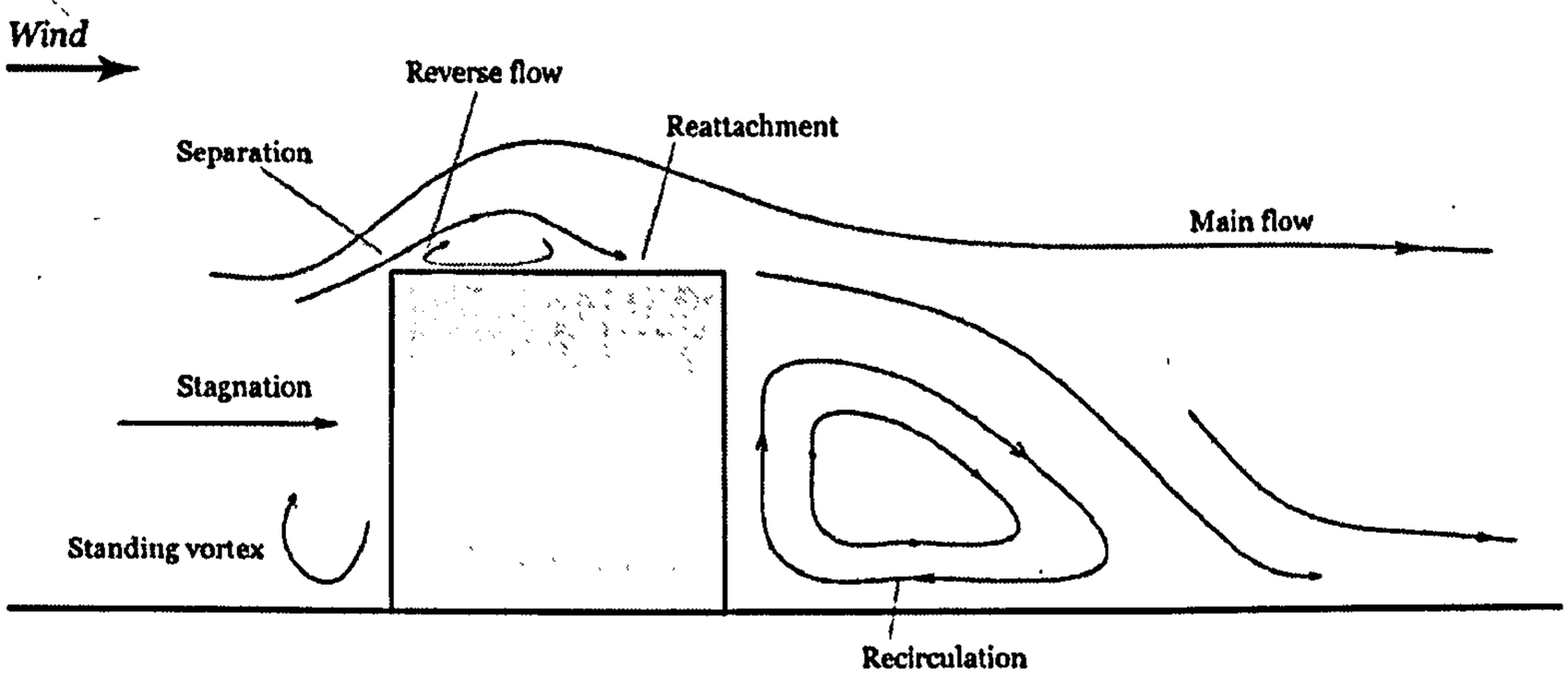

Figure 5.2: The airflow around a cubic building

It can be seen from Figure 5.2 that, for a sealed building, the oncoming wind blows from the left hand side and separates at the roof level when it meets the building because of the sharp corner. This results in a stagnation area at the lower level near the ground in front of the

building, and as the main flow over the building has an angle from the top surface rather than being parallel to it, a reverse flow is produced between the main flow and the roof. The flow will reattach to the roof after a certain distance and a recirculation is formed behind the building. (Tutar and Oguz 2002)

If a triangular roof is employed instead of the flat roof, then several different scenarios would occur depending on the roof angle. When the roof angle is very large, the roof will intrude into the main flow and thus the separation point will move from the left intersection corner of the roof and the windward wall to the peak of the roof. Under this circumstance, if openings are incorporated, part of the main flow of the wind will enter the building and go directly through the roof openings and drive a recirculation in the space, as illustrated in Figure 5.3 (I). This airflow pattern is actually the same as the one named "skimming flow" by Oke (1988) introduced in Chapter Two. However, when the roof angle is small, the separation point for the inflow is still at the corner of the roof and the windward wall. In this situation the airflow is induced by the airflow below the main flow (suction) such as reattaching flow and reverse flow if openings are provided on the roof. Depending on the direction of the air velocity at the inlet opening, two airflow patterns can be identified: for the one shown in Figure 5.3 (II), the air coming through the inlet goes vertically to the bottom of the space, whilst for the one shown in Figure 5.3 (III), the air flows horizontally forming a small recirculation at the roof level and the air movement in the space is driven by a secondary recirculation.

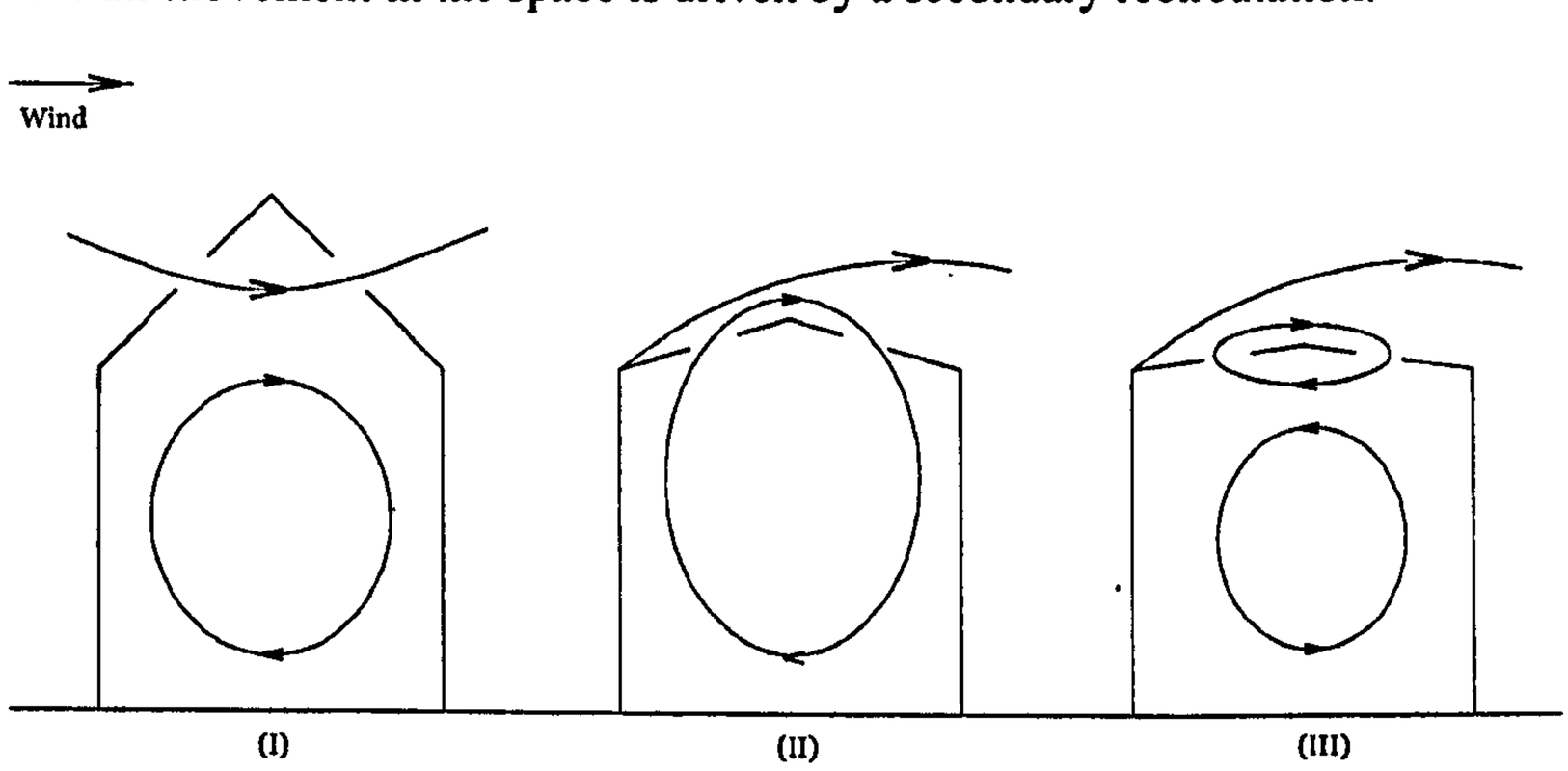

Figure 5.3: Three possible airflow patterns for wind-induced natural ventilation in atrium buildings with two roof openings

These three airflow patterns may have very different performances for creating cooling effects. Apparently the main flow is much stronger than the reverse flow and "tunnel effect[1]" will take place enhancing the airflow going through the openings. Thus the flow pattern (I) perhaps induces the highest air velocity at the occupants' level in the space, compared to the

[1] The air speed increases considerably between the obstacles to the wind. This is known as "tunnel effect".

other two. As regards flow patterns (II) and (III), the air velocity magnitude is significantly influenced by the height of the centre of the recirculation and magnitude of the horizontal momentum driving the recirculation. A recirculation can be generally considered as a symmetric ellipse, and hence the air velocity at the bottom of a recirculation can be regarded similar to that at the top with a reduction coefficient which is mostly influenced by the vertical size of the recirculation. Therefore, for the same momentum driving the flow, more recirculations usually mean more reduction for the air velocity from the main flow. In addition, it is also interesting to note that the directions of the air movement at the bottom of the space for the three flow patterns are different: that of the first two are opposite to the wind direction whilst the last one is the same as the wind direction.

It can also be inferred from the above analysis that roof angle is a very important factor for the airflow pattern, since it determines the location of the separation point of surfaces exposed to positive and negative pressures and also it can influence the reverse flow and reattaching flow. This also suggests that additional windward adjacent buildings will have very significant impacts on the ventilation performance of the space as their presence can change the separation point. Nevertheless, the above analysis does not show the full picture and is generally quite crude for the use as design guides. For instance, the factors affecting the transition between the flow patterns (II) and (III), and the effects of the recirculation behind the building still remain unclear. In order to bridge the gap, CFD simulations are carried out for more detailed understanding of the problem and to make clear the effects of the parameters involved.

5.3 Impacts of roof shape

The ventilation performance of atrium spaces with three common types of roofs is investigated in this part of study, including triangular roof, saw-tooth roof and barrel vault roof. The impacts of triangular roof are examined firstly, followed by the study of the other two kinds of roofs.

5.3.1 Triangular roof

CFD simulation is performed for the atrium spaces with a number of different roof angles including 0° (flat roof), 5°, 7°, 10°, 12°, 15°, 18°, 20°, 22°, 25°, 30°, 45°, 60° and one without roof, i.e. a courtyard in order to gain an appreciation of the general airflow patterns and their performance in the space. The simulations are only 2-D and it is assumed that the wind is perpendicular to the roof edge. The openings are located in the centre of each pitch of the roof and have the same width of 1m. There are no adjacent buildings beside the atrium space.

Figure 5.4 illustrates the typical airflow patterns of the wind-induced natural ventilation for atrium spaces selected from the simulations. It is observed that the airflow pattern (I) will take place for the atrium buildings with roof angle over 25°; the airflow patterns for roof angles from 10° to 15° correspond to flow pattern (II); and the courtyard and the atrium spaces with roof angles from 0° to 7° and from 18° to 20° have the flow pattern (III).

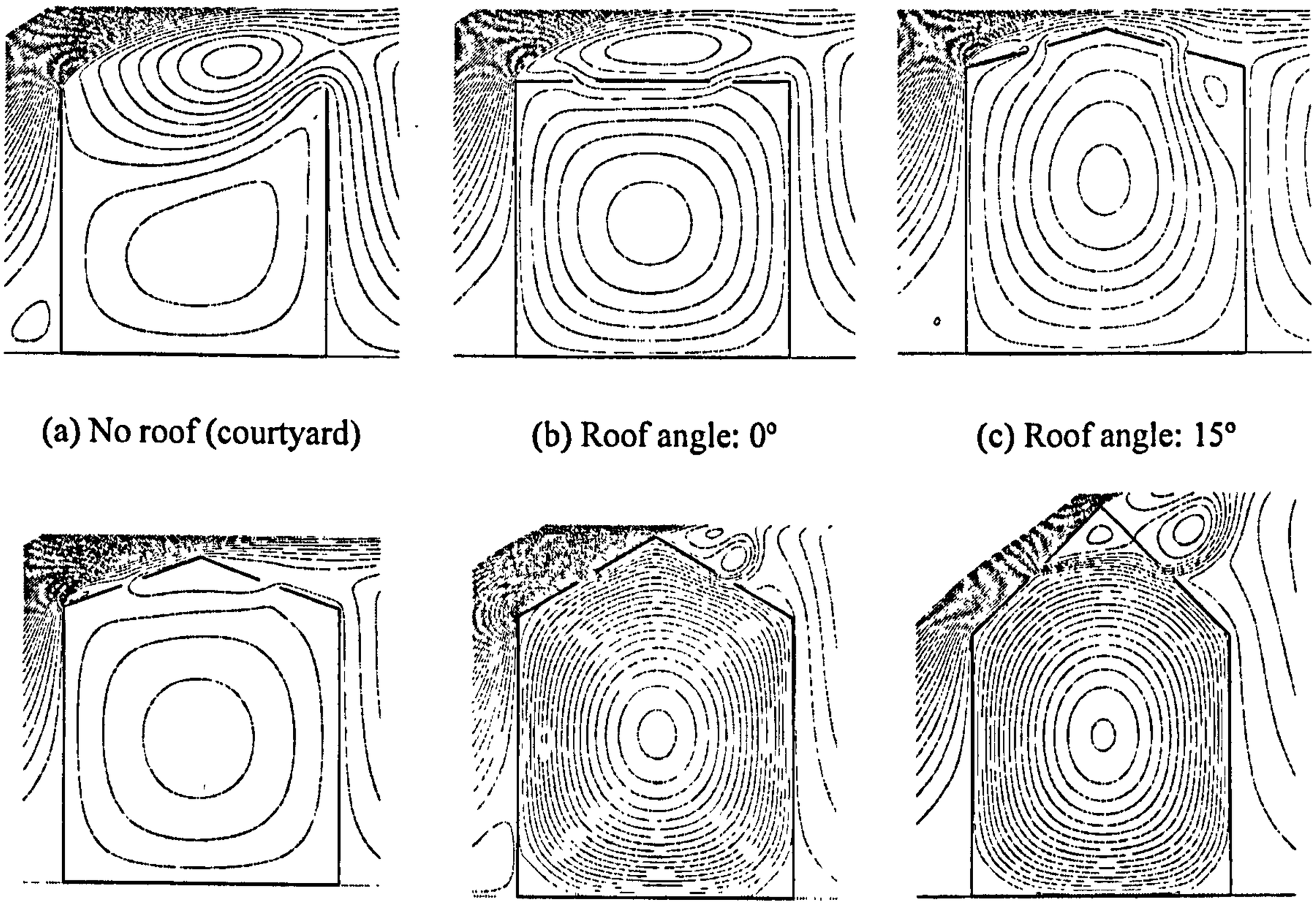

(a) No roof (courtyard) (b) Roof angle: 0° (c) Roof angle: 15°

(d) Roof angle: 20° (e) Roof angle: 30° (f) Roof angle: 45°

Figure 5.4: Airflow patterns of wind-induce natural ventilation for atria without a roof (courtyard) and with a roof angle of 0°, 15°, 20°, 30° and 45°

This figure also confirms the preliminary analysis in Section 5.2: the separation point for (a) to (d) is located at the top corner of the windward wall when the roof angle is small whilst it is located at the roof peak for (e) and (f) when the roof intrudes into the main flow. It is also shown from (b) to (f) that, with the increase of the roof angle, the main flow becomes closer to the roof and the reverse flow is gradually compressed and finally disappears when flow pattern (I) takes place. The separated flow at the windward corner will reattach on the leeward pitch for the roof angle 10°-15°(Fig 5.4c), and on the windward pitch for roof angle 18°-20° but the reattaching flow is not found for any other roof angles.

It is interesting to note that, with the increase of the roof angle, flow pattern (III) occurs twice: initially when the roof angle is very small, i.e. from 0° to 7° (Figure 5.4b) and then when the roof angle is 18°-20° (Figure 5.4d). Nevertheless, a further review shows that they are

incurred for different reasons. When the roof is nearly flat, the recirculation at the roof level is actually driven by the reverse flow above the roof in conjunction with the back flow from the recirculation behind the building and they assist with each other. However, when the roof angle increases, the main flow becomes closer to the roof and the reverse flow almost disappears, whilst the influences of the recirculation behind the building increase. In addition, when the roof angle is 20°, the reattaching flow will separate at the peak of the roof again resulting in a shade area at the leeward pitch. Thus the airflow pattern (III) for the 20° roof case is mostly the effect of the back flow from the recirculation behind the atrium (see Figure 5.4d), which is also the mechanism that occurs for the courtyard case. According to this analysis, two types of flow pattern (III) can be distinguished in terms of the driving mechanism for later investigations: flow pattern (III).a which is driven by the collective effects of the reverse flow and the back flow, and flow pattern (III).b which is dominated by the back flow from the recirculation behind the atrium.

Figure 5.5 shows the air velocity distributions at the occupants' level for the atria with roof angles of 0°, 15°, 20°, 30°, 45°, 60° and the courtyard. The velocity coefficient is defined as the ratio between the local air velocity and the reference wind velocity defined in Chapter Three (4*m/s* at the roof level which has a height of 12*m*). The occupants' level is defined as the level 1.6*m* higher than the ground. It can be seen that, atrium buildings with all the roof angles generally share a similar air velocity distribution at the occupants' level: the maximum velocity is obtained in the centre of the space and the distribution is generally symmetric with lowest velocities at the corners. It is also observed that, the airflow pattern (I) generally has the highest air velocity among all three flow patterns with the air velocity quite evenly distributed for the majority of the area at the occupants' level; the air velocity obtained for flow pattern (III).a is the second highest and is approximately half of that of roof angle 30° and 35% of that of roof angle 45° and 60°; the air velocity of the flow pattern (II) is slightly slower than the flow pattern (III).a, and the flow pattern (III).b, which takes place in the courtyard and the atrium with 20° roof, has the weakest performance with the highest velocity coefficient less than 0.08. Therefore, based on the above discussions, the air velocity for each pattern can be generally summarised as follows although it may be not very precise for transitional phase:

$$(I) > (III).a > (II) > (III).b$$

This order also reveals the main factors determining the ventilation performance. For flow pattern (III).b, as has been pointed out, it is dominated by the back flow from the recirculation behind the building with two recirculations in the space, and more importantly, the size of the recirculation at the roof level is quite large, which results in a significant reduction of air velocity compared to the main flow. This discussion also suggests that, if strategies can be employed to influence the back flow, the ventilation performance can be significantly changed. For the courtyard, for instance, if the height of the leeward wall is increased which prevents the

back flow, the flow pattern of the courtyard will change to (II) and the air velocity at occupants' level in the courtyard can be greatly enhanced (see Figure 5.6).

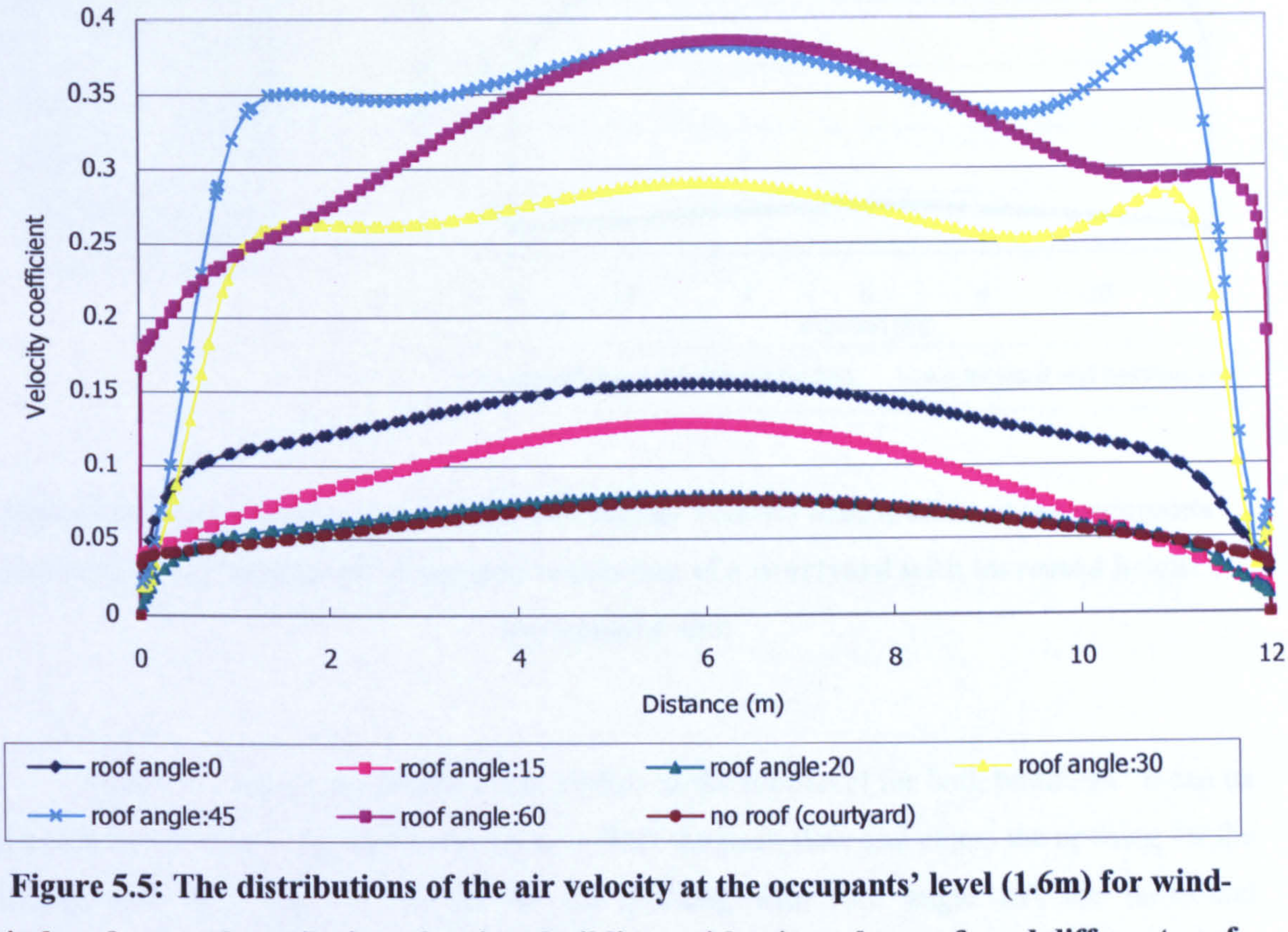

Figure 5.5: The distributions of the air velocity at the occupants' level (1.6m) for wind-induced natural ventilation of atrium buildings with triangular roofs and different roof angles

A comparison between the ventilation performance of atrium buildings with roof angles of 0° and 15° can provide a deep insight into the difference of the mechanism for flow patterns (II) and (III).a. As can be seen from Figure 5.5, the air velocity at the occupants' level of an atrium building with a roof angle of 0°, in which the airflow pattern is (III).a, is higher than that of an atrium with a roof angle of 15° that has a flow pattern (II). The reason for this is that, for the building with a roof angle of 15°, the wind shear caused at the opening on the roof, together with the opposite flow from the recirculation behind the building significantly weakens the horizontal momentum driving the airflow in the space, whilst the air can come in and out of the building quite smoothly for the atrium with a roof angle of 0°.

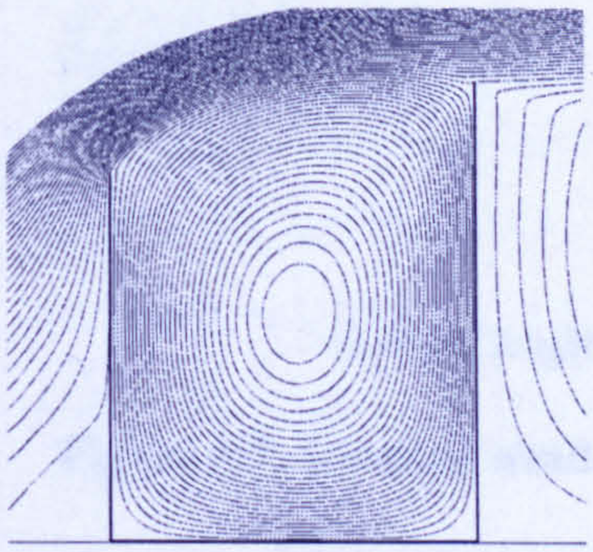

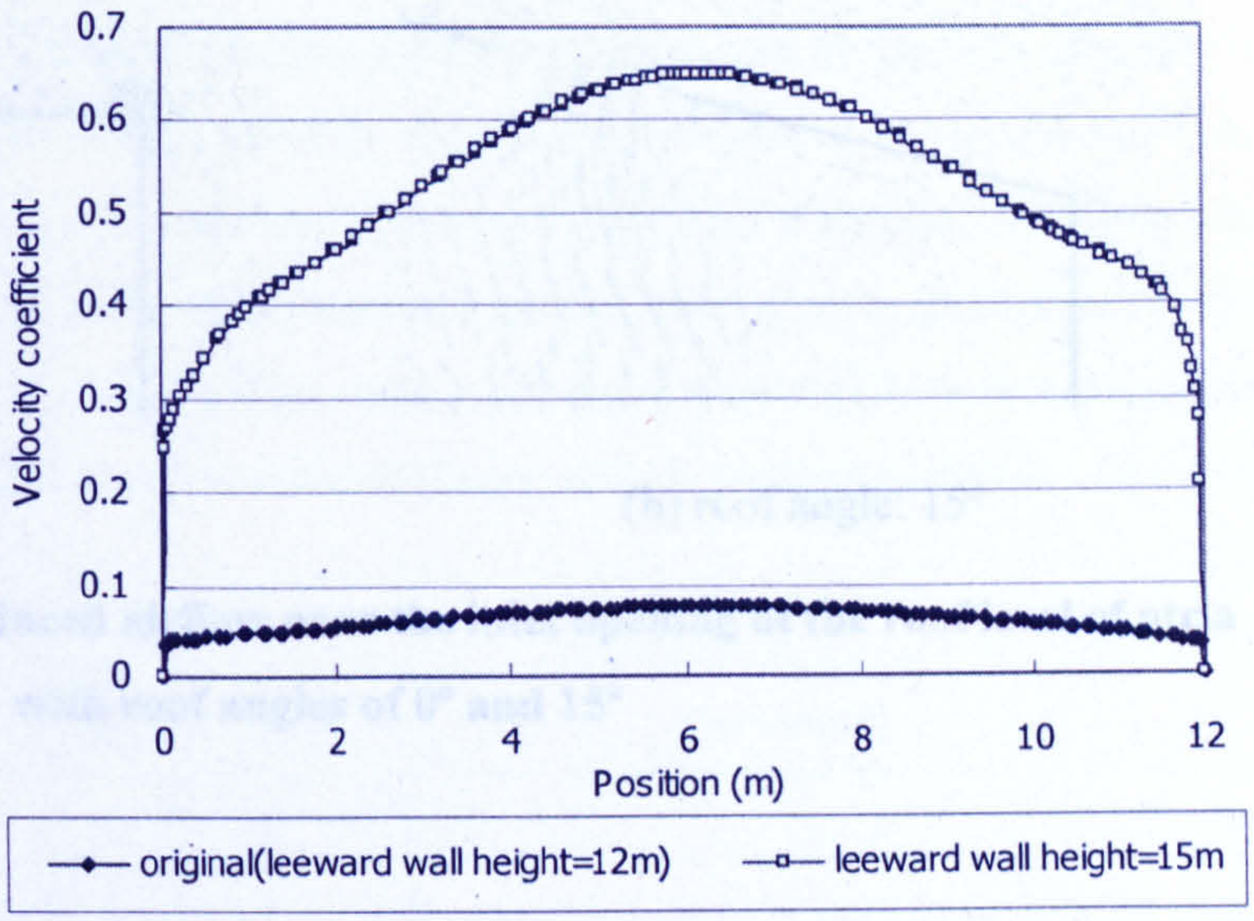

Figure 5.6: The airflow pattern (left) and the air velocity distribution at the occupants' level (right) for wind-induced natural ventilation of a courtyard with increased height of the leeward wall

Figure 5.7 shows the details of the airflow at the roof level for both buildings. It can be seen that the air speeds up with the assistance from the back flow and enters the opening for the building with roof angle 0°, whilst for the building with roof angle 15°, the horizontal momentum of the reattaching wind neutralises the momentum from the recirculation behind the building resulting very weak air movement near the opening. The wind shear caused at the roof level also leads to significant production of turbulent kinetic energy (TKE) and hence higher turbulence intensity, which is then advected from the roof level to the bottom of the space. Figure 5.8 compares the TKE and the turbulence intensity at the occupants' level of atria with roof angle 0° and 15°, and as can be seen, both the TKE and the turbulence intensity produced by the 15° roof are much higher than that of 0° roof. Therefore, from thermal comfort point of view, the conditions of the 0° roof will be more favourable, as it can bring on higher air velocity with less turbulence intensity for the occupants.

With respect to the flow pattern (I), the effects of the recirculation behind the building are entirely overwhelmed by the main flow. Thus, from the physics point of view, the main factors influencing the four flow patterns can be summarised as follows: flow pattern (I) is dominated by the main flow entering through the windward opening; flow pattern (II) is the result of the interaction of the reattaching flow and the opposing back flow from the recirculation behind the building but the reattaching flow is stronger; the reverse flow and the back flow assist each other for the flow pattern (III).a, and the back flow from behind the building governs flow pattern (III).b.

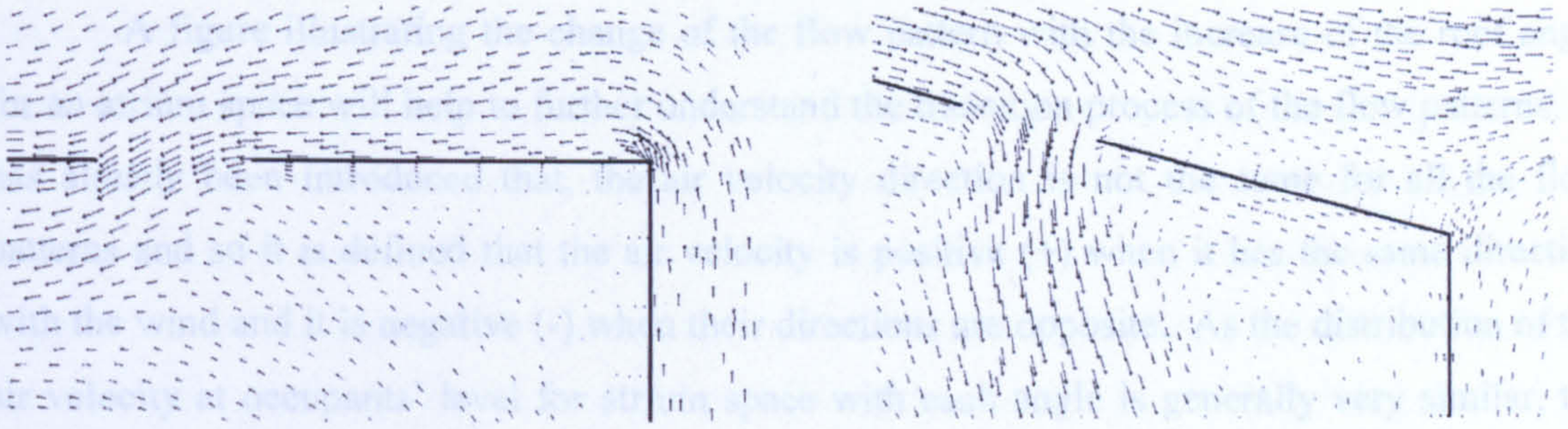

(a) roof angle: 0°　　(b) roof angle: 15°

Figure 5.7: Detailed wind-induced airflow near the inlet opening at the roof level of atria with roof angles of 0° and 15°

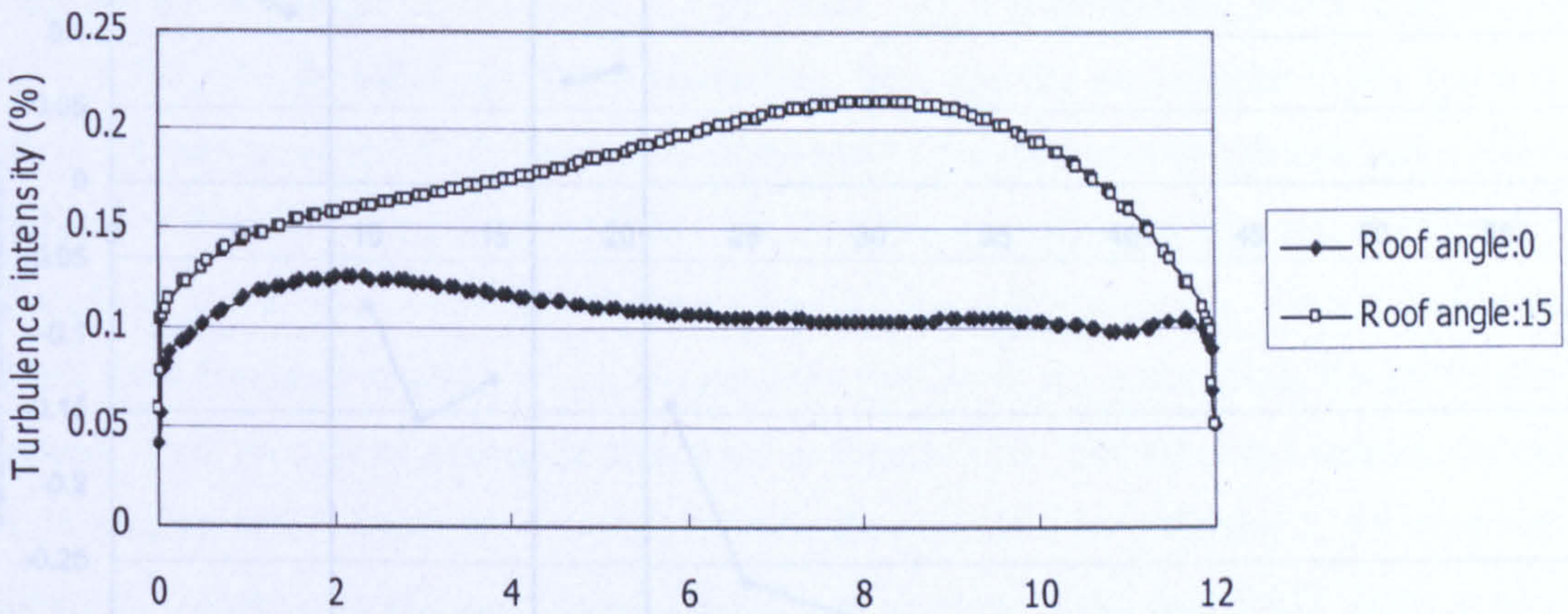

(a) Comparison of turbulence intensity

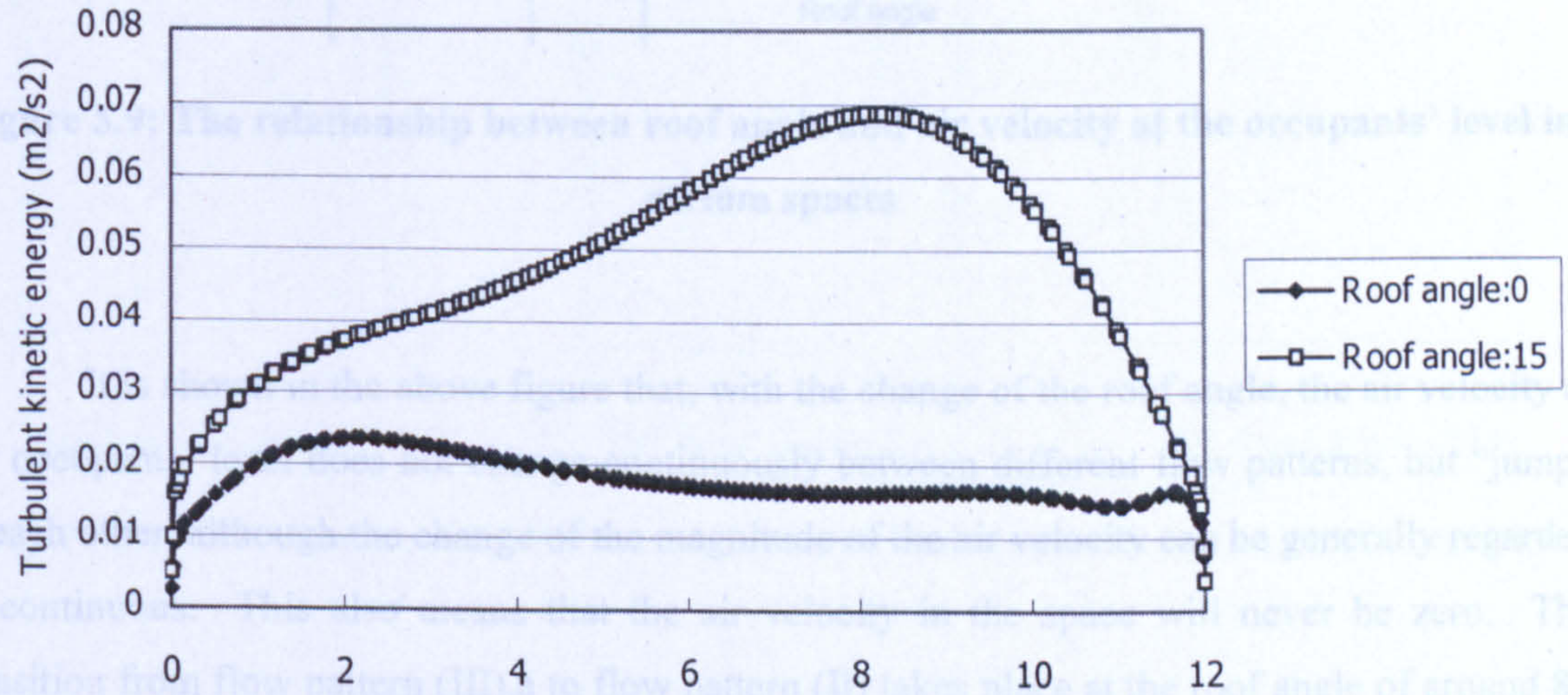

(b) Comparison of turbulent kinetic energy (TKE)

Figure 5.8: Comparison of the turbulence intensity (a) and the turbulent kinetic energy (TKE) (b) at the occupants' level of atria with roof angles of 0° and 15°

A figure illustrating the change of the flow pattern with the increase of the roof angle for an atrium space will help to further understand the transition process of the flow patterns. It has already been introduced that, the air velocity direction is not the same for all the flow patterns and so it is defined that the air velocity is positive (+) when it has the same direction with the wind and it is negative (-) when their directions are opposite. As the distribution of the air velocity at occupants' level for atrium space with each angle is generally very similar, the maximum velocity is employed for the evaluation of the ventilation performance here. Thus we can obtain Figure 5.9 as follows.

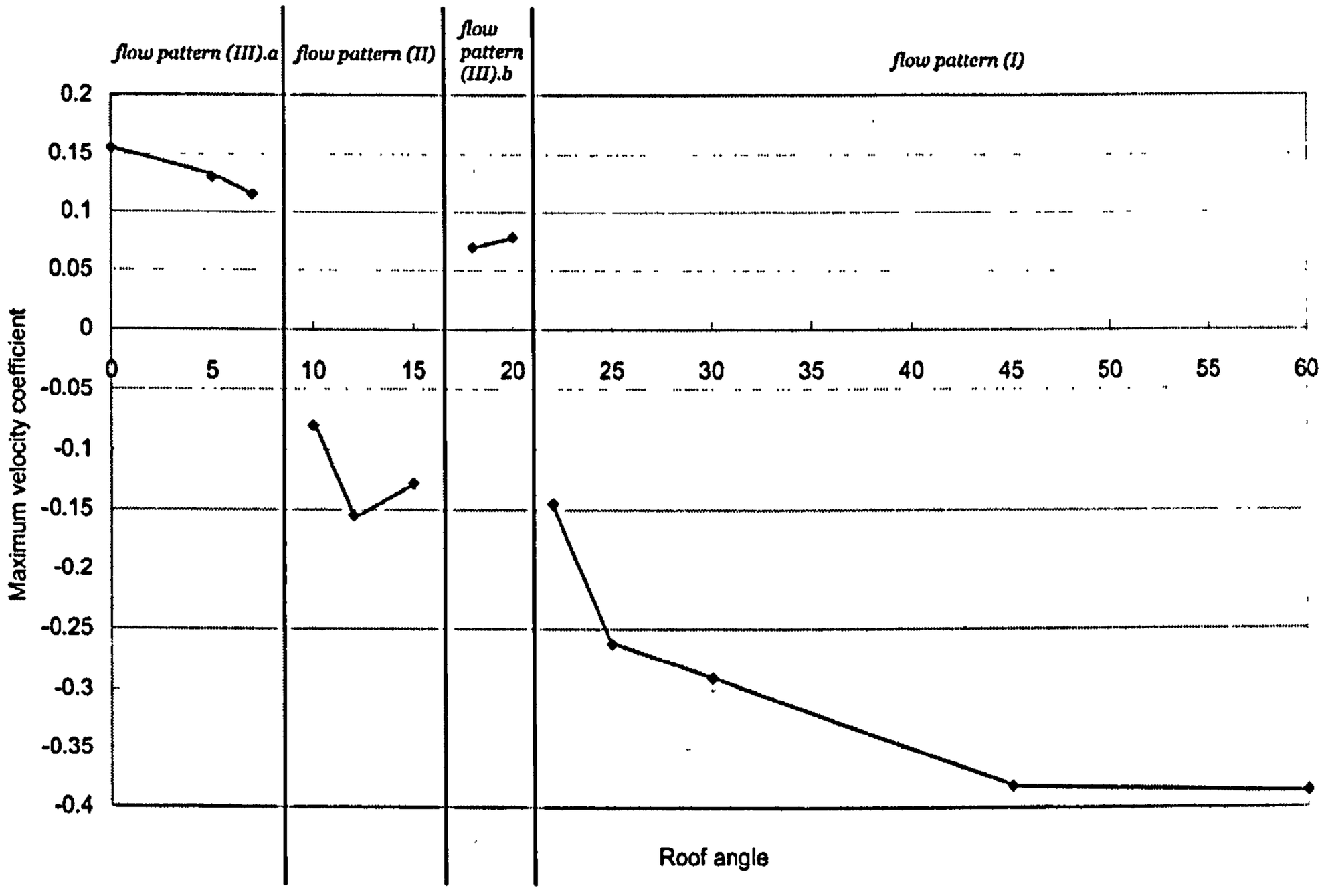

Figure 5.9: The relationship between roof angle and air velocity at the occupants' level in atrium spaces

It is shown in the above figure that, with the change of the roof angle, the air velocity at the occupants' level does not change continuously between different flow patterns, but "jump" to each other, although the change of the magnitude of the air velocity can be generally regarded as continuous. This also means that the air velocity in the space will never be zero. The transition from flow pattern (III).a to flow pattern (II) takes place at the roof angle of around 8°; and 17° for the transition from (II) to (III).b; and 21° for the transition from (III).b to (I). When the roof angle is below 21°, the maximum velocity coefficient for the occupants' level will be below 0.16. It can also be seen that, the air movement in the space will be driven by suction if the roof angle is smaller than 20°, which is in compliance with the experimental observations of van Straaten et al. (1965), who found that, with a low-pitched roof, both leeward and windward

sides of the roof are subject to suction and the air stream approaching the building turned upwards at a roof angle which varies from about 18° to 25° depending on the height of the wall.

Having made clear the dominating force for each flow pattern, it is generally quite easy to understand the trend of the change of the air velocity in the space with the change of the roof angle when the flow pattern is not changed. For flow pattern (III).a, when the roof angle is increased, the area between the roof and the reverse flow will reduce. Thus the effects of the reverse flow are weakened resulting in lower air movement. For flow pattern (II), the change of the air velocity in the space is a little more complicated: initially the air velocity will increase but then start to decrease at about 12°. The reason for this is related to the development of the reattaching flows. When the roof angle is very low and the reverse flow just disappears (around 7-10°), the reattaching flow does not develop sufficiently and thus the horizontal momentum driving the air movement in the space is very weak. As a consequence, increase of the roof angle will help the development of the reattaching flow and the air velocity in the space will increase. However, after 12°, the triangular shape makes the roof quite rough and hence reduces the effects of the reattaching flow, and the back flow becomes stronger with the increase of the roof angle as it can reach more area of the roof which has a low pressure. Thus the difference between them becomes smaller, which weakens the airflow in the space when the roof angle is increased. This process of change is illustrated in Figure 5.10. For this latter reason, the trend for flow pattern (III).b which is controlled by back flow can also be understood. Flow pattern (I) is generally governed by the main flow, and with the increase of the roof angle, more wind can directly enter into the building and thus lead to stronger air movement at the occupants' level.

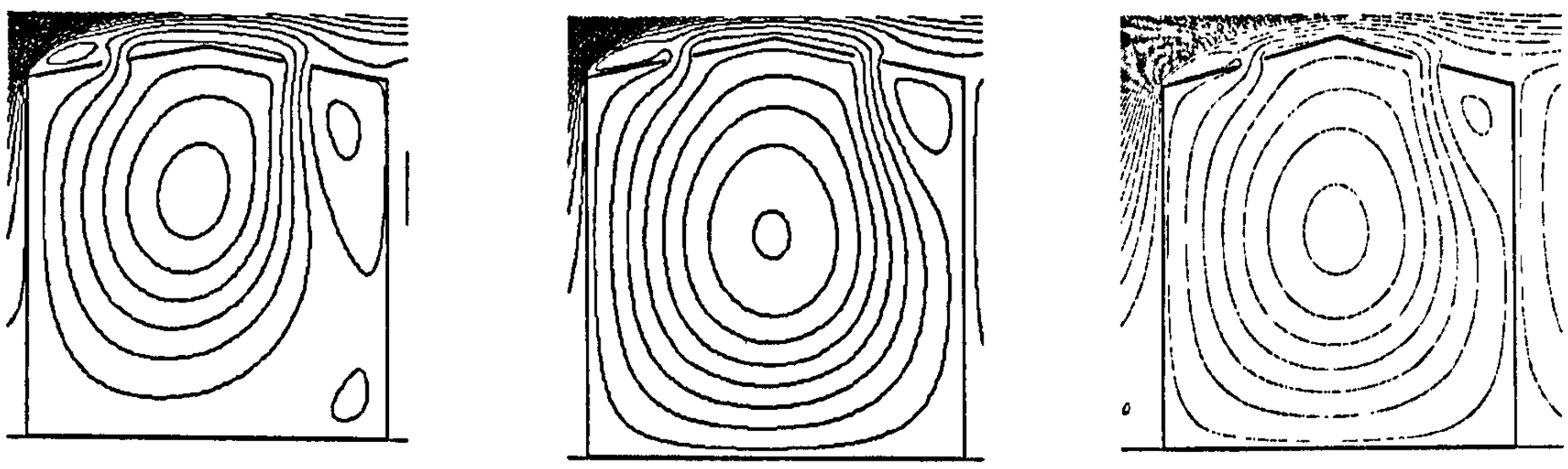

(a) Roof angle: 10° (b) Roof angle: 12° (c) Roof angle: 15°

Figure 5.10: Flow pattern (II) for atria with three different roof angles: 10°, 12° and 15°

Nevertheless, it is of interest to notice that the building with a roof angle of 60° does not have a better performance than that of 45°: the highest air velocity at the occupants' level is nearly the same as that of 45° and the average air velocity magnitude is significantly smaller (see Figure 5.5). This is because, when the roof angle is 60°, the centre of the recirculation in the space becomes very high due to the higher level of openings locations and the elliptical recirculation becomes more prolate. This does not bring on any difference for the maximum air

velocity in the middle of the occupants' level; however it significantly influences the air movement at lower corners where larger "shade" area results. A further investigation on the comparison of the turbulence properties of atria with roof angles of 45° and 60° shows that the atrium with 60° roof generates higher TKE and turbulence intensity for the occupants' level (Figure 5.11), which means that the 60° angle does not have any advantage in improving the thermal comfort level of the space, compared to the atrium with 45° roof when airflow is required. The reason for this is the same as explained earlier for the difference of the turbulence properties for roof angles of 0° and 15°: a higher roof pitch causes stronger wind shear resulting in more turbulent kinetic energy and higher turbulence intensity.

As a consequence, it can be generally concluded from the above simulations and discussions that the atrium with a roof angle of around 45° (flow pattern I) leads to the highest air velocity for the occupants' level with the maximum velocity coefficient of 0.38 and relatively lower turbulence intensity than atrium buildings with higher roof pitches. Flow pattern (III).a provides a similar air velocity at the occupants' level as flow pattern (II) with the maximum velocity coefficient of around 0.1 – 0.15 but generates much lower turbulence intensity and less TKE. Flow pattern (III).b, which occurs for the courtyard and the atrium with 18°-20° roof, has the lowest air velocity in the space with the maximum velocity coefficient lower than 0.1.

It is also worth mentioning the fact that the courtyard, which can be considered as an atrium of any roof angle with the largest opening has a poor ventilation performance. This implies that opening size has significant impacts on the air movement in the space. This issue will be discussed in a later section particularly concerned with opening characteristics.

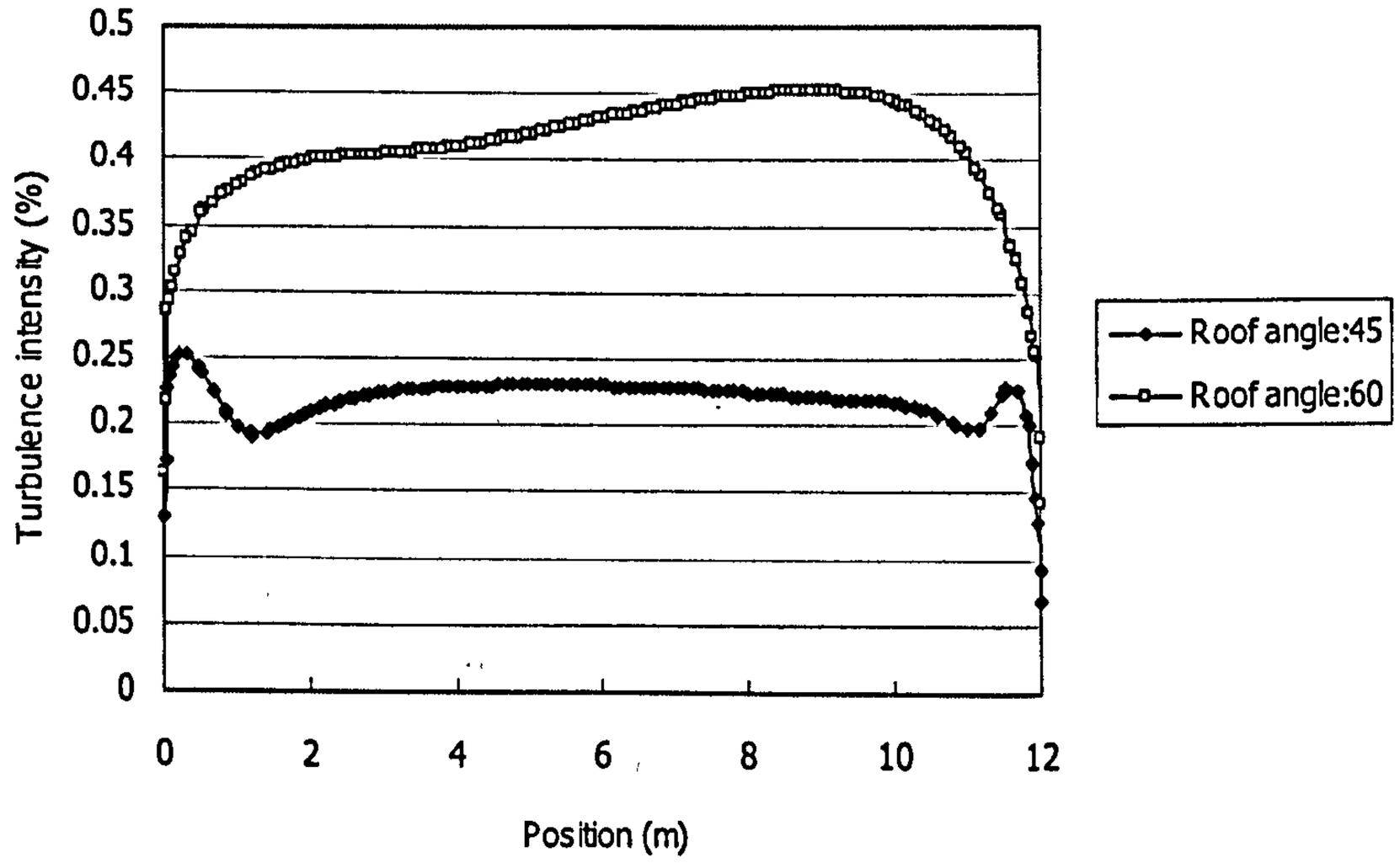

(a) Comparison of turbulence intensity

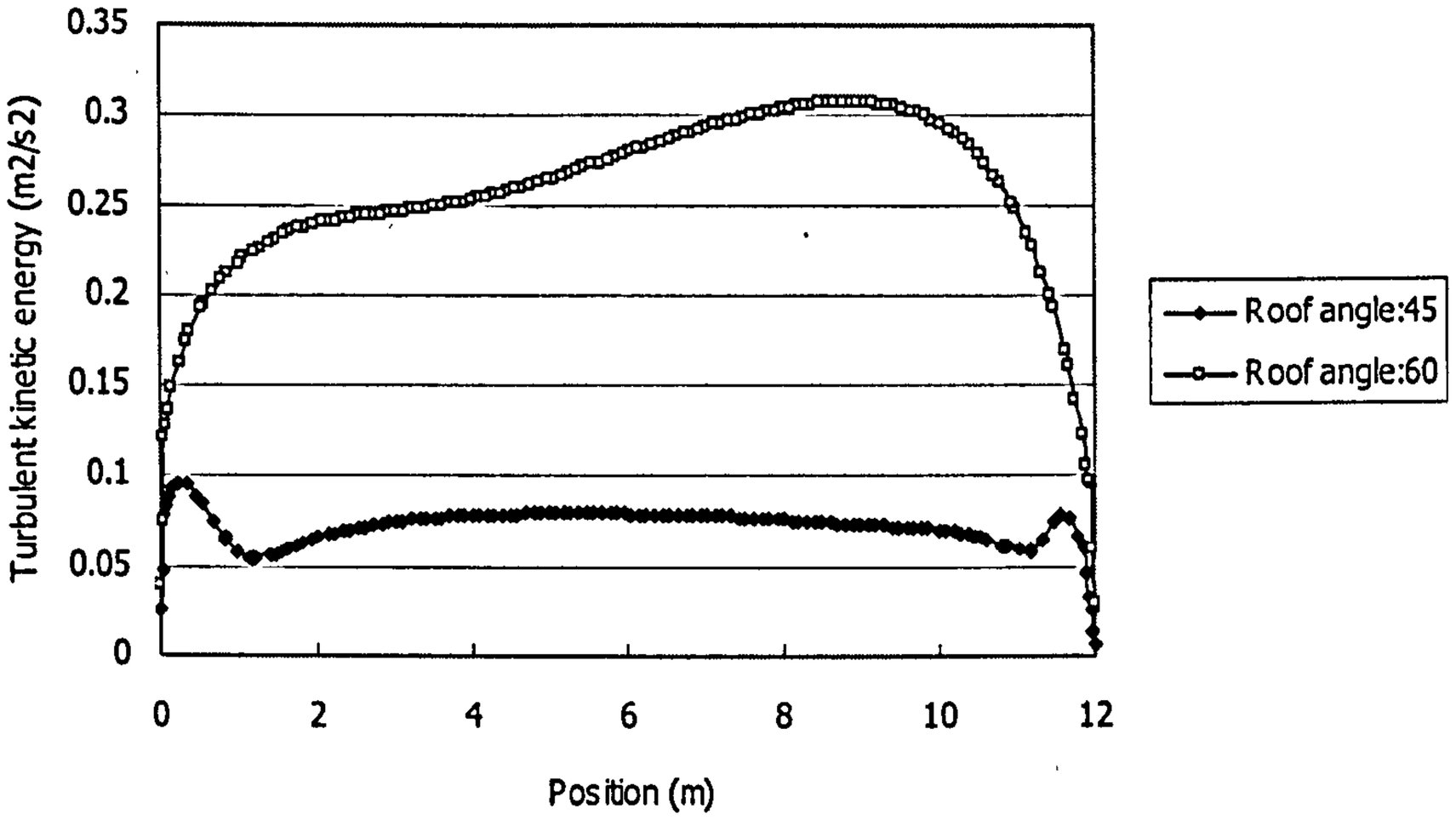

(b) Comparison of turbulent kinetic energy (TKE)

Figure 5.11: Comparison of the turbulence intensity (a) and the turbulent kinetic energy (TKE) (b) at the occupants' level of atria with roof angles of 45° and 60°

5.3.2 Barrel vault roof

A barrel vault roof is usually characterised with an arched shape. For ease of investigation, only a roof shape as part of a circle is considered in this part of study, notwithstanding the existence of other types of vault roofs in reality. The shape of the vault roof can be governed by any of the geometrical parameters shown in Figure 5.12 including the roof angle α, the tangential angle which is 2α according to geometry, the roof height h and the radius R. The roof/tangential angle is employed in this part of study to keep consistency with previous studies.

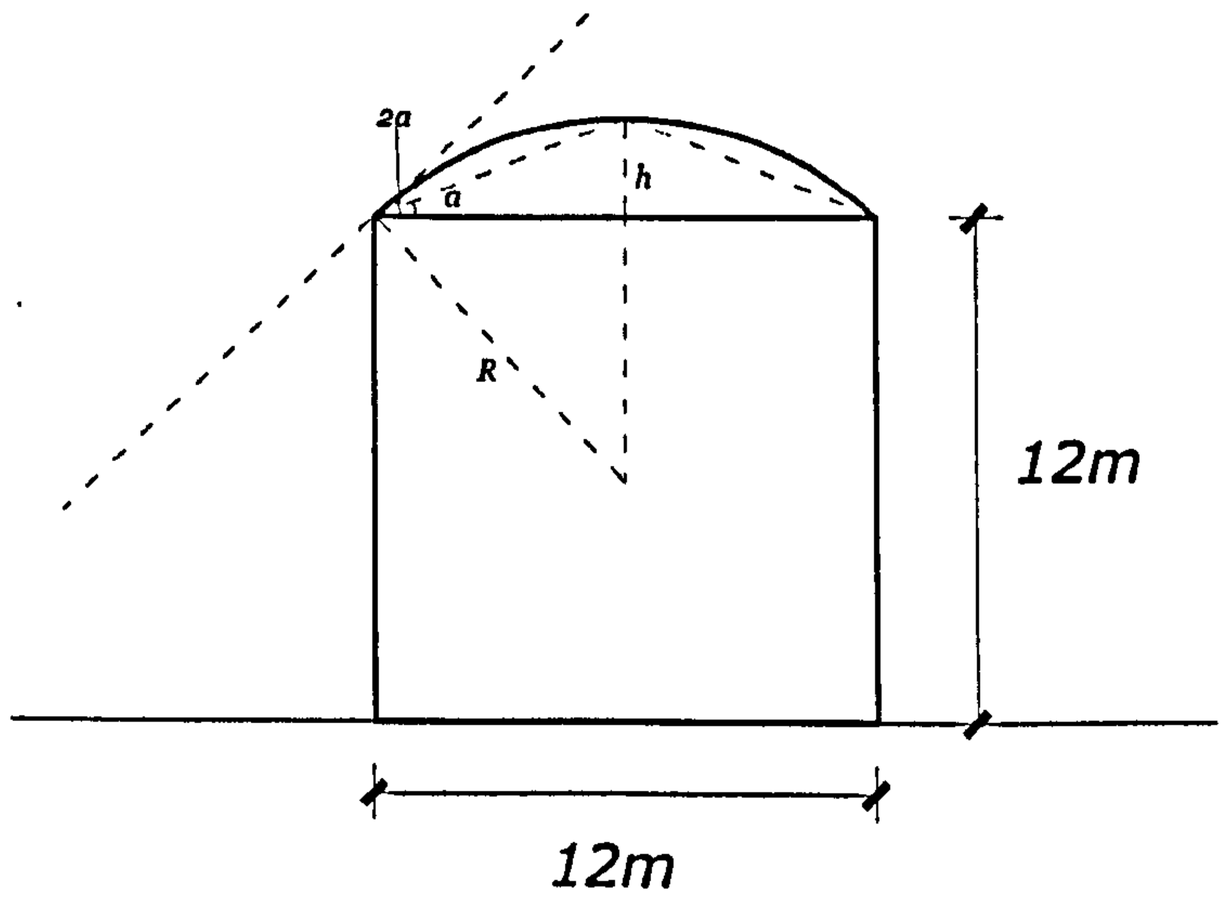

Figure 5.12: Geometrical characteristics of a barrel vault roof

Figure 5.13 shows the flow patterns of the atrium spaces with a number of different angles for vault roof. It is shown that, when the roof angle is below 5°, the flow pattern (III).a occurs and atrium spaces with roof angle over 7° have the flow pattern (II). Other flow patterns are not found. The separation of the main flow is only observed for atrium spaces with angle below 10°. Although these quantitative critical values for roof angles are not in compliance with those of triangular roofs for distinguishing flow patterns, further inspection shows that the tangential angle for vault roof correspond to the results on the separation point for triangular roofs: as described earlier, the separation point will move to the peak of the roof at around 20° for triangular roofs.

It should also be noted that, the main flow will not separate at the peak of the roof for the vault roof atria even if the roof angle becomes very high. In other words, the air movement in the space can only be driven by suction for barrel vault roofs. This is basically because of the shape employed for the roof: as a vault roof, there is no sharp corner on the roof and thus flow can move smoothly along its boundary. Therefore, the flow pattern (I) and (III).b, which occurs with the separation point located at the peak of the roof pitch will not occur.

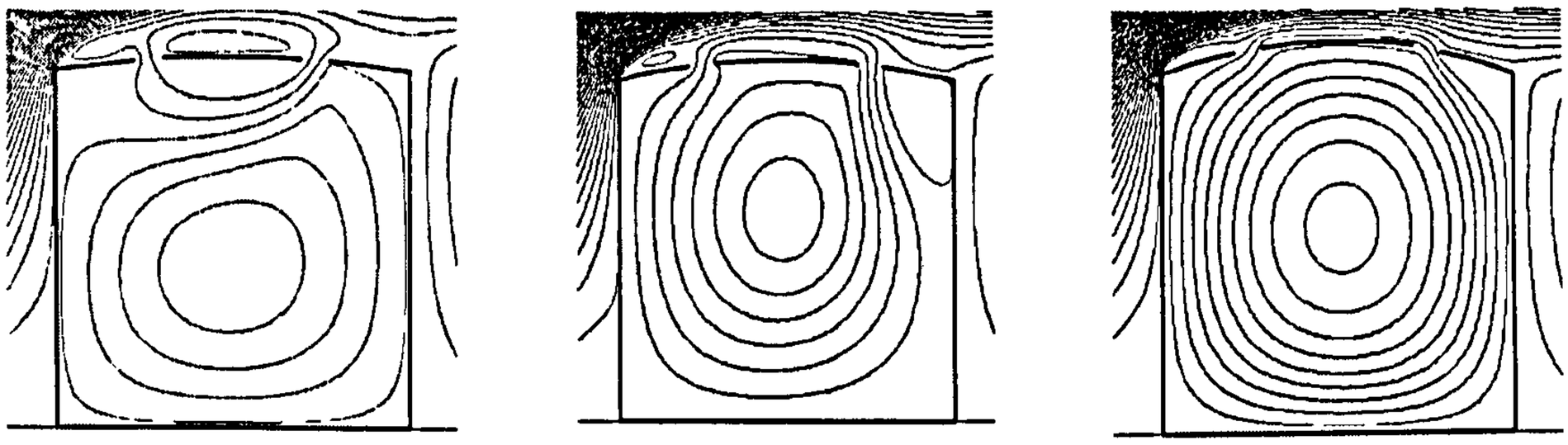

(a) Roof angle: 5° (Tangential angle:10°)

(b) Roof angle: 7° (Tangential angle:14°)

(c) Roof angle: 10° (Tangential angle:20°)

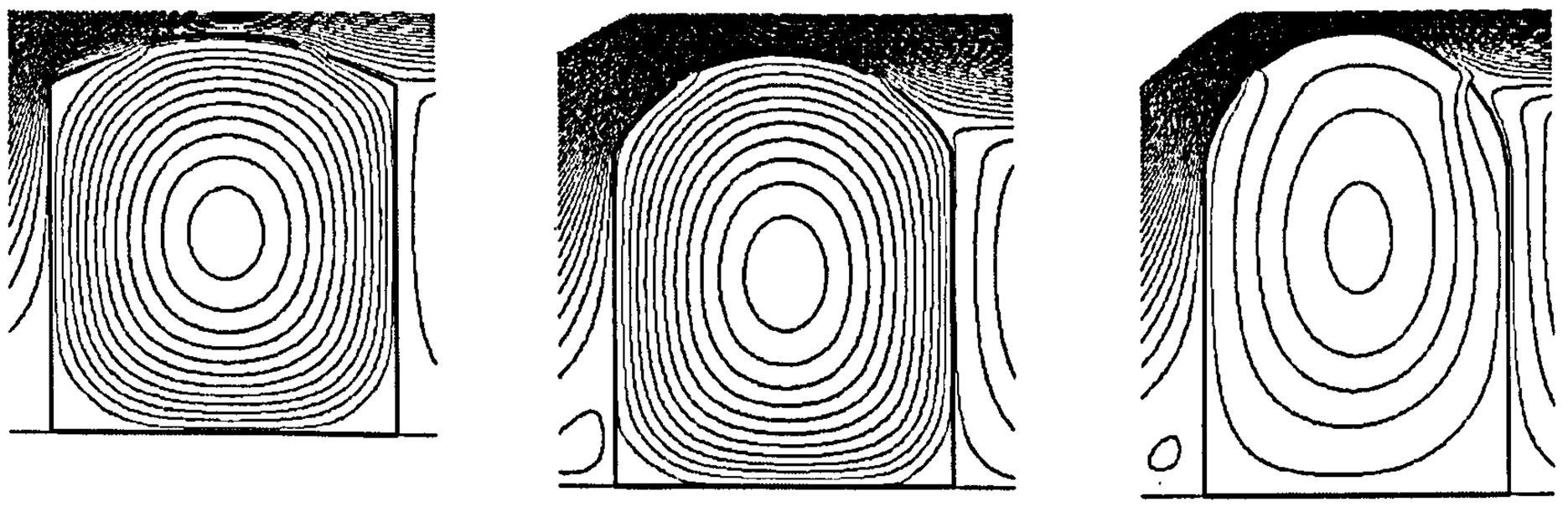

(d) Roof angle: 15° (Tangential angle:30°)

(e) Roof angle: 30° (Tangential angle:60°)

(f) Roof angle: 45° (Tangential angle:90°)

Figure 5.13: Airflow patterns of wind-induce natural ventilation for atria with a vault roof (roof angle: 5°, 7°, 10°, 15°, 30° and 45°)

The relationship between roof angle and air velocity at the occupants' level in atrium spaces with barrier vault roofs is plotted in Figure 5.14. It can be found that, the atria with angle 5° vault roof generally has the same performance with the atria with triangular roof of the same angle: they have the same velocity direction and similar value of maximum velocity. However, if the roof angle continues to increase afterwards, the velocity distributions at the occupants' level of atria with vault roofs differ significantly with those of atria from triangular roofs. The maximum velocity coefficient continues to increase with the increase of the roof angle until the angle reaches 15° and then starts to decrease. When the roof angle is 45°, the maximum velocity coefficient reduces to less than 0.06.

Further investigation into the mechanism of the airflow shows the reason for the above observation. Although atria with roof angle over 7° share the same flow pattern, the main flow still separates for the atria with angle 7° and 10° vault roof and as a result the flow is driven by the reattachment. This is also the mechanism for atria with triangular roofs when flow pattern (II) takes place. However, when the roof angle is above 10°, the flow is driven by the main flow rather than the reattachment, which causes more significant air movement in the space. As has been pointed out before, the back flow from the recirculation behind the building has a negative effect for the flow pattern (II), and this effect becomes greater with the increase of the roof angle, which explains why the ventilation performance becomes weaker when the roof angle is over 15°.

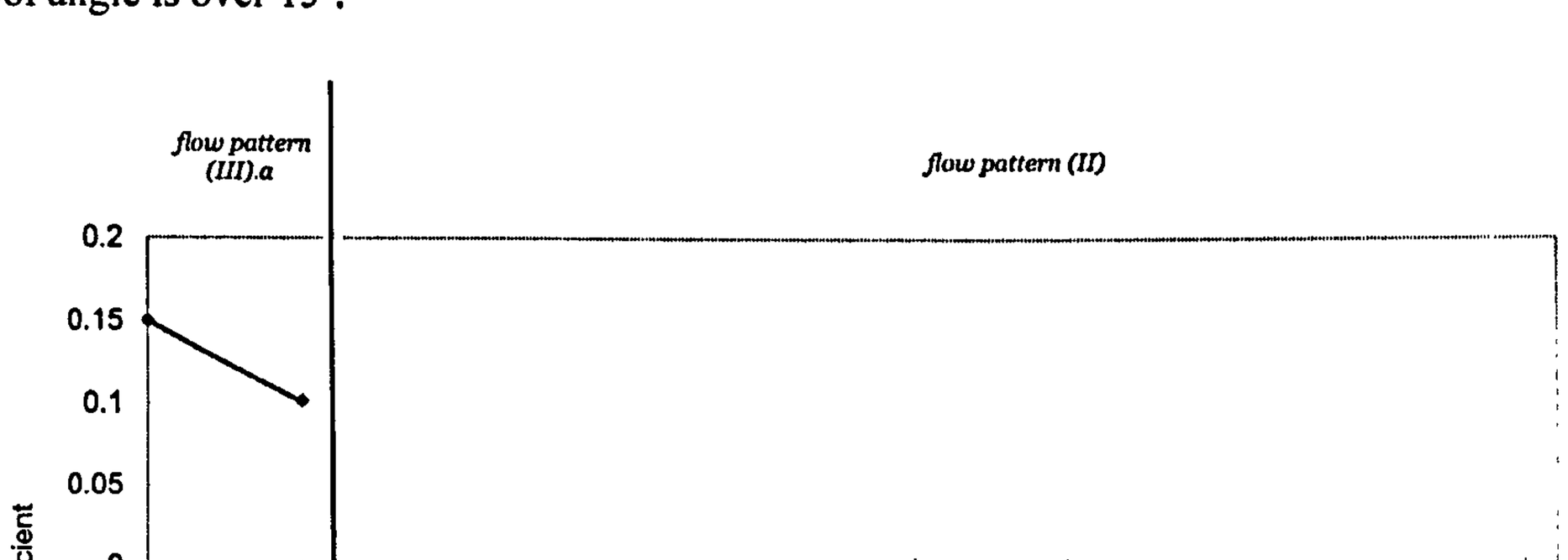

Figure 5.14: The relationship between roof angle and air velocity at the occupants' level in atrium spaces with barrier vault roofs

Figure 5.15 shows the turbulence intensity distribution at the occupants' level for each angle of vault roof. Generally speaking, the turbulence intensity caused by vault roofs is less than 20% except when the roof angle is 7°, i.e. when the reattachment drives the airflow and it is much less than that from the triangular roofs (See Figures 5.8 and 5.11). The turbulence intensity of very low roof angles (5°) is nearly the same as that of the correspondent triangular roofs, which, together with the observation that each pair has similar air velocity distribution, suggests that the ventilation performance of the atria with very low roof pitch (below 5°) is not sensitive to the roof shape and in this situation the vault roof atria can be considered as triangular ones with the same triangular angle.

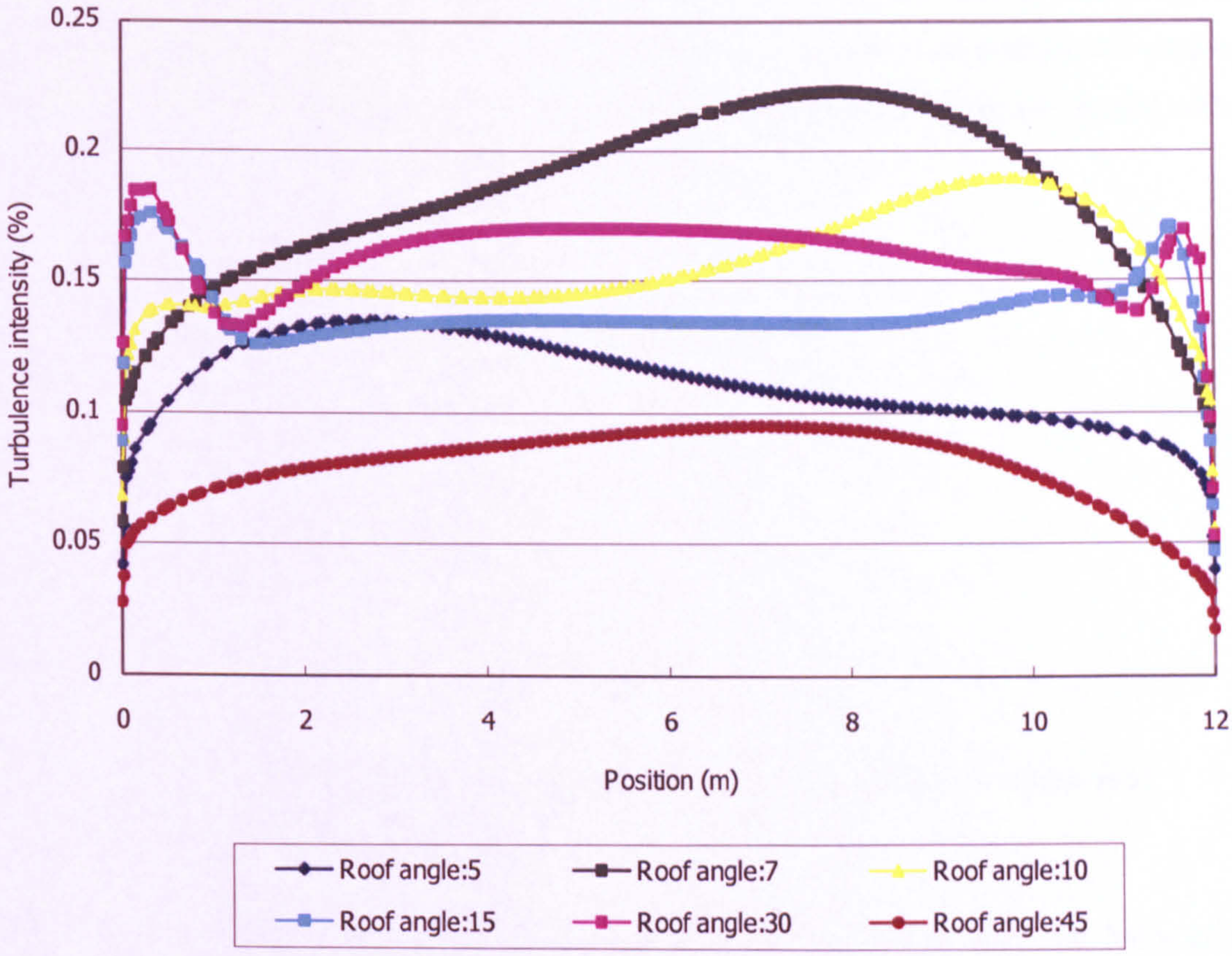

Figure 5.15: The distributions of the turbulence intensity at the occupants' level for wind-induced natural ventilation of vault roof atrium buildings with different angles

From the above discussions, it can be summarised that only two kinds of flow patterns can occur for atria with barrel vault roofs, flow pattern (II) and (III).a, which are distinguished at roof angle of around 6°; the highest air velocity in the space is induced when the roof angle is around 15° with the maximum velocity coefficient of 0.28; the turbulence intensity at the occupants' level induced by the vault roof is weaker than that by triangular roofs due to the less shear stress caused by its shape.

5.3.3 Sawtooth roof

Having studied two simple types of roofs in the previous two subsections, this subsection will move onto the more complicated sawtooth roof, which is often seen in industrial buildings and has also been incorporated in atrium buildings, such as the National Trust Central Office Swindon (RIBA Awards, 2006). The geometry of an atrium with a sawtooth roof that is employed for this part of study is illustrated in Figure 5.16. Three design variables are investigated, including the angle of the roof pitch in the roof (supposing all pitches have the same angle), the number of the "teeth" and the opening distributions. Four roof angles are chosen to represent the possible flow patterns according to previous studies, including 5°, 15°, 20° and 45°; the number of the teeth in the roof is either three or six; and three opening distributions are considered: only the leftmost and rightmost openings are opened; all windward openings are opened with all leeward ones closed; and all leeward openings are opened with all windward ones closed. Thus, overall 24 simulations are carried out.

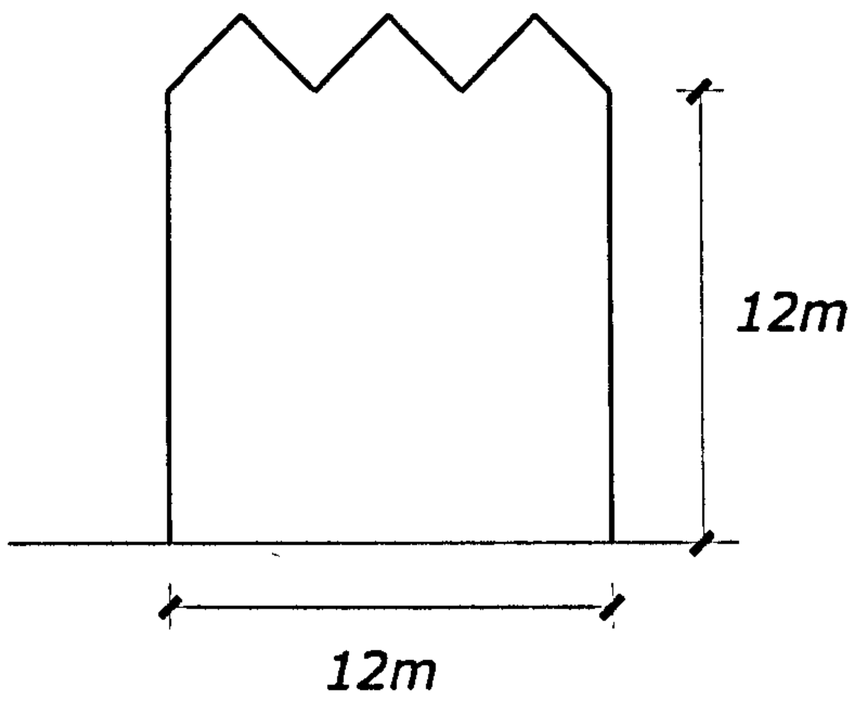

Figure 5.16: Geometrical configuration of an atrium with a sawtooth roof

Let us consider the simplest opening distribution first: when only the leftmost and rightmost openings are opened. Figure 5.17 illustrates the flow pattern of each scenario with this type of opening distribution. It is shown that under this circumstance roof angle is not very sensitive to the flow pattern in atria with a sawtooth roof, especially when the number of the teeth is large. It can be seen that, when the number of the teeth is 6, the roof can be generally regarded as flat for the prediction of the flow pattern; when the number of the teeth is 3, flow pattern (III).a still occurs for all the scenarios except the situation for the atrium with 45° angle roof because its leftmost roof pitch intrudes into the main flow.

With the same flow pattern, the atria with less teeth lead to stronger air movement due to the relatively larger openings. As has been pointed out before, the flow pattern (III).a is driven by the conjunction of the reverse flow and the back flow from behind the building, and the sawtooth has significant impacts on both of them. On one hand, the increase of the pitch angle will make the roof "rougher" thus increasing the difficulty of forming reverse flow; on the

other hand, as stated earlier, higher roof pitch can increase the effects of the back flow. These two effects are contrary and the importance of each of them depends on the roof angle. When the roof pitch is low, the latter effect is more important and thus the air movement is enhanced with the increase of the roof angle (see Figure 5.17a-f); when the roof angle is very large, the former effect will be more significant and the air movement will be weakened by increasing the roof angle (see Figure 5.17h).

The air velocity and turbulence intensity at the occupants' level quantitatively comply with previous findings for triangular roofs, with highest air velocity coefficient smaller than 0.15 and turbulence intensity less than 12% for flow pattern (III).a.

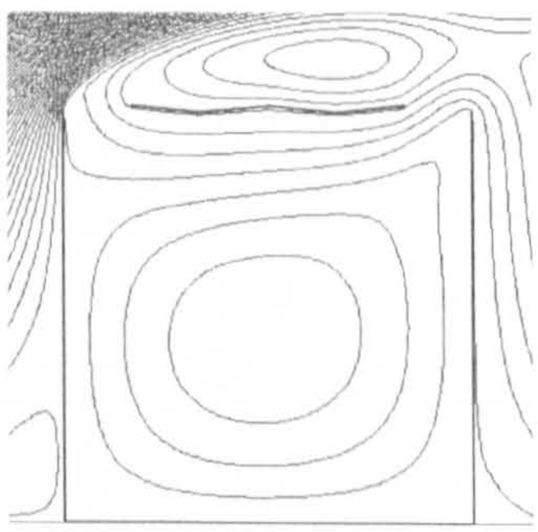

(a) Roof angle: 5°; tooth number: 3

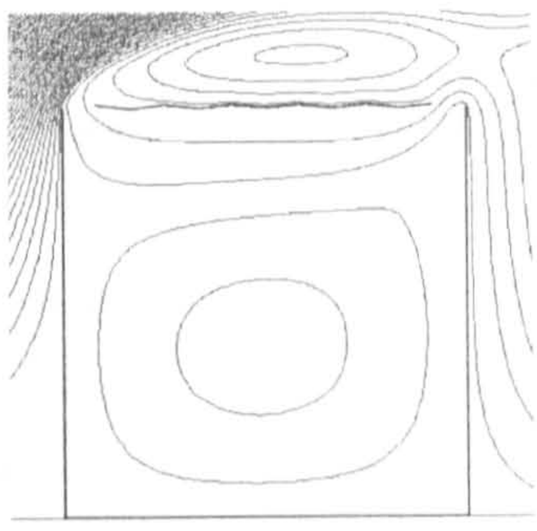

(b) Roof angle: 5°; tooth number: 6

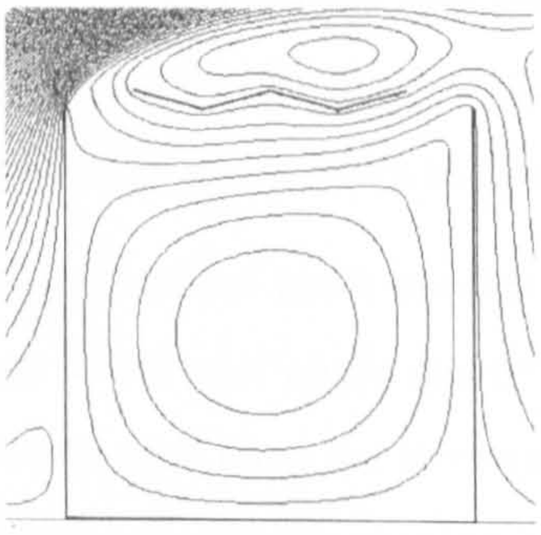

(c) Roof angle: 15°; tooth number: 3

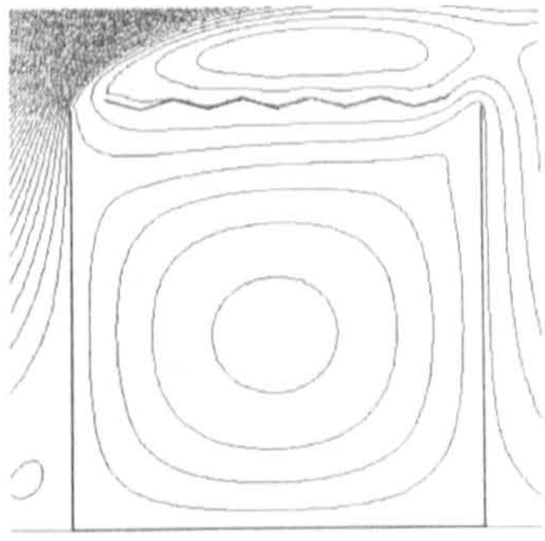

(d) Roof angle: 15°; tooth number: 6

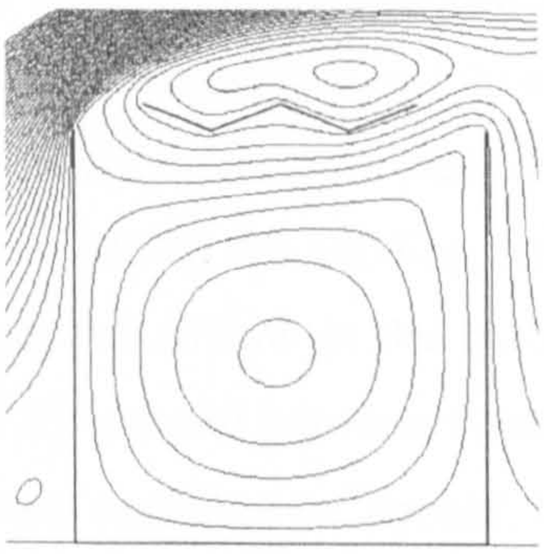

(e) Roof angle: 20°; tooth number: 3

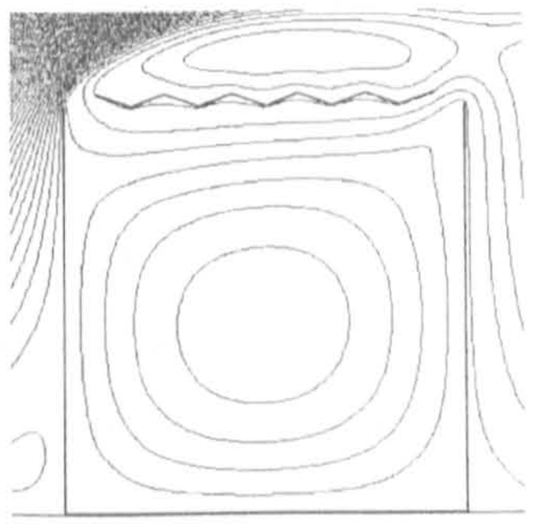

(f) Roof angle: 20°; tooth number: 6

(g) Roof angle: 45°; tooth number: 3

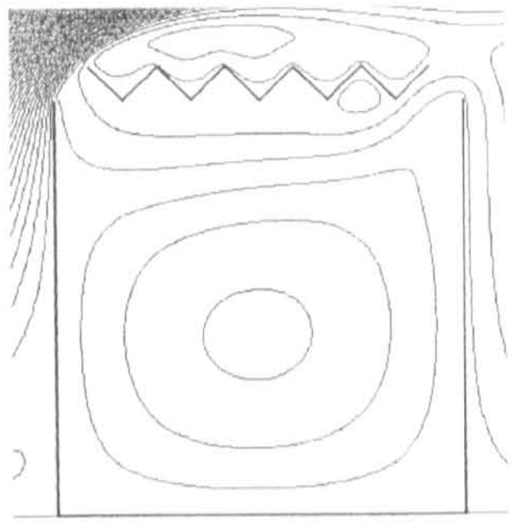

(h) Roof angle: 45°; tooth number: 6

Figure 5.17: Airflow patterns of wind-induce natural ventilation for atria with sawtooth roofs (when only the leftmost and rightmost openings are opened)

Figure 5.18 shows the flow patterns when all leeward openings are opened and all windward openings are closed. It can be seen that, when the tooth number is 6, the flow pattern is (III).a no matter what roof angle is and when the tooth number is 3, the flow pattern alters with the change of the roof angle: flow pattern (III).a occurs for 5° roof and changes to (II) when the roof angle increases to 20° and then (III).b for atrium with 45° roof. This transition process of the flow patterns clearly shows the effects of the roof angle: it helps to increase the size of the recirculation at the roof level. With more evenly distributed openings (when tooth number is 6), the level of the increase of the recirculation is generally small with the increase of the roof angle, whilst the level of the increase of the recirculation can significantly change the flow pattern in the space when the tooth number is 3 (see Figure 5.7).

When the roof tooth number is 6, the air velocity at the occupants' level increases with the increase of the roof angle due to the increased impacts of the back flow and the atrium with a 45° sawtooth roof have the strongest air movement with the maximum velocity coefficient of 0.17. When the roof tooth number is 3, the recirculation at the roof level may be so large that it reaches the bottom of the space, which will significantly reduce the air velocity at the occupants' level. As a consequence, the air velocity at occupants' level for 3-teeth sawtooth roof atria will decrease first and then increase until the separation point changes from the corner of the windward wall to the peak of the roof pitch, at which moment the back flow from the recirculation behind the building occupies the whole area between the main flow and the roof and induces the airflow in the space. This also sheds some light on the mechanism of the airflow of a courtyard introduced earlier (see Figure 5.4a). For atria with 3-teeth sawtooth roof, if all leeward openings are opened, the best ventilation performance is achieved when the roof angle is around 20°.

The effect of the roof angle introduced above to enlarge the recirculation at the roof level is also found when the windward openings are opened, but it is more significant when the number of the teeth is larger (see Figure 5.19). For 6-teeth atria, the flow pattern will switch

from (III).a to (II) when the roof angle is over 20° and the air velocity will decrease initially and then increase for the same reason explained as for 3-teeth leeward openings cases. For 45° 6-teeth atria, the maximum velocity coefficient can reach up to 0.18. As regards the 3-teeth atria, the air velocity at the occupants' level will reduce with the increase of the roof angle, which is different from the trend of 6-teeth leeward openings atria. This is because the impacts of the recirculation behind the building change very little as the leeward openings are closed and thus with the increase of the size of the recirculation at the roof level, the air movement is reduced. When the roof pitch can intrude into the main flow, flow pattern (I) (or II, there is no difference for this case) will be incurred and the air movement at occupants' level will be greatly enhanced with the maximum velocity coefficient of 0.3.

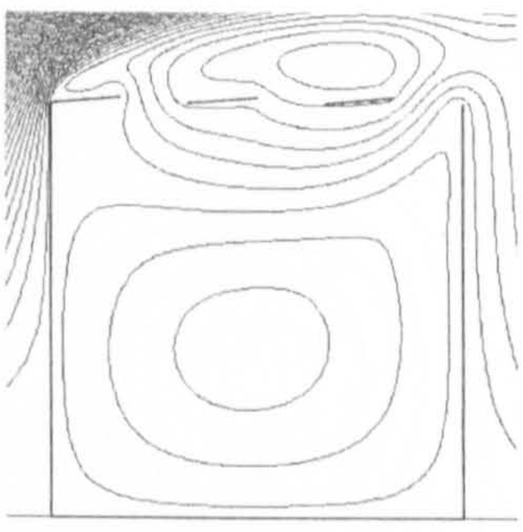

(a) Roof angle: 5°; tooth number: 3

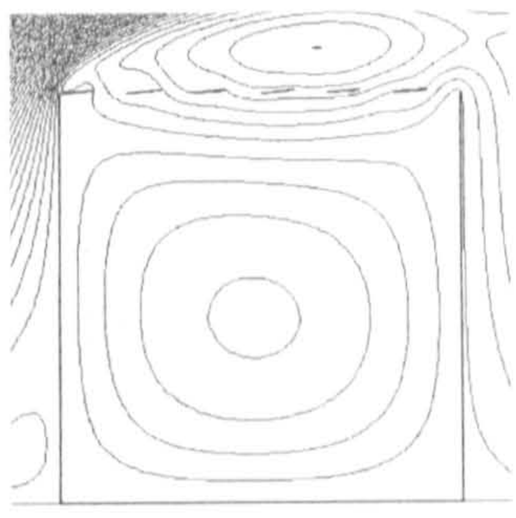

(b) Roof angle: 5°; tooth number: 6

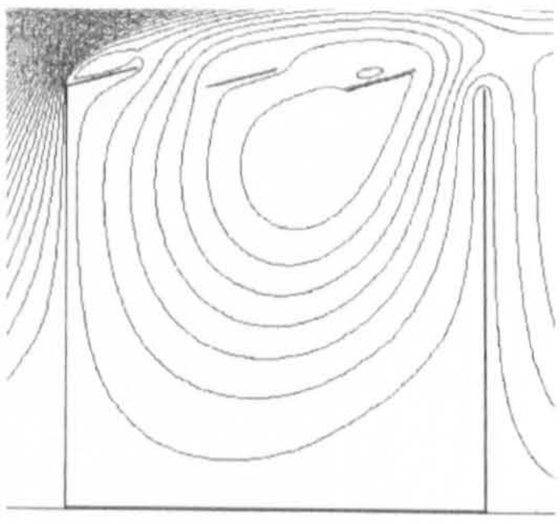

(c) Roof angle: 15°; tooth number: 3

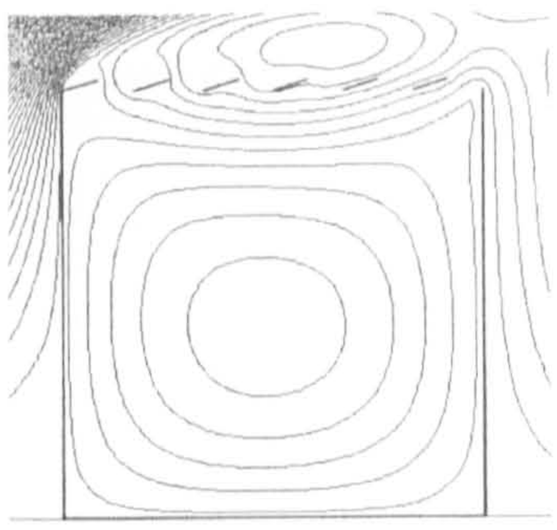

(d) Roof angle: 15°; tooth number: 6

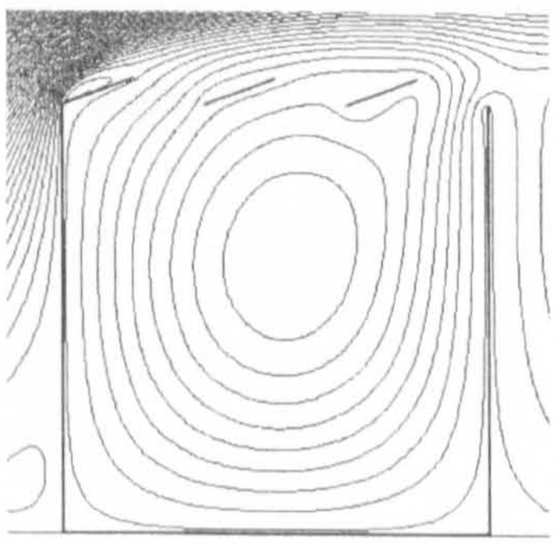

(e) Roof angle: 20°; tooth number: 3

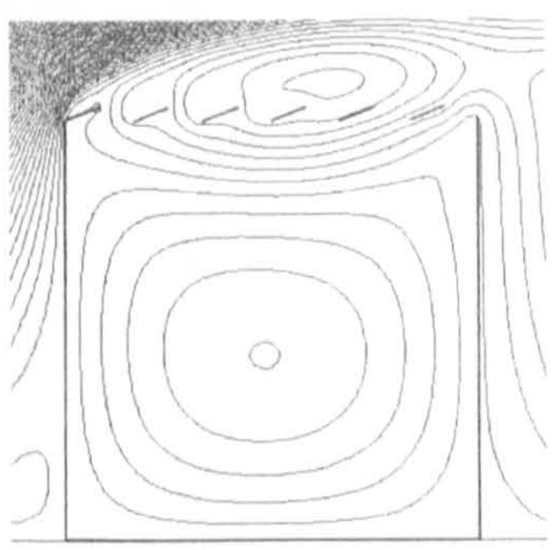

(f) Roof angle: 20°; tooth number: 6

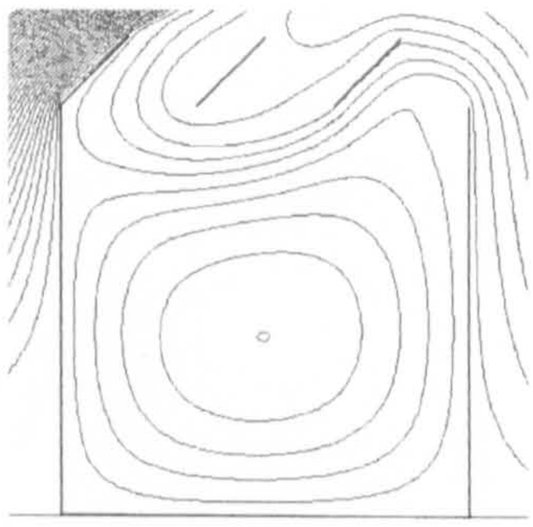

(g) Roof angle: 45°; tooth number: 3

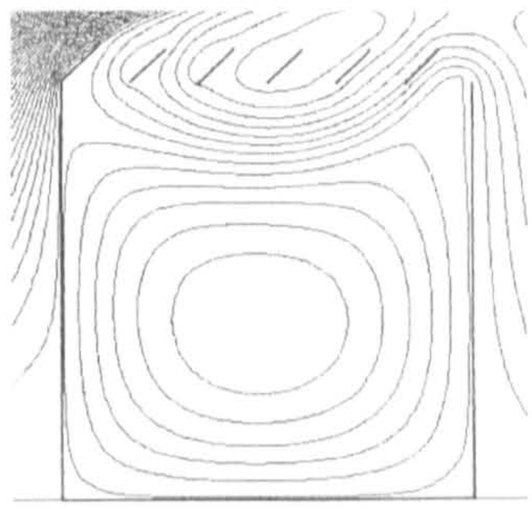

(h) Roof angle: 45°; tooth number: 6

Figure 5.18: Airflow patterns of wind-induce natural ventilation for atria with sawtooth roofs (when all leeward openings are opened and all windward openings are closed)

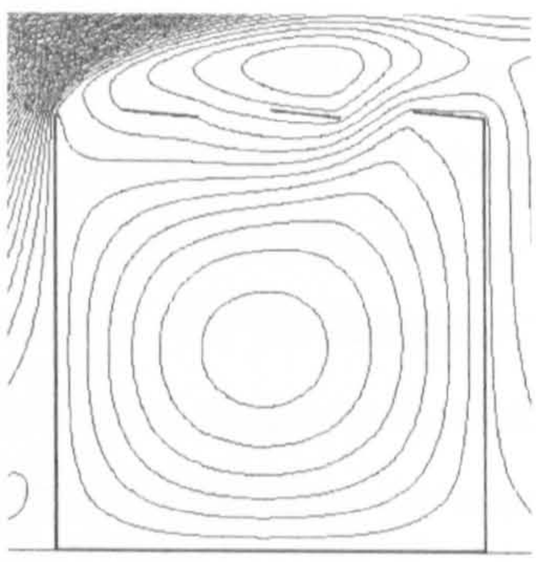

(a) Roof angle: 5°; tooth number: 3

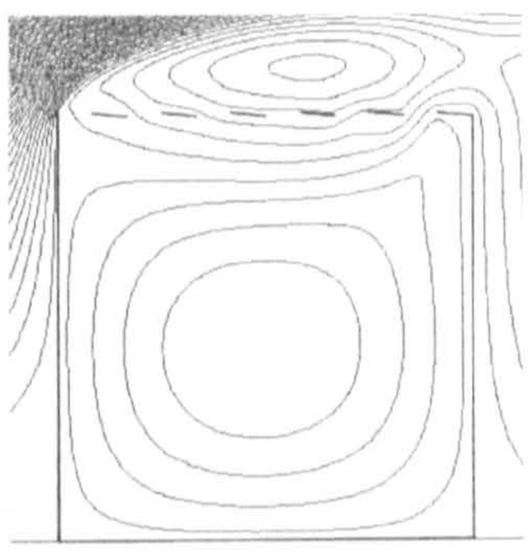

(b) Roof angle: 5°; tooth number: 6

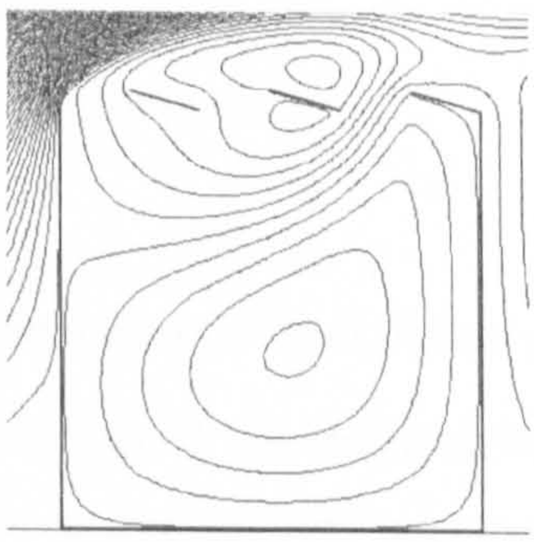

(c) Roof angle: 15°; tooth number: 3

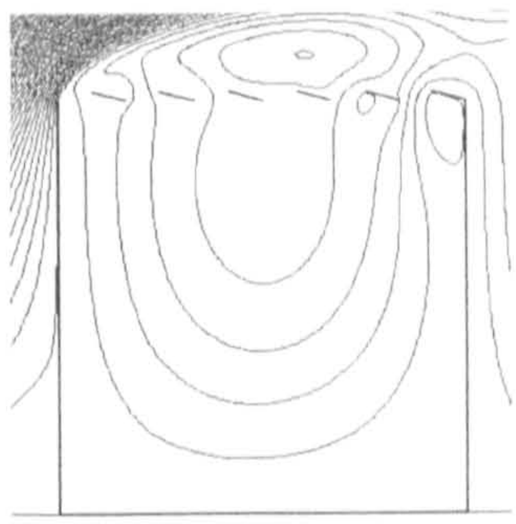

(d) Roof angle: 15°; tooth number: 6

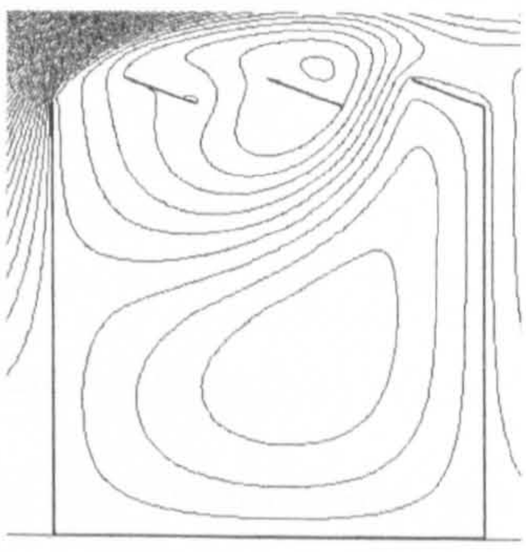

(e) Roof angle: 20°; tooth number: 3

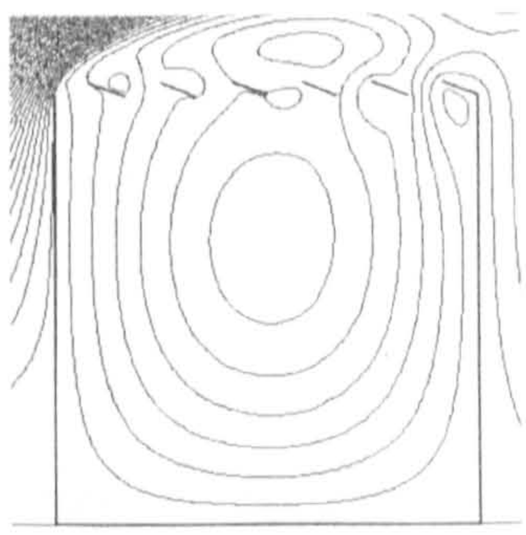

(f) Roof angle: 20°; tooth number: 6

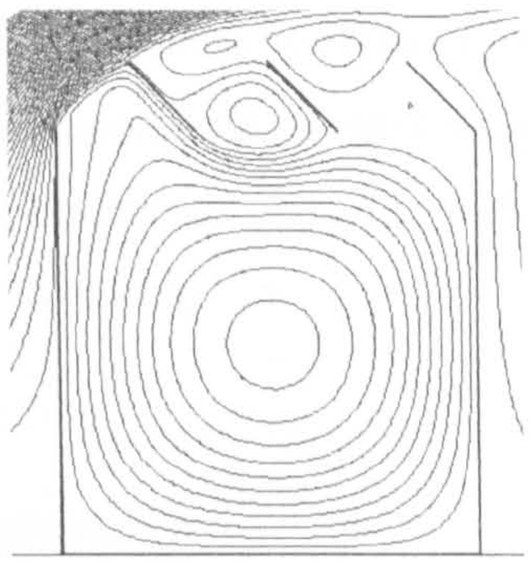

(g) Roof angle: 45°; tooth number: 3

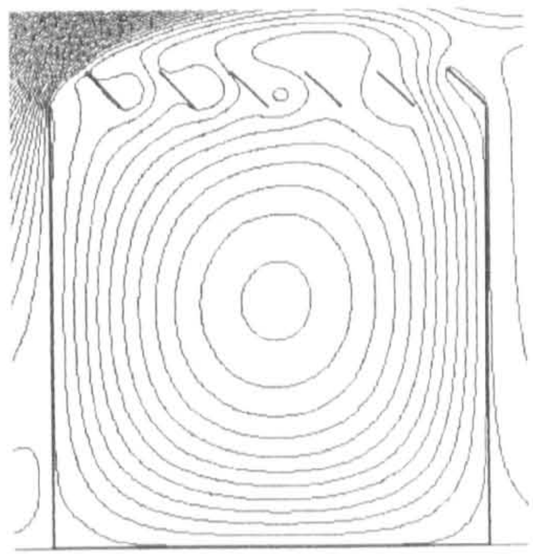

(h) Roof angle: 45°; tooth number: 6

Figure 5.19: Airflow patterns of wind-induce natural ventilation for atria with sawtooth roofs (when all windward openings are opened and all leeward openings are closed)

It can be summarised from the above discussions that all three variables that have been investigated, namely the roof angle, opening locations and number of teeth can significantly influence the ventilation performance of an atrium with a sawtooth roof and their impacts are not independent. For the situations where either all leeward or windward openings are opened, a higher roof pitch is generally more favourable if the sawtooth number is large, although the flow pattern is not the same for windward and leeward conditions: (II) for the former and (III).a for the latter. If the sawtooth number is small, higher pitch will be more suitable when the windward openings are opened, and 20° roof will lead to stronger air movement when the leeward openings are opened, which is also the case when two openings are provided at each end of the sawtooth roof.

5.3.4 Guidance on the roof design of atrium spaces

This section has identified the possible flow patterns for the wind-induced ventilation in atrium spaces through roof openings. Based on the findings on the effects of three types of roofs on the wind-induced ventilation performance of atrium spaces, guidance can be developed for different design objectives and Figures 5.9, 5.14 and 5.17-19 are particularly useful for this purpose. Below are some examples of various conditions and relevant design guidance developed.

- *Shape based design*

For this circumstance, the shape of the roof, i.e. either triangular or barrel vault or sawtooth has already been decided at earlier stage but the roof angle needs to be determined (and sawtooth number and openings location for sawtooth roof need to be determined too). It can be seen that, the best angle for triangular roof atria is 45°, and that for barrel vault roof atria

is 15°. If a sawtooth roof has to be used for an atrium, there will be three variables to be determined including sawtooth number, opening location and roof angle, and the recommendations made at the end of subsection 5.3.3 (the first paragraph of the last page) should be followed.

- *Flow pattern based design*

Sometimes the ventilation strategy should be used to assist the other passive or active strategies, such as buoyancy-driven ventilation or HVAC systems and consequently a certain flow pattern is required. If flow pattern (I) is needed, either triangular roof with roof angle above 21°, or sawtooth roof with a small number of teeth and roof angle above 20° should be employed, and the openings in the sawtooth roof should be placed on the windward side. However, barrel vault roof cannot be used to obtain flow pattern (I). If flow pattern (II) is required, all three roofs can be used but the roof angle should be 8° to 17° for triangular roofs and above 7° for barrel vault ones; with respect to sawtooth roof, if the openings are placed on the leeward side of the roof, the roof angle should be around 15° - 20° and if the openings are on the windward side, the roof angle should be larger than 15°. The openings should not be provided at two ends in a sawtooth roof in order to achieve flow pattern (II). For other roof angles not mentioned above, the flow pattern will be (III).

- *Design with limited height of the space*

Usually the building site may have certain limitations on the height the building cannot exceed, such as those historical areas or those with control of population density. In this situation, the design guidance can be obtained by comparing Figures 5.9 and 5.14 (only triangular and vault roofs are considered here for ease of demonstration): if the limitation can still hold a triangular roof with an angle above 21°, then triangular roof should be chosen to induce flow pattern (I); if the limitation can only hold a triangular roof with an angle between 8°-18°, the vault roof should be used and flow pattern (II) will result; if the limited height is extremely close to the roof level, the two roof shapes generally do not have any difference.

5.4 Impacts of opening characteristics

Having studied the impacts of the roof shape in the previous section, this section will move onto the investigation of the effects of opening characteristics on the wind-induced ventilation performance in atrium spaces. The most commonly used type of roof, i.e. triangular roof, has been selected for the majority of the investigation of this section, and three characteristics of openings, including location, size and opening methods are considered. The

location of the openings is investigated first, followed by the discussion on the size of the openings, and finally the impacts of the opening methods are studied. Research has also been extended to other types of roofs after the triangular roof cases are understood.

5.5.1 Opening locations

It can be anticipated from previous studies that, the upper part of the roof has certain effects on the formation of the reverse flow and the reattaching flow, because a roof with a lower pitch results in stronger reverse flow, and additionally, the sawtooth roofs, which can be seen as similar to reducing the height of middle part of the triangular roof can easily lead to reverse flow on the roof (see Figures 5.17-19). Thus openings at the upper part of the roof may impact on the reverse flow and reattaching flow. The simulations for the sawtooth roofs also show that the incorporation of the leeward bottom openings influences the effects of the back flow from the recirculation behind the building. As both the reverse flow and the back flow can act as the driving force for the indoor air movement, the location of the openings will therefore have significant impacts on the ventilation performance.

In order to reduce the number of simulations and hence simplify the investigation, each roof pitch is equally divided into 5 parts and marked as A to E respectively as shown in Figure 5.20. Thus 5 simulations are carried out for each roof angle firstly with two openings at the same level, and then additional simulations based on the alteration of the five simulations are also performed for the further investigation of effects of the location of the openings on the dominating forces of each flow pattern. Atria with four different roof angles which represent different flow patterns of the airflow in the space, including 5°, 15°, 20° and 45° are chosen for the study. Adjacent buildings are not considered in this part.

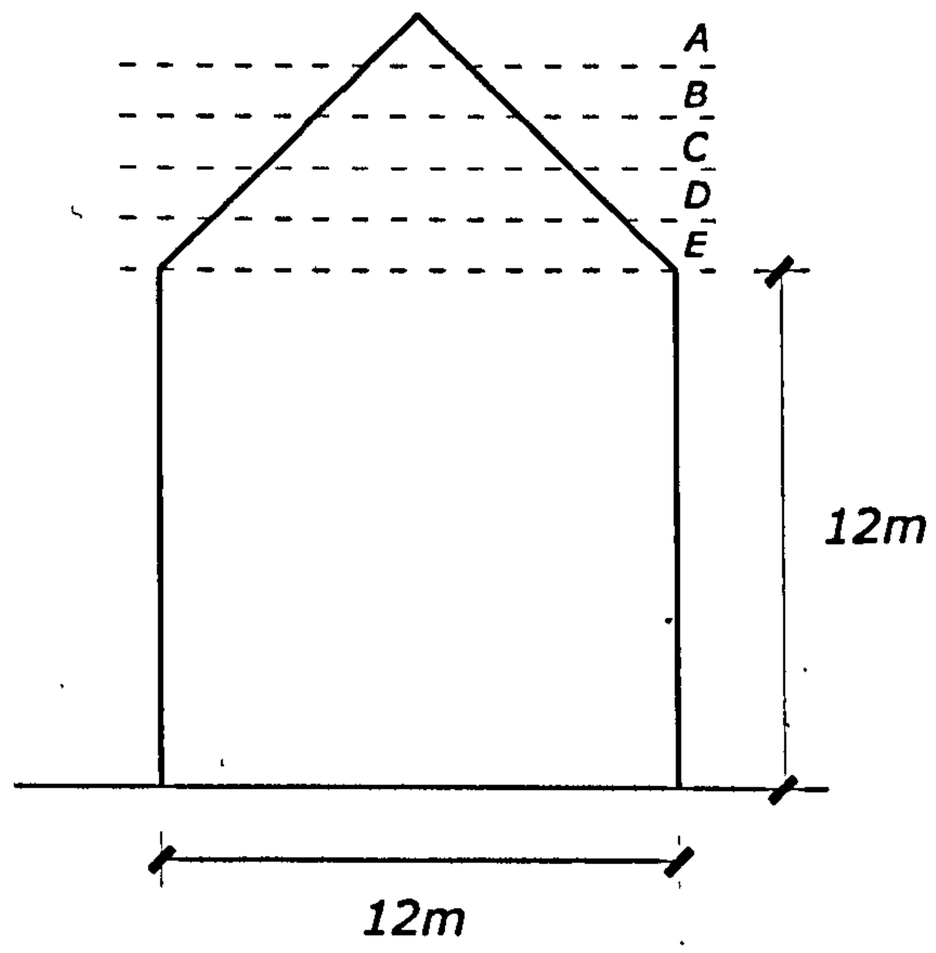

Figure 5.20: Illustration of the opening locations that are investigated in this research

• *5° roof*

Figure 5.21 shows the airflow pattern of atrium spaces with 5° roof and different opening locations. It can be observed that, the width of the reverse flow above the roof is determined by the distance between the openings; the effects of the back flow will be enhanced by placing the leeward opening closer to the back recirculation, as more flow from the recirculation will come into the building. It is also of interest to note that, the flow pattern (III).a occurs for opening locations A-D whilst it changes to (II) when the opening is provided at the bottom of the leeward roof. The reason for this can be understood by looking at the detailed air movement at the inlet opening. As identified earlier, flow pattern (III).a is driven by the collective effects of both reverse flow and back flow, and the horizontal momentums generated by these two forces assist each other. However, the reverse flow needs some distance on the roof behind the opening for the generation of horizontal momentum, as the direction of the air velocity over the inlet is generally vertical (consider the tangential direction of a vertex of a major axis of an ellipse). In addition, the development of the horizontal momentum from back flow also requires some distance on the solid roof. As a result, when the opening is placed at the bottom of the leeward pitch, there will be little horizontal momentum generated from both flow and hence the direction of the air velocity at the inlet is generally vertical, whereby flow pattern (II) takes place. Nevertheless, this seems contradictory to the findings for sawtooth roof atria: it has been demonstrated in Figure 5.18 that flow pattern (III).a occurs when the leeward opening is provided at the bottom of the pitch. This discrepancy is attributed to the roof shape: the upward shape of the sawtooth roof near the inlet opening helps the generation of the horizontal momentum from the back flow and flow pattern (III) appears as a result, whilst the downward orientation of the triangular shape of the leeward roof does the opposite and thus flow pattern (II) takes place instead.

It can also be expected from the above analysis that, more horizontal momentum will be induced resulting in stronger indoor air movement when the reverse flow becomes more egg shaped (compare a&f; c&g in Figure 5.21). In other words, in order to achieve higher air velocity at the occupants' level in the space with flow pattern (III).a, it would be good practice to place one opening at the bottom of the windward roof as outlet, provided that inlet opening is not placed at the bottom of the leeward roof. The best location for the inlet seems to be at the top of the roof, because in this way the peak of the roof does not disturb the development of the reverse flow.

However, if flow pattern (II) occurs, i.e. when there is opening at the bottom of the leeward roof, opening at the bottom of the windward roof will not be a good choice, as seen in Figure 5.21(e). Two more simulations are performed regarding to the location of the outlet

opening (see Figure 5.21h, i), and it shows that the opening in the middle of the windward roof results in a slightly higher air velocity at the occupants' level.

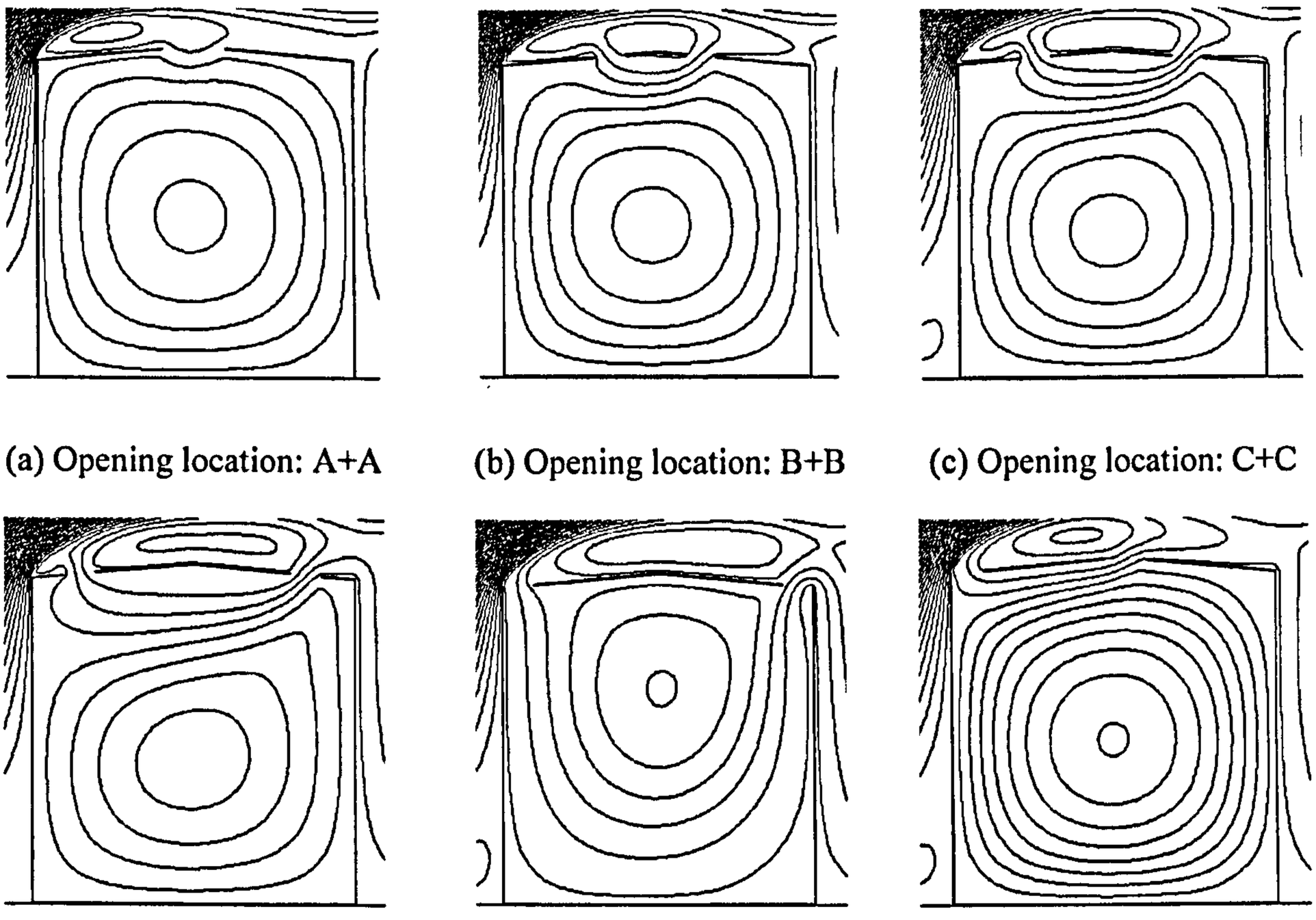

Figure 5.21: Airflow patterns of wind-induce natural ventilation for atria with 5° roof and different opening locations

- *15° roof*

The airflow patterns of the atria with 15° triangular roof and several different settings of openings are illustrated in Figure 5.22, which shows that flow pattern (II) is the most popular

opening (see Figure 5.21h, i), and it shows that the opening in the middle of the windward roof results in a slightly higher air velocity at the occupants' level.

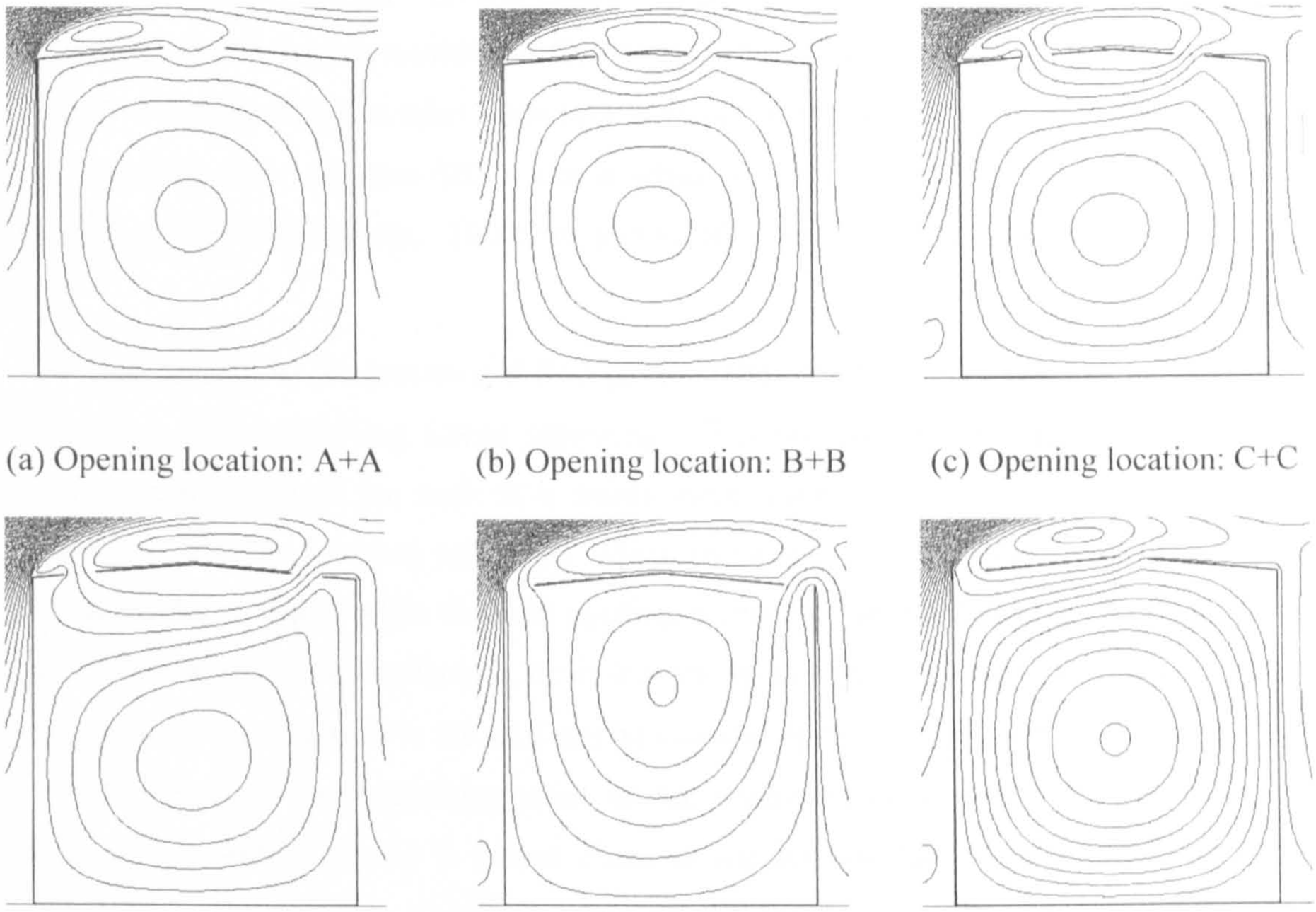

(a) Opening location: A+A (b) Opening location: B+B (c) Opening location: C+C

(d) Opening location: D+D (e) Opening location: E+E (f) Opening location: E+A

(g) Opening location: E+C (h) Opening location: A+E (i) Opening location: C+E

Figure 5.21: Airflow patterns of wind-induce natural ventilation for atria with 5° roof and different opening locations

- *15° roof*

The airflow patterns of the atria with 15° triangular roof and several different settings of openings are illustrated in Figure 5.22, which shows that flow pattern (II) is the most popular

among all except the last one. It has already been identified earlier that the driving force for the air movement of atria with this roof angle is the interaction between the reattaching flow and the back flow from the recirculation behind the building. Mostly the former flow overwhelms the latter such as Figure 5.22 (a) - (g) but Figure 5.22(h) shows that the opposite can also happen under certain circumstances resulting in the occurrence of flow pattern (III). It should be noted that the flow pattern (III) that takes place here is driven by reattaching flow and is different from those other two flow patterns (III) a and b which are induced mainly by reverse flow and recirculation flow respectively. This flow pattern is defined as flow pattern (III).c for further use.

The reason for the presence of flow pattern (III).c for this roof angle can be understood by analysing the two driving forces separately. Previous studies have pointed out that the horizontal momentum of the back flow needs some distance to develop but its effects will reduce if the distance becomes too large. These two phenomena together mean that the back flow will be the strongest when the inlet opening is placed near the middle of the leeward roof pitch. With respect to the reattaching flow, it is shown in Figure 5.22(a) – (e) that the position for the main flow to reattach to the roof can be changed by the location of the outlet opening in the windward pitch: the reattaching point on the windward pitch will move upwards if the location of the outlet opening is placed closer to the bottom due to the vertical momentum brought within the outgoing air which enhances the separation at the leftmost corner. This upward vertical momentum can also bring the horizontal momentum generated upwards and thus make the reattaching flow weaker. As a consequence, when the inlet opening is provided near the middle of the leeward opening and outlet opening is placed at the bottom, the horizontal momentum of the back flow will be the strongest and that of the reattaching flow will be the weakest, under which condition flow pattern (III).c will result and the air movement at the occupants' level will be considerably weakened, as seen in Figure 5.22(i).

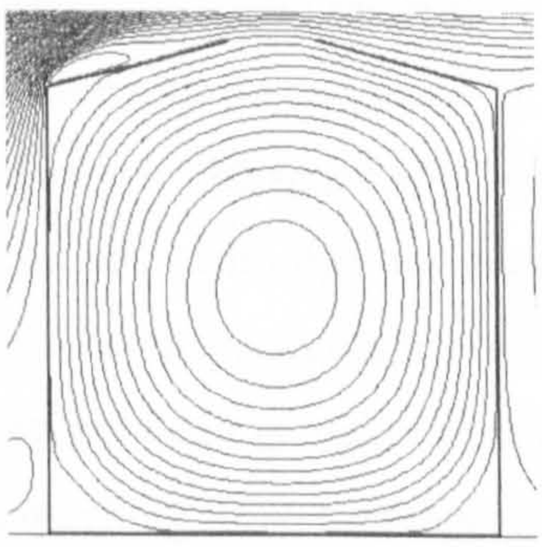

(a) Opening location: A+A

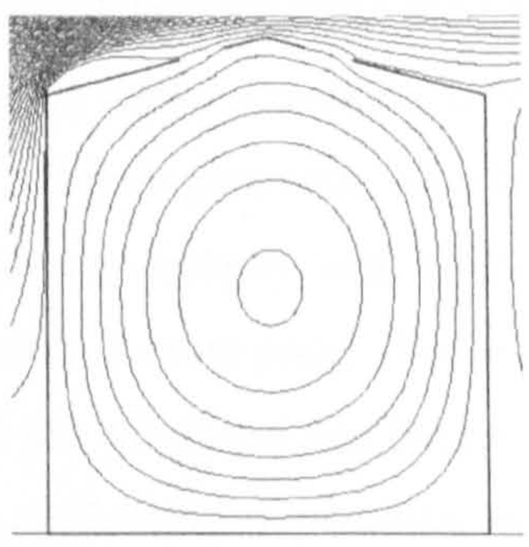

(b) Opening location: B+B

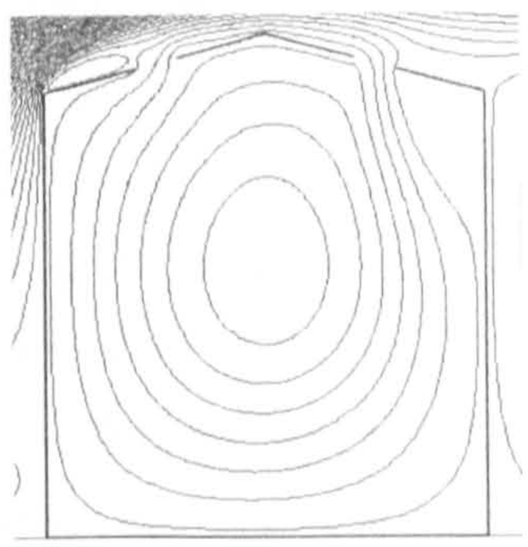

(c) Opening location: C+C

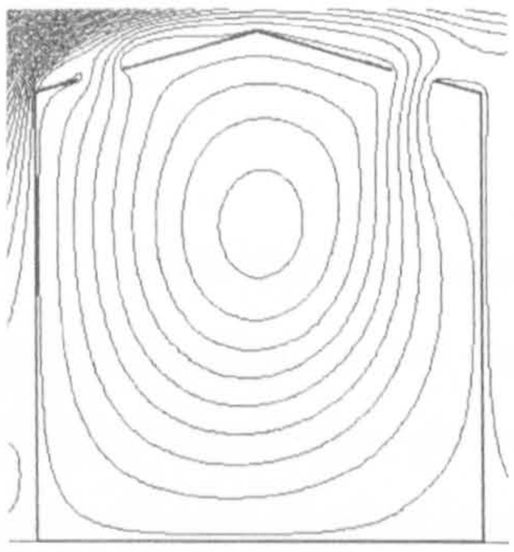

(d) Opening location: D+D

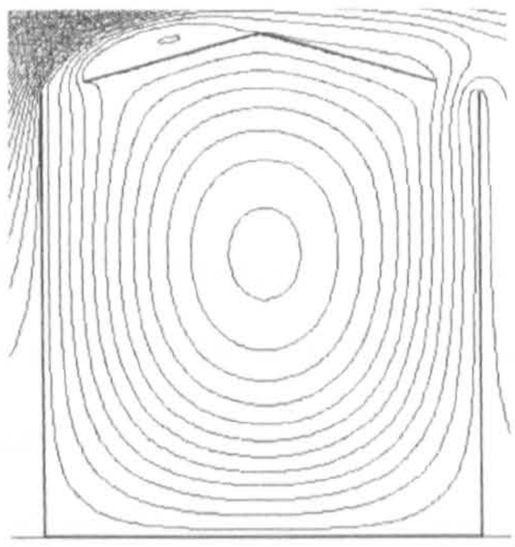

(e) Opening location: E+E

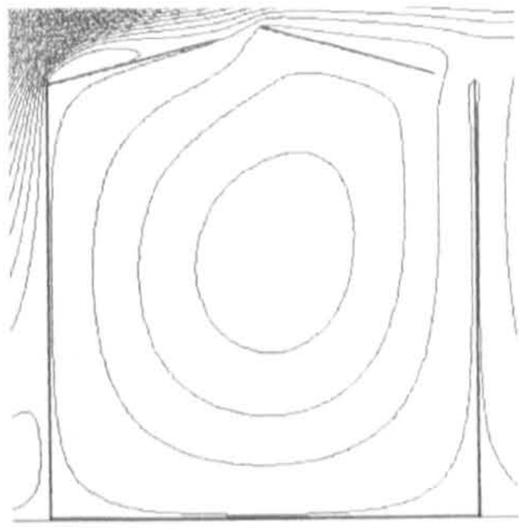

(f) Opening location: A+E

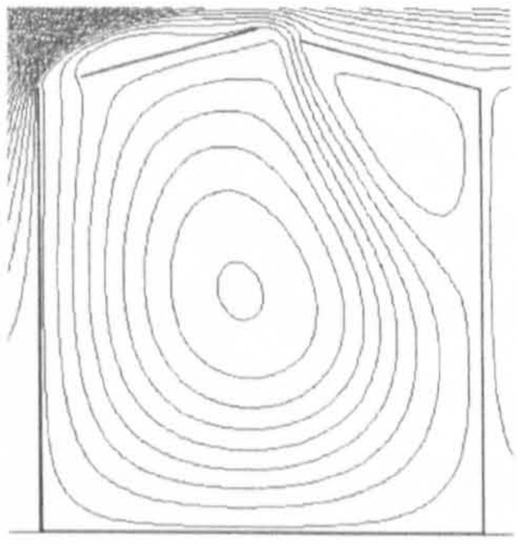

(g) Opening location: E+A

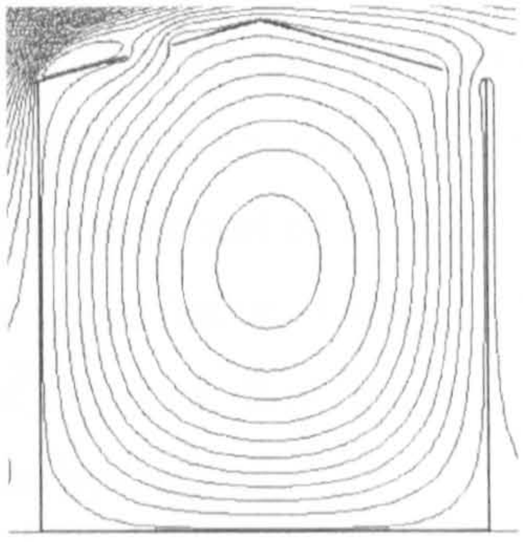

(h) Opening location: C+E

(i) Opening location: E+C

Figure 5.22: Airflow patterns of wind-induce natural ventilation for atria with 15° roof and different opening locations

Based on the above analysis, higher air velocities at the occupants' level can be achieved by either reducing the effects of the back flow or reinforcing the reattaching flow or both. Thus, the inlet opening should be located at the top or bottom level of the leeward pitch and the outlet opening should be placed at the top or middle level of the windward pitch. This conclusion can be further demonstrated by comparing the ventilation performance of different scenarios shown in Figure 5.22: scenario (a) has both virtues introduced above and hence the highest air velocities at the occupants' level; reducing the levels of both openings will decrease the velocity down (see a-c); when the leeward opening is located at the bottom or top, the air velocity in the space will be enhanced (compare c&h, e&g&i). However, there is one exception here: atria with opening location (f) also comply with both of the conditions mentioned above for a better performance but the result is quite poor. The reason for this is that the peak of the leeward pitch is higher than that of the windward one because of the outlet opening and thus the reattaching flow, together with the outflow from the outlet will separate when encountering with the leeward pitch, which significantly weakens the reattaching flow driving the airflow in the space (see Figure 5.22f).

• *20° roof*

When the roof angle continues to increase, the windward side of the roof will have more significant effects on the separation of main flow at the windward corner. It is shown in Figure 5.23 that the airflow pattern of the wind-induced ventilation of atria with 20° roof is very sensitive to the opening locations. It can be seen that, when the openings are placed near the top level, flow pattern (I) occurs, such as (a) and (b); then the pattern changes to (III).b when the openings are located near the middle and atria with openings at the bottom of the roof pitches lead to flow pattern (II). This is basically because of the pressure distribution on the windward roof pitch resulted from the relationship between the main flow and the windward roof pitch: positive pressure can be caused at the upper part of the pitch with the pressure of the lower part still remained negative due to the more inclined roof. Consequently, when the windward opening is located near the top of the roof, flow pattern (I) will be incurred; otherwise air movement in the space will be driven by suction.

Nevertheless, scenario (a) and (b) also show that very little flow will enter into the building but move quite smoothly along the sharp peak of the roof. As seen also in other scenarios (e.g. Figure 5.23f), this phenomenon helps to avoid the generation of the shear stress between the roof and the flow and is favourable for the development of the airflow pattern (I) resulting in higher air velocities in the space.

Similar to governing force for the atria with 15° roof, the suction airflow for atria with 20° roof is also induced by the interaction between the reattaching flow and the back flow from the recirculation behind the building. However, due to the higher pitch, the flow for 20° roof may separate at the peak of roof resulting in a significant reduction of the reattaching flow and thus when the leeward opening is provided near the middle of the leeward roof pitch which back flow has significant effects on, the back flow will be stronger and will be the primary source driving the air movement in the space (see Figure 5.23c, d). If the level of both openings continue to reduce to the bottom of the pitches, the effects of the back flow will reduce as explained before and flow pattern (II) will result (see Figure 5.23e).

The location of the windward opening also has similar effects on the reattaching flow as discussed for the 15° roof. When it is located near the top, the reattaching flow can move smoothly as mentioned above; when the location is reduced to the middle of the windward pitch, the reattaching point would be moved upwards to the peak of the roof causing significant separation of the flow there and hence reduction of its capacity to drive the flow in the space (see Figure 5.23 c, h); if the windward opening is at the bottom, the vertical momentum of the outgoing air can help to reduce the separation (see Figure 5.23e, g, i). The airflow pattern for this circumstance is dependent of the strength of the back flow and becomes very complicated: when the inlet opening is placed near the bottom of the leeward roof and the back flow is not

sufficiently developed, flow pattern (II) will take place, as shown for scenario (e); and when the inlet opening is placed near the upper area of the leeward pitch, as the peak of the roof does not bring too much disturbance, the reattaching flow can move smoothly around it and enter the building driving the flow in the space with the occurrence of flow pattern (III).c, as seen for scenarios (g) and (i).

It can be seen from the above discussions that the airflow of atria with 20° roof is very complicated covering a wide range of flow patterns defined earlier, and this implies that this range of angles from 18° to 20° is more like a transitional phase where the performance of the airflow in and around the building is very sensitive to small changes. According to the above observation and analysis, in order to achieve higher air velocities in the space, the leeward opening should be placed near the top with the windward opening provided at the bottom if flow pattern (III).c is needed, whilst both openings should be located near the top if flow pattern (I) is more favourable and the location of the windward opening is more crucial. Other flow patterns, including (II) and (III).b, generally lead to very weak performance.

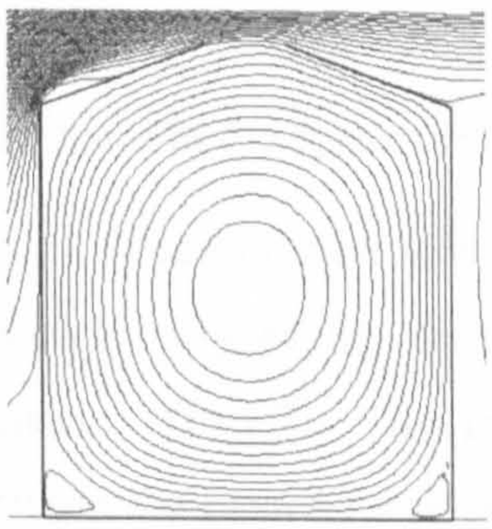

(a) Opening location: A+A

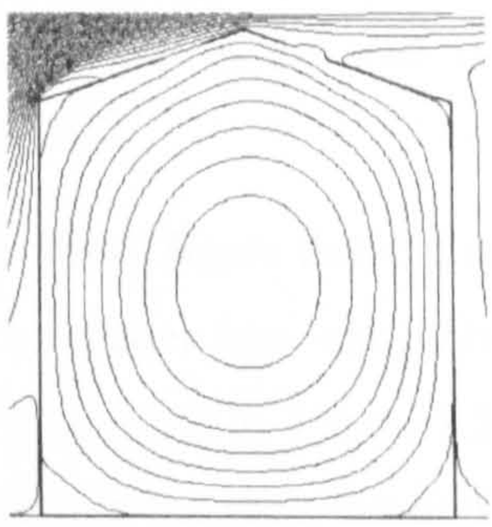

(b) Opening location: B+B

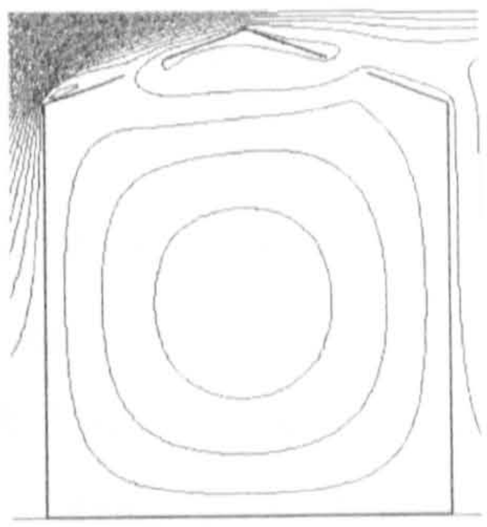

(c) Opening location: C+C

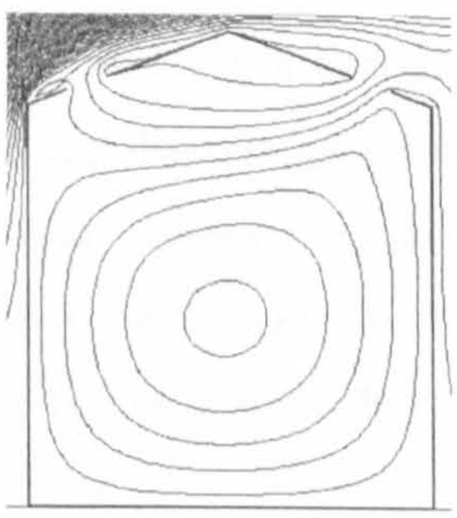

(d) Opening location: D+D

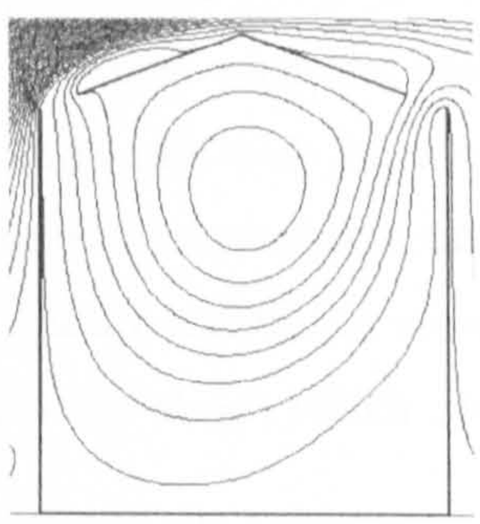

(e) Opening location: E+E

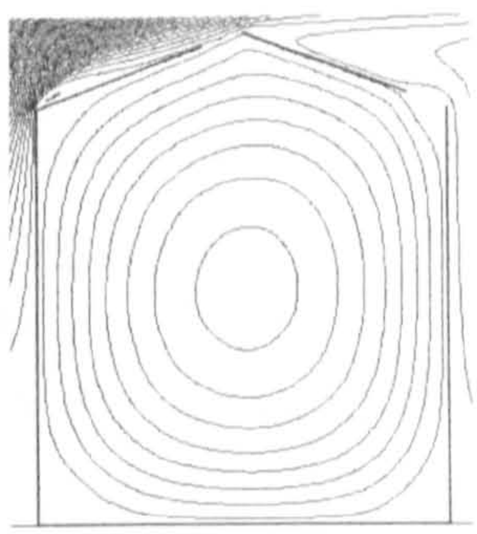

(f) Opening location: A+E

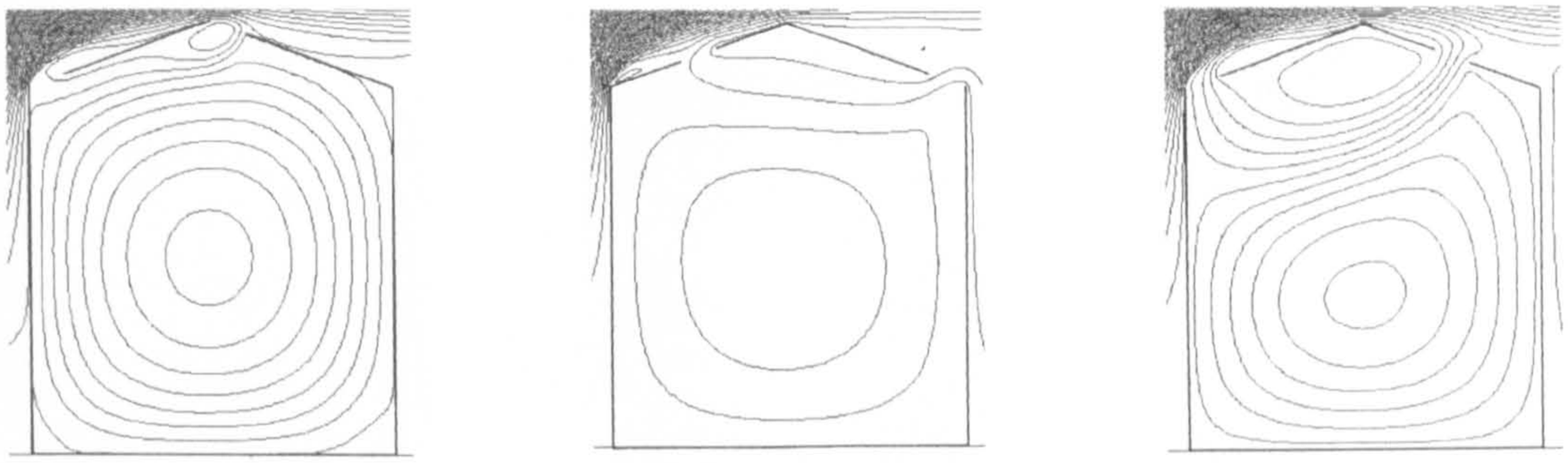

(g) Opening location: E+A (h) Opening location: C+E (i) Opening location: E+C

Figure 5.23: Airflow patterns of wind-induce natural ventilation for atria with 20° roof and different opening locations

• *45° roof*

Figure 5.24 illustrates the airflow patterns of the wind-induced ventilation of atria with 45° triangular roof and different settings of openings. All the scenarios have flow pattern (I) except scenario (a), in which flow pattern (III).b occurs resulting in a very weak performance, because the main flow separates at the top of the roof and the back flow dominates the air movement in the space (see Figure 5.24a).

It can also be seen from the above figure that the air velocity at the occupants' level is generally very evenly distributed, no matter how unevenly the openings are located, such as scenarios (f) to (i). This is further confirmed by Figure 5.25, which illustrates the relationship between the local air velocity coefficients and their location at the occupants' level. It is shown that, the air velocities in the space achieve the highest when both openings are located in the middle of the pitches such as scenario (b) and (c). This is because, the "tunnel effect", which flow pattern (I) is based on, is the strongest when the openings are on the same line and the wind can directly go through them. The atria with the windward opening at the bottom of the pitch have weaker performance than other scenarios: scenario (g) and (i) have the lowest air velocity coefficients among all simulations, and the air velocity of scenario (e) at the occupants' level is lower than that of scenarios (b) to (d) which also have "directly-through" opening locations.

It can be summarised from the above discussion that, flow pattern of the atria with 45° roof is (I) except the both openings on the windward and leeward pitches are at the top. In order to achieve the highest air velocity in the space, both openings should be located in the middle of each roof pitch and it is not good practice to place the windward opening at the bottom of the roof pitch.

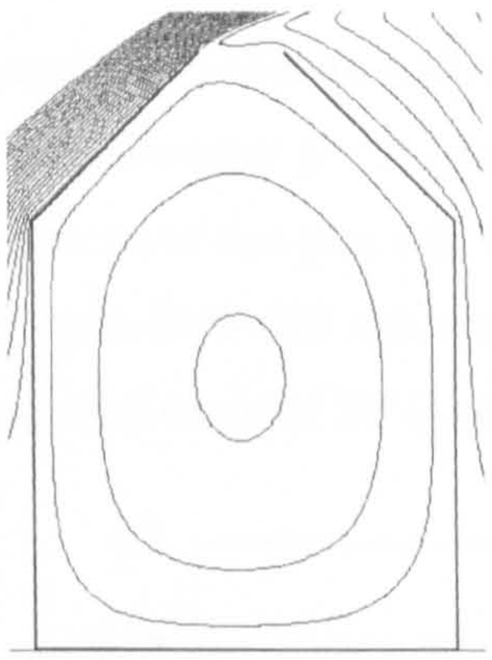

(a) Opening location: A+A

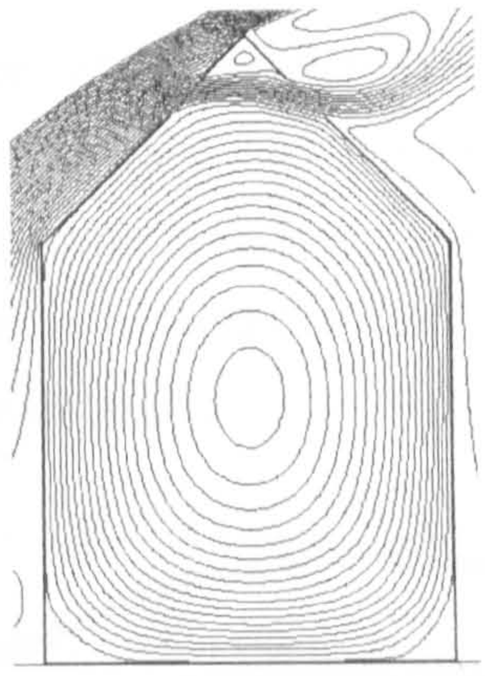

(b) Opening location: B+B

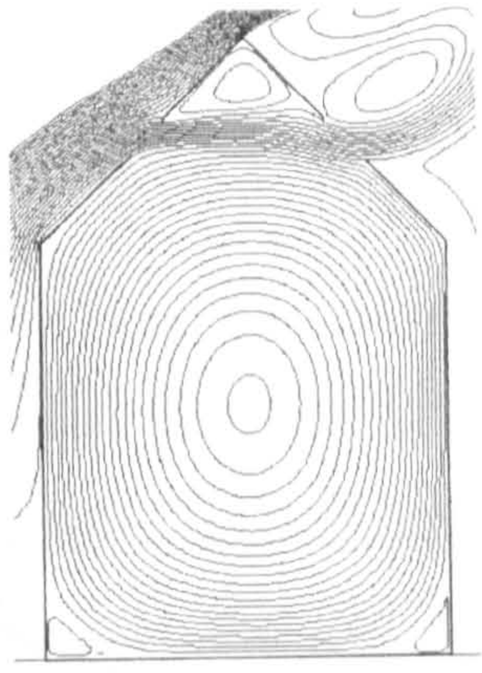

(c) Opening location: C+C

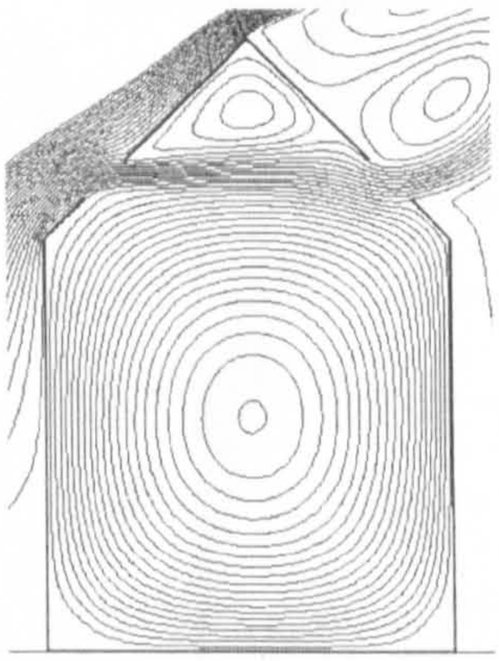

(d) Opening location: D+D

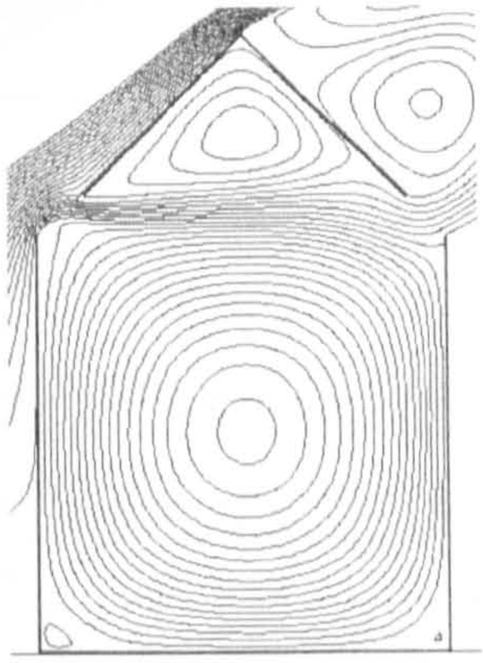

(e) Opening location: E+E

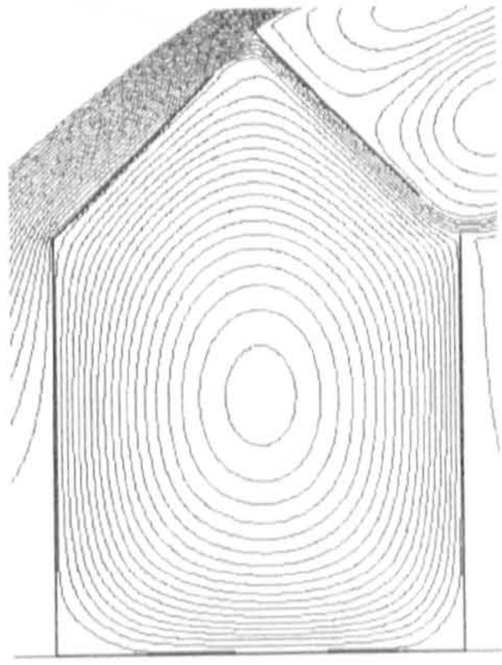

(f) Opening location: A+E

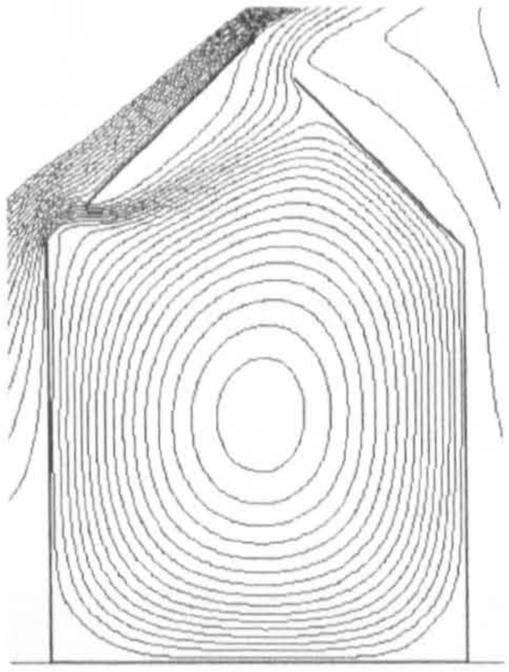

(g) Opening location: E+A

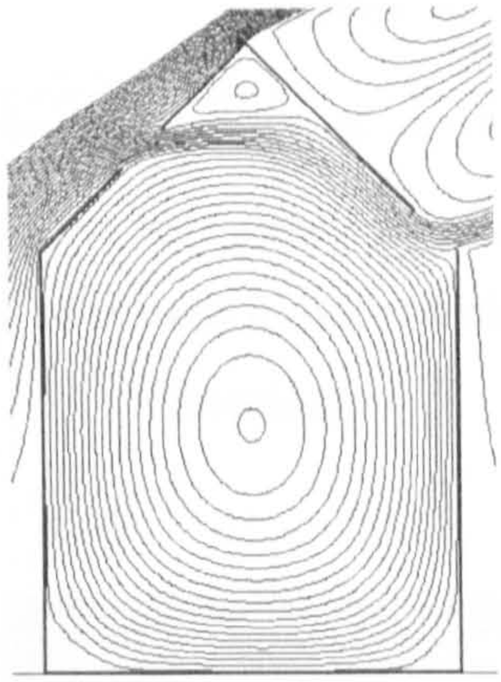

(h) Opening location: C+E

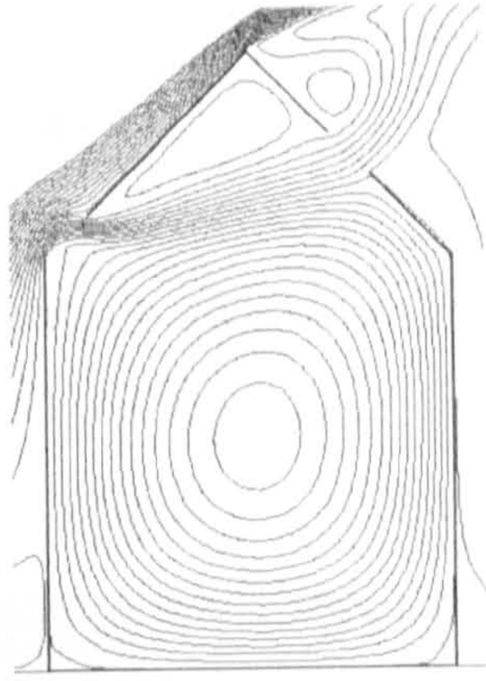

(i) Opening location: E+C

Figure 5.24: Airflow patterns of wind-induce natural ventilation for atria with 45° roof and different opening locations

• *Barrel vault roof*

It has been pointed out that, when the roof angle is below 20°, the main flow will separate at the top corner of the windward wall and the ventilation performance in the atrium space is generally similar to the correspondent triangular case that has the same flow pattern.

Therefore, the opening characteristics of this group of atria will also have the similar effects as described earlier for 5° and 15° roof atria and there is no need to repeat the investigation here. The focus of this part will be the vault roof atria with a tangential angle of more than 20° where the main flow will not separate before meeting the atrium roof. The barrel vault roof with a tangential angle of 30° is chosen for the study.

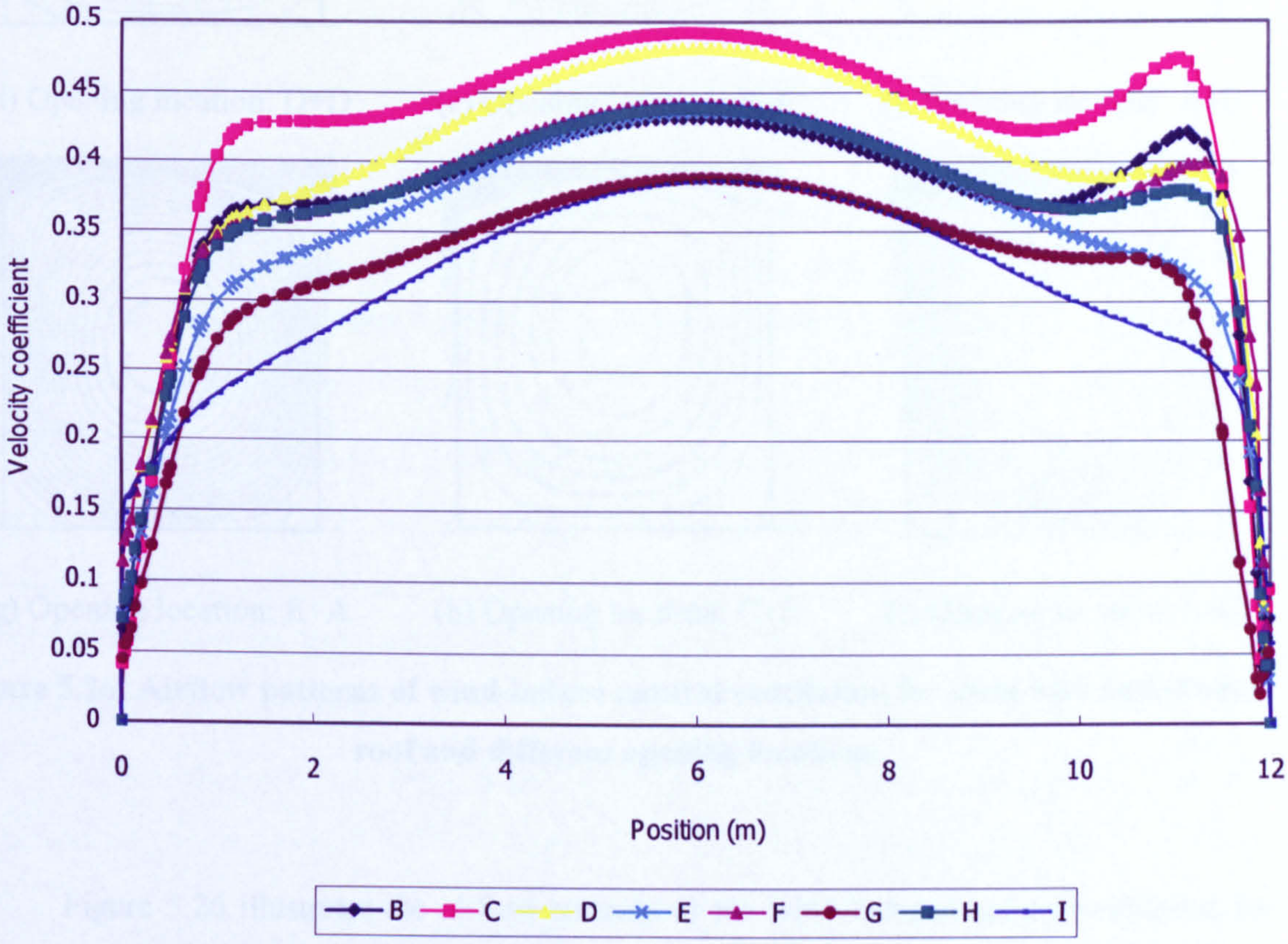

Figure 5.25: The distributions of the air velocity coefficients at the occupants' level for wind-induced natural ventilation of atrium buildings with 45° roof and different opening locations

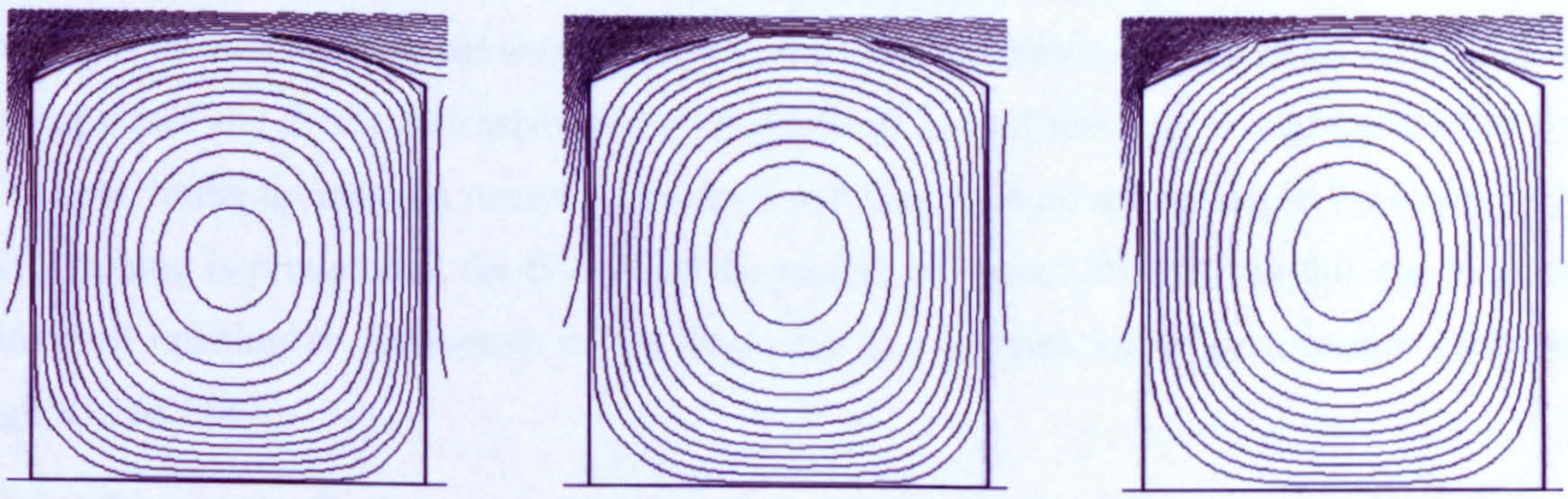

(a) Opening location: A+A (b) Opening location: B+B (c) Opening location: C+C

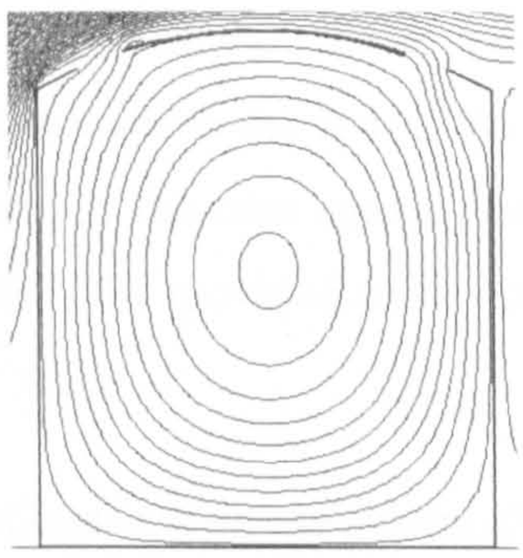

(d) Opening location: D+D

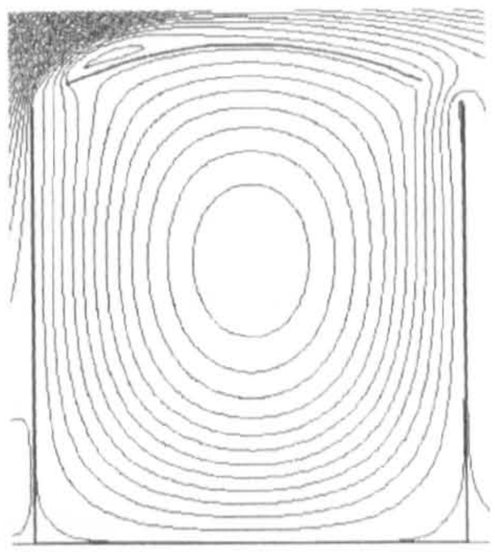

(e) Opening location: E+E

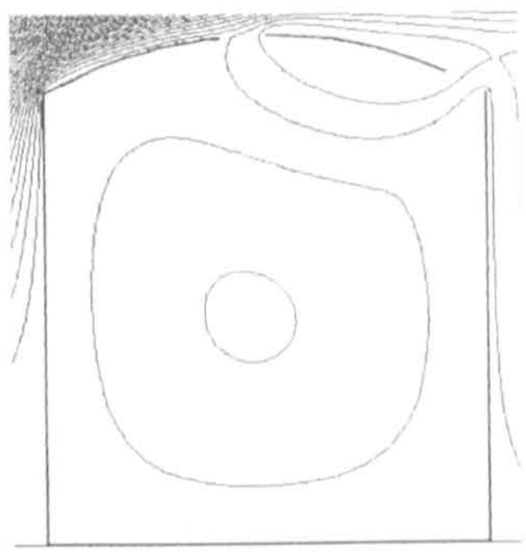

(f) Opening location: A+E

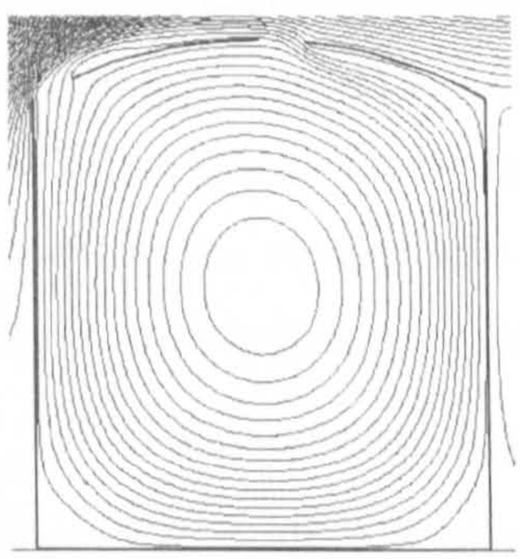

(g) Opening location: E+A

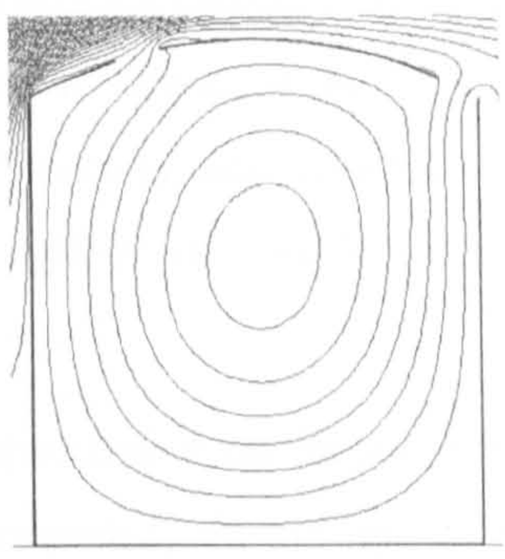

(h) Opening location: C+E

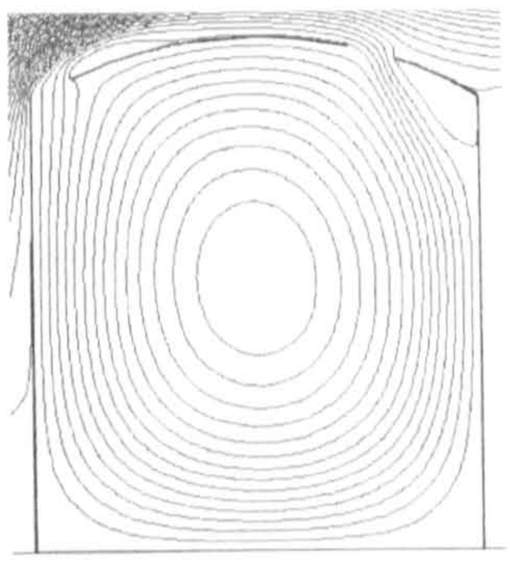

(i) Opening location: E+C

Figure 5.26: Airflow patterns of wind-induce natural ventilation for atria with barrel vault roof and different opening locations

Figure 5.26 illustrates the airflow patterns of the wind-induced natural ventilation for atria with barrel vault roof and several different opening locations. It is shown that flow pattern (II) is the most popular among all scenarios, which means that the reattaching flow is the dominating force. It has been pointed out in the analysis for the flow pattern of 15° triangular roof atria that the reattaching flow is influenced by the location of the outlet opening in the windward side and this phenomenon is also observed for this part of study. When the outlet opening is located in the upper area of the roof, the vertical momentum can bring the reattaching flow upwards and even cause separation at the peak of the roof resulting in significant reduction of the horizontal momentum near the roof level and hence the air movement in the space, if the inlet opening is provided at the bottom of the roof (see Figure5.26f&h). In this situation, the windward opening at the bottom of the pitch can give a much better performance (compare Figure5.26e&f&h).

In scenario (f), the separation is too strong and the horizontal momentum from the back flow drives the airflow in the space causing the occurrence of flow pattern (III).b. This analysis also suggests that the inlet opening at the top of the roof will help to enhance the airflow, as the reattaching flow at the peak of the roof has very strong horizontal momentum. This can be seen by comparing scenario (e), (g) and (i).

Based on the above discussion, it can be summarised that, in order to induce stronger air movement in the space, the inlet opening on the leeward roof should be placed near the upper area. If the inlet opening has to be positioned at the bottom of the roof, the windward opening should be provided at the bottom of the roof as well for a better performance.

• *Guidance on the design of the openings locations*

The above investigations were concerned with the identification of possible flow patterns for each typical roof angle and the effects of the location of two small openings on the controlling forces of each flow pattern. Based on the relevant findings, design guidance can be developed for different design objectives and conditions, and Figures 5.21 to 5.24, 5.26 illustrating the comparisons of the airflow patterns for different scenarios of openings locations are particularly useful for this purpose.

If the roof angle has been specified at earlier stage and the openings locations need to be designed to achieve a better performance, the design guidance provided at the end of each subsection dealing with each roof angle should be followed, which can be summarised as follows (only triangular and vault roofs are considered here and it is assumed that only two openings are used on the roof):

• If the triangular roof angle is below 8°, either of the openings should be provided at the bottom of the roof pitches but they cannot be placed at the bottom of the roof at the same time;

• If the triangular roof angle is between 8°-17°, both openings should be placed at the top or bottom of the roof;

• If the triangular roof angle is between 17°-21°, at least either of the openings should be placed at the top of the roof and it would be better if both of them are positioned there;

• If the triangular roof angle is above 21°, both openings should be placed at the same level, and for the best, they should be positioned in the middle of the roof;

• If vault roof is used and the roof angle is below 21°, correspondent guidelines above for the triangular roofs should be followed; if the roof angle is above 21°, only one condition should be avoided, which is that, the windward opening is placed near the top of the roof pitch when the leeward opening is at the bottom. Otherwise good ventilation performance will be generally achieved.

If a certain flow pattern is the design requirement, it should be noted that triangular roof atria with roof angle below 8° can only produce airflow pattern (II) and (III) depending on the location of leeward opening. Those with roof angle 8° -17° generally have flow pattern (II) except when the windward opening is at the bottom and the leeward opening is in the middle.

The airflow pattern in triangular roof atria with roof angle 17° to 21° covers a very wide range and is very sensitive to the openings locations. It is therefore not recommended to use atria with this range of roof angle for the control of flow pattern. Atria with roof angle above 21° mostly generates flow pattern (I), and the airflow pattern in vault roof atria with angle above 21° is generally (II).

5.5.2 Opening size

As has been pointed out, the atria with the largest opening size, namely the courtyards have a very weak ventilation performance and its flow pattern, (III).b is not commonly seen in atria with small openings. In addition, this phenomenon is quite different from ordinary buildings with cross ventilation, where larger openings usually result in higher air velocities in the space. These suggest that the opening size may have significant impacts on the ventilation performance of atria and its effects are quite different from those of simple plane buildings. This will be the main concern of this part of investigation.

Previous studies have made clear the possible flow patterns for the prototype atria with each typical roof angle and their associated controlling forces. Based on these findings, this subsection will concentrate on how opening size affect the airflow patterns and the air velocity at the occupants' level. Similar to the last subsection, this subsection is still divided into five parts, each of which deals with one typical roof angle respectively. As has also been shown, openings located at the top, middle or bottom of a roof pitch may have very different attributions and thus they will be studied separately in each part.

- *5° roof*

As has been found out earlier, two possible flow patterns may occur for atria with 5° triangular roof and two small openings: (III).a and (II), and the effects of large openings on them are discussed respectively as follows. Let us first consider the atrium with two small opening in the middle of the roof pitches. It has a flow pattern of (III).a, as shown in Figure 5.27 (a). If the size of the leeward opening is enlarged, the back flow from the recirculation behind the building will increase and then dominate the airflow at the roof level resulting in the flow pattern (III).b. However, with the increase of the leeward opening size, the horizontal momentum of the reverse flow is significantly weakened because of the less distance on the leeward side of the opening for the development of the reverse flow. Furthermore, the size of the recirculation at the roof level is also significantly increased. It can be seen that, in this situation the air velocity in the space is significantly reduced, as shown in Figure 5.27 (b) and (c). On the contrary, if the windward opening is enlarged, the back flow will not be influenced

but more horizontal momentum will be generated by the reverse flow enhancing the air movement in the space (see Figure 5.27d&e).

However, if both openings are located at the top forming a larger opening, it will not lead to flow pattern (III).b. When the large opening is on the leeward side, the main flow has already started to move downwards over the windward roof pitch and reattach to the roof level, which overwhelms the back flow from behind the building resulting in flow pattern (II) (see Figure 5.27g); when the larger opening is on the windward side, the same will happen as for middle openings and the reverse flow will drive the air movement in the space (see Figure 5.27h). It can be seen that the air velocities at the occupants' level for both of the above two scenarios are higher than the original (see Figure 5.27f), which suggests that, the ventilation performance of a courtyard can be improved with a shelter at the roof level that has certain length.

As regards flow pattern (II), i.e. when the leeward opening is placed at the bottom of the roof pitch, enlarging the opening on the windward roof cannot change the flow pattern either and higher air velocities will be induced in the space, as the effects introduced above; the increase of the size of the leeward opening will lead to flow pattern (III).b with the air velocity in the space reduced, which also have similar effects as mentioned above.

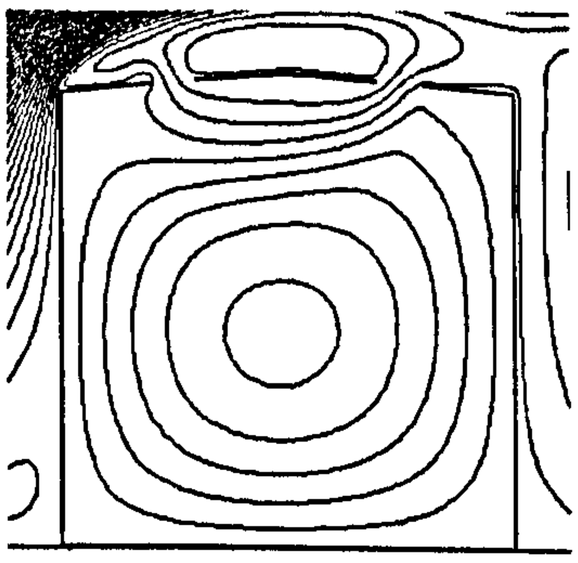

(a) Opening size: C+C

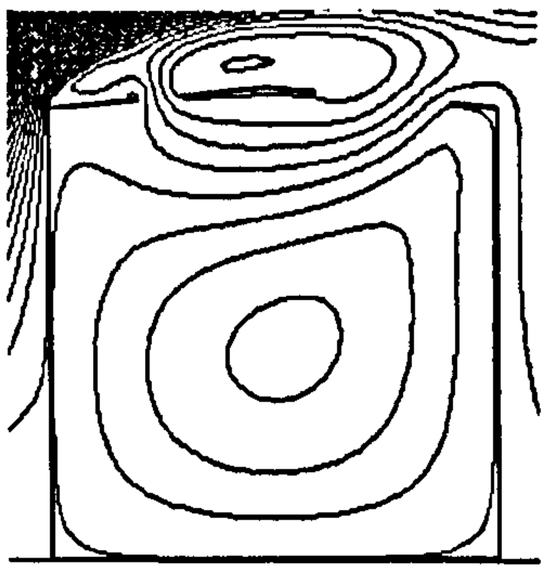

(b) Opening size: C+3C

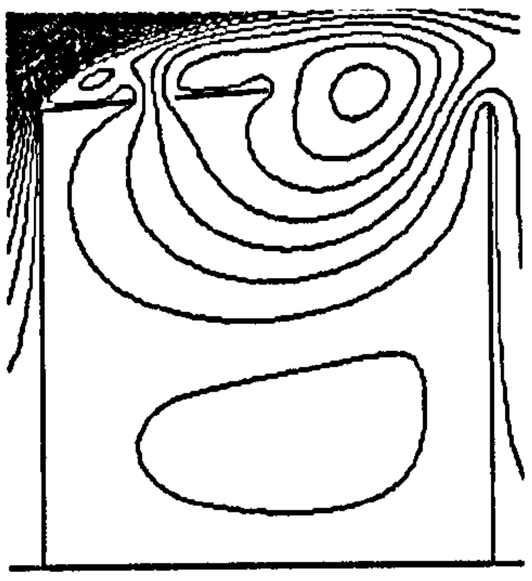

(c) Opening size: C+5C

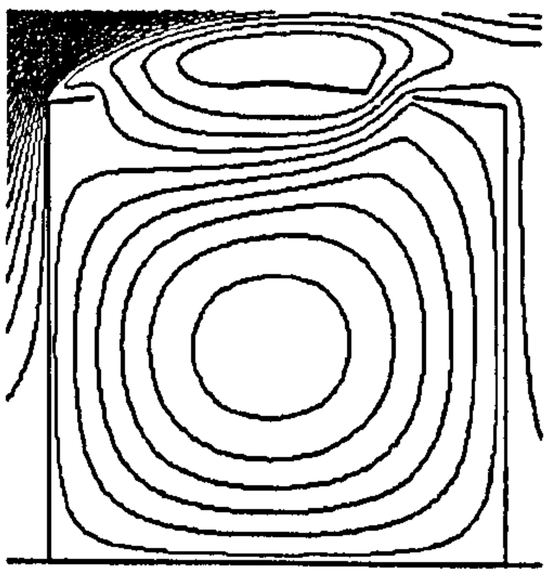

(d) Opening size: 3C+C

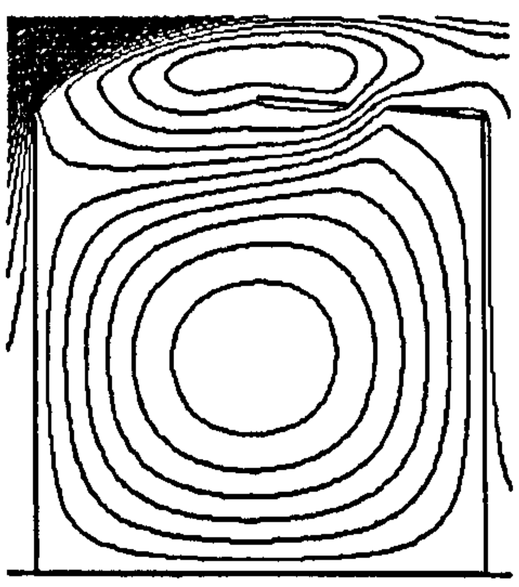

(e) Opening size: 5C+C

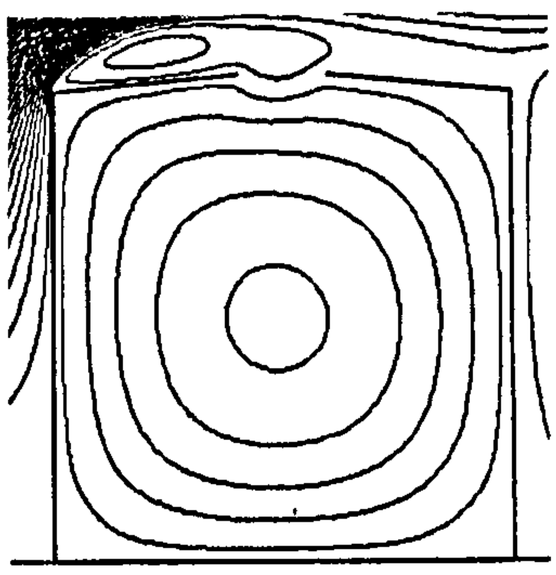

(f) Opening size: A+A

but more horizontal momentum will be generated by the reverse flow enhancing the air movement in the space (see Figure 5.27d&e).

However, if both openings are located at the top forming a larger opening, it will not lead to flow pattern (III).b. When the large opening is on the leeward side, the main flow has already started to move downwards over the windward roof pitch and reattach to the roof level, which overwhelms the back flow from behind the building resulting in flow pattern (II) (see Figure 5.27g); when the larger opening is on the windward side, the same will happen as for middle openings and the reverse flow will drive the air movement in the space (see Figure 5.27h). It can be seen that the air velocities at the occupants' level for both of the above two scenarios are higher than the original (see Figure 5.27f), which suggests that, the ventilation performance of a courtyard can be improved with a shelter at the roof level that has certain length.

As regards flow pattern (II), i.e. when the leeward opening is placed at the bottom of the roof pitch, enlarging the opening on the windward roof cannot change the flow pattern either and higher air velocities will be induced in the space, as the effects introduced above; the increase of the size of the leeward opening will lead to flow pattern (III).b with the air velocity in the space reduced, which also have similar effects as mentioned above.

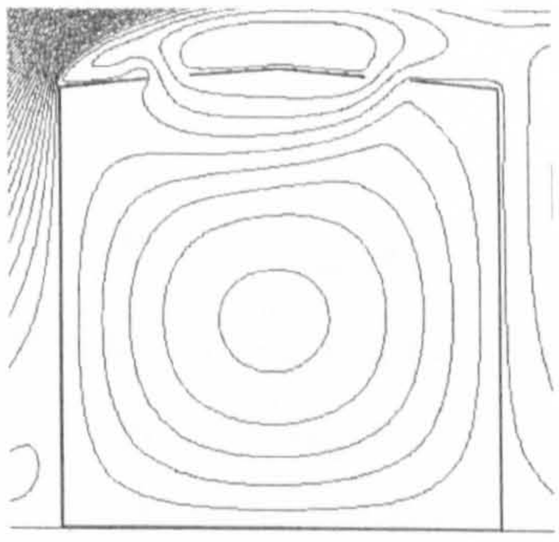

(a) Opening size: C+C

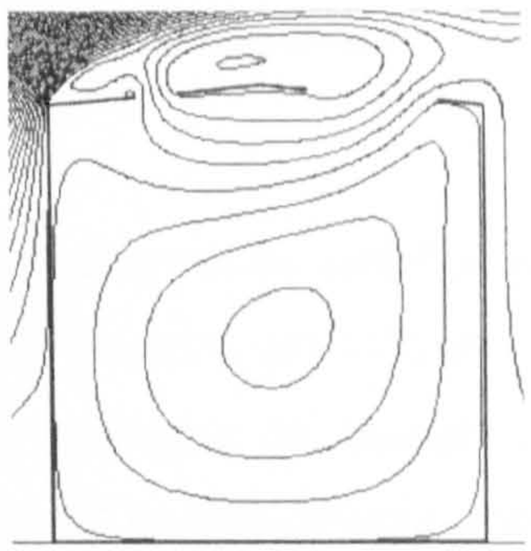

(b) Opening size: C+3C

(c) Opening size: C+5C

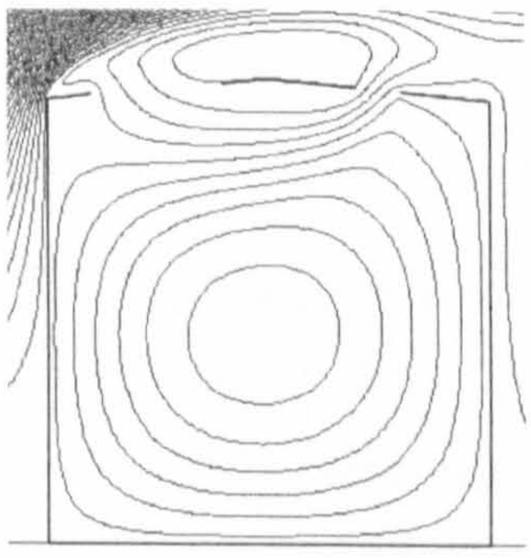

(d) Opening size: 3C+C

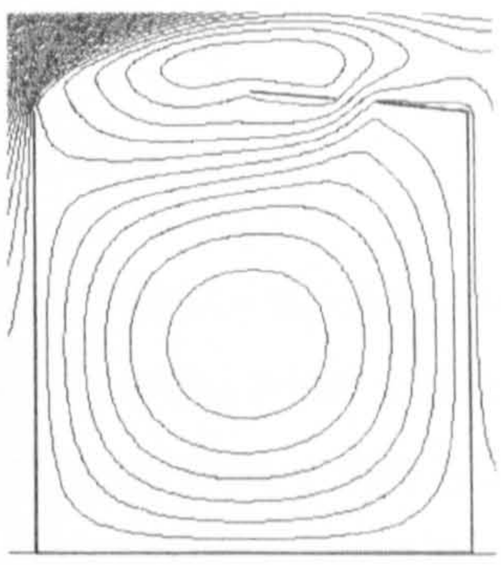

(e) Opening size: 5C+C

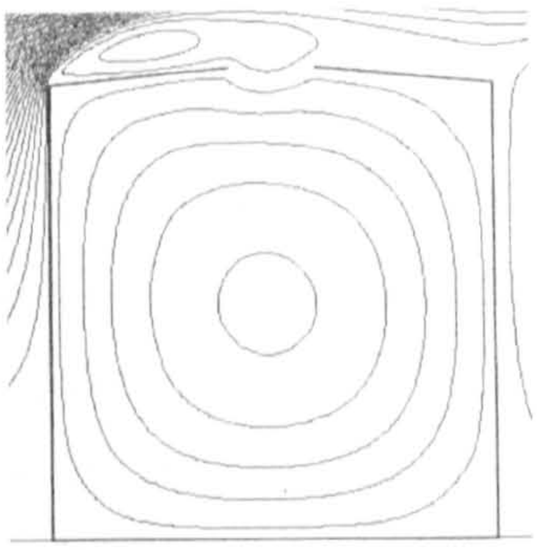

(f) Opening size: A+A

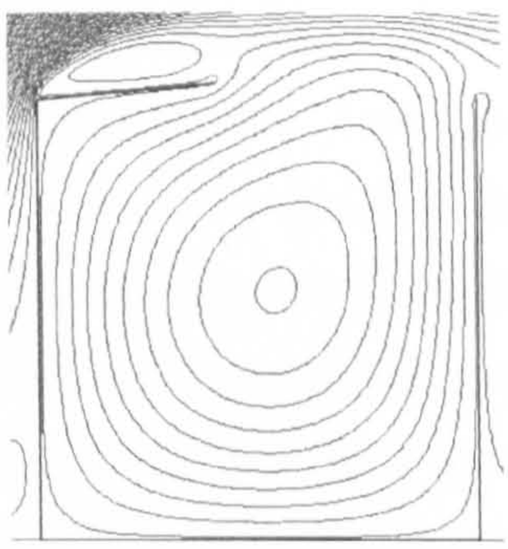

(g) Opening size: A+5A

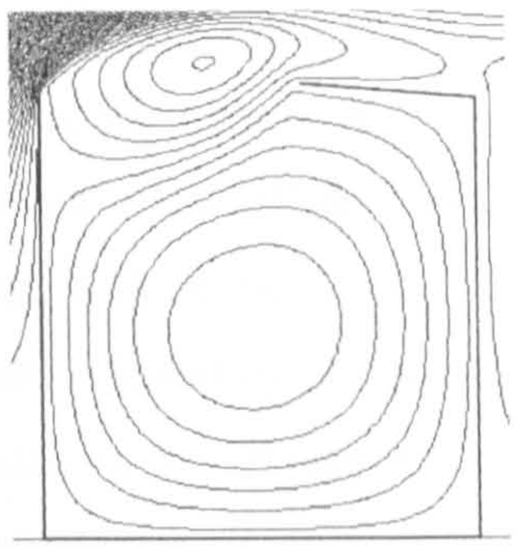

(h) Opening size: 5A+A

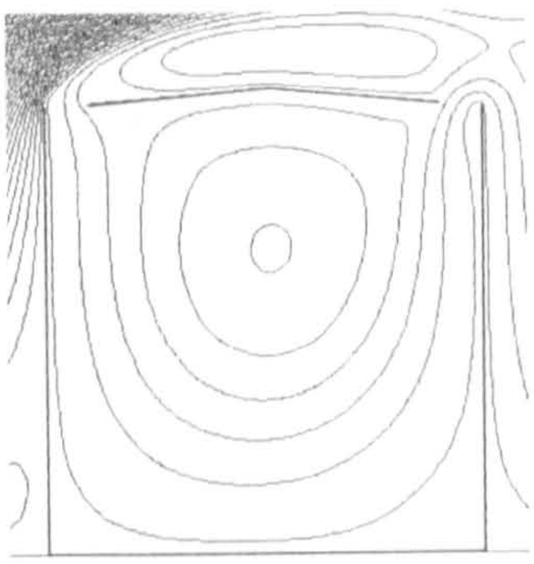

(i) Opening size: E+E

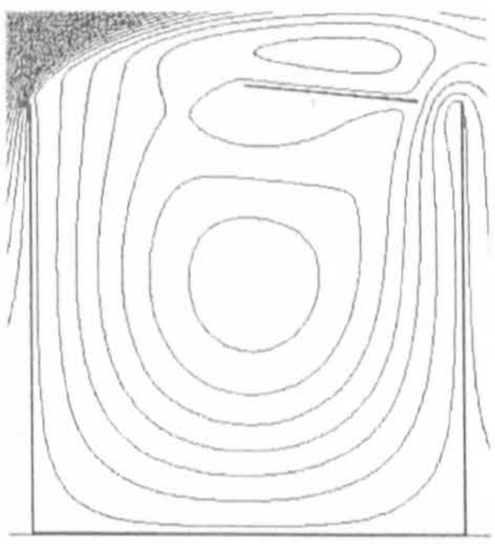

(j) Opening size: 5E+E

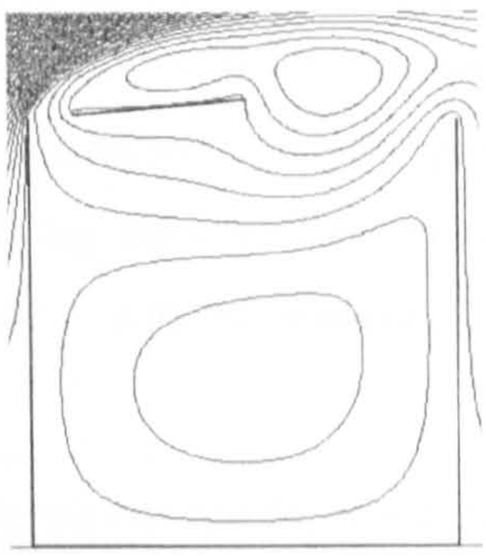

(k) Opening size: E+5E

Figure 5.27: Airflow patterns of wind-induce natural ventilation for atria with 5° roof and different opening locations and sizes (scenarios a, f &i are reproduced from Figure 5.21 for comparison)

Thus, according to the above observations and discussions, it can be summarised that the size of the windward opening does not have any influence on the airflow pattern and larger size result in stronger air movement; enlarging the leeward opening may induce flow pattern (III).b and air velocity in the space will be significantly reduced, except when the windward opening is placed at the top under which circumstance the openings on both sides form a bigger opening on the roof.

- *15° roof*

Recall that the two possible flow patterns that may occur for atria with 15° roof and two small openings are (III).c and (II) and it is the result of the interaction of two counteractive forces: the back flow and the reattaching flow. The former occurs when the horizontal momentum generated by the back flow is stronger than that by the reattachment, i.e. only when the inlet opening is placed in the middle of the leeward roof and the outlet opening is provided at the bottom of the windward roof (see precious subsection for more details). Otherwise flow pattern (II) will take place.

Let us still start from the atria with this roof angle and two small openings in the middle of the roof pitches. Enlarging the leeward opening cannot change the flow pattern, but it seems that the airflow velocity at the occupants' level will decrease first and then increase (see Figure 5.28b&c). The reason for this is that, both of the driving forces for this flow pattern, i.e. the reattaching flow and the back flow are affected by the size of the leeward opening in the same trend. Since both flows need distances on the leeward pitch for their developments, enlarging the opening from the middle will weaken both of them. This also shows that the leeward bottom area is of great importance for ensuring a stronger internal air movement of this roof angle, which is further confirmed by the scenarios (g), (h) and (j), as with this bottom opening, the horizontal momentum of the back flow will be the weakest. Increasing the size of the windward opening can result in the occurrence of flow pattern (III).c, as by doing this the horizontal momentum of the reattaching flow will be brought upwards due to the vertical momentum from the outlet and thus it will be weakened near the roof level (see Figure 5.28d&e).

Since the reattachment is quite significant for the airflow of atria with this roof angle, a continuous roof pitch over a certain distance will be very beneficial for a good ventilation performance. As shown in Figure 5.28 (f) to (k), the main flow can reattach to the leeward roof pitch after separation at the leftmost corner and bring on a good ventilation performance at the occupants' level with flow pattern (II).

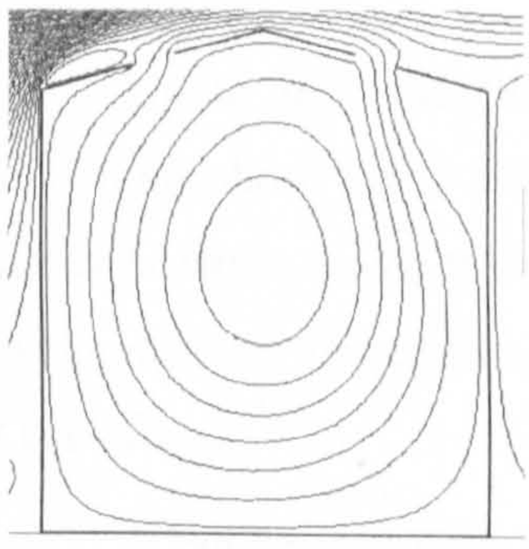

(a) Opening size: C+C

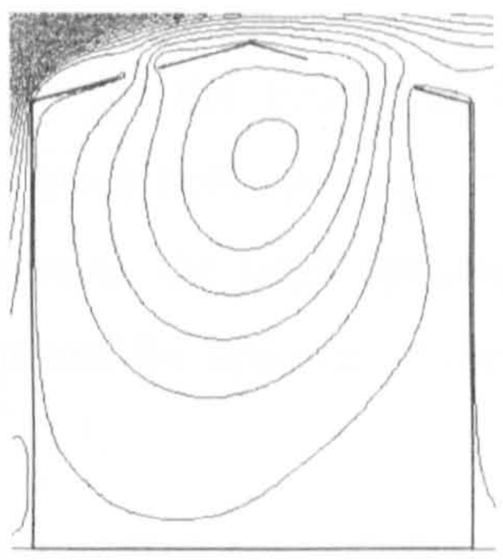

(b) Opening size: C+3C

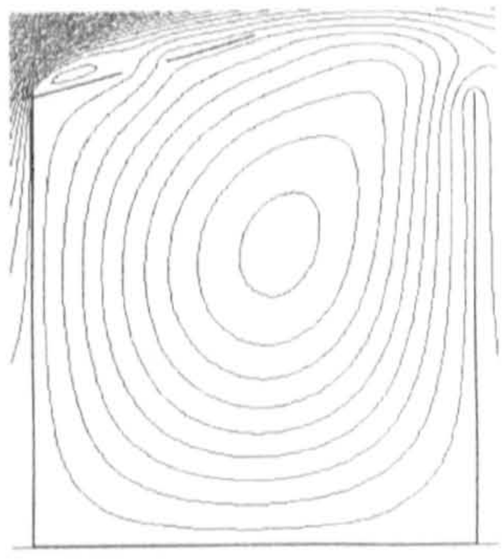

(c) Opening size: C+5C

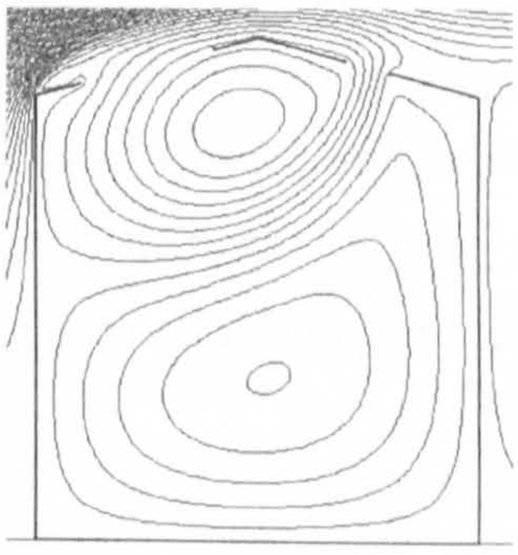

(d) Opening size: 3C+C

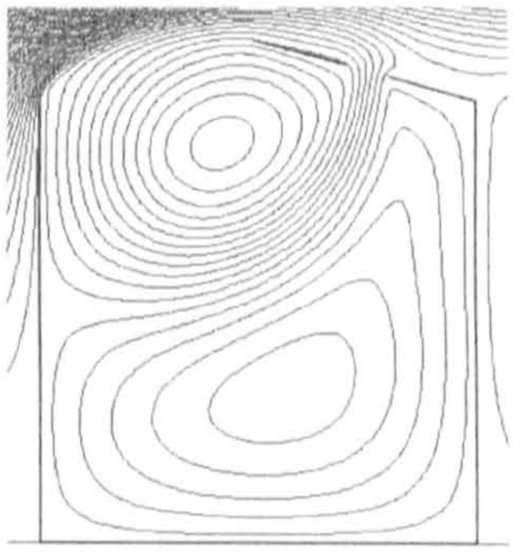

(e) Opening size: 5C+C

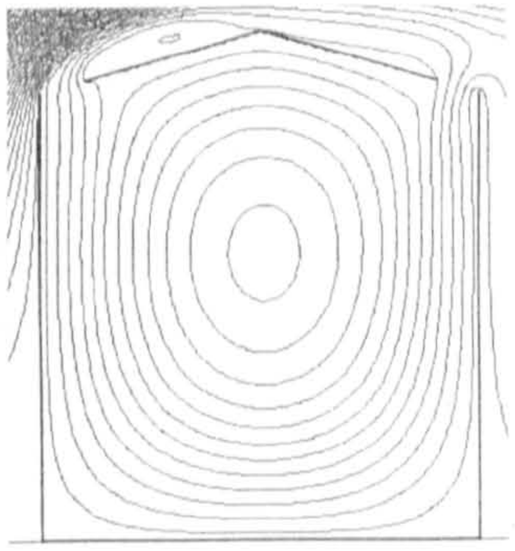

(f) Opening size: E+E

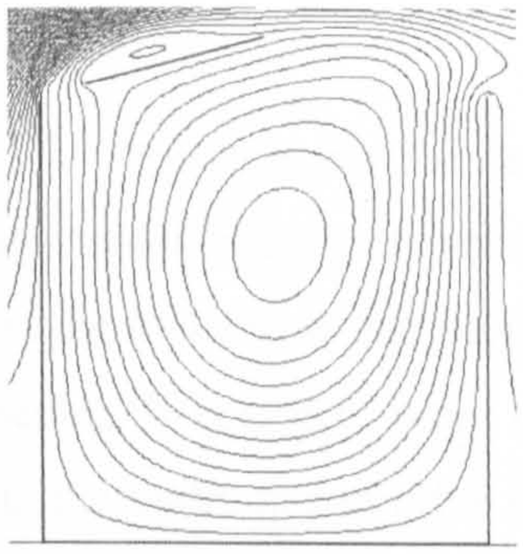

(g) Opening size: E+5E

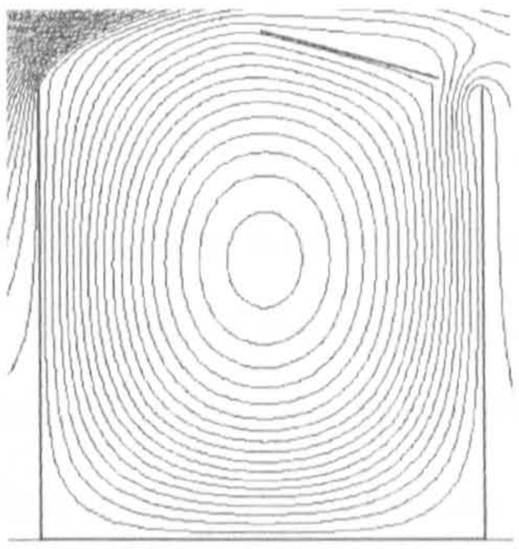

(h) Opening size: 5E+E

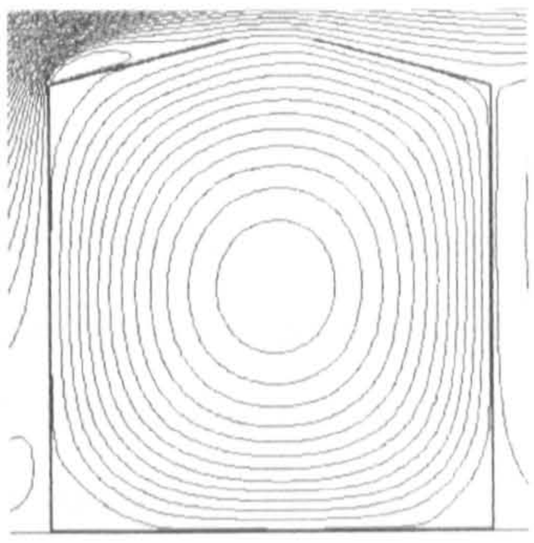

(i) Opening size: A+A

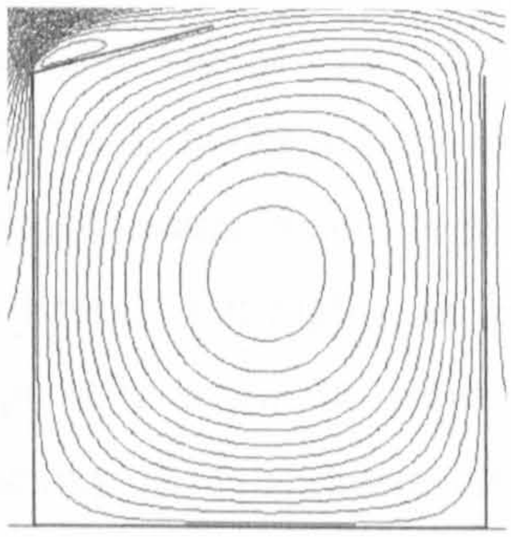

(j) Opening size: A+5A

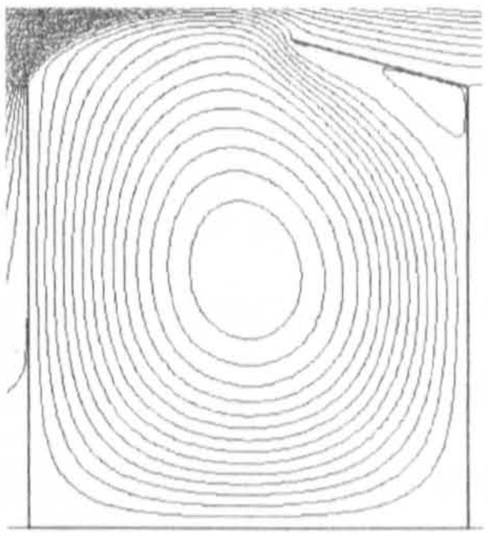

(k) Opening size: 5A+A

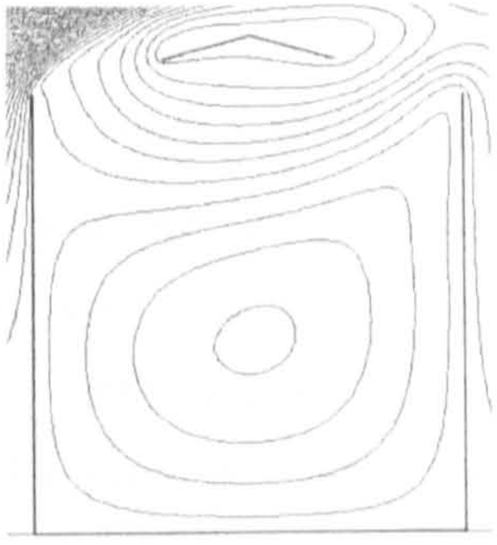

(j) Opening size: 3E+3E

Figure 5.28: Airflow patterns of wind-induce natural ventilation for atria with 15° roof and different opening locations and sizes (scenarios a, f &i are reproduced from Figure 5.22 for comparison)

Up to now the flow pattern for the courtyard, (III).b has not appeared. Further simulations show that it will occur when both openings are large, as seen in Figure 5.28 (J). This is because, under this circumstance, the large opening on the windward side breaks the development of the reattaching flow and the opening on the leeward side attracts large amount of back flow.

It can be seen from the above analysis suggests that, the airflow pattern of atria with this roof angle is quite complicated and it depends on the size of both openings. Flow pattern (III).c occurs when the leeward opening is small and is placed in the middle of the roof pitch, and the size of the windward opening for this circumstance does not have any influence; flow pattern (III).b is incurred only when both openings are large; flow pattern (II) will take place for all other conditions. In order to achieve higher air velocity in the space, longer continuous roof pitch on one side is preferred which helps the development of the reattaching flow.

• *20° roof*

Previous studies on the ventilation performance of atria with this roof angle have suggested that the pressure near the top of the windward pitch will be positive, and this means that the main flow can separate at the peak of the roof. As a consequence, when the leeward opening is enlarged, more back flow of the recirculation from behind the building will come into the building and drive the airflow in the space resulting in flow pattern (III).b, as shown in Figure 5.29 (b), (c), (g) and (j).

Increasing the size of the opening on the windward roof cannot change the flow pattern (compare Figure 5.29f&h, i&k), except when it is located at the middle of the pitch (see Figure 5.29d&e), under which condition the flow pattern changes from (III).b to (III).c because stronger reattachment is induced by the larger opening. For other situations flow pattern (II) will result and higher air velocities in the space can be induced by larger windward opening, especially when the leeward opening is at the top and all the windward roof is used as an opening. In fact, this result suggests an efficient way for improving the ventilation performance of a courtyard by using a shelter from the leeward side. By comparing the ventilation performance of shelters with different angles (see Figures 5.27h, 5.28k, 5.29k), it is shown that shelter with an angle of 20° results in the highest air velocities in the space with the maximum velocity coefficient of 0.63, which is even higher than that induced by 45° roof with two openings (see Figure 5.25, maximum less than 0.5). Later study will show that further increase of the angle of the shelter will be inefficient in enhancing the airflow in the courtyard.

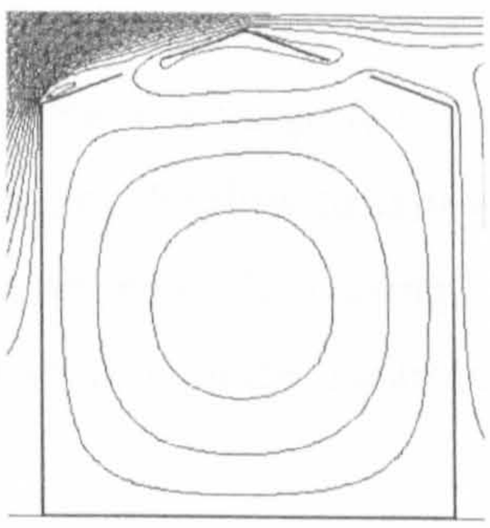

(a) Opening size: C+C

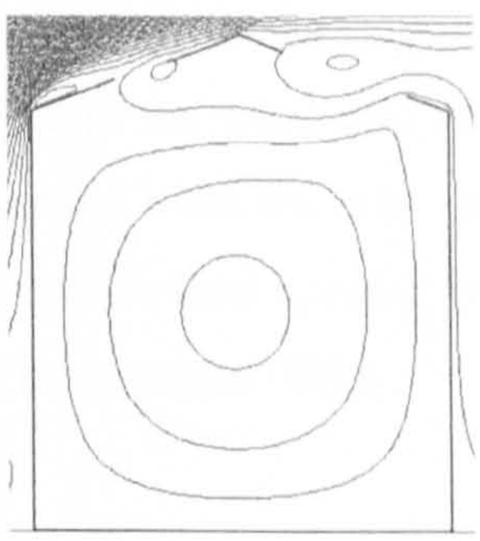

(b) Opening size: C+3C

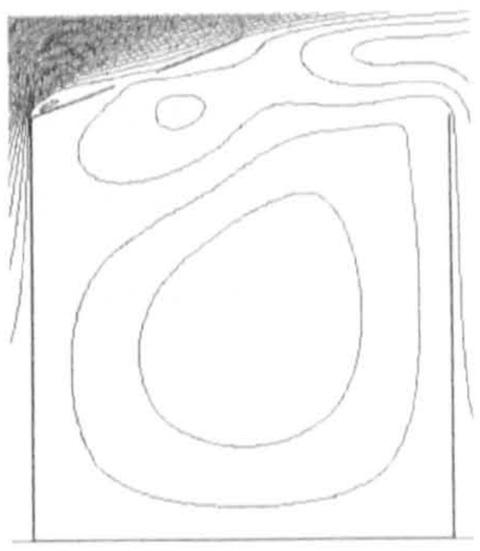

(c) Opening size: C+5C

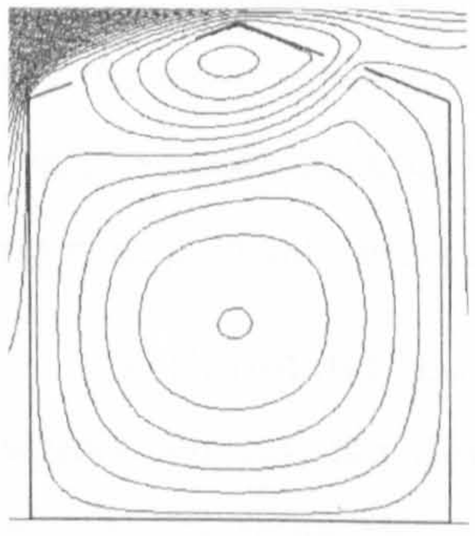

(d) Opening size: 3C+C

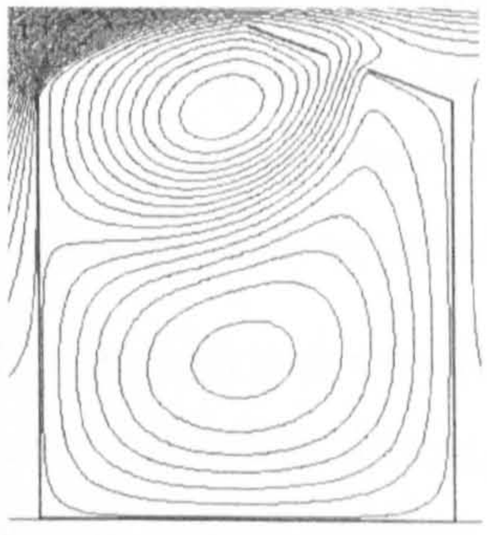

(e) Opening size: 5C+C

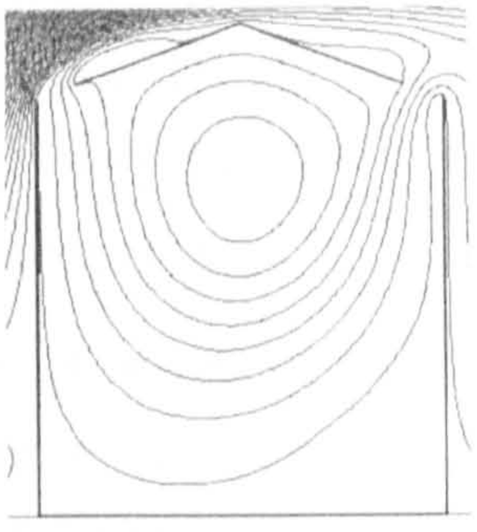

(f) Opening size: E+E

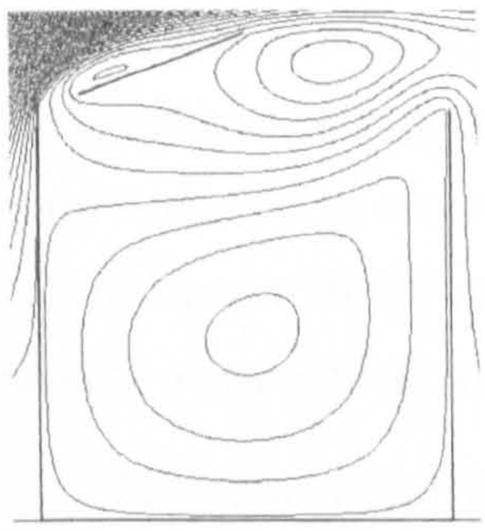

(g) Opening size: E+5E

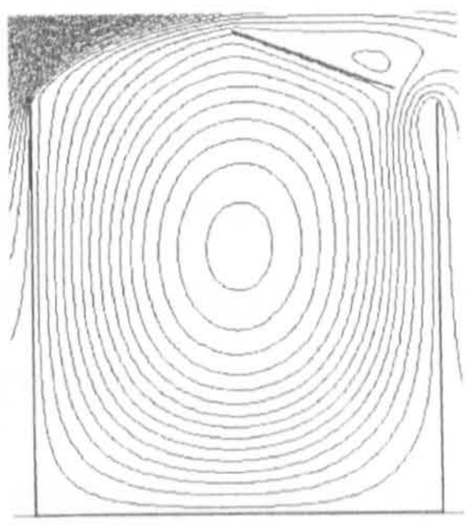

(h) Opening size: 5E+E

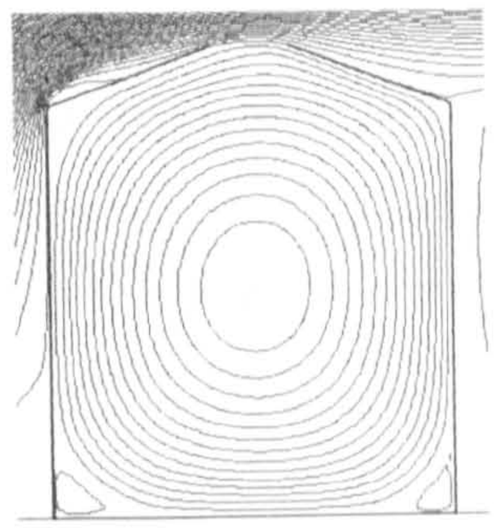

(i) Opening size: A+A

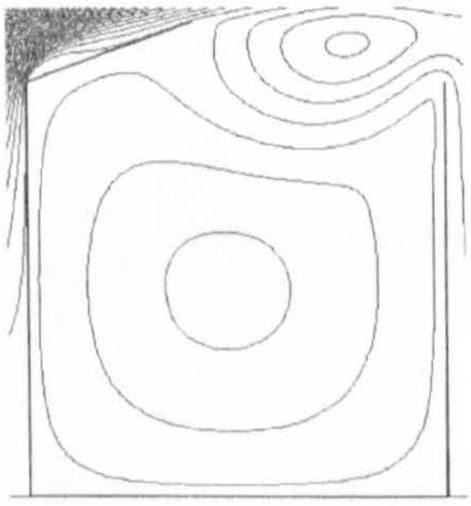

(j) Opening size: A+5A

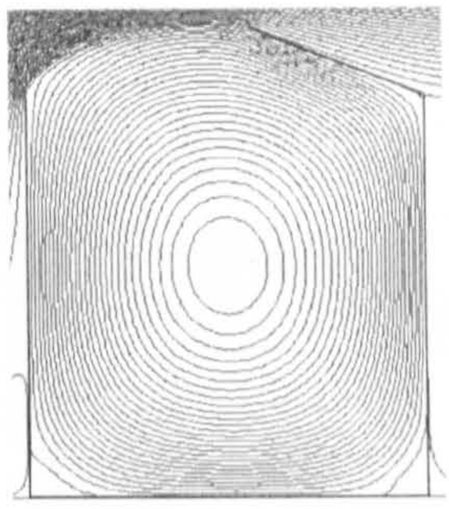

(k) Opening size: 5A+A

Figure 5.29: Airflow patterns of wind-induce natural ventilation for atria with 20° roof and different opening locations and sizes (scenarios a, f &i are reproduced from Figure 5.23 for comparison)

According to the above discussion, to enhance the airflow in the space, it is good practice to enlarge the outlet opening in the windward roof but it should be noticed that by doing so the flow pattern will be changed when the inlet opening is placed in the middle of the leeward roof. Increasing the size of the leeward opening will result in weaker air movement in the space with the occurrence of the flow pattern (III).b.

- *45° roof*

The investigation of the opening location of atria with 45° roof has indicated that the top part is the most important for the airflow pattern and it has been suggested that, only when the top part has been occupied by openings, the airflow flow pattern will change from (I) to (III).b. This result is further verified by the following study of the effects of the opening size.

As shown in Figure 5.30 (d), even with both very large openings on both windward and leeward openings, the flow pattern (I) still occurs driving in the air movement in the space. Although enlarging the opening size is able to increase the air velocity in the space, the increment is generally very small: the maximum velocity coefficients induced by scenarios (b) and (c) which have 3 times bigger openings on windward side or leeward side are only 15% and

10% more than that by (a) respectively. With 4 times as the size of the openings employed in scenario (a), scenario (d) generates the maximum velocity coefficient of 0.7, which is 40% more than (a) does. These observations show that two small openings are quite effective for inducing the air movement in the space and the efficiency will reduce with the increase of the openings, especially when only the size of one opening is increased.

The scenario (e) shows the airflow pattern of a courtyard with a shelter of 45° and the maximum velocity coefficient is around 0.55, which is less than that of the courtyard with a 20° shelter (0.63) as described earlier. This shows that a shelter with an angle of 20° will be more efficient in inducing wind-driven natural ventilation in the space.

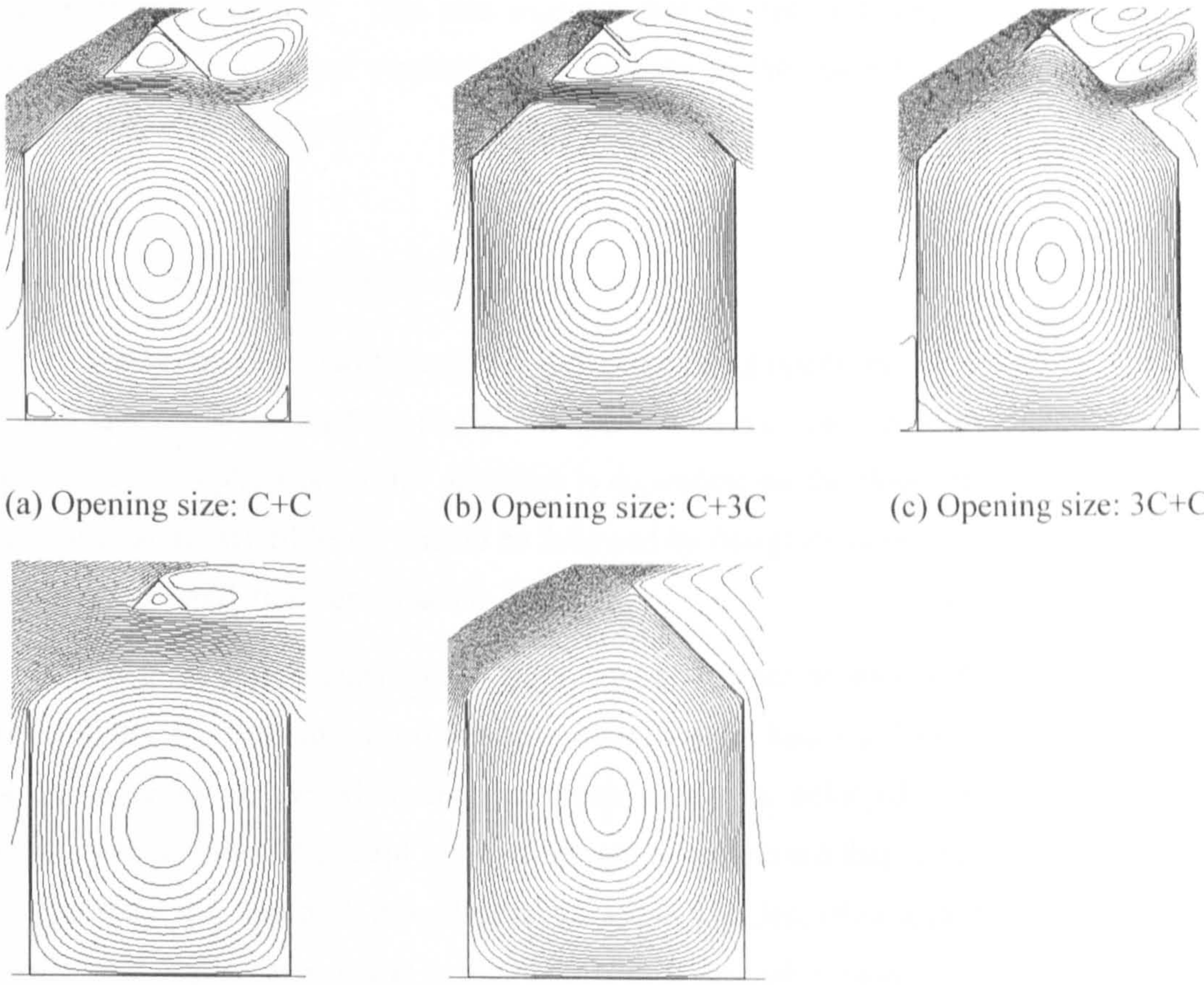

(a) Opening size: C+C (b) Opening size: C+3C (c) Opening size: 3C+C

(d) Opening size: 4E+4E (e) Opening size: 5A+A

Figure 5.30: Airflow patterns of wind-induce natural ventilation for atria with 45° roof and different opening locations and sizes (scenario a is reproduced from Figure 5.24)

• *Barrel vault roof*

Barrel vault roof atria with a tangential angle of 30° are employed for the study of the effects of the opening size. Figure 5.31 illustrates the airflow patterns of the atria with vault roof with different sizes of openings provided at the roof level. Since the reattaching flow is the driving force, the roof pitch on the leeward side that helps the continuous movement of the reattaching flow near the roof level is quite important. It is shown in scenarios (c), (g) and (j),

when the whole leeward pitch is used as an opening, the reattaching flow will separate from the peak of the roof causing significant reduction of the air velocity in the space. In particular, when the windward opening is placed at the top as well, the horizontal momentum of the reattaching flow near the roof level will be overwhelmed by that from the back flow of the recirculation behind the building and as a result flow pattern (III).b will be incurred (see scenario j).

Enlarging the windward opening size seems a good way of improving the ventilation performance of vault roof atria. By comparing scenarios (a), (d) and (e), (f) and (h), (i) and (k), it is shown that higher air velocity in the space can be induced and the flow pattern does not change with this variation. This also suggests that the leeward part is the most important component to ensure a good ventilation performance in the space for vault roof atria with a tangential roof angle above 20°.

• *Guidance on the design of the openings sizes*

Usually designers have the intuition that enlarging openings can always be an efficient approach to increase the airflow rate in the space; however, the investigations of this section suggest that the application of this approach is dependent on the flow pattern in the space and the guidance summarised below should be followed by designers in order to use larger openings to improve the ventilation performance:

• when the air movement in the atrium space is driven by suction flows resulting in flow pattern (II) or (III), i.e. triangular roof atria with roof angle below 21° and all types of vault roof atria, the opening on the windward roof pitch should be enlarged and the opening on the leeward roof pitch should be kept small; (it should be mentioned that this is not the only way for the purpose but this approach is applicable for all roof angles; other approaches exclusively for particular roof angle can be found in the summaries at the end of each subsection)

• when flow pattern (I) takes place, i.e. when the triangular roof angle is more than 21°, traditional design guidelines on opening sizes can be used: increasing the size of either opening can help improve the airflow in the space but the ventilation performance is generally determined by the size of the small opening.

5.5.3 Opening methods

Treated as "holes" in the roof, openings in previous investigations can be generally regarded as retractable or roll-up windows. Although this kind of opening is common in reality, there are also some other openings whose opening method may have significant impacts on the airflow in and around the building. In fact, in addition to the empty area for the air to come in, a

window also provides opening surfaces and edges that can also affect the airflow because they may enhance or block the movement of the air around the opening. One example that has been mostly adopted in practice is pivoting windows whose edges can intrude into the airflow and certainly have some influences as apparently they are not parallel to the streamlines.

This subsection will focus on this issue and study two types of pivoting openings in terms of the pivoting axis: when the axis is in the middle and when it is on the edge. The atria with 5°, 15°, 20° and 45° triangular roof and two small openings are chosen to represent flow pattern (III).a, (III).b, (II) and (I) respectively. The pivoting opening can be used either in the windward roof or in the leeward roof or both.

In order to enhance the natural ventilation in the space, the opening edges should be used in such a way that the driving force can be reinforced and/or the counterforce can be weakened when they are opened. With this principle and the airflow patterns identified earlier, it is therefore not difficult to understand the effects of the opening methods on the ventilation performance of atria with each roof angle. Figures 5.32 to 5.35 present the airflow patterns of the wind-induced ventilation in typical triangular roof atria with different angles which are incorporated with various settings of pivoting windows.

For atria with 5° roof where the airflow is driven by the reverse flow in conjunction with the back flow from behind the space and these two forces support each other (see scenario a), incorporation of pivoting window on the leeward roof pitch with the upper edge as the pivoting axis can enhance the reverse flow coming into the building and hence the internal air movement if the opening angle is appropriate (compare b&g). When pivoting window is used on the windward pitch and the upper edge is still the pivoting axis, the opening angle should be generally larger for better ventilation performance as it results in larger opening area for the outlet (see c&i). If the pivoting window is used in such a way that the air is blocked for coming in or going out of the building compared to (a), the flow pattern will change depending on the opening angle. For instance, when the leeward opening is a pivoting window with lower edge as its pivoting axis (see f), apparently the opening edge blocks the reverse flow that comes from the right hand side of the opening and the direction of the air velocity at this opening has changed to vertical resulting in the occurrence of flow pattern (II). It can also be seen that, for this situation, pivoting windows as inlets will be more efficient than as outlets as they control the driving force (compare f&h). Similar examples include scenario (h) where the outlet pivoting opening blocks the air to get out of the space. The pivoting windows with the axis in the middle of the opening may have both positive and negative effects on the airflow described above and their effects are very similar to those with the axis on one extreme edge but which one depends on its opening angle. It can be seen that, scenarios (e), (j) and (k) are similar to (d), (i) and (f) respectively but the flow is slightly weaker.

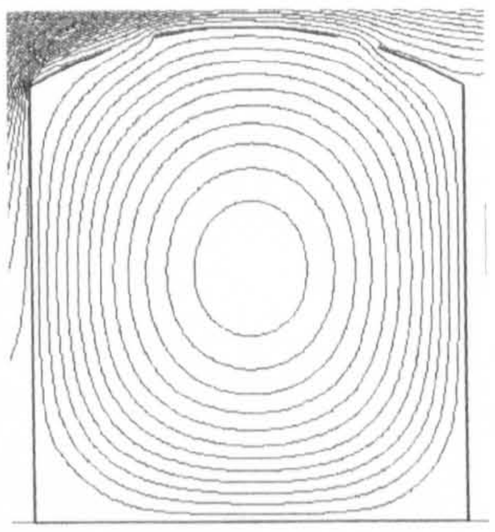

(a) Opening size: C+C

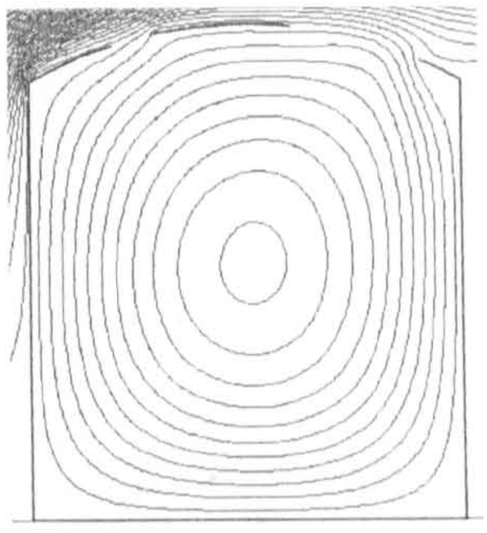

(b) Opening size: C+3C

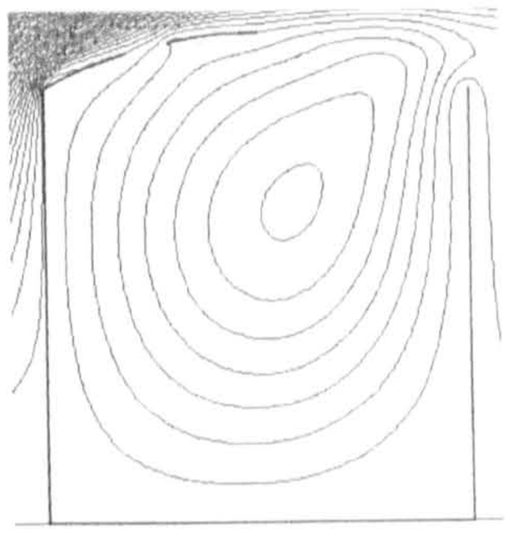

(c) Opening size: C+5C

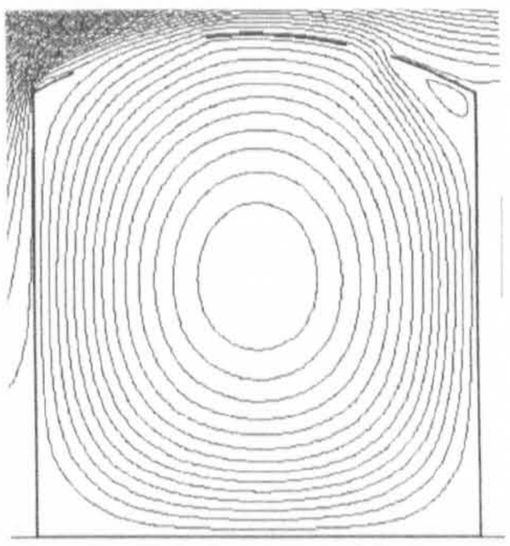

(d) Opening size: 3C+C

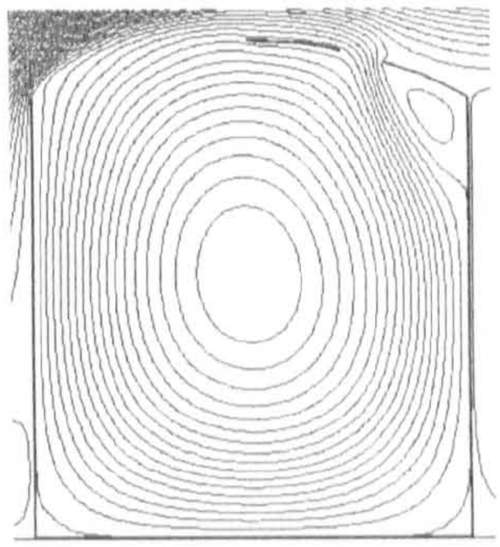

(e) Opening size: 5C+C

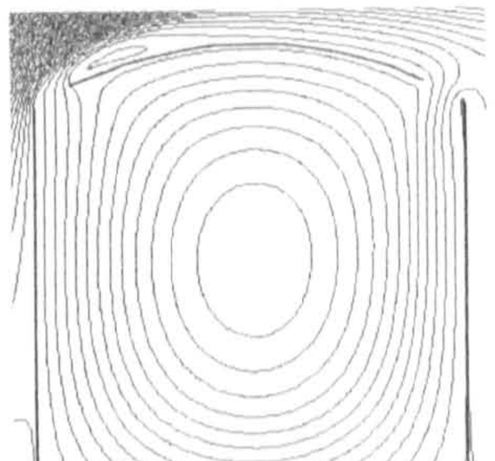

(f) Opening size: E+E

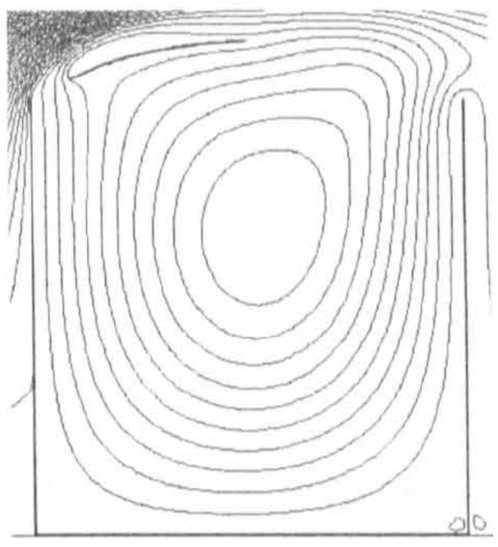

(g) Opening size: E+5E

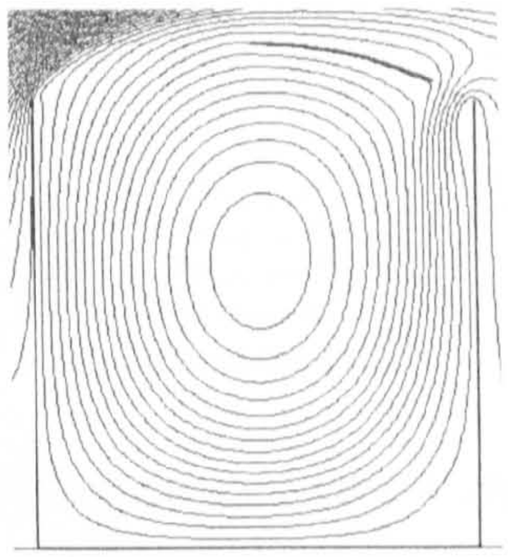

(h) Opening size: 5E+E

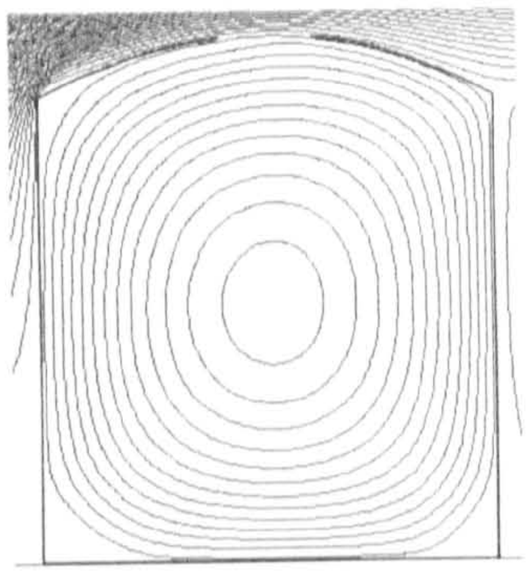

(i) Opening size: A+A

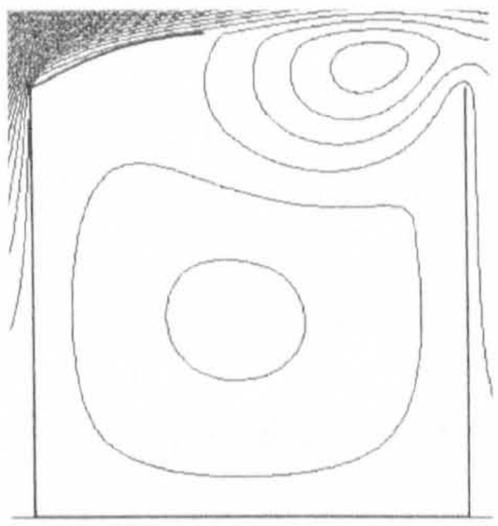

(j) Opening size: A+5A

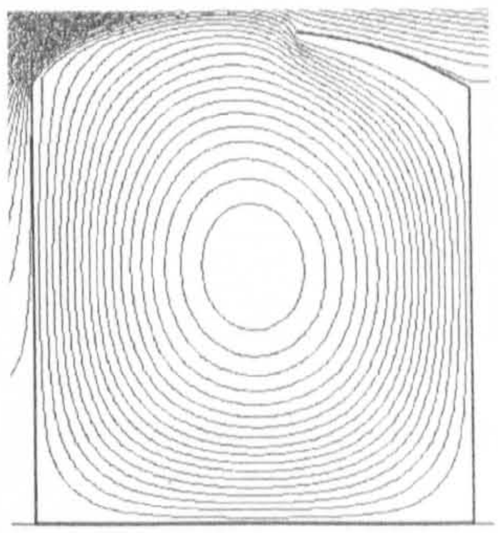

(k) Opening size: 5A+A

Figure 5.31: Airflow patterns of wind-induce natural ventilation for atria with barrel vault roof and different opening locations and sizes

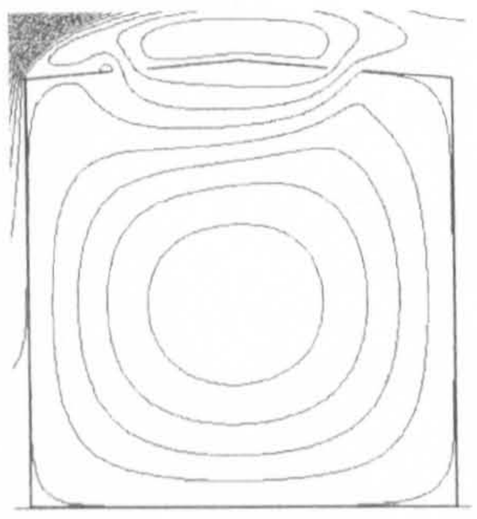

(a) original

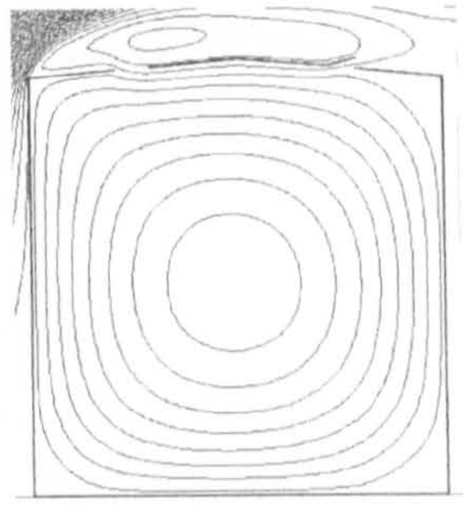

(b) right pivoting (upper edge)

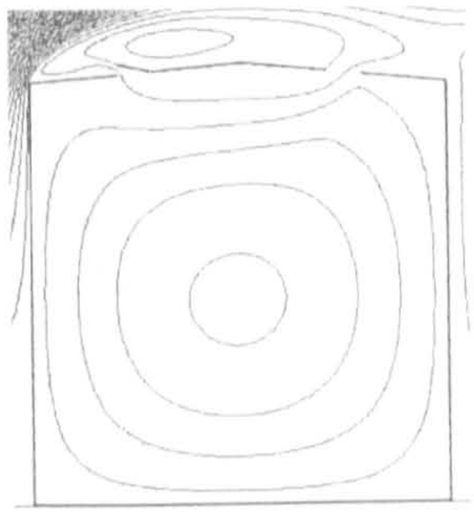

(c) left pivoting (upper edge)

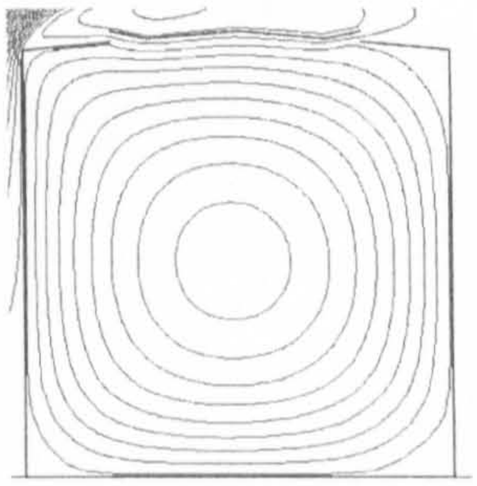

(d) both pivoting (upper edge)

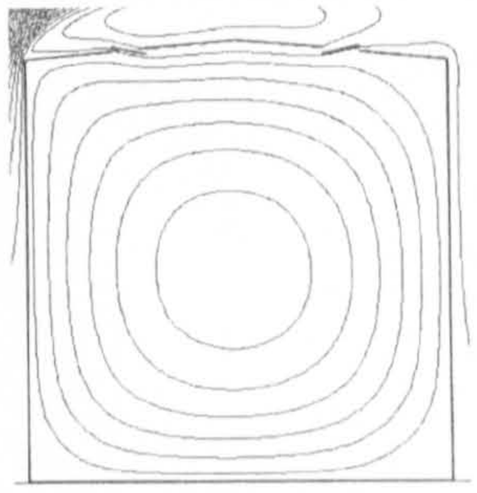

(e) both pivoting (middle)

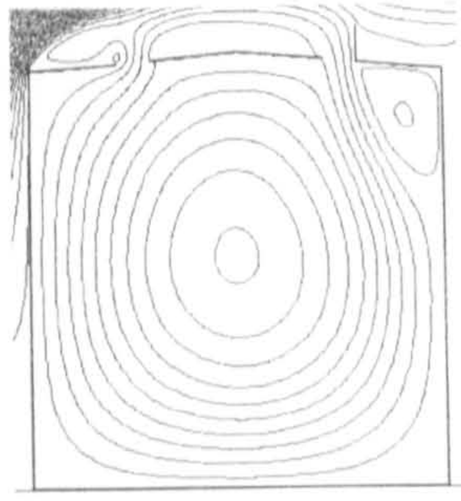

(f) right pivoting (lower edge)

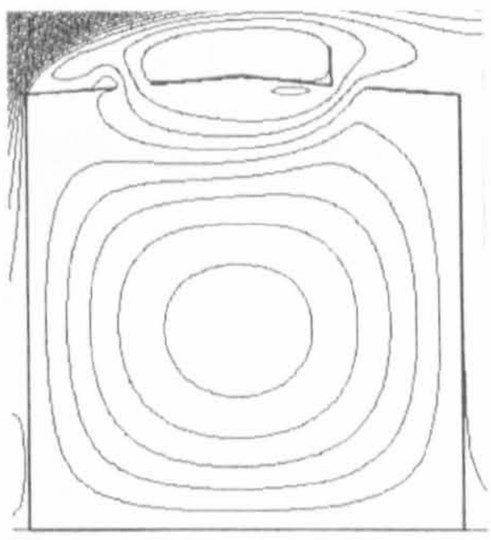

(g) right pivoting (upper edge)

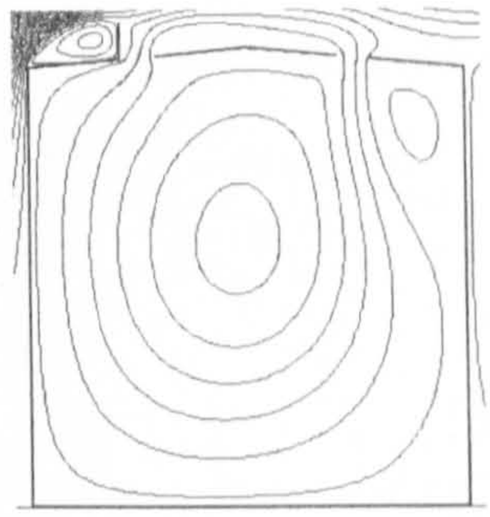

(h) left pivoting (lower edge)

(i) left pivoting (upper edge)

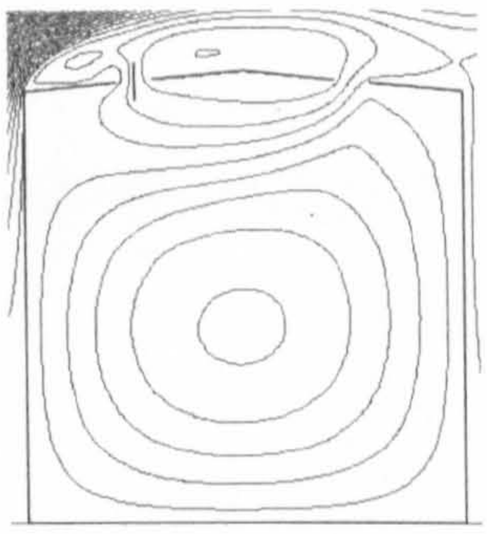

(j) left pivoting (middle)

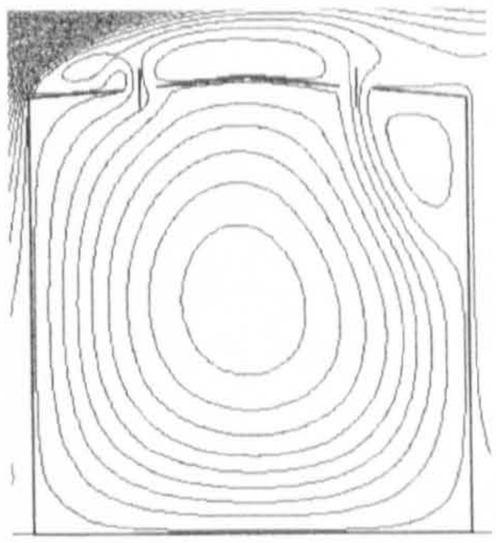

(k) both pivoting (middle)

Figure 5.32: Airflow patterns of wind-induce natural ventilation for atria with 5° triangular roof and pivoting openings

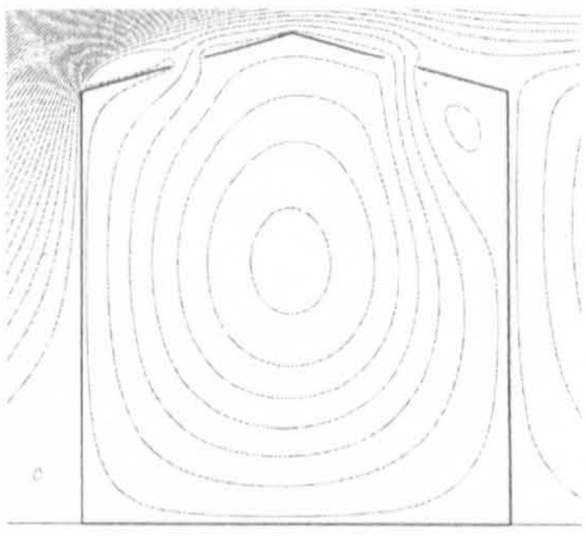

(a) original

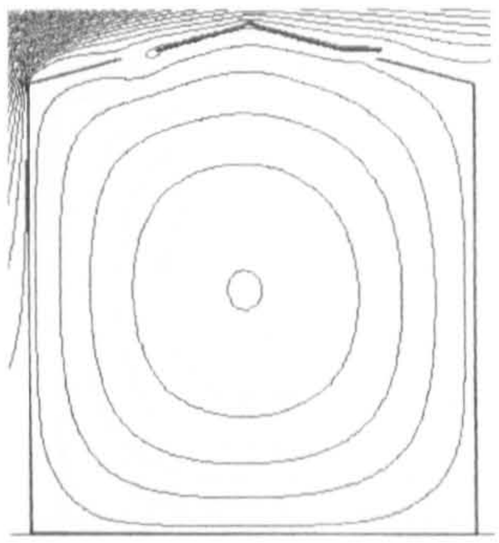

(b) right pivoting (upper edge)

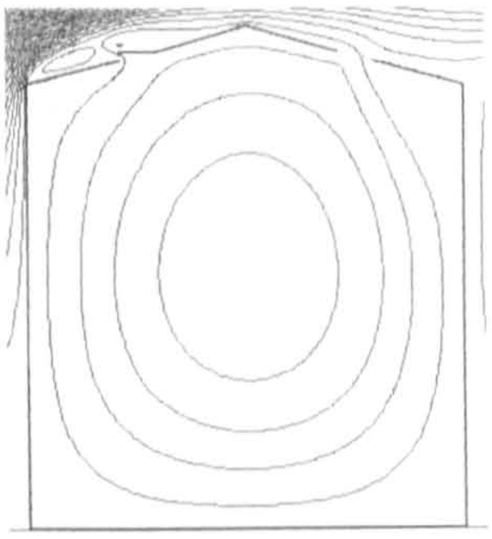

(c) left pivoting (upper edge)

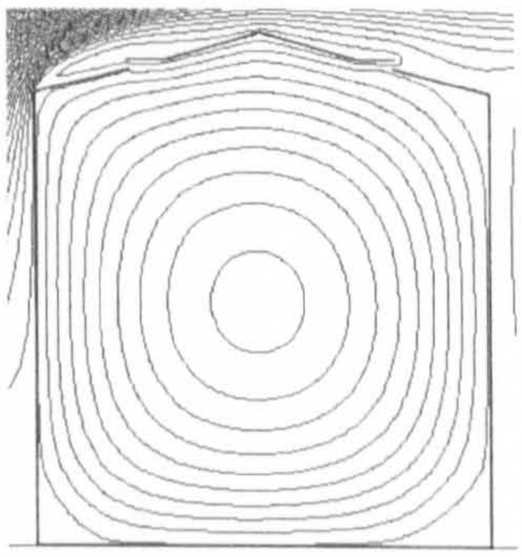

(d) both pivoting (upper edge)

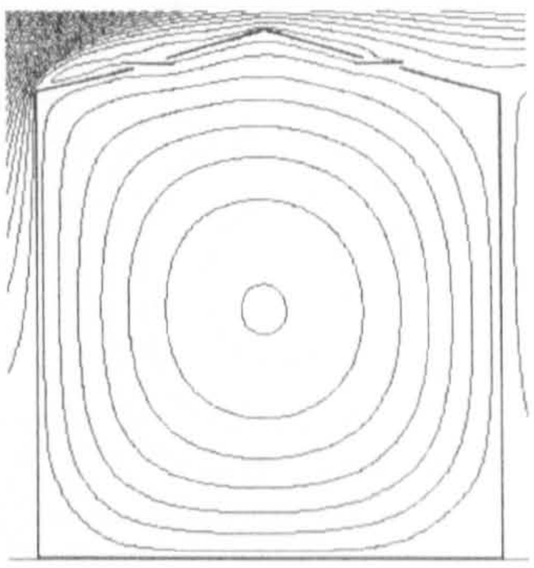

(e) both pivoting (middle)

(f) right pivoting (lower edge)

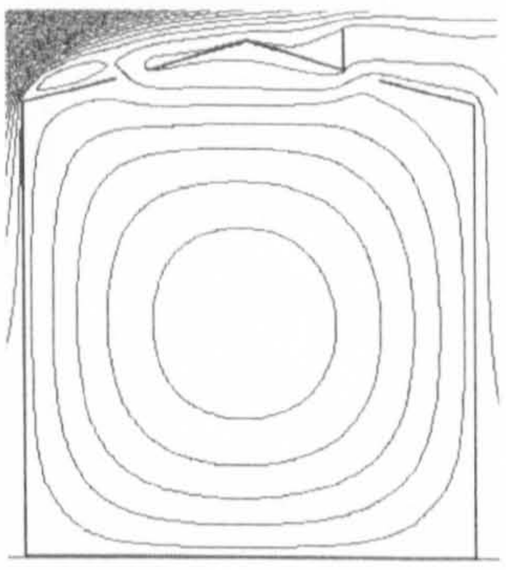

(g) right pivoting (upper edge)

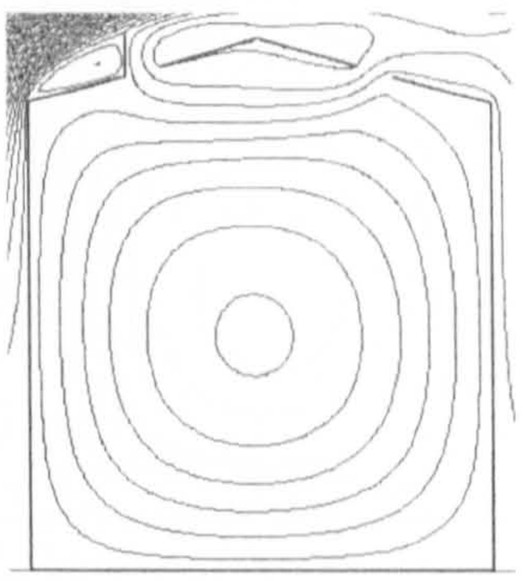

(h) left pivoting (lower edge)

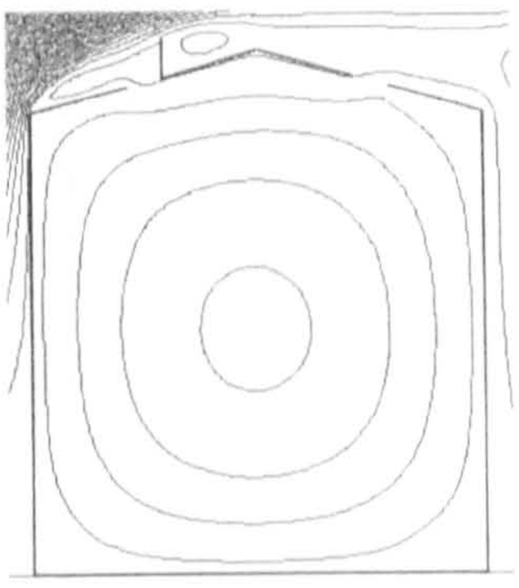

(i) left pivoting (upper edge)

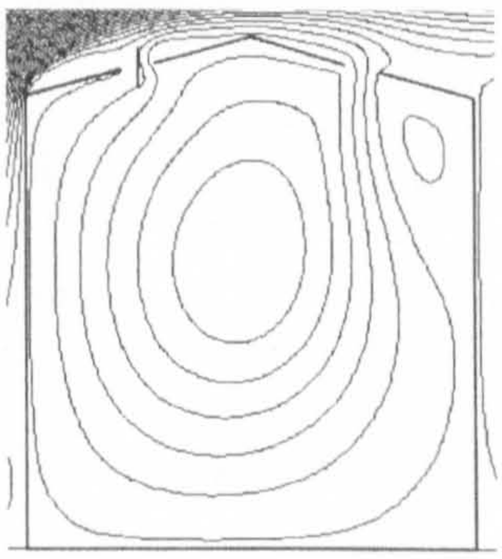

(j) left pivoting (middle)

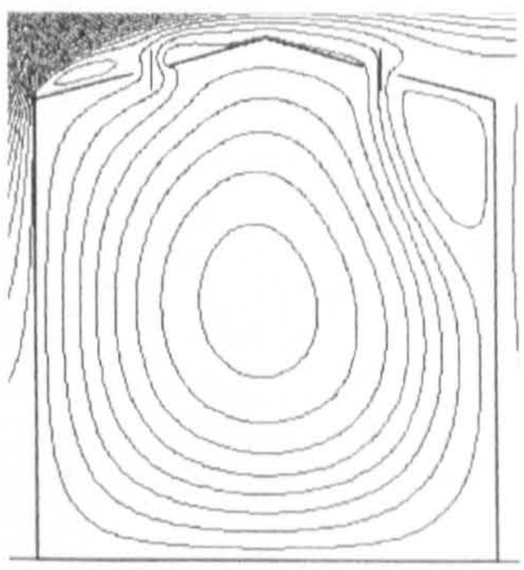

(k) both pivoting (middle)

Figure 5.33: Airflow patterns of wind-induce natural ventilation for atria with 15° triangular roof and pivoting openings

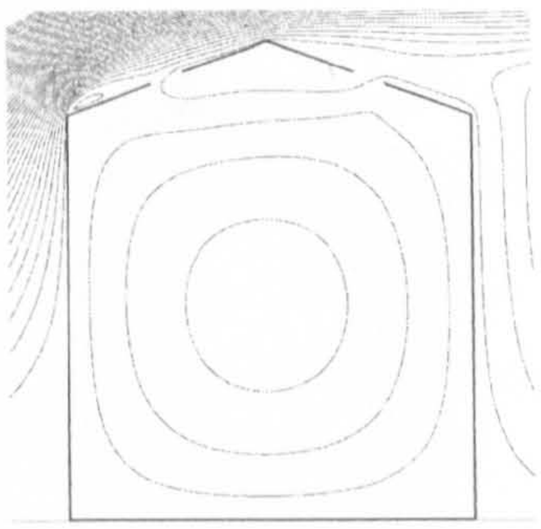

(a) original

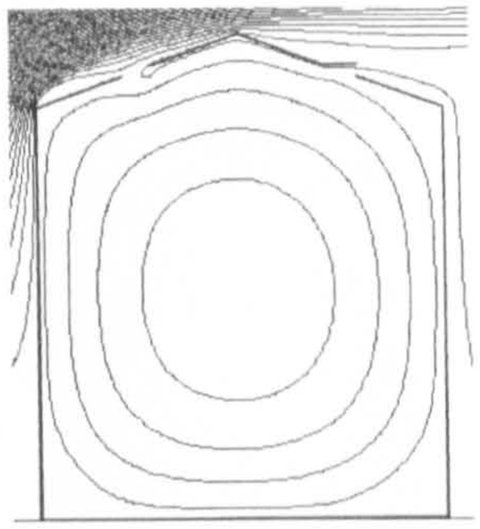

(b) right pivoting (upper edge)

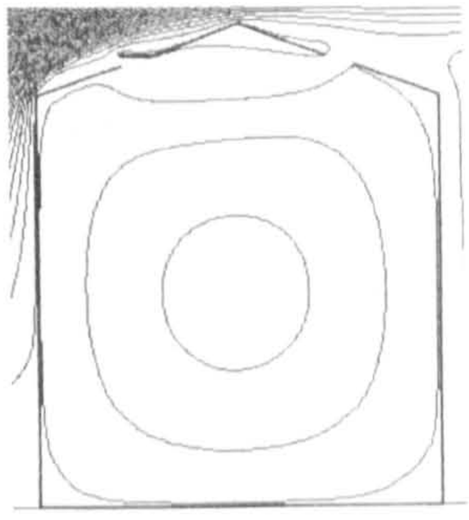

(c) left pivoting (upper edge)

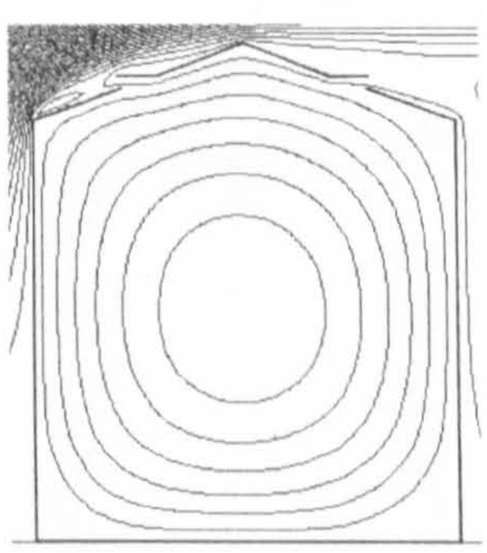

(d) both pivoting (upper edge)

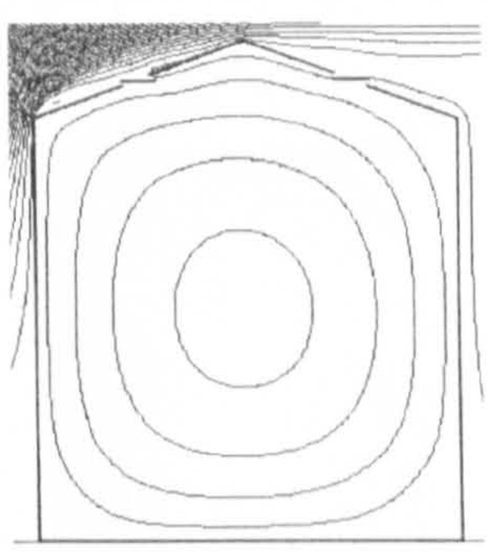

(e) both pivoting (middle)

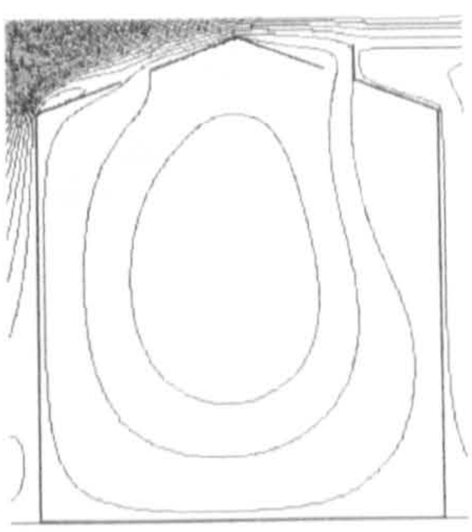

(f) right pivoting (lower edge)

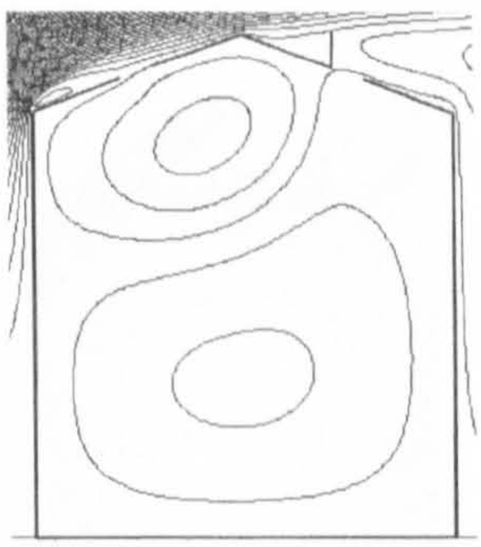

(g) right pivoting (upper edge)

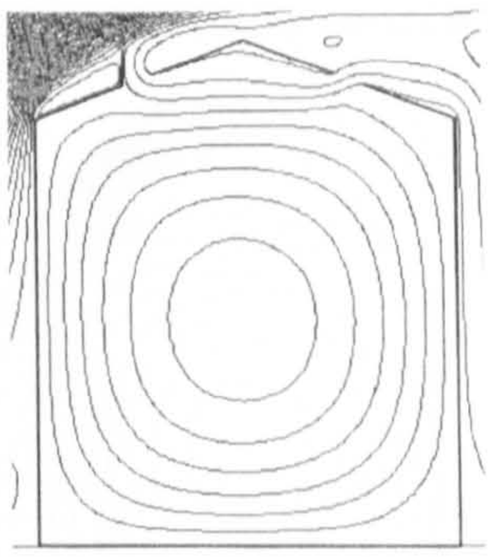

(h) left pivoting (lower edge)

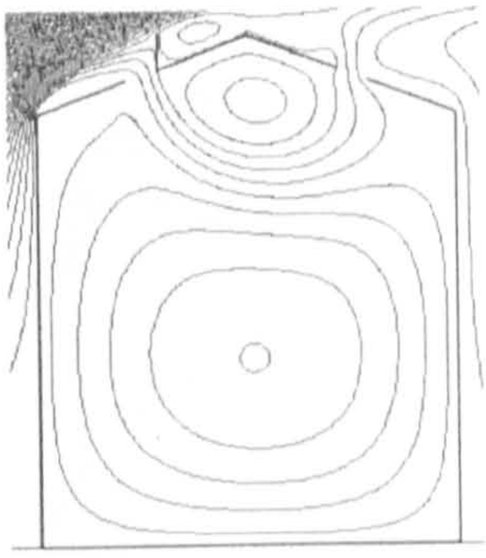

(i) left pivoting (upper edge)

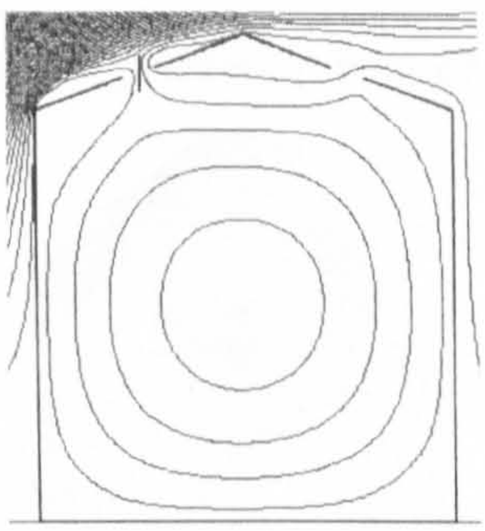

(j) left pivoting (middle)

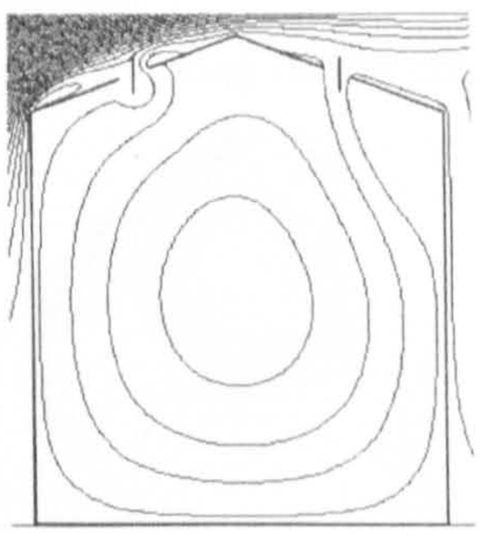

(k) both pivoting (middle)

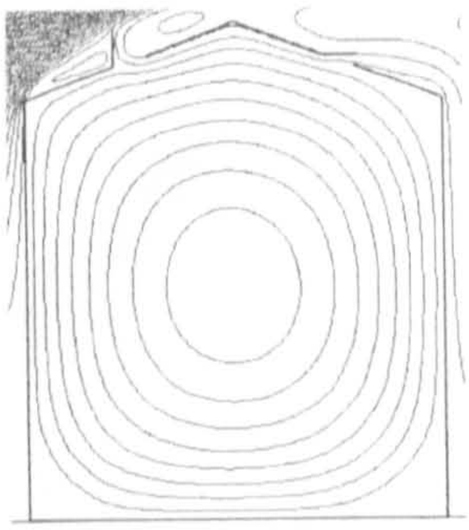

(l) both pivoting

Figure 5.34: Airflow patterns of wind-induce natural ventilation for atria with 20° triangular roof and pivoting openings

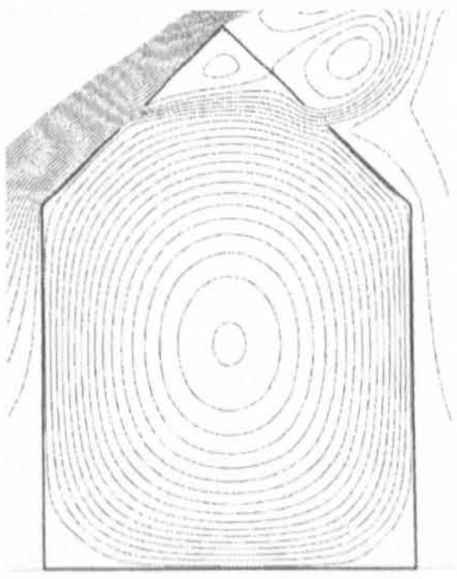

(a) original

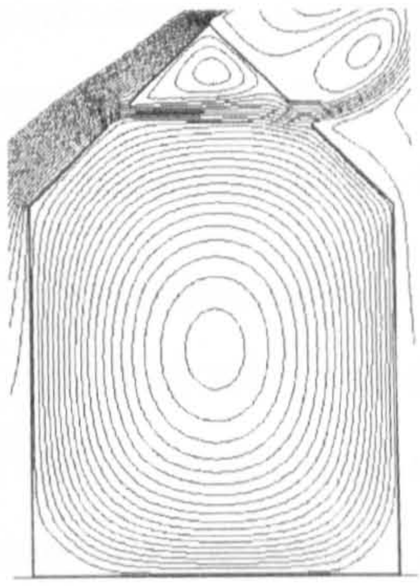

(b) right pivoting (upper edge)

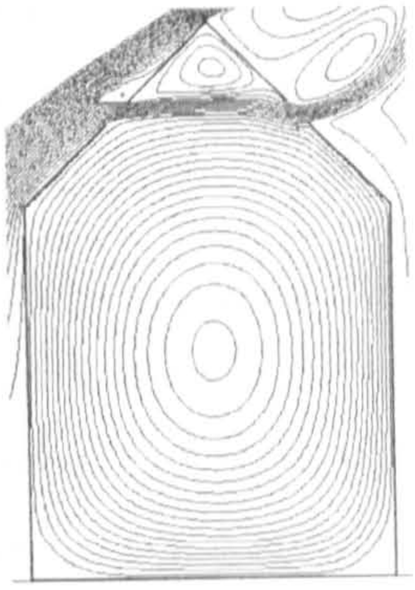

(c) left pivoting (upper edge)

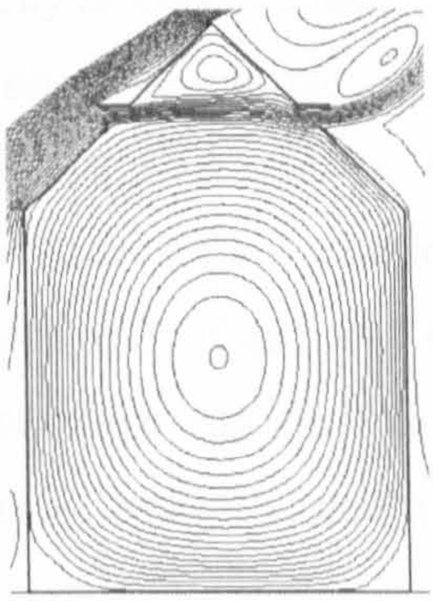

(d) both pivoting (upper edge)

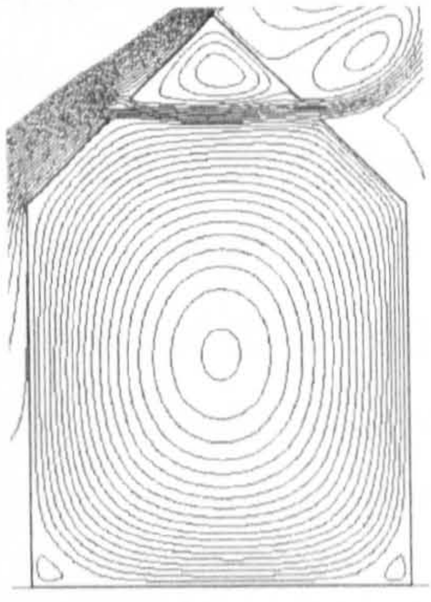

(e) both pivoting (middle)

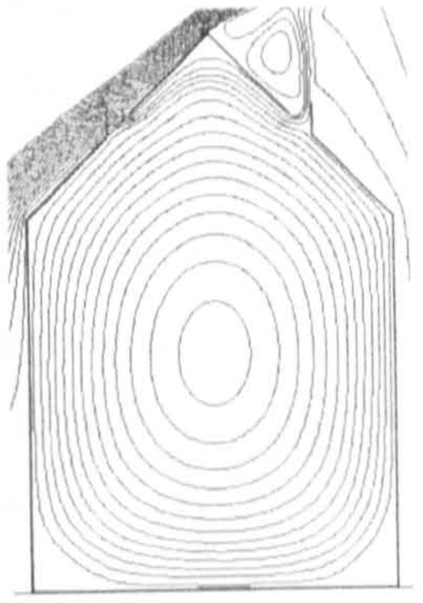

(f) right pivoting (lower edge)

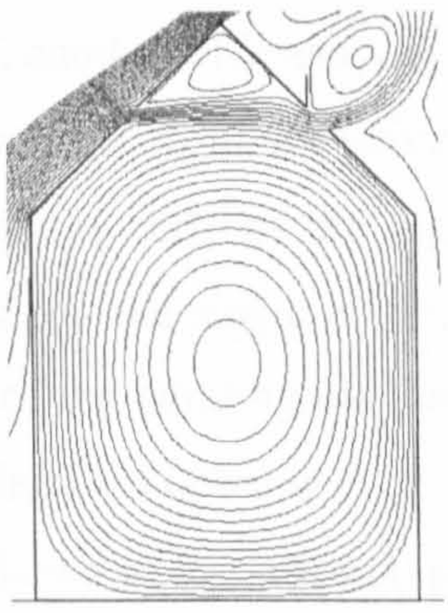

(g) right pivoting (upper edge)

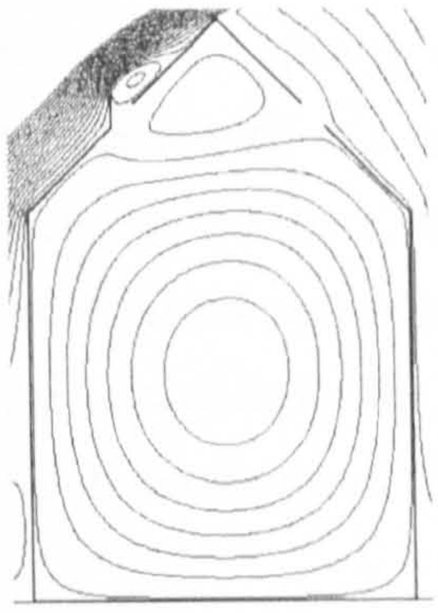

(h) left pivoting (lower edge)

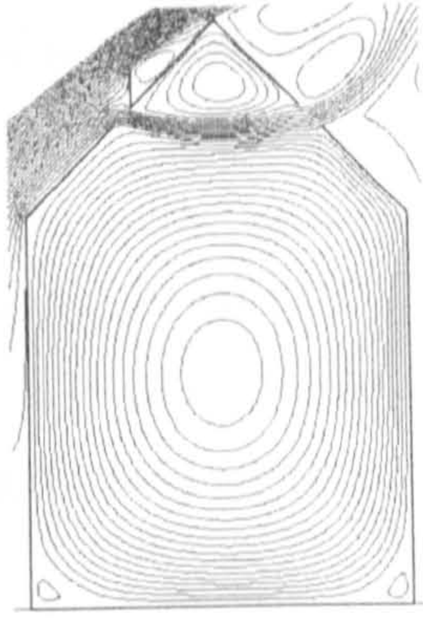

(i) left pivoting (upper edge)

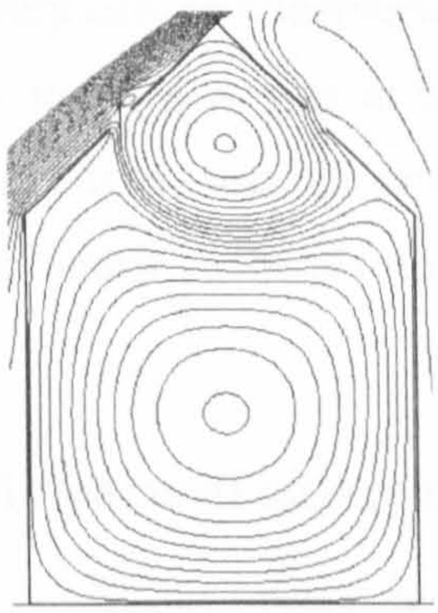

(j) left pivoting (middle)

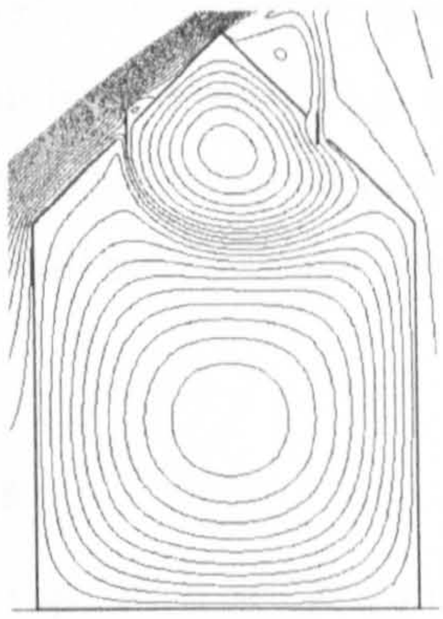

(k) both pivoting (middle)

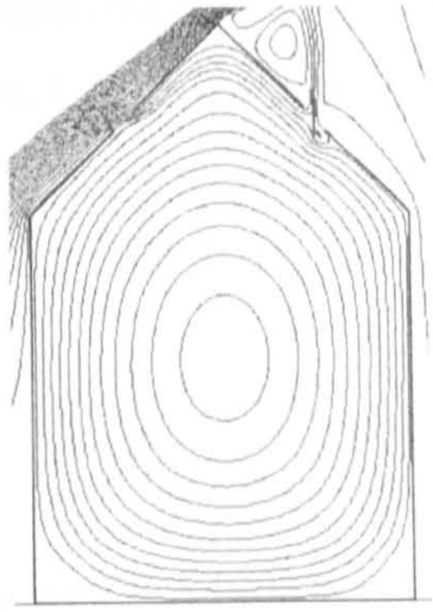

(l) right pivoting (middle)

Figure 5.35: Airflow patterns of wind-induce natural ventilation for atria with 45° triangular roof and pivoting openings

Based on the above discussions, it can be summarised that, in order to use pivoting windows to improve the ventilation performance, the edge of the window should be able to enhance the driving force, i.e. the reverse flow, if the flow pattern is to be kept unchanged; otherwise changing flow pattern to (II) by opening edges will also be a good choice.

The observations for the ventilation performance of 5° roof atria can also apply for 15° roof atria. It can be seen from Figure 5.33 that, when the driving force of the flow in the space, i.e. the reattaching flow is blocked by the opening edges, such as scenarios (b), (c), (g) and (j), the airflow will be significantly weakened; on the contrary, if the opening edge can obstruct the counteracting force, i.e. the back flow, or enhance the reattaching flow, the magnitude of the air velocity at the occupants' level in the space will be increased, such as scenarios (f) and (k). It is also observed that the separation of the main flow can be caused due to the opening edge on the windward pitch and the back flow will dominate the internal air movement resulting in the occurrence of flow pattern (III).b. An interesting scenario is (d), which can be considered as a composition of (b) and (c). Although either (b) or (c) does not have a good ventilation performance and their flow patterns are different, their combination leads to a much better situation, basically because of the enhanced "tunnel effects" formed by the two opening edges.

For 20° roof atria (Figure 5.34), in order to improve the ventilation performance of the space, apart from enhancing the back flow like scenarios (b) and (e) on the leeward side of the roof, another efficient way is to use the windward opening edge to cause separation of the main flow, as seen in scenarios (h) and (i). Scenario (l) is a combination of the above mentioned strategies and has the highest air velocity in the space, but scenario (h) should be the most efficient: the single pivoting window on the windward side can not only induce the flow to get out of the building but also result in the separation for the main flow. It is also observed that, the leeward opening edge can also bring on the change of flow pattern if it blocks the back flow, as shown in scenarios (f) and (k).

The effects of the pivoting windows on the ventilation performance of the 45° roof atria are very easy to understand (see Figure 5.35): when the opening edges block the oncoming main flow, the airflow rate in the space will be weakened (e.g. scenarios f, h, j, k; l); when they are parallel to the wind direction, the air velocity at the occupants' level will be increased (e.g. b, c, d, e); otherwise the pivoting windows will not have significant impacts (e.g. scenarios g&i).

5.5 Impacts of adjacent buildings

As has been pointed out, the separation of the main flow at the windward top corner of the atrium space has significant effects on the ventilation performance of the space, and it is easy to understand that the presence of the windward adjacent buildings can block the wind and move the separation point forward. The leeward adjacent buildings will occupy the area for

developing the recirculation behind the building and hence may have influence on the back flow. Consequently, it is anticipated that the adjacent buildings on both sides will have certain impacts on the ventilation performance of atria and this is the main concern of this section. The impacts of the windward adjacent buildings are investigated first, followed by the study of the effects of the leeward adjacent buildings. The typical atrium roofs used before will also be employed for this part of study. It is assumed that the height of the adjacent building is the same as that of the roof level, 12*m*.

5.5.1 Windward adjacent buildings

• *Triangular roof*

It can be envisaged that, if the windward adjacent building is very wide, the main flow will separate at the most windward top corner and then fully reattach to the top surface of the windward adjacent building before meeting the atrium roof pitch. In this situation, the windward roof pitch will expose to positive pressure and flow pattern (I) will result regardless of the roof angle. This is illustrated in Figure 5.36. It is also observed that the width of the adjacent building that enables the full reattachment of the main flow is not the same for all roof angles but increases with the increase of the roof angle. The width needed is around 14m when the roof angle is 5°; 20m for 15°; 24m for 20° and 45° roof will require around 32m for the full reattachment.

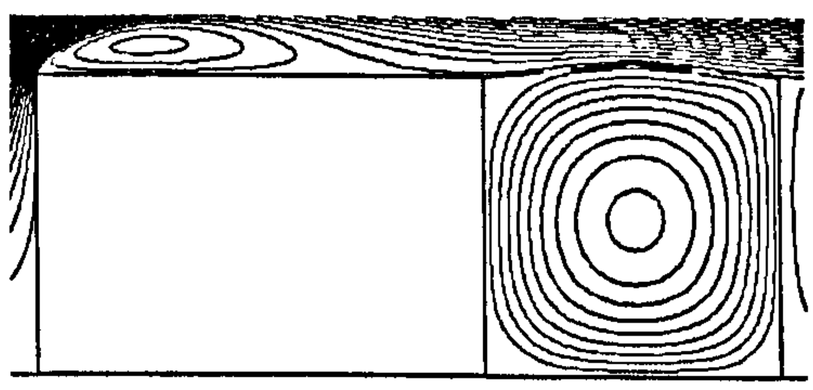

(a) roof angle: 5°; width of the windward adjacent building: 18m

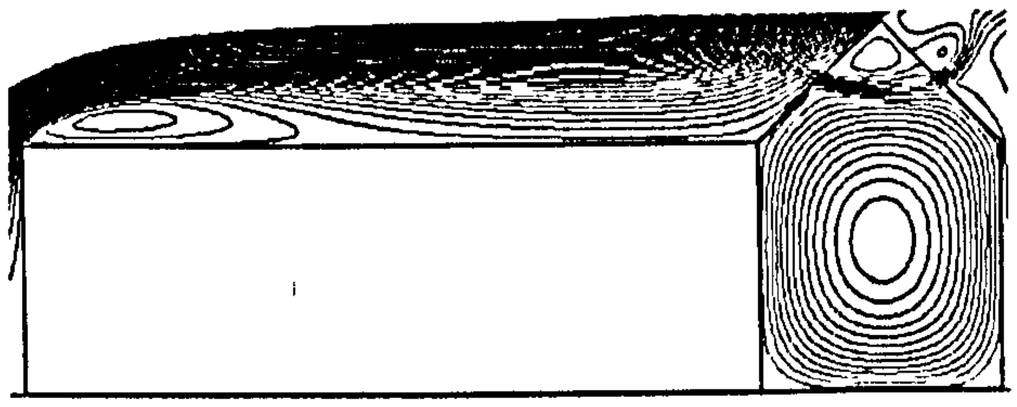

(b) roof angle: 45°; width of the windward adjacent building: 36m

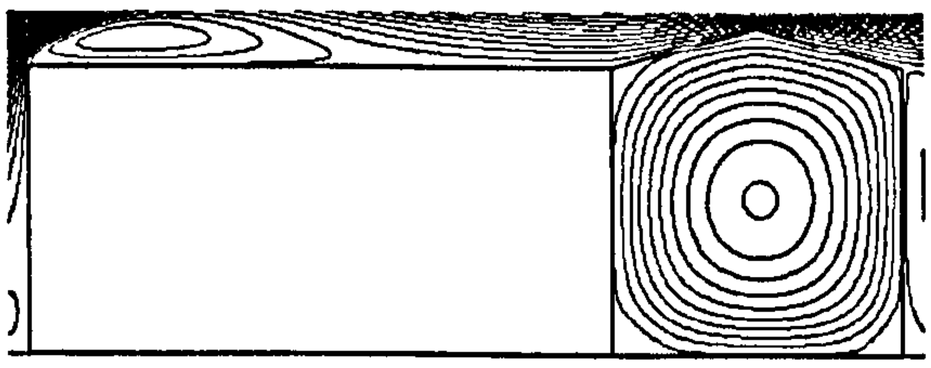

(c) roof angle: 15°; width of the windward adjacent building: 24m

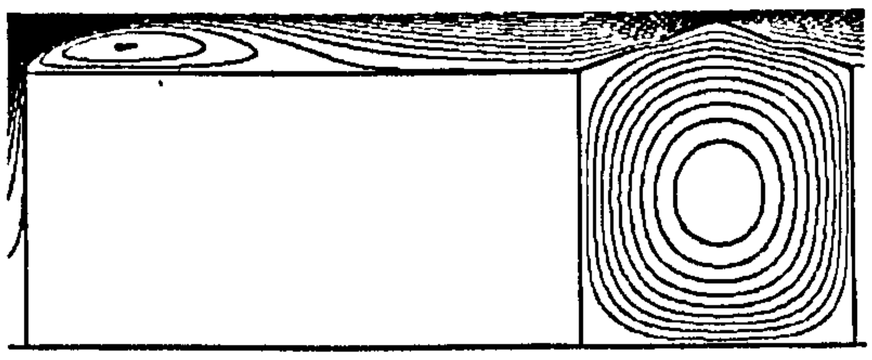

(d) roof angle: 20°; width of the windward adjacent building: 24m

Figure 5.36: Airflow patterns of wind-induce natural ventilation for atria with triangular roofs and windward adjacent buildings

developing the recirculation behind the building and hence may have influence on the back flow. Consequently, it is anticipated that the adjacent buildings on both sides will have certain impacts on the ventilation performance of atria and this is the main concern of this section. The impacts of the windward adjacent buildings are investigated first, followed by the study of the effects of the leeward adjacent buildings. The typical atrium roofs used before will also be employed for this part of study. It is assumed that the height of the adjacent building is the same as that of the roof level, 12*m*.

5.5.1 Windward adjacent buildings

• *Triangular roof*

It can be envisaged that, if the windward adjacent building is very wide, the main flow will separate at the most windward top corner and then fully reattach to the top surface of the windward adjacent building before meeting the atrium roof pitch. In this situation, the windward roof pitch will expose to positive pressure and flow pattern (I) will result regardless of the roof angle. This is illustrated in Figure 5.36. It is also observed that the width of the adjacent building that enables the full reattachment of the main flow is not the same for all roof angles but increases with the increase of the roof angle. The width needed is around 14m when the roof angle is 5°; 20m for 15°; 24m for 20° and 45° roof will require around 32m for the full reattachment.

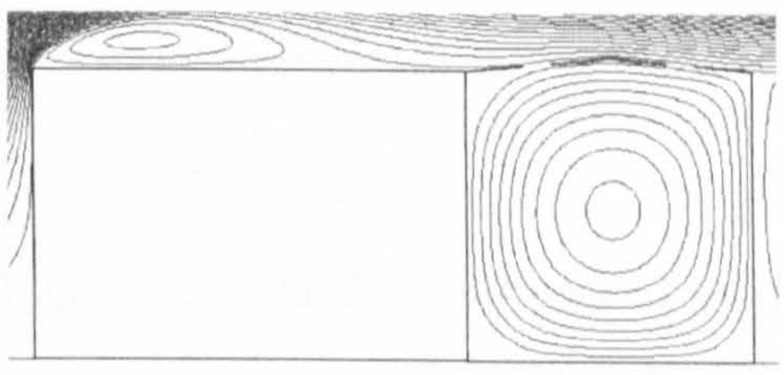

(a) roof angle: 5°; width of the windward adjacent building: 18m

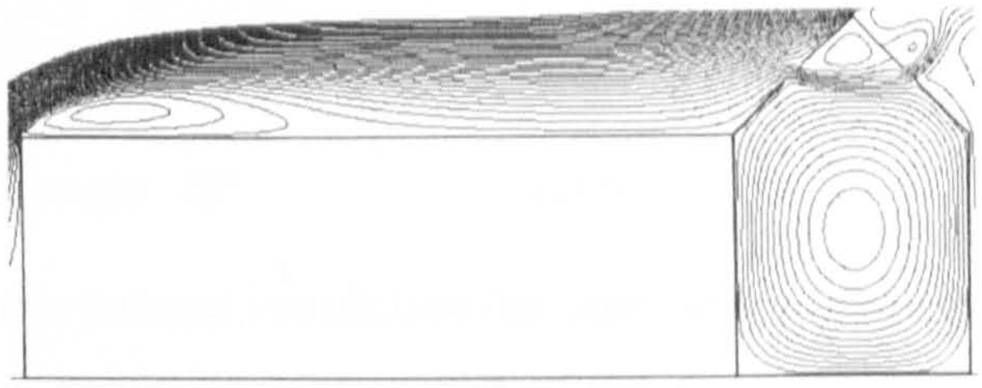

(b) roof angle: 45°; width of the windward adjacent building: 36m

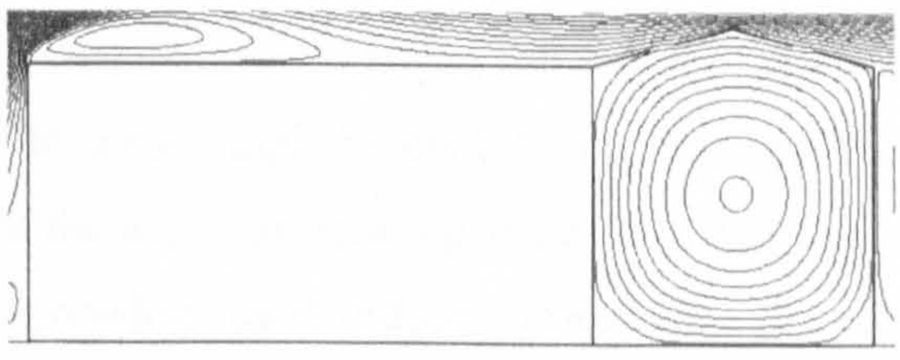

(c) roof angle: 15°; width of the windward adjacent building: 24m

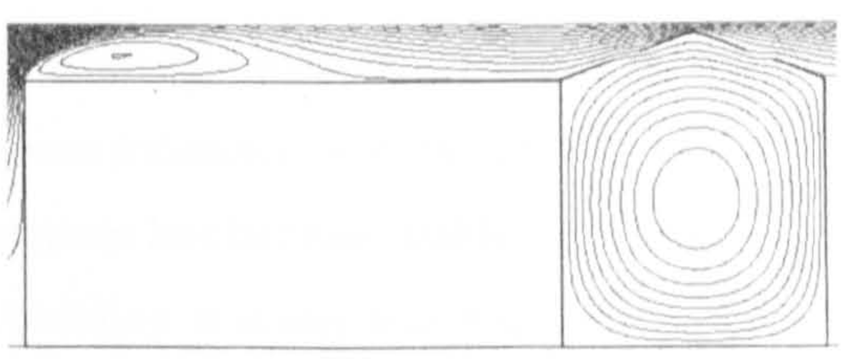

(d) roof angle: 20°; width of the windward adjacent building: 24m

Figure 5.36: Airflow patterns of wind-induce natural ventilation for atria with triangular roofs and windward adjacent buildings

As has already been made clear, for roof angle below 21°, the ventilation of the prototype atria is driven by suction when there is no adjacent building beside the atrium and the flow pattern is (III).a, (II) and (III).b for 5°, 15° and 20° roof respectively. Thus, there must be a transition process for the airflow pattern of atria with these roof angles if adjacent buildings are added. Figure 5.37 illustrates the airflow patterns for the atria with these roof angles when the adjacent building is not wide enough to change the flow pattern to (I). It is shown that a reverse flow will be induced between the windward opening and the leftmost top corner, and flow pattern (II) occurs for atria with all three different roof angles. It can be seen that, the presence of the windward adjacent building brings the separation point forward and the main flow has already begun to reattach to the roof level from above the windward opening. Thus, for 5° roof, its horizontal momentum at the inlet opening can easily overwhelm that from the back flow and becomes the driving force for the air movement in the space. For 15° and 20° roofs, the main flow can reattach the roof from a higher position due to earlier separation than that of the single stand-alone atrium building and thus the flow will reattach to the roof more smoothly resulting in higher air velocity in the space.

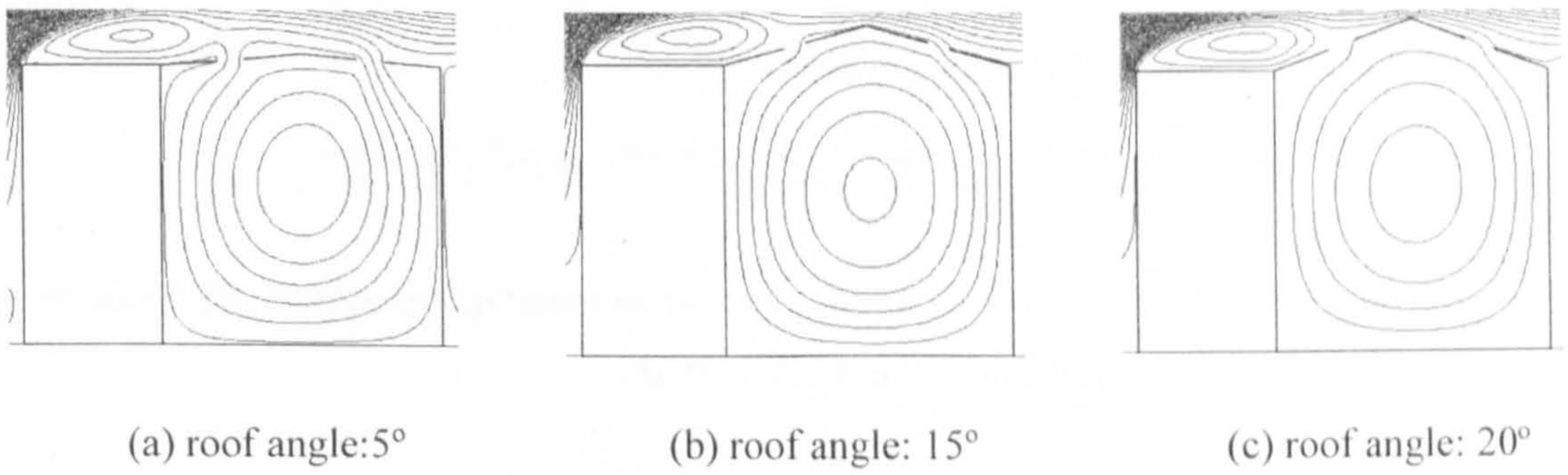

(a) roof angle:5° (b) roof angle: 15° (c) roof angle: 20°

Figure 5.37: Airflow patterns of wind-induce natural ventilation for atria with triangular roofs and windward adjacent buildings of a width of 6m

Figure 5.38 presents the relationship between the maximum air velocity coefficient at the occupants' level and the width of the windward adjacent building. It shows that, for atria with a roof angle below 20°, the air velocity in the space increases with the increase of the width of the adjacent building, especially when the flow pattern has become stable. Nevertheless, the increasing speed reduces down when the adjacent building is wider and it becomes zero when the main flow fully attaches to the roof. However, for atria with 45° roof, the air velocity at the occupants' level will decrease first and then increase if the width of the adjacent building is continuously increased. This is because, when there is no adjacent building, the main flow will directly enter into the building through the windward opening; however, when the width of the adjacent building is intermediate, the main flow will separate at the most windward corner and

only part of the separated flow enters into the building and as a result the airflow in the space will be weaker; when the adjacent building is very wide, the main flow can fully reattach to the roof level and enables more air to get in the building, thus enhancing the airflow in the space. However, due to the friction of the roof, the flow is still much weaker than the situation when no adjacent building exists. The airflow patterns of these three situations are illustrated in Figure 5.39.

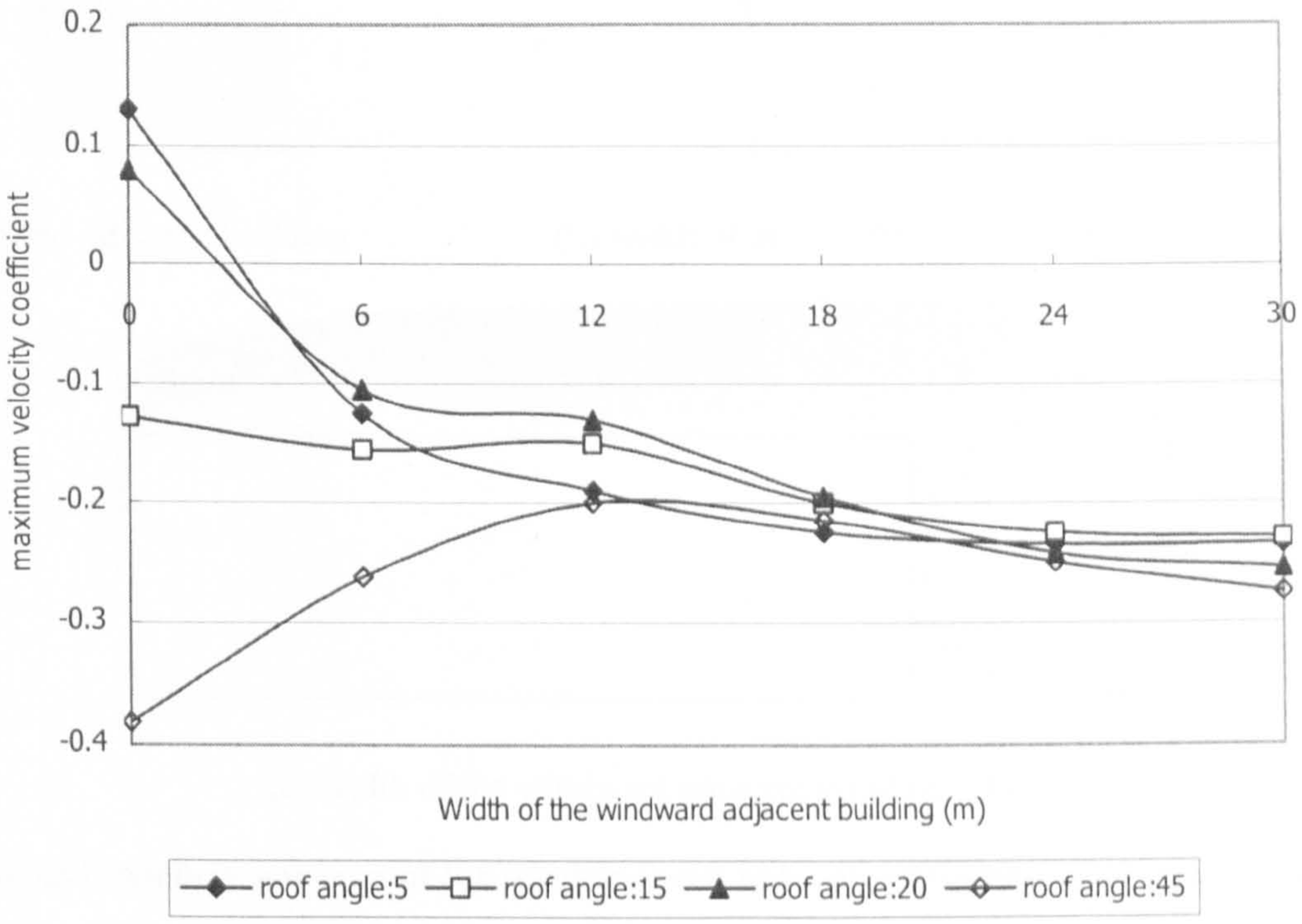

Figure 5.38: Relationship between the maximum air velocity coefficient and the width of the windward adjacent building

It can also be seen that, when the adjacent building is very wide (no less than 18m), the air velocities of different roof angles become very similar to each other with a discrepancy less than 15%. When the airflow becomes stabilised and does not change with the increase of the width of the adjacent building, the order of the magnitude of the air velocity is the same as that of the roof angle since higher roof pitch has larger vertical opening area. This analysis actually suggests that, when the adjacent building becomes very wide, the ventilation performance of the atria will become insensitive to the roof angle.

According to the above discussions, it can be summarised that, over the whole process of increasing the width of the windward adjacent building, the airflow pattern for all roof angles will be finally (I) with the occurrence of (II) during the transitional process. For atria with lower roof angles where the ventilation is driven by suction, the windward adjacent building can help to enhance the air movement in the space. However, with respect to the atria with high

roof angle where flow pattern (I) occurs, it is not good practice to place any adjacent building on the windward side of the space for promoting internal airflow.

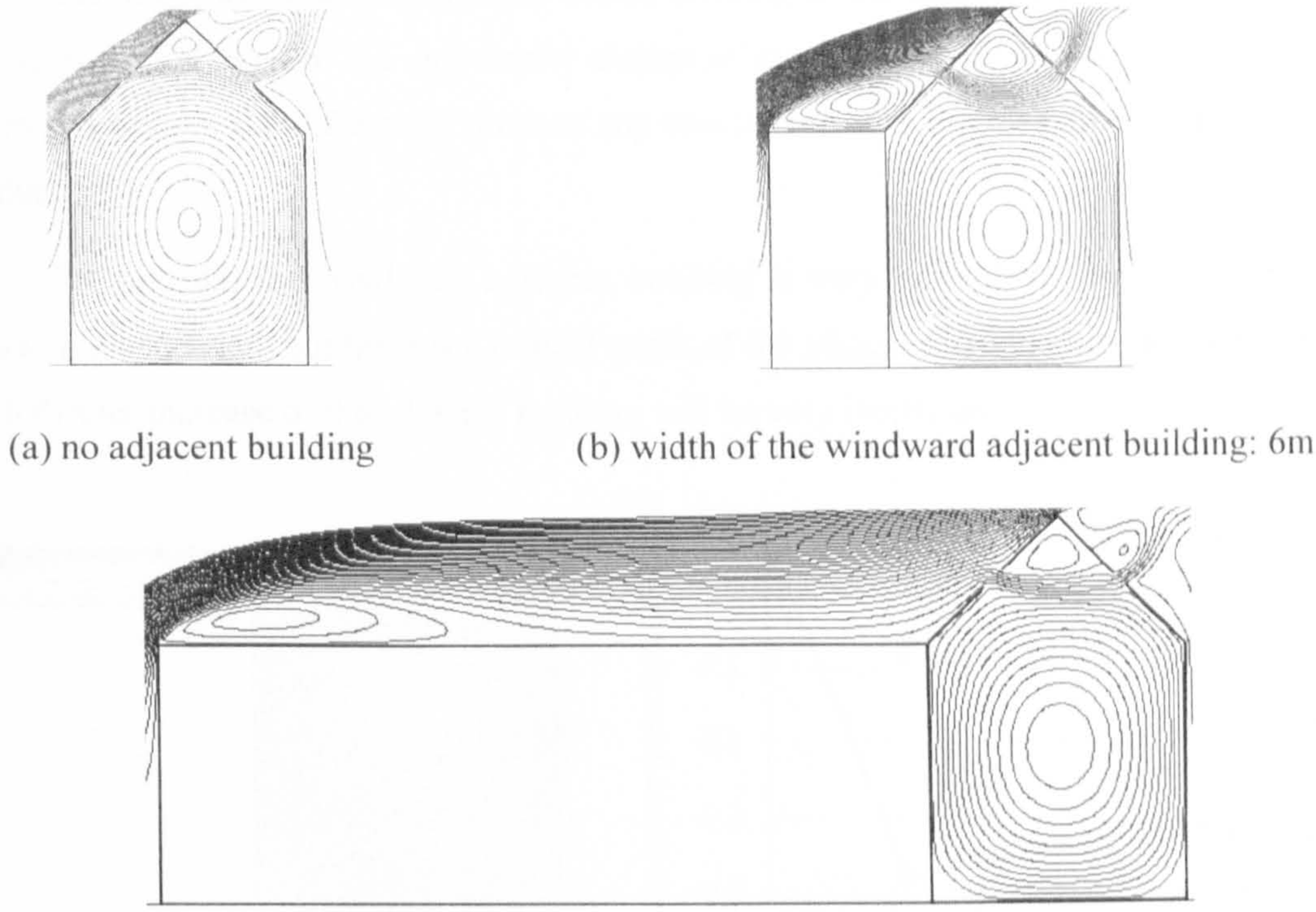

(a) no adjacent building

(b) width of the windward adjacent building: 6m

(c) width of the windward adjacent building: 36m

Figure 5.39: Airflow patterns of the wind-induced natural ventilation of 45° roof atria with different widths of windward adjacent building

• *Courtyard*

The results on the effects of the windward adjacent building obtained in above studies are still applicable for courtyards: the separation point is moved forward; the main flow starts to reattach to the roof level earlier, thus increasing the horizontal momentum of the main flow at the roof level. Therefore, its impact is very similar to that of increasing the height of the leeward wall and the ventilation performance can be greatly improved with the flow pattern changed from (III).b to (II) (see Figure 5.40).

It is also observed that, when the flow pattern has been changed to (II), the variation trend of the air velocity in the space includes two different parts which distinguish when the adjacent building is 18m wide. For the first part, the main flow has not fully reattached to the roof level and the flow direction above the courtyard is downward and windward, i.e. both horizontal and vertical momentums are strong. In this way, the flow has more intention to reach to the bottom of the space and drive the air movement there. As a consequence, wider adjacent building reduces the downward momentum and hence the air velocity at the occupants' level.

When the adjacent building is wide enough, the flow can fully reattach to the roof before meeting the courtyard. Because of the roof, part of vertical momentum disappears and the other part is transferred to horizontal momentum. This process also needs certain distance and wider roof means more horizontal momentum before arriving at the stabilisation point. This is also the reason for the trend of the air velocity change of the second part. Nevertheless, when flow pattern (II) occurs, the difference between any two scenarios is quite small with a variation of less than 16%.

To sum up, the windward adjacent building is very helpful for the enhancement the airflow in a courtyard, but there is a critical width of the adjacent building for this purpose, over which further increase of the adjacent building will be very inefficient.

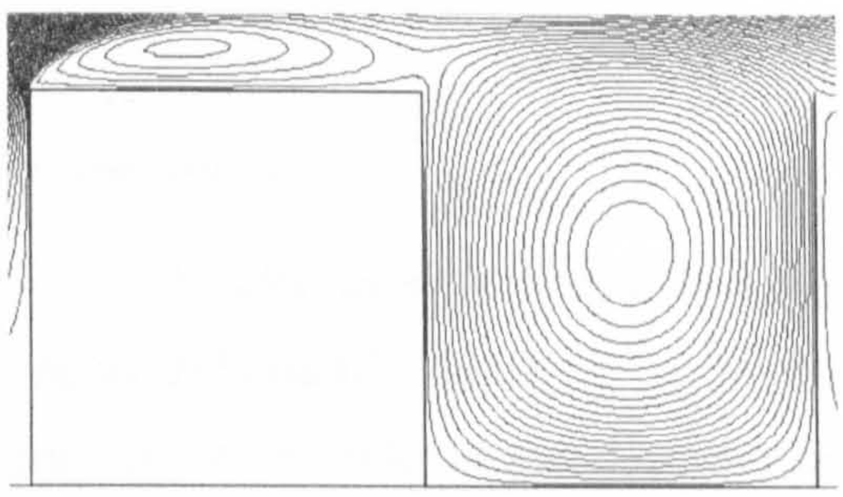

(a) airflow pattern for a courtyard with a windward adjacent building of 12m

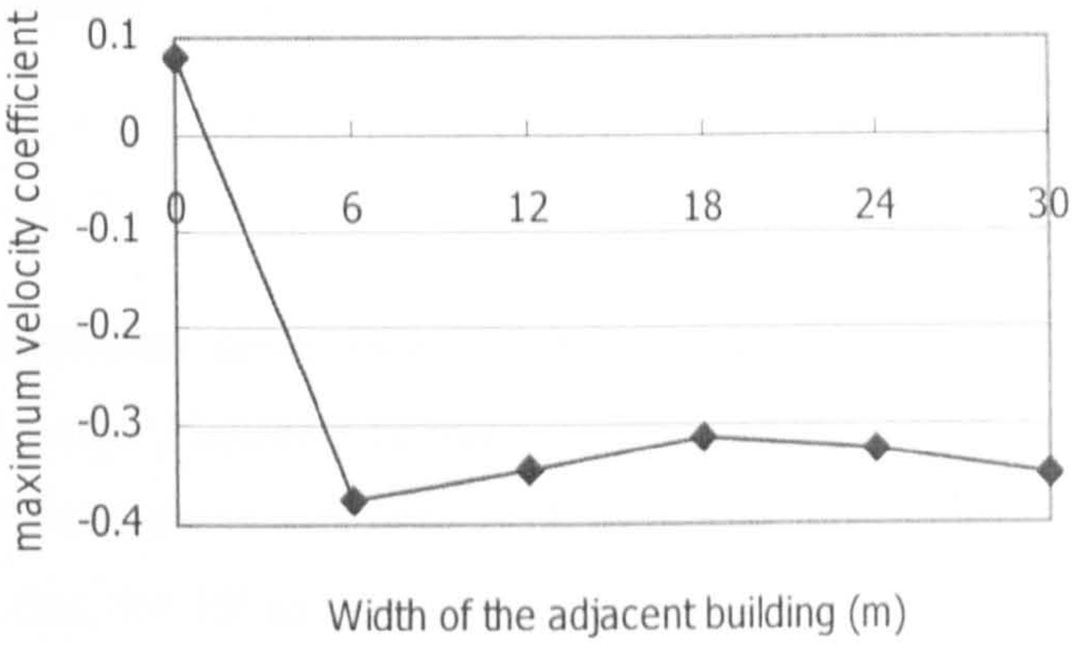

(b) relationship between maximum velocity coefficient and the width of the adjacent building

Figure 5.40: investigation of the impacts of the windward adjacent buildings on the ventilation performance of a courtyard

• *Barrel vault roof*

The study of the vault roof atria with a tangential angle below 20° can refer to previous studies for 5° and 15° and will not be repeated here. Vault roof atria with a tangential angle of 30°, which were also used before, are employed for this part of investigation.

Figure 5.41 compares the airflow patterns of a stand-alone vault roof atrium and another vault roof atrium with a windward adjacent building. It is observed that the windward adjacent building does not have any effect on the flow pattern of the wind-induced air movement of atria with vault roofs, even when it is very wide and the main flow can fully reattach to the roof. With respect to the magnitude of the air velocity at the occupants' level, it generally has the same trend as that for atria with 45° triangular roof, because they have the same effects on the main flow in terms of the separating and reattaching phenomenon, and thus windward adjacent building cannot significantly improve the ventilation performance of the space.

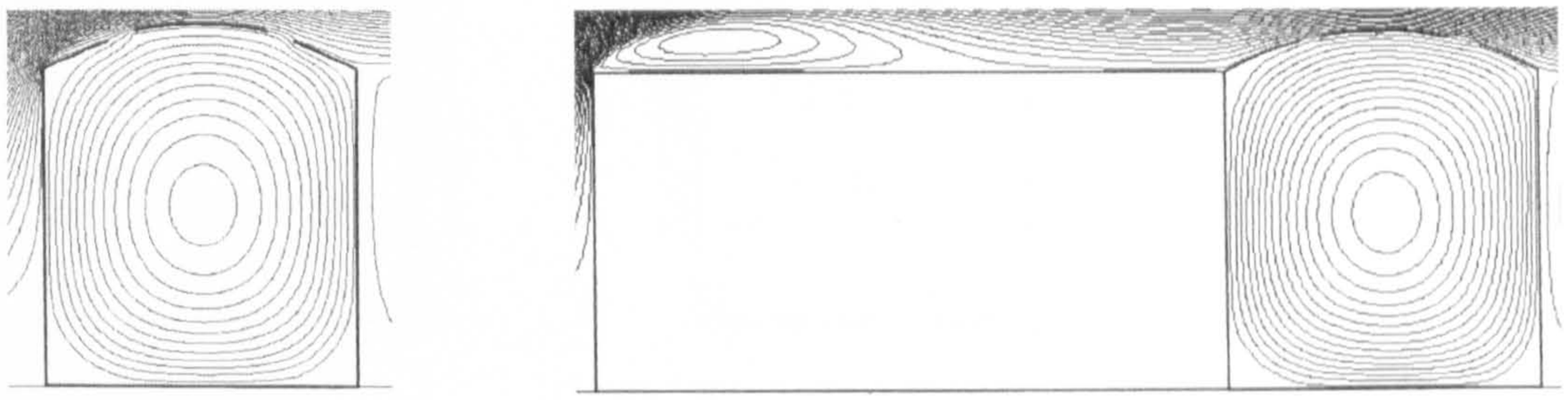

(a) no adjacent building

(b) width of the windward adjacent building: 24m

Figure 5.41: Comparison of airflow patterns of the wind-induced natural ventilation of an stand-alone vault roof atrium and one vault roof atrium with a windward adjacent building

• *Sawtooth roof*

Finally let us take a look at the complicated sawtooth roof. Atria with typical roof angles, 15° and 45°, have been chosen for the study. Figures 5.32 and 5.43 compare the airflow patterns of the wind-induced ventilation of stand-alone sawtooth roof atria and those with windward adjacent buildings. It can be seen that, for 15° sawtooth roof atria where the airflow in the space is driven by suction, the windward adjacent building can help with the enhancement of the internal air movement for both tooth number conditions (see scenarios a to c in both figures), because it reduces the separating effects at the left top corner of the atrium, thus resulting in stronger horizontal momentum that drives the indoor airflow.

Situations for 45° sawtooth roof are much more complicated. When all leeward openings are opened with windward openings closed, the effects of adjacent buildings are not very significant as separation still occurs due to the high roof pitch (see scenario d in both figures), and the flow pattern remains as (III).b. If all windward openings are opened with leeward openings closed, although flow pattern (I) is incurred due to the adjacent buildings, the internal airflow is not significantly enhanced as well. This is basically because of the shape of the roof: there is no directly through path for the main flow for such shape of roof, which the basis of flow pattern (I) "tunnel effect" relies on. With regards to the bottom openings situations, the air flow rate at the occupants' level can be increased by windward adjacent buildings. The reason for this varies for different tooth numbers. When tooth number is 3, the adjacent building can change the flow pattern from (III).b to (I), which is the similar to the case of 20° triangular roof; when the tooth number is 6, the reason is the same as explained for sawtooth roof atria with leeward openings at the beginning of this passage.

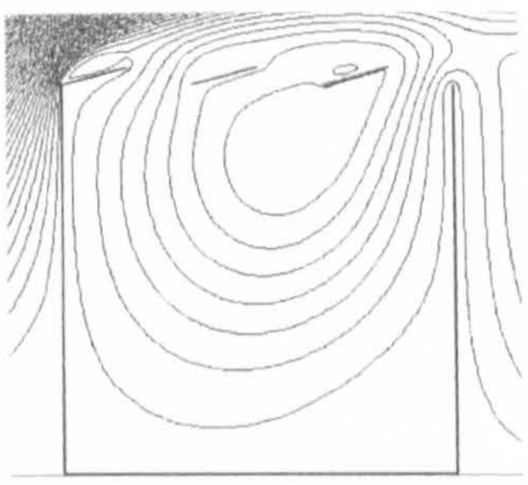

(a) 15°, leeward openings

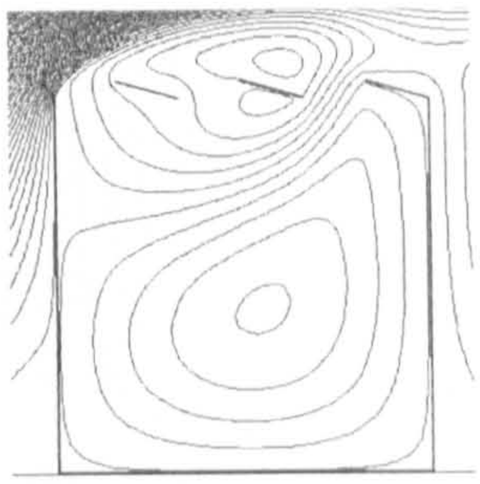

(b) 15°, windward openings

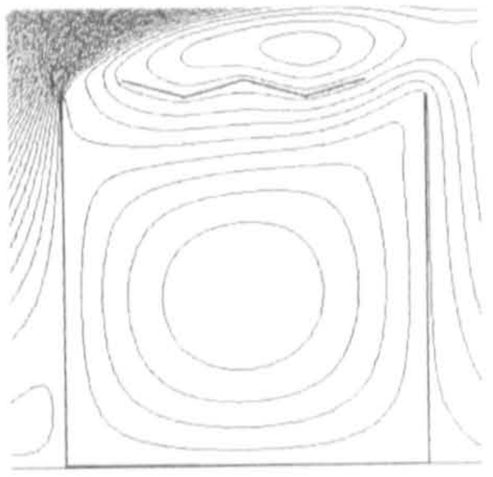

(c) 15°, bottom openings

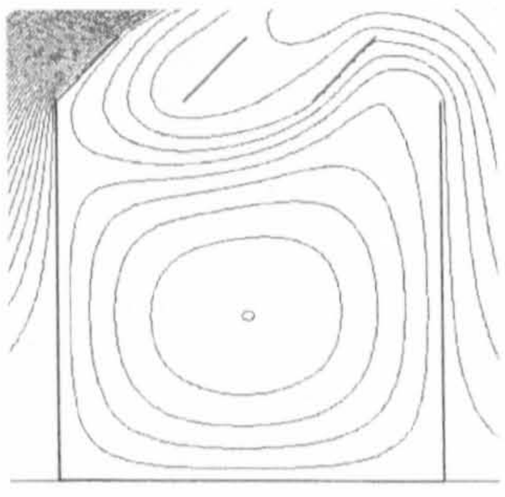

(d) 45°, leeward openings

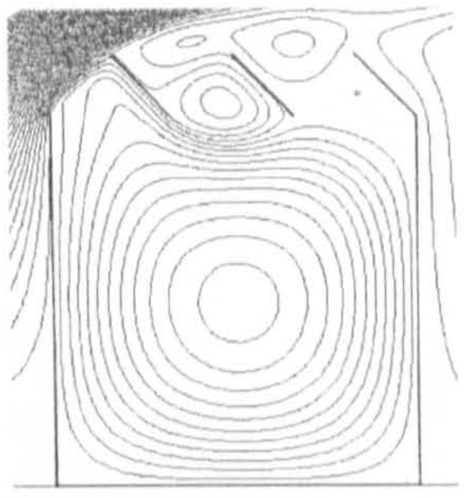

(e) 45°, windward openings

(f) 45°, bottom openings

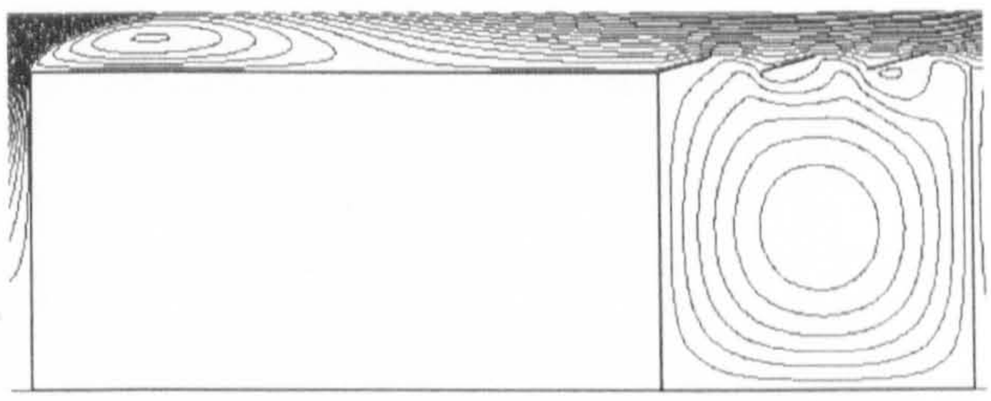

(a) + 24m windward adjacent building

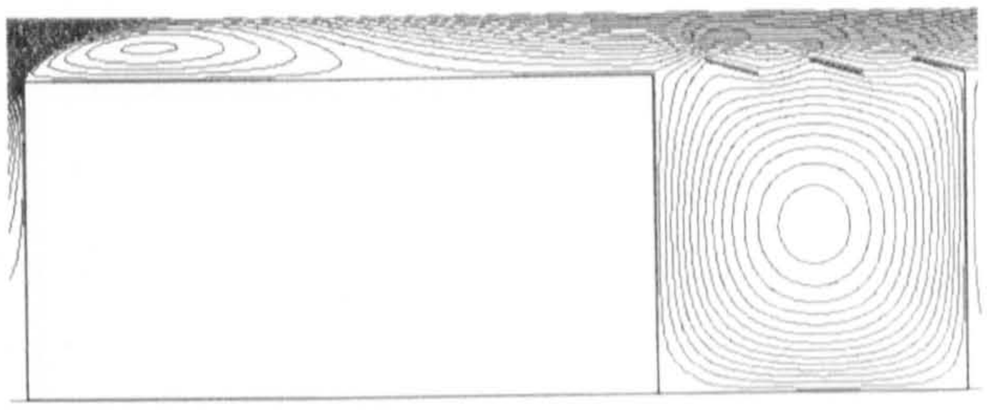

(b) + 24m windward adjacent building

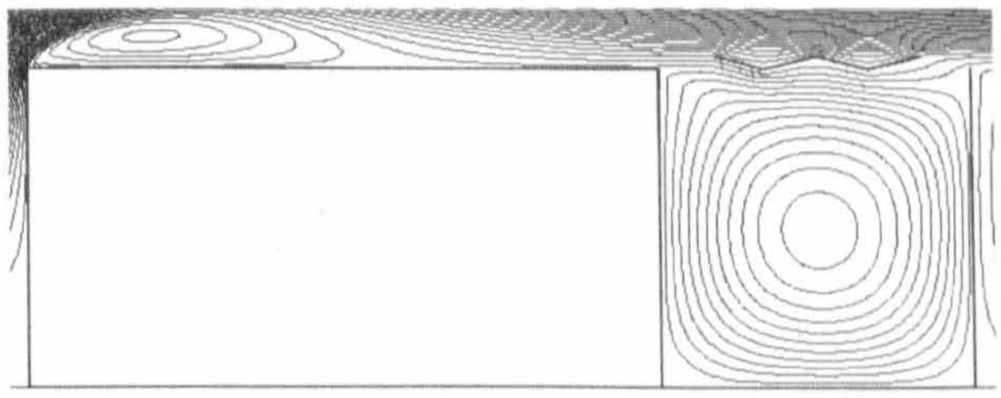

(c) + 24m windward adjacent building

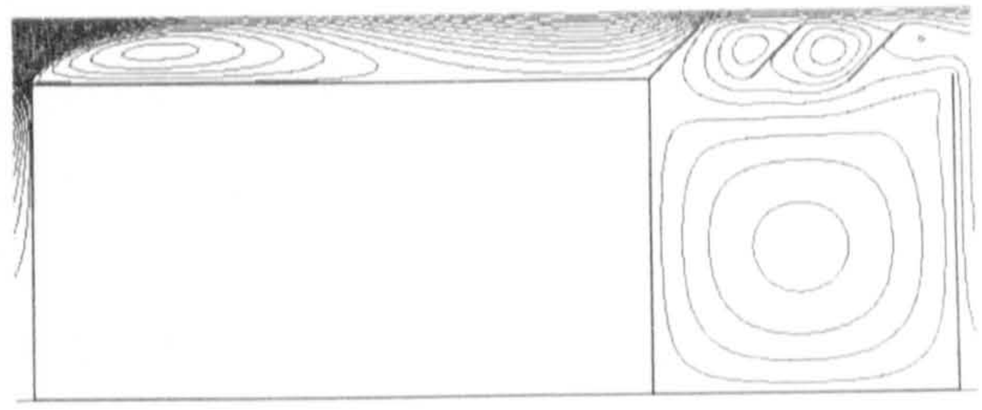

(d) + 24m windward adjacent building

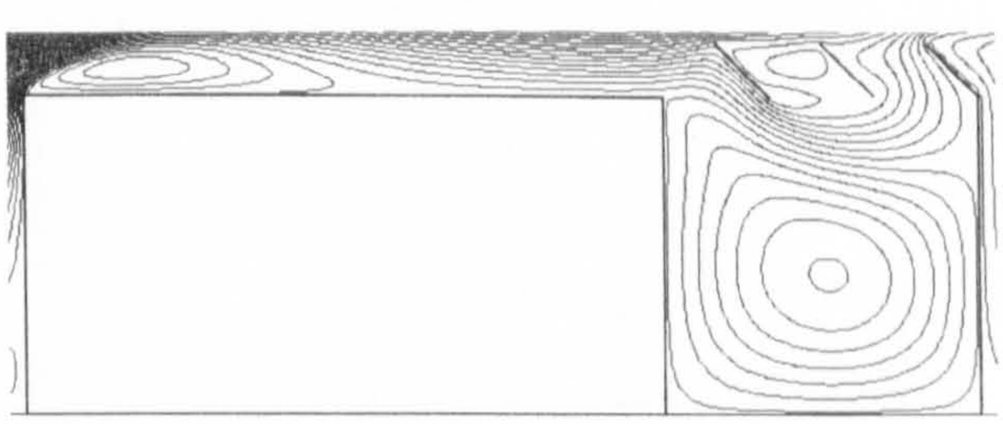

(e) + 24m windward adjacent building

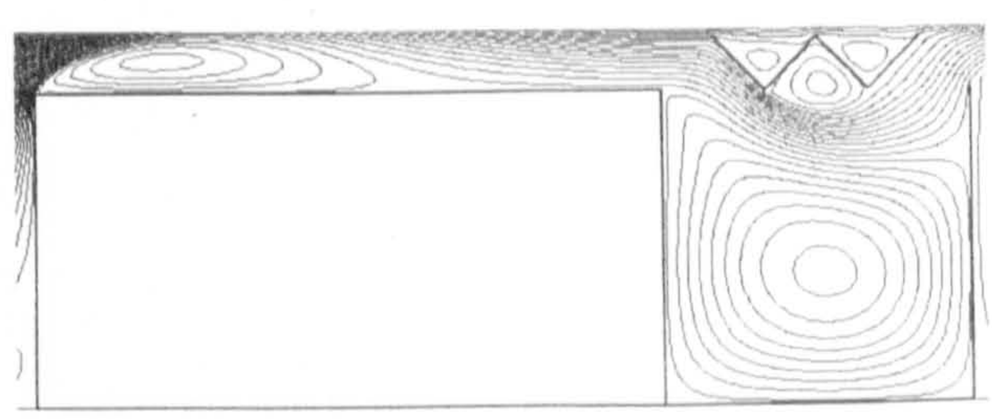

(f) + 24m windward adjacent building

Figure 5.42: Airflow patterns of the wind-induced natural ventilation of sawtooth roof atria with windward adjacent building (tooth number: 3)

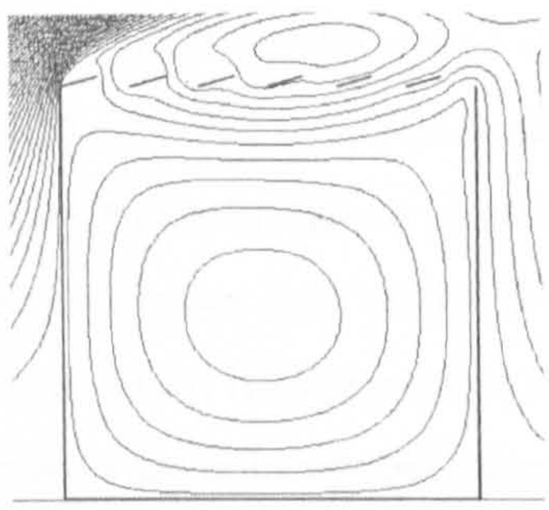

(a) 15°, leeward openings

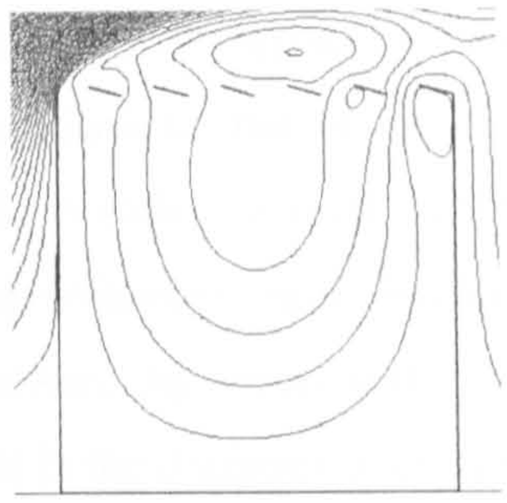

(b) 15°, windward openings

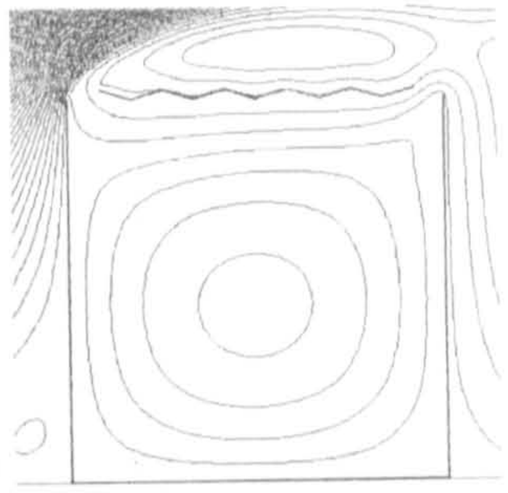

(c) 15°, bottom openings

(d) 45°, leeward openings

(e) 45°, windward openings

(f) 45°, bottom openings

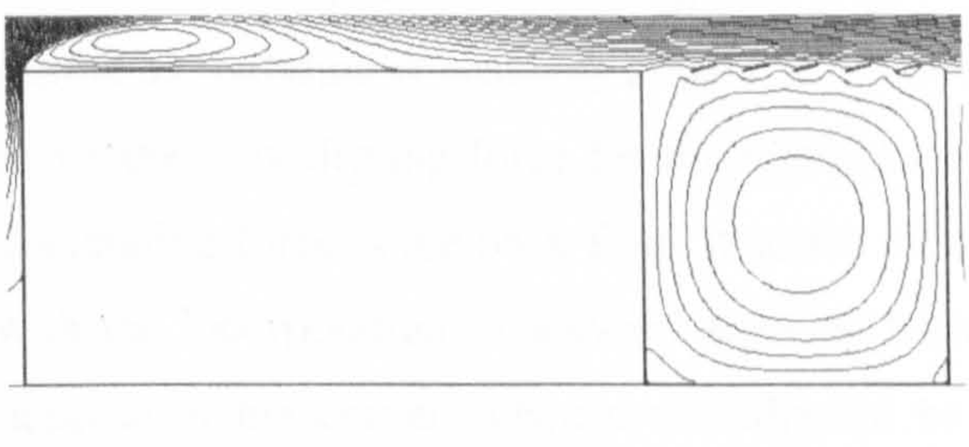

(a) + 24m windward adjacent building

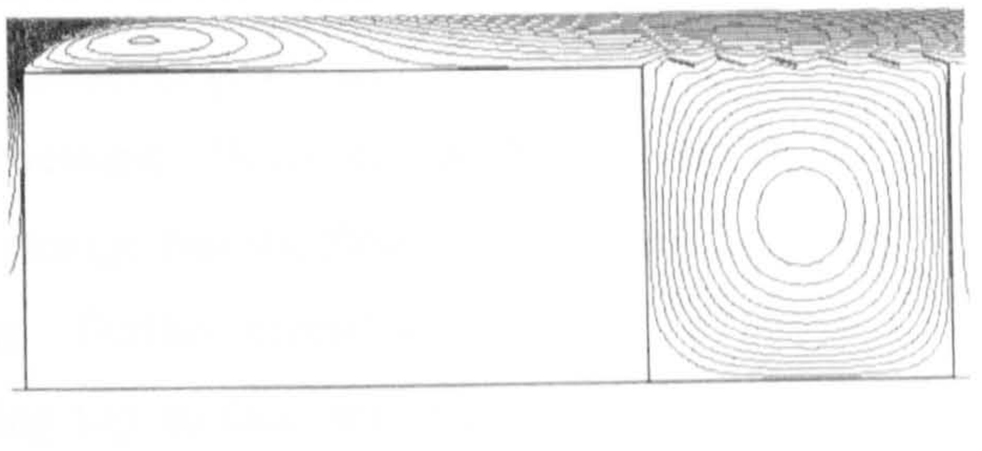

(b) + 24m windward adjacent building

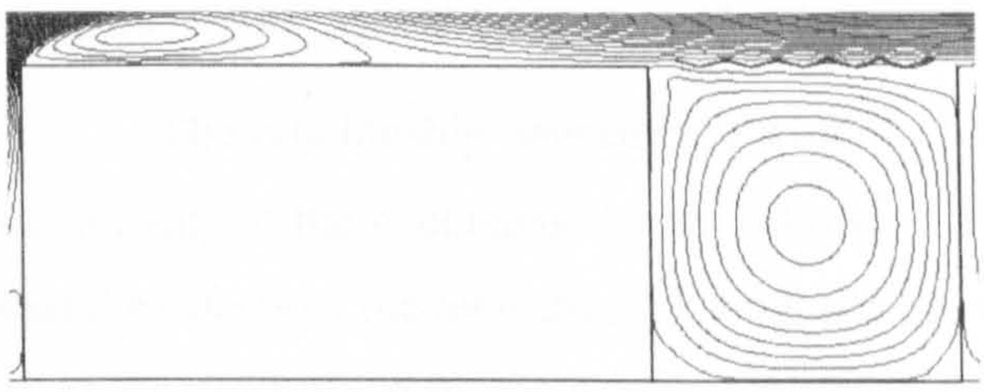

(c) + 24m windward adjacent building

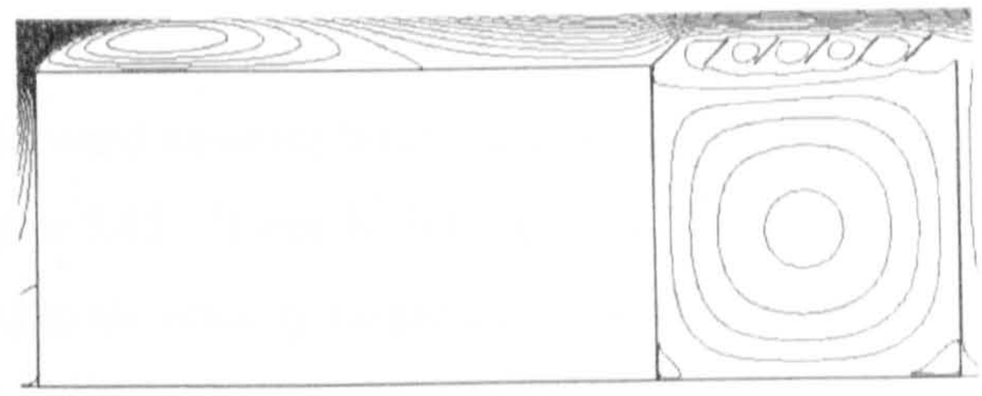

(d) + 24m windward adjacent building

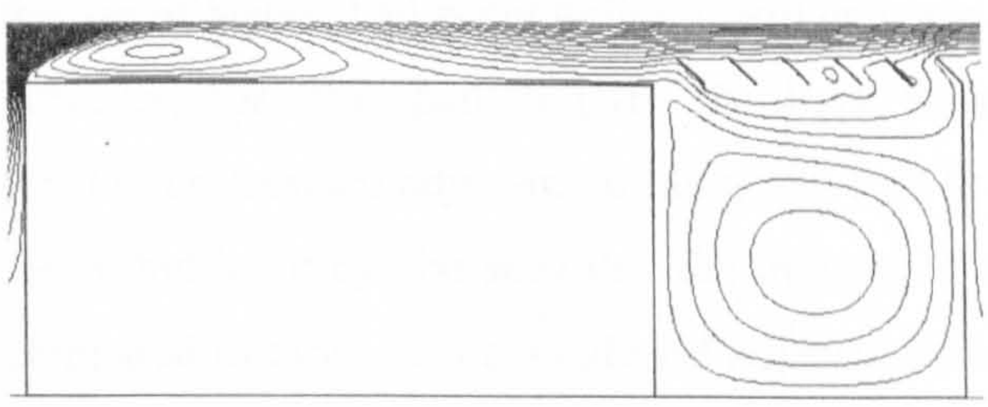

(e) + 24m windward adjacent building

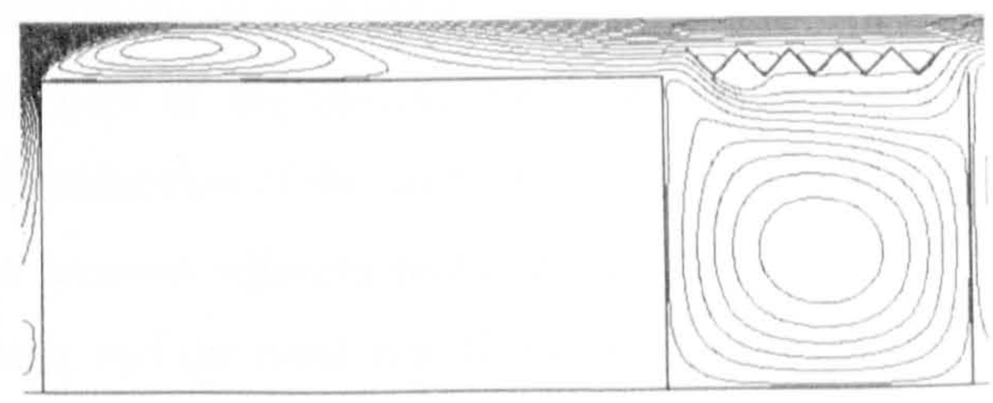

(f) + 24m windward adjacent building

Figure 5.43: Airflow patterns of the wind-induced natural ventilation of sawtooth roof atria with windward adjacent building (tooth number: 6)

Based on the above discussions about the effects of windward adjacent buildings on several different forms of roofs, the conditions for the use of adjacent buildings to improve the ventilation performance of atrium buildings with two small openings in the roof (also including courtyard cases and sawtooth roof atria with roof angle less than 20°) can be summarised as follows: main flow separates at the windward top corner if the atrium is stand-alone and the use of windward adjacent building can result in the disappearance of the separation above the atrium roof level. For sawtooth roof atria with roof angle above 20°, among the three openings distributions tested, the adjacent buildings are useful for bottom openings situations only.

5.5.2 Leeward adjacent buildings

• *Triangular roof*

Figure 5.44 illustrates the airflow patterns of triangular roof atria that have different roof angles and 12m leeward adjacent building. It can be seen that, for all roof angles, the flow pattern remains the same as that of the related stand-alone atrium space. This is easy to understand for atria with roof angle of 5°, 15° and 45°, as the effect of the back flow from behind the building is basically assist (i.e. 5°) or counteract (e.g. 15° and 45°) other forces and it is not the only driving force for the internal air movement. However, for 20° roof where the dominating force is the back flow, it seems a little strange that the flow pattern is not changed with the incorporation of leeward adjacent building. Further investigation shows that this is because of the corner between the adjacent building top surface and the leeward roof pitch where recirculation is formed since there is an angle between the main flow and the leeward pitch due to the separation at the peak of the roof.

The relationship between the width of the leeward adjacent building and the maximum air velocity at the occupants' level is shown in Figure 5.45. It can be inferred from the figure that the effects of the leeward adjacent buildings on the air velocity magnitude at the occupants' level are determined by the role that the back flow plays in driving the internal air movement. As identified earlier, for flow pattern (I) and (II), the back flow acts as the counterforce and thus the use of leeward adjacent building will enhance the airflow, as seen for roof angle 15° and 45°; however, for flow pattern (III), the back flow is part of the driving force and therefore employing leeward adjacent building will lead to the reduction of the air flow rate in the space. Nevertheless, it can be seen that the impacts of the leeward adjacent buildings are quite small compared to those of the windward adjacent buildings, and the most significant one takes place for the 15° roof where the two counteracting forces that induces the airflow, the reattaching flow and the back flow are similar in scale, which means the reduction of the back flow can contribute more to the internal flow than other cases. It can also be observed that only a small width is needed for the realisation of the impacts (6m for this case) and further increase of the width of the adjacent building has no effects on the ventilation performance of the space.

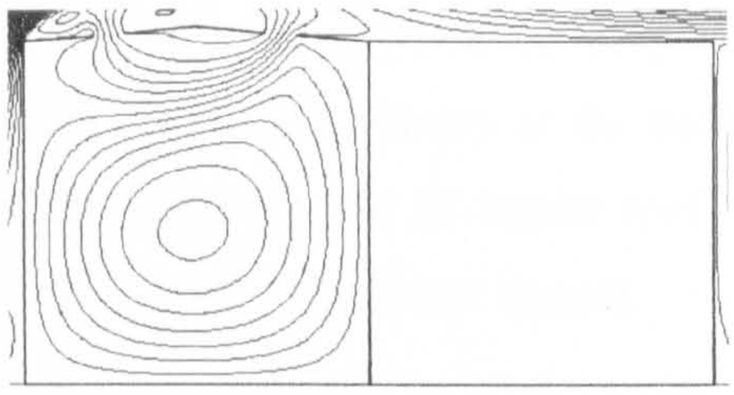

(a) roof angle: 5°

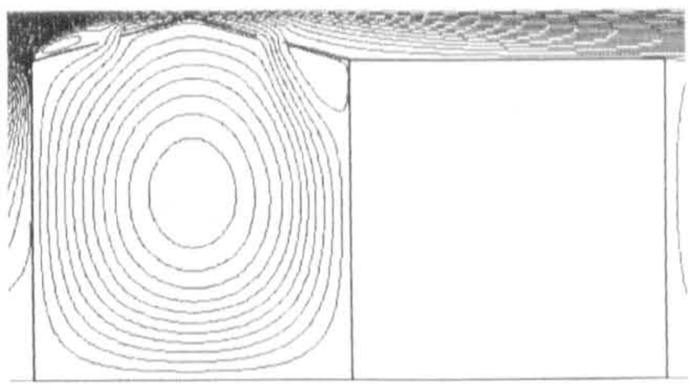

(b) roof angle: 15°

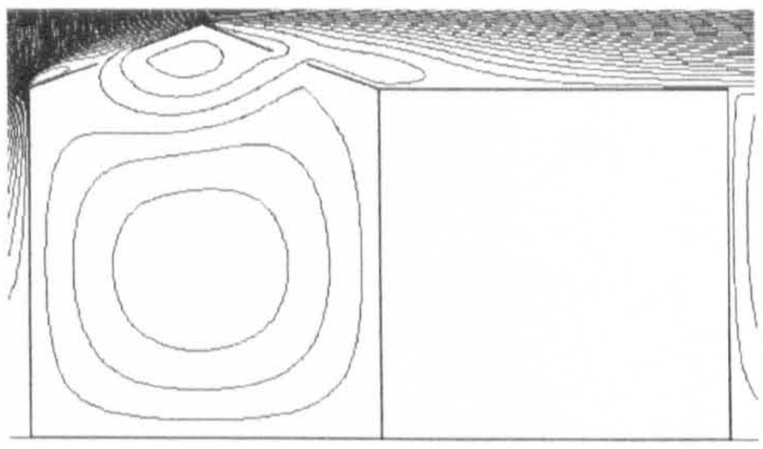

(c) roof angle: 20°

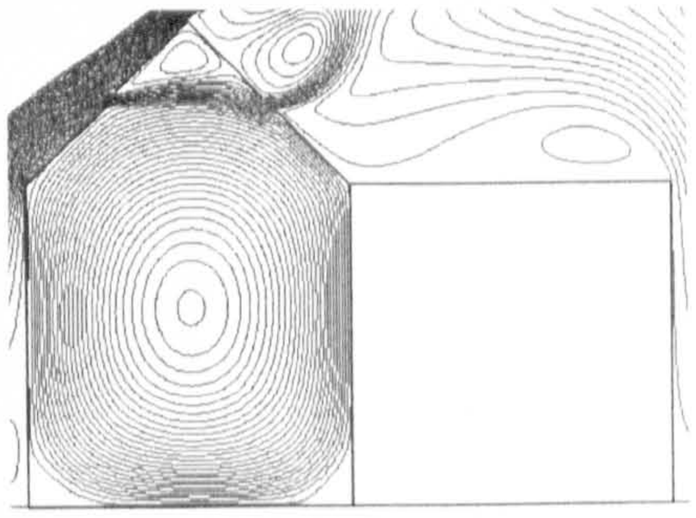

(d) roof angle: 45°

Figure 5.44: Airflow patterns of the wind-induced natural ventilation of triangular roof atria

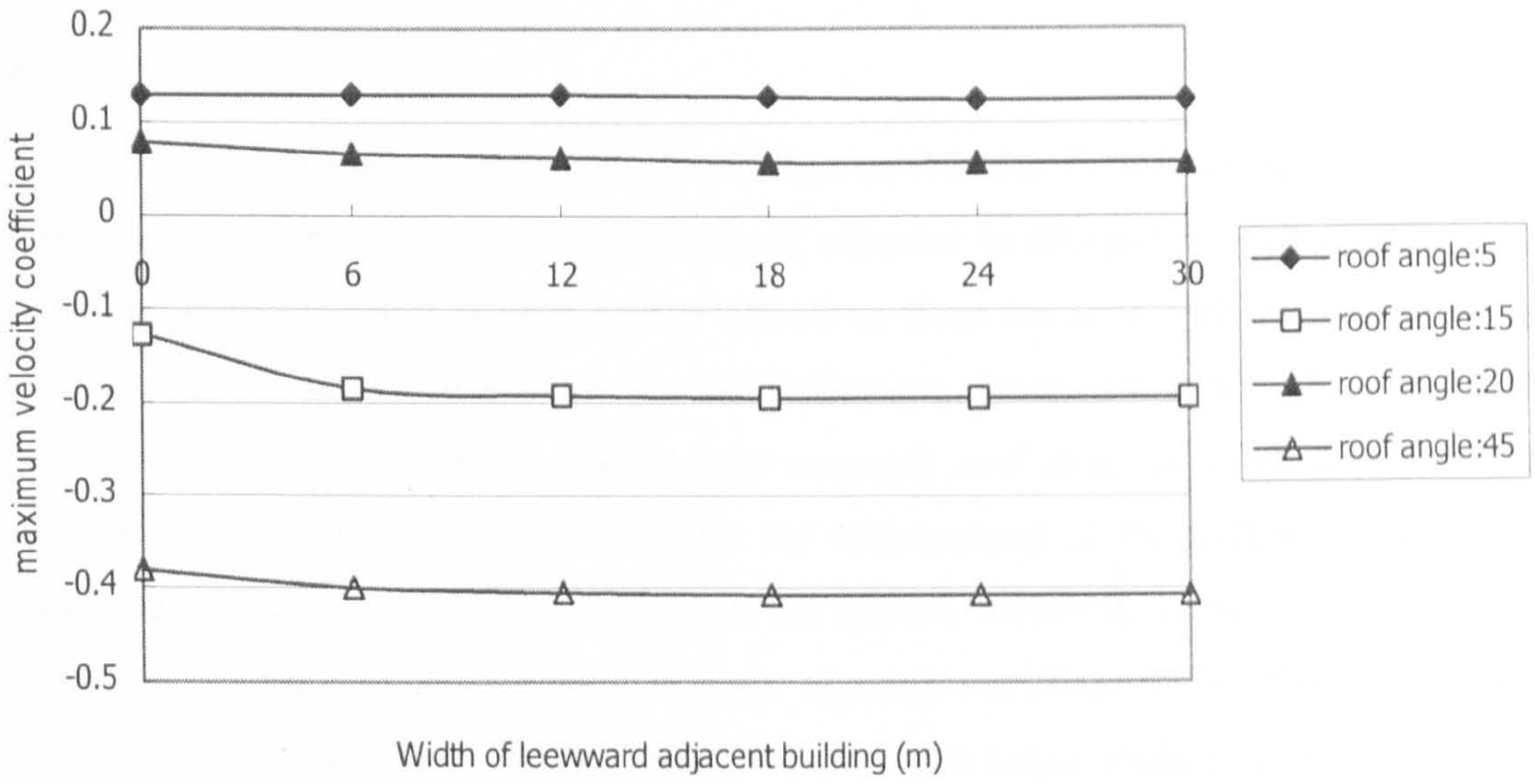

Figure 5.45: Relationship between the maximum air velocity coefficient and the width of the leeward adjacent building

• *Courtyard*

Although courtyards and 20° roof atria have the same flow pattern (III).b, the leeward adjacent buildings will have very different impacts on them because the corner between the top surface of the leeward adjacent building and the leeward roof pitch for 20° case will not be formed as a courtyard does not any roof pitch at all. It can be seen from Figure 5.46 that, with the leeward adjacent building, the ventilation performance of the courtyard can be greatly enhanced and the flow pattern changes from (III).b to (II), since the back flow vanishes away

due to the leeward adjacent building. The effects of the leeward adjacent building on the magnitude of the air velocity at the occupants' level of a courtyard are generally the same as described above for the triangular roof atria: it is very effective initially but further increase does not have any significant impact.

(a) a stand-alone courtyard (b) a courtyard with a 12m wide leeward adjacent building

Figure 5.46: Comparison of the airflow patterns of a stand-alone courtyard and a courtyard with a leeward adjacent building

• *Other roofs*

The effects of the leeward adjacent buildings on the back flow discussed above are also observed for atria with other roofs. The leeward adjacent buildings for vault roof atria with tangential angle above 20° will have similar effects as those for atria with 45° triangular roof and does not significantly influence the internal airflow, as shown in Figure 5.47. Figures 5.48 and 5.49 further demonstrate more examples for sawtooth roof atria. It is still shown that, the incorporation of leeward adjacent building for the enhancement of the airflow in the space is only sensible for the cases where flow pattern (II) occurs, including scenarios (a) for 3-tooth roof atria and (b) for 6-tooth roof atria; it is not of much significance for other flow patterns although it can get rid of the effects of the back flow and hence slightly change the internal airflow rate.

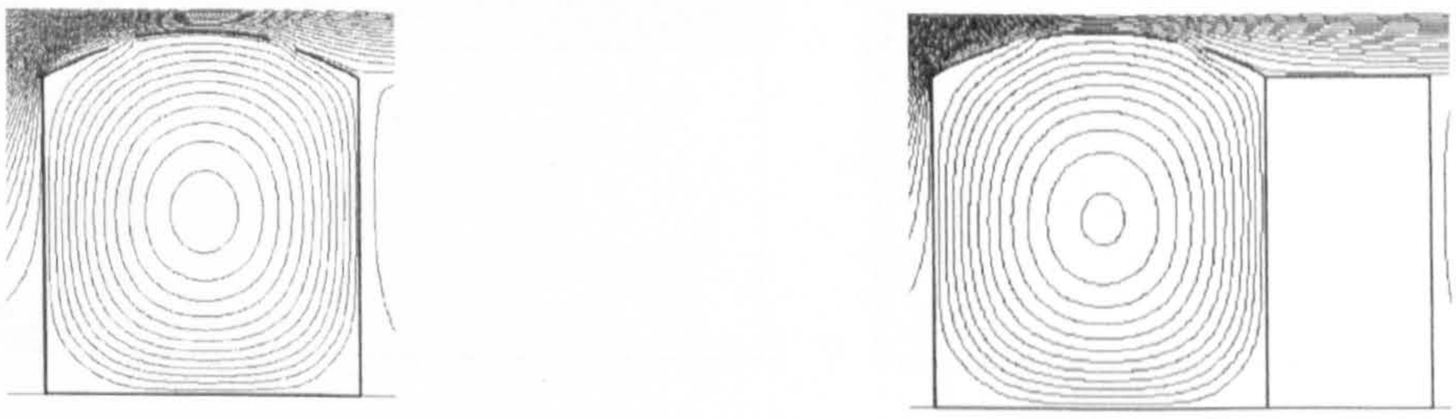

(a) a stand-alone vault roof atria (15°) (a) + 6m wide leeward adjacent building

Figure 5.47: Comparison of the airflow patterns of a stand-alone vault roof atrium and a vault roof atrium with a leeward adjacent building

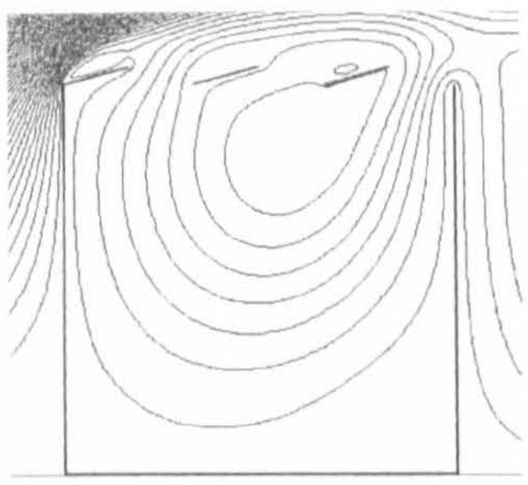

(a) 15°, leeward openings

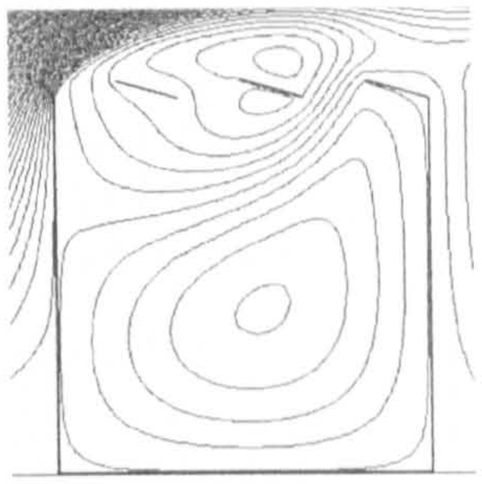

(b) 15°, windward openings

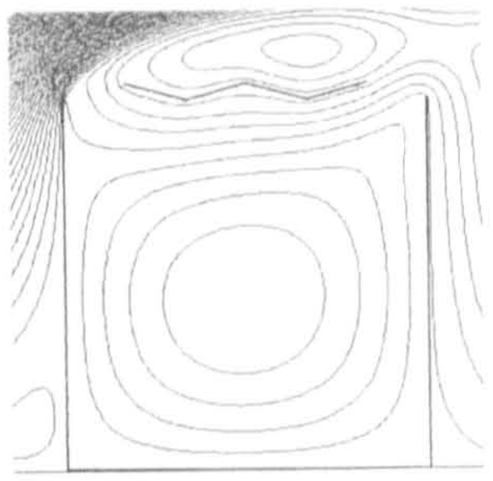

(c) 15°, bottom openings

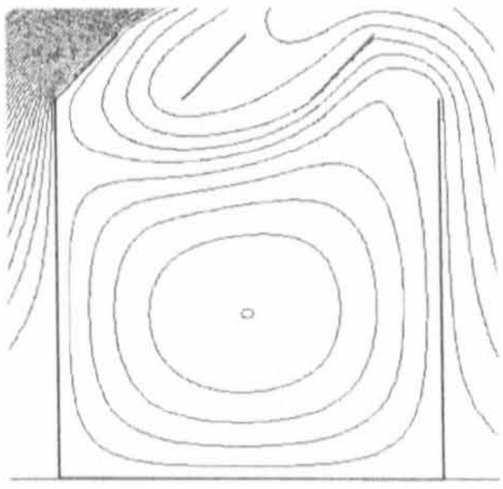

(d) 45°, leeward openings

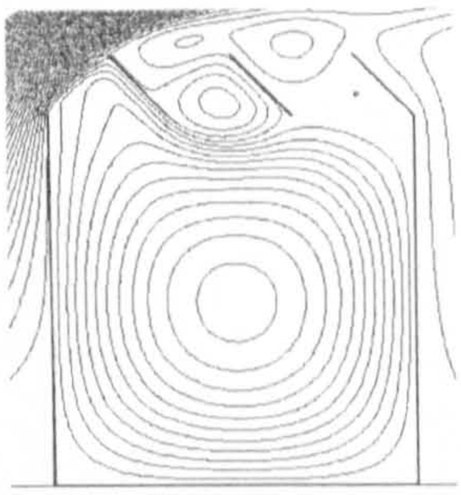

(e) 45°, windward openings

(f) 45°, bottom openings

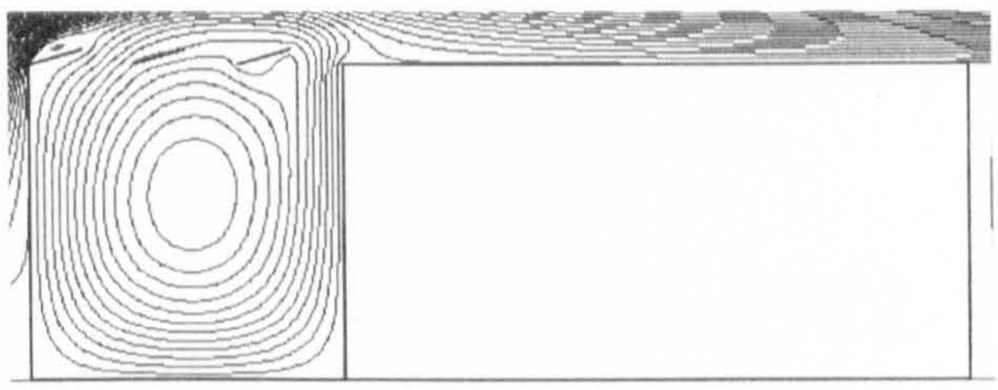

(a) + 24m leeward adjacent building

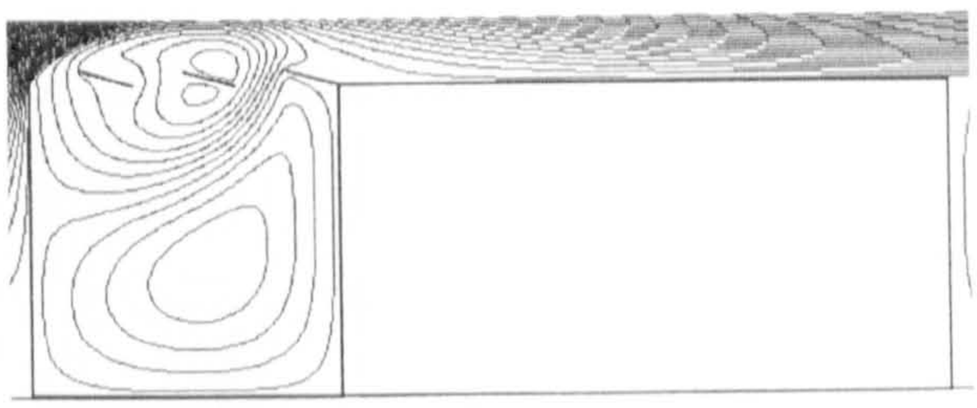

(b) + 24m leeward adjacent building

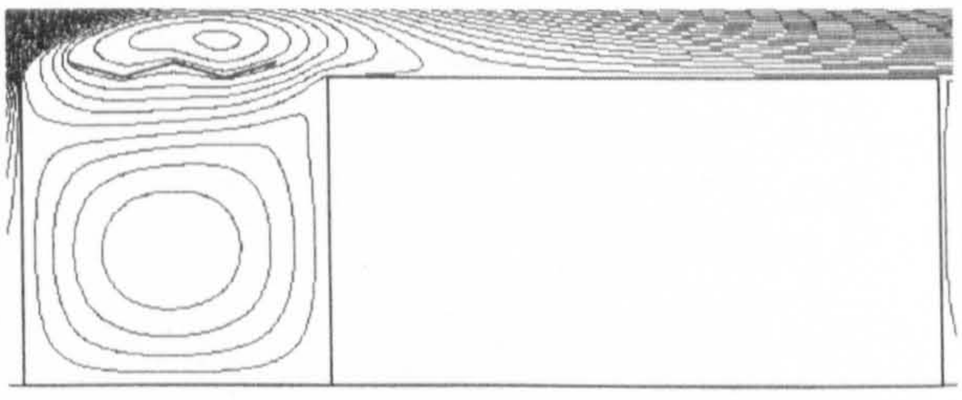

(c) + 24m windward adjacent building

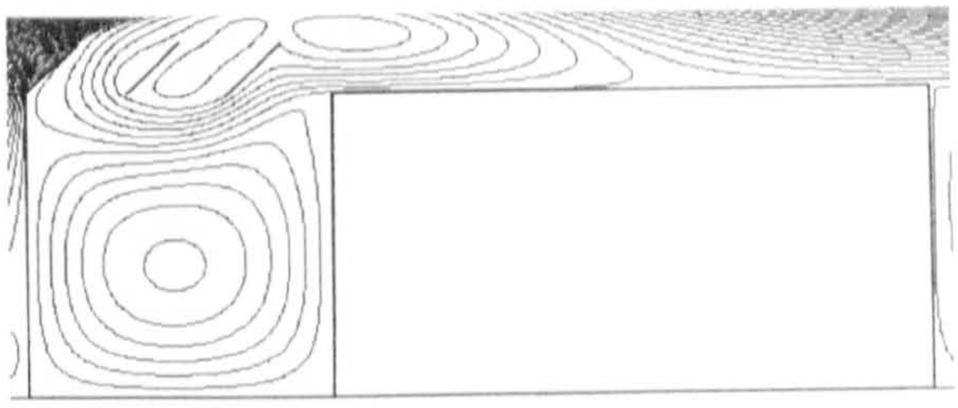

(d) + 24m windward adjacent building

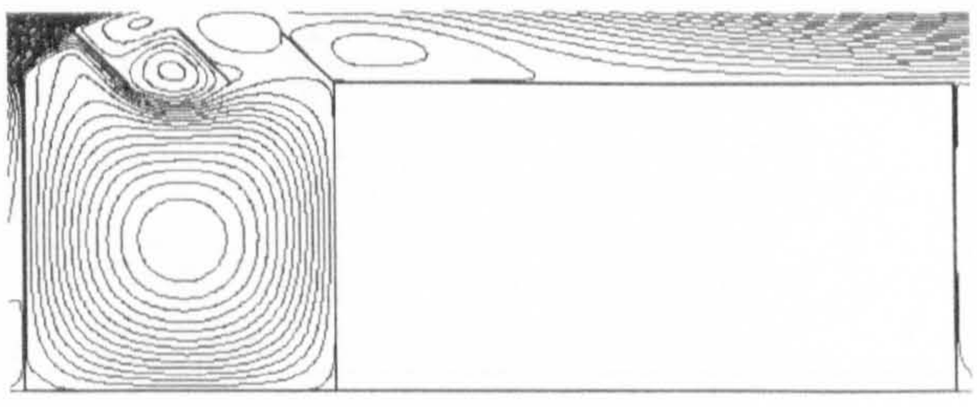

(e) + 24m windward adjacent building

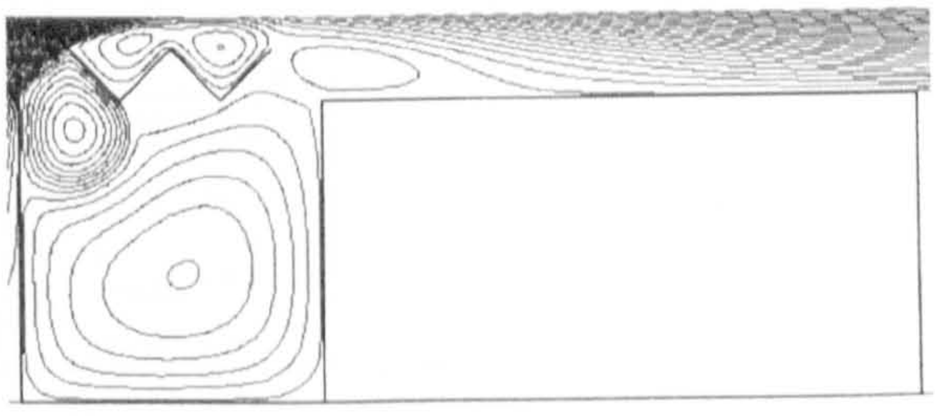

(f) + 24m windward adjacent building

Figure 5.48: Airflow patterns of the wind-induced natural ventilation of sawtooth roof atria with leeward adjacent building (tooth number: 3)

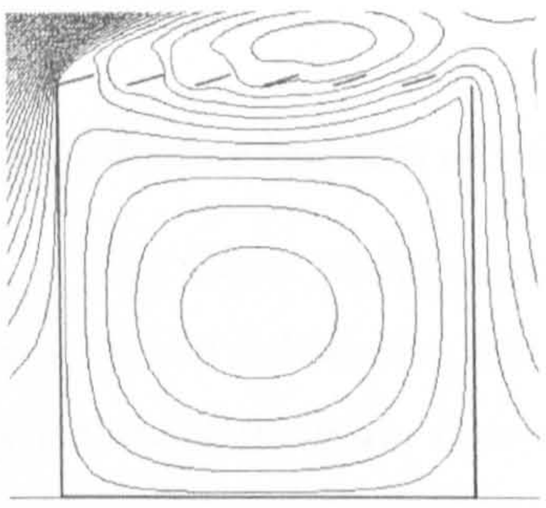

(a) 15°, leeward openings

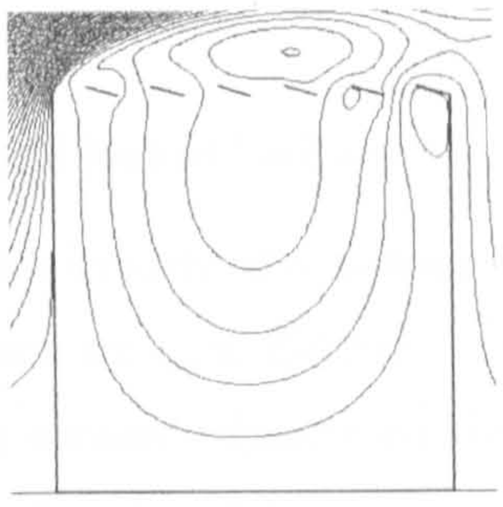

(b) 15°, windward openings

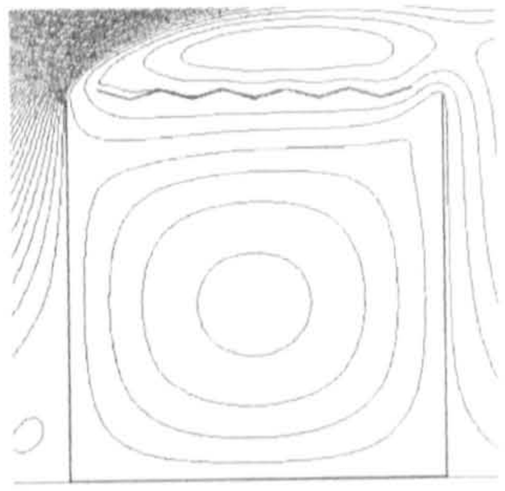

(c) 15°, bottom openings

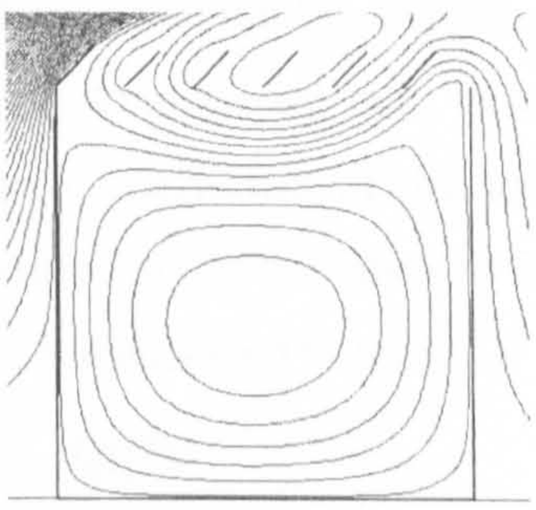

(d) 45°, leeward openings

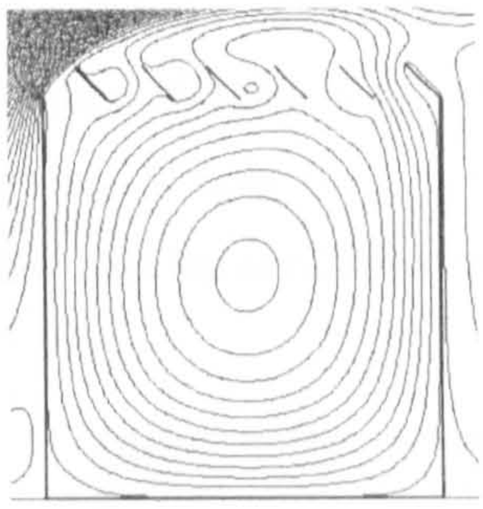

(e) 45°, windward openings

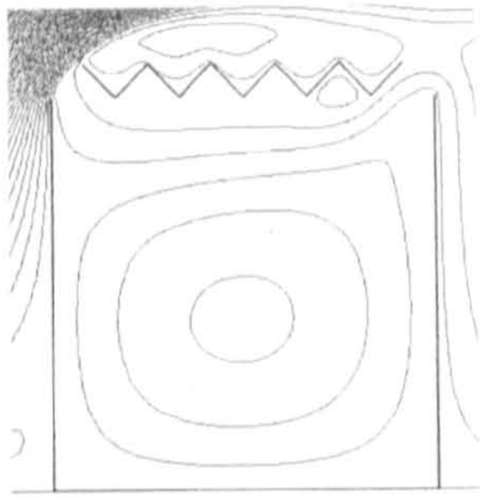

(f) 45°, bottom openings

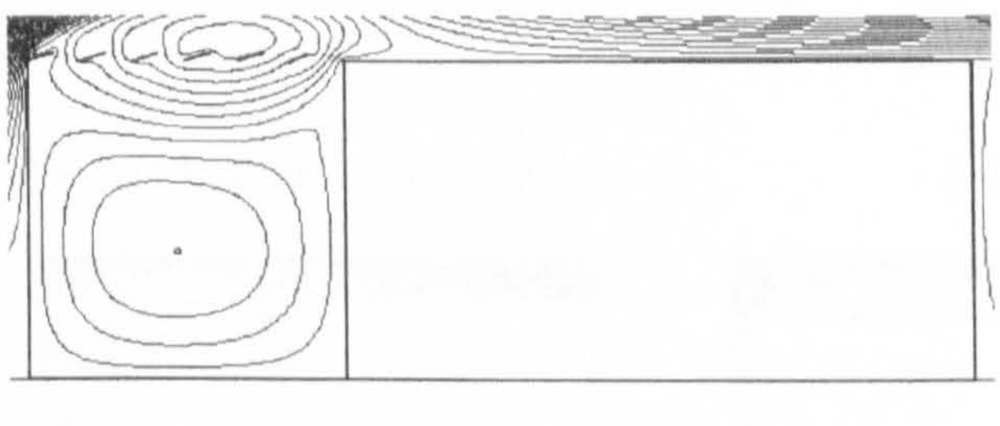

(a) + 24m windward adjacent building

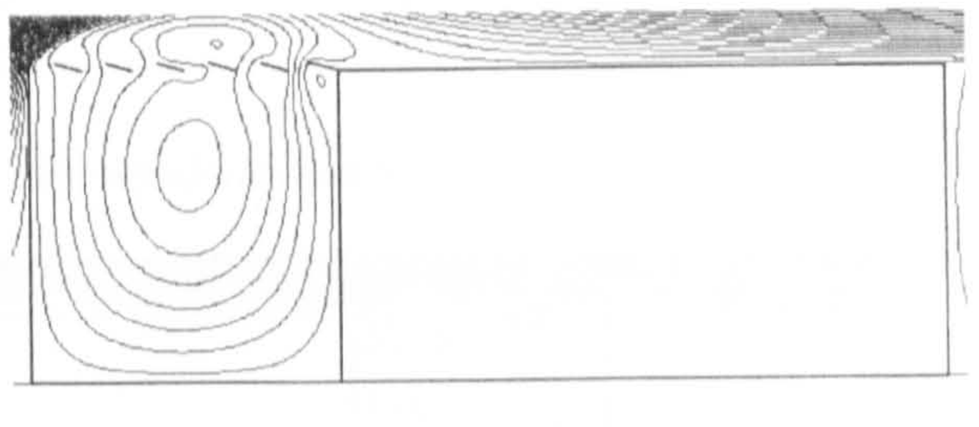

(b) + 24m windward adjacent building

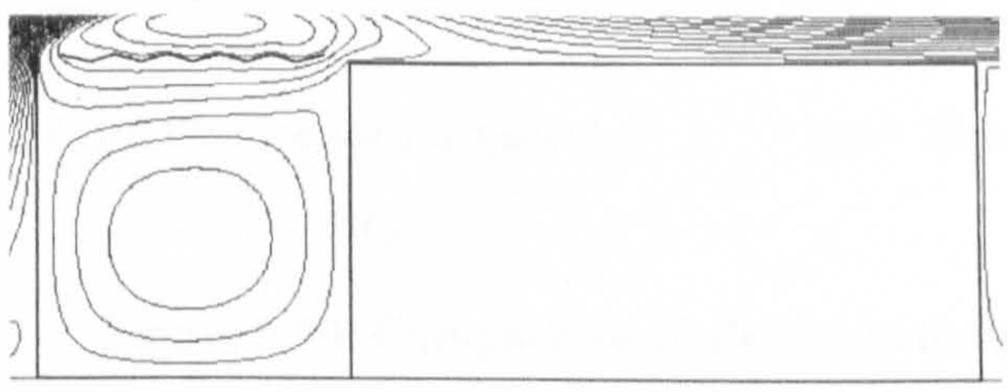

(c) + 24m windward adjacent building

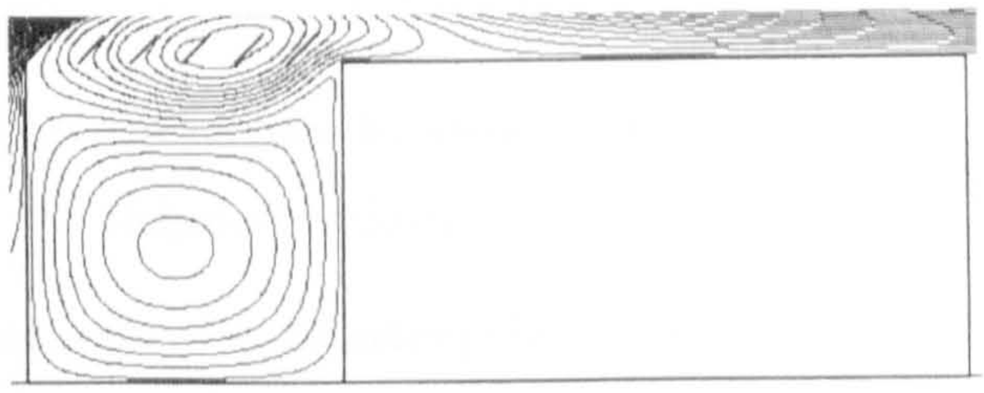

(d) + 24m windward adjacent building

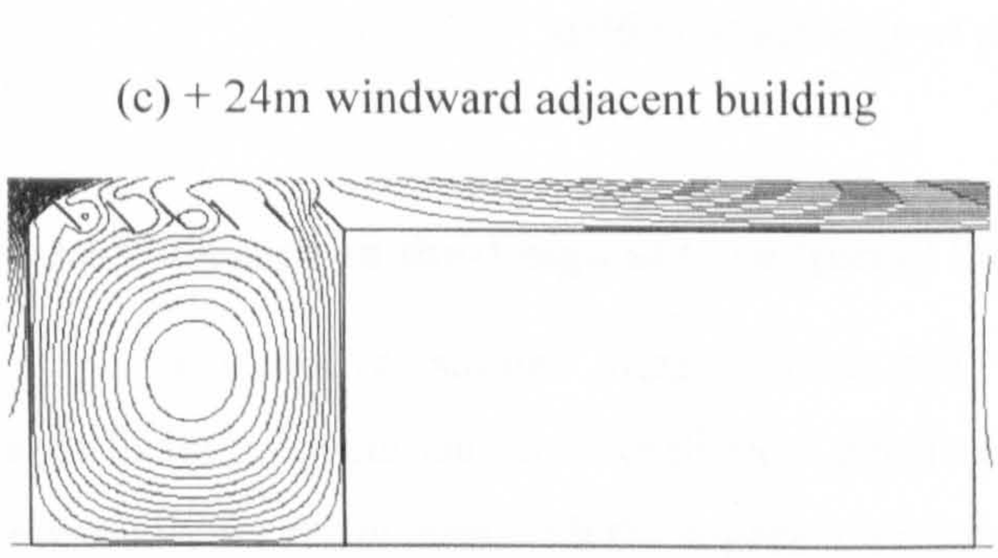

(e) + 24m windward adjacent building

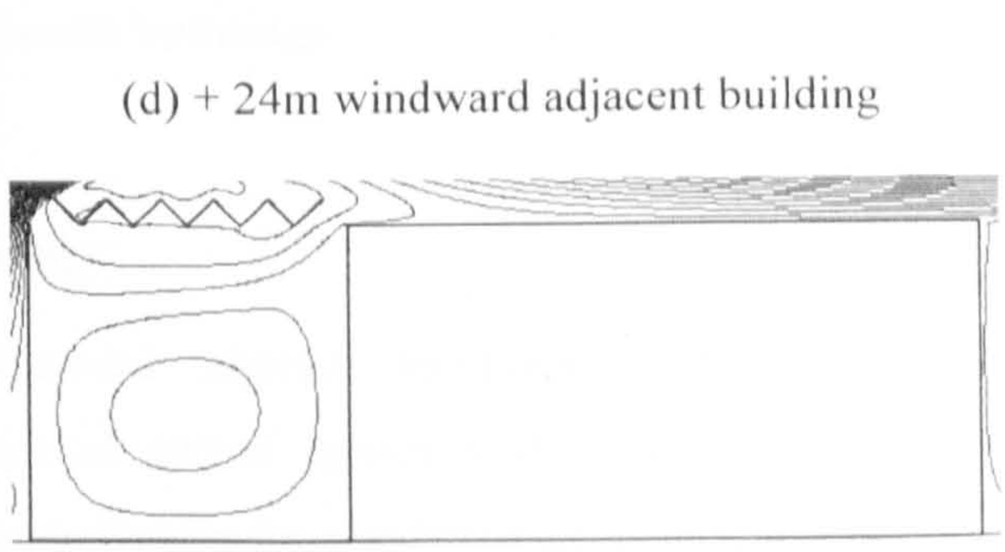

(f) + 24m windward adjacent building

Figure 5.49: Airflow patterns of the wind-induced natural ventilation of sawtooth roof atria with leeward adjacent building (tooth number: 6)

5.5.3 Collective impacts of windward and leeward adjacent buildings

The above studies investigated the impacts of windward and leeward adjacent buildings separately and it is shown that their effects are quite different: the windward adjacent buildings only influence the main flow whilst the leeward adjacent buildings affect the back flow. It is therefore envisaged that, if both of windward and leeward adjacent buildings are employed, their collective effects can be simply predicted by adding their separate effects together. Figure 5.50 shows a simple example of the wind-induced ventilation of an atrium with a 15° triangular roof to demonstrate this. It can be seen that, if there is no adjacent building, the maximum velocity coefficient of the stand-alone atrium is only 0.12; with the 24m windward adjacent building only, it increases to 0.22; with the 12m leeward adjacent building only, it is 0.18; with both, it reaches up to 0.25.

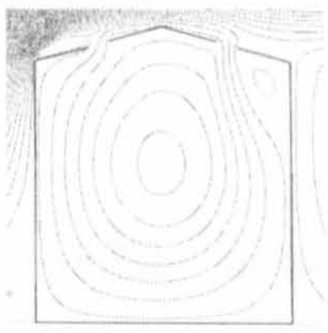

(a) a stand-alone 15° roof atrium

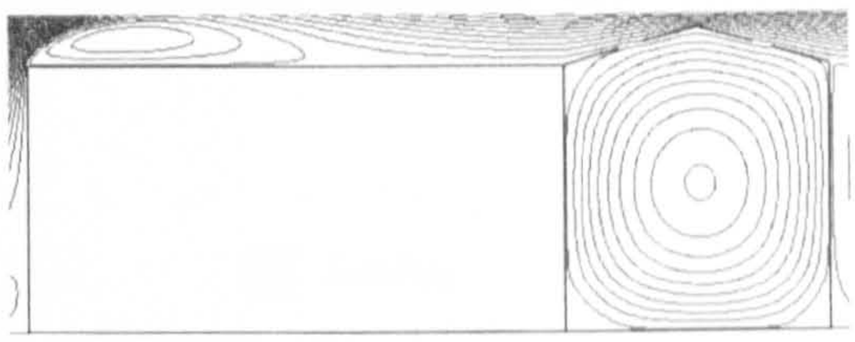

(a) + 24m windward adjacent building

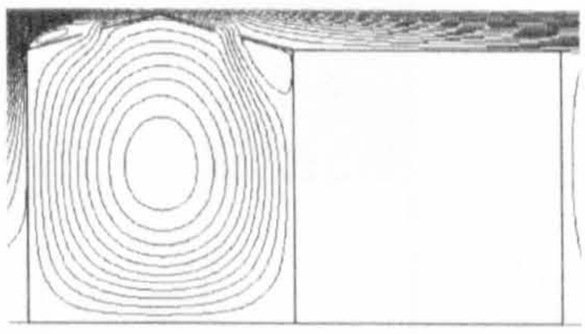

(a) + 12m leeward adjacent building

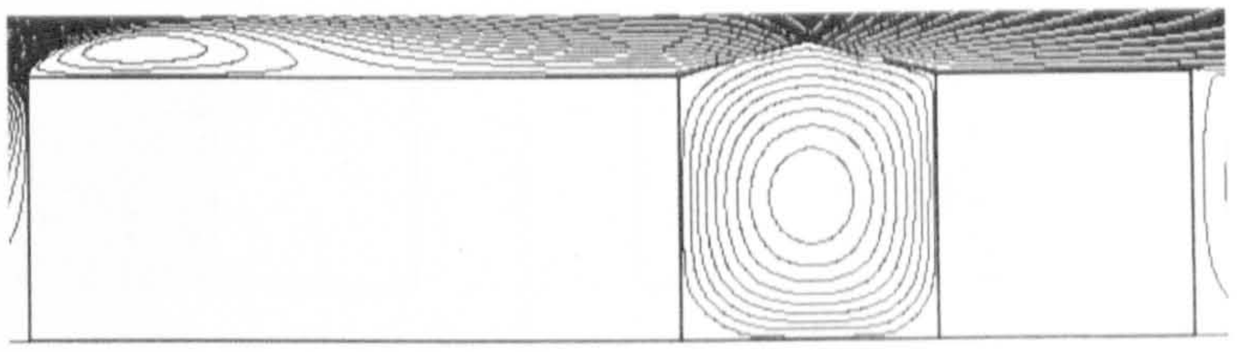

(a) + 24m windward adjacent building + 12m leeward adjacent building

Figure 5.50: Comparison of airflow patterns of atria with 15° triangular roofs and different settings of adjacent buildings

5.5.4 Guidance on the design of the adjacent buildings

The above studies suggest that, the windward adjacent buildings usually have significant impacts on the ventilation performance of atrium spaces with roof openings, especially for those atria with the separation of the main flow at the windward top corner, whilst the effects of the leeward adjacent buildings can be generally ignored. Based on these findings, guidance on the design of the adjacent buildings can be developed for different design objectives, and Figures 5.38 and 5.45 that illustrate the relationship between the width of adjacent buildings and the air velocity in the space are very valuable for this purpose. Some

commonly seen conditions and related design guidance developed are shown below (only atrium spaces with two roof openings are considered here unless specified). It should be mentioned that the guidelines developed below are all for adjacent buildings with the same height of the atrium space.

• *Roof shape based design*

Sometimes the roof shape, i.e. either triangular or barrel vault or sawtooth or no roof (courtyard) has already been determined at earlier stage but the width of the adjacent buildings needs to be determined for the enhancement of ventilation performance.

• For a courtyard, either windward or leeward adjacent buildings can significantly enhance the airflow of the space. This also suggests that courtyard should not be placed alone along the wind direction if it is incorporated to induce more significant ventilation, as shown in Figure 5.51.

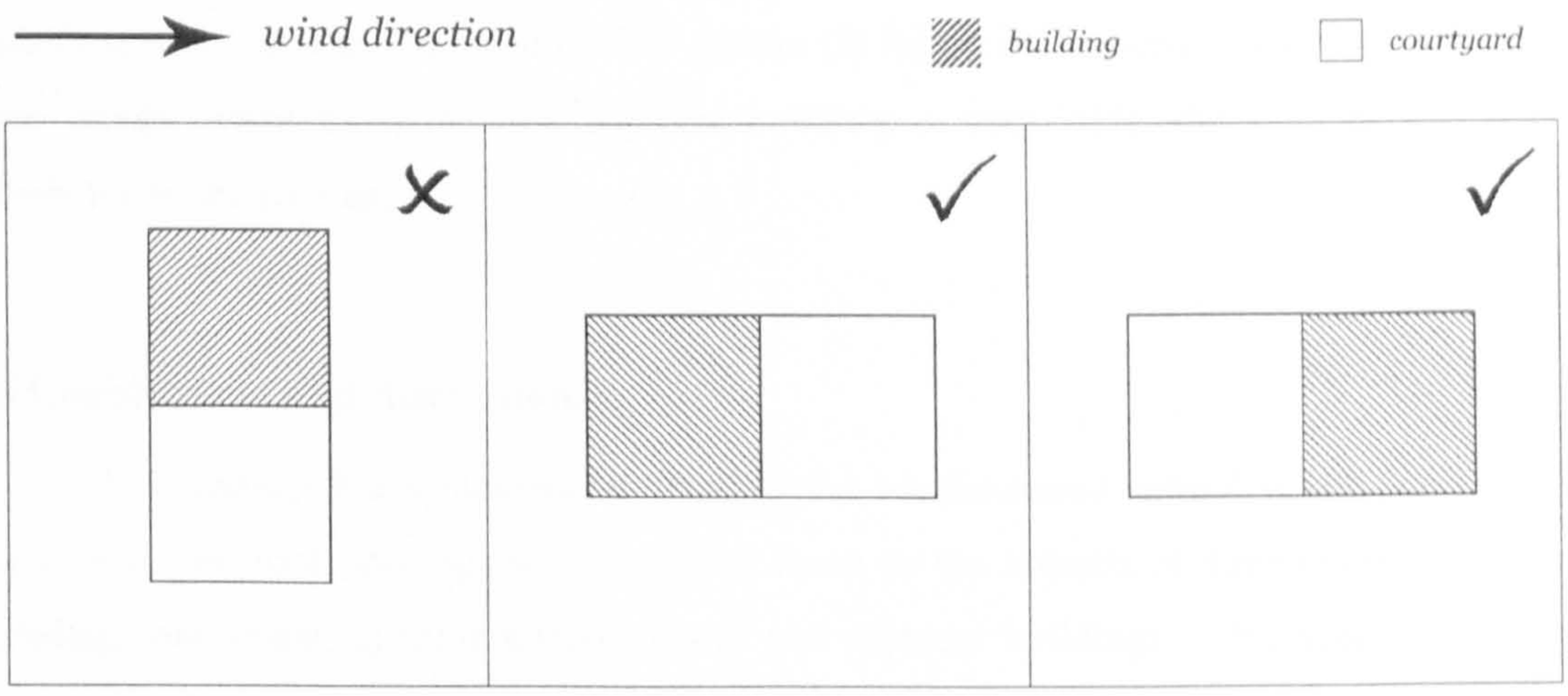

Figure 5.51: Comparison of the ventilation performance of three layouts of a building with a courtyard

• If the triangular roof angle is below 8°, the incorporation of windward adjacent building can help to enhance the ventilation in the space but its width should exceed that of the atrium building; the effects of leeward adjacent building can be generally ignored;

• If the triangular roof angle is between 8°-17°, adjacent buildings on either side can be used to improve the ventilation performance in the space;

• If the triangular roof angle is between 17°-21°, only the adjacent building on the windward side of the atrium space can have significant positive impacts;

• If the triangular roof angle is above 21°, windward adjacent building will have negative effects, and the impacts of leeward buildings can be ignored;

• If vault roof is used and the roof angle is below 21°, correspondent guidelines introduced above for the triangular roofs are still applicable; if the roof angle is above 21°, the effects of the adjacent buildings are similar to those for triangular roof atria with angle above 21°;

• With respect to atrium spaces with sawtooth roofs, the effects of leeward adjacent buildings are generally ignorable with very few exceptions (see Page 173 for details). Windward adjacent buildings are useful if the roof angle is below 21° but their effects will be dependent of the opening distributions if the roof angle is above 21°.

• *Flow pattern based design*

It was already made clear that, the incorporation of leeward adjacent building will not change the flow pattern in the atrium space, whilst the windward adjacent building can move the separation point forward and lead to flow pattern (I) for all roof angles if it is wide enough. In other words, when the windward adjacent building is very wide, the flow pattern will be insensitive to the roof angle.

5.6 Conclusions and discussions

This chapter has systematically studied the wind-induced natural ventilation of atrium spaces with two roof openings with particular focus on the impacts of three design parameters, including roof shape, opening characteristics and adjacent buildings. This section sets out to summarise the physics for this ventilation strategy and develop design guidance for the incorporation of the strategy based on the understandings obtained from the detailed investigations earlier. The limitations of this strategy will also be discussed at the end of this section.

5.6.1 Physics of the model

It has been known from the analysis of the airflow around a cubic box that, when the oncoming wind meets a building with sharp corners, the main flow will separate at the windward top corner resulting in reverse flow and reattaching flow above the roof level, and a recirculation flow will be incurred behind the building. These flows will be the primary forces that drive the ventilation if openings are provided in the roof of the building.

For the wind-induced ventilation of the prototype atrium illustrated at the beginning of this chapter (see Figure 5.1), which has the same width and height of 12m and an opening in each roof pitch, five different flow patterns can be defined in terms of the driving forces and the air movement as follows. Figure 5.52 repeats some typical flow patterns used before for demonstration.

Flow pattern (I): the main flow enters the space through the windward opening and leaves from the leeward opening, and thus the internal airflow can be regarded as being driven by "tunnel effect". As the main flow does not separate at the windward top corner, the reverse flow and the reattaching flow will not appear at the roof level in this flow pattern. Back flow from the recirculation behind the building acts as a counterforce but it is very weak compared to the main flow. This flow pattern generally induces the highest airflow rate at the occupants' level in the space among all five flow patterns, because the main flow has much stronger horizontal momentum than other flows.

Flow pattern (II): the main flow separates before meeting the windward opening and the internal air movement is driven by the reattaching flow on the leeward pitch of the roof. The back flow still acts as a counterforce for this flow pattern. The air coming into the building through the leeward opening has a vertical direction and it will directly go to the bottom of the space. This movement of air requires that the horizontal momentum of the reattaching flow should overwhelm or at least equate to that of the back flow. It can also envisaged that this flow pattern usually have the largest turbulence intensity at the occupants' level as the turbulence caused by the shear at the roof level is convected to the bottom of the space.

Flow pattern (III).a: the three type (III) flow patterns are quite similar: they are all driven by secondary recirculation because the direction of the momentum of the air that enters the building through the leeward opening is horizontal towards the opposite direction of the wind. However, the dominating flows for each of them are quite different. Flow pattern (III).a is driven by the cooperation of reverse flow and back flow, and the two driving forces assist each other.

Flow pattern (III).b: this flow pattern is driven by the back flow. Since the back flow is not strong, the air velocity induced in this flow pattern is usually very weak and thus should be avoided.

Flow pattern (III).c: this flow pattern is very similar to flow pattern (III).b. The only difference is that is that, in this flow pattern most of the air coming into the building is from the reattaching flow whilst it is from the back flow. Sometimes transitional flow pattern may occur in-between these two patterns, i.e. part of the air is from the back flow and the other part is from the reattaching flow. They are not distinguished in this research as the main concern of this thesis is the driving force rather than the mass flow. Since the driving force is the same as that

of flow pattern (III).c, the air velocity of this flow pattern at the occupants' level is very low as well.

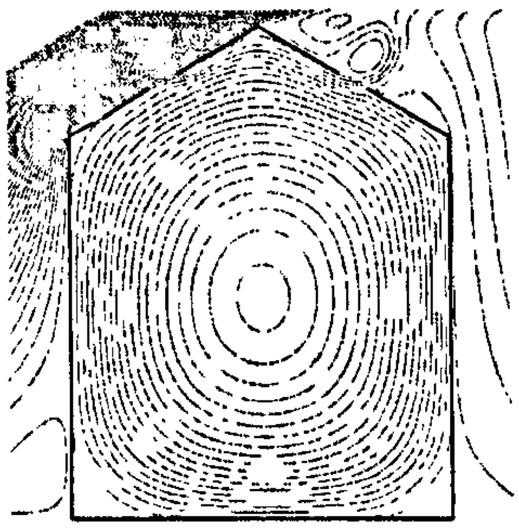

(a) Flow pattern (I)

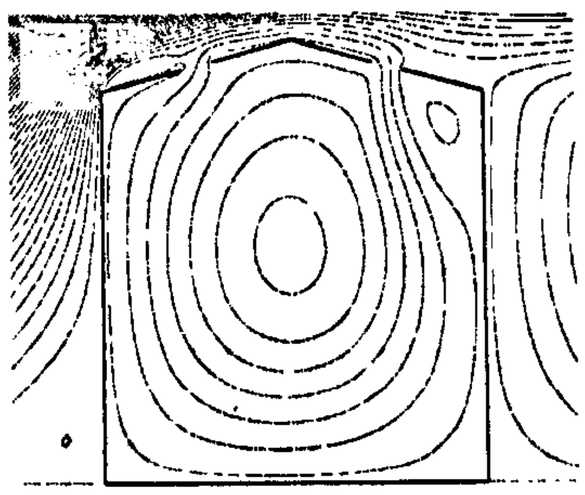

(b) Flow pattern (II)

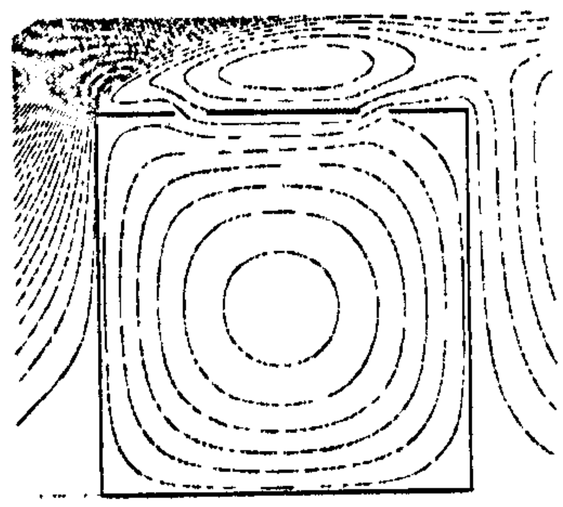

(c) Flow pattern (III).a

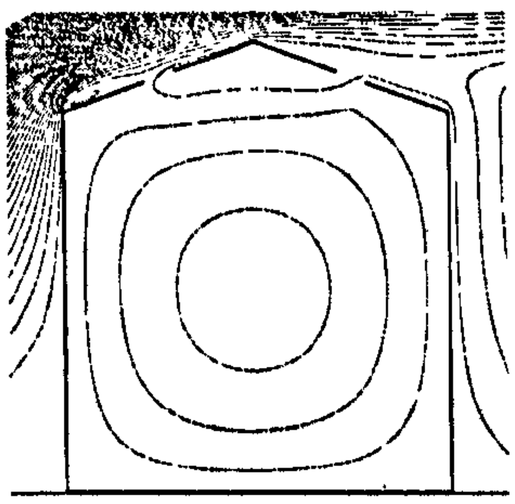

(d) Flow pattern (III).b

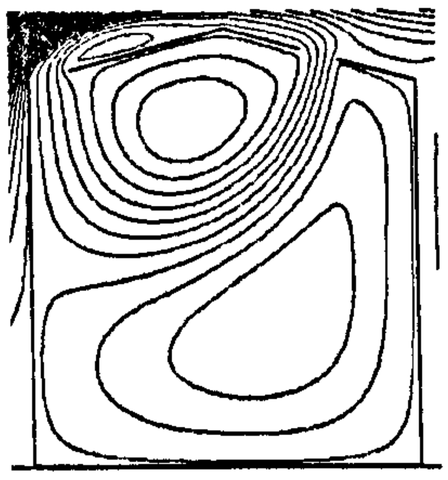

(d) Flow pattern (III).c

Figure 5.52: Possible airflow patterns of wind-induce natural ventilation for the prototype atrium space (which has a triangular roof and one small opening in each roof pitch)

The above identifications of the possible flow patterns suggest that the air movement in and around an atrium space is driven by the interaction of the main flow, reattaching flow, reverse flow and the back flow around the building. It can be seen that, only flow pattern (I) is driven by the positive pressure caused by main flow and all the others are driven by "suction". In other words, the windward opening is inlet for flow pattern (I), whilst it is outlet for all other flow patterns. Reverse flow only occurs for flow pattern (III).a and all other flow patterns are the interaction of the reattaching flow and the back flow. Back flow appears in all flow patterns with positive effects on patterns (III).a&b&c but negative effects on patterns (I) and (II).

Understanding how design parameters affect these flows will be very important for the prediction of the airflow pattern and evaluation of the ventilation performance at the early design stage, and this is elaborated in terms of each flow.

Main flow is essentially "original" flow of the oncoming wind. Separation caused by the sharp corner before the wind enters the windward opening can significantly weaken the main flow near the roof level and even cause the main flow to go over the windward roof pitch rather than enter the windward building, under which condition the internal flow will be driven

by suction. It is also observed that not all shape corners will cause separation of the main flow and this is dependent of the angle between the two surfaces that form the corner.

These descriptions mean that, whether flow pattern (I) can take place for the prototype atrium is determined by the interrelationship between the location of the corner, the location of the opening and roof angle. According to simulation, the flow pattern (I) will occur when the roof angle is above 21° and not both openings are at the top; or when the roof angle is 18° to 20° and openings are placed near the upper area; and when there is wide windward adjacent building so that the separated main flow can fully reattach to the top surface of the windward adjacent building before meeting the opening in the windward roof pitch of the atrium. Flow pattern (I) will never occur for barrel vault roof atria due to its roof shape, and it takes place for sawtooth roof atria if the width of the windward adjacent building is very large and an opening is provided on the most windward roof pitch, or if the roof has a small tooth number, an angle over 21° and an opening on the most windward pitch.

Reattaching flow is intrinsically main flow too but it is the main flow that has separated and then reattached to the roof level. Two important factors that determine the effects of the reattaching flow are the reattaching point and the distance along which the reattaching flow develops after the reattaching point. If the main flow reattaches onto the windward pitch near the peak of the roof after separation at the windward top corner of the atrium, the flow may separate again at the peak of the roof and this will result in very weak reattaching flow on the leeward roof pitch, which is the case for many scenarios with 20° triangular roof (see Figure 5.23c&d&h) or vault roof with large angles (see Figure 5.26f) which has a flow pattern of (III).b. If the flow can reattach to the leeward pitch of the roof but there is not much distance available for the development of the flow, such as the situation where roof angle is 15° and the leeward opening is too large, the reattaching flow can be overwhelmed by the back flow, thus resulting in the flow pattern (III).c (see Figure 5.22i). The position of the windward inlet can also affect the strength of the reattaching flow, as the vertical momentum within the air going through the opening can bring the horizontal momentum near the roof upwards, thus weakening the horizontal momentum of the reattaching flow that drives the internal airflow. Examples of this have been shown in the study of the opening location of the atria with 15° triangular roof (see Figure 5.22) and those with vault roof (see Figure 5.26). When the momentum of the reattaching flow has well developed, flow pattern (II) will occur.

Back flow is the airflow that is from the back of the atrium space, i.e. it has an opposite direction of the oncoming wind. This usually results from the "wind shade" behind the building or the corner between roof and the top surface of the leeward adjacent building. The back flow only has effects on the leeward roof pitch which are determined by the roof angle and the opening location and area. It has been made clear that the effects will more significant on higher roof pitch and/or larger opening. The back flow also needs some distance for its

development but too far distance from the bottom of the roof pitch will weaken its effects. As a result its impacts will reduce from the middle of the leeward roof pitch to the two ends.

As introduced before, the collective effects of design parameters on the reattaching flow and the back flow determine the flow pattern (II) and it takes place when the former is stronger than the latter. In other words, flow pattern (II) will occur when the reattaching flow has developed better than the back flow has. Simulation results have shown that, for the stand-alone prototype atrium with two small openings, flow pattern (II) will take place when the roof angle is below 18° and when the inlet opening is placed at the bottom of the leeward roof pitch; under the same condition for 18° to 20° but the outlet opening is not at the upper area of the windward roof pitch (otherwise flow pattern (I) will occur as introduced above); when the roof angle is 8° to 15°, and the conditions that the inlet opening is in the middle of the leeward roof pitch, and that the outlet is at the bottom of the windward pitch do not happen simultaneously. Flow pattern (II) is also the dominating pattern for vault roof atria with a tangential angle over 21° and two small openings, and the only exception happens when the windward opening is placed at the top with the leeward opening in the middle of the roof pitch. It also occurs for sawtooth roof atrium buildings when leeward openings are opened and tooth number is small or when windward openings are opened and tooth number is large.

Reverse flow is the small recirculation at the roof level that develops when there is large room between the separated main flow and the roof surface. This definition actually suggests that the reverse flow only occurs when the roof angle is very small. In order for the reverse flow to develop horizontal momentum, there should also be enough distance on the leeward side of the inlet opening, which also means that the reverse flow will not be the driving force for the internal air movement if the leeward opening is provided at the bottom of the roof pitch. These discussions also suggest the conditions for the occurrence of flow pattern (III).a. Simulation has shown that it occurs when the roof angle is below 8° for the prototype atrium and the leeward opening should include some middle or upper area. It also takes place for atria with sawtooth roofs when tooth number is large and windward openings are opened, or when tooth number is small and leeward openings are opened (see Figures 5.18&5.19). It is also envisaged that the vertical size of the reverse flow at the roof level has significant effects on the magnitude of the air velocity in the space and larger size usually result in higher reduction from the main flow. Consequently, the distance of the two openings should be kept larger in order to induce stronger air movement in the space.

It has to be mentioned that the conditions listed above for each flow pattern to take place is not complete and it is next to impossible to do so, since there are too many parameters involved and even more variations for the combination of these parameters. In order to gain a precise appreciation of the flow pattern for a real case, it is suggested that readers should refer to the figures in the previous detailed studies.

5.6.2 Design guidance

Based on the understanding of the controlling forces for each flow pattern, plenty of strategies can be employed for the enhancement of the airflow of the prototype atrium space. Examples that have been introduced in this chapter include using pivoting windows, changing opening size, relocating the windows, employing adjacent buildings and modifying roof shapes and angles. Their effects on the internal air movement are generally summarised as follows:

Roof angle is perhaps the most important design parameter for the ventilation performance of the stand-alone prototype atrium. When the openings are located in the middle of the both pitches, roof angle will determine the flow pattern of the space: flow pattern (I) will occur roof angle above 21°; (II) for 8°-17°; (III).a for 0°-7°; (III).b for 18°-20°. High roof pitch will also lead to more significant impacts from the back flow. Roof angle around 45° induce the highest air velocity in the space and further increase of the roof angle will lead to higher turbulence intensity. However, if windward adjacent buildings are employed, especially when they are very wide, the roof angle will become insensitive to the ventilation performance of the space. The relationship between the roof angle and the air velocity in the space for triangular and vault roof atria is illustrated in Figure 5.9 and 5.14 respectively.

The **opening location** should vary for different flow patterns in order to achieve the best ventilation performance of the prototype triangular roof atrium. For roof angle above 21° with flow pattern (I), the two opening should be on the same level of each roof pitch to enhance the "tunnel effect" and simulation also shows that the best position should be in the middle of the roof. For roof angle 8°-17° with flow pattern (II), the inlet opening should be located at the top or bottom level of the leeward pitch to reduce the effects of back flow whilst the outlet opening should be placed at the top or middle level of the windward pitch so that the reattaching point is not too close to the peak of the roof. For roof angle below 8° with flow pattern (III).a, the leeward opening should be located at the upper area of the pitch to allow the development of the reverse flow and the windward opening should be positioned near the bottom of the pitch to enlarge the distance between the two openings for more horizontal momentum. Another option for this roof angle is to change the flow pattern to (II) by placing the leeward opening at the bottom of the leeward opening which impedes the development of the reverse flow and for this circumstance the windward opening location should follow the guidelines of flow pattern (II) introduced above. With respect to roof angle between 18° and 20°, both openings should be placed near the top to change flow pattern to (I). For vault roof atria with a tangential angle above 21°, the leeward opening should be placed in the upper area of roof pitch to avoid the separation of the main flow. Figures 5.21-5.24 and 5.26 compare the airflow patterns in atrium spaces with various opening locations of the typical roof angles.

Enlarging **opening size** does not necessarily improve the ventilation performance of the space and similar to the opening location, different approaches should be adopted for different flow patterns. For atria with roof angle above 21° with flow pattern (I), increasing the size of both openings' size will enhance the air velocity in the space if the both openings do not occupy the top area at the same time; for roof angle 8°-17° with flow pattern (II), continuous roof pitch will help the development of the reattaching flow and thus for the improvement of the ventilation performance it will be favourable to locate both openings together or place them at the bottom of the roof pitch; for flow patterns (III).a and (III).c with roof angle 0°-8° and 18°-20° respectively, enlarging the windward opening will make the ventilation performance even worse as the recirculation at the roof level will be bigger resulting in more reduction from the main flow; and thus the windward opening should be enlarged instead to enhance the internal airflow. This strategy has also proven efficient for the barrel vault roof atria with tangential roof angle above 21°. Figures 5.27 – 5.31 show the comparisons of the ventilation performance of atrium spaces with different sizes of openings for several typical roof angles.

Incorporating other **opening methods,** such as the opening edges of the pivoting windows is also an efficient approach to enhance the ventilation in the space. The pivoting windows can be used in two ways: either it can be used to enhance the controlling forces of each flow pattern, such as those used for flow patterns (I) and (II) or it can be employed to change the flow pattern, especially when the original flow pattern does not induce a good ventilation performance, such as those for flow pattern (III). In order to enhance the controlling forces, the opening edges should be parallel to the flow it is intended to reinforce or blocks the counterforce. To change the pattern (usually to flow pattern II), the window edges should be opened to the vertical direction. Relevant comparisons of the flow patterns in the atrium spaces with different opening methods are shown in Figures 5.32 – 5.35.

Adjacent buildings can also be helpful for the internal air movement. Windward adjacent buildings can move the separation point forward and allow the main flow to reattach to the top surface of the adjacent building before meeting the atrium roof. In this way it changes the flow pattern to (I) for the triangular roof atria no matter the roof angle and as a consequence significantly improve the ventilation performance of the prototype atria with roof angle smaller than 21°. However it does not help atria with roof angle over 21°, and in addition, wide windward adjacent buildings make the roof angle insensitive to the airflow in the space. Leeward adjacent building is helpful for atria with all roof angles in spite of its limited effectiveness as it weakens the back flow. Simulation also shows that either windward or leeward adjacent buildings can greatly improve the ventilation performance of a courtyard. The relationship between the air velocity in the space and the width of the windward/leeward adjacent building is illustrated in Figure 5.38 and Figure 5.45 respectively.

The above guidelines are made assuming that all other parameters are fixed expect the one that is being discussed and some detailed guidance can be found at the end of each section. Nevertheless, it has to be admitted that it is not possible to include all design conditions in this piece of work and develop relevant design guidance. However, it is believed that, with the understanding of effects of related design parameters introduced above and those valuable graphs made illustrating the relationship between the ventilation performance and different variables, designers should be able to develop their own design guidelines for other more complicated situations.

5.6.3 Other discussions

This part of study is focused on the wind-induced ventilation of atria through roof openings and it is assumed that there are no openings available at the occupants' level. This condition is not only encountered in atrium spaces but it can also be seen in many other types of buildings such as some large scale industrial buildings where security concerns may not allow people to open windows at the occupants' level, and also the attic of a house with skylights. It is therefore believed that the findings of this research will also be of some benefit for these applications in addition to atrium type buildings.

It has to be admitted that cross ventilation through the openings at the occupants' level is much more efficient. As shown in Figure 5.53, with an additional opening on the leeward wall, the airflow rate at the occupants' level is significantly increased compared to those scenarios without it. It is suggested that the openings at the occupants' level will always be the first choice whenever possible. However, there are many occasions where openings at the occupants' level cannot be incorporated and the ventilation has to be induced from the roof level: such as when there is too much noise and air pollution from the outdoor traffic; or the wind is too heavy and is not suitable for direct use; or the opening is too far away such as the condition in the middle of a very long shopping street; or there are too many obstructions near the opening, etc.

It should also be noted that the airflows investigated in this chapter are all driven by recirculation rather than direct flow and it was shown that recirculation can be effective in producing cooling effects if appropriately designed. In fact, the use of recirculation can be quite commonly seen in our everyday life. Consider a single-sided office as shown in Figure 5.54a, the windows are only available on the right hand side and the left hand side is attached with a corridor. If the wind direction is parallel to the opening, the ventilation will be driven by the recirculation induced by wind and it can be envisaged that the cooling effects under this circumstance will be better than the situation where the wind is perpendicular to the building facade. Figure 5.54b illustrates another example of using recirculation for cooling purposes in a room where the space between the window and the entrance forms the path for the main flow

and the airflow around the occupant is driven by recirculation. It is anticipated that the guidelines developed in this chapter will also be useful for these circumstances, such as the facade design for the former case.

Finally, it should also be mentioned that there are many limitations for this part of study. As introduced in Chapter Two, the aspect ratio of the width to height is quite crucial for its application: the primary recirculation is formed when the aspect ratio is between 0.7 and 1.3 over which the airflow at the bottom will be driven by secondary recirculation which will significantly weaken the air movement at the occupants' level. In addition, the number of the conditions considered in the study is quite limited and it is impossible to cover all of them since there are too many variations. Furthermore, quite a few quantitative values were suggested in the study but it should be noted that they are only for the atrium with the shape illustrated at the beginning of this chapter, i.e. 12m wide and 12m high, and they are from 2D simulations.

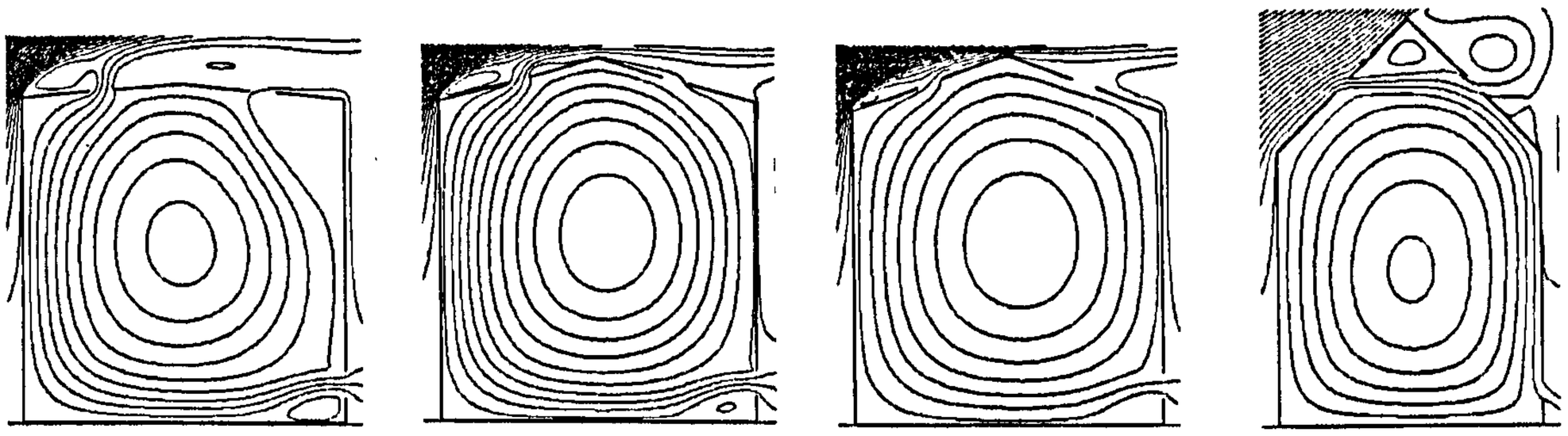

(1) 5° roof (2) 15° roof (3) 20° roof (4) 45° roof

Figure 5.53: Airflow patterns of wind-induce natural ventilation for the prototype atria when an additional opening is provided at the occupants' level

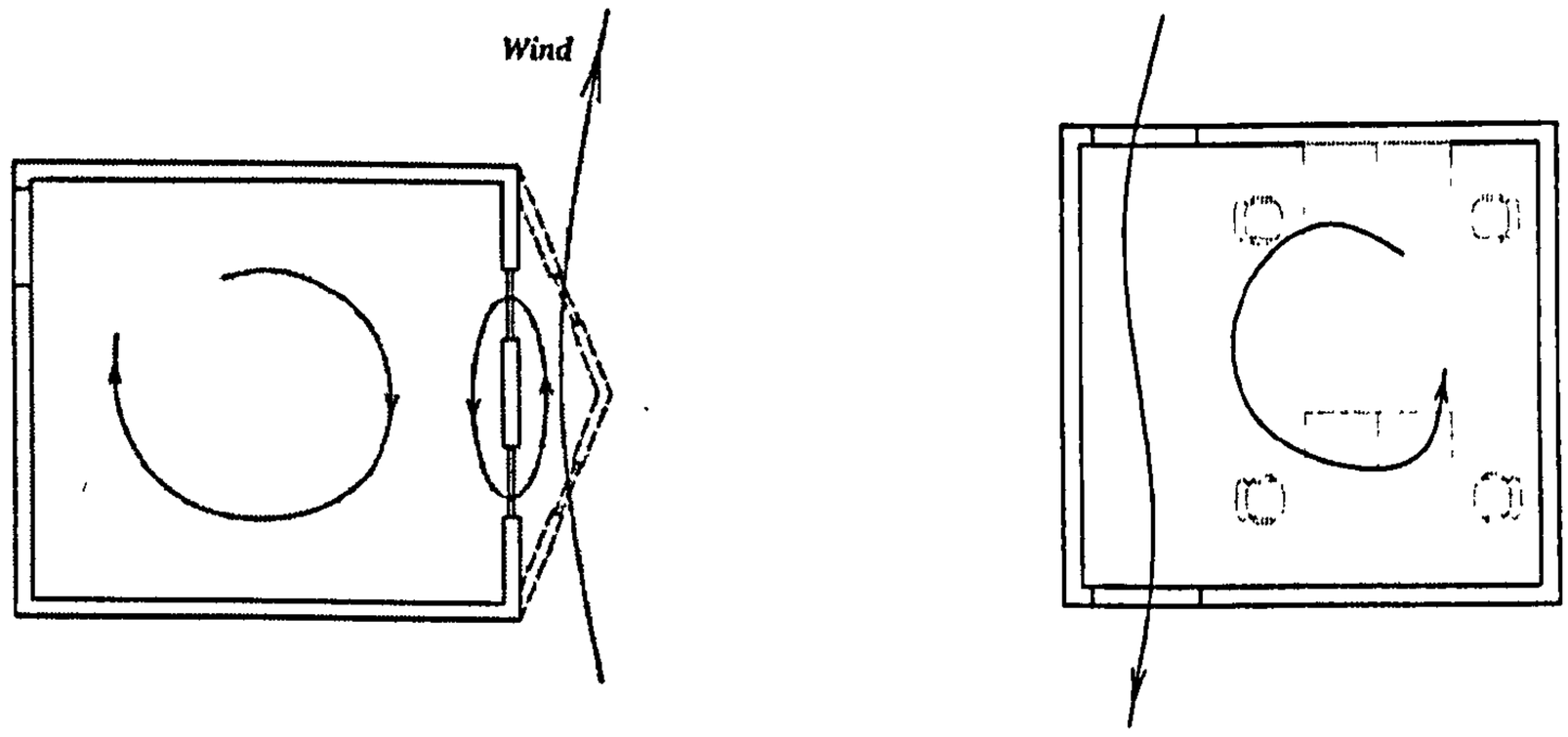

(a) ventilation of a single-sided office (plan) (b) cooling ventilation by recirculation

Figure 5.54: Two examples illustrating use of recirculation for ventilation

6

BUOYANCY-DRIVEN NATURAL VENTILATION IN ATRIUM SPACES

6.1 Introduction

Having examined the impacts of atrium design parameters on the performance of wind-induced ventilation in the previous chapter, this chapter is intended for the study of buoyancy-driven natural ventilation in atrium spaces as a passive cooling strategy. Compared to wind-induced airflow which is significantly influenced by the external forces such as back flow, reattaching flow, reverse flow, etc, buoyancy-driven flow is mostly affected by internal forces, i.e. the static pressure difference generated by the difference between the indoor and outdoor air temperatures, and as a result its effects are less sensitive to the design parameters that are only relevant to the outside forces such as the roof and adjacent buildings. This difference between the two ventilation regimes also means that the methods used to investigate them are not the same: instead of parametric study employed for the wind-induced ventilation studies, the investigation of the airflow driven by buoyancy forces in this part will be more focused on the physics of the ventilation and the applicability of the generalised algorithms for different circumstances, based on which the impacts of the design parameters are further studied.

As has been pointed out in Chapter One, the study on buoyancy-driven natural ventilation in this chapter will be concerned with two issues in relation to the thermal and geometrical characteristics of atrium spaces. Firstly, the effects of the heat sources on the ventilation performance will be studied, especially when they are located on the vertical wall

irradiated by the sun, and this will be the main topic of Section 6.2. Secondly, the impacts of large openings on the level of the neutral plane will be investigated in Section 6.3 so that the neutral plane can be controlled in order to aid the ventilation of adjacent buildings. Design guidance is also developed respectively regarding to each issue at the end of each section, and finally a summary of this chapter is provided in Section 6.4.

6.2 Impacts of heat sources

In order to simplify the investigation in a logical and scientific way and reduce the number of the simulations that have to be carried out, three prototypes are employed as the basis models based on the two basic flow regimes identified in Chapter Two, i.e. displacement ventilation and mixing ventilation, as illustrated in Figure 6.1: the first two are for the study of displacement ventilation (cross displacement ventilation and single-sided displacement ventilation respectively) whilst the last is for that of mixing ventilation. The atrium building to be studied has the same geometrical dimensions as the one used for the study of the wind-induced ventilation in the previous chapter, i.e. it is still a 2D cubic model with a width of 12m and a height of 12m. For displacement ventilation, the openings have a height of 1m and are located 1m away from the nearest horizontal surfaces (which is the top surface for upper openings and the bottom surface for the lower openings), as shown in Figure 6.1 (I) and (II). The opening for the mixing ventilation is 2m high and is placed in the middle of a vertical wall, as seen in Figure 6.1 (III). Both the location and the intensity of the heat source will have certain effects on the ventilation performance, and their impacts will be studied in terms of each prototype.

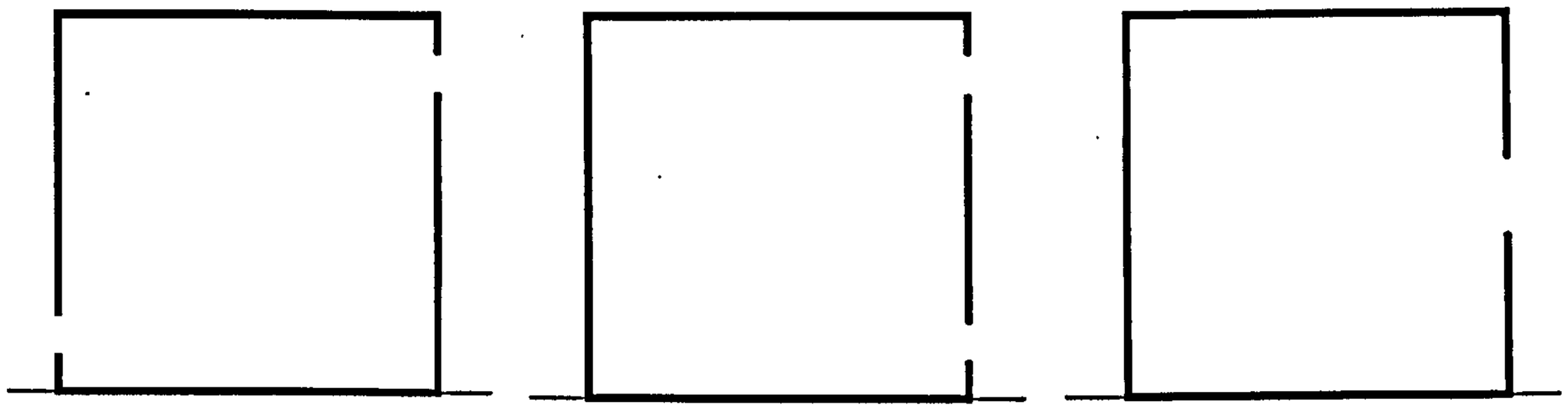

(I) cross displacement ventilation | *(II) single-sided displacement ventilation* | *(III) mixing displacement ventilation*

Figure 6.1: Three prototypes for the investigation of the buoyancy-driven natural ventilation of atrium spaces

6.2.1 Cross displacement ventilation

In order to investigate the effects of the location of the heat source, the whole surface of the building is divided into a number of small edges that are of equal length (3m), and each of them work as the source emitting a heat flux of 60W/m^2 for a different scenario, as shown in Figure 6.2. The outside air temperature is specified as 17°C (290K). These values are the same as those used for validation studies. Thus a total number of 14 simulations are carried out for initial investigation, apart from which additional simulations will also run for further comparison and analysis.

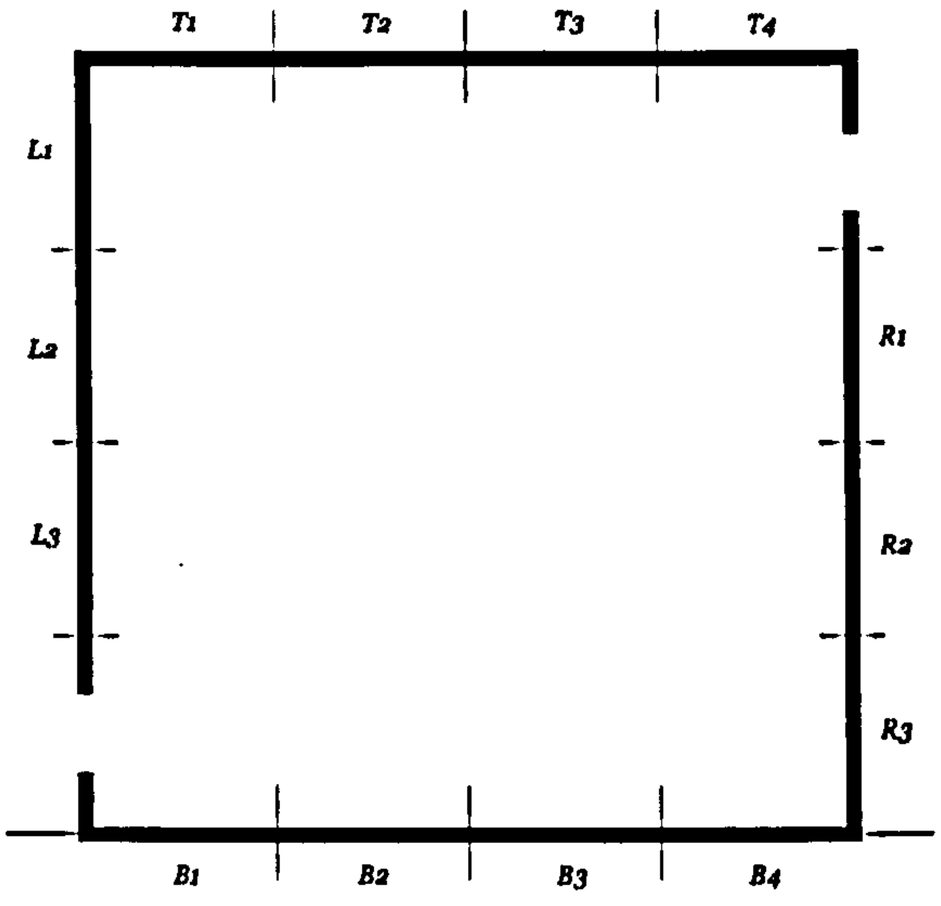

Figure 6.2: The locations of the heat sources simulated in the study of cross displacement ventilation

Chapter Two has introduced a generalised algorithm for the calculation of airflow rates of buoyancy-driven natural ventilation with a uniformly distributed indoor air temperature (Equation 2.11). Using this equation, a reference airflow rate for the model illustrated above in Figure 6.2 can be obtained as 0.25m/s. In fact this airflow rate is the highest for the heat flux available as all energy is used to induce the air movement and no energy accumulates in the space. By defining the airflow rate coefficient as the ratio of the airflow rate simulated by CFD to the reference airflow rate, we can plot the airflow rate coefficients of the buoyancy driven natural ventilation for different locations of the heat source in Figure 6.3. The tendency of the efficiency of the heat source with the variation of its location is discussed below.

Vertical tendency of the efficiency of the heat source

It can be seen that, the heat source located at the similar vertical height generally has similar performance, such as those located on the floor or the ceiling, and the discrepancies between them are less than 12%. However, the efficiency of the heat source reduces

significantly with the increase of its height: the heat sources located on the ground level can be more than three times as efficient as those on the ceiling.

This can be understood by plotting the vertical temperature profiles for scenarios with different locations of the heat source, as shown in Figure 6.4. According to energy conservation laws, the energy emitted from the heat source is transferred to heat up the air coming into the building from lower opening and raise its temperature from lower outside temperature to the higher temperature near the upper opening (actually part of the energy is also used to provide the kinetic energy for the air movement, but this part is very small compared to the other used for heat energy and thus can be ignored). This can be expressed by Equation (2.24):

$$E = \rho C_p q (T_i - T_o) \tag{2.24}$$

In this way, it can be inferred that, high air temperature at the upper part of the space will result in a lower airflow rate. As shown in Figure 6.4, higher location of the heat source will lead to a higher air temperature near the upper opening and hence a lower airflow rate.

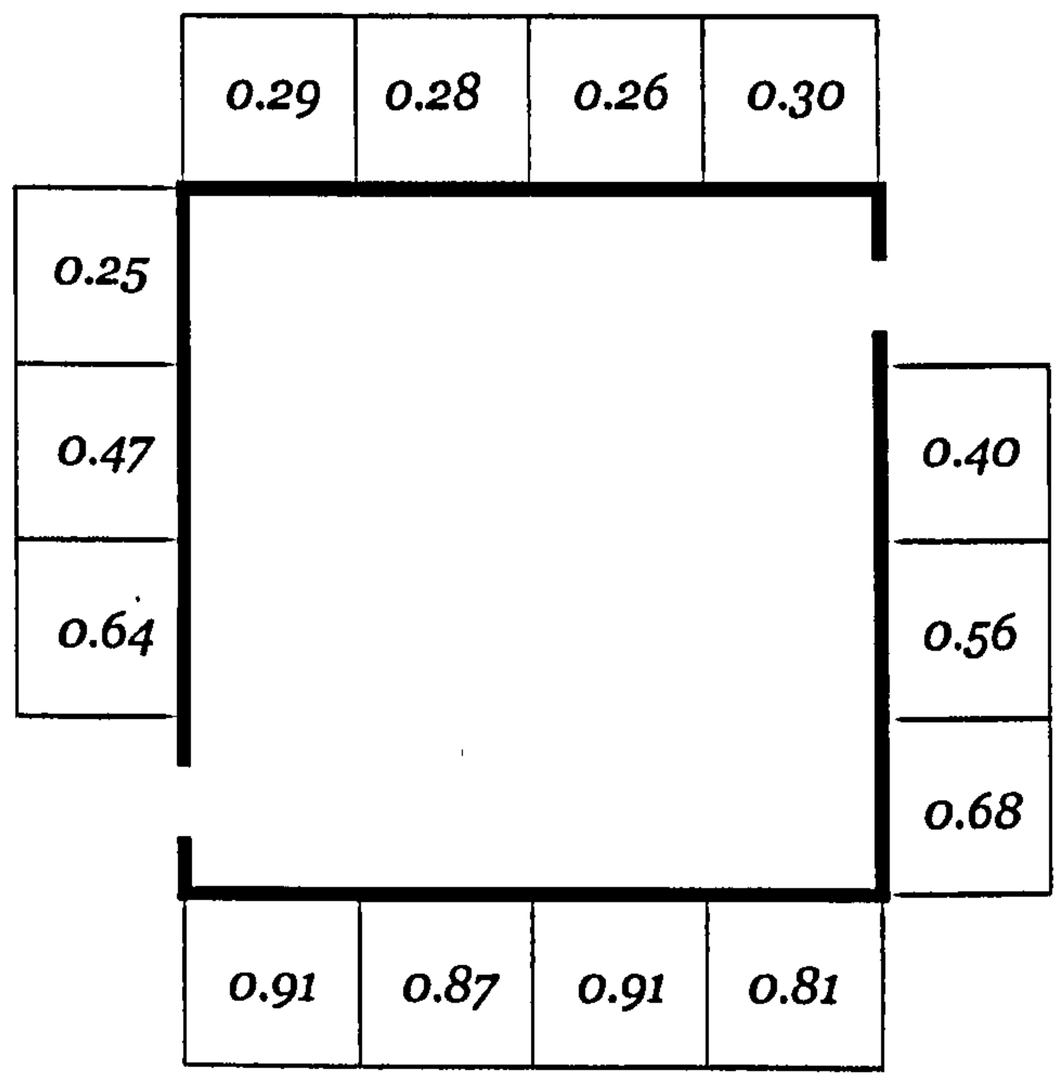

Figure 6.3: The airflow rate coefficients of the buoyancy-driven cross ventilation for different locations of the heat source

In addition, in relation to the high temperature near the top of the building opening caused by the heat sources located very high, bi-directional flow may occur for the upper opening, which essentially reduce the effective opening area (as defined in Chapter Two, Section 2.6.2) and hence the airflow rate. This is demonstrated in Figure 6.4 which compares the airflow fields with two different locations of the heat source. It is shown that, when the heat source is located on the floor, the lower opening will act as inlet and the upper opening as outlet

(as seen in Figure 6.5a); however, when the heat source is placed at the upper area of the space, the lower opening is still inlet but the upper opening works as both inlet and outlet (as seen in Figure 6.5b).

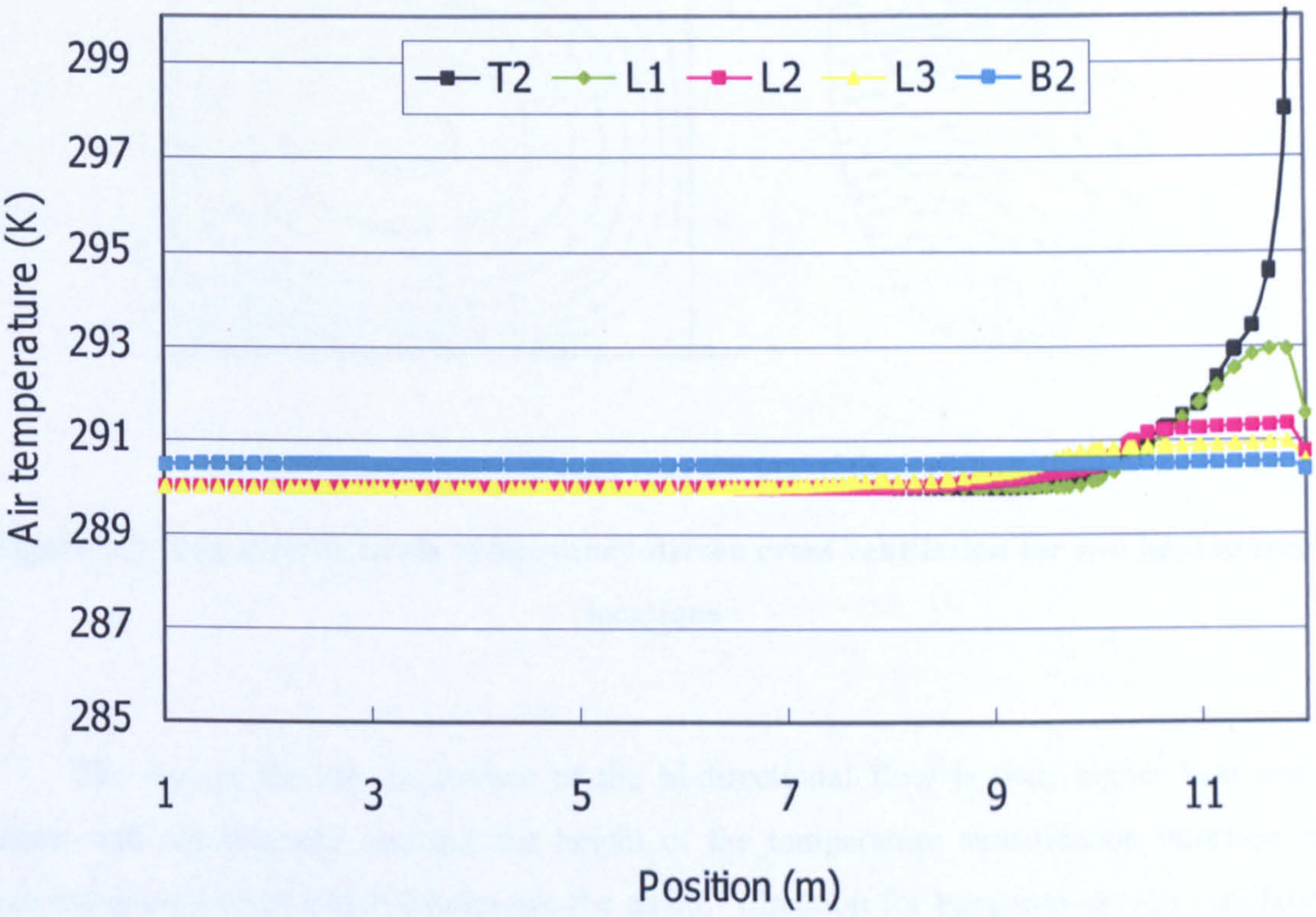

Figure 6.4: Vertical temperature profiles of the buoyancy-driven cross ventilation for different locations of the heat source

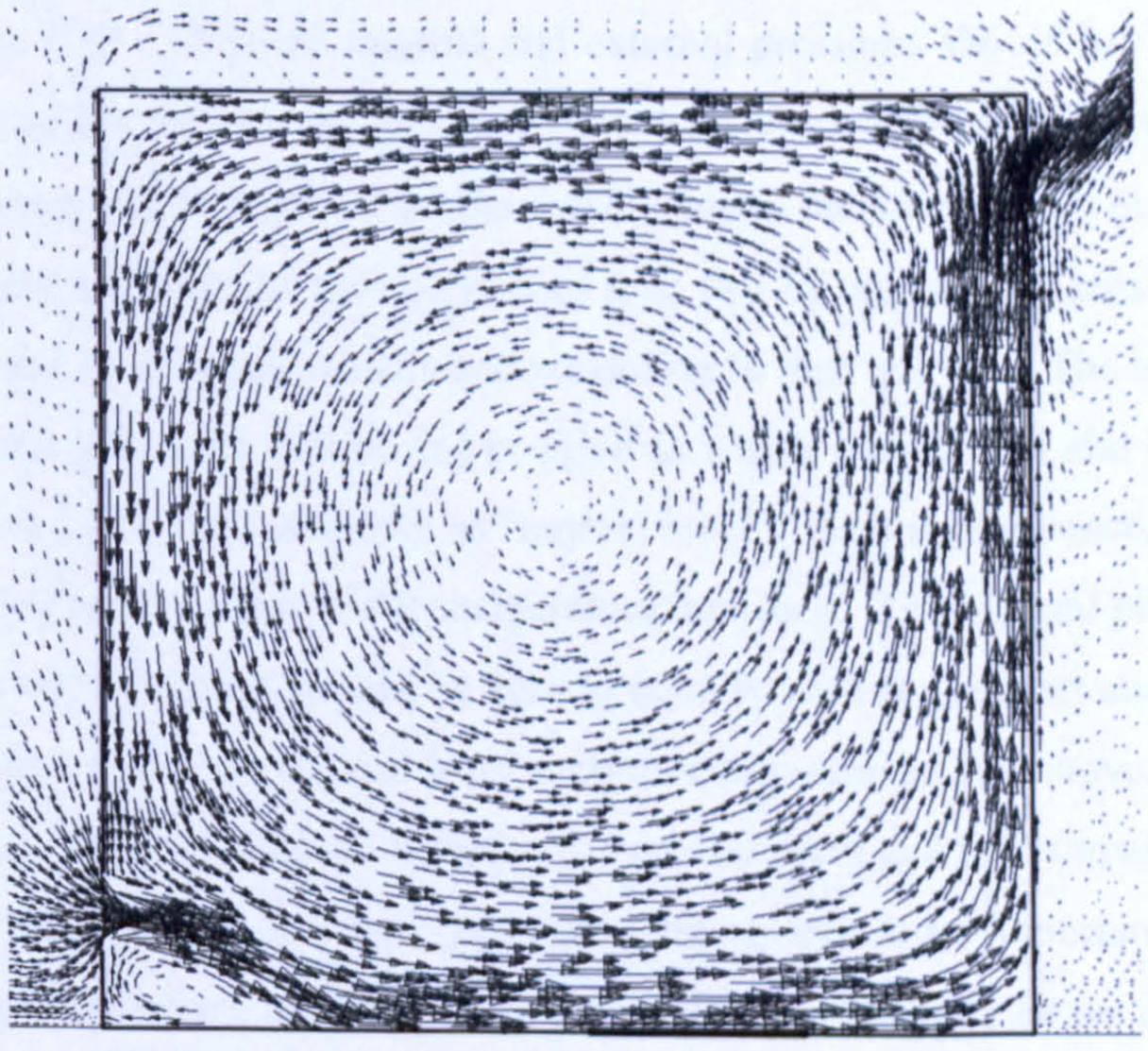

(a) the heat source is located on the floor (B3)

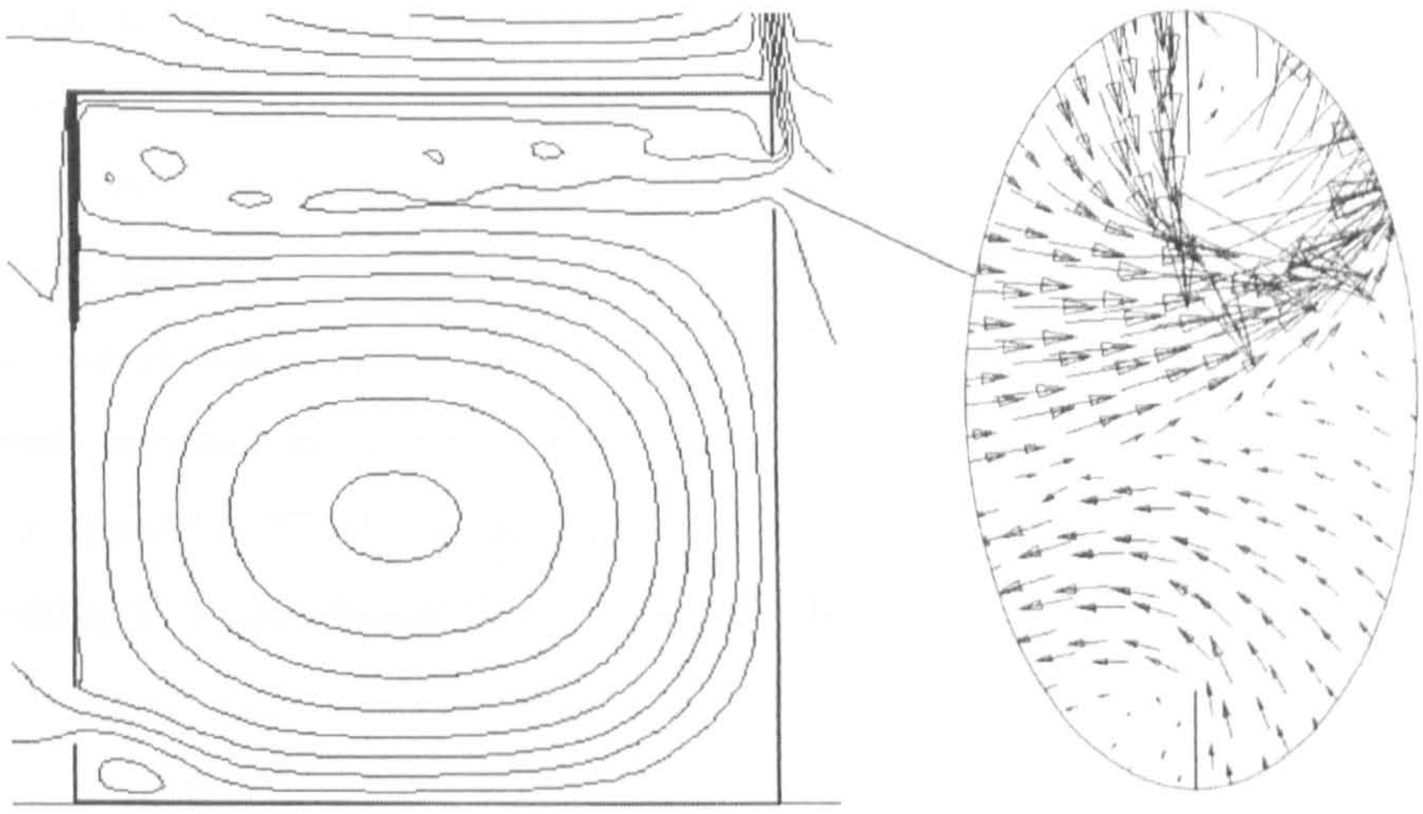

(b) the heat source is located near the top of the building (L1)

Figure 6.5: The airflow fields of buoyancy-driven cross ventilation for two heat source locations

The reason for the occurrence of the bi-directional flow is that, higher heat source location will significantly increase the height of the temperature stratification interface and hence the neutral level which determines the airflow direction for buoyancy-driven ventilation, and when the neutral level intersects with an opening, bi-directional flow will take place.

A diagram illustrating this process in detail based on the pressure difference analysis is presented in Figure 6.6. It is known that, when the heat source is located at the upper area of the building, the air temperature at lower levels of the building will be the same as the outside (also as shown in Figure 6.4). Thus the internal and external pressures should have the same slope below the temperature interface, as seen in Figure 6.6. Above the temperature interface, the indoor air temperature will be higher than the outside due to the energy from the heat source and the slope of the external pressure will be steeper than that of the internal pressure since higher air temperature result in lower air density and according to idea gas law. The intersection of the internal and external pressures will be the position at which the internal and external pressure difference is zero and this level is known as "neutral level". As a consequence, the neutral level should always be higher than that of the temperature interface. The integral pressure difference generated through two openings should be zero to comply with the conservation laws, and as a result the shaded area below the neutral level should be the same as that above the neutral level. This in fact suggests that the distance between the neutral level and the temperature interface is dependent on the size of both openings, because opening area is an important factor affecting the integral pressure difference of an opening. Generally speaking, the larger the upper opening, the higher the neutral level.

It is also known that, the level of the temperature interface is determined by the location of the heat source if the building height and the areas and the locations of the openings do not vary. When the location of the heat source is not very high, the temperature interface will be far below the lower edge of upper opening and the neutral level will not intersect with the upper opening. As a result bi-directional flow will not occur (as seen in Figure 6.6a). However, when the temperature interface is already very close to the upper opening (such as the case when the heat source is located at T2 or L1, see Figure 6.4), the neutral level will easily intersect with the opening resulting in bi-directional flow (as seen in Figure 6.6b).

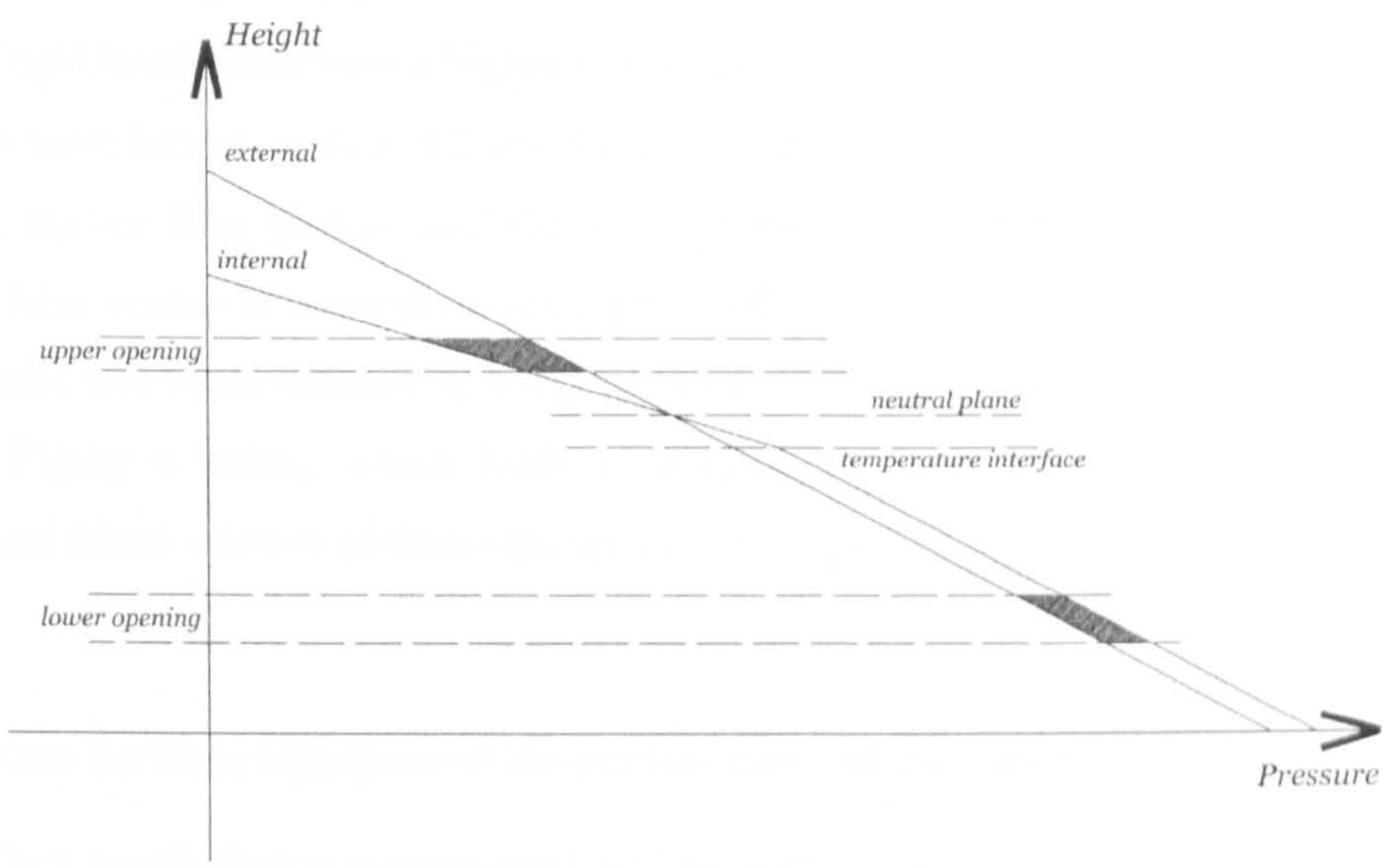

(a) When the temperature interface is not very high (neutral level does not intersect with the upper opening and bi-directional flow does not occur)

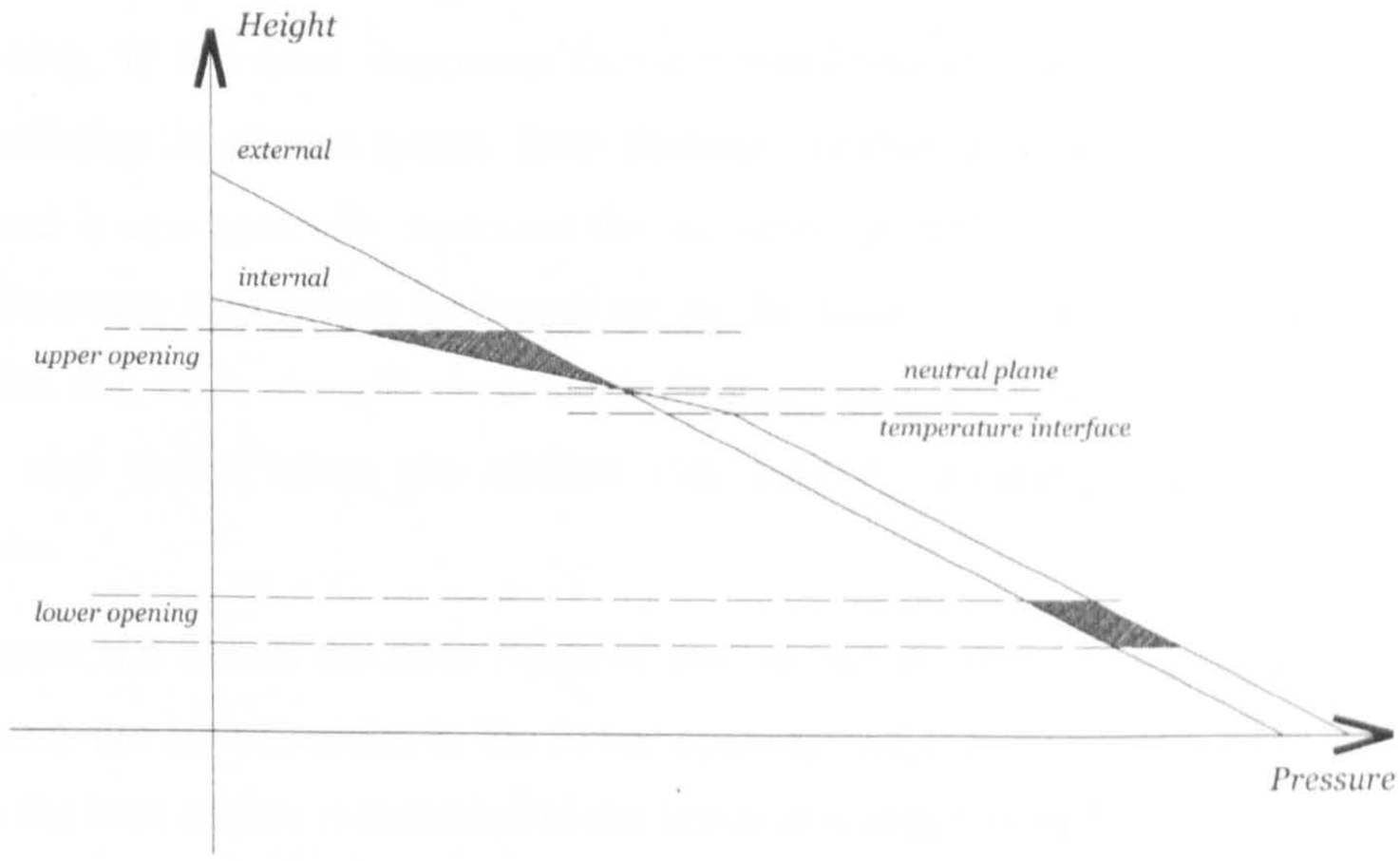

(b) When the temperature interface is very high (neutral level intersects with the upper opening and bi-directional flow occurs)

Figure 6.6: The vertical pressure distributions for buoyancy-driven cross ventilation

It is also known that, the level of the temperature interface is determined by the location of the heat source if the building height and the areas and the locations of the openings do not vary. When the location of the heat source is not very high, the temperature interface will be far below the lower edge of upper opening and the neutral level will not intersect with the upper opening. As a result bi-directional flow will not occur (as seen in Figure 6.6a). However, when the temperature interface is already very close to the upper opening (such as the case when the heat source is located at T2 or L1, see Figure 6.4), the neutral level will easily intersect with the opening resulting in bi-directional flow (as seen in Figure 6.6b).

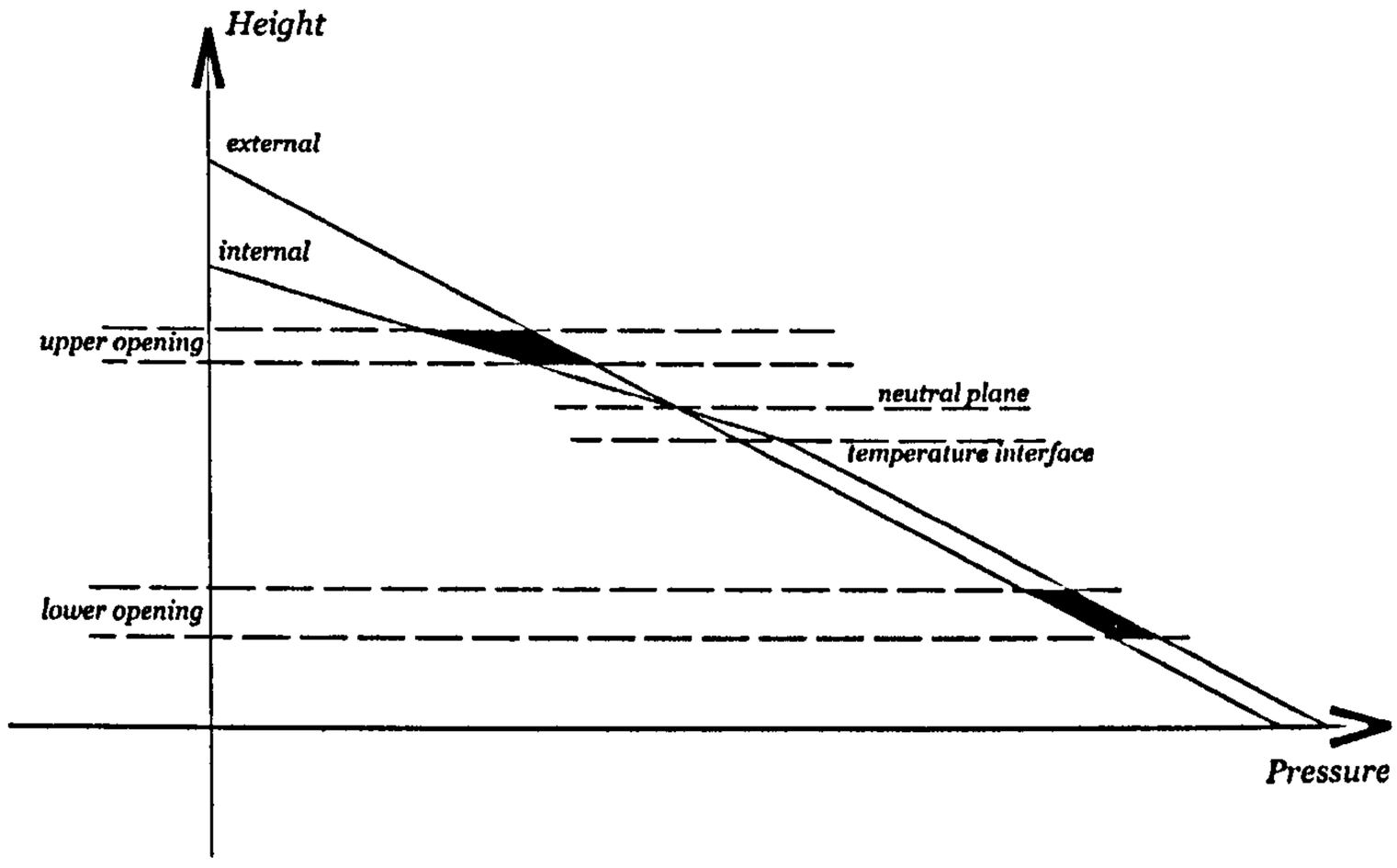

(a) When the temperature interface is not very high (neutral level does not intersect with the upper opening and bi-directional flow does not occur)

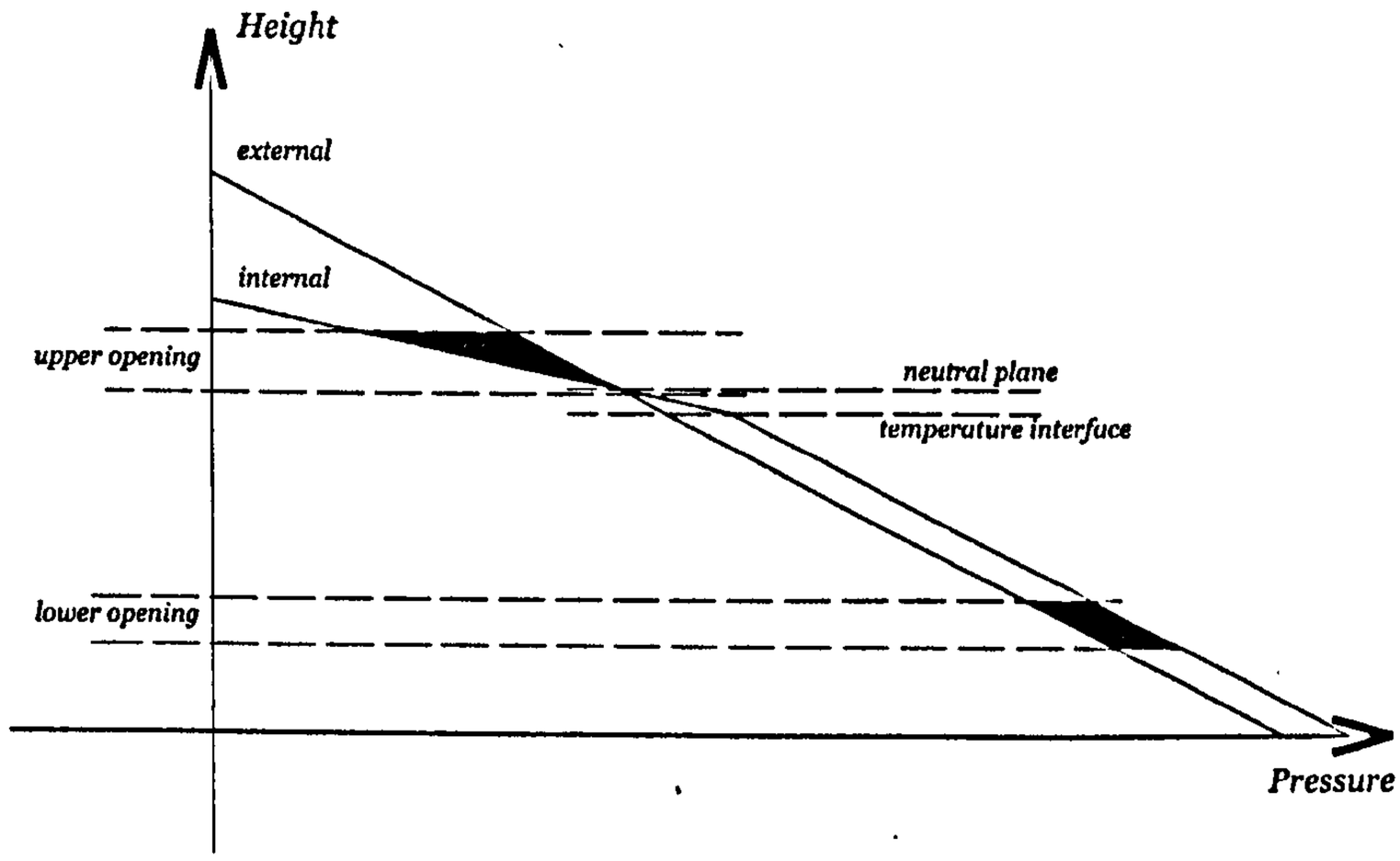

(b) When the temperature interface is very high (neutral level intersects with the upper opening and bi-directional flow occurs)

Figure 6.6: The vertical pressure distributions for buoyancy-driven cross ventilation

It has already been described in Chapter Two that, the conventional generalised algorithms used for the prediction of the airflow rate and the neutral level are based on the assumption of small openings over which the pressure is uniformly distributed. In other words, they will not be applicable for large openings with bi-directional flows. This issue will not be further discussed here but will be the topic of a later section.

Horizontal tendency of the efficiency of the heat source

It is also observed that, for the heat sources located on vertical walls, those on the outlet side wall (right hand side) have a higher effectiveness than those on the opposite wall (left hand side) at the same height, such as L2 and R1, L3 and R2. The reason for this can be explained by examining the air flow pattern and the air temperature distributions near the upper opening. When the heat source is located on the right hand side wall, the air coming into the building from the inlet will more efficiently bring the heat emitted to the upper openings by convection (compare Figure 6.7a&b), which leads to a generally higher air temperature at the upper openings and hence a lower airflow rate(see Figure 6.7c).

Other indices for the evaluation of the performance of buoyancy-driven ventilation

When ventilation is incorporated and an opening is provided at the lower level, the air temperature will be almost the same as the outside air temperature due to convection (also see Figure 6.4: the air temperature at 1.6m level is generally the same as outside) and mostly airflow rate, which can also be regarded as the air velocity coming into the building through the lower opening, is the most important factor determining the performance of the buoyancy-driven ventilation in atrium spaces from thermal comfort point of view, because under this circumstance it can generally represent the air velocity at the occupants' level. In addition, higher airflow rate also means that more air can be exchanged between the inside and outside environment, and more excessive heat can be brought out. However, it should be noted that one exception also exists when the airflow rate cannot accurately represent the ventilation performance.

Figure 6.8 shows the flow fields of two scenarios with different heat source locations and compares the air velocities at the lower opening and the occupants' level. It can be seen that, when the heat source is extended to the lower opening, the airflow rate will be increased as the size of the heat source is increased (see Figure 6.8c). However, the air velocities at the occupants' level are significantly reduced to less than 0.08m/s for the increase of the size of the heat source, which is only one third of those without heat source extension (see Figure 6.8d). The reason for this can be understood by examining the airflow fields shown in Figure 6.8a&b. When the heat source is very close to the inlet, such as shown in Figure 6.8b, the energy emitted

from the heat source will be directly transferred to the air coming through the lower opening, and the air temperature at the lower opening will be higher than the inside. As a consequence the air will go upwards from an earlier point near the lower opening due to the buoyancy forces compared to the scenario where the heat source is kept away from the inlet. This also means that, higher airflow rate does not necessarily induce higher air velocities at the occupants' level and it would not be good practice to use the heat source too close to the lower opening to generate ventilative cooling effects.

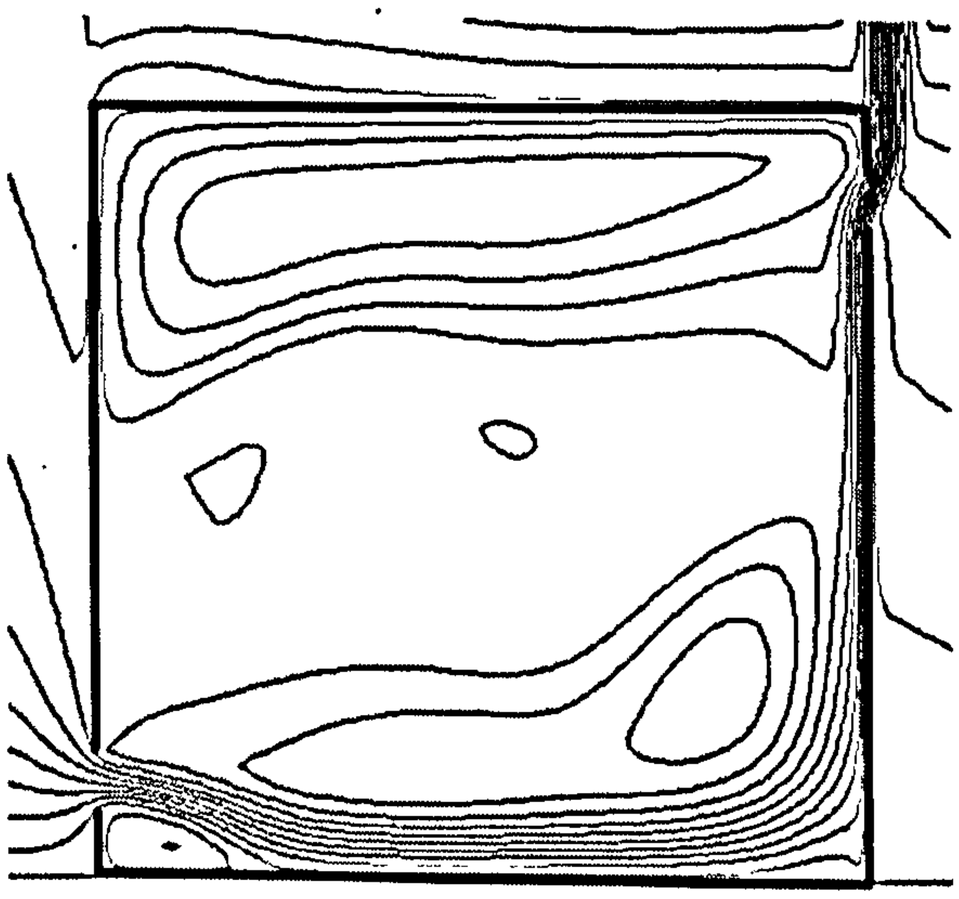

(a) heat source location: R2

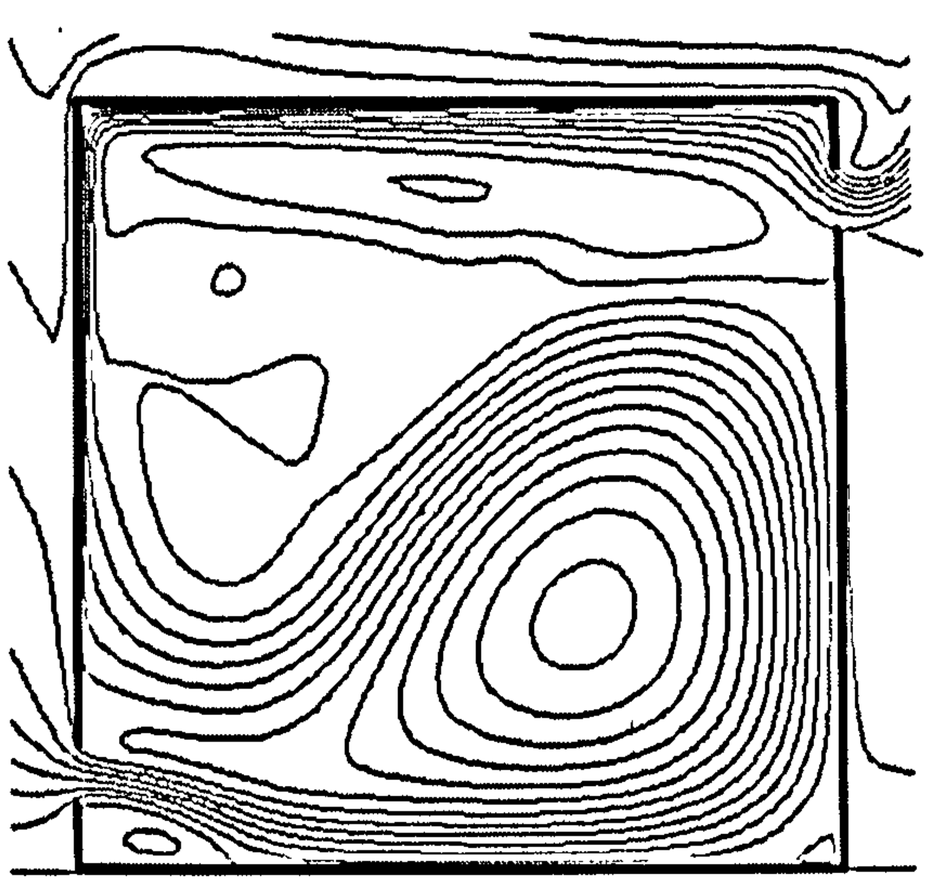

(b) heat source location: L3

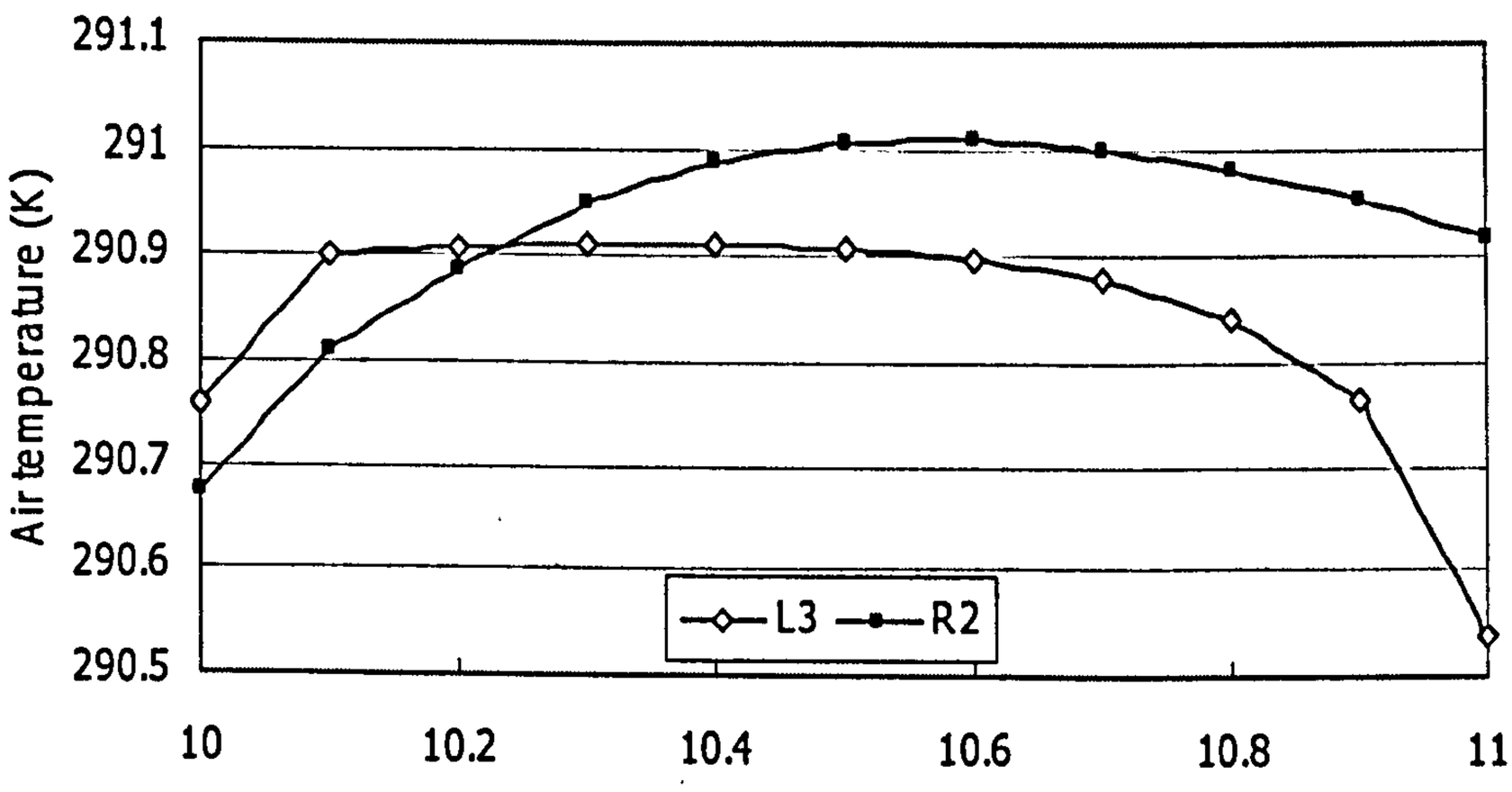

(c) comparison of the air temperature at the upper opening

Figure 6.7: The airflow fields and temperature distributions at the outlet for the buoyancy-driven cross ventilation of two different heat source locations

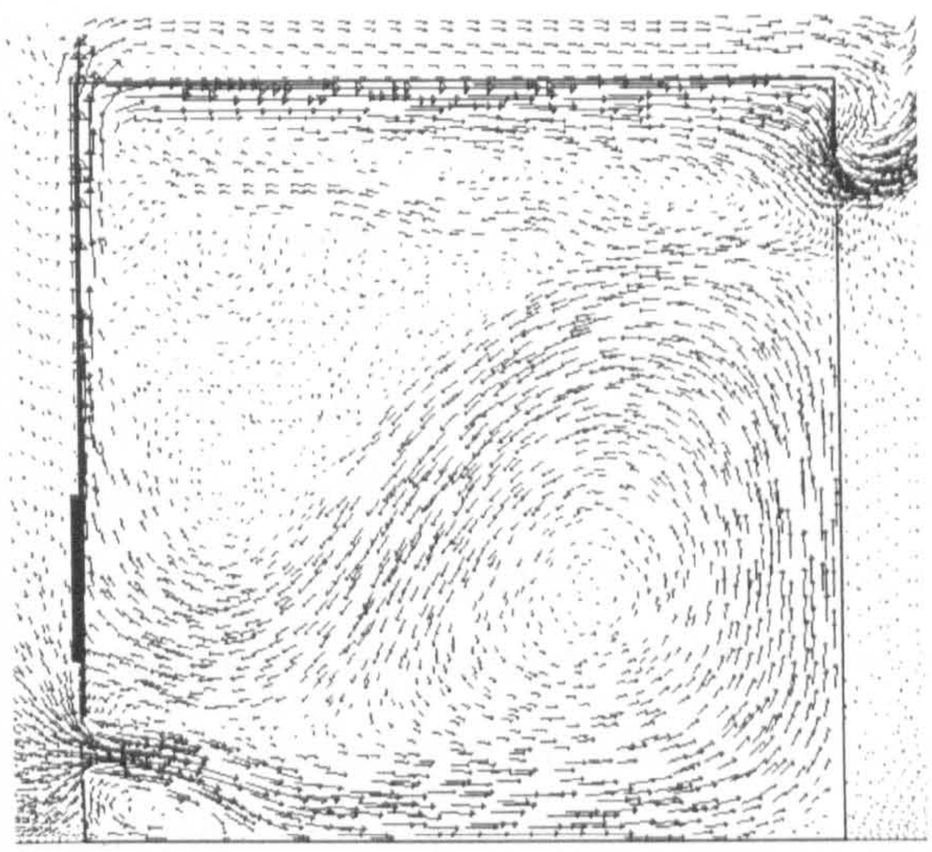

(a) heat source location: L3

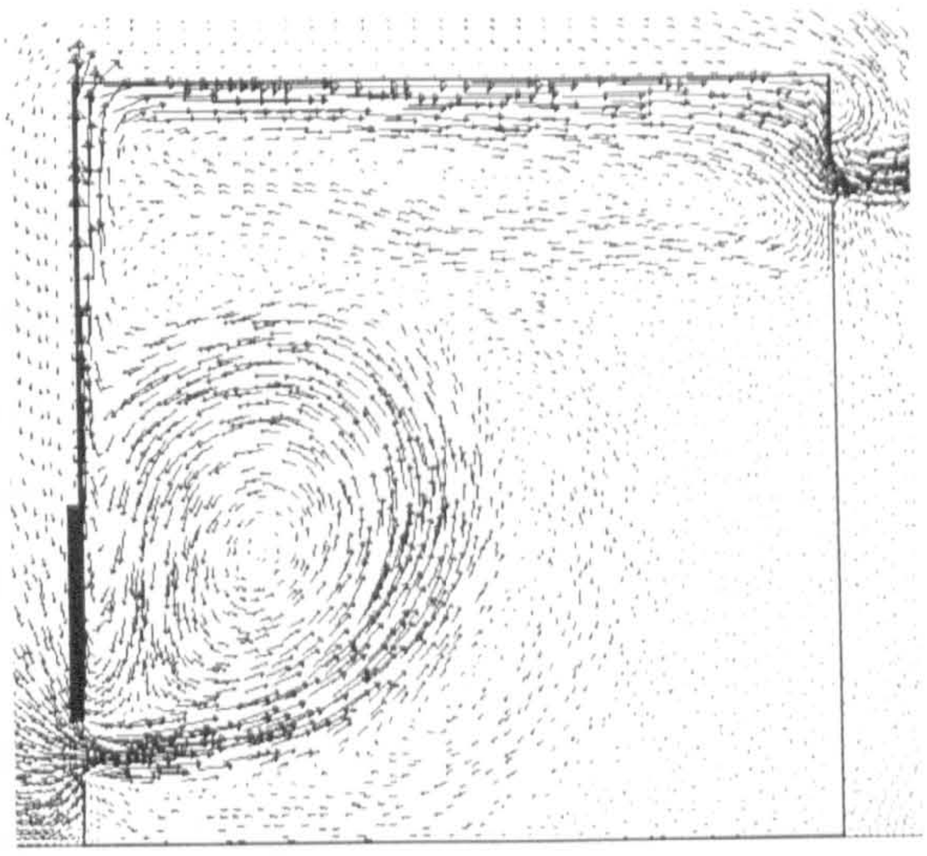

(b) heat source location: L3 + extension to the lower opening

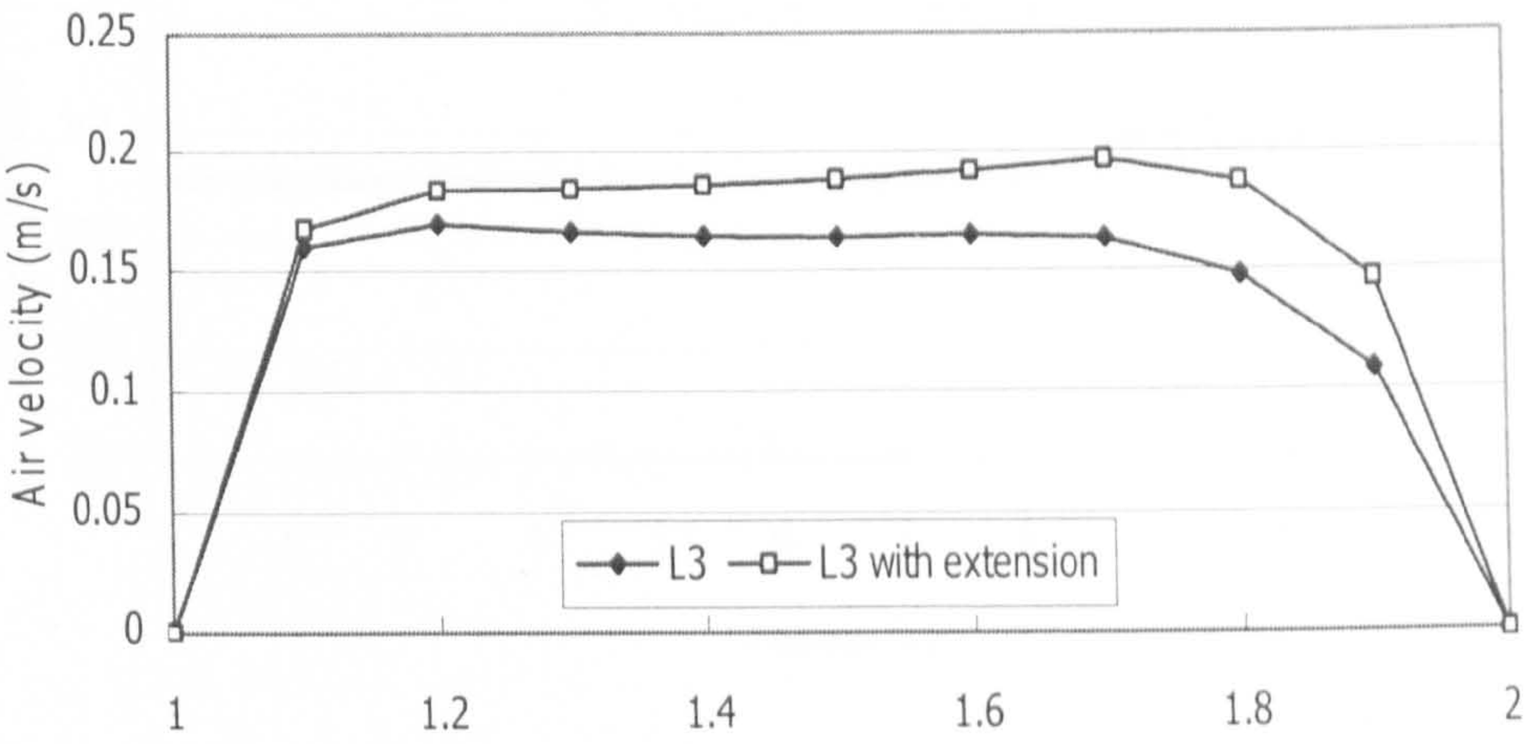

(c) air velocities at the lower opening

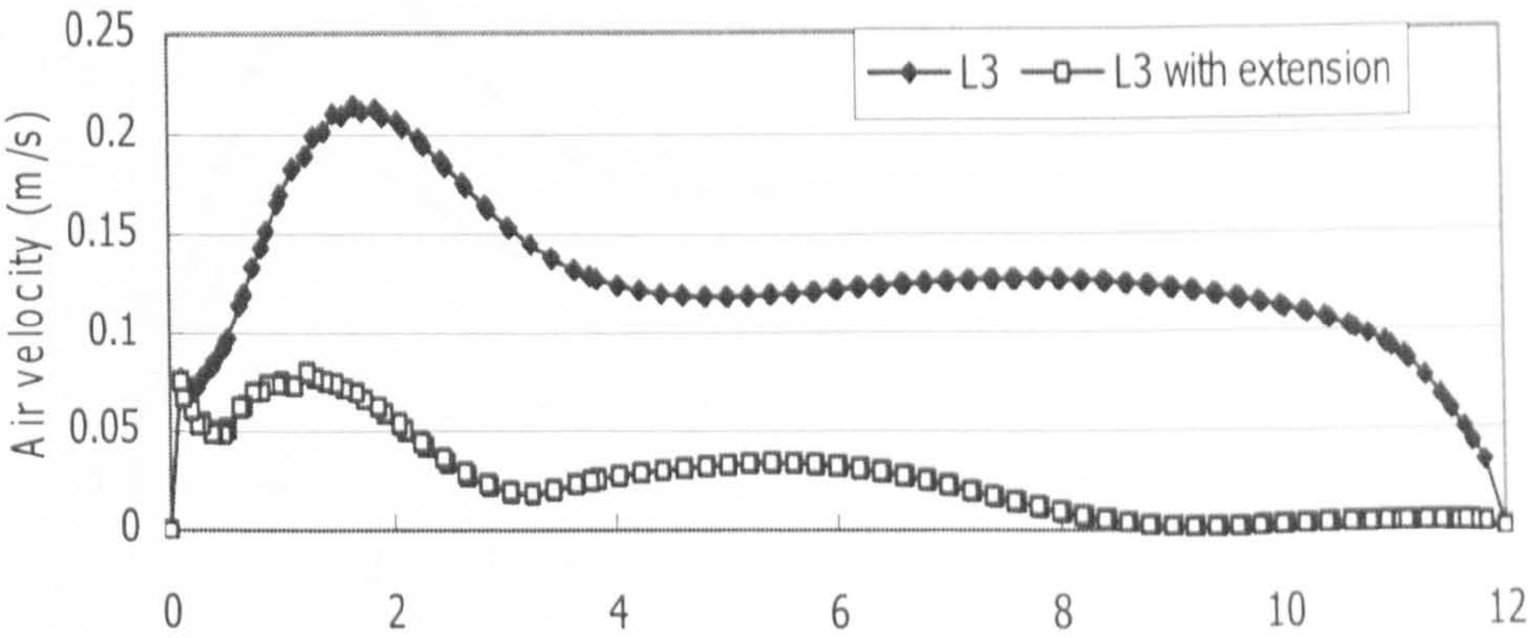

(d) air velocity distributions at the occupants' level

Figure 6.8: Comparison of the airflow fields and velocity distributions for two scenarios of buoyancy-driven natural ventilation

Intensity of the heat source

Figure 6.9 presents a comparison between two scenarios of buoyancy-driven natural ventilation with the same the heat source location (L3) but with different intensity. It is shown that the intensity of heat source can only affect the magnitude of the air velocities and temperatures in the space but it has little to do with the general patterns of the air movement and temperature/velocity distributions at the occupants' level. This result is the same for that of point heat source (plume) obtained by Linden et al. (1990). It can also be seen that even if the heat source is very intensive (200W/m^2 means that the ground should be nearly 50°C higher than the air temperature), the indoor air temperature at the occupants' level is still the same as outside, which shows the efficiency of ventilation in modifying the indoor thermal conditions.

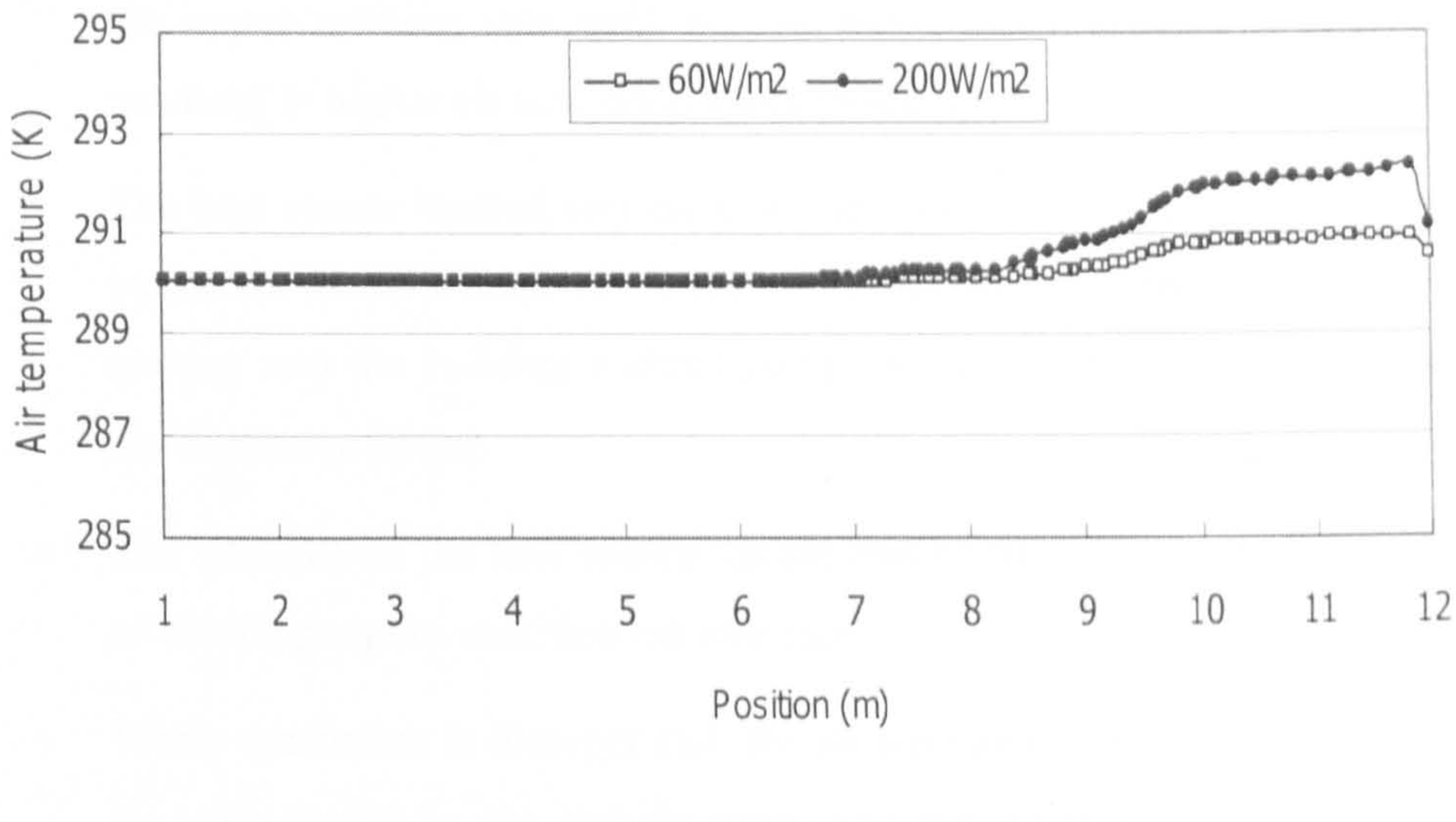

(a) vertical temperature profiles

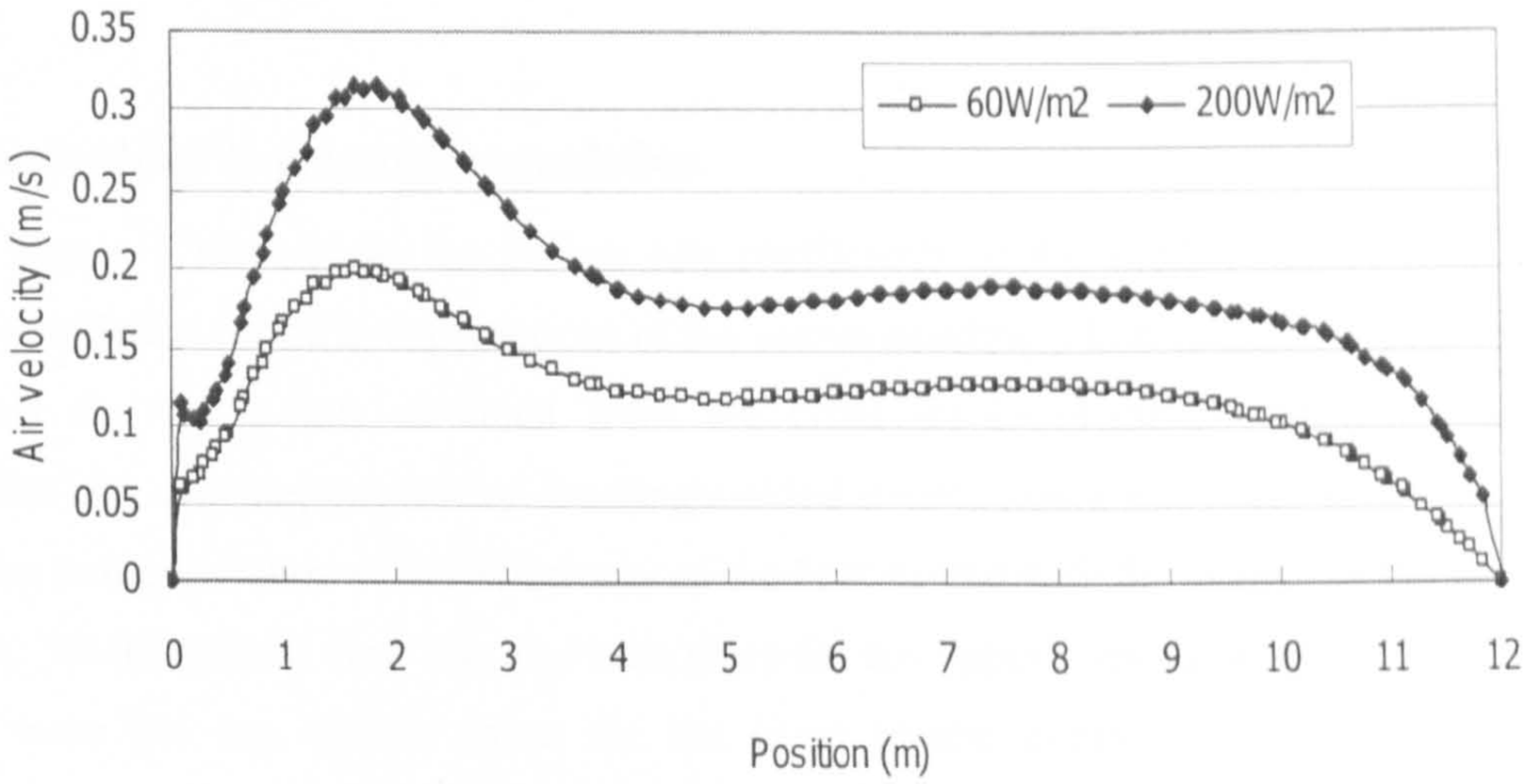

(b) air velocity distributions at the occupants' level

Figure 6.9: Comparison of two scenarios of buoyancy-driven natural ventilation with different intensities of the heat source

The above investigations in relation to the effects of the heat source can be generally summarised by the following key points:

- The efficiency of the heat source reduces with the increase of the height of its location, because more heat will be accumulated at the upper area of the space and thus less energy can be used for the provision of the kinetic energy of the air. In addition, it is also observed that bi-directional flow can occur for the upper opening when the heat source is located very high.
- For heat sources located on vertical walls, those on the upper opening side wall will have a higher efficiency than those on the opposite side at the same level. The reason for this is that when the energy emitted by the heat source located on the upper opening side wall will be more easily brought to the outlet, thus resulting in higher air temperature and hence lower airflow rate.
- The heat source located very close to the lower opening may lead to very low air velocities at the occupants' level, since the air will directly go upwards once coming into the building without going into the deep inside of the space due to the buoyancy forces.
- The intensity of the heat source cannot change the airflow pattern and the height of the temperature stratification interface.
- When ventilation is incorporated, the air temperature at the occupants' level will be very similar to the outside regardless the intensity or location of the heat source.

6.2.2 Single-sided displacement ventilation

Figure 6.10 presents the airflow rate coefficients of the single-sided buoyancy-driven natural ventilation for different locations of the source emitting a heat flux of 60W/m^2. It can be seen that the key points obtained from the cross displacement buoyancy-driven natural ventilation are also applicable for the single-sided displacement buoyancy-driven ventilation regarding to the variation of the efficiency of the heat source with the change of the heat source location. Bi-directional flow can also take place for the upper opening when the heat source is located near the top of the space for the same reason explained earlier. The detailed investigation and analysis of the single-sided displacement ventilation is excluded here as it is generally the same as that of the cross displacement ventilation.

6.2.3 Mixing ventilation

Figure 6.11 shows the airflow rate coefficients of the mixing type buoyancy-driven ventilation with heat sources emitting a heat flux of 60W/m^2 located at different areas of the space. It can be seen that mixing type buoyancy-driven natural ventilation has a number of different characteristics from displacement ventilation studied in the previous subsection (the reference airflow rate is 0.12m/s, as calculated using Equation 2.18, which is around half of that for displacement ventilation).

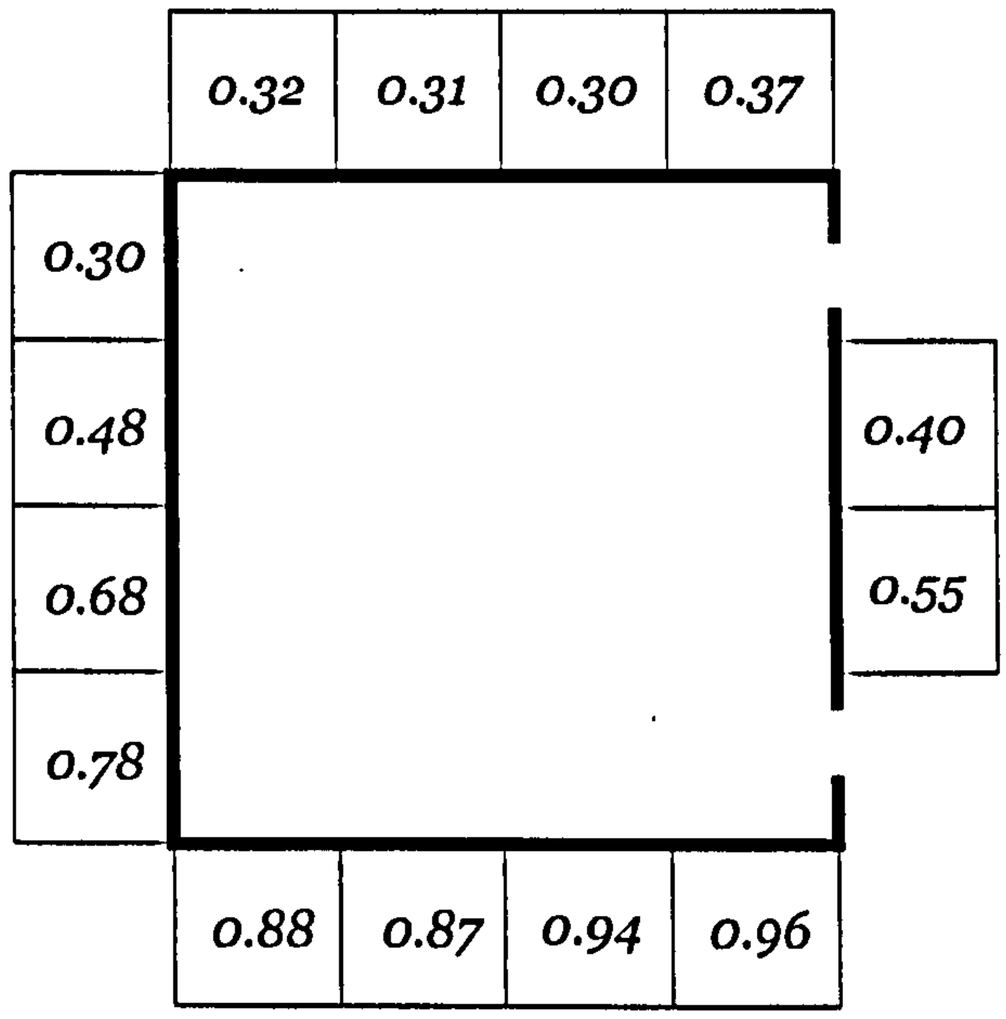

Figure 6.10: The airflow rate coefficients of the single-sided buoyancy-driven ventilation for different locations of the heat source

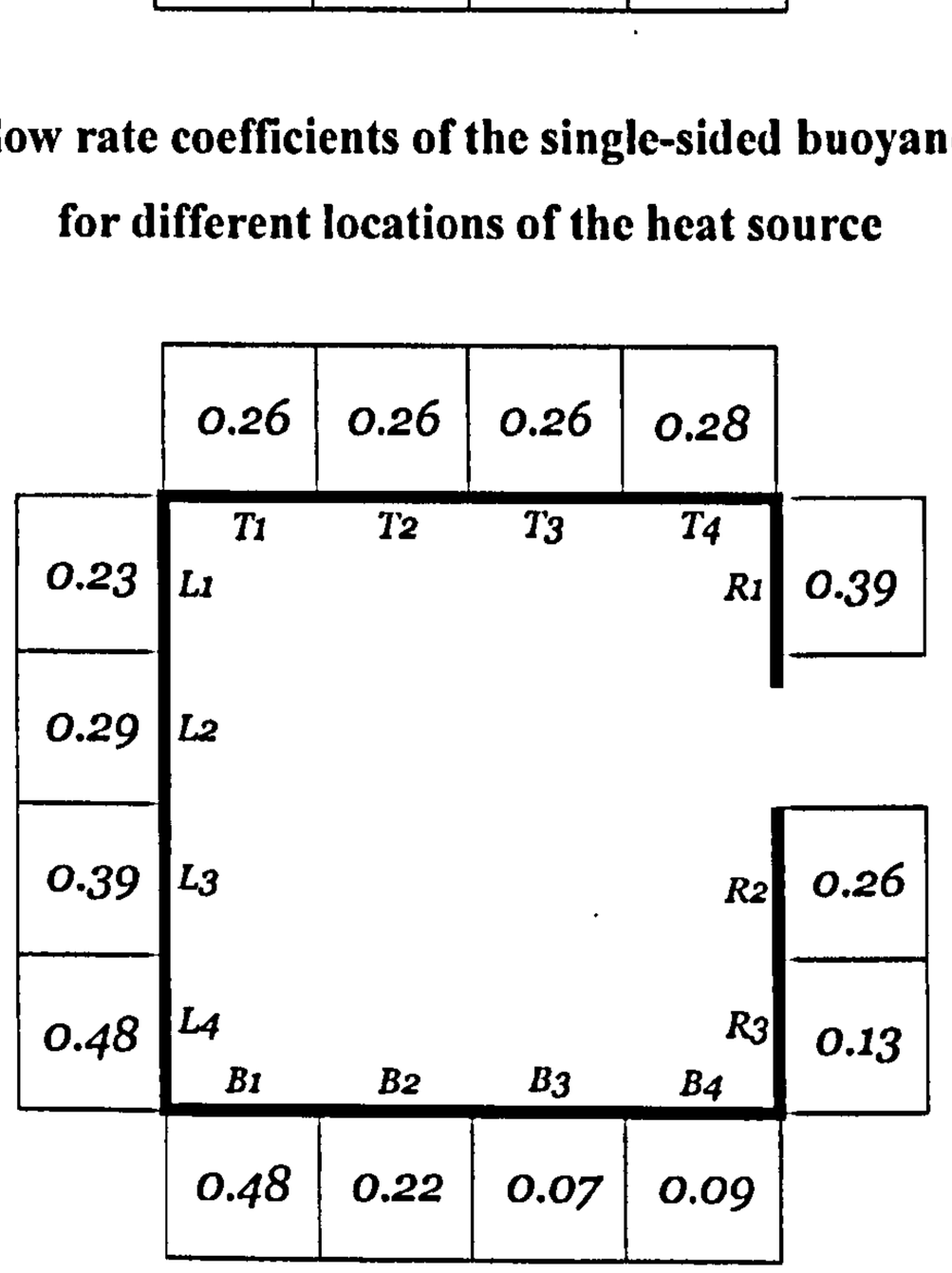

Figure 6.11: The airflow rate coefficients of the mixing buoyancy-driven ventilation for different locations of the heat source

Firstly, it is shown in Figure 6.11 that the conventional algorithm significantly over-predicts the airflow rate: the highest airflow rate that can be achieved by plain heat source located on the building surface is less than half of the reference airflow rate. The reason for this inefficiency of the heat source is that vertical temperature stratification traps much energy at the upper area. In this way, the underlying assumption for the use of the algorithm, i.e. the uniform distribution of the air temperature is violated. As shown in Figure 6.12, the vertical temperature stratification is still very strong even when the heat source is located at the bottom (B1), for which circumstance the air temperature of the displacement ventilation is uniformly distributed. This actually means that, mixing type ventilation does not result in a "well-mixed" air temperature in the space, and its ventilation performance is much weaker than that of the displacement ventilation.

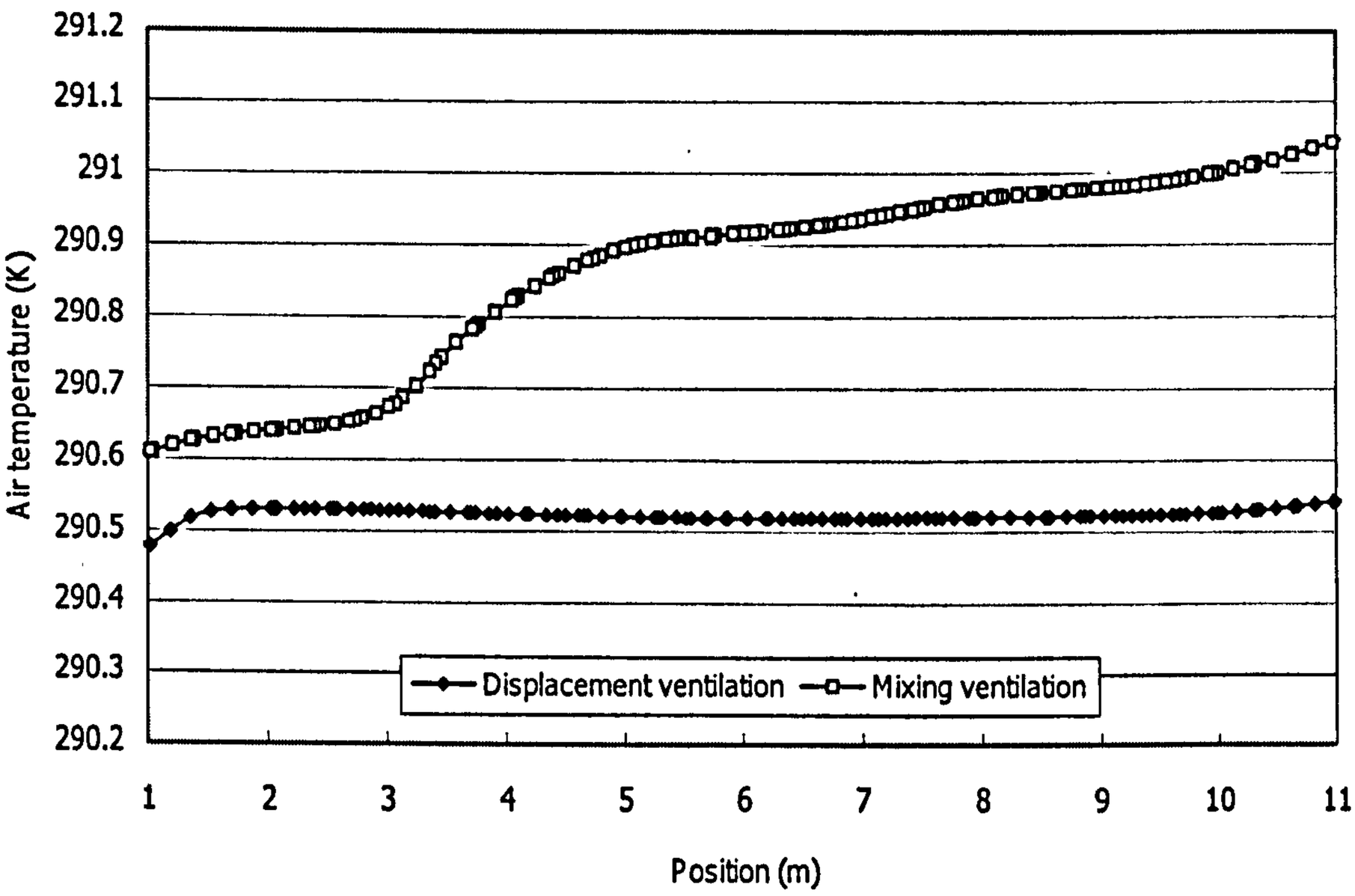

Figure 6.12: Vertical temperature profiles of the mixing and displacement buoyancy-driven ventilation when the heat source is located at the bottom (B1)

Secondly, although the variation of the airflow rate of the mixing ventilation with the height of the heat source on the left hand side wall is the same as that of the displacement ventilation, it is observed that the heat sources located at the right bottom corner lead to extremely low airflow rate, which is less than 10% of the reference airflow rate. The reason for this is attributed to the flow patterns these heat sources result in. Figure 6.13 illustrates the detailed airflow fields of the mixing buoyancy-driven natural ventilation of two different heat source locations, B1 and B3. It can be seen that, due to the different locations of the heat source,

the airflow patterns for the mixing buoyancy-driven ventilation can be just the opposite: when the heat source is located at B1, the air in the space moves clockwise and the outside air can come in through the lower part of the opening resulting in a higher airflow rate, as seen in Figure 6.13a; when the heat source is located at B3, the indoor air moves anticlockwise and very little outside air can get into the building because the air movement brings the energy from the heat source to the opening by convection, as seen in Figure 6.13b&c. It is shown that, for heat source located at B3, the air temperature over the whole opening is higher than the outside temperature, which impedes the external air to come into the space. These two flow patterns can be schematically illustrated by the diagram shown in Figure 6.14.

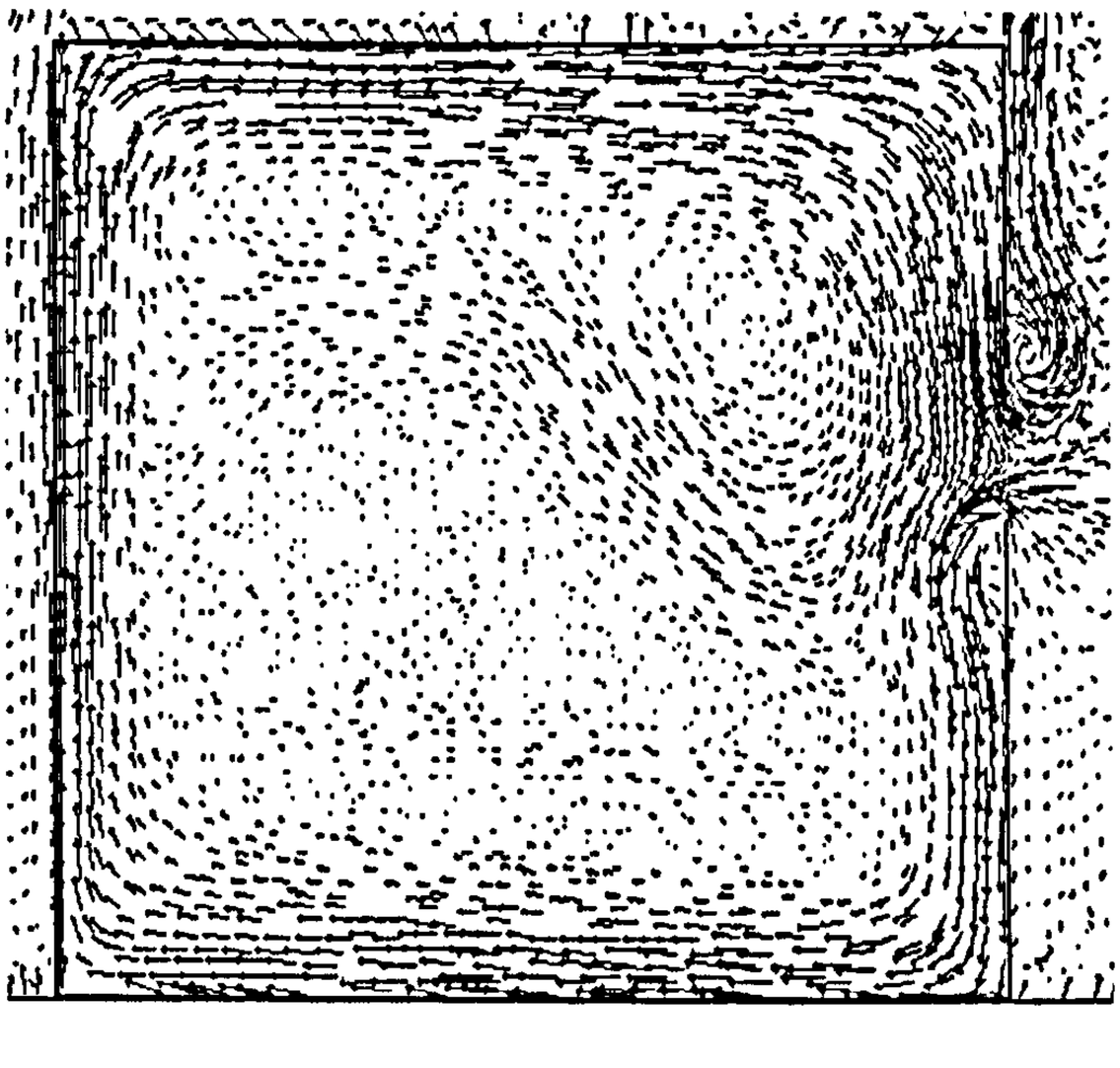

(a) heat source location: B1

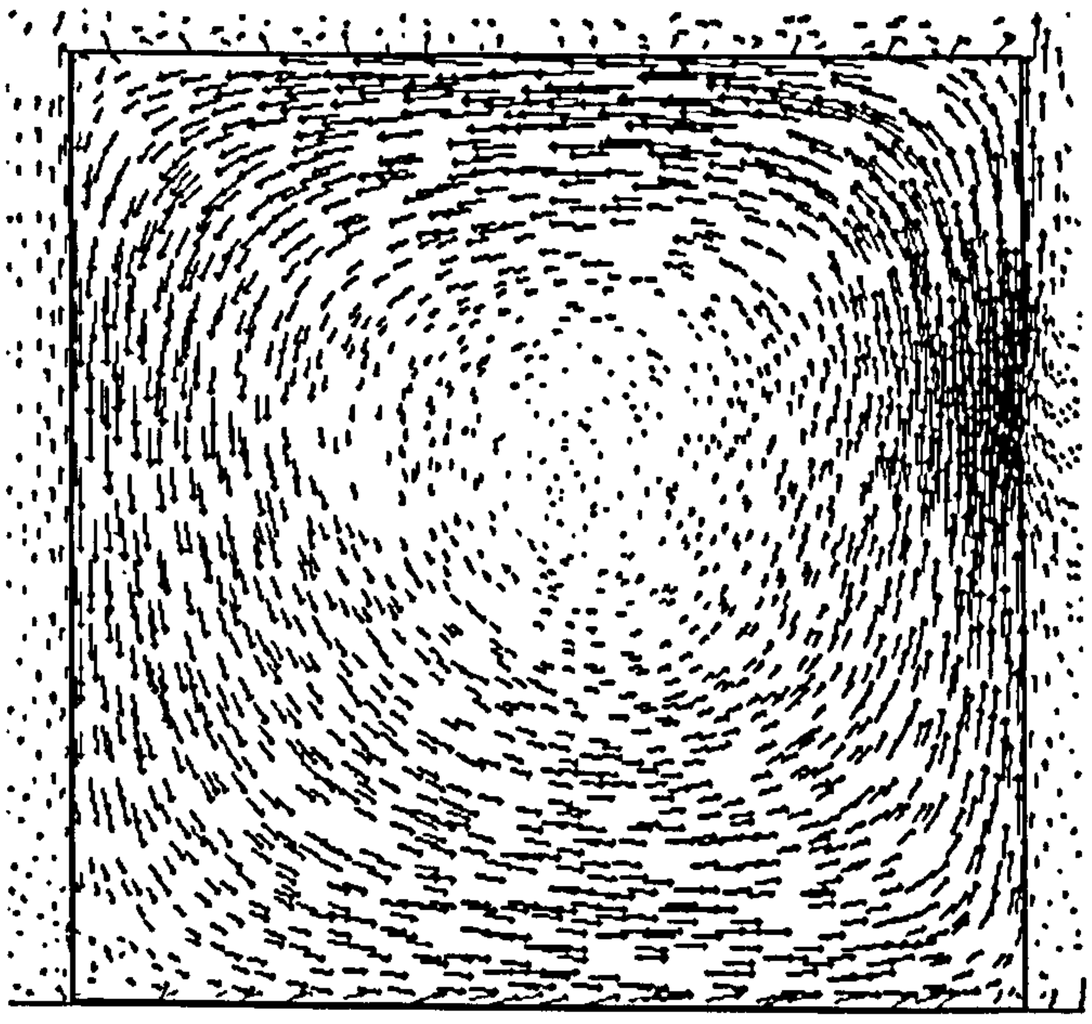

(b) heat source location: B3

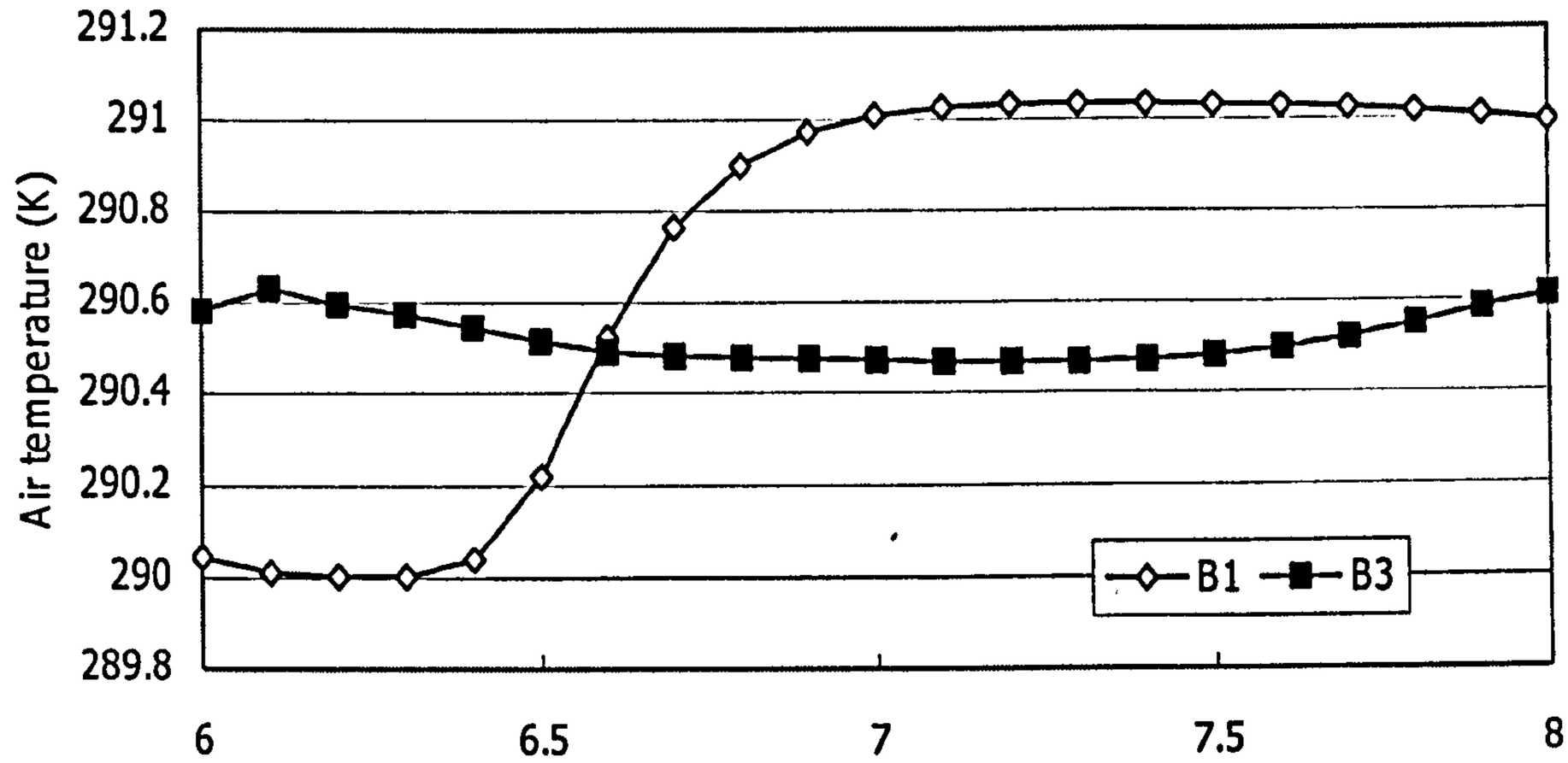

(c) comparison of the air temperature distribution at the opening

Figure 6.13: Two different airflow patterns of the mixing buoyancy-driven natural ventilation

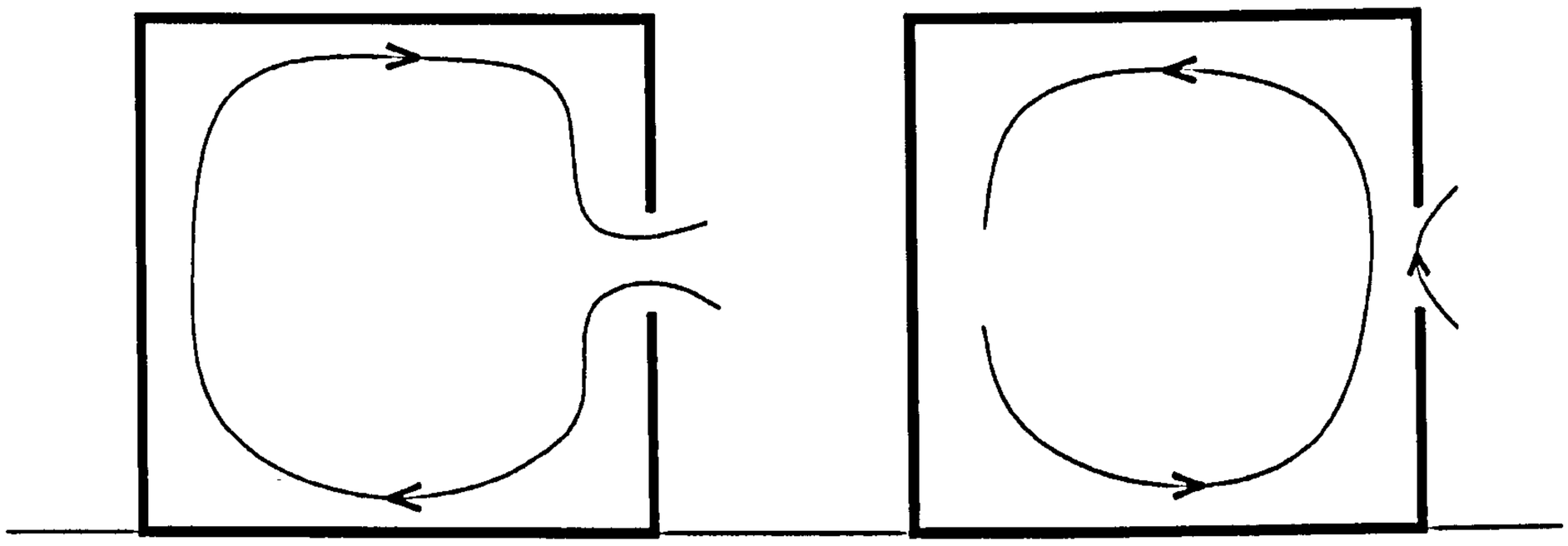

Figure 6.14: Schematic illustration of the two different airflow patterns of the mixing buoyancy-driven natural ventilation

This result suggests that the airflow rate is very sensitive to the flow pattern, and it is necessary to convect the air with high temperature to the opening from the upper side in order to gain a higher airflow rate and hence enhance the efficiency of the heat source. To achieve this, the optimised heat source should be on the opposite side of the wall with the opening or the upper area of the space or the far corner of the lower level from the opening; the heat source located beneath the opening should be avoided.

Thirdly, the air velocities at the occupants' level are not always related to the airflow rate. As shown in the above Figure 6.13a&b, although the two flow patterns illustrated above generate different airflow rates, they seem to produce similar magnitudes of the air velocities at the occupants' level. This is further investigated by plotting the air velocity distributions of more heat source locations (see Figure 6.15). It can be seen that, the air velocities at the occupants' level are at maximum when the heat source is located at the bottom of the space (See B1 to B4) but then reduce significantly with the increasing of the height of the heat source. The air velocity becomes very small when the heat source is located near the top of the building, such as L1 and R1. It should be also noted that, the air velocities achieved by heat sources located at the bottom of the space are actually very high and the maximum air velocity can be twice as the reference airflow rate (0.12m/s), which is similar in scale with that of displacement ventilation with the heat source of the same intensity (see Figure 6.9b for comparison).

The above investigation means that mixing type ventilation is able to generate high air velocities for occupants despite of the low air exchange rate. Nevertheless, it is also suggested that, if the opening is not located at the occupants' level, the heat source has to be placed at the lower level to "suck" the air from the inlet to provide cooling effects for occupants. However, if the opening is provided at the occupants' level, the air velocity at the occupants' level can still be acceptable even if the heat source is located near the top of the building (see Figure 6.16).

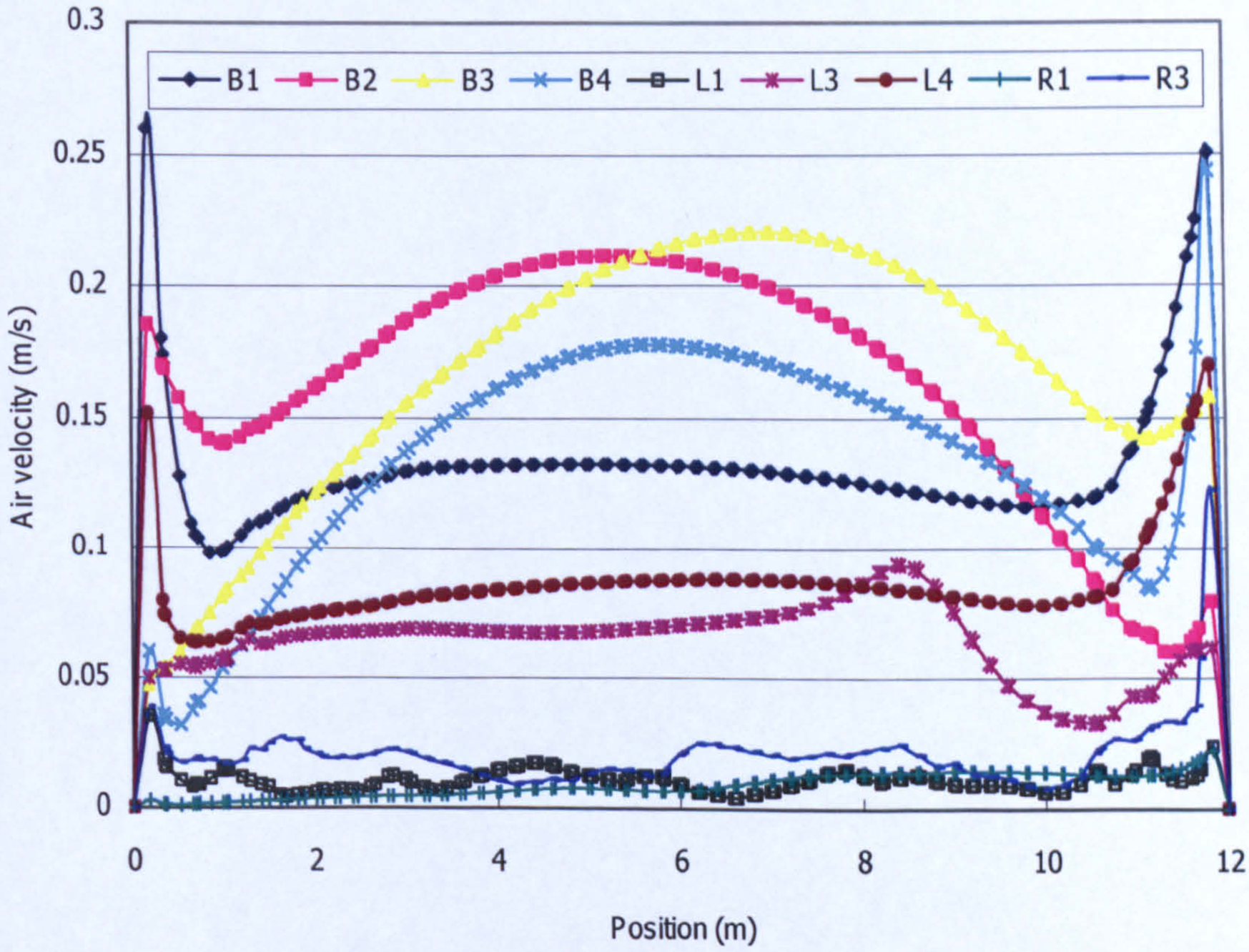

Figure 6.15: Air velocity distributions of the mixing buoyancy-driven natural ventilation for different heat source locations

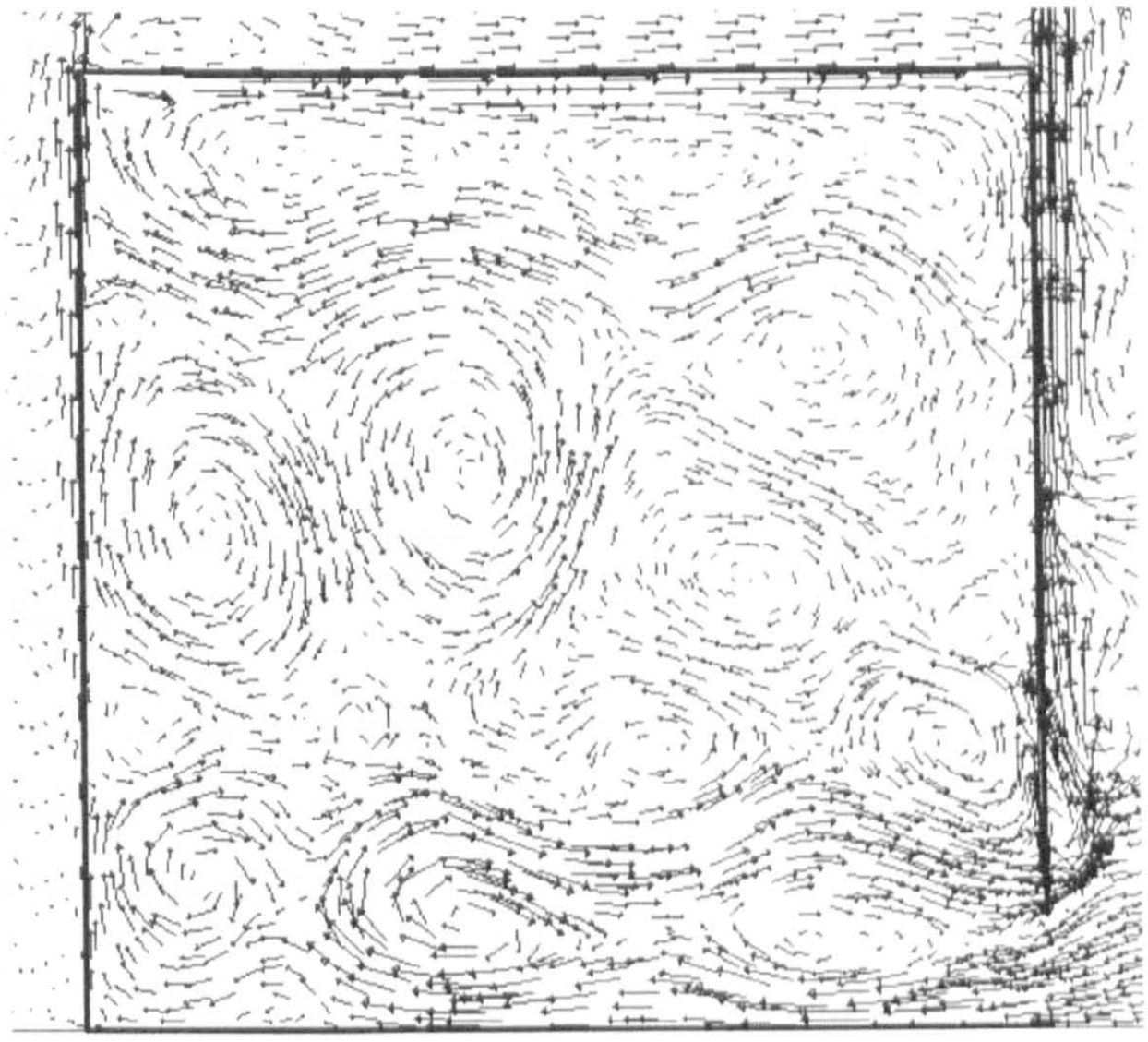

(a) airflow field of the space

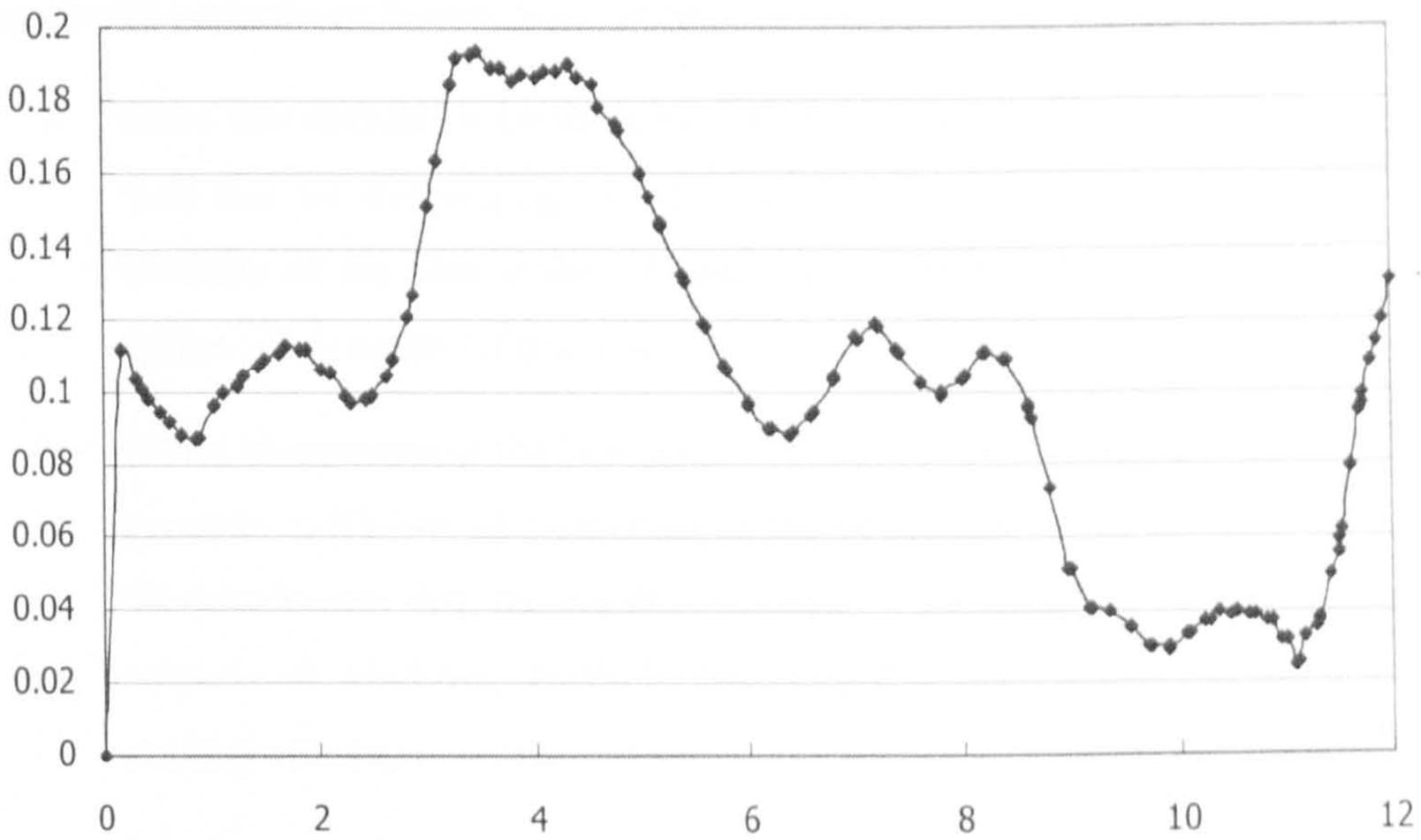

(b) air velocity distribution at the occupants' level

Figure 6.16: Airflow pattern and velocity distribution at the occupants' level of the mixing buoyancy-driven natural ventilation when the opening is located at the occupants' level and the heat source is located at L1

By summarising the above studies, several key points can be obtained with regard to the effects of the heat source on the ventilation performance of the mixing buoyancy-driven natural ventilation:

- The vertical temperature stratification always exists for mixing type buoyancy-

driven natural ventilation, even when the heat source is located at the bottom of the space, which results in a much lower airflow rate compared to displacement ventilation.

- Two different airflow patterns can be distinguished for the internal air movement of the mixing type buoyancy-driven ventilation, and they have very significant impacts on the airflow rate. The flow pattern is determined by the location of the heat source: the heat source located beneath the opening can result in a very low airflow rate.
- In spite of the low airflow rate, mixing type ventilation can create strong air movement for the occupants' level if either the opening or the heat source or both are located at the bottom of the space.

6.2.4 Design guidance and discussions

Having separately investigated the effects of the heat source on the two flow regimes of buoyancy-driven natural ventilation, some general design guidelines can be obtained as follows:

- Since the ventilation performance of the displacement ventilation is much better than that of the mixing ventilation if both have the same opening area and intensity of the heat source, displacement ventilation should always be the first option for designers if possible;
- Either an opening or the heat source should be located near the ground in order to generate sufficient air velocities at the occupants' level for both flow regimes; this also means that, the bottom openings of the atrium to the outside, such as the entrance or windows, should be encouraged to open during the warm weather for cooling effects;
- It is better to locate the heat source on the opposite wall of the outlet opening as this reduces the heat accumulated around the outlet consuming more energy from the source for the heat transfer;
- The heat source should not be placed too close to the lower opening to avoid low air velocities at the occupants' level due to direct heating of the air coming into the space;
- The building roof should be the last option to be used as the heat source, since not only does it have a very low efficiency, it also causes very high temperature for the upper area of the building which may lead to overheating problems for the occupants in adjacent parts.

It should be note that, although designers cannot directly locate the heat source for passive strategies, the results obtained above regarding to the effects of heat sources can be used to help designers with the selection and location of the materials for building surfaces in order to incorporate buoyancy-driven natural ventilation for the cooling of the space. Two issues are the main concerns for this purpose: the thermal comfort of the occupants' level and the efficiency of the heat source. Thus, on one hand, the lower occupants' level should not be irradiated directly by the sun in order to avoid too high MRT and hence overheating of the space. On the other hand, the heat source should be located at the lower part of the building to enhance its efficiency. Considering these two issues and also the conditions obtained earlier, the optimised locations of the heat source for each flow regime can be illustrated as Figure 6.17.

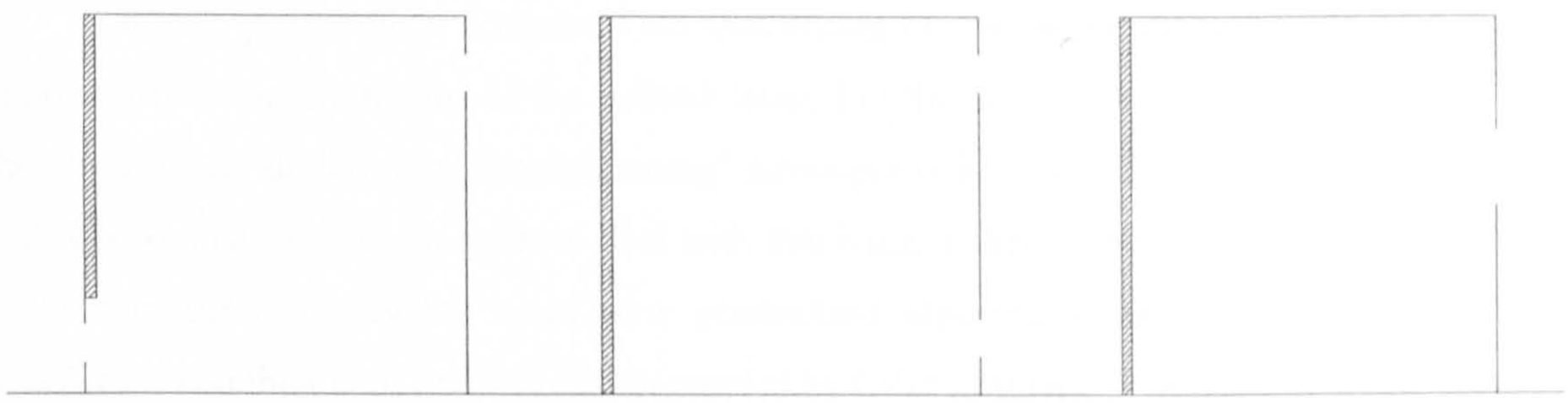

Figure 6.17: Optimised locations for the heat source for different flow regimes of buoyancy-driven natural ventilation (shaded areas are the locations of the heat sources)

Lightweight materials that can be easily heated with significant increase of its temperature, such as timber and metal should be placed at these areas for creating the heat source. Then the location of the transparent materials can be determined according to the position of the sun to allow the sunshine to penetrate into the space and heat the lightweight materials. Shading should be provided to prevent the sun from directly irradiating the occupants, and thermal mass can be used at the bottom to reduce the temperature fluctuation at the occupants' level and also avoid the unnecessary heat loss/gain. In addition, the material of the roof should either be reusing thermal mass or transparent: lightweight materials should be generally avoided from thermal comfort point of view because this may accumulate large amount of energy at the upper area of the space.

Nevertheless, it should be noted that the above decisions are made for immediate cooling effects, but in the long run, the thermal effects of these materials will certainly interact with each other, which may affect the thermal environment at the occupants' level and alter the suggestions above. This issue is far beyond this research since thermal simulation has to be used for this purpose and will it be addressed in future work.

6.3 Impacts of large openings

The previous section is primarily concerned with the ventilation performance of the atrium space itself whilst this section sets out to study the use of atrium space as the buffer zone to aid the ventilation of the adjacent spaces. It has been demonstrated in Chapter One that, one of the most important factors for this purpose is the neutral level, which should be higher than the uppermost opening in order to "suck" the air from adjacent buildings so that the high temperature air from the atrium building will not get in the adjacent building causing overheating problems. This section is in particular interested in the neutral level of displacement ventilation, since the neutral plane will certainly intersect with the opening for mixing type ventilation.

It was proposed in Chapter Two that enlarging the upper opening will be a feasible approach to raise the height of the neutral level, but this would incur bi-directional flow and thus violate the underlying "small-opening" assumption for the prediction of the neutral level and related airflow rate. In order to deal with this issue, a theoretical analysis is performed first in Section 6.3.1 to develop some new generalised algorithms that can be used for "large openings", and then their applicability is studied by CFD simulations in Section 6.3.2.

6.3.1 Theoretical analysis

Consider the simple prototype illustrated in Figure 6.18. This model in fact is the same as that used for the displacement buoyancy-driven natural ventilation study in Section 2.1.1. It is a building with two openings, and the openings sizes and the distance between the openings can be seen in the figure. The indoor and outdoor air temperature are both regarded as uniformly distributed and they are T_i and T_o respectively. For summer cases, T_i is usually higher than T_o. The neutral level is defined as the distance between the neutral plane and the lower edge of the inlet. Only 2D situation is considered here but the result will also be extended to 3D later.

Chapter Two has introduced the conventional algorithms for the conditions where there are only small openings, i.e. the pressure over the opening is uniformly distributed, and the neutral level for this circumstance can be calculated as:

$$h_n = \frac{\gamma^2}{1+\gamma^2} h \tag{2.13}$$

where γ is the opening ratio and is calculated by $\gamma = C_{Du} A_u / C_{Dl} A_l$. Thus, the neutral plane will vary between zero and the distance between the openings, h, with the variation of the size of the upper opening and this process is monotonic. However, this will never become practical because the neutral plane may intersect with one opening when it becomes very close to the

upper or lower extreme, and the openings cannot be assumed as small openings any more as bi-directional flow is incurred. As a consequence an approach that can be used to deal with non-uniform pressure distribution is needed for this situation.

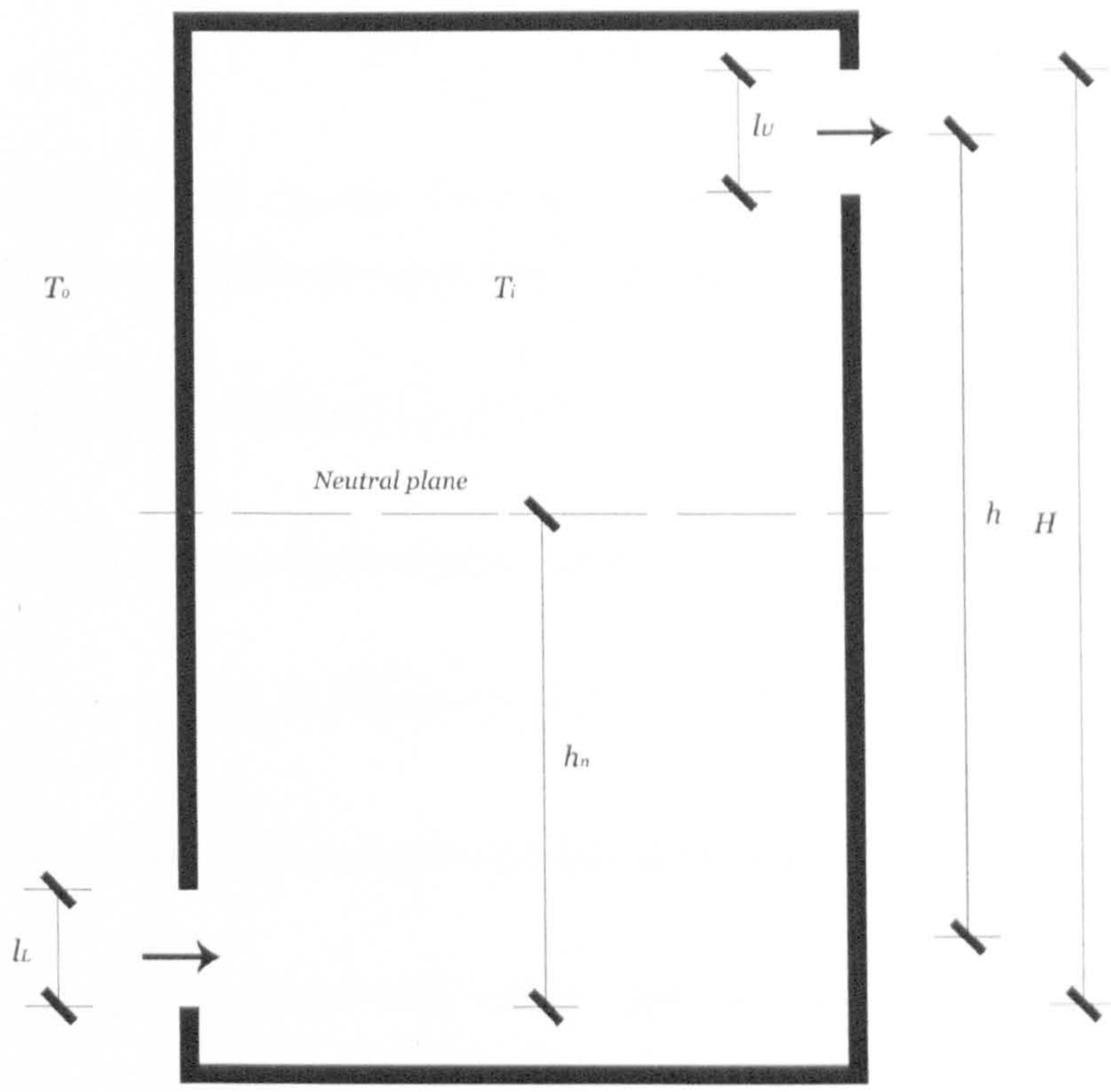

Figure 6.18: Schematic illustration of the simple physical model considered in this study ($T_i > T_o$)

It can be seen from the above analysis that, there are three flow modes in terms of the position of the neutral level as follows:

(I) when the neutral height is at intermediate level of the lower opening;

(II) when the neutral height has no intersection with openings;

(III) when the neutral height is at the intermediate level of the higher opening.

The pressure distributions inside and outside the building for these three modes can be illustrated in Figure 6.19. As the pressure distributions for large openings cannot be assumed as constant, a multiple element approach has to be adopted, i.e. an opening is divided into small parallel sub-openings and flow rates are calculated individually for each sub-opening, thus the overall airflow rate can be considered as the integration of that of all the small elements. Detailed description of the basic theory for the analysis of large openings is introduced by Li et al. (2000).

Define that H is overall vertical distance from the lower edge of the lower opening to the upper edge of the higher opening and D is the depth of the room. For flow mode (I), the pressure difference at the higher opening can be obtained by:

$$\Delta p = \int_{H-h_n-l_U}^{H-h_n} \Delta\rho g dh \tag{6.1}$$

where l is the height of the opening. Thus by substituting Equation (6.1) into (2.6) and by integration, the airflow rate through upper opening can be calculated as:

$$q_U = \frac{2}{3}(C_D D\sqrt{2\Delta\rho g/\rho_o})\left[(H-h_n)^{\frac{3}{2}} - (H-h_n-l_U)^{\frac{3}{2}}\right] \tag{6.2}$$

Likewise, the airflow rate through the lower opening can be expressed as:

$$q_L = \frac{2}{3}(C_D D\sqrt{2\Delta\rho g/\rho_o})\left[h_n^{\frac{3}{2}} - (l_L-h_n)^{\frac{3}{2}}\right] \tag{6.3}$$

Thus, by equating the airflow rates through higher and lower openings, we have:

$$h_n^{\frac{3}{2}} - (l_L-h_n)^{\frac{3}{2}} = (H-h_n)^{\frac{3}{2}} - (H-h_n-l_U)^{\frac{3}{2}} \tag{6.4}$$

The airflow rate of the building can be expressed by the airflow rate below the neutral level, i.e. the incoming flow rate:

$$q = \frac{2}{3}(C_D D\sqrt{2\Delta\rho g/\rho_o})h_n^{\frac{3}{2}} \tag{6.5}$$

Considering the energy balance equation for the building and boussinesq approximation, we have (also seen as Equation 2.24):

$$E = \rho C_p q \Delta T \tag{6.6}$$

$$\Delta\rho/\rho_o = \Delta T/T_o \tag{6.7}$$

By substituting Equations (6.6) and (6.7) into (6.5), it can be obtained that:

$$q = (\frac{2}{3}C_D D)^{\frac{2}{3}}(\frac{2gE}{T_o C_p \rho})^{\frac{1}{3}} h_n \tag{6.8}$$

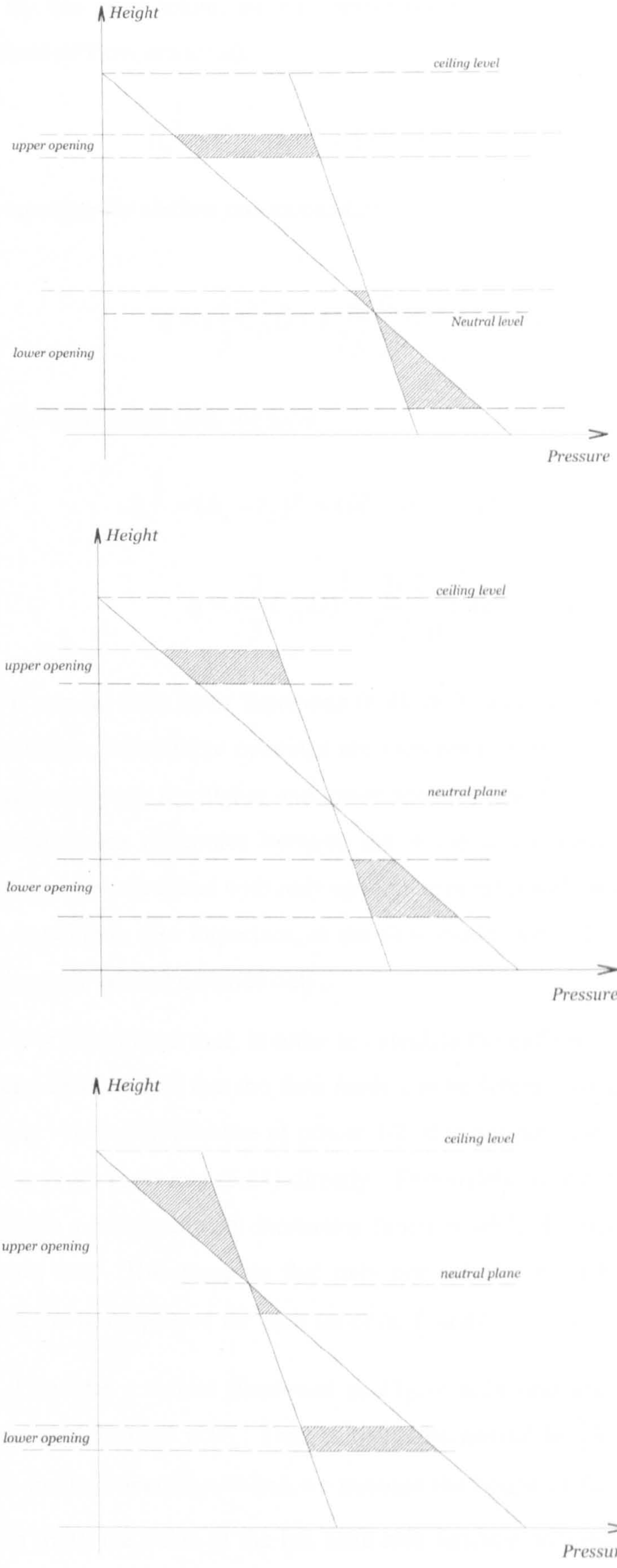

(a) flow mode (I)

(b) flow mode (II)

(c) flow mode (III)

Figure 6.19: The pressure distributions of the three flow modes of buoyancy-driven natural ventilation with large openings

By the same token, we can obtain the following equation for the prediction of the neutral level of flow mode (II):

$$h_n^{\frac{3}{2}} - (h_n - l_L)^{\frac{3}{2}} = (H - h_n)^{\frac{3}{2}} - (H - h_n - l_U)^{\frac{3}{2}} \tag{6.9}$$

and the equation for airflow rate calculation:

$$q = (\frac{2}{3} C_D D)^{\frac{2}{3}} (\frac{2gE}{T_o C_p \rho})^{\frac{1}{3}} \left[h_n^{\frac{3}{2}} - (h_n - l_L)^{\frac{3}{2}} \right]^{\frac{2}{3}} \tag{6.10}$$

For flow mode (III), we have:

$$h_n^{\frac{3}{2}} - (h_n - l_L)^{\frac{3}{2}} = (H - h_n)^{\frac{3}{2}} - (h_n + l_U - H)^{\frac{3}{2}} \tag{6.11}$$

$$q = (\frac{2}{3} C_D D)^{\frac{2}{3}} (\frac{2gE}{T_o C_p \rho})^{\frac{1}{3}} (H - h_n) \tag{6.12}$$

It can be seen from Equations (6.4), (6.9) and (6.11) that, similar to the situation of small openings, when large openings are incorporated, the neutral level is still determined by the distance between the higher and lower openings and the opening sizes, and it is not related to the temperature difference between the inside and outside air. Nevertheless, the neutral height cannot be calculated with only opening area ratio and overall height. The absolute height of each opening is also important, as the flow mode cannot be decided with the opening ratio and the overall vertical distance only.

It is also shown that, in order to calculate the airflow rate, it is necessary to make clear the neutral level first so that the flow mode can be determined and the appropriate equation can be chosen. However, because of power 3/2, it is not possible to obtain analytical solution for Equations (6.4), (6.9) and (6.11) directly. Fortunately, it is noted that, for all of them, the left hand side is a monotonically increasing function while the right hand side is a monotonically decreasing one. This suggests that only one solution exist for each of them and numerical approach can be employed for each set of H, l_L and l_U.

Consider a model illustrated as Figure 6.18 and start with the situation when both openings are of equal size. Thus initially the neutral height is exactly at the middle level between the two openings. When we increase the height of the lower opening l_L, according to Equation (6.9), the value of the left hand side function will increase, and thus the neutral level will reduce in order to increase the value of function of the right hand side to keep the equation. The further increase of the lower opening area will further result in the reduction of the neutral height and at some point the neutral plane will meet with the upper edge of the lower opening. At this stage, $h_n = l_L$, and equations (6.9) and (6.4) become the same.

If we continue to increase the lower opening area, the equation (6.4) applies and by the similar analysis of above, it could be inferred that the neutral height will increase because the sign of l_L in Equation (6.4) is opposite to that of Equation (6.9). This means that, if the height of the higher opening l_U and the overall vertical distance H are fixed, there is a lowest position for neutral plane and this occurs when the neutral plane is of the same height with the upper edge of the lower opening. For the same reason, when the lower opening size and the overall vertical distance are fixed, there would be a highest level of neutral plane if we increase the area of the upper opening.

More interestingly, if we substitute l_U with l_L and l_L with l_U for all equations regarding to the neutral height, it can be easily find that the new solution for these equations have the following relationship with original solution:

$$h_n = H - h_{n,original} \tag{6.13}$$

This means that, by exchanging the location of the two openings, the flow mode will not be changed. Comparison between Equations (6.8) and (6.12) suggests that the airflow rate will not be altered as well by doing so. The whole airflow is just 'rotated' an angle of 180°.

It can also be seen that, with the increase of lower opening area, the air flow rate will increase as well, no matter which mode the airflow is. Nevertheless, different flow modes have different increasing rate, as Equation (6.8), (6.10) and (6.12) differ from each other. Equations (6.8) and (6.12) show that, when bi-directional flows occur, the airflow rate will be linearly proportional to the height of the neutral level. It is also worth mentioning that, when large openings are incorporated, the airflow rate may not be influenced very significantly by smaller openings, as bi-directional flow can occur and some part of the larger opening can complement the area shortage of the small opening.

6.3.2 CFD simulation

The basic geometry and settings used in CFD simulations has the same configuration of the one employed for buoyancy-driven cross ventilation, as illustrated in Figure 6.2. The heat source is located on the floor to produce a uniform air temperature distribution in the space. Two groups of simulations are performed. In the first group, the size of the higher opening is fixed as 1m and the area of the lower changes from 1m to 7m. In the other group the size of lower opening is fixed as 1m and the area of the higher opening changes from1m to 7m.

Figures 6.20 to 6.23 show the airflow fields of the buoyancy-driven natural ventilation with different openings sizes. It can be seen that, when the opening area ratio is big/small enough, bi-directional flow occurs for larger openings (See Figures 6.21 and 6.23), although the flow patterns inside the buildings for them are quite different. When the opening area ratio is at

intermediate level then the airflow will be the displacement ventilation (See Figures 6.20 and 6.22). These results confirm the theoretical analysis on the general flow regime performed earlier.

Figure 6.24 presents quantitatively the height of neutral plane and the airflow rate predicted by both theoretical calculation with formulae developed earlier and CFD simulation when the height of the upper opening is 1m and the size of the lower opening varies. It is shown that good agreement between the two methods has been achieved with only minor discrepancies for the prediction of the neutral plane when lower opening area is small. The flow mode for these situations is simple displacement ventilation without bi-directional flow for both openings, i.e. flow mode (II). The discrepancy is partly attributed to the fact there is no simple and direct approach to determine the neutral height for CFD simulation. In this study, this is done by comparing the vertical static pressure distribution of the central line in the building and that of far field. However, as the flow has significant impacts on the pressure distributions, the result is very sensitive to the selection of the lines for comparison. This problem does not exist for bi-directional flow modes (I) and (III), because for these circumstances the neutral level can be easily determined by the position on the opening where the x-velocity is zero. But still, general trend of the change of the height of neutral plane with the increase of the lower opening size is clearly shown.

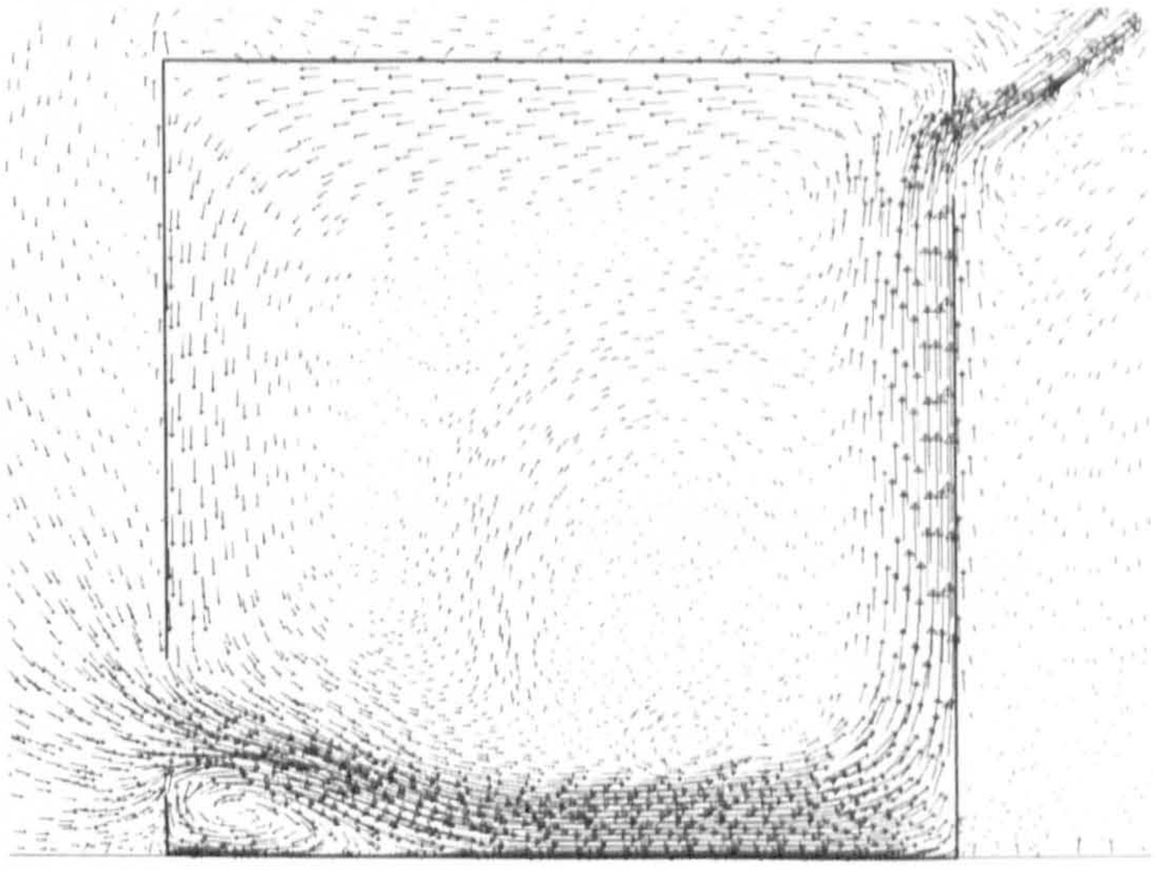

Figure 6.20: Airflow field of buoyancy-driven natural ventilation when the lower opening height is 2m and the upper opening is 1m

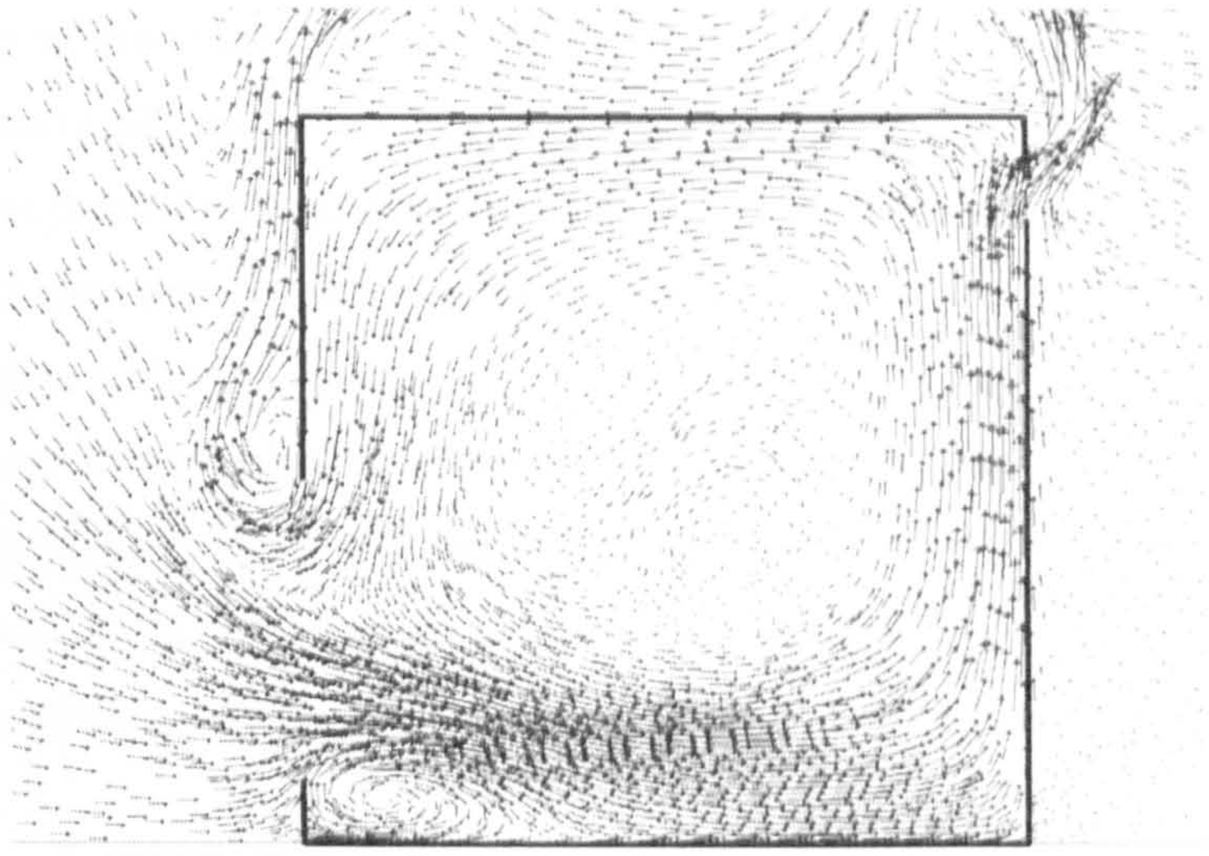

Figure 6.21: Airflow field of buoyancy-driven natural ventilation when the lower opening height is 5m and the upper opening is 1m

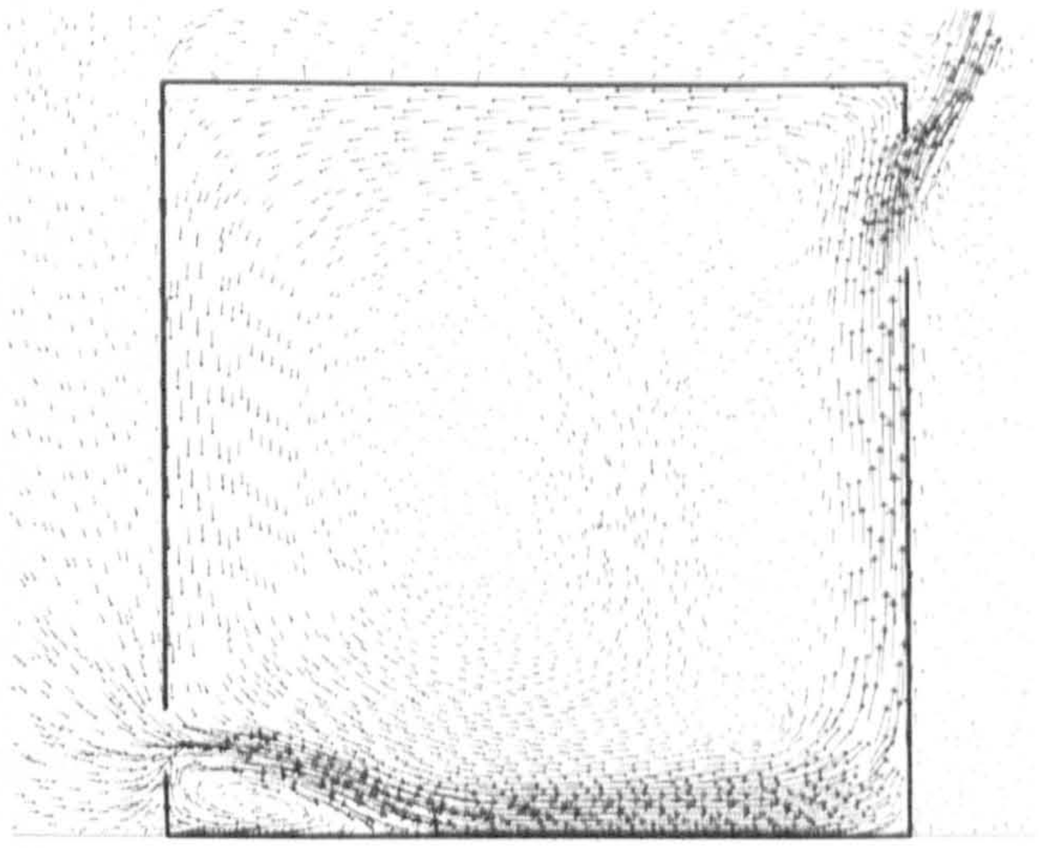

Figure 6.22: Airflow field of buoyancy-driven natural ventilation when the lower opening height is 1m and the upper opening is 2m

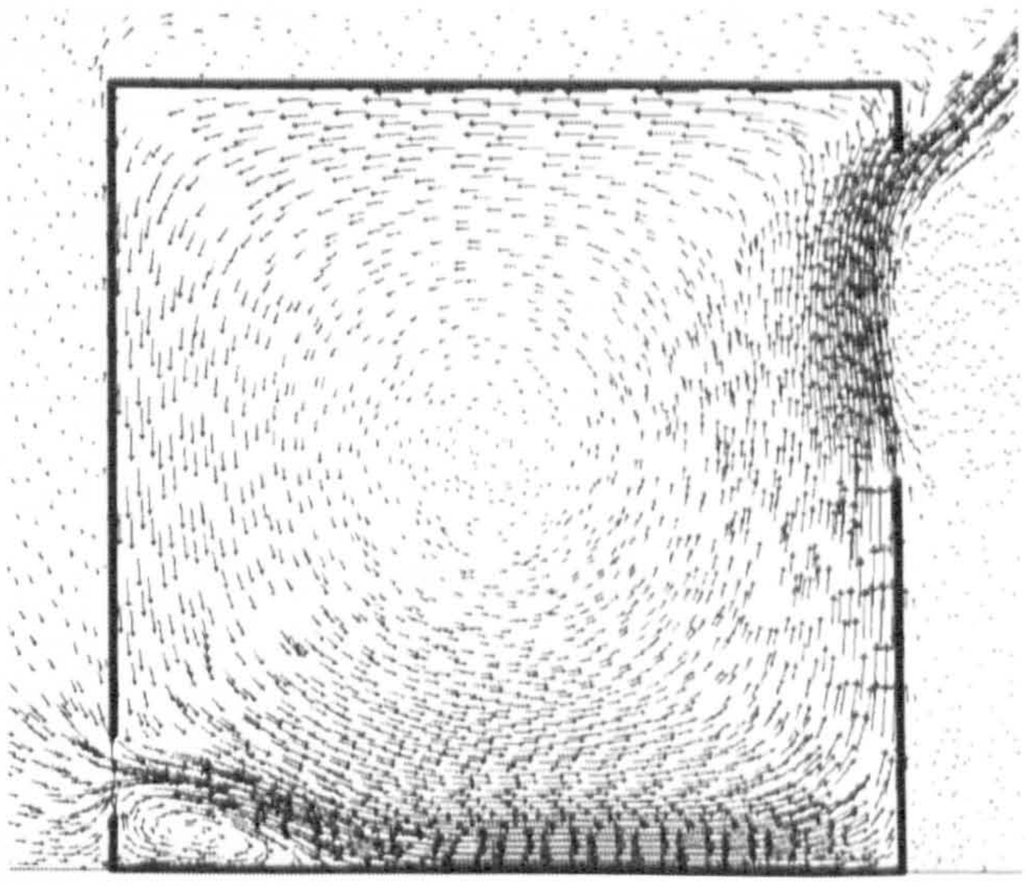

Figure 6.23: Airflow field of buoyancy-driven natural ventilation when the lower opening height is 1m and the upper opening is 5m

It can also be seen that, with the increase of the lower opening area from 1m, the neutral level reduces dramatically and when the opening area increases to about 2.5m, the neutral level reaches to the lowest level and the flow mode switches from (II) to (I). Then the height of the neutral plane increases almost linearly with the increase of the area of the lower opening. The airflow rate continuously increases with the increase of the lower opening area and the increasing rate keeps nearly constant all the time, even when the opening area ratio is very small (1/10). This confirms the results of former theoretical analysis and suggests that increasing the area of larger openings may be still an efficient way to enhance the airflow rate because the flow mode has changed and the part of the larger opening can assist the small opening.

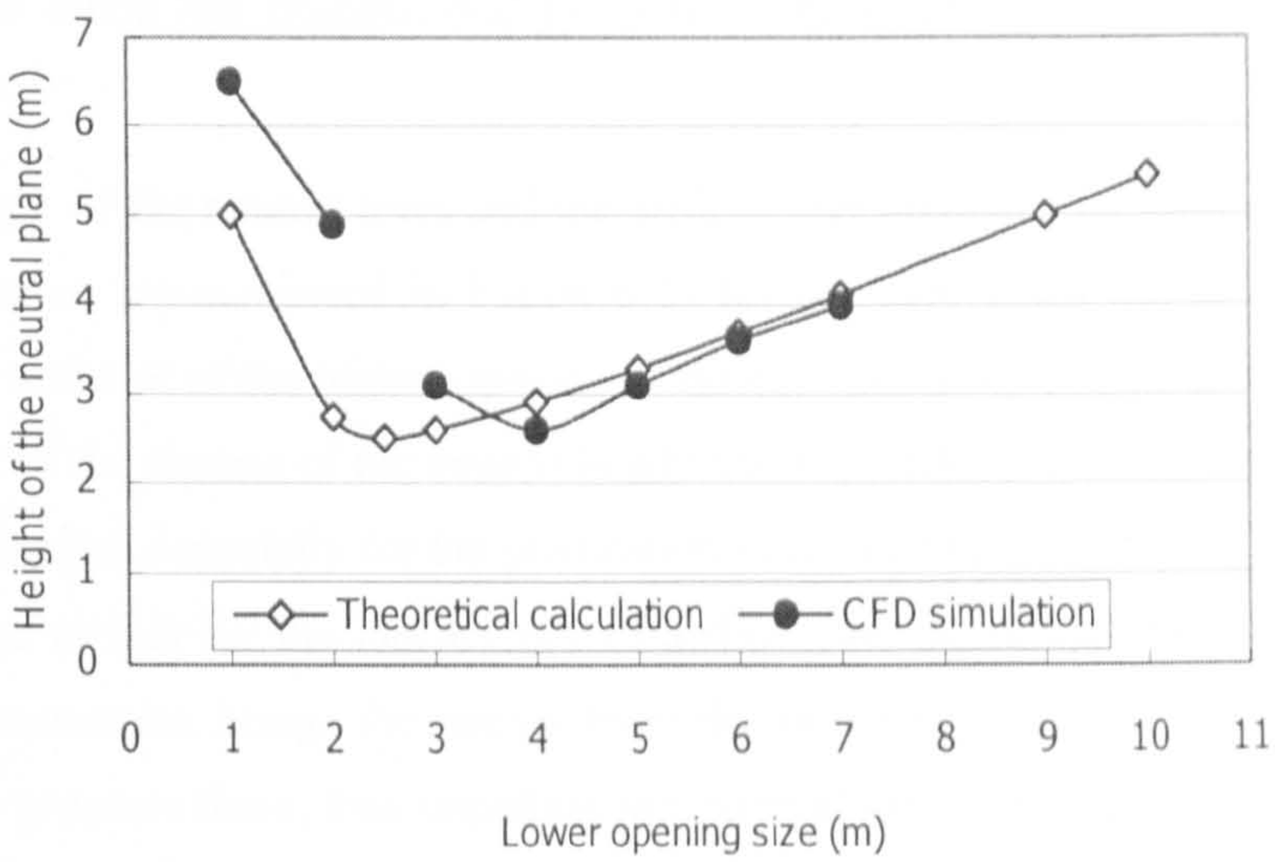

(a)The neutral level predicted by theoretical analysis and CFD simulation

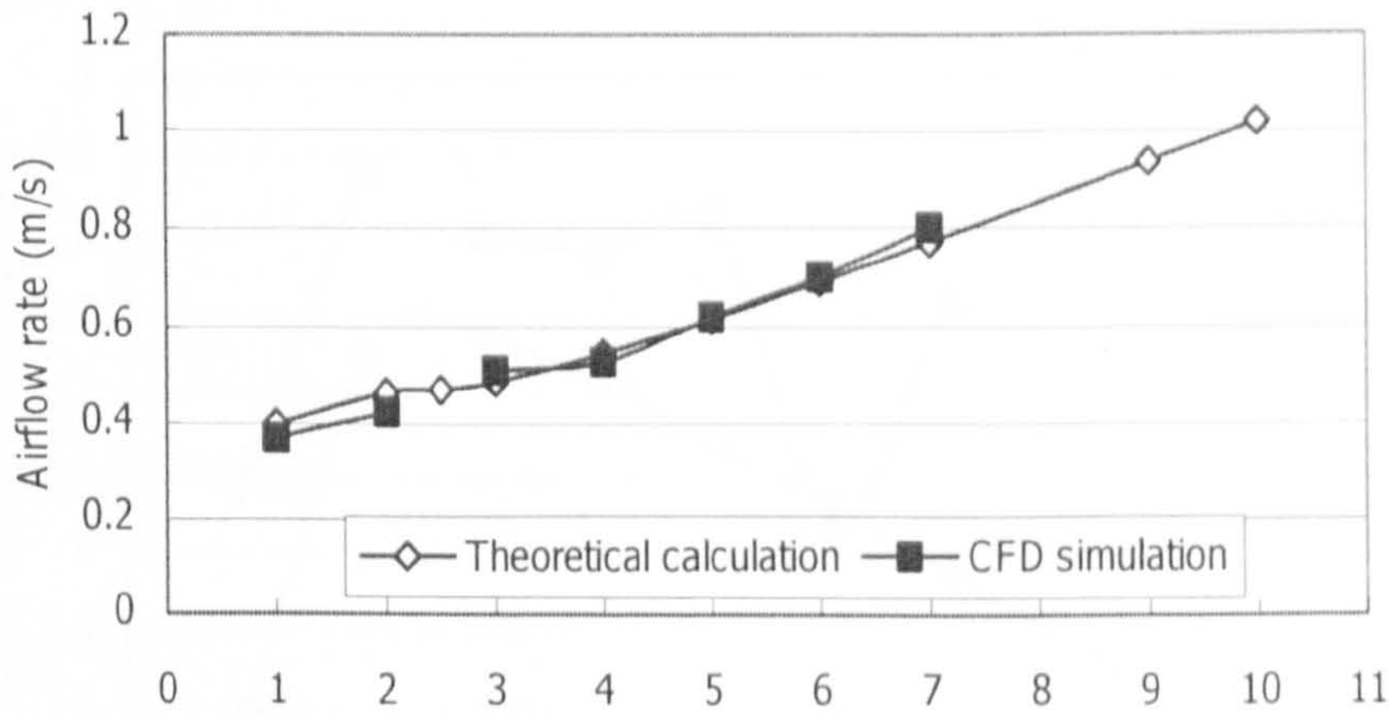

(b)The airflow rate predicted by theoretical analysis and CFD simulation

Figure 6.24: Comparison of the neutral level and airflow rate obtained from theoretical calculation and CFD simulation for buoyancy-driven natural ventilation when the size of the lower opening varies (the height of the upper opening is constantly 1m)

The above figure also shows that, with the increase of the lower opening height from 1m, the neutral level reduces dramatically and when the opening area increases to about 2.5m, the neutral level reaches to the lowest level and the flow mode switches from (II) to (I). Then the height of the neutral plane increases almost linearly with the increase of the area of the lower opening. The airflow rate continuously increases with the increase of the lower opening area and the increasing rate keeps nearly constant all the time, even when the opening area ratio is very small (1/10). This confirms the results of former theoretical analysis and suggests that increasing the area of larger openings may be still an efficient way to enhance the airflow rate because the flow mode has changed and the part of the larger opening can assist the small opening.

The height of the neutral level and the airflow rate predicted by theoretical calculation and CFD simulation are compared in Figure 6.25 for the case when the height of the lower opening is fixed and that of the higher opening is varied. Generally speaking, agreement on the qualitative trend of the change of the neutral height and the airflow rate is shown but significant discrepancy does exist, especially for the predication of the neutral height. The reason for this is actually the same as that for the inefficiency of airflow rate the mixing ventilation introduced earlier: the air movement brings the energy from the heat source to the upper opening which increases the air pressure there, thus impeding the external air coming into the building. Please see Figure 6.23 for the flow pattern in the space, and the temperature distributions of two spaces with large openings (one with lower large opening and the other with upper large opening) are illustrated in Figure 6.26.

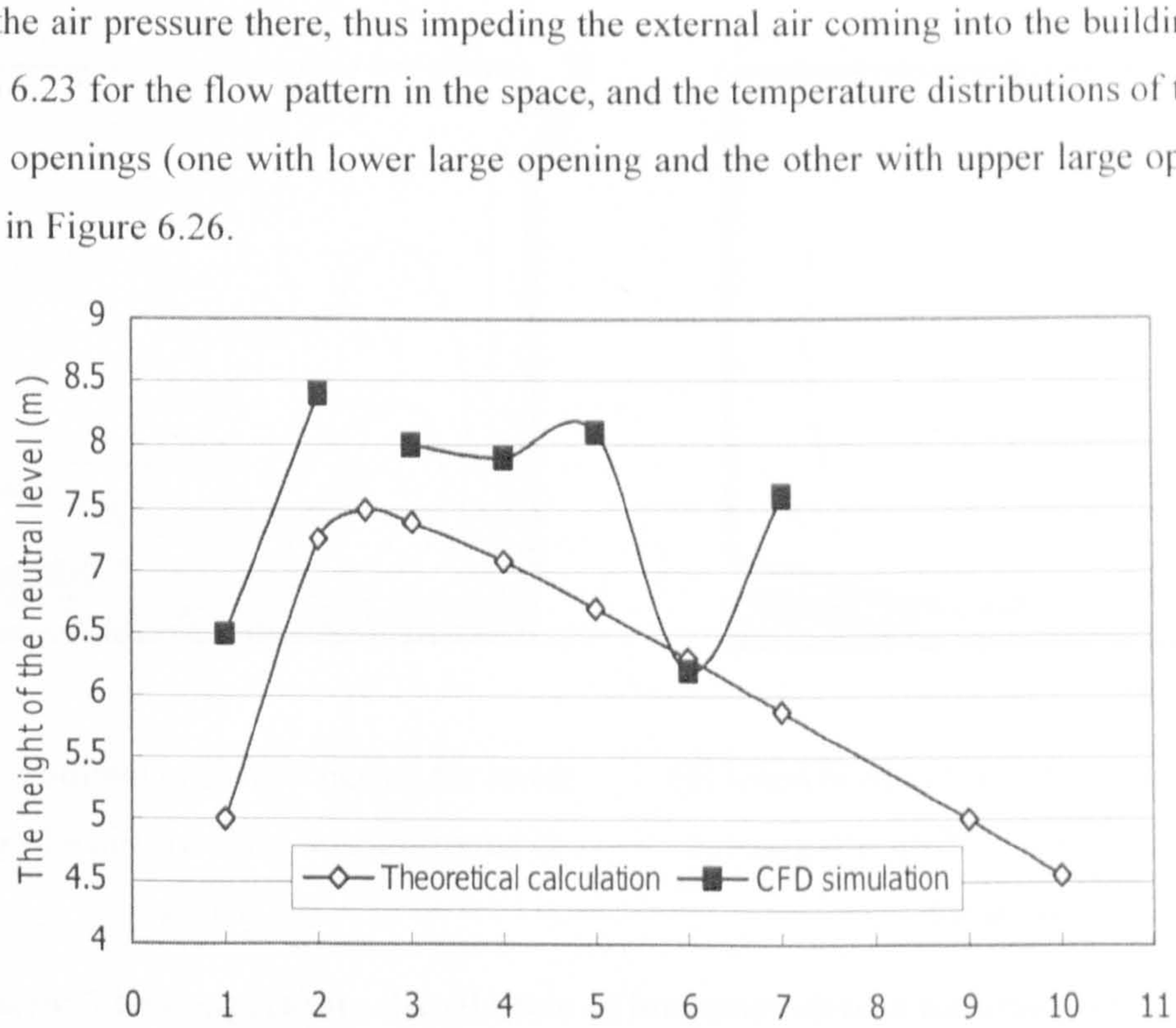

(a) The neutral level predicted by theoretical analysis and CFD simulation

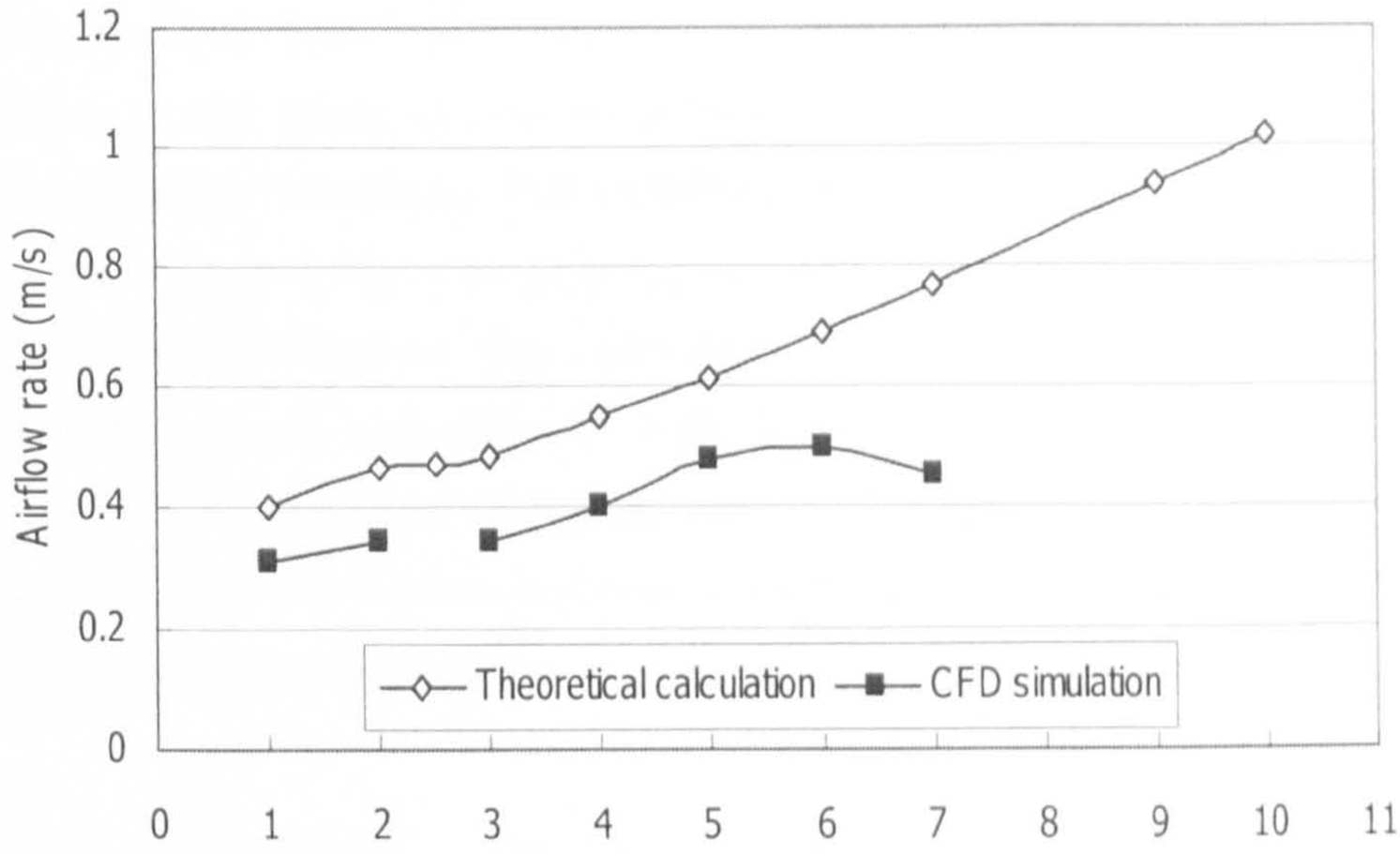

(b) The airflow rate predicted by theoretical analysis and CFD simulation

Figure 6.25: Comparison of the neutral level and airflow rate obtained from theoretical calculation and CFD simulation for buoyancy-driven natural ventilation when the size of the upper opening varies (the height of the lower opening is constantly 1m)

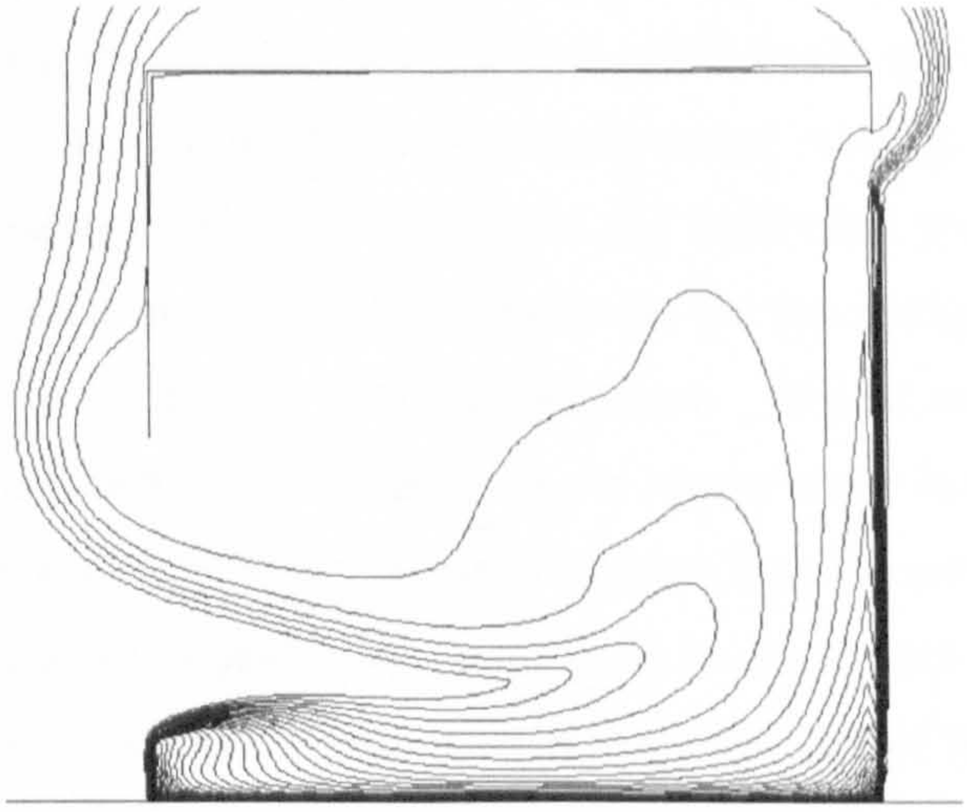

(a) when bi-directional flow occurs for lower opening (the airflow field was illustrated in Figure 6.19)

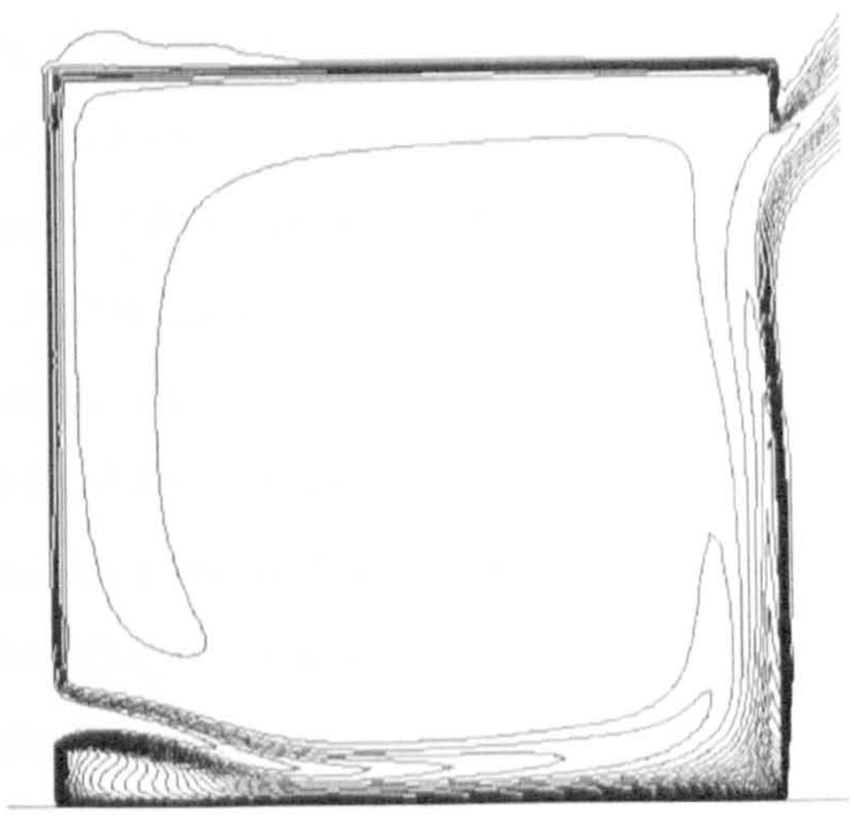

(b) when bi-directional flow occurs for upper opening (the airflow field was illustrated in Figure 6.21)

Figure 6.26: The temperature distribution of buoyancy-driven natural ventilation with large openings (lines are the temperature contours)

It can be seen from Figure 6.26 that, when bi-directional flow occurs for the lower opening, there is still strong vertical temperature stratification there since the temperature contours are generally horizontal. This means that the temperature of the air coming into the building is relatively cool whilst the air going out of the building from this opening is warmer. However, when the bi-directional flow takes place at the upper opening, the air temperature at the large opening is nearly uniformly distributed in the vertical direction, and it is warmer than either the inside or the outside of the building, as seen in Figure 6.26b. As a consequence, this layer of air with high temperature becomes a barrier between the building and the external environment reducing the air exchange.

6.3.3 Conclusions and design guidance

In order to predict the neutral level and the airflow rate for the space where bi-directional airflow occurs, a number of new generalised algorithms have been developed based on a multiple element approach which divides a large opening into small parallel sub-openings and hence enables the treatment of the openings with non-uniform pressure distribution. In fact, these new algorithms can take the place of those conventional ones because all openings can be regarded as "large openings", no matter whether bi-directional flow occurs.

CFD simulation was performed in order to verify the theoretical analysis, and good agreement was achieved both qualitatively and quantitatively for flow mode (I), i.e. when the neutral level intersects with the lower opening. However, there are significant discrepancies between the CFD simulation and theoretical prediction for flow mode (III), although to some extent they show the same trend for the change of airflow rate and neutral height when the upper opening increases/decreases. This is attributed to the airflow pattern and associated temperature distribution in the space: when bi-directional flow occurs for the upper opening (flow mode III), the energy emitted from the source will be convected to the opening forming a barrier impeding the outside air to come into the building, which significantly reduces the airflow rate and causes erroneous prediction of the neutral level.

With regard to the control of the neutral level, it should be noted that, for a fixed lower opening, there is a highest neutral level which is achieved when it is at the same height with the lower edge of upper opening. Further increase of the opening size will lead to the reduction of the neutral level. In addition, when bi-directional flow occurs, the ventilation efficiency will be significantly reduced. Fortunately this problem can be mitigated if considered from a 3D perspective.

In essence, from the pressure point view, the basic strategy to raise the height of the neutral plane is to increase/decrease the pressure difference between the inside and outside at the upper/lower opening but increasing the pressure difference at the upper opening will be

more favourable since reducing the pressure difference will cause the reduction of airflow rate. As introduced earlier in the subsection of the theoretical analysis, for a large opening, the edge farther sway from neutral level (the lower edge of the lower opening and the upper edge of the upper opening) can generate larger pressure difference. This means that, in order to increase the pressure difference on the two sides of an opening, it will be better to increase the depth of an opening than to increase its height: as seen in Figure 6.27, the opening on the left building will lead to a higher pressure difference and hence higher neutral level and airflow rate than the one on the right building will if they have the same size and the upper edges are on the same level. As a consequence, it can be concluded that, horizontal/vertical strip window can be used for the upper/lower opening in order to increase the neutral level from a 3D point of view and this will not result in the bi-directional flow reducing the efficiency of the openings. Nevertheless, it should be noted that, the underlying assumption for this conclusion is that the inside air temperature is uniformly distributed. When temperature stratification exists, the vertical air pressure is distributed as shown in Figure 6.6, and it can be seen that the shape of the lower opening cannot change the pressure difference, because the air temperature below the temperature interface is generally identical.

Further to this, it can be easily inferred that openings on the roof level, i.e. openable skylights, can generate the largest pressure difference, since this is the farthest level available from the neutral plane, and this means that, openable skylights can help to increase the neutral level for displacement ventilation. The area of the opening will be the only crucial factor affecting the neutral level and its shape will be of little significance because the static pressure difference is the same everywhere at this level.

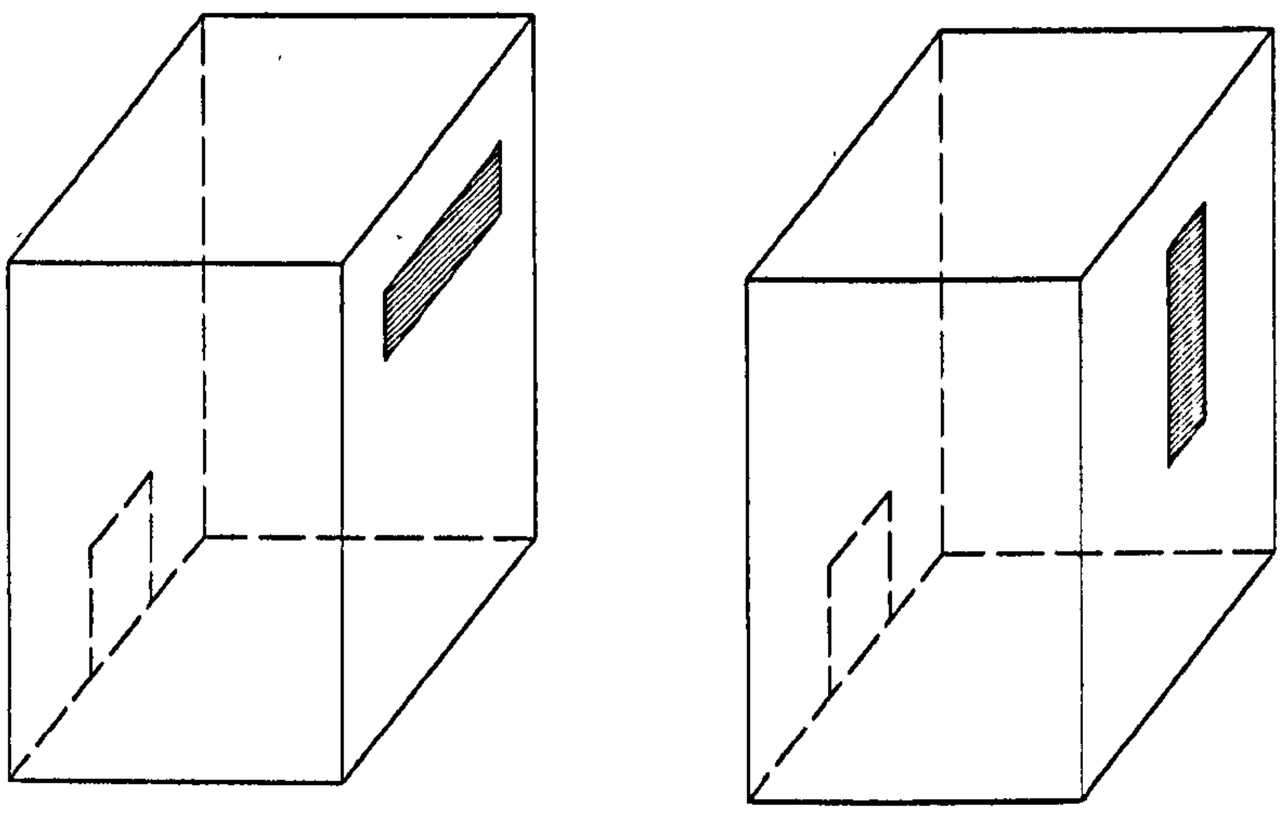

Figure 6.27: Increasing the height (left) or increasing the depth (right) of an opening for improving the performance of the buoyancy-driven natural ventilation

The above descriptions are focused on the control of the neutral level for displacement ventilation. With respect to mixing type ventilation, the neutral level will be certainly in-between the lower and upper edges of the opening as bi-directional flow always occurs. Thus, in order to raise the height of the neutral plane, the opening has to be placed very high, and it has been suggested before that, under this condition the heat source has to be located very near to the bottom to achieve acceptable air velocities at the occupants' level, which may bring on the risk of thermal discomfort because of overheating at the bottom.

6.4 Summary

This chapter studied the buoyancy-driven natural ventilation for the use of two purposes: (I) to generate cooling effects for itself; (II) to aid the ventilation of adjacent buildings. For the first purpose, the impacts of the heat sources were studied in terms of their effects on the airflow rate and air velocity distribution at the occupants' level. The optimised heat source location for different flow regimes was identified, and guidelines for the location of heat source and associated building materials were developed. It was also shown that displacement ventilation is a very efficient approach to reduce the air temperature at the occupants' level down to the outside level. As regards the second purpose, it was suggested that neutral level is the most important factor and some new algorithms for the prediction of the airflow rate and neutral level when the neutral level intersects with openings were developed and then compared with CFD simulations. It was found that neutral level is mostly affected by geometrical parameters including the openings' locations and sizes and the distance between the openings when the indoor and outdoor temperature profiles has been determined, and the new algorithms can be very effective when bi-directional flow occurs for lower opening but less effective when bi-directional flow takes place for upper opening. Design guidelines for the increase of the height of the neutral level were also provided.

7

COMBINED WIND AND BUOYANCY DRIVEN NATURAL VENTILATION IN ATRIUM SPACES

7.1 Introduction

Chapters Five and Six have studied the ventilation performance of atrium spaces when either wind forces or buoyancy forces dominate the air movement. However, the two forces can often work together in similar scale in reality, such as when the oncoming wind is not strong and the solar radiation is very intensive, and in this situation the airflow is driven by the combination of them.

The review in Chapter Two has introduced that previous studies on the airflows driven by combined forces have suggested that an interesting characteristic for this type of flow is that multiple stable solutions may exist for the same set of physical and geometrical parameters depending on different initial conditions when the two forces oppose with each other. It was also noticed that most research was focused on the investigation of the situations where two forces entirely oppose each other based on analytical methods. The prototype employed in this group of research was illustrated in Figure 7.1b (repeated from Figure 2.16). This chapter sets out to extend the research of this area to another common situation: when the two forces partly assist each other whilst partly oppose each other. In other words, in this situation, the stronger force cannot entirely overwhelm the weaker one and even assist the weaker force. The study in this part is particularly interested in two fundamental prototypes, both of which can be regarded as based on the prototypes of Figure 7.1:

(1) The first prototype has the same wind direction and building configuration as the model where two forces assist each other (see Figure 7.1a) and the only difference is the location of the heat source: previous studies presume that the heat source is at the bottom but here it is on the vertical wall, which is quite common for atrium spaces. This is schematically illustrated in Figure 7.2a.

(2) The second prototype is similar to the original opposed model of Figure 7.1b and the only difference is that large openings are incorporated, as shown in Figure 7.2b.

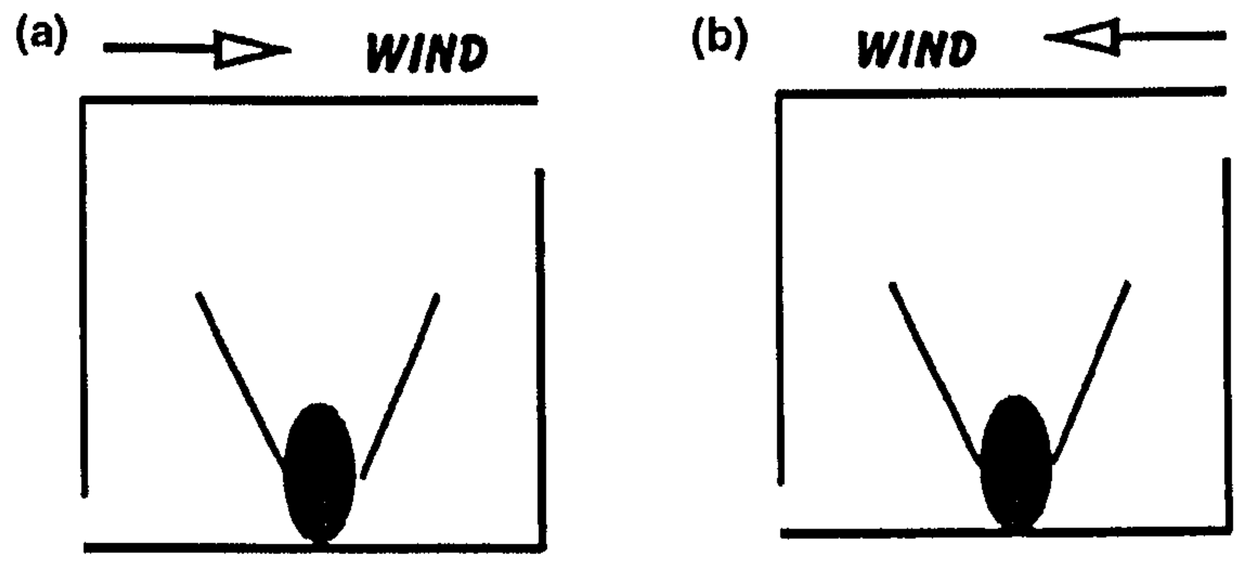

Figure 7.1: A schematic diagram illustrating the conditions for which wind and buoyancy forces assist (a) or oppose (b) each other (Heiselberg et al. 2004) (repeated from Figure 2.16)

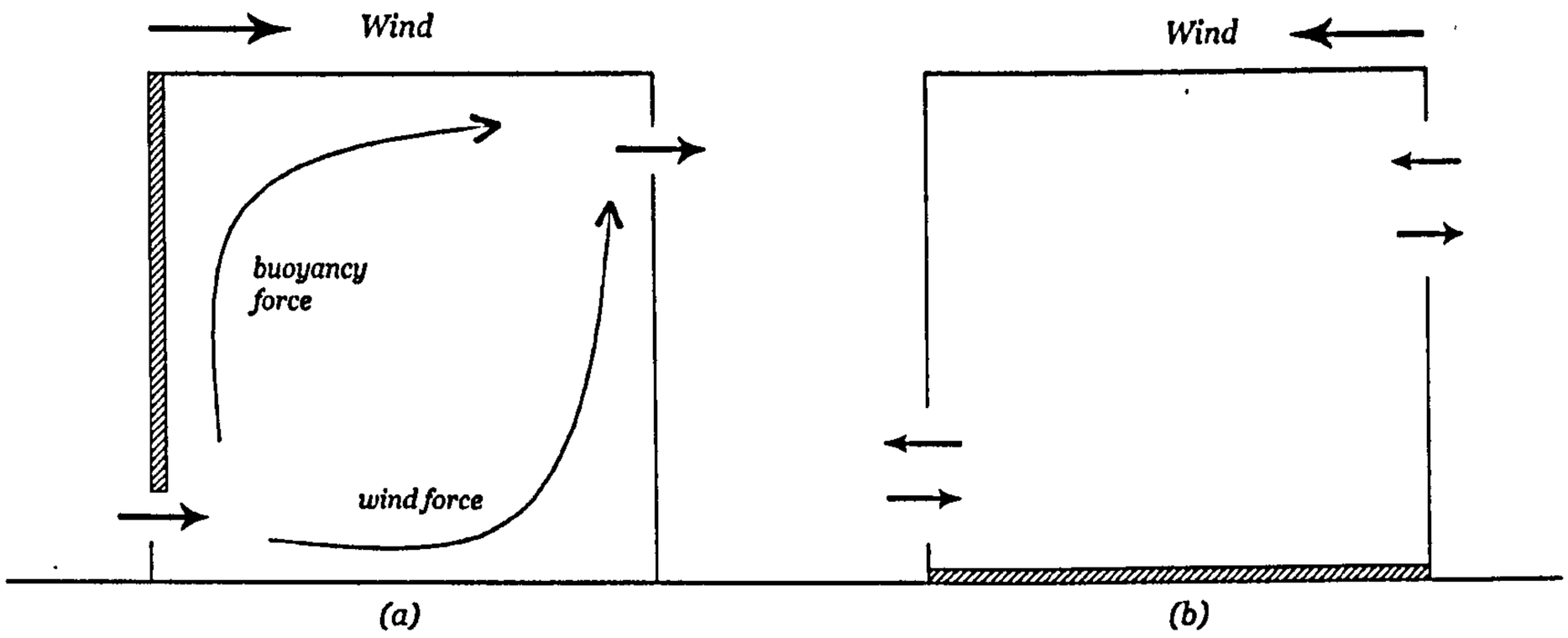

Figure 7.2: Two prototypes employed for the study of combined buoyancy and wind driven natural ventilation (shaded areas are the locations of the heat sources)

It can be seen that, for prototype (I), although the bulk flows of the wind forces and buoyancy forces assist each other at the openings, the internal airflow patterns driven by the two forces are opposite. As regards prototype (II), the flow direction will become opposite when the wind forces overwhelms the buoyancy forces, and this transition process will result in bi-

directional flows due to the large opening incorporated (this will be introduced in detail later). As a result the external wind forces will assist the part of flow at each opening that has the same direction of the wind direction whilst oppose the other part of flow.

This research will first study whether multiple solutions still exist for each prototype, and then investigate whether this has any significant influence on the evaluation of the cooling effects at the occupants' level, based on which relevant design guidelines can be developed. Section 7.2 will focus on the first prototype shown in Figure 7.2a, and the second one is dealt with in Section 7.3. A preliminary analysis is performed for each section, and then CFD simulations are carried out, followed by the discussions and design guidelines drawn at the end of each section based on the investigations. A summary of the chapter is finally provided in Section 7.4.

7.2 Combined ventilation with small openings only (prototype 1)

7.2.1 Preliminary analysis

Let us consider the ventilation performance of the space when only one force dominates the air movement. Figure 7.3 illustrates the airflow patterns driven by buoyancy forces and wind forces respectively. It is shown that, although the bulk flows driven by the two forces have the same direction and they should assist each other, but the detailed directions of the internal air movement of the two forces differ for some areas: for instance, the air near the top of the building moves towards the right for the buoyancy-driven flow due to the heat source located on the left hand side wall whilst it moves towards the left for the wind-driven flow as the recirculation induced by the main flow going across the building.

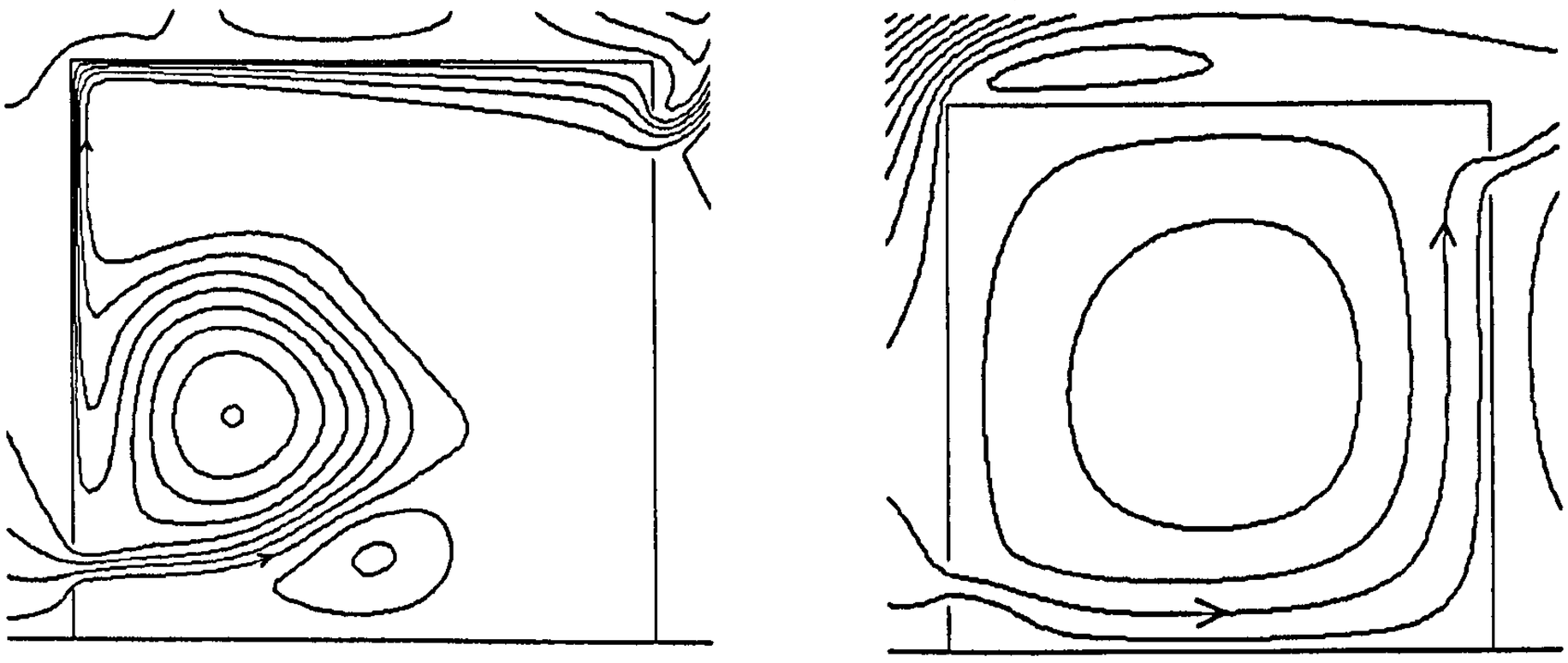

(a) buoyancy forces dominate the airflow (b) wind forces dominate the airflow

Figure 7.3: The airflow patterns of combined ventilation prototype (I) driven by buoyancy forces (a) and wind forces (b) (direction arrows are shown for this figure but will be omitted for the rest figures of this section as they are the same)

The above description suggests that, when the two forces work together, there must be competition between the two forces near the top of the space to determine the airflow direction and hence which direction the energy is convected. As a consequence, from the flow pattern point of view, the two forces oppose each other for prototype (I), although the two forces should assist each other from the bulk flow point of view.

It should be noted that, for this circumstance, the competition is not between the main flows driven by the two forces, but between the recirculation of one flow and the main flow of the other. As has been introduced in Chapter Five, the recirculation airflow is usually much weaker than the main flow, and this actually means that, it will be very difficult for one force to dominate the flow, because in order to do so, the recirculation driven by this force should still be much stronger than the main flow of the other force. As a result this force has to be much stronger than the other, which requires either extremely intensive solar radiation or extremely high wind speed, and this will not be common in reality. Recall that Chapter Two has introduced that multiple solutions can exist when the two forces are opposite and one cannot overwhelm the other. Thus the above analysis may suggest that prototype (I) will have a much broader range of environmental conditions for the existence of solution multiplicity due to the difficulty of one force to entirely defeat the other.

It can also be seen from Figure 7.3 that, the two flow patterns generated by two forces have very different air velocity distributions at the occupants' level and hence different cooling effects. As introduced in the previous chapter, the cooling effects are poor when the heat source is located very close to the lower opening, but the wind-driven airflow can provide sufficient air movement for occupants. Thus it will be very interesting to know how these two forces together influence the thermal comfort at the occupants' level, and in particular, whether different solutions have different performance to generate cooling effects if multiple solutions do exist.

It is also worth mentioning that, as the counteractive force for one driving force (either buoyancy forces or wind forces) is the recirculation of another force, it will be not possible to implement the study with conventional analytical methods such as those introduced in Section 2.5.3, because there are still no widely recognised ways to express the recirculation airflows in an analytical form. Instead CFD simulations will be carried out to test the points made above.

7.2.2 CFD simulations

The building configurations employed in the CFD simulations are the same as that for the buoyancy-driven natural ventilation. It is a 2-D rectangular building 12m wide and 12m high. Both of the openings have a height of 1m and are located 1m away from the nearest

horizontal surfaces. The heat source on the left vertical wall constantly emits a heat flux of 200W/m^2, which generates an airflow rate of around 0.3m/s if no wind presents. The wind profile used is the same of that for the wind-induced ventilation study and the reference velocity changes from 0.1m/s to 0.9m/s with a step of 0.1m/s. Thus both of the conditions where wind forces are stronger and those where buoyancy forces are stronger can be simulated. The two-way approach introduced in Chapter Three (Section 3.4.5) is also used here to test the existence of the multiple solutions, i.e. the initial conditions which emphasise the wind forces will be used for the first group of simulations (which means that the airflow is dominated by wind forces at the preceding moment), and the second group tries to find the solutions emphasising the buoyancy forces (which means that buoyancy forces dominate the airflow at the preceding moment).

• *Existence of multiple solutions*

Figure 7.4 illustrates the flow patterns for the first group of simulations and it is shown that, for all wind speeds, the wind can generally dominate the air movement at the bottom of the space: the wind blows deeply into the space and then moves upwards along the inside wall. This is very similar to the wind-dominated situation as shown in Figure 7.3b. However, the airflow near the upper area of the building is quite different depending on the wind speed. When the wind speed is lower than 0.2m/s, the wind forces are much weaker than the buoyancy forces and the air going upwards near the right vertical wall driven by the wind will be overwhelmed by the airflow induced by the buoyancy forces. As a result the outgoing flow across the upper opening is entirely from the buoyancy flow, as seen in Figure 7.4(a) and (b). The airflow of the wind forces can only lead to recirculations at the bottom of the space, which impedes the outside air to come into the building.

When the wind speed is higher than 0.3m/s, wind forces can overcome the recirculation of the buoyancy-driven flow and thus part of the outgoing flow is driven by the airflow from the wind. The proportion of the airflow from the wind out of the overall outgoing flow increases with the increase of the wind speed, as seen in Figure 7.4(c) to (i). The flow pattern becomes stable when the wind speed exceeds 0.6m/s. It is also observed that, the recirculation of the wind cannot overwhelm the buoyancy forces and therefore the air near the heat source located on the left vertical wall always moves upwards.

Figure 7.5 shows the airflow patterns of the CFD simulations for the second group which emphasises the buoyancy forces. It can be seen that, all flow patterns obtained by the simulations of this group are fundamentally different from the corresponding flow patterns with the same wind velocity and the airflow at the bottom of the space is controlled by buoyancy forces: the air coming into the building will be directly sucked up without going deeply into the

space and all the flow patterns show significant similarity with the flow pattern of buoyancy-dominated situation as shown in Figure 7.3a.

It can also be observed that, the simulations for the second group have a number of characteristics identified earlier for the first group of simulations: for instance, when the wind velocity is low, the outgoing air is only driven by buoyancy forces, and wind forces will gradually dominate the outgoing air when the wind speed increases.

(a) v = 0.1m/s (b) v = 0.2m/s (c) v = 0.3m/s

(d) v = 0.4m/s (e) v = 0.5m/s (f) v = 0.6m/s

(g) v = 0.7m/s (h) v = 0.8m/s (i) v = 0.9m/s

Figure 7.4: The airflow patterns of combined ventilation prototype (I): when the wind forces are emphasised for the initial conditions settings

space and all the flow patterns show significant similarity with the flow pattern of buoyancy-dominated situation as shown in Figure 7.3a.

It can also be observed that, the simulations for the second group have a number of characteristics identified earlier for the first group of simulations: for instance, when the wind velocity is low, the outgoing air is only driven by buoyancy forces, and wind forces will gradually dominate the outgoing air when the wind speed increases.

(a) v = 0.1m/s (b) v = 0.2m/s (c) v = 0.3m/s

(d) v = 0.4m/s (e) v = 0.5m/s (f) v = 0.6m/s

(g) v = 0.7m/s (h) v = 0.8m/s (i) v = 0.9m/s

Figure 7.4: The airflow patterns of combined ventilation prototype (I): when the wind forces are emphasised for the initial conditions settings

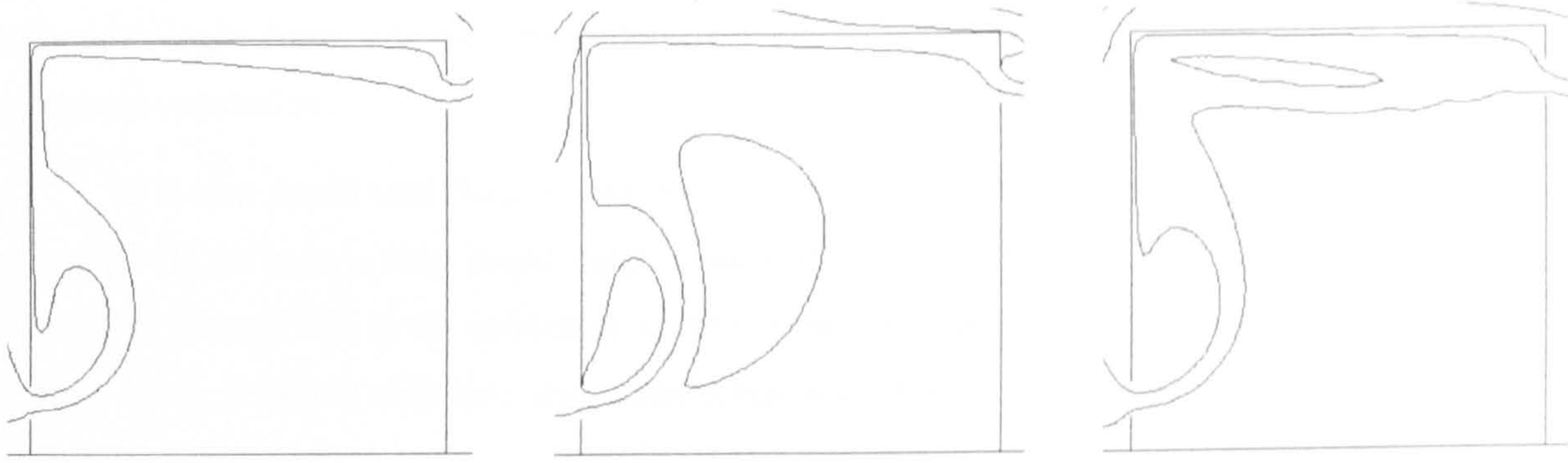

(a) v = 0.1m/s (b) v = 0.2m/s (c) v = 0.3m/s

(d) v = 0.4m/s (e) v = 0.5m/s (f) v = 0.6m/s

(g) v = 0.7m/s (h) v = 0.8m/s (i) v = 0.9m/s

Figure 7.5: The airflow patterns of combined ventilation prototype (I): when the buoyancy forces are emphasised for the initial conditions settings

The above analysis shows that multiple solutions do exist for the prototype (I) of combined ventilation and it is observed that the airflow pattern for the actual solution tends to be similar to that at the preceding moment: if the wind forces are dominant at the preceding moment, the airflow pattern for combined ventilation will be highly associated with that for the wind-dominated situation and if the dominating force at the preceding moment is the buoyancy forces, the airflow pattern for combined ventilation will show great similarity to that for the buoyancy-dominated situation. This result also suggests that, the analysis of the airflow pattern

with one single force will be very helpful for the determination of the flow pattern of the combined ventilation.

It is also found that the environmental conditions for solution multiplicity to occur for prototype (I) do have a very broad range since different flow patterns are found for all wind velocities. (Recall that in the validation studies of the CFD settings for combined ventilation in Section 3.4.5, multiple solutions only exist when wind forces and buoyancy forces are quite similar in scale.)

• *Influence of solution multiplicity on the evaluation of ventilation performance*

Figure 7.6 shows the airflow rates predicted by the two groups of simulations. It can be seen that the CFD simulations with both initial conditions settings predict the same tendency of the airflow rate with the variation of the reference wind velocity, although discrepancies exist at some points (less than 15%), especially between when the reference wind velocity is very high or very low. This is because, when the wind speed is very low, the initial conditions with the emphasis of wind forces will result in the recirculation of the wind-driven flow at the bottom of the space which impedes the air to come into the building, as shown in Figure 7.4(a); when the wind speed becomes very high, the initial conditions with the emphasis of the wind forces will bring more energy out of the building and result in lower air temperature (also see Figure 7.5a) and hence lower airflow rate. Nevertheless, these discrepancies are still generally acceptable at the early design stage for prediction purposes, and this means that, when the bulk flows of the wind forces and buoyancy forces assist each other, the airflow rate can be calculated at this stage regardless of the initial conditions.

However, the CFD simulations with different initial conditions show very different performance on providing cooling effects for the occupants' at the bottom of the space. As has been suggested earlier, the air movement near the ground level of the building tends to be similar to that at the preceding moment and it has also been made clear in the preliminary analysis that the cooling effects generated by the two single forces are quite different (see Figure 7.3). These descriptions suggest that solution multiplicity of combined ventilation may have significant influence on the evaluation of the thermal comfort at the occupants' level and the effects generated by the related passive strategies.

Figure 7.7 further demonstrates this by comparing the velocity distributions at the occupants' level and the vertical temperature profiles in the space for the two simulations with different initial conditions when reference wind velocity is 0.5m/s. It is shown that, although the vertical temperature profiles are quite similar, the air velocity distributions at the occupants' level are very different.

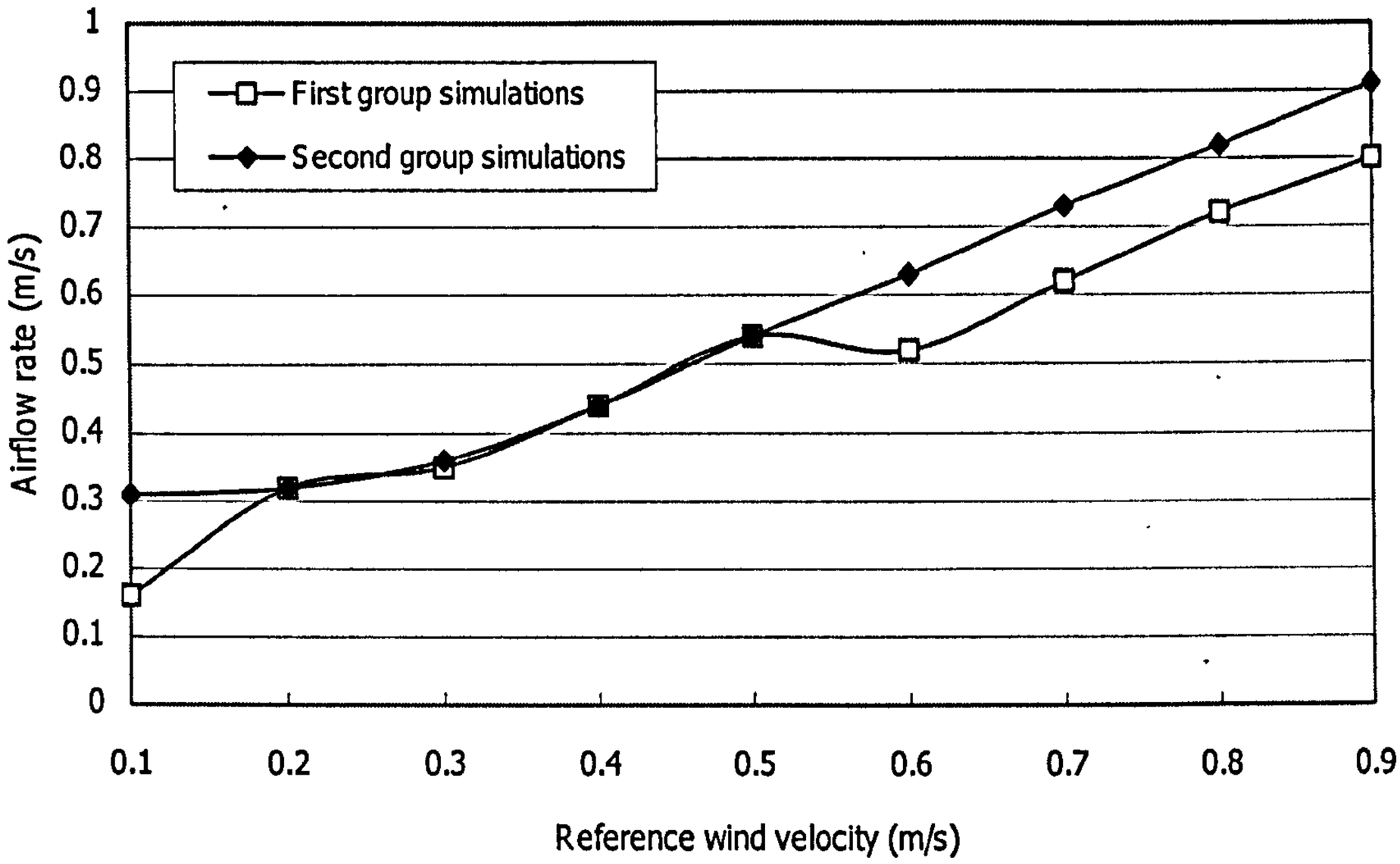

Figure 7.6: Comparison of the airflow rates of combined ventilation prototype (I) predicted from CFD simulations and analytical solutions

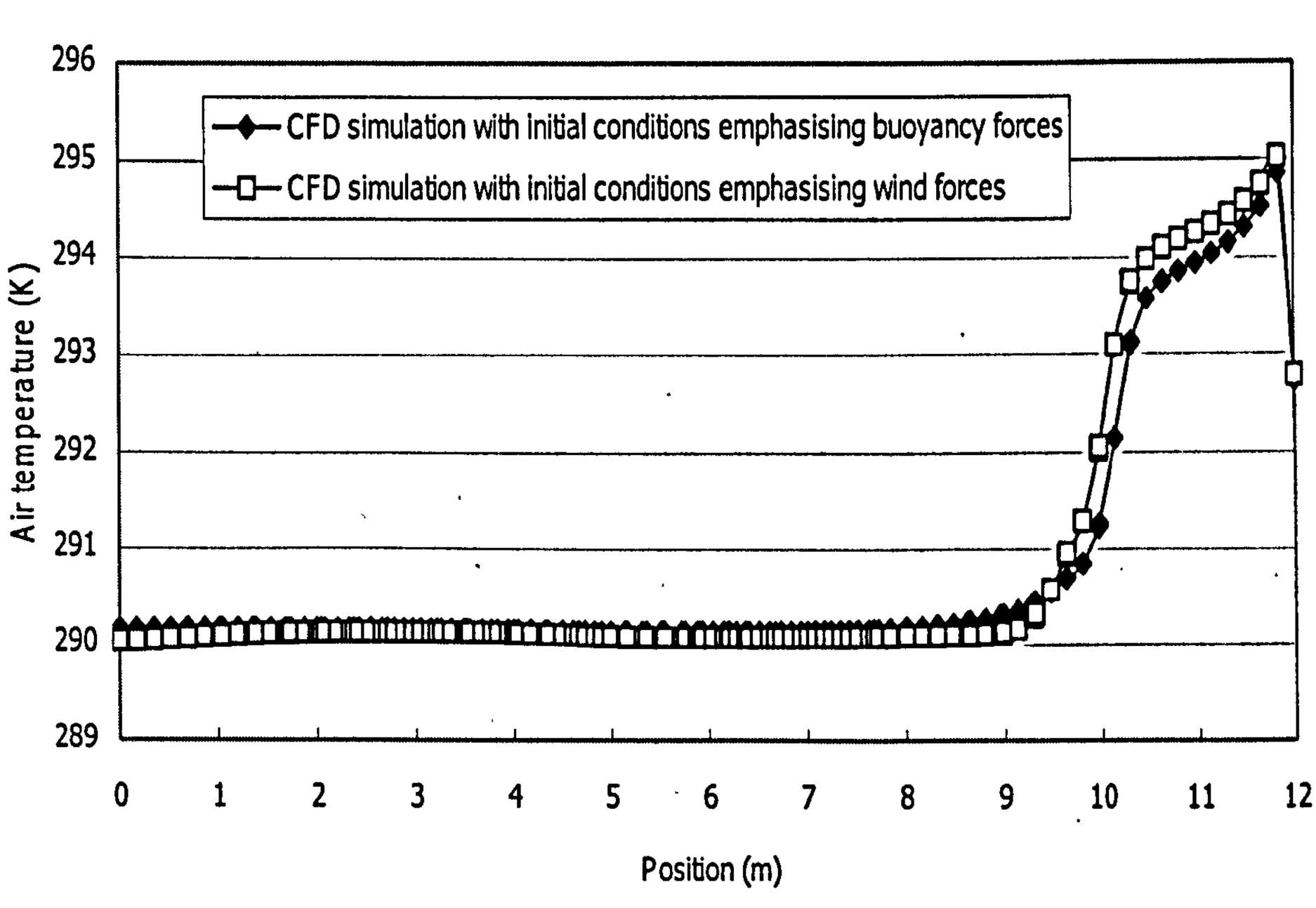

(a) comparison of the vertical temperature profiles

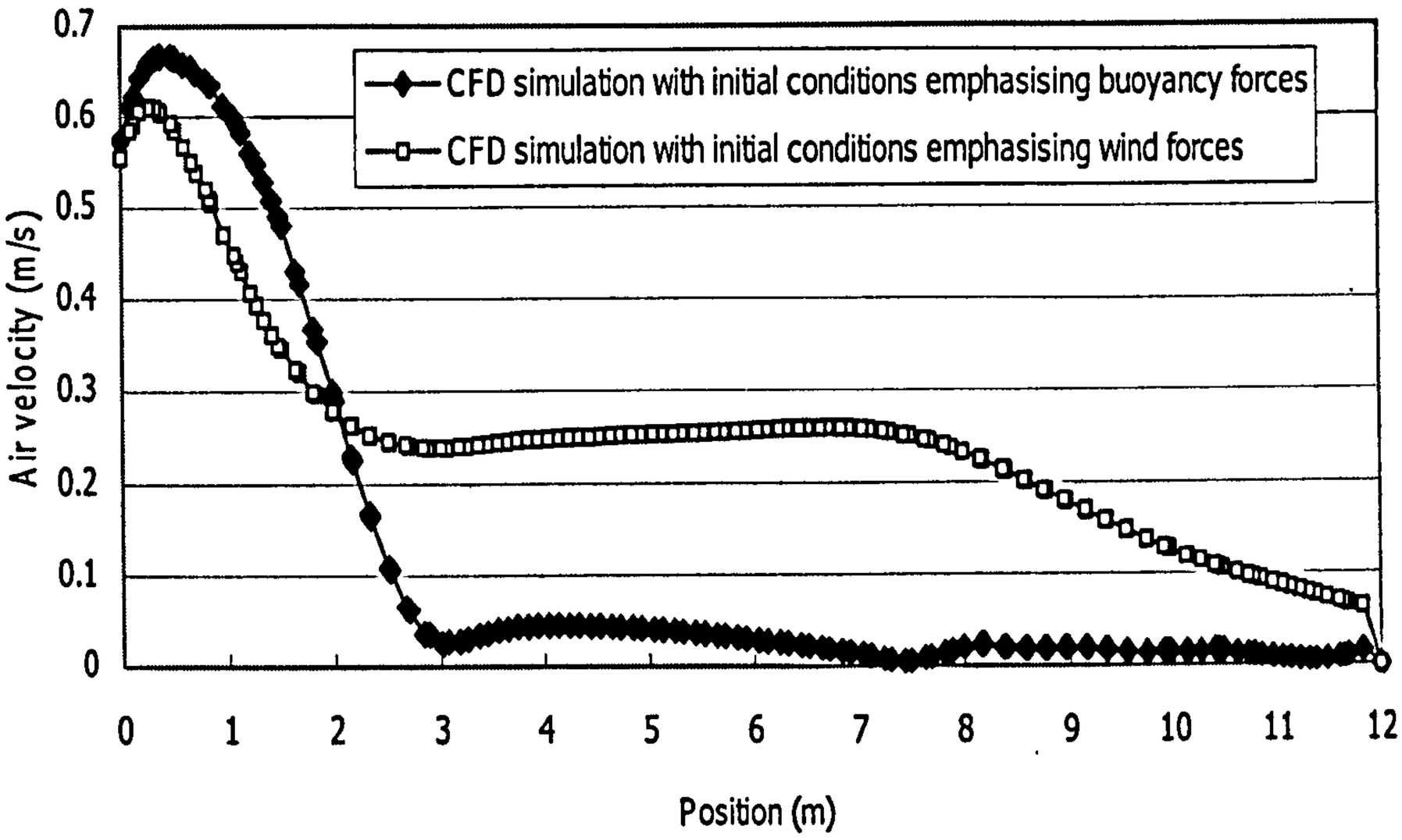

(b) comparison of the air velocity distributions at the occupants' level

Figure 7.7: Comparison of the vertical temperature profiles and velocity distributions at the occupants' level of combined ventilation prototype (I) predicted from CFD simulations with different initial conditions (the reference wind velocity is 0.5m/s)

7.2.3 Discussions and design guidance

The significance of the above investigations can be summarised and discussed as follows. Firstly, in addition to the airflows driven by opposed forces, multiple solutions also exist for assisting flows. In fact, all airflows driven by combined forces are opposed flows in the sense that the driving forces cannot assist each other everywhere in the flow field. It is quite clear that the directions of the momentums driven by the buoyancy forces and wind forces are different: it is upward for the buoyancy force whilst it is along the wind direction (usually not upward) for the wind forces. As a result it is very probable that the flow patterns generated by the single force to oppose each other even if the bulk flows have the same direction. These descriptions actually suggest that solution multiplicity should be a very widely applied characteristic for combined airflows other than a special feature of ventilation with opposed bulk flows (the details of the mechanism of solution multiplicity will be further discussed in the next section). The relationship between the bulk flows of different driving forces cannot be used as the main factor to judge the existence of the multiple solutions.

Secondly, different solutions of a combined ventilation problem may have very different effects on the thermal comfort of the space, which suggests that, to understand the initial conditions for combined ventilation problems is very important for precise evaluation of the ventilation performance. In other words, combined ventilation problems should be

considered in an unsteady context other than in a steady one. It should be noted that, when the bulk flows are assisting, different solutions can produce similar airflow rates but different flow patterns; when the bulk flows are opposing, the airflow rates predicted by different solutions are different. Related to this, it is found that the study of the ventilation performance when the possible single forces are dominate will be very helpful as the flow pattern of one solution is very similar to that when a certain single force controls the flow.

Thirdly, the CFD simulations also suggest that the initial conditions may bring on either positive or negative effects for the ventilation performance, and this means that, effective incorporation of a ventilation strategy also depends on the ventilation performance at the preceding moment. For instance, at a certain moment only buoyancy-driven ventilation is available and it is incorporated. It is also known from forecast that wind will be coming and thus wind-induced ventilation can be used. However, if the wind-driven ventilation is directly used, the performance would be not effective as the initial conditions emphasise buoyancy forces and the flow pattern illustrated in Figure 7.5 rather than in Figure 7.4 will result. This means that the buoyancy forces have negative effects for the next moment although they are positive at the time being. As a consequence, in order to better utilise the wind-induced ventilation, the effects of the buoyancy-driven natural ventilation should be reduced before the wind comes. This also shows the significance of precise control of each strategy for a more controllable indoor environment, especially when combined ventilation occurs very frequently.

7.3 Combined ventilation with large openings (prototype 2)

It has been made clear in the last section that, multiple solutions exist for combined ventilation with small openings where no bi-directional flows occurs regardless of the relationship of the bulk flows driven by different forces. This section will extend the study of small openings to the situation where large openings are incorporated and bi-directional flows take place, and see whether multiple solutions still exist and how they affect the evaluation of the ventilation performance, based on which the mechanism for solution multiplicity is discussed.

7.3.1 Preliminary analysis

Let us consider the analysis of combined ventilation with small openings first and then extend the result to large opening cases. For a prototype building illustrated in Figure 7.8a, when no wind presents, the neutral level will be in-between the vertical distance of the two openings, as also shown in the previous chapter. The indoor and outdoor pressure distribution along the vertical direction for this circumstance is shown in Figure 7.8b. When there is wind blowing from the upper opening side, the outdoor pressure on the windward side wall will

increase and as a result the height of neutral plane, where the indoor and outdoor pressure equals, has to rise because the indoor pressure should become greater than the outdoor pressure to keep the balance. For the same reason, the wind will also reduce the outdoor pressure on the leeward wall as the wind pressure is negative on this side, and thus the neutral level will reduce.

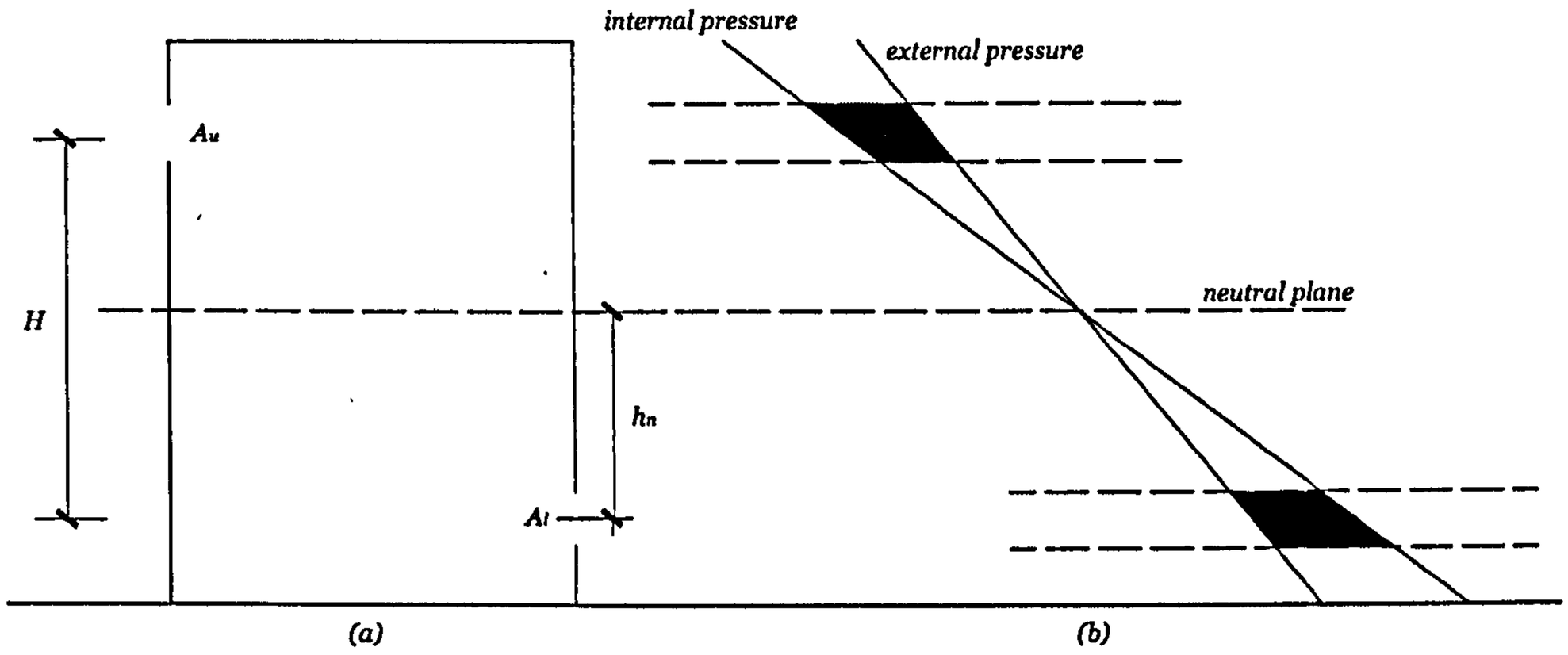

Figure 7.8: Schematic illustration of a prototype building when no wind presents and only buoyancy forces dominate the flow

This analysis in fact suggests that, neutral plane is not unique when wind forces present in buildings, and each wall has its own neutral plane. The positive wind pressure will push the neutral plane upwards whilst the negative wind pressure will push the neutral plane downwards. Duan and Li (2005) derived following equations for the calculation of the height of the neutral planes for both windward and leeward walls:

$$h_{n,w} = \frac{A_u^2}{A_u^2 + A_l^2} H + \frac{A_l^2}{A_u^2 + A_l^2} KH \tag{7.1}$$

$$h_{n,l} = \frac{A_u^2}{A_u^2 + A_l^2} H - \frac{A_l^2}{A_u^2 + A_l^2} KH \tag{7.2}$$

where $K = \frac{\Delta P_w}{\Delta P_B}$, which expresses the relative intensity of the pressures generated by two forces, i.e. wind forces and buoyancy forces. The tendency of the neutral levels on windward and leeward walls with the variation of the wind pressure can also be seen from the above two equations.

The above equations also suggest that, when the wind pressure increases to certain level, the neutral planes of two walls may intersect with the openings if both openings are large

enough, and bi-directional flows will be incurred. In fact, this is very similar to the analysis on the buoyancy-driven natural ventilation with large openings in the previous chapter. The pressure generated by the buoyancy forces over the opening will not be uniform due to the large openings but the wind pressure can be generally considered as uniformly distributed there. As a result the wind pressure cannot equate to the static pressure difference everywhere on the opening and thus bi-directional flows can take place. If wind pressure further increases, the neutral planes will get over the openings and flow directions for both openings will be reversed. This process is illustrated in Figure 7.9. Nevertheless, it would be very difficult to obtain the analytical solutions for the neutral levels and airflow rates for combined ventilation with large openings like those for buoyancy-driven airflows, because there are too many unknowns (several neutral planes may exist which make the airflow pattern very complicated).

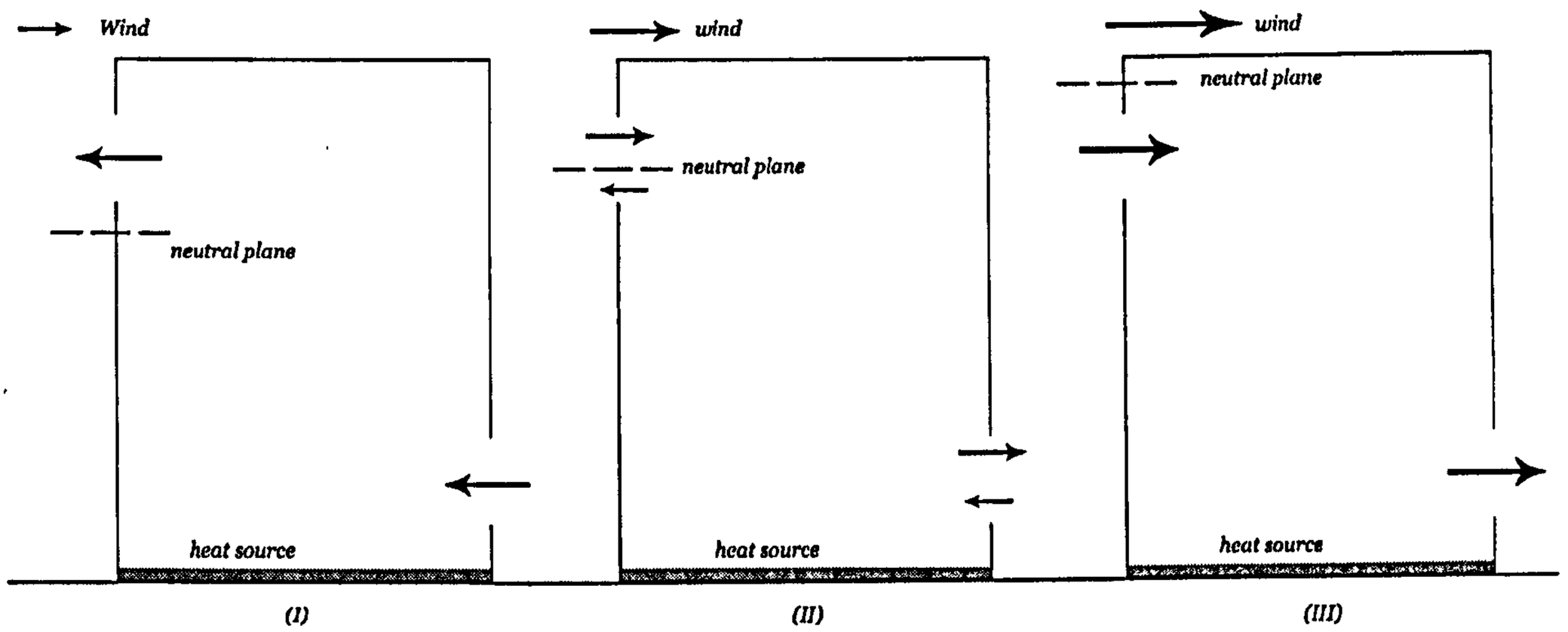

Figure 7.9: Schematic illustration of the movement of the neutral plane with the increase of the wind pressure (only the neutral plane on the windward wall is shown)

Recall the conditions for the existence of multiple solutions introduced in Chapter Two: basically this is because the airflow has to comply with both mass conservation and energy conservation. For small openings cases, when the buoyancy forces and wind forces are equal to each other, the airflow will have to stop because the pressure difference is zero (also see Equation 2.6), which will never be possible as this violates the energy conservation laws: the energy from the heat source is mostly transferred to heat the exchanging air. As a result the airflow direction will be reversed suddenly without reaching to zero when one force overwhelms the other, and in this way multiple solutions will occur with hysteresis behaviour.

However, for buildings with large openings, the air movement through an opening will never stop according to the above analysis because the wind pressure and the static pressure over an opening cannot be exactly opposite. From this point of view, solution multiplicity will

not occur for combined ventilation with large openings as the airflow direction can change smoothly and there is no sudden reverse of flow directions.

7.3.2 CFD simulations

The building configuration used for the CFD simulations in this part is the same of the prototype of the previous section: it is 12m high and 12m wide. Two large openings with the same height of 4m are incorporated at upper and lower levels. They are placed 1m away from the nearest horizontal edge. The oncoming wind blows from the upper opening side and the reference velocity increases from 0.1m/s to 0.9m/s with a step of 0.1m/s. The log-law wind profile introduced in Chapter Three is also used here. The heat source is located on the floor with a constant flux of 100W/m^2 which can induce an airflow rate of around 0.3m/s when no wind presents. The two-way approach for the initial conditions settings used before is also employed to seek the multiple solutions.

The flow patterns when either of the two forces dominates the air movement are shown first in Figure 7.10 and it can be easily known that the airflow directions for the two flow patterns are opposite. It is found that the flow pattern will be very close to that shown in Figure 7.10 (a) when the reference wind velocity is not higher than 0.2m/s, whilst it will be very similar to that illustrated in Figure 7.10 (b) when the reference wind velocity is higher than 0.5m/s. When the wind velocity is between 0.3m/s to 0.5m/s, bi-directional flows are observed for both types of settings of initial conditions and multiple solutions are found for all situations where bi-directional flows take place. Figure 7.11 illustrates the detailed airflow fields of the two simulation results when the wind reference velocity is 0.3m/s. In this situation the buoyancy forces are slightly stronger than the wind forces.

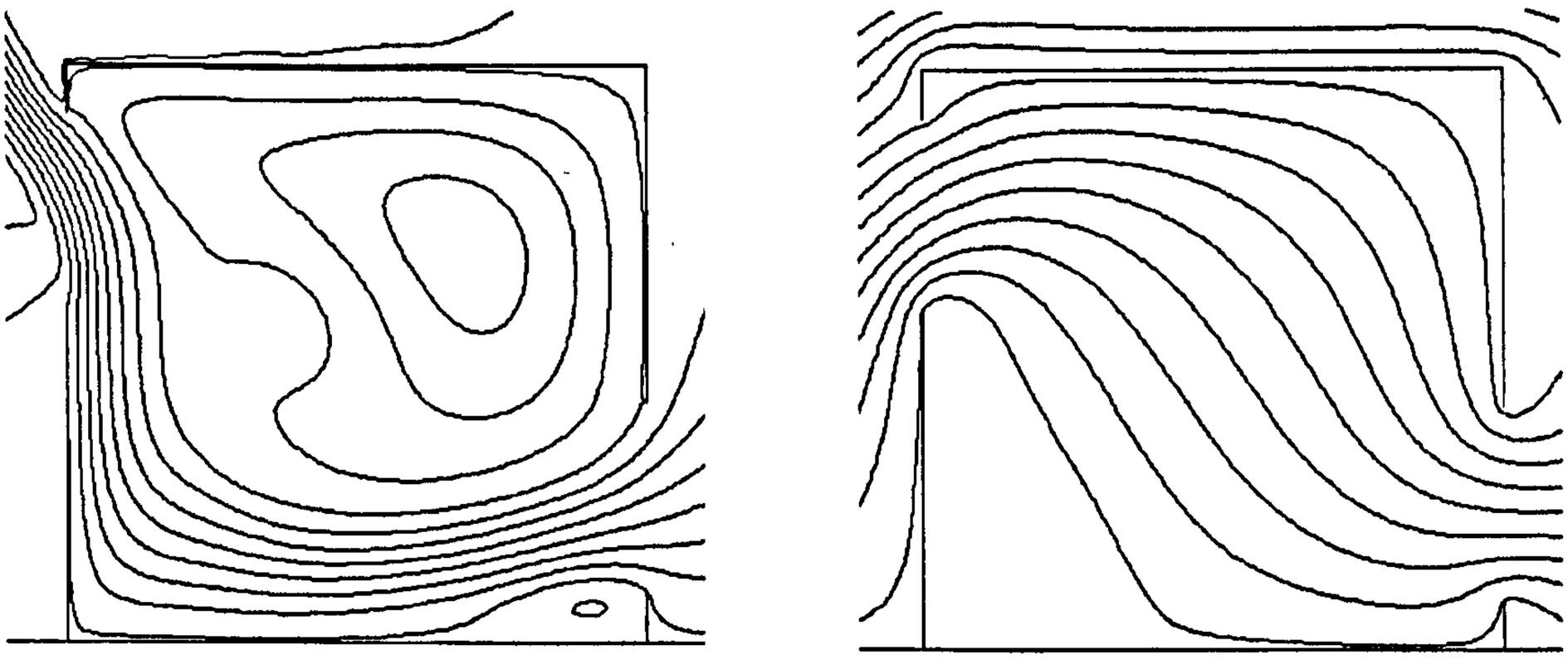

(a) buoyancy-dominated airflow (b) wind-dominated airflow

Figure 7.10: Airflow patterns when either of the two forces dominates the air movement

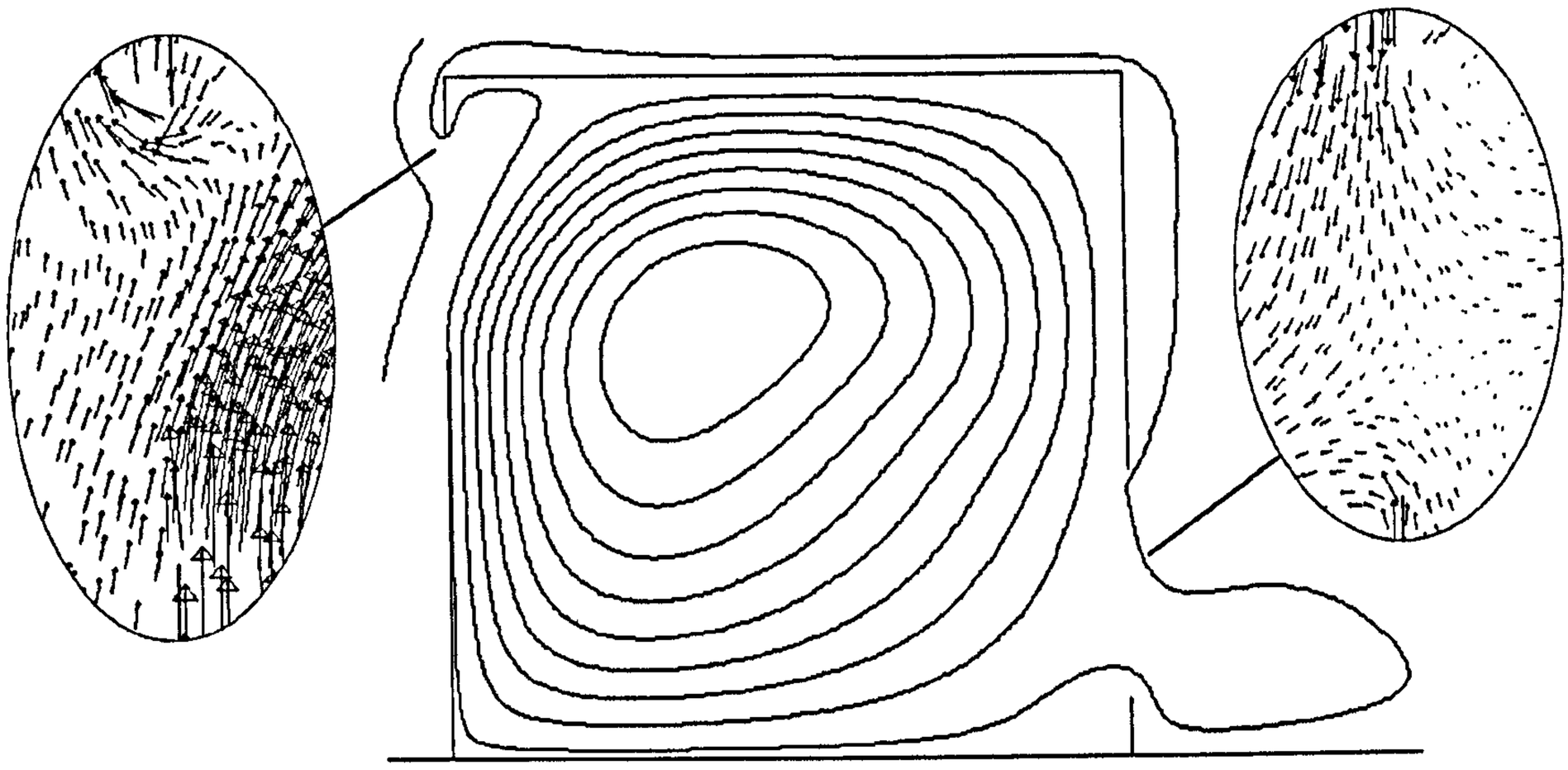

(a) when the wind forces are emphasised by the initial conditions

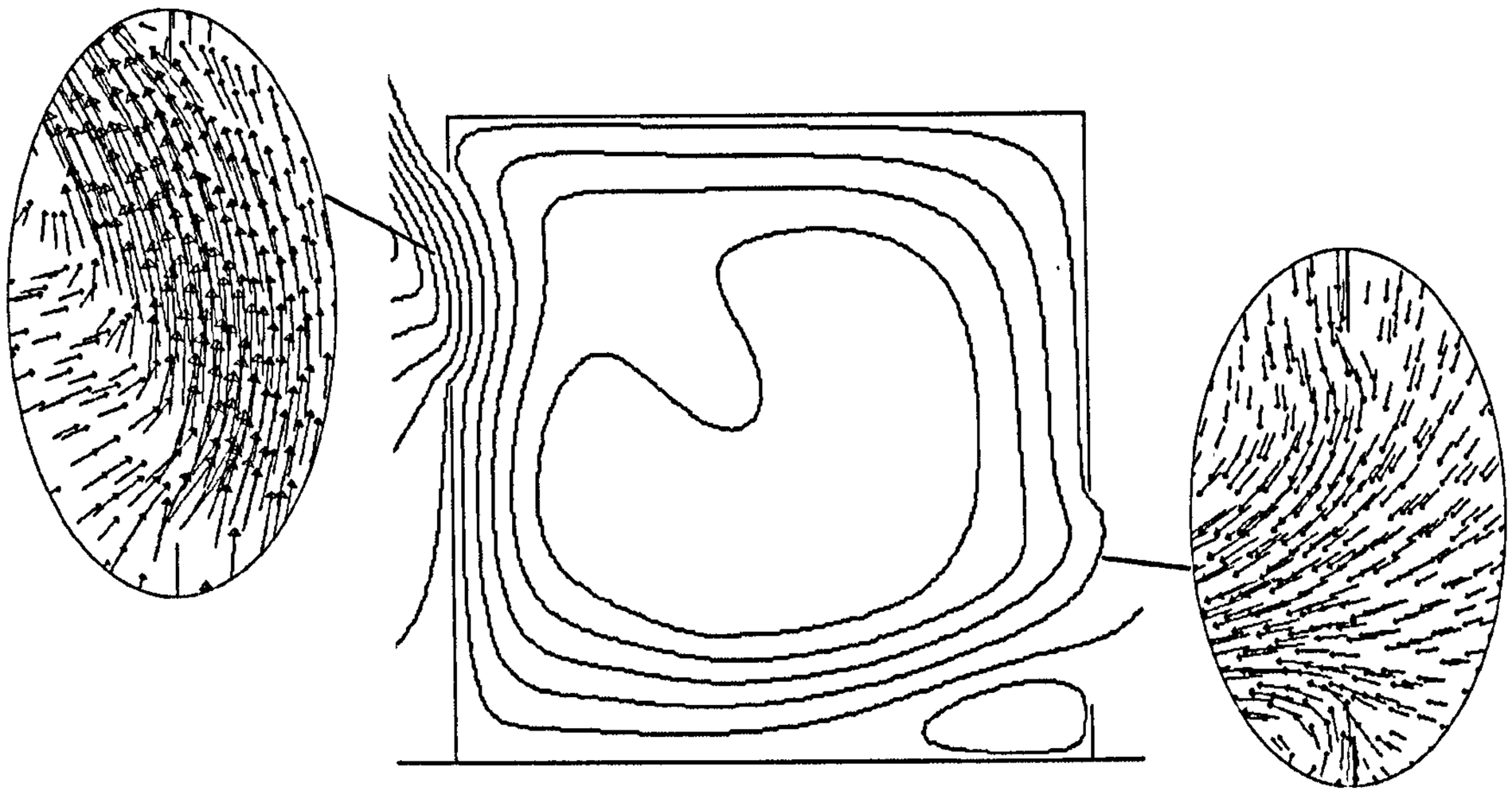

(b) when the buoyancy forces are emphasised by the initial conditions

Figure 7.11: Airflow fields for combined ventilation prototype (II) with different settings of initial conditions when the reference wind velocity is 0.3m/s

Apparently the above two flow patterns are quite different and it can be observed that the airflow is driven by the forces emphasised by the initial conditions: the first flow illustrated in Figure 7.11 (a) is driven by the wind forces whilst the second one is driven by buoyancy forces as shown in Figure 7.11 (b). This can also be seen by examining the main inflow openings for both situations: for scenario (a), the inlet is not very clear because recirculation flows take place for both openings, and the net airflow rate through each opening is only

0.03m/s, but clearly the lower opening will be the main inlet for scenario (b) because no recirculation occurs for lower opening and most air coming into the upper opening just directly goes out. For this situation the net airflow rate is 0.15m/s, which is much higher than scenario (a). The two scenarios also predict very different temperature profiles in the space as shown in Figure 7.12, and the velocity distributions at the occupants' level are compared in Figure 7.13.

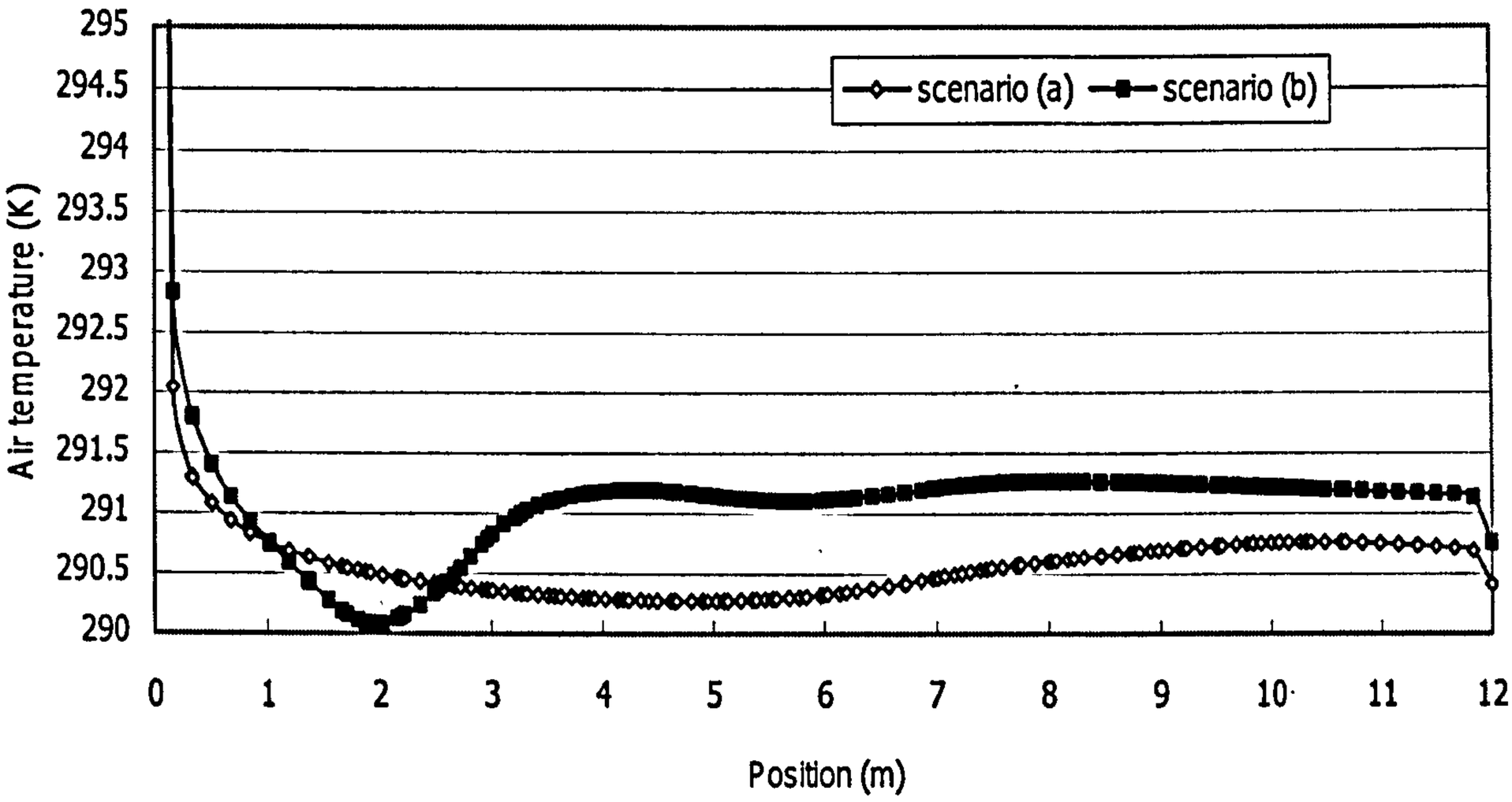

Figure 7.12: Comparison of vertical air temperatures at the centre of the space for prototype (II) of combined ventilation

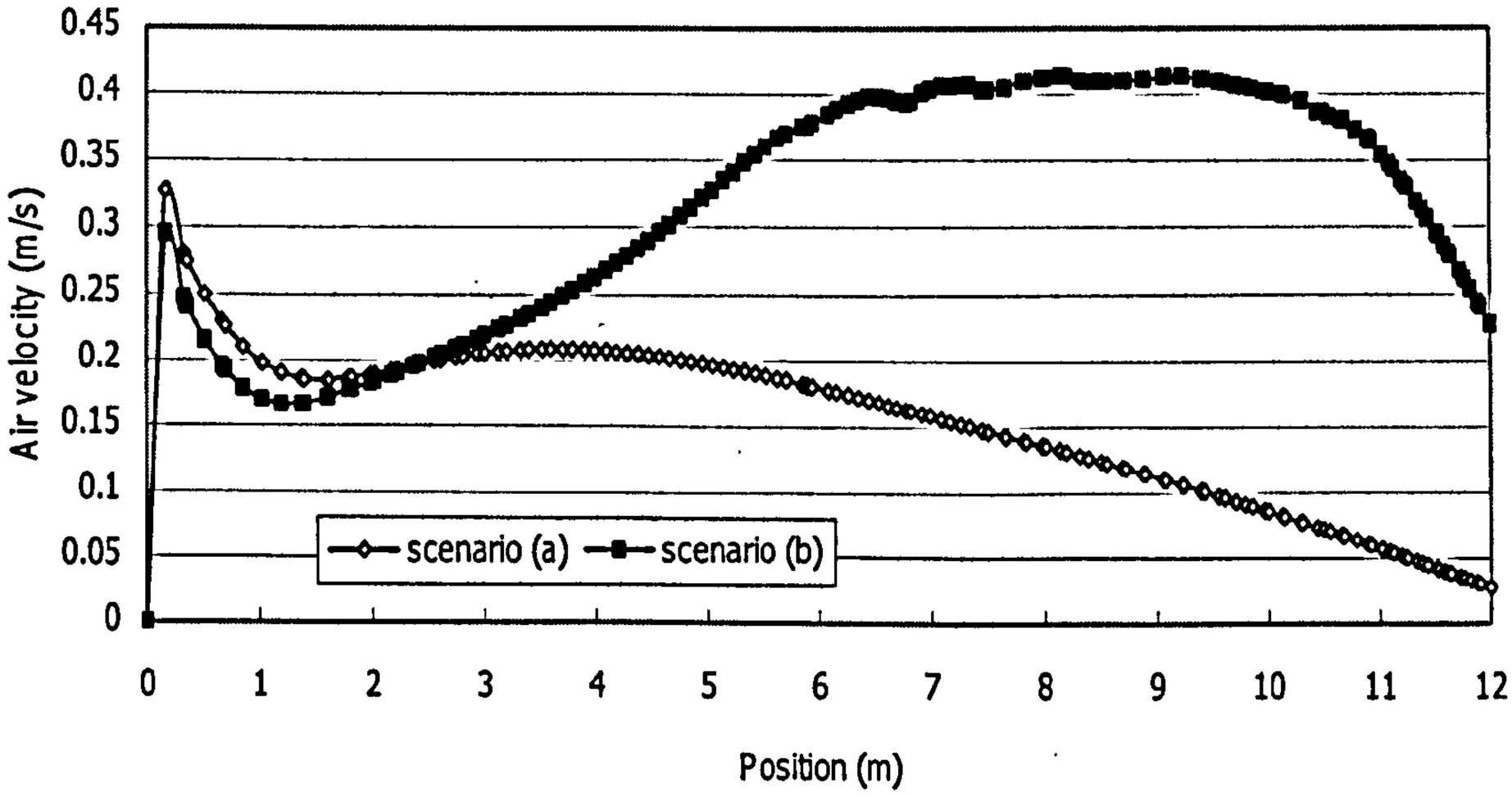

Figure 7.13: Comparison of air velocities at the occupants' level for prototype (II) of combined ventilation

It can be seen from the above two figures that, the results simulated with two different initial conditions significantly differ from each other. The scenario (b), which emphasises buoyancy forces, produces higher air temperature in the space and thus stronger buoyancy forces, which result in higher air velocities at the occupants' level as buoyancy forces are still the main forces driving the air movement in the space for this wind velocity.

7.3.3 Discussions

The main points of the investigations performed above can be summarised and discussed as follows. Firstly, the transition process for prototype (II) of the combined ventilation with the increase of the wind velocity has been identified. The wind pressure can push up the neutral plane on the windward wall and push it down on the leeward wall. When the neutral plane intersects with an opening, bi-directional flow will occur and further increase of the wind velocity will allow the neutral plane go over the opening resulting in the entire reverse of the flow direction. The whole transition process has also been observed by CFD simulations.

Related to this, it should be noted that bi-directional flows may be an important characteristic for combined airflows when the two forces are similar in scale and large openings are incorporated. Here large openings are defined as those over which the static pressure cannot be considered as uniformly distributed. This may lead to difficulties for the prediction of the ventilation performance for combined ventilation at the early stage because there is still no analytical approach available, and computational methods, either multi-zone approaches (e.g. Duan and Li 2005) or CFD simulations have to be resort to. It is also shown that the study of the ventilation situation with one single dominating force will be of help for the investigation of the performance of combined ventilation because the result airflow pattern will be very similar to the situation where the forces emphasised by the initial conditions dominate the flow.

Secondly, the above study also provides evidence to show that multiple solutions do exist for bi-directional flows even if no sudden reverse of the flow direction occurs. This seems contradictory to the mechanism for the presence of solution multiplicity but actually it does not. Although the sudden reverse of the airflow direction will not occur for an opening, this may take place for a grid in the computational domain of CFD. Basically the conservation laws that are used in macroscopic approach in Chapter Two for the analysis of solution multiplicity are also applicable for any grid in CFD (see those basic equations of CFD in Chapter Three). Thus when the sudden reverse of the flow direction occurs for a grid (this will at least occur at the grids on the neutral plane because the pressure difference there is always zero), multiple solutions will exist for the simulation results of this small element, and the information of this grid will also propagate to other areas in the whole computational domain resulting in different flow patterns for different initial conditions.

7.4 Summary

This chapter extended the research of combined ventilation on conventional models to another common situation where the two forces partly assist with each other and partly oppose each other, and two prototypes are employed for the investigation: one is that the two bulk flows assist each other but the recirculation flow of one force opposes the main flow of the other; the other is that two forces oppose each other and large openings are incorporated resulting in bi-directional flow.

It was found that different solutions present for both prototypes depending on the settings of initial conditions, and this provides evidence that solution multiplicity is an important characteristic for combined airflows regardless of the relationship of the bulk flows of different driving forces or the occurrence of the bi-directional flows. The reason for this is revealed by examining the combined ventilation with large openings: even a small element in the whole flow field has encountered equal driving forces and result in sudden reverse of the flow direction due to conservation laws, multiple solutions for the whole domain will be incurred. This also suggests that solution multiplicity should exist for a very wide range of airflows driven by combined forces since it is very difficult for different forces to entirely assist each other everywhere in the flow field.

It was also shown that different solutions generated very different ventilation performance. This means that, for combined ventilation, the effects of a ventilation strategy will also be dependent on the conditions at the preceding moment and in addition, a strategy may bring positive effects for this moment but may be negative for the next one. As a consequence, the combined ventilation problems should be considered in an unsteady manner other than a steady one, and precise control of the ventilation strategies will be very important in order to achieve a higher efficiency. It is also suggested that the study on the ventilation performance when only one single force dominates the airflow will be very valuable for the investigation of that of combined ventilation as they are closely related.

CONCLUSIONS AND RECOMMENDATIONS

8.1 Conclusions

The purpose of this research has been to develop design guidelines and relevant prediction tools for the incorporation of natural ventilation in atrium spaces as a passive cooling strategy. Focused on the thermal and geometrical characteristics of atrium spaces, the stated objectives of the research were (repeated from Chapter One):

- To develop a new approach for the thermal comfort assessment of atrium spaces taking the impacts of solar radiation into account;
- To investigate the wind-induced natural ventilation through roof openings of atrium spaces;
- To study the effects of the heat sources on the buoyancy-driven natural ventilation and to develop algorithms for the prediction and adjustment of the neutral level, especially when large openings are incorporated;
- To examine combined natural ventilation when buoyancy forces and wind forces partly oppose each other and partly assist each other.

These objectives have been realised in Chapter Four to Chapter Seven respectively and the major findings for each of them can be summarised as follows:

1. Chapter Four developed a new method for the assessment of thermal comfort level of atrium spaces taking solar radiation into account by using MATLAB as a data

exchanging platform. A code for the calculation of mean radiant temperature (MRT) was developed first enabling the treatment of the contribution of solar radiation to MRT, and CFD was used to predict the air temperature and velocity at the occupants' level. All the data obtained were then put together in MATLAB for PPD/PMV calculation. Based on this new approach, it was found that MRT could be a more significant factor leading to the overheating of atrium spaces, especially when the sun could directly irradiate the occupants' level, which means that the most important passive cooling strategy for this circumstance would be the provision of shading devices. In addition, it was also shown that the air temperature at the occupants' level is mostly affected by the temperatures of the surfaces at lower levels and the temperatures at the roof level and the upper areas generally have little influence on the air temperature at the occupants' level. These findings together in fact suggest that the upper surfaces of the space irradiated by the sun can work as the heat source driving the buoyancy-driven natural ventilation in the space if needed, in which way both the MRT and the air temperature at the occupants' level can be avoided becoming too high due to the location of the heat source.

2. Chapter Five studied the wind-induced ventilation through roof openings by CFD simulations; in essence, this type of ventilation is driven by the recirculation of the main flow rather than the direct use of the oncoming wind. It was identified that the main forces controlling the air movement include the main flow from the wind, the back flow from behind the building, the reverse flow and the reattaching flow at the roof level. The possible flow patterns were also defined and the dominating forces for each of them can be considered as different organisations of the above forces. It was observed by CFD simulations that the ventilation performance is closely associated with the pattern of the flow: the recirculation driven by the main flow will be the strongest whilst that driven by the back flow will be the weakest. Based on these identifications of the flow pattern and the relevant controlling forces, the effects of the design parameters, such as the roof shape and angle, the width of the adjacent buildings and the openings' size and location were investigated and a number of valuable graphs were drawn for the use of designers, including Figures 5.19 and 5.14 illustrating the relationship between the roof angle and the ventilation performance for different roof shapes; Figures 5.38 and 5.45 illustrating the relationship between the width of the adjacent buildings and the ventilation performance; Figures 5.27 – 5.31 illustrating the relationship between the opening size and the ventilation performance; Figures 5.21-5.24 and 5.26 illustrating the relationship between the opening location and the ventilation performance and Figures 5.32 – 5.35 illustrating the relationship between the

opening methods and the ventilation performance. According to these graphs, guidelines were also developed for various design purposes such as shape based design, flow pattern based design and other more complicated basis. Details regarding to these guidelines can be found in relevant sections.

3. In Chapter Six which dealt with buoyancy-driven natural ventilation, the effects of the location of heat source and the control of the neutral level when bi-directional flow occurs were studied. It was shown that the efficiency of the heat source on driving the airflow is very sensitive to its location, and graphs were made for illustrating the relationship between the location of the heat source and the airflow rate coefficients (See Figures 6.3, 6.10 and 6.11). It was found that the heat source located on the opposite wall of the outlet opening has a higher efficiency than that on the same side wall of the outlet opening as this reduces the heat accumulated around the outlet consuming more energy from the source for the heat transfer, and the heat source placed too close to the lower opening will avoid low air velocities at the occupants' level due to direct heating of the air coming into the space. The heat source located at the top area of the space will result in bi-directional flows and hence a very low airflow rate. Based on these findings, the optimised location of the heat source in order to driven buoyancy-driven natural ventilation was determined for each flow regime, and the guidelines on the selection of the surfaces materials were also developed accordingly. As regards the control of the neutral level, the possible flow patterns were identified for the situations with large openings, and a number of new generalised algorithms for the prediction of the airflow rates and the neutral level were developed based on pressure difference analysis. The new algorithms agreed with the CFD simulations when the lower opening is larger but significant discrepancies existed when bi-directional flow occurs for the upper opening due to the high air temperature there which is advected from the bottom heat source. The algorithms also suggested that, in order to raise the height of the neutral plane, horizontal/vertical strip window can be used for the upper/lower opening if the areas of the openings are fixed.

4. The investigation of the combined ventilation associated with Chapter Seven studied two prototypes where wind forces and buoyancy forces partly assist each other and partly oppose each other. It was observed that multiple solutions still existed for both prototypes, which provided evidence that solution multiplicity is an important characteristic for combined ventilation problems regardless of the relationship between the bulk flows or the occurrence of bi-directional flows. It was also found that different solutions had different ventilation performance and hence different cooling effects depending on the initial conditions. As a result, for combined ventilation, the effects of a ventilation strategy would also be dependent

on the conditions at the preceding moment and in addition, a strategy with positive effects for this moment might be negative for the next moment. These descriptions meant that the combined ventilation problems should be considered in an unsteady manner rather than a steady one, and precise control of the ventilation strategies will be very important in order to achieve a higher efficiency. It was also shown that the study on the ventilation performance when only one single force dominates the airflow would be very valuable for the investigation of that of combined ventilation because the flow pattern of the combined ventilation would be very similar to that dominated by the forces emphasised by the initial conditions.

5. Apart from the above findings regarding to the incorporation of natural ventilation, this study has also provided valuable validations of several common research methods for air movement. Generally two different research methods were employed for this project: CFD simulations and generalised theoretical methods. It could be seen that, with appropriate settings, not only can CFD be used to predict the airflow pattern and relevant velocity and temperature values, it can also be employed to investigate some sophisticated characteristics of air movement, including convective heat transfer, separation effects of wind-driven airflows, bi-directional flows through large openings and solution multiplicity of combined airflows. It should be noted that, in order to study natural ventilation, the computational domain usually has to be extended to include part of the outside environment and "fictitious walls" will have to be used. The detailed CFD settings for these purposes can be found in Section 3.4 and they can also be used as guidelines or references for similar simulation objectives. Generalised models developed based on the pressure difference analysis for large openings generally agreed with CFD simulations and they were also very useful for the prediction of the neutral level and airflow rate at the early design stage. However, it was also shown that the generalised models can only apply to very simple geometries and usually also very simple situations such as uniform environment. It is also worth mentioning that MATLAB is also an important research tool for the exchange of the data from different sources and this research integrates the data from CFD and those from another code calculating MRT. It is hoped that this tool can be further used for the data analysis of interdisciplinary research, such as the interaction between acoustic, lighting and thermal aspects.

The above findings are obtained in terms of different ventilation strategies, but in reality they usually have to be used together and adapted into the existing well-established processes.

Generally speaking, the findings of this research are of significance for the practice in the following relevant areas:

• *Process of climatic sensitive atrium design*

It is clear that the purpose of incorporating passive strategies is to make the occupants thermally comfortable. As a consequence, in order to incorporate passive cooling strategies for a building in warm weather to cope with overheating problems, the thermal comfort evaluation method developed should be used first with the data from thermal simulations (mainly the surface temperatures) to diagnose the main causes for the overheating: if MRT is the main problem then shading should take the priority and if air temperature is the most significant reason, then natural ventilation will be more efficient (only strategies with immediate effects are considered here). Since the design of shading is generally easy from thermal point of view, the following will be dealing with the latter condition.

It can be seen that the influential factors determining the performance of the wind-driven and buoyancy-driven ventilation significantly differ due to their different mechanisms: wind-driven ventilation is mostly influenced by wind and thus very sensitive to those parameters related to the shape of the space, such as the adjacent buildings, the roof shape and angle, the opening location and size whilst the buoyancy-induced natural ventilation is driven by internal forces and thus insensitive to the roof shape and adjacent buildings but significantly affected by the openings' sizes and locations and the selection of materials for internal surfaces. The combined ventilation will be influenced by both parameters introduced for wind-induced ventilation and for buoyancy-driven ventilation.

These descriptions suggest that, before designing the ventilation strategies, it is necessary to clarify the driving forces of airflow in and around the atrium building in order to identify the dominating flow regimes in the building so that the design guidelines developed before regarding to each flow regime can be followed. A simple and easy-to-use way of doing this is to use the equations introduced in Chapter Two or CFD to roughly obtain the airflow rates at each time step for single forces (solar radiation or wind). The values from different forces are then compared to determine the dominating flow regime for each time step. Finally statistical methods can be used for the whole overheating period to judge which flow regime will be the most significant one the design should focus on.

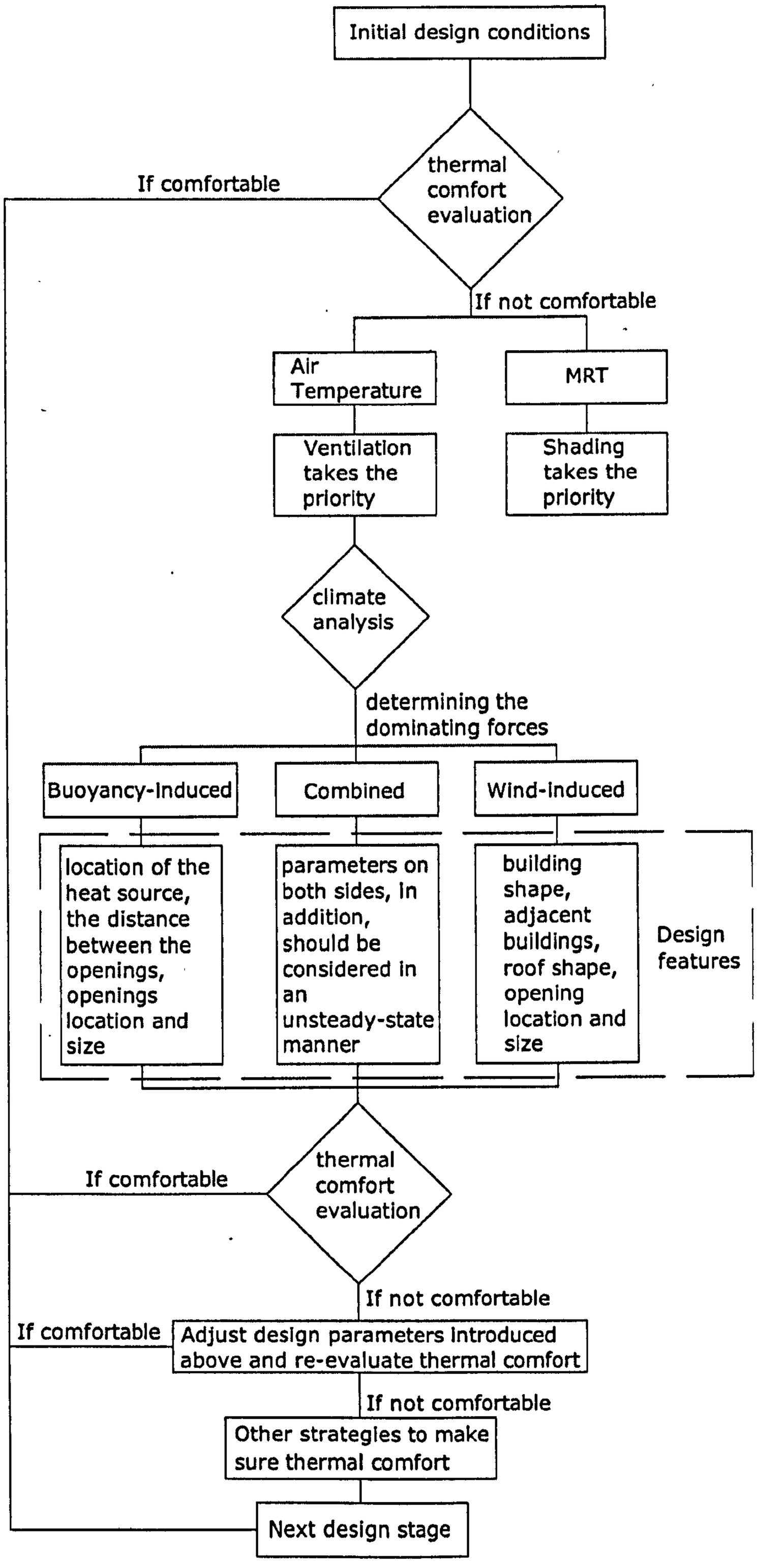

Figure 8.1: Process of the climatic sensitive building design

The effects of ventilation strategy designed can then be checked with the thermal comfort assessment method to see whether acceptable thermal comfort level has been achieved. If not, the design strategies should be improved or other strategies should be considered such as night cooling or even HVAC systems. The whole process for the climatic sensitive atrium design is illustrated in Figure 8.1. It is easy to understand that this process also applies to the design of all other types of buildings and the only thing that may change is the thermal comfort criteria.

• *Passive strategies for large-volume spaces*

Large-volume spaces are characterised as those with non-uniform thermal environment, and in particular the spaces where the thermal conditions at the occupants' level are not the same as those at other areas. For this type of spaces, there is no need to make sure every area of the space is comfortable and only the thermal comfort of the occupied areas needs to be taken care of. Conventional methods usually assume a space as a small one with uniformly distributed thermal properties, such as air temperature and velocity, and apparently these methods will not be suitable for the design of non-uniform large spaces. This research proposed a new approach by combining CFD and other codes based on MATLAB as a data exchange platform which enabled the treatment of non-uniform environment to monitor the specific areas in need for thermal comfort. Sometimes other areas may also be occupied in addition to the bottom, and this approach can also be easily extended to deal with these conditions.

According to the thermal characteristics of large-volume spaces, it can also be known that the design of the lower level of the large-volume space will focus on the control of the air temperature and velocities whilst the design of the upper level should avoid the intensive solar radiation and use the surfaces there as the source to induce the airflow. Based on this idea, lower levels should incorporate more thermal mass to reduce the fluctuation of the thermal environment at the occupants' level and some new passive cooling strategies that cannot be used in ordinary small spaces can be incorporated in large-volumes space, such as the use of recirculation of the wind or the use of upper walls irradiated by the sun as the heat source to generate the air movement for cooling effects of the ground level. This is illustrated in Figure 8.2. and design guidelines regarding to these issues can be referred to in the chapters dealing with them respectively. The investigation of the recirculation flows should be also of interest to other situations with similar flow mode, such as the facade design of the single-sided buildings for wind-induced ventilation purposes, and the guidelines developed earlier will also be applicable for the corresponding parameters.

• *Building energy management*

This research also shows the significance of the control of the design parameters to ensure good performance of the passive strategies, especially for the airflows when buoyancy forces are of significance, because wind-induced flow pattern is generally independent of the Reynolds number whilst the sun moves all the time which changes the location of the heat source in the space affecting the airflow rate and the neutral plane, as has been indicated in the research. In addition, the study on combined ventilation suggests that the conditions at the preceding moment will affect the performance of the ventilation strategies to be employed for the next moment.

In order to realise the control of the relevant design parameters to achieve a more comfortable environment with less energy consumption, control algorithms have to be developed for the implementation of the management. The thermal comfort program and the generalised algorithms for the prediction of the neutral plane and airflow rate derived in this research, in addition to those design guidelines developed can be used to help monitor and control the thermal conditions in the buildings and change the status of relevant building components accordingly, such as openings and shadings.

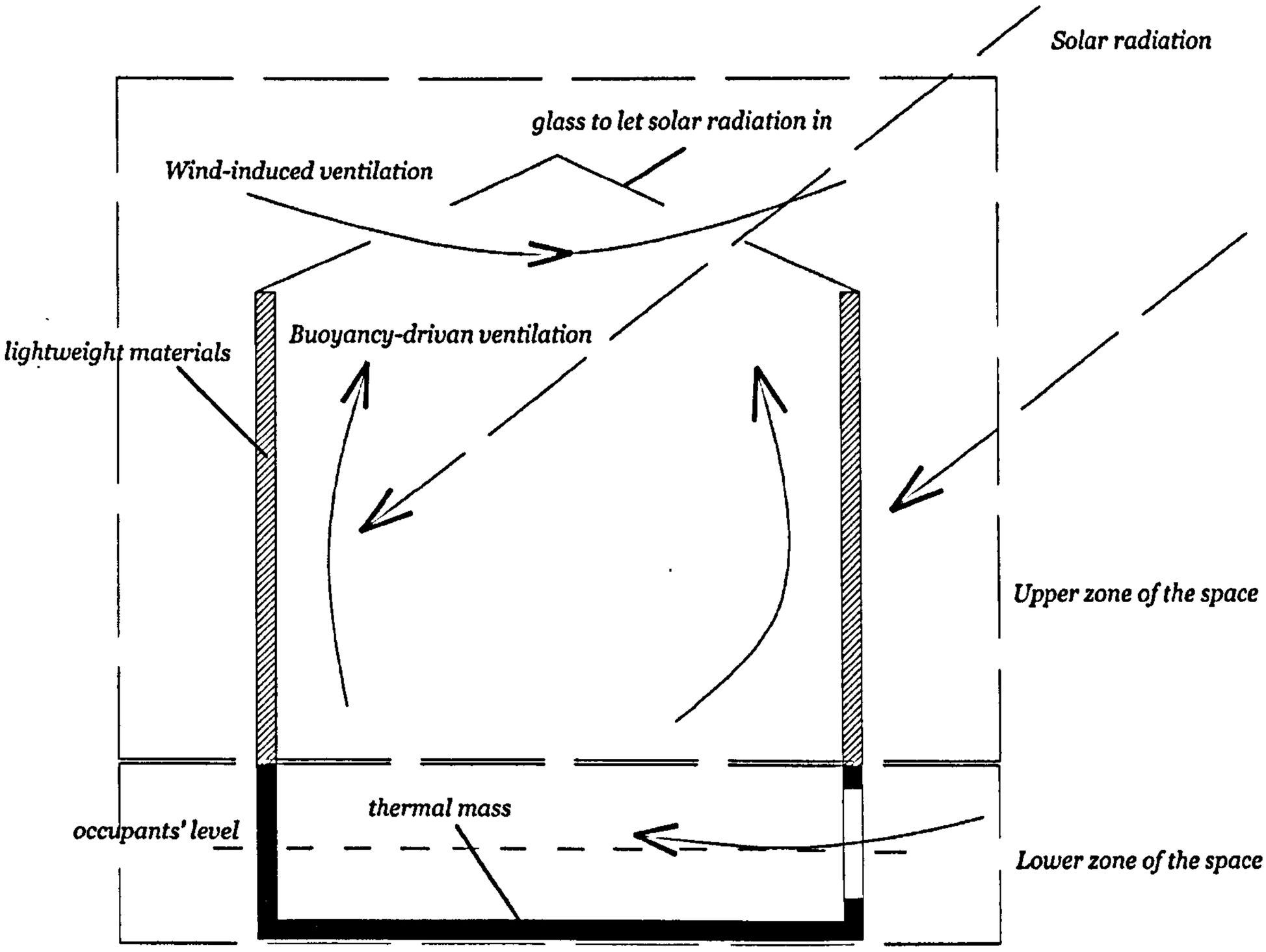

Figure 8.2: Passive strategies for large-volume spaces

• *New building component development*

The outcomes of this research in fact suggest that skylight is an important component for the passive design of atrium spaces. Its shape, and the size and location of the openings in it are very important for the incorporation of wind-induced ventilation; it will be also of significance for the performance of the buoyancy-driven natural ventilation and the control of the neutral level. In addition, it also allows the solar radiation to penetrate into the space so that the heat source on the internal surface is impacted upon or modified.

The guidelines developed in this research also reveal that the performance of a skylight is also dependent on other design parameters including the adjacent buildings and building shape for the wind-induced ventilation, or the size of the lower opening for the buoyancy-driven natural ventilation, which means that different design conditions may need very different kinds of skylights to achieve the highest efficiency. It was shown that, when flow pattern (I) occurs for wind-induced airflow, the openings should placed to be able to "see" each other and encourage the "tunnel effect" enhancing the airflow but the openings locations are different for other flow patterns when the airflow is driven by "suction". These findings mean that other types of skylights can be developed for energy saving reasons as alternatives to the conventional ones (e.g. the one illustrated in Figure 1.1). Nevertheless, it has also been indicated that, although skylights are of great significance for the passive design, openings at the occupants' level are also very important and should be incorporated wherever possible.

8.2 Recommendations for future work

This research has identified a number of areas worthy of further work and has provided a platform for future research. Although the work documented in this thesis represents a contribution towards the passive design of atrium spaces, much work remains. Some recommendations are provided below.

• *Thermal comfort of atrium spaces*

Chapter Four developed a new thermal comfort assessment approach based on the well known PPD/PMV system. It should be noted that mostly this system is only used for indoor spaces and it has been well established that the outdoor thermal evaluation method is very different. However, due to the large areas of glazing incorporated, atrium spaces are usually identified as "grey spaces" (also like the corridor with roof attached to the outside of a building) (Kurokawa 1988) which means that atrium type spaces may be neither indoor spaces nor outdoor spaces but in-between them. As a consequence, it is interesting to know whether there is another special thermal comfort assessment system suitable for the use of this type of spaces. Questionnaires and field surveys may need to be carried out for this purpose.

• *Natural ventilation of atrium spaces*

This research only performed 2D simulations for the investigation of the natural ventilation strategies, and further 3D simulations and physical experiments need to be performed to verify the results obtained. In addition, this study only focused on the steady-state conditions, but unsteady-state effects of airflows were not considered. It has been known that the fluctuating effects of the wind, i.e., the turbulence effects do have certain impacts on the thermal comfort level of the occupants, and although possible, it is not easy to observe and measure the fluctuation by the methods available at present. Furthermore, the buoyancy-driven ventilation usually has a very large timescale for the establishment of the steady state due to its weakness and this implies that design criteria should also account for the transient behaviour rather than just simply on the final steady-state conditions. All these issues need to be addressed in the future in order to give a full picture for the passive design of atrium spaces, and furthermore the applicability of these research results should be tested in real buildings before intensive use.

• *Thermal simulation of atrium spaces*

It was mentioned in previous chapters that thermal mass or night cooling may be incorporated as passive strategies for atrium spaces, and in order to study the effects of these strategies, long-term energy simulation has to be carried out. Conventional methods for the thermal simulation of buildings, such as Esp-r of the UK and Energyplus of the US, usually employ the assumption that the temperature for the air in the space and the temperature for each surface are uniformly distributed, because only one node is commonly used to represent each surface and the whole air volume. However, as discussed earlier, as large-volume spaces, atria usually have a very large height causing temperature stratification, and as a result the uniform air temperature will not be valid for this circumstance. In addition, the solar radiation penetrating into the space may warm up small part of the internal walls other than the whole space and the temperature of any surface inside may not be uniform as well. As a result new approaches have to be adopted to account for these issues.

• *Other environmental aspects of atrium spaces*

This research is mainly concerned with the thermal issues of atrium spaces including thermal comfort and natural ventilation. However, practitioners usually consider design as a collective decision-making process, and consequently it will be useful to bring the information from acoustic and lighting aspects together with that from the thermal aspects obtained from this research to generate some new guidelines for the design of the space or some special

components of the space such as the roof (some work has already been carried out on the acoustic and lighting aspects of atrium spaces in the School of Architecture, the University of Sheffield, such as (Kang et al. 2007) and (Samant and Sharples 2004)).

REFERENCES

Alamdari, F. and G. P. Hammond (1983). "Improved data correlations for buoyancy-driven convection in rooms." Building Services Engineering Research and Technology **4**(3): 106-112.

Allocca, C., Q. Chen and L. R. Glicksman (2003). "Design analysis of single-sided natural ventilation." Energy and Buildings **35**(8): 785-795.

Alvarez, S., F. Sanchez and J. L. Molina (1998). Air flow patterns at courtyards. Proceedings of Passive and Low Energy Architecture, Lisbon, Portugal.

Andersen, K. T. (2007). "Airflow rates by combined natural ventilation with opposing wind - unambiguous solutions for practical use." Building and Environment **42**(2): 534-542.

Anderson, K. T. (2003). "Theory for natural ventilation by thermal buoyancy in one zone with uniform temperature." Building and Environment **38**(11): 1281-1289.

Aschehoug, O., A. G. Hestnes, M. Thyholt and T. Jacobsen (1990). An Advanced Case Study for IEA Solar Heating and Cooling - Task XI (Passive and Hybrid Solar Commercial Buildings), Trondheim.

ASHRAE (2001). 2001 ASHRAE handbook : Fundamentals. Atlanta, GA., ASHRAE.

Assimakopoulos, V. D., H. M. ApSimon and N. Moussiopoulos (2003). "A numerical study of atmospheric pollutant dispersion in different two-dimentional street canyon configurations." Atmospheric Environment **37**(29): 4037-4049.

Auliciems, A. (1981). "Towards a psychophysiological model of thermal perception." International Journal of Biometeorol **25**: 109-122.

Awbi, H. (1998). "Calculation of convective heat transfer coefficients of room surfaces for natural convection." Energy and Buildings **28**(2): 219-227.

Awbi, H. B. (1996). "Air movement in naturally-ventilated buildings." Renewable Energy **8**(1-4): 241-247.

Awbi, H. B. (2003). Ventilation of buildings. London, New York, Spon Press, Taylor & Francis Group.

Axley, A. (1998). Introduction to the design of natural ventilation systems using loop equations. Proceedings of 19th AIVC conference, Oslo, Norway.

Ayata, T., E. Arcakiloglu and O. Yildiz (2007). "Application of ANN to explore the potential use of natural ventilation in buildings in Turkey." Applied Thermal Engineering **27**(1): 12-20.

Ayoob, A. N. and J. L. Izard (1994). "Study of comfort in atrium design." Renewable Energy **5**(5-8): 1002-1005.

Baker, A. J. (1983). Finite element computational fluid mechanics. Washington [D.C.] ; London, Hemisphere Pub. Corp.

Baker, N. and P. F. Linden (1991). Physical modelling of airflows - a new design tool. Welwyn, England, CICC Publications.

Baker, N. and K. Steemers (2000). Energy and environment in architecture: a technical design guide. London, E & FN Spon.

Barthakur, A. (1996). Thermal bahavior of atria: A comparative study between measured data and a computational fluid dynamics model. Department of Architecture, University of Southern California.

Bartzanas, T., T. Boulard and C. Kittas (2004). "Effect of vent arrangement on windward ventilation of a tunnel greenhouse." Biosystems Engineering **88**(4): 479-490.

Bauman, F., D. Ernest and E. Arens (1988). "The effect of surrounding buildings on wind pressure distributions and natural ventilation in long building rows." ASHRAE Transactions **94**(2): 1670 - 1695.

Beausoleil-Morrison, I. (2000). The adaptive coupling of heat and air flow modelling within dymanic whole-building simulation. Glasgow, UK, The University of Strathclyde.

Bednar, M. J. (1986). The new atrium. London; New York, McGraw-Hill.

Bejan, A. (1995). Convection heat transfer. New York ; Chichester, J. Wiley.

Boussinesq, J. (1877). "Essai sur la theorie des eaux courantes." Mem. Presentes Acad. Sci.

Boyer, L. L. and K. S. Kim (1988). "Empirically-based algorithms for preliminary prediction of daylight performance in top-lighted atriums." ASHRAE Transactions **90**(1): 765-781.

Bryn, I. and P. A. Schilfloe (1996). Atrium models for the analysis of thermal comfort and energy use. IEA Task 12.

BS5925 (1991). Code of practice for ventilation principles and designing for natural ventilation. London, British Standards Institution.

Butera, F. M. (2005). Glass architecture: is it sustainable? Passive and low energy cooling for the built environment, Santorini, Greece.

Castro, I. P. (2003). "CFD for external aerodynamics in the built environment." The QNET-CFD Network Newsletter **2**(2): 4-7.

Chen, Q. (1995). "Comparison of different k-e models for indoor airflow computations." Numerical Heat Transfer **28**: 353-369.

Chen, Q. and N. T. Chao (1996). Prediction of buoyant plume and displacement ventilation with different turbulence model. Proceedings of the 7th international conference on indoor air.

Chen, Q. and Z. Jiang (1992). "Significant questions in predicting room air flow." ASHRAE Transactions **98**(1): 929-939.

Chen, Q., A. Moser and A. Huber (1990). "Prediction of buoyant, turbulent flow by a low-Reynolds-number k-e model." ASHRAE Transactions **98**(1): 564-573.

Chen, Q. and W. Xu (1998). "A zero-equation turbulence model for indoor airflow simulation." Energy and Buildings **28**(2): 137-144.

Chen, Z. D. and Y. Li (2002). "Buoyancy-driven displacement natural ventilation in a single-zone building with three-level opening." Building and Environment **37**(3): 295-303.

CIBSE (1988). CIBSE Guide. Chartered institute of Building Services Engineering, UK.

Clements-Croome, D. (1997). Naturally Ventilated Buildings: Buildings for the Senses, The Economy and Society, E & FN Spon.

Cook, M. J. (1998). An evaluation of computational fluid dynamics for modelling buoyancy-driven displacement ventilation. Leicester, De Montfort University.

Cook, M. J., Y. Ji and G. Hunt (2005). CFD modelling of buoyancy-driven natural ventilation opposed by wind. Proceedings of 9th IBPSA Conference, Montreal, Canada.

Cook, M. J., Y. Ji and G. R. Hunt (2003). "CFD modelling of natural ventilation: combined wind and buoyancy forces." International Journal of Ventilation **1**(3): 169-179.

Cook, M. J. and K. J. Lomas (1997). Guidance on the use of computational fluid dynamics for modelling buoyancy driven flows. Proceedings of IBPSA 6th meeting, Prague, Czech Republic.

Cooper, P. and P. F. Linden (1996). "Natural ventilation of an enclosure containing two buoyancy sources." Journal of Fluid Mechanics **311**: 153-176.

Denton, R. A. and I. R. Wood (1979). "Turbulent convection between two horizontal plates." International Journal of Heat and Mass Transfer **22**(10): 1339-1346.

Douvlou, E. D. (2003). Climatic responsive design & occupant comfort: The case of the Mediterranean climate. Department of Architecture. Sheffield, the UK, the University of Sheffield.

Duan, S. and Y. Li (2005). "An example of solution multiplicity in a building with bi-directional flow openings." Indoor and Built Environment **14**(5): 359-369.

Emmerich, S. (1997). Use of computational fluid dynamics to analyses indoor air quality issues. Report NISTIR 5997, National Insititute of Standards and Technology, USA.

Emmerich, S. J. and K. B. McGrattan (1998). "Application of a large eddy simulation model to study airflow." ASHRAE Transactions **104**(1): 1-9.

Ernest, D. (1991). Predicting wind-induced indoor air motion, occupant comfort and cooling loads in naturally ventilated buildings. Department of Architecture. California, University of Carlfornia, Berkley.

Etheridge, D. and M. Sandberg (1996). Building ventilation : theory and measurement. Chichester ; New York, John Wiley & Sons.

Fanger, P. O. (1970). Thermal comfort: Analysis and applications in environment engineering. New York, McGraw-Hill Book Company.

Favarolo, P. A. and H. Manz (2005). "Temperature-driven single-sided ventilation through a large rectangular opening." Building and Environment **40**(5): 689-699.

Ferreira, A. D., A. C. M. Sousa and D. X. Viegas (2002). "Prediction of building interference effects on pedestrian level comfort." Journal of Wind engineering and Industrial Aerodynamics **90**(4-5): 305-319.

Fitzgerald, S. D. and A. W. Woods (2004). "Natural ventilation of a room with vents at multiple levels." Building and Environment **39**(5): 505-521.

FLUENT (1996). Fluent : user's guide. Lebanon, N.H., Fluent Incorporated.

Fox, R. W., A. T. McDonald and P. J. Pritchard (2006). Introduction to fluid mechanics, Hoboken : Wiley.

Franke, J., C. Hirsch, A. G. Jensen, H. W. Krus and M. Schatzmann (2004). Recommendations on the use of CFD in predicting pedestrian wind environment. COST Action 14.

Gan, G. (1995). "Numerical investigation of local thermal discomfort in offices with displacement ventilation." Energy and Buildings **23**(2): 73-81.

Gayev, Y. A. and E. Savory (1999). "Influence of street obstructions on flow processes within urban canyons." Journal of Wind Engineering and Industrial Aerodynamics **82**(1-3): 89-103.

Geist, J. F. (1983). Arcade. Cambridge, Mass., MIT Press.

Gennusa, M. L., A. Nucara, M. Pietrafesa and G. Rizzo (2006). "A model for managing and evaluating solar radiation for indoor thermal comfort." Solar Energy **81**(5): 594-606.

Givoni, B. (1969). Man, climate, and architecture. Amsterdam ; New York, Elsevier.

Givoni, B. (1976). Man, climate and architecture. London, Applied Science Publishers.

Gladstone, C. and A. W. Woods (2001). "On buoyancy-driven natural ventilation of a room with a heated floor." Jounal of Fluid Mechanics **441**: 293-314.

Goulding, J., J. O. Lewis and T. C. Steemers (1992). Energy in architecture: the European passive solar handbook. London, B.T. Batsford for the Commission of the European Communities, Directorate General XII for Science, Research and Development.

Hall, R. C. (1997). Evaluation of modelling uncertainty. CFD modelling of near-field atmospheric dispersion. Project EMU final report. Surrey, WS Atkins Consultants Ltd.

Hamilton, D. C. and W. R. Morgan (1952). Radiant interchange configuration factors. NASA TN 2836.

Hargreaves, D. M. and N. G. Wright (2006). "On the use of the k-e model in commercial CFD software to model the neutral atmospheric boundary layer." Journal of Wind engineering and Industrial Aerodynamics **95**(5): 355-369.

Haslavsky, V., J. Tanny and M. Teitel (2006). "Interaction between the mixing and displacement modes in a naturally ventilated enclosure." Building and Environment **41**(12): 1755-1761.

Heiselberg, P., Y. Li, A. Anderson, M. Bjerre and Z. Chen (2004). "Experimental and CFD evidence of multiple solutions in a naturally ventilated building." Indoor Air **14**: 43-54.

Hix, J. (1974). The Glass house. London, Phaidon.

Holford, J. M. and G. R. Hunt (2003). "Fundamental atrium design for natural ventilation." Building and Environment **38**(3): 409-426.

Houghten, F. C. and C. P. Yagloglou (1923). Determination of comfort zone. ASHVE Research Report.

Huang, H., Y. Akutsu, M. Arai and M. Tamura (2000). "A two-dimensional air quality model in an urban street canyon: evaluation and sensitivity analysis." Atmospheric Environment **34**(5): 689-698.

Hunt, G. R. and P. F. Linden (1999). "The fluid mechanics of natural ventilation - displacement ventilation by buoyancy-driven flows assisted by wind." Building and Environment **34**(6): 707-720.

Hunt, G. R. and P. F. Linden (2001). "Steady-state flows in an enclosure ventilated by buoyancy forces assisted by wind." Jounal of Fluid Mechanics **426**: 355-386.

Hunt, G. R. and P. F. Linden (2004). "Displacement and mixing ventilation driven by opposing wind and buoyancy." Journal of Fluid Mechanics **527**: 27-55.

ISO7730 (2005). Ergonomics of the thermal environment : analytical determination and interpretation of thermal comfort using calculation of the PMV and PPD indices and local thermal comfort criteria. Geneva, International Organization for Standardization.

Izard, J.-L. and F. Frusta (1998). Thermal comfort in atria: thermal stratification and architectural design. Proceedings of PLEA, Lisbon, Portugal.

Jeong, S. J. and M. J. Andrews (2002). "Application of the k-e turbulence model to the high Reynolds number skimming flow field of an urban street canyon." Atmospheric Environment **36**(7): 1137-1145.

Ji, Y., M. J. Cook and V. Hanby (2007). "CFD modelling of natural displacement ventilation in an enclosure connected to an atrium." Building and Environment **42**(3): 1158-1172.

Jiang, Y. (2002). Study of natural ventilation in buildings with large eddy simulation, Massachusetts Institute of Technology, USA.

Jiang, Y. and Q. Chen (2003). "Buoyancy-driven single-sided natural ventilation in buildings with large openings." International Journal of Heat and Mass Transfer **46**(6): 973-988.

Jones, P. J. and G. E. Whittle (1992). "Computational fluid dynamics for building air flow prediction - current status and capabilities." Building and Environment **27**(3): 321-338.

Judkoff, R. and J. Neymark (1995). International Energy Agency Building Energy Simulation Test and Diagnostic Method. IEA Energy Conservation in Buildings and Community Systems Programme Annex 21 and IEA Solar Heating and Cooling Programme Task 12.

Kang, J., P. L. Yap, Y. Meng and B. Chen (2007). Acoustics in large atrium spaces. Proceedings of the 14th International Congress on Sound and Vibration, Cairns, Australia.

Kastner-Klein, P. and E. J. Plate (1999). "Wind-tunnel study of concentration fields in street canyons." Atmospheric Environment **33**(24-25): 3973-3979.

Khalifa, A. J. N. and R. H. Marshall (1990). "Validation of heat transfer coefficients on interior building surfaces using a real-sized indoor test cell." International Journal of Heat and Mass Transfer **33**(10): 2219-2236.

Khaoua, S. A. O., P. E. Bournet, C. Migeon, T. Boulard and G. Chasseriaux (2006). "Analysis of greenhouse ventilation efficiency based on computational fluid dynamics." Biosystems Engineering **95**(1): 83-98.

Kindangen, J., G. Krauss and P. Depecker (1997). "Effects of roof shapes on wind-induced air motion inside buildings." Building and Environment **32**(1): 1-11.

Kurokawa, K. (1988). Rediscovering Japanese space, Weatherhill.

La Gennusa, M., A. Nucara, G. Rizzo and G. Scaccianoce (2005). "The calculation of the mean radiant temperature of a subject exposed to the solar radiation - a generalised algorithm." Buiding and Environment **40**(3): 367-375.

Lam, C. K. G. and K. Bremhorst (1981). "A modified form of the k-e model for predicting wall turbulence." Journal of Fluids Engineering, Transactions of the ASME **103**: 456-460.

Laouadi, A. and M. R. Atif (1999). "Comparison between computer and field measured thermal parameters in an atrium building." Building and Environment **34**(1999): 129-138.

Laouadi, A., M. R. Atif and A. Galasiu (2001). "Towards developing skylight design tools for thermal and energy performance of atriums in cold climates." Building and Environment **37**(2002): 1289-1316.

Laouadi, A., M. R. Atif and A. Galasiu (2003). "Methodology towards developing skylight design tools for thermal and energy performance of atriums in cold climates." Building and Environment **38**(1): 117-127.

Launder, B. E. and D. B. Spalding (1974). "The numerical computation of turbulent flows." Computer Methods in Applied Mechanics and Engineering **3**(2): 269-289.

Lebrun, J. (1970). Physiological requirements and physical conditions for air conditioning by concentrated static source, University de Liege, France.

Leschziner, M. (1991). "Modelling engineering flows with reynolds stress turbulence closure." Journal of Wind engineering and Industrial Aerodynamics **35**(1-3): 21-47.

Levermore, G. J. (2000). Building energy management systems: applications to low-energy HVAC and natural ventilation control. London, E & FN Spon.

Li, X.-X., C.-H. Liu, D. Y. C. Leung and K. M. Lam (2006). "Recent progress in CFD modelling of wind field and pollutant transport in street canyons." Atmospheric Environment **40**(29): 5640-5658.

Li, Y. (2000). "Buoyancy-driven natural ventilation in a thermally stratified one-zone building." Building and Environment **35**(3): 207-214.

Li, Y. and A. Delsante (2001). "Natural ventilation induced by combined wind and thermal forces." Building and Environment **36**(1): 59-71.

Li, Y., A. Delsante, Z. Chen, M. Sandberg, A. Andersen, M. Bjerre and P. Heilselberg (2001). "Some examples of solution multiplicity in natural ventilation." Building and Environment **36**(7): 851-858.

Li, Y., A. Delsante and J. Symons (2000). "Prediction of natural ventilation in buildings with large openings." Building and Environment **35**(3): 191-206.

Liddament, M. W. (1991). A review of building air flow simulation. AIVC Technical Note 33, AIVC, UK.

Liddament, M. W. (1996). A guide to energy efficient ventilation. Coventry, Air Infiltration and Ventilation Centre.

Lienhard, J. H. (2004). A heat transfer textbook. London, [s.n.].

Linden, P. F. (1999). "The fluid mechanics of natural ventilation." Annual Reviews of Fluid mechanics **31**: 201-238.

Linden, P. F. and P. Cooper (1996). "Multiple sources of buoyancy in a naturally ventilated enclosure." Jounal of Fluid Mechanics **311**: 177-192.

Linden, P. F., G. F. Lane-Serff and D. A. Smeed (1990). "Emptying filling boxes: the fluid mechanics of natural ventilation." Jounal of Fluid Mechanics **212**: 309-335.

Livermore, S. R. and A. W. Woods (2007). "Natural ventilation of a building with heating at multiple levels." Building and Environment **42**(3): 1417-1430.

Mabb, J. A. (2001). Modification of atrium design to improve thermal and daylighting performance. Centre for Medical, Health and Environmental Physics, Queensland University of Technology.

Montero, J. I., A. Anton, R. Kamaruddin and B. J. Bailey (2001). "Analysis of thermally driven ventilation in tunnel greenhouses using small scale models." Journal of Agriculture Engineering 79(2): 213-222.

Moser, A. (1992). Numerical simulation of room thermal convection - review of IEA Annex-20 results. Proceeding of International Symposium on Room Air Convection and Ventilation Effectiveness.

Murakami, S. (1993). "Comparison of various turbulence models applied to a bluff body." Journal of Wind engineering and Industrial Aerodynamics **46-47**: 21-36.

Murakami, S., S. Kato, S. akabayashi and Y. Tominaga (1992). "Velocity-pressure field of cross ventilation with open windows analyzed by wind tunnel and numerical simulation." Jounal of Wind Engineering and Industrial Aerodynamics 44(1-3): 2575-2586.

Nielsen, P. V. (1974). Flow in air-conditioned rooms. Copenhagen, Denmark, Technical University of Denmark.

Nielsen, P. V. (1989). Progress and trends in air infiltration and ventilation research. Proceedings of 10th AIVC Conference, Coventry.

Nielsen, P. V. (1998). "The selection of turbulence models for prediction of room airflow." ASHRAE Transactions **104**(1B): 1119-1127.

Niu, J. and J. van der Kooi (1992). Grid-optimisation for k-e turbulence model simulation of natural convection in rooms. Proceedings of ROOMVENT, Aalborg Denmark.

Oke, T. R. (1988). "Street design and urban canopy layer climate." Energy and Buildings **11**(1-3): 103-113.

Olson, D. A., L. R. Glicksman and H. M. Ferm (1990). "Steady-state natural convection in empty and partitioned enclosures at high rayleigh numbers." Journal of Heat Transfer **112**: 640-647.

Papakonstantinou, K. A., C. T. Kiranoudis and N. C. Markatos (2000). "Numerical simulation of air flow field in single-sided ventilated buildings " Energy and Buildings **33**(1): 41-48.

Patankar, S. V. (1980). Numerical heat transfer and fluid flow. [Great Britain], Taylor & Francis.

Patankar, S. V. and D. B. Spalding (1972). "A calculation procedure for heat, mass and momentum transfer in three-dimensional parabolic flows." International Journal of Heat and Mass Transfer **15**(10): 1787-1806.

Rafailidis, S. (1997). "Influence of building area density and roof shape on the wind characteristics above a town." Boundary Meteorology **85**(2): 255-271.

Rapoport, A. (1969). House Form and Culture. Englewood Cliffs, N.J.

Richards, P. J. and R. P. Hoxey (1993). "Appropriate boundary conditions for computational wind engineering models using the k-e turbulence model." Journal of Wind engineering and Industrial Aerodynamics **46-47**: 145-153.

Riskowski, G. L., S. E. Ford and K. O. Mankell (1998). "Laboratory measurements of wind effects on ridge vent performance." ASHRAE Transactions **104**(1A): 495-501.

Roache, P. J. (1972). Computational fluid mechanics. Albuquerque, New Mexico.

Rodi, W. (1980). Turbulence models and their application in hydraulics : a state of the art review, by Wolfgang Rodi. Delft, International Association for Hydraulic Research.

Russell, J. A. (2000). "Building types study." Architectural Record **188**.

Samant, S. and S. Sharples (2004). "Surface reflectance distributions and its effect on average daylight factor values in atrium buildings." Architectural Science Review **47**(2): 177-182.

Santamouris, M., F. Allard, E. European Commission. Directorate-General for and A. Programme (1998). Natural ventilation in buildings : a design handbook. London, James and James (Science Publishers) Ltd.

Saxon, R. (1983). Atrium buildings : development and design. London, Architectural Press.

Saxon, R. (1994). The atrium comes of age. Harlow, Longman.

Schild, P. (1997). Accurate prediction of indoor climate in glazed enclosures, Norwegian University of Science and Technology, Trondheim Norway.

Schild, P. G., P. O. Tjelflaat and D. Aiulfi (1995). "Guidelines for CFD modelling of atria." ASHRAE Transactions **101**(2): 1311 - 1332.

Schlichting, H. (1968). Boundary-layer theory. New York ; London, McGraw-Hill.

Seifert, J., Y. Li, J. Axley and M. Rosler (2006). "Calculation of wind-driven cross ventilation in buildings with large openings." Jounal of Wind Engineering and Industrial Aerodynamics **94**(12): 925-947.

Setty, B. S. (1983). "Atriums: the HVAC factor." ASHRAE Journal **25**(7): 40-45.

Shao, L., R. R. Walker and M. Woolliscroft (1993). Natural ventilation via courtyards: the application of CFD. Proceedings of 14th AIVC Conference, Copenhagen.

Sharples, S. and R. Bensalem (2001). "Airflow in courtyard and atrium building in the urban environment: a wind tunnel study." Solar Energy **70**(3): 237-244.

Shih, T. H., W. W. Liou, A. Shabbir, Z. Yang and J. Zhu (1995). "A new k-e eddy-viscosity model for high reynolds number turbulent flows - model development and validation " Computers and Fluids **24**(3): 227-238.

Smith, P. F. and A. C. Pitts (1997). Energy : building for the third millennium. London, Batsford.

Spengler, J. D. and Q. Chen (2000). "Indoor air quality factors in designing a healthy building." Annual Review of Energy and the Environment **25**: 567-600.

Tennekes, H. and J. L. Lumley (1972). A first course in turbulence. Cambridge [Mass.] ; London, M.I.T. Press.

Tutar, M. and G. Oguz (2002). "Large eddy simulation of wind flow around parallel buildings with varying configurations." Fluid Dynamics Research **31**(5-6): 289-315.

van Straaten, J. F. (1967). Thermal performance of buildings, Elsevier.

van Straaten, J. F., S. J. Richards, F. J. Lotz and E. N. van Deventer (1965). Ventilation and thermal considerations in school building design. Pretoria, N. B. R. I.

Versteeg, H. K. and W. Malalasekera (1995). An introduction to computational fluid dynamics : the finite volume method. Harlow, Longman Scientific & Technical.

Voeltzel, A., F. R. Carrie and G. Guarracino (2000). "Thermal and ventilation modelling of large highly-glazed spaces." Energy and Buildings **33**(2001): 121-132.

Walker, R. R., L. Shao and M. Woolliscroft (1993). Natural ventilation via courtyards: theory and measurement. Proceedings of 14th AIVC Conference, Copenhagen.

Wall, M. (1996). Climate and Energy Use in Glazed Spaces. Institute of Technology, Department of Building Science. Lund, Sweden, Lund University.

Wang, L. and N. H. Wong (2006). "The impacts of ventilation strategies and facade on indoor thermal environment for naturally ventilated residential buildings in Singapore " Building and Environment **42**(12): 4006-4015.

Watson, D. (1982). "The energy within the space within." Progressive Architecture **July 1982**: 97-102.

Whittle, G. E. (1986). "Computation of air movement and convective heat transfer within buildings." International Journal of Ambient Energy 7(2): 151-164.

Winslow, C. E. A., L. P. Herrington and A. P. Gagge (1937). "Relations between atmospheric conditions, Physiological reactions and sensations of pleasantness." American Journal of Physiology **26**: 103-115.

Yakhot, V., S. A. Orszag, S. Thangam, T. B. Gatski and C. G. Speziale (1992). "Development of turbulence models for shear flows by a double expansion technique." Physics of Fluids A 4(7): 1510-1520.

Yuan, X., A. Moser and P. Suter (1993). "Wall functions for numerical simulation of turbulent natural convection along vertical plates." International Journal of Heat and Mass Transfer **36**(18): 4477-4485.

Zhai, Z. (2003). Developing an integrated building design tool by coupling building energy simulation and computational fluid dynamics programs. Department of Architecture, MIT.

Zhai, Z. and Q. Chen (2004). "Numerical determination and treatment of convective heat transfer coefficient in the coupled building energy and CFD simulation " Building and Environment **39**(8): 1001-1009.

Zhai, Z., Q. Chen, P. Haves and J. H. Klems (2002). "On approaches to couple energy simulation and computational fluid dynamics programs." Building and Environment **37**(8-9): 875-864.

Zhang, Y. Q., A. H. Huber, S. P. S. Arya and W. H. Snyder (1993). "Numerical simulation to determine the effects of incident wind shear and turbulence level on the flow around a building." Journal of Wind Engineering and Industrial Aerodynamics **46-47**: 129-134.

APPENDIX A

Thermophysical properties of air

Table A.1: Thermophysical properties of air at atmospheric pressure (101325 Pa) (Lienhard 2004)

T (K)	ρ (kg/m^3)	c_p (J/kg·K)	μ (kg/m·s)	ν (m^2/s)	k (W/m·K)	α (m^2/s)	Pr
			Air				
100	3.605	1039	0.711×10^{-5}	0.197×10^{-5}	0.00941	0.251×10^{-5}	0.784
150	2.368	1012	1.035	0.437	0.01406	0.587	0.745
200	1.769	1007	1.333	0.754	0.01836	1.031	0.731
250	1.412	1006	1.606	1.137	0.02241	1.578	0.721
260	1.358	1006	1.649	1.214	0.02329	1.705	0.712
270	1.308	1006	1.699	1.299	0.02400	1.824	0.712
280	1.261	1006	1.747	1.385	0.02473	1.879	0.711
290	1.217	1006	1.795	1.475	0.02544	2.078	0.710
300	1.177	1007	1.857	1.578	0.02623	2.213	0.713
310	1.139	1007	1.889	1.659	0.02684	2.340	0.709
320	1.103	1008	1.935	1.754	0.02753	2.476	0.708
330	1.070	1008	1.981	1.851	0.02821	2.616	0.708
340	1.038	1009	2.025	1.951	0.02888	2.821	0.707
350	1.008	1009	2.090	2.073	0.02984	2.931	0.707
400	0.8821	1014	2.310	2.619	0.03328	3.721	0.704
450	0.7840	1021	2.517	3.210	0.03656	4.567	0.703
500	0.7056	1030	2.713	3.845	0.03971	5.464	0.704
550	0.6414	1040	2.902	4.524	0.04277	6.412	0.706
600	0.5880	1051	3.082	5.242	0.04573	7.400	0.708
650	0.5427	1063	3.257	6.001	0.04863	8.430	0.712
700	0.5040	1075	3.425	6.796	0.05146	9.498	0.715
750	0.4704	1087	3.588	7.623	0.05425	10.61	0.719
800	0.4410	1099	3.747	8.497	0.05699	11.76	0.723
850	0.4150	1110	3.901	9.400	0.05969	12.96	0.725
900	0.3920	1121	4.052	10.34	0.06237	14.19	0.728
950	0.3716	1131	4.199	11.30	0.06501	15.47	0.731
1000	0.3528	1142	4.343	12.31	0.06763	16.79	0.733
1100	0.3207	1159	4.622	14.41	0.07281	19.59	0.736
1200	0.2940	1175	4.891	16.64	0.07792	22.56	0.738
1300	0.2714	1189	5.151	18.98	0.08297	25.71	0.738
1400	0.2520	1201	5.403	21.44	0.08798	29.05	0.738
1500	0.2352	1211	5.648	23.99	0.09296	32.64	0.735

APPENDIX B

Algorithms for buoyancy-driven ventilation of a building with non-uniform temperature distribution

1. Airflow rate

Consider a simple building as shown in Figure B.1, in which the parameters involved in the development of the algorithms are also defined. A_u and A_l are the areas of the upper and lower openings; T_i and T_o are the indoor and outdoor air temperatures and T_i varies vertically; P_1 and P_4 are the outdoor pressures at the lower and upper openings; P_2 and P_3 are the indoor pressures at the lower and upper openings; h is the distance between the two openings; h_n is the neutral level.

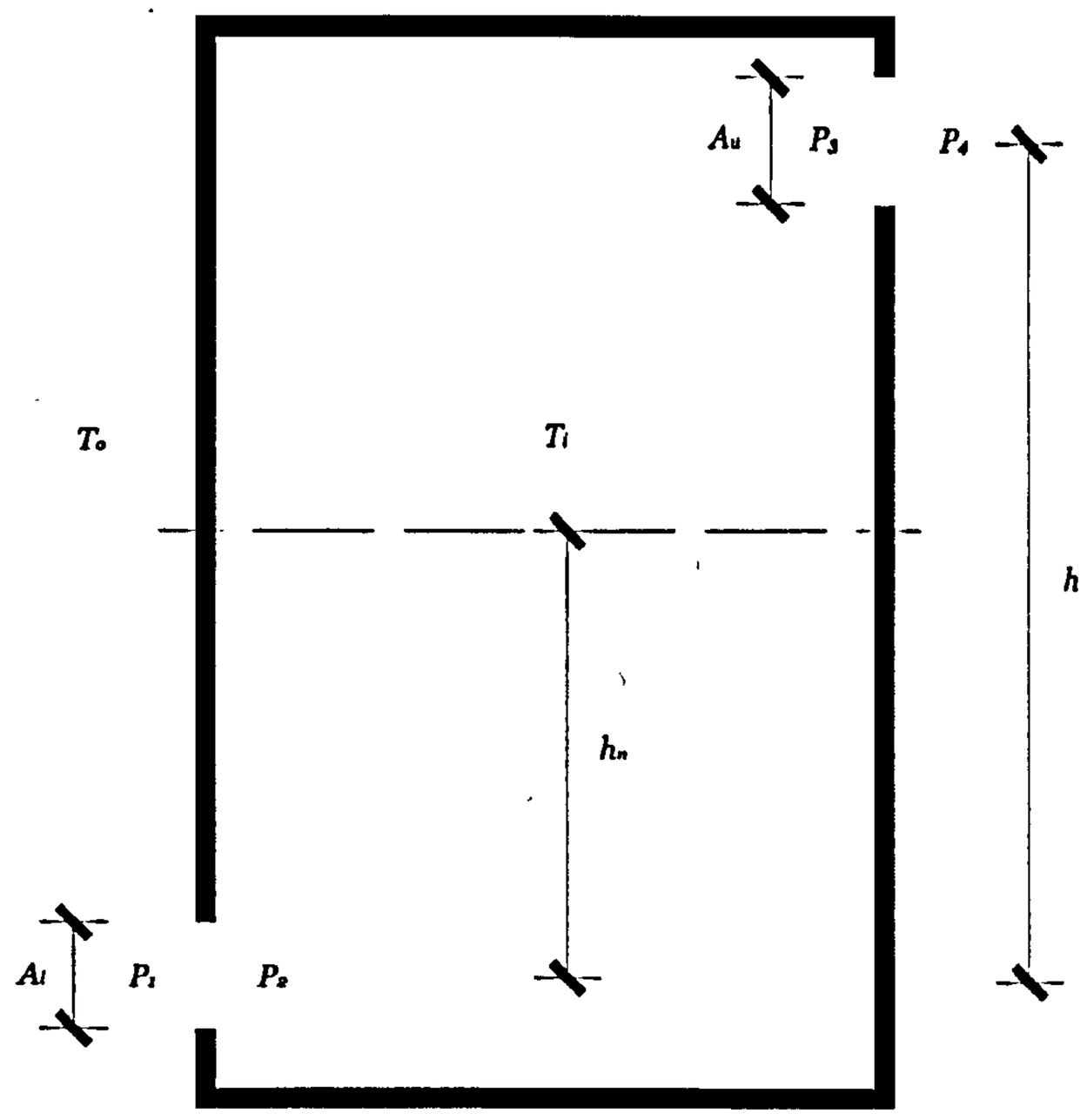

Figure B.1: Schematic illustration of the simple physical model considered in this appendix ($T_i > T_o$)

It has been introduced that, the airflow through an opening approximates to a simple square root law as expressed in Equation (B.1) (Etheridge and Sandberg 1996):

$$q = C_D A\sqrt{2\Delta p/\rho} \tag{B.1}$$

Thus, for the upper opening, we have:

$$q_u = (C_D A)_u\sqrt{2(P_3 - P_4)/\rho} \tag{B.2}$$

and for the lower opening we have:

$$q_l = (C_D A)_l\sqrt{2(P_1 - P_2)/\rho} \tag{B.3}$$

With Equations (B.2) and (B.3), we can obtain:

$$(P_1 - P_2) + (P_3 - P_4) = \frac{\rho(q_l)^2}{2[(C_D A)_l]^2} + \frac{\rho(q_u)^2}{2[(C_D A)_u]^2} \tag{B.4}$$

The outdoor static pressure difference between the levels of the upper and lower openings can be expressed as:

$$P_1 - P_4 = \rho_o g h \tag{B.5}$$

As the indoor air temperature is non-uniformly distributed, the internal air pressure cannot be assumed as uniform according to ideal gas law. The indoor static pressure difference between the levels of the upper and lower openings can be calculated as:

$$P_2 - P_3 = \int_0^h \rho_i g dh \tag{B.6}$$

According to mass conservation, the airflow rates through upper and lower openings are the same, thus:

$$q_l = q_u \tag{B.7}$$

Substituting (B.5) to (B.7) into (B.4), Equation (B.4) will become:

$$\rho_o g h - \int_0^h \rho_i g dh = \frac{1}{2}\rho_o q^2 \frac{1}{[(C_D A)^*]^2} \tag{B.8}$$

where
$$(C_D A)^* = \left[\frac{1}{[(C_D A)_l]^2} + \frac{1}{[(C_D A)_u]^2}\right]^{-\frac{1}{2}} \tag{B.9}$$

Assuming that the air temperature is inversely proportional to the pressure, the equation (B.8) becomes:

$$q = (C_D A)^* \sqrt{2gh(1 - \frac{1}{h}\int_0^h \frac{T_o}{T_j} dy)} \tag{B.10}$$

where T_j is the air temperature at vertical point j.

2. Neutral level

The neutral level is the defined as the distance from the lower opening to the neutral plane where the internal air pressure equals to the external air pressure. Substitute Equation (B.10) into Equation (B.3), the pressure difference at the lower opening can be calculated as:

$$P_1 - P_2 = \frac{\rho_o gh(1 - \frac{1}{h}\int_0^h \frac{T_o}{T_j} dy)[(C_D A)^*]^2}{[(C_D A)_t]^2} \tag{B.11}$$

This pressure difference can also be calculated by following equation considering the vertical pressure increment from the neutral level:

$$P_1 - P_2 = \int_0^{h_n} (\rho_o - \rho_i) g dy \tag{B.12}$$

Equating Equations (B.11) and (B.12), we have:

$$\int_0^{h_n} (1 - \frac{T_o}{T_i}) dy = \frac{h(1 - \frac{1}{h}\int_0^h \frac{T_o}{T_j} dy)[(C_D A)^*]^2}{[(C_D A)_t]^2} \tag{B.13}$$

By defining:

$$A_u^* = \frac{[(C_D A)_t]^2}{[(C_D A)_t]^2 + [(C_D A)_w]^2} \tag{B.14}$$

we can finally have:

$$\int_0^{h_n} (1 - \frac{T_o}{T_i}) dy = A_u^* (h - \int_0^h \frac{T_o}{T_j} dy) \tag{B.15}$$

APPENDIX C

Code for the calculation of the Mean Radiant Temperature at the occupants' level

```
% Calculate MRT;
display('This code can be used to predict the mean radiant temperature at the height of 1.6m');
display('Input the Parameters of the Sun Position:');
az=input('The Sun Position - the Azimuth:');
al=input('The Sun Position - the Altitude:');
display('Input the Parameters of the Atrium Space:');
L=input('Length:');
W=input('Width:');
H=input('Height:');
or=input('The Orientation of the Space:');
a=cos((az-or)*pi/180);
b=-sin((az-or)*pi/180);
c=tan(al*pi/180);
display('How Many Units do you want to Divide the Surface:');
N=input('Division Number:');
%% Determine the the glass surface(s) the sun impings on!
% Initialise the value of Diffuse Radiation Intensity;
Id1=0;
Id2=0;
Id3=0;
Id4=0;
Id5=0;
Id6=0;
R=input('Please Input the Number of the glass surface(s) the sun impingings on:');
if R==0
   P1=0;
   P2=0;
   P3=0;
   P4=0;
   P5=0;
end
if R==1
display('Please Input the Index (the Number) of the glass surface(s) the sun impingings on:');
display('A1B1C1D1 - 1;');
display('ABB1A1 - 2;');
display('CDD1C1 - 3');
display('ADD1A1 - 4');
display('BCC1B1 - 5');
R1=input('Please Input the Plane:','s');
if R1=='1'
  P1=1;
  P2=0;
```

APPENDIX C

Code for the calculation of the Mean Radiant Temperature at the occupants' level

```
% Calculate MRT;
display('This code can be used to predict the mean radiant temperature at the height of 1.6m');
display('Input the Parameters of the Sun Position:');
az=input('The Sun Position - the Azimuth:');
al=input('The Sun Position - the Altitude:');
display('Input the Parameters of the Atrium Space:');
L=input('Length:');
W=input('Width:');
H=input('Height:');
or=input('The Orientation of the Space:');
a=cos((az-or)*pi/180);
b=-sin((az-or)*pi/180);
c=tan(al*pi/180);
display('How Many Units do you want to Divide the Surface:');
N=input('Division Number:');
%% Determine the the glass surface(s) the sun impings on!
% Initialise the value of Diffuse Radiation Intensity;
Id1=0;
Id2=0;
Id3=0;
Id4=0;
Id5=0;
Id6=0;
R=input('Please Input the Number of the glass surface(s) the sun impingings on:');
if R==0
   P1=0;
   P2=0;
   P3=0;
   P4=0;
   P5=0;
end
if R==1
display('Please Input the Index (the Number) of the glass surface(s) the sun impingings on:');
display('A1B1C1D1 - 1;');
display('ABB1A1 - 2;');
display('CDD1C1 - 3');
display('ADD1A1 - 4');
display('BCC1B1 - 5');
R1=input('Please Input the Plane:','s');
if R1=='1'
  P1=1;
  P2=0;
```

```
  P3=0;
  P4=0;
  P5=0;
  Id1=input('Please input the Diffuse Radiation Intensity:');
end
if R1=='2'
  P1=0;
  P2=1;
  P3=0;
  P4=0;
  P5=0;
  Id2=input('Please input the Diffuse Radiation Intensity:');
end
 if R1=='3'
  P1=0;
  P2=0;
  P3=1;
  P4=0;
  P5=0;
  Id3=input('Please input the Diffuse Radiation Intensity:');
 end
 if R1=='4'
  P1=0;
  P2=0;
  P3=0;
  P4=1;
  P5=0;
  Id4=input('Please input the Diffuse Radiation Intensity:');
 end
  if R1=='5'
   P1=0;
   P2=0;
   P3=0;
   P4=0;
   P5=1;
   Id5=input('Please input the Diffuse Radiation Intensity:');
  end
end
if R==2
  display('Please Input the Index (the Number) of the the glass surface(s) the sun impingings
on:');
  display('A1B1C1D1 & ABB1A1 - 1;');
  display('A1B1C1D1 & CDD1C1 - 2;');
  display('A1B1C1D1 & ADD1A1 - 3');
  display('A1B1C1D1 & BCC1B1 - 4');
  display('ABB1A1 & BCC1B1 - 5');
  display('BCC1B1 & CDD1C1 - 6');
  display('CDD1C1 & ADD1A1 - 7');
  display('ADD1A1 & ABB1A1 - 8');
  R1=input('Please Input the surface:','s');
  if R1=='1'
   P1=1;
   P2=1;
   P3=0;
   P4=0;
   P5=0;
   Id1=input('Please input the Diffuse Radiation Intensity for A1B1C1D1:');
```

```
  Id2=input('Please input the Diffuse Radiation Intensity for ABB1A1:');
end
if R1=='2'
  P1=1;
  P2=0;
  P3=1;
  P4=0;
  P5=0;
  Id1=input('Please input the Diffuse Radiation Intensity for A1B1C1D1:');
  Id3=input('Please input the Diffuse Radiation Intensity for CDD1C1:');
end
 if R1=='3'
  P1=1;
  P2=0;
  P3=0;
  P4=1;
  P5=0;
  Id1=input('Please input the Diffuse Radiation Intensity for A1B1C1D1:');
  Id4=input('Please input the Diffuse Radiation Intensity for ADD1A1:');
end
if R1=='4'
  P1=1;
  P2=0;
  P3=0;
  P4=0;
  P5=1;
  Id1=input('Please input the Diffuse Radiation Intensity for A1B1C1D1:');
  Id5=input('Please input the Diffuse Radiation Intensity for BCC1B1:');
end
if R1=='5'
  P1=0;
  P2=1;
  P3=0;
  P4=0;
  P5=1;
  Id2=input('Please input the Diffuse Radiation Intensity for ABB1A1:');
  Id5=input('Please input the Diffuse Radiation Intensity for BCC1B1:');
end
if R1=='6'
  P1=0;
  P2=0;
  P3=1;
  P4=0;
  P5=1;
  Id3=input('Please input the Diffuse Radiation Intensity for CDD1C1:');
  Id5=input('Please input the Diffuse Radiation Intensity for BCC1B1:');
end
if R1=='7'
  P1=0;
  P2=0;
  P3=1;
  P4=1;
  P5=0;
  Id3=input('Please input the Diffuse Radiation Intensity for CDD1C1:');
  Id4=input('Please input the Diffuse Radiation Intensity for ADD1A1:');
end
if R1=='8'
```

```
    P1=0;
    P2=1;
    P3=0;
    P4=1;
    P5=0;
    Id2=input('Please input the Diffuse Radiation Intensity for ABB1A1:');
    Id4=input('Please input the Diffuse Radiation Intensity for ADD1A1:');
  end
end
if R==3
  display('Please Input the Index (the Number) of the the glass surface(s) the sun impingings
on:');
  display('A1B1C1D1 & ABB1A1 & BCC1B1 - 1;');
  display('A1B1C1D1 & BCC1B1 & CDD1C1 - 2;');
  display('A1B1C1D1 & CDD1C1 & ADD1A1 - 3;');
  display('A1B1C1D1 & ADD1A1 & ABB1A1 - 4;');
  R1=input('Please Input the surface:','s');
  if R1=='1'
    P1=1;
    P2=1;
    P3=0;
    P4=0;
    P5=1;
    Id1=input('Please input the Diffuse Radiation Intensity for A1B1C1D1:');
    Id2=input('Please input the Diffuse Radiation Intensity for ABB1A1:');
    Id5=input('Please input the Diffuse Radiation Intensity for BCC1B1:');
end
if R1=='2'
    P1=1;
    P2=0;
    P3=1;
    P4=0;
    P5=1;
    Id1=input('Please input the Diffuse Radiation Intensity for A1B1C1D1:');
    Id3=input('Please input the Diffuse Radiation Intensity for CDD1C1:');
    Id5=input('Please input the Diffuse Radiation Intensity for BCC1B1:');
end
 if R1=='3'
    P1=1;
    P2=0;
    P3=1;
    P4=1;
    P5=0;
    Id1=input('Please input the Diffuse Radiation Intensity for A1B1C1D1:');
    Id3=input('Please input the Diffuse Radiation Intensity for CDD1C1:');
    Id4=input('Please input the Diffuse Radiation Intensity for ADD1A1:');
 end
 if R1=='4'
    P1=1;
    P2=1;
    P3=0;
    P4=1;
    P5=0;
    Id1=input('Please input the Diffuse Radiation Intensity for A1B1C1D1:');
    Id2=input('Please input the Diffuse Radiation Intensity for ABB1A1:');
    Id4=input('Please input the Diffuse Radiation Intensity for ADD1A1:');
end
```

```
end
Ib=input('Please input the Direct Radiation Intensity:');
display('Please input the temperature of each surface(K):');
T1=input('The temperature of Surface A1B1C1D1:');
T2=input('The temperature of Surface ABB1A1:');
T3=input('The temperature of Surface CDD1C1:');
T4=input('The temperature of Surface ADD1A1:');
T5=input('The temperature of Surface BCC1B1:');
T6=input('The temperature of Surface ABCD:');
%% Calculate the coordinates of each division unit;
DIV=zeros(N,N,2);
for i=1:N
   for j=1:N
      DIV(i,j,1)=L/2/N+(i-1)*L/N;
      DIV(i,j,2)=W/2/N+(j-1)*W/N;
   end
end
%% Calculate the coordinates of the intersections with each surface of the
%% house;
CO=zeros(N,N,5,2);
VA=zeros(N,N,5,1); % valide value;
for i=1:N
   for j=1:N
      m=DIV(i,j,1);
      n=DIV(i,j,2);
      CO(i,j,1,1)=(H-1.6)*a/c+m;
      CO(i,j,1,2)=(H-1.6)*b/c+n;
      CO(i,j,2,1)=-a*n/b+m;
      CO(i,j,2,2)=-c*n/b;
      CO(i,j,3,1)=(W-n)*a/b+m;
      CO(i,j,3,2)=(W-n)/b*c;
      CO(i,j,4,1)=-m*b/a+n;
      CO(i,j,4,2)=-m*c/a;
      CO(i,j,5,1)=(L-m)*b/a+n;
      CO(i,j,5,2)=(L-m)*c/a;
      if (((CO(i,j,1,1)>=0)&(CO(i,j,1,1)<=L))&((CO(i,j,1,2)>=0)&(CO(i,j,1,2)<=W)))
         VA(i,j,1,1)=1;
      else
         VA(i,j,1,1)=0;
      end
      if (((CO(i,j,2,1)>=0)&(CO(i,j,2,1)<=L))&((CO(i,j,2,2)>=-1.6)&(CO(i,j,2,2)<=H-1.6)))
         VA(i,j,2,1)=1;
      else
         VA(i,j,2,1)=0;
      end
      if (((CO(i,j,3,1)>=0)&(CO(i,j,3,1)<=L))&((CO(i,j,3,2)>=-1.6)&(CO(i,j,3,2)<=H-1.6)))
         VA(i,j,3,1)=1;
      else
         VA(i,j,3,1)=0;
      end
      if (((CO(i,j,4,1)>=0)&(CO(i,j,4,1)<=W))&((CO(i,j,4,2)>=-1.6)&(CO(i,j,4,2)<=H-1.6)))
         VA(i,j,4,1)=1;
      else
         VA(i,j,4,1)=0;
      end
      if (((CO(i,j,5,1)>=0)&(CO(i,j,5,1)<=W))&((CO(i,j,5,2)>=-1.6)&(CO(i,j,5,2)<=H-1.6)))
         VA(i,j,5,1)=1;
```

```
      else
        VA(i,j,5,1)=0;
      end
    end
end
%% Finally get the information that whether a grid is being lighted or not;
LIGHTING=zeros(N,N,1);
for i=1:N
  for j=1:N
    X=P1*VA(i,j,1,1)+P2*VA(i,j,2,1)+P3*VA(i,j,3,1)+P4*VA(i,j,4,1)+P5*VA(i,j,5,1);
    if X==0
      LIGHTING(i,j,1)=0;
    else
      LIGHTING(i,j,1)=1;
    end
  end
end
LIGHT=LIGHTING;
%%display('LIGHT is a Matrix Denoting ////////////////////////');
%%display('LIGHT=');
%%LIGHT
%%  Calculate View Factor F;
VF1=zeros(N,N,1); % for surface A1B1C1D1;
VF2=zeros(N,N,1); % for surface ABB1A1;
VF3=zeros(N,N,1); % for surface CDD1C1;
VF4=zeros(N,N,1); % for surface ADD1A1;
VF5=zeros(N,N,1); % for surface BCC1B1;
VF6=zeros(N,N,1); % for surface ABCD;
% For surface A1B1C1D1
for i=1:N
  for j=1:N
    aa=L/2/N+(i-1)*L/N;
    bb=W/N/2+(j-1)*W/N;
    cc=H-1.6;
    % calculate VF1 for A1B1C1D1;
    aa1=aa;
    bb1=bb;
    cc1=cc;
    A=aa1/cc1;
    B=bb1/cc1;
    F11=1/2/pi*(A/sqrt(1+A^2)*atan(B/sqrt(1+A^2))+B/sqrt(1+B^2)*atan(A/sqrt(1+B^2)));
    aa1=L-aa;
    A=aa1/cc1;
    F12=1/2/pi*(A/sqrt(1+A^2)*atan(B/sqrt(1+A^2))+B/sqrt(1+B^2)*atan(A/sqrt(1+B^2)));
    bb1=W-bb;
    B=bb1/cc1;
    F13=1/2/pi*(A/sqrt(1+A^2)*atan(B/sqrt(1+A^2))+B/sqrt(1+B^2)*atan(A/sqrt(1+B^2)));
    aa1=aa;
    A=aa1/cc1;
    F14=1/2/pi*(A/sqrt(1+A^2)*atan(B/sqrt(1+A^2))+B/sqrt(1+B^2)*atan(A/sqrt(1+B^2)));
    F1=F11+F12+F13+F14;
    VF1(i,j,1)=F1;
    % Calculate VF2 for ABB1A1;
    aa2=cc;
    bb2=aa;
    cc2=bb;
    A=aa2/bb2;
```

```
C=cc2/bb2;
Y=sqrt(A^2+C^2);
F21=1/2/pi*(atan(1/C)-C/Y*atan(1/Y));
aa2=cc;
bb2=L-aa;
cc2=bb;
A=aa2/bb2;
C=cc2/bb2;
Y=sqrt(A^2+C^2);
F22=1/2/pi*(atan(1/C)-C/Y*atan(1/Y));
aa2=1.6;
bb2=L-aa;
cc2=bb;
A=aa2/bb2;
C=cc2/bb2;
Y=sqrt(A^2+C^2);
F23=1/2/pi*(atan(1/C)-C/Y*atan(1/Y));
aa2=1.6;
bb2=aa;
cc2=bb;
A=aa2/bb2;
C=cc2/bb2;
Y=sqrt(A^2+C^2);
F24=1/2/pi*(atan(1/C)-C/Y*atan(1/Y));
F2=F21+F22+F23+F24;
VF2(i,j,1)=F2;
% Calculate VF3 for CDD1C1;
aa3=cc;
bb3=aa;
cc3=W-bb;
A=aa3/bb3;
C=cc3/bb3;
Y=sqrt(A^2+C^2);
F31=1/2/pi*(atan(1/C)-C/Y*atan(1/Y));
aa3=cc;
bb3=L-aa;
cc3=W-bb;
A=aa3/bb3;
C=cc3/bb3;
Y=sqrt(A^2+C^2);
F32=1/2/pi*(atan(1/C)-C/Y*atan(1/Y));
aa3=1.6;
bb3=aa;
cc3=W-bb;
A=aa3/bb3;
C=cc3/bb3;
Y=sqrt(A^2+C^2);
F33=1/2/pi*(atan(1/C)-C/Y*atan(1/Y));
aa3=1.6;
bb3=L-aa;
cc3=W-bb;
A=aa3/bb3;
C=cc3/bb3;
Y=sqrt(A^2+C^2);
F34=1/2/pi*(atan(1/C)-C/Y*atan(1/Y));
F3=F31+F32+F33+F34;
VF3(i,j,1)=F3;
```

```
% Calculate VF4 for ADD1A1;
aa4=cc;
bb4=bb;
cc4=aa;
A=aa4/bb4;
C=cc4/bb4;
Y=sqrt(A^2+C^2);
F41=1/2/pi*(atan(1/C)-C/Y*atan(1/Y));
aa4=cc;
bb4=W-bb;
cc4=aa;
A=aa4/bb4;
C=cc4/bb4;
Y=sqrt(A^2+C^2);
F42=1/2/pi*(atan(1/C)-C/Y*atan(1/Y));
aa4=1.6;
bb4=bb;
cc4=aa;
A=aa4/bb4;
C=cc4/bb4;
Y=sqrt(A^2+C^2);
F43=1/2/pi*(atan(1/C)-C/Y*atan(1/Y));
aa4=1.6;
bb4=W-bb;
cc4=aa;
A=aa4/bb4;
C=cc4/bb4;
Y=sqrt(A^2+C^2);
F44=1/2/pi*(atan(1/C)-C/Y*atan(1/Y));
F4=F41+F42+F43+F44;
VF4(i,j,1)=F4;
% Calculate VF5 for BCC1B1;
aa5=1.6;
bb5=bb;
cc5=L-aa;
A=aa5/bb5;
C=cc5/bb5;
Y=sqrt(A^2+C^2);
F51=1/2/pi*(atan(1/C)-C/Y*atan(1/Y));
aa5=1.6;
bb5=W-bb;
cc5=L-aa;
A=aa5/bb5;
C=cc5/bb5;
Y=sqrt(A^2+C^2);
F52=1/2/pi*(atan(1/C)-C/Y*atan(1/Y));
aa5=cc;
bb5=bb;
cc5=L-aa;
A=aa5/bb5;
C=cc5/bb5;
Y=sqrt(A^2+C^2);
F53=1/2/pi*(atan(1/C)-C/Y*atan(1/Y));
aa5=cc;
bb5=W-bb;
cc5=L-aa;
A=aa5/bb5;
```

```
C=cc5/bb5;
Y=sqrt(A^2+C^2);
F54=1/2/pi*(atan(1/C)-C/Y*atan(1/Y));
F5=F51+F52+F53+F54;
VF5(i,j,1)=F5;
%Calculate VF6 for ABCD;
aa6=aa;
bb6=bb;
cc6=1.6;
A=aa6/cc6;
B=bb6/cc6;
F61=1/2/pi*(A/sqrt(1+A^2)*atan(B/sqrt(1+A^2))+B/sqrt(1+B^2)*atan(A/sqrt(1+B^2)));
aa6=L-aa;
bb6=bb;
cc6=1.6;
A=aa6/cc6;
B=bb6/cc6;
F62=1/2/pi*(A/sqrt(1+A^2)*atan(B/sqrt(1+A^2))+B/sqrt(1+B^2)*atan(A/sqrt(1+B^2)));
aa6=L-aa;
bb6=W-bb;
cc6=1.6;
A=aa6/cc6;
B=bb6/cc6;
F63=1/2/pi*(A/sqrt(1+A^2)*atan(B/sqrt(1+A^2))+B/sqrt(1+B^2)*atan(A/sqrt(1+B^2)));
aa6=aa;
bb6=W-bb;
cc6=1.6;
A=aa6/cc6;
B=bb6/cc6;
F64=1/2/pi*(A/sqrt(1+A^2)*atan(B/sqrt(1+A^2))+B/sqrt(1+B^2)*atan(A/sqrt(1+B^2)));
F6=F61+F62+F63+F64;
VF6(i,j,1)=F6;
  end
end
VF1=VF1/2;
VF2=VF2/2;
VF3=VF3/2;
VF4=VF4/2;
VF5=VF5/2;
VF6=VF6/2;
TT=zeros(N,N,1);
for i=1:N
  for j=1:N
    if LIGHT(i,j,1)==0

VWFV=VF1(i,j,1)*Id1+VF2(i,j,1)*Id2+VF3(i,j,1)*Id3+VF4(i,j,1)*Id4+VF5(i,j,1)*Id5+VF6(i,j
,1)*Id6;
      TT(i,j,1)=(VF1(i,j,1)*T1^4+VF2(i,j,1)*T2^4+VF3(i,j,1)*T3^4+VF4(i,j,1)*T4^4+...
        VF5(i,j,1)*T5^4+VF6(i,j,1)*T6^4+0.7*10^8/5.67/0.97*VWFV)^0.25;
    else

VWFV=VF1(i,j,1)*Id1+VF2(i,j,1)*Id2+VF3(i,j,1)*Id3+VF4(i,j,1)*Id4+VF5(i,j,1)*Id5+VF6(i,j
,1)*Id6;
      TT(i,j,1)=(VF1(i,j,1)*T1^4+VF2(i,j,1)*T2^4+VF3(i,j,1)*T3^4+VF4(i,j,1)*T4^4+...

VF5(i,j,1)*T5^4+VF6(i,j,1)*T6^4+0.7*10^8/5.67/0.97*VWFV+(0.24*0.7*10^8*Ib/0.97/5.67))
^0.25;
```

```
      end
   end
end
TT=TT';
for i=1:N
   for j=1:N
      T(i,j,1)=TT(N-i+1,j,1);
   end
end
VF1=VF1';
for i=1:N
   for j=1:N
      VF1(i,j,1)=VF1(N-i+1,j,1);
   end
end
display('T=');
T
%END
```